NASA Conference Publication 3159

23rd Annual Precise Time and Time Interval (PTTI) Applications and Planning Meeting

Proceedings of a meeting held at
the Ritz-Carlton Huntington Hotel
Pasadena, California
December 3–5, 1991

NASA

NASA Conference Publication 3159

23rd Annual Precise Time and Time Interval (PTTI) Applications and Planning Meeting

Editorial Committee Chairman
Richard L. Sydnor
Jet Propulsion Laboratory
Pasadena, California

Proceedings of a meeting sponsored by the U.S. Naval Observatory, the NASA Goddard Space Flight Center, the Jet Propulsion Laboratory, the Space and Naval Warfare Systems Command, the Naval Research Laboratory, the Army Electronics Technology and Devices Laboratory, the Rome Laboratory, and the Air Force Office of Scientific Research and held at the Ritz-Carlton Huntington Hotel
Pasadena, California
December 3–5, 1991

NASA
National Aeronautics and Space Administration
Office of Management
Scientific and Technical Information Program
1992

PRECISE TIME AND TIME INTERVAL (PTTI) APPLICATIONS AND PLANNING MEETING

ORDER FORM FOR THE PROCEEDINGS

	Year	Cost	Available	Unavailable
1	1969			X
2	1970	$25.00	X	
3	1971	$25.00		X
4	1972	$25.00	X	
5	1973	$25.00	X	
6	1974	$25.00	X	
7	1975	$25.00	X	
8	1976			X
9	1977			X
10	1978	$25.00	X	
11	1979	$25.00	X	
12	1980	$25.00	X	
13	1981	$25.00	X	
14	1982	$25.00		X
15	1983	$25.00	X	
16	1984	$25.00	X	
17	1985	$25.00	X	
18	1986	$20.00	X	
19	1987	$25.00	X	
20	1988	$35.00	X	
21	1989	$65.00	X	
22	1990	$70.00	X	
23	1991	$85.00	X	

Please circle copy(ies) requested and make the check payable to "Treasurer, PTTI". **Please do not add personal names or addresses to the pay line on the check. We cannot accept invoices.** Please return the check and the Order Form to:

Mrs. Sheila Faulkner
Chairman, PTTI Executive Committee
U. S. Naval Observatory
Time Service Department
34th and Massachusetts Avenue, NW
Washington, DC 20392-5100
(202) 653-1460 FAX: 202/653-0909

It is with great regret that we must announce we can no longer absorb the cost of air mailing to international addresses; therefore, the Proceedings will be shipped by Surface Mail. However, if you wish to pay the air mail postage, we will notify you of the cost before mailing. For example, Air Mail to Europe is currently estimated at $27.90 for the first 5 pounds. Each additional pound is $4.00.

When you register for the PTTI Meeting or order the Proceedings, your name is added to the PTTI Mailing list to automatically receive future meeting information.

EXECUTIVE COMMITTEE

Sheila C. Faulkner, Chairman
U.S. Naval Observatory

Paul Bergschneider
Space and Naval Warfare Systems Command

James A. Buisson
U.S. Naval Research Laboratory

Morton A. Dubinsky
Space and Naval Warfare Systems Command

Hugh S. Fosque
NASA Headquarters

Raymond Granata
NASA Goddard Space Flight Center

Dr. Helmut Hellwig
Air Force Office of Scientific Research

Dr. William J. Klepczynski
U.S. Naval Observatory

Mr. Paul H. Kuhnle
NASA/Jet Propulsion Laboratory

Dr. Richard L. Sydnor
NASA/Jet Propulsion Laboratory

Dr. John R. Vig
Army Electronics Technology and Devices Laboratory

Dr. Joseph D. White
U.S. Naval Research Laboratory

Dr. Gernot M.R. Winkler
U.S. Naval Observatory

Dr. Nicholas F. Yannoni
Rome Air Development Center

Ms. Nicolette Jardine
Support Assistance
U.S. Naval Observatory

OFFICERS

GENERAL CHAIRMAN

DR. MARTIN W. LEVINE

Smithsonian Astrophysical Observatory

TECHNICAL PROGRAM COMMITTEE CHAIRMAN

MR. S. CLARK WARDRIP

Bendix Field Engineering Corporation

ASSISTANT TECHNICAL PROGRAM COMMITTEE CHAIRMAN

MRS. DEBRA COLEMAN

Bonneville Power Administration

ASSISTANT TECHNICAL PROGRAM COMMITTEE CHAIRMAN

DR. SIGFRIDO LESCHIUTTA

Politechnico Di Torino

TECHNICAL PROGRAM COMMITTEE MEMBERS

DR. LEONARD S. CUTLER
Hewlett-Packard

DR. HENRY F. FLIEGEL
The Aerospace Corporation

MR. PAUL F KUHNLE
Jet Propulsion Laboratory

DR. MARTIN W. LEVINE
Smithsonian Asrophysical Observatory

MR. TERRY N. OSTERDOCK
Stellar Navigation, Incorporated

DR. RICHARD L. SYDNOR
Jet Propulsion Laboratory

MR. PHILIP E. TALLEY

The Aerospace Corporation

EDITORIAL COMMITTEE CHAIRMAN

DR. RICHARD L. SYDNOR

Jet Propulsion Laboratory

EDITORIAL COMMITTEE MEMBERS

Mr. T. Tucker
Jet Propulsion Laboratory
California Institute of Technology

Dr. M. Calhoun
Jet Propulsion Laboratory
California Institute of Technology

Mr. Albert Kirk
Jet Propulsion Laboratory
California Institute of Technology

Dr. G. J. Dick
Jet Propulsion Laboratory
California Institute of Technology

PUBLICITY AND EXHIBITS CHAIRMAN

MR. FRANCIS MULLEN

Frequency and Time Systems, Incorporated

TECHNICAL ASSISTANCE

MR. PAUL KUSHMEIDER

Bendix Field Engineering Corporation

MR. JEFFREY S. INGOLD

Bendix Field Engineering Corporation

INVITED SPEAKERS

DR. DONALD B. PERCIVAL

University of Washington

MR. ROBERT E. WILSON

University of Idaho

SESSION CHAIRMEN

SESSION IA
Mr. William J. Riley
EG&G

SESSION IB
Dr. John R. Vig
Army Electronics Technology and Devices Laboratory

SESSION II
Mr. James L. Wright
Computer Science Raytheon

SESSION IIIA
Dr. Joseph D. White
Naval Research Laboratory

SESSION IIIB
Mr. Paul F. Kuhnle
Jet Propulsion Laboratory

SESSION IV
Dr. Henry F. Fliegel
Aerospace Corporation

SESSION V
Dr. Leonard S. Cutler
Hewlett-Packard Company

SESSION VI
Dr. Claudine Thomas
BIPM

SESSION VII
Dr. Giovanni Busca
Observatoire Cantonal de Neuchâtel

SESSION VIII
Dr. Gernot M.R. Winkler
U.S. Naval Observatory

ARRANGEMENTS

Sheila C. Faulkner
Paul F. Kuhnle
Dr. Richard L. Sydnor
Paul J. Kushmeider

FINANCE COMMITTEE

Dr. William J. Klepczynski
Sheila C. Faulkner

RECEPTIONISTS

The receptionists at the 23rd Annual PTTI meeting were:

Ms. Maddie Green, Jet Propulsion Laboratory
Ms. Kathy Hibbard, Datum
Ms. Nicolette Jardine, U.S. Naval Observatory
Mrs. Aline Kuhnle, Jet Propulsion Laboratory
Mrs. Mary Levine, Smithsonian Astrophysical Observatory
Mrs. Betty Wardrip, Bendix Field Engineering Corporation

PTTI ADVISORY BOARD COMMITTEES
1992

OFFICE	NAME	ORGANIZATION
Chairman	Mr. S. Clark Wardrip	BFEC
Vice Chairman	Mr. Martin B. Bloch	FEI
Finance Committee	Mr. Martin B. Bloch, Chairman	FEI
	Mr. S. Clark Wardrip	BFEC
	Mr. James L. Wright	CSR
	Mr. Gary Smith	KODE
Exhibits Committee	Mr. Francis Mullen, Chairman	FTS
	Dr. Martin W. Levine	SAO
	Mr. Ron C. Roloff	Austron
	Mr. Jack McNabb	TRAK
	Mr. William J. Riley	EG&G
	Dr. Robert F. C. Vessot	SAO
	Mr. Michael R. Tope	Truetime
Guest Speaker Committee	Mr. Robert H. Kern, Chairman	KERNCO
	Professor Carroll O. Alley	University of MD
	Dr. Leonard S. Cutler	HP
	Professor Bradford Parkinson	Stanford University
	Dr. Victor S. Reinhardt	Hughes
	Dr. Samuel R. Stein	Timing Solutions
	Dr. Richard L. Sydnor	JPL
Reports Committee	Mr. Terry N. Osterdock, Chairman	STI
	Mr. Paul F. Kuhnle	JPL
	Mr. Paul J. Kushmeider	BFEC
	Professor Harry Robinson	Duke University
	Mr. Philip E. Talley	Aerospace
	Dr. James A. Barnes	Austron
1991 PTTI Officers		
	General Chairman	
	Dr. Martin W. Levine	SAO
	Program Chairman	
	Mr. S. Clark Wardrip	BFEC
	PTTI Editorial Chairman	
	Dr. Richard L. Sydnor	JPL

NOTE: NON-GOVERNMENT OFFICERS OF THE PTTI ARE AUTOMATICALLY MEMBERS OF THE PTTI ADVISORY BOARD FOR THE YEAR(S) THAT THEY ARE IN OFFICE.

1991 ADVISORY BOARD MEMBERS
Mr. S. Clark Wardrip, Chairman

Bendix Field Engineering Corporation

Professor Carroll O. Alley
University of Maryland

Dr. James A. Barnes
Austron, Inc.

Mr. Martin B. Bloch
Frequency Electronics, Inc.

Mrs. Mary Chiu
Johns Hopkins University
Applied Physics Laboratory

Dr. Leonard S. Cutler
Hewlett-Packard Company

Dr. Henry F. Fliegel
The Aerospace Corporation

Mr. Robert H. Kern
Kernco, Inc.

Mr. Paul J. Kushmeider
Bendix Field Engineering Corp.

Mr. Jack McNabb
TRAK Microwave

Mr. Donald Mitchell
Austron, Inc.

Mr. Francis Mullen
Frequency and Time Systems, Inc.

Mr. Jerry Norton
Johns Hopkins University
Applied Physics Laboratory

Mr. Allen W. Osborne
Allen Osborne Associates

Mr. Terry N. Osterdock
Stellar Navigation, Inc.

Professor Bradford W. Parkinson
Stanford University

Dr. Victor S. Reinhardt
Hughes Aircraft

Mr. William J. Riley
EG&G, Inc.

Professor Harry Robinson
Duke University

Mr. Ron Roloff
FTS/Austron (DATUM)

Mr. Gary Smith
KODE

Dr. Samuel R. Stein
Timing Solutions Corporation

Mr. Philip E. Talley
The Aerospace Corporation

Mr. Michael R. Tope
Truetime

Dr. Robert F. C. Vessot
Smithsonian Astrophysical
Observatory

Mr. S. Clark Wardrip
Bendix Field Engineering Corp.

Mr. James L. Wright
Computer Sciences/Raytheon

CONTENTS

SESSION IA
Time Synchronization
Chairman: William J. Riley
EG&G

SESSION IB
Panel Discussion - Vendor and User Problems
Moderator: John R. Vig
AETDL

SESSION II
Tutorials
Chairman: James L. Wright
CSR

SESSION IIIA
Applications of PTTI
Chairman: Joseph D. White
U.S. Naval Research Laboratory

SESSION IIIB
Poster Session
Chairman: Paul F. Kuhnle
Jet Propulsion Laboratory

SESSION IV

Frequency Standard Performance

Chairman: Henry F. Fliegel
The Aerospace Corporation

SESSION V

Workshop - Applications of Optical Techniques to Frequency and Time Systems

Chairman: Leonard S. Cutler
Hewlett-Packard

SESSION VI

International Time Keeping: Status, Performance and Results

Chairman: Claudine Thomas
Bureau International des Poids et Mesures

SESSION VII

Scientific Applications of Frequency and Time

Chairman: Giovanni Busca
Observatoire de Neuchatel

THE NEED FOR GPS STANDARDIZATION

W. Lewandowski, G. Petit and C. Thomas
Bureau International des Poids et Mesures
Pavillon de Breteuil
92312 Sèvres Cedex
France

Abstract

A desirable and necessary step for improvement of the accuracy of GPS time comparisons is the establishment of common GPS standards. For this reason, the CCDS proposed the creation of a special group of experts with the objective of recommending procedures and models for operational time transfer by GPS common-view method.

Since the announcement of the implementation of Selective Availability at the end of last spring, action has become much more urgent and this CCDS Group on GPS Time Transfer Standards has now been set up. It operates under the auspices of the permanent CCDS Working Group on TAI and works in close cooperation with the Sub-Committee on Time of the CGSIC.

Taking as an example the implementation of SA during the first week of July 1991, this paper illustrates the need to develop urgently at least two standardized procedures in GPS receiver software: monitoring GPS tracks with a common time scale and retaining broadcast ephemeris parameters throughout the duration of a track. Other matters requiring action are the adoption of common models for atmospheric delay, a common approach to hardware design and agreement about short-term data processing. Several examples of such deficiencies of standardization are presented.

INTRODUCTION

In recent years the operational GPS worldwide time transfer by C/A code receivers in common-view mode [1] has seen significant progress in both precision and accuracy [2]. The accuracy of GPS time links within continents now approaches two nanoseconds on an operational basis. Between continents, the accuracy of operational links is between 10 and 20 nanoseconds. Some recent studies, however, have shown that, when using an accurate homogeneous reference frame for antenna coordinates, ionospheric measurements and post-processed precise satellite ephemerides, these long-distance time comparisons can be achieved with an accuracy of a few nanoseconds [3].

But when approaching such a level of accuracy other problems arise. These are mainly due to the lack of standardization in the software and hardware of commercial receivers which, for example, process raw data differently or treat the input signal to the antenna in different ways. There is, in addition, a need to remove the effects of SA degradation of GPS signals.

The first section of this paper presents an analysis of the effects of SA with the example of its implementation during the beginning of July 1991. We show here the absolute necessity of strict

common views and of data post-processing with precise satellite ephemerides to overcome SA effects. There is a consequent need for unified procedures in the design of GPS time receivers.

The second section deals with some other deficiencies of GPS time transfer which could be reduced in the framework of an international standardization. Several examples are given and are illustrated by the diversity of GPS time receiver types now in operation at the BIPM and national centers.

The third section of this paper briefly reports on the roles of the formal bodies concerned with GPS standardization: the CGSIC Subcommittee on Time and the CCDS Group on GPS Time Transfer Standards.

IMPLEMENTATION OF SA, JULY 1-4 1991

The GPS system was designed with an optional facility to degrade the GPS signals available to non- cleared users. The degradation is called 'Selective Availability' (SA). In addition to SA, there is also Anti-Spoofing (AS).

The activation of SA and AS makes the GPS Precise Positioning Service (PPS), which contains the full accuracy of GPS, inaccessible to those without encryption keys (authorized users). However, the Clear Access (C/A) 1.023 MHz code on L1 frequency remains available for all users and provides the GPS Standard Positioning Service (SPS). In case of SA, the SPS has a stated 95% accuracy in two dimensions of 100 meters in position and 167 ns in time [4].

According to the information available to the civil community, the degradation brought about by SA concerns only Block II satellites and consists of a phase jitter in the satellite clock and a changeable bias in the broadcast ephemerides. For the civil users, SA causes peak-to-peak inaccuracies of several hundreds of nanoseconds in the direct extraction of GPS time from Block II satellites [5].

This was observed for four consecutive days at the beginning of July 1991. Figure 1 shows an example of raw GPS data taken at Paris Observatory (Paris, France): a time modulation as high as 200ns is added to the usual noise affecting the GPS data.

Use of post-processed precise ephemerides

The effect of a changeable bias in the broadcast ephemerides can be overcome if precise post-processed ephemerides are available. Such precise ephemerides are produced by the Defense Mapping Agency (DMA) and the National Geodetic Survey (NGS) [6]. They are received on a regular basis at the BIPM, the delay before access being several weeks. Their estimated accuracy is of order 3m.

In practice, computations with precise ephemerides require knowledge of the broadcast ephemerides used by the receiver software in order to apply differential corrections [7], so it is necessary to collect regularly GPS broadcast ephemerides, at least at some sites in the world. Another difficulty is the possible change of ephemeris parameters during the usual 13-minute tracking period. This makes it necessary to modify the software of current GPS receivers in order to retain a single set of ephemeris parameters for the full duration of the track.

At the BIPM the software of one commercial GPS receiver has been modified to permit a 13-minute freezing of ephemeris parameters and the recording of broadcast ones. We are thus in position to

Figure 1. [UTC(OP) - GPS time]

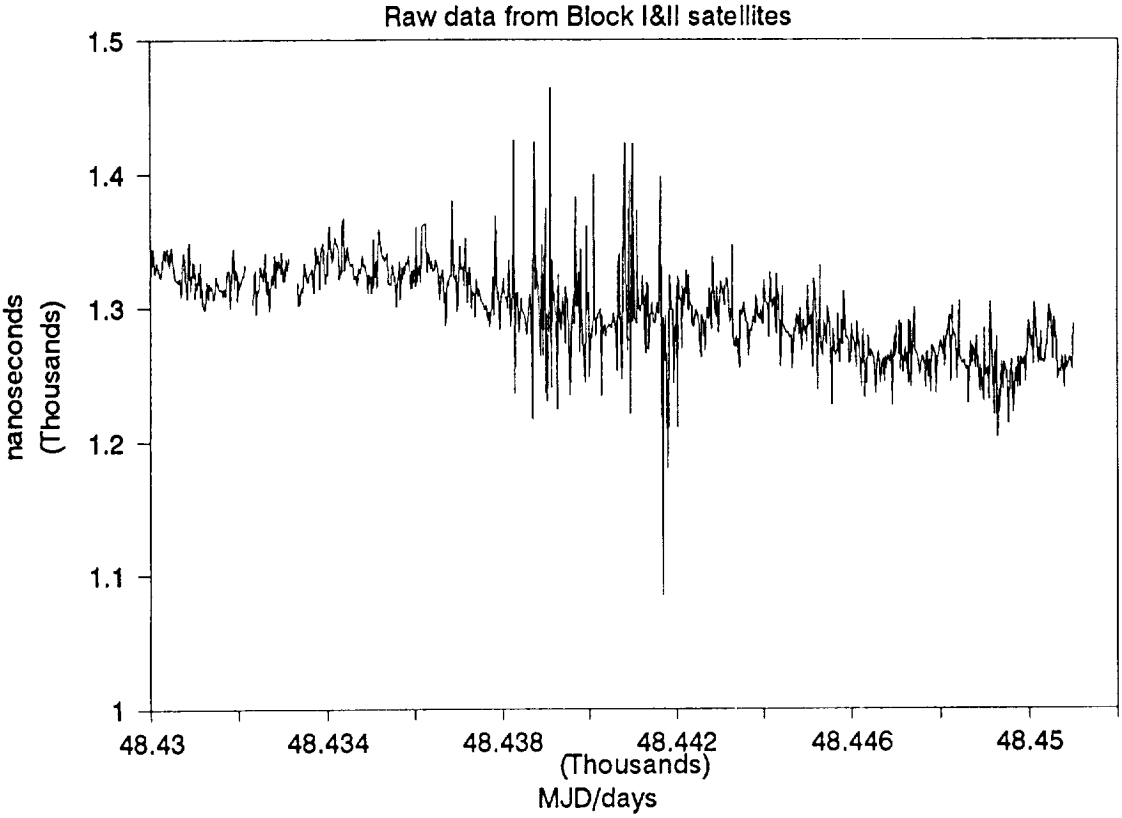

correct raw GPS data for precise satellite ephemerides [8].

The raw data taken at Paris Observatory at the beginning of July 1991 are repeated in Figure 2-a for Block I satellites and in Figure 2-b for a selection of Block II satellites, those for which we can effectively process an ephemeris correction. The results of this correction process are shown in Figures 3-a and 3-b, together with the smoothed values [UTC(OP) - GPS time] obtained from Block I satellites only, through a Vondrak smoothing with a cut-off period of about 3 days [9].

The use of precise ephemerides improves the precision of time extraction from Block I satellites, and removes major errors from Block II satellites. For the 4- day period (1-4 July 1991) the root mean square of the residuals to the smoothed values [UTC(OP) - GPS time] is equal to 15.4ns for Block I satellites and to 29.9ns for Block II satellites. Such a high value for the Block II satellites implies that the specific implementation of SA used in this period consists not only in the degradation of satellite ephemerides but also in the activation of on-board clock jitter.

It is interesting to make a quantitative evaluation of the amount of noise brought about by SA during these four days:

* The degradation of ephemerides can be estimated from the root mean square of the differential time corrections between broadcast and precise ephemerides. From the values computed at the BIPM for the period 1-4 July 1991, we obtain about 39ns. However, this value is probably

an under-estimate as the differential corrections for satellite 21, one of those most affected by SA, is unavailable (no recording of its broadcast ephemerides at that time).

* The noise observed for Block II satellites corrected for precise ephemerides (Fig. 3-b) comes both from clock jitter brought about by SA and from the usual noise of time extraction. This latter can be estimated from data taken from Block I satellites (Fig. 3-a). Thus this gives a rough estimation of the root mean square of the clock-jitter deviation of about 26ns.

Computation of strict common views

It is possible to eliminate on-board clock jitter in the comparison of remote clocks on the Earth. This supposes that strict common-view observations are available [**1**,**5**], that is observations having:

* same track length (780s),
* same start time (within 1s).

These conditions on timing express the need for a common reference time scale for monitoring tracks. This is not always the case at present: the BIPM international schedule refer to UTC time but some commercial receivers refer to GPS time or even mix UTC time and GPS time.

To complete the example of SA described here, we have computed the long-distance time comparisons [UTC(OP) - UTC(NIST)] for 21 consecutive days covering the period 1-4 July 1991. The residuals to smoothed values (Vondrak smoothing with a 3-day cut-off period [**9**]) are shown in Figure 4-a from strict common views. They show that on- board clock jitter noise is canceled, but ephemerides degradation is still present. After applying corrections for precise ephemerides (Fig. 4-b) the effect of SA become indiscernible: the root mean square of the residuals to smoothed values drops to 5.2ns for the 21- day period. Figure 4-c, where correction for measured ionospheric delay on both branches of the link is applied [**8**], is yet more striking: the precision of the time transfer (root mean square of the residuals) is a remarkable 2.7ns.

Conclusions

The particular example of SA chosen here does not correspond to the full specification of SA given in official documents [**4**]. The civil community must be then prepared to face even more serious problems. At least we know how to overcome SA in a post-processed mode: we use precise satellite ephemerides and strict common-view observations.

The impact on the need for GPS Standardization is now very clear: local GPS time receivers should, at least, use the same reference time for monitoring track start time and retain ephemeris parameters over the 13- minute duration of a track. It may also be wise to follow, strictly, the international schedule for common- view time transfer issued by the BIPM.

EXAMPLES OF DEFICIENCIES IN GPS TIME-TRANSFER CAUSED BY A LACK OF STANDARDIZATION

In this section we give some examples of deficiencies in GPS time transfer caused by a lack of standardization. We report briefly on recent progress and underline residual difficulties. Some of these points have already been discussed in [10] so we have chosen here to focus on topics pointed out more recently.

Homogenization of antenna coordinates

At one time, errors in antenna coordinates contributed one of the largest terms to the global error budgets of GPS time links [2]. These errors were first reduced for continental links [11,12], then, in 1990, a global homogenization of coordinates was realized in one of the most accurate reference frames, the ITRF (IERS Terrestrial Reference Frame) [13]. The BIPM continues this effort of homogenization by providing accurate coordinates in ITRF (uncertainties range from 10cm to 1m) to new laboratories equipped with GPS time receivers and contributing to TAI. The last GPS antenna position determined by the BIPM is installed near Moscow in the VNIIFTRI: it is the first ITRF point in USSR, the uncertainty of the determination is 1m [14].

Receiver hardware

A recent study [15] has shown one particular GPS time receiver type to be sensitive to external temperature. This sensitivity has been shown to depend on the length of antenna cables. With a 100m antenna cable the peak-to-peak deviations can reach 20ns.

Recently a sensitivity to signal power has been discovered at the NIST (National Institute of Standards and Technology, Boulder, Colorado) [16]: when a 10dB pad is added to the antenna, the measured receiver delay is modified. Generally this change is of order 1ns, but for one receiver tested at the NIST the change was much higher.

At present time, the reasons for such discrepancies are not completely understood but it is already clear that a standardization in hardware design may be necessary.

Receiver software

A typical example

Colleagues from the Laboratoire Primaire du Temps et des Fréquences (LPTF, Paris, France), responsible for the production of TA(F) and UTC(OP), have recently drawn the attention of the BIPM to an example of non-uniformity in the treatment of GPS signals by different GPS receivers operating in France.

Figures 5-a, 5-b and 5-c summarize the situation. The LPTF operates on site three receivers from different manufacturers A, B and C. Raw GPS data [UTC(OP) - GPS time] obtained by receivers A and B are in good agreement except for satellite 19 (Fig. 5-a) which provides raw values with a

spread of about 15ns. Raw GPS data obtained by receivers C and B are in good agreement even for satellite 19 (Fig. 5-b).

The CNES (Centre National d'Etudes Spaciales, Toulouse, France) operates one receiver of type A. When computing the time link [UTC(CNES) - UTC(OP)] with receiver A in CNES and B in LPTF, values given from observing satellite 19 are too small by about 15ns (Fig. 5-c).

It may be that receivers of type A perform an incorrect treatment of data from satellite 19 for some reason at present unknown, while receivers of types B and C handle it correctly. But there is an alternative: satellite 19 data may be treated correctly by receiver of type A, while all other values are wrong.

Sampling of short-term GPS data

For most of GPS time receivers, short-term data are taken every 15s. For others short-term data are taken every 6s but offer an option which allows the choice of 6s or 15s for basic observations. Another receiver, recently put in operation at the BIPM, uses 1s intervals short-term measurement. In addition short-term raw data are not treated identically. This could make it difficult to define the actual start times of tracks when strict common views are necessary.

Sampling of short-term measurement is one important element of receiver software which is not standardized, but other points are questionable, among them the models which are used for estimation of the ionospheric and tropospheric delays of GPS signals, and also the regular updates of constants used in receiver software.

GPS data format

At present time most GPS receivers use the so-called 'NBS format' initially developed for 'NBS type' receivers in 1983.

Until early 1990, this standard format has fully played its role. The problem of defining a new format for GPS data files arose when ionospheric measurement systems began to operate in tandem with current time receivers. The automatic correction of GPS data by ionospheric measurements raised several questions, in particular the need to provide additional data columns for ionospheric measurements and the corresponding statistical parameters. The values of the tropospheric model should also be present in the output files.

In addition to these new questions, there is an incoherence in the usual data format: the quantities issued are not referenced to the same instant of the track. 'START TIME' is given for the beginning of the track while 'ELEVATION' and 'AZIMUTH' of the satellite refer to its position at the end of the track. The useful data 'REF-GPS' is referenced to any of the beginning, the mid-point or the end of the track, among which, statistically, the mid-point value is the most reliable. In fact all the values given in GPS data files should be referenced to the mid-point of the track.

The choice of unit is also questionable. It has become necessary to specify time values in tenths of nanoseconds rather than in nanoseconds. The elevation and azimuth of the satellite should also be given in tenths of degrees.

Finally, it must be remembered that the arrangement of the columns is only the visible part of the work. It is also necessary to agree on and to distribute the corresponding software. Setting up a

new format also means that users need to be informed about its meaning for the best use of data.

Most discussion about the GPS data format is now opened. Receiver manufacturers and the staff of the national time laboratories are invited to give their opinions and suggestions. Agreement on the format may constitute the first concrete output of the official bodies set up to deal with the problem of GPS standardization.

FORMAL BODIES FOR GPS STANDARDIZATION

Two formal bodies are concerned with GPS coordination and standardization, they are the CGSIC Subcommittee on Time and the CCDS Group on GPS Time Transfer Standards [11].

The Subcommittee on Time of the Civil GPS Service Interface Committee (CGSIC) is mainly a forum for the exchange of information between military and civilian elements. It cannot undertake formal decisions. On the one hand, the Subcommittee provides up to date information to the civil timing community , as presently reports on progress in the computation of precise satellite ephemerides and their availability. On the other hand, it promotes the needs of the civil community, especially about SA, during general meetings of the CGSIC.

The CCDS Group on GPS Time Transfer Standards (CGGTTS) operates under the auspices of the permanent Working Group on TAI of the Comité Consultatif pour la Définition de la Seconde (CCDS). This Group can initiate formal procedures as the CCDS could choose to submit its recommendations and standards to the approbation of the Comité International des Poids et Mesures (CIPM) and then to the Conférence Générale des Poids et Mesures (CGPM). The Group on GPS Time Transfer Standards was set up during the summer of 1991. Its first formal meeting was held on 2 December 1991 during the 23rd PTTI meeting in Pasadena, California.

The CGSIC Subcommitee on Time and the CCDS Group on GPS Time Transfer Standards are indispensable and are complementary.

CONCLUSIONS

Accuracy of a few nanoseconds in GPS time transfer is now possible even for long-distance links using post- processed corrections. Further improvements are feasible through international coordination and standardization of receiver hardware and software. Joint action is required to overcome the SA degradation of GPS signals. Two complementary formal bodies are concerned with these matters, the CGSIC Subcommitee on Time and the CCDS Group on GPS Time Transfer Standards. At the end of 1991, the prime activities of these two committees are, respectively, providing information on SA to the civil timing community and initiating a widespread debate on GPS data format.

ACKNOWLEDGMENTS

The authors wish to thank Dr. Granveaud and R. Tourde from LPTF for kindly providing the Figures 5-a, 5-b and 5-c of this paper.

References

1. D. W. Allan and M. A. Weiss, *"Accurate Time and Frequency Transfer during Common-View of a GPS Satellite"*, Proc. 34th Annual Symposium on Frequency Control, pp. 334-346, 1980.

2. W. Lewandowski and C. Thomas, *"GPS Time Transfer"*, IEEE Special Issue on Time and Frequency, 79, pp. 991-1000, 1991.

3. W. Lewandowski, G. Petit and C. Thomas, *"Accuracy of GPS Time Transfer Verified by Closure around the World"*, accepted in Proc. 23rd Annual Precise Time and Time Interval (PTTI) Applications and Planning Meeting, 1991.

4. NATO Standardization Agreement (STANAG) 4294 (1 August 1990), Arinc Research Corporation, 2551 Riva Road, Annapolis, MD 21401, United States, Publication 3659-01- 01-4296.

5. D. W. Allan, M. Granveaud, W. J. Klepczynski and W. Lewandowski, *"GPS Time Transfer with Implementation of Selective Availability"*, in Proc. 22nd Annual Precise Time and Time Interval (PTTI) Applications and Planning Meeting, pp. 145-156, 1990.

6. W. Lewandowski, G. Petit and C. Thomas, *"Precise GPS Ephemerides from DMA and NGS Tested by Time Transfer"*, accepted in Proc. 23rd Annual Precise Time and Time Interval (PTTI) Applications and Planning Meeting, 1991.

7. W. Lewandowski and M. A. Weiss, *"The Use of Precise Ephemerides for GPS Time Transfer"*, in Proc. 21st Annual Precise Time and Time Interval (PTTI) Applications and Planning Meeting, pp. 95-106, 1989.

8. W. Lewandowski, G. Petit, C. Thomas and M. A. Weiss, *"The Use of Precise Ephemerides, Ionospheric Data and Corrected Antenna Coordinates in a long-distance GPS Time Transfer"*, in Proc. 22nd Annual Precise Time and Time Interval (PTTI) Applications and Planning Meeting, pp. 547-558, 1990.

9. J. Vondrak, *"A Contribution to the Problem of Smoothing Observational Data"*, Bull. Astron. Inst. Czechoslovakia, 20, pp. 349-355, 1969.

10. W. Lewandowski, C. Thomas and D. W. Allan, *"CGSIC Subcommittee on Time and CCDS Group of Experts on GPS Standardization"*', in Proc. ION GPS-91 4th International Technical Meeting, in press, 1991.

11. B. Guinot and W. Lewandowski, *"Improvement of the GPS Time Comparisons by Simultaneous Relative Positioning of the Receiver Antennas"*, in Bulletin Géodésique, 63 pp. 371-386, 1989.

12. W. Lewandowski, R. J. Douglas, W. J. Klepczynski, W. Strange, J. Suter and M. A. Weiss, *"Positioning of GPS Antennas in Time-Keeping Laboratories of North America"*, in Proc. 43rd Annual Symposium on Frequency Control, pp. 218-224, 1989.

13. W. Lewandowski, *"High Accuracy Ground-Antenna Coordinates for GPS Time Transfer"*, in Proc. IAG Symposium G2-Permanent Satellite Tracking Networks for Geodesy and Geodynamics, Vienna, August 1991, in press.

14. W. Lewandowski, G. Petit and C. Thomas, *"Comparison of GLONASS and GPS Time Transfers between University of Leeds and VNIIFTRI"*, accepted in Proc. 23rd Annual Precise Time and Time Interval (PTTI) Applications and Planning Meeting, 1991.

15. W. Lewandowski and R. Tourde, *"Sensitivity to the External Temperature of some GPS Time Receivers"*, in Proc. 22nd Annual Precise Time and Time Interval (PTTI) Applications and Planning Meeting, pp. 307-316, 1990.

16. D. Davis, NIST, Boulder, Colorado, USA, personal communication.

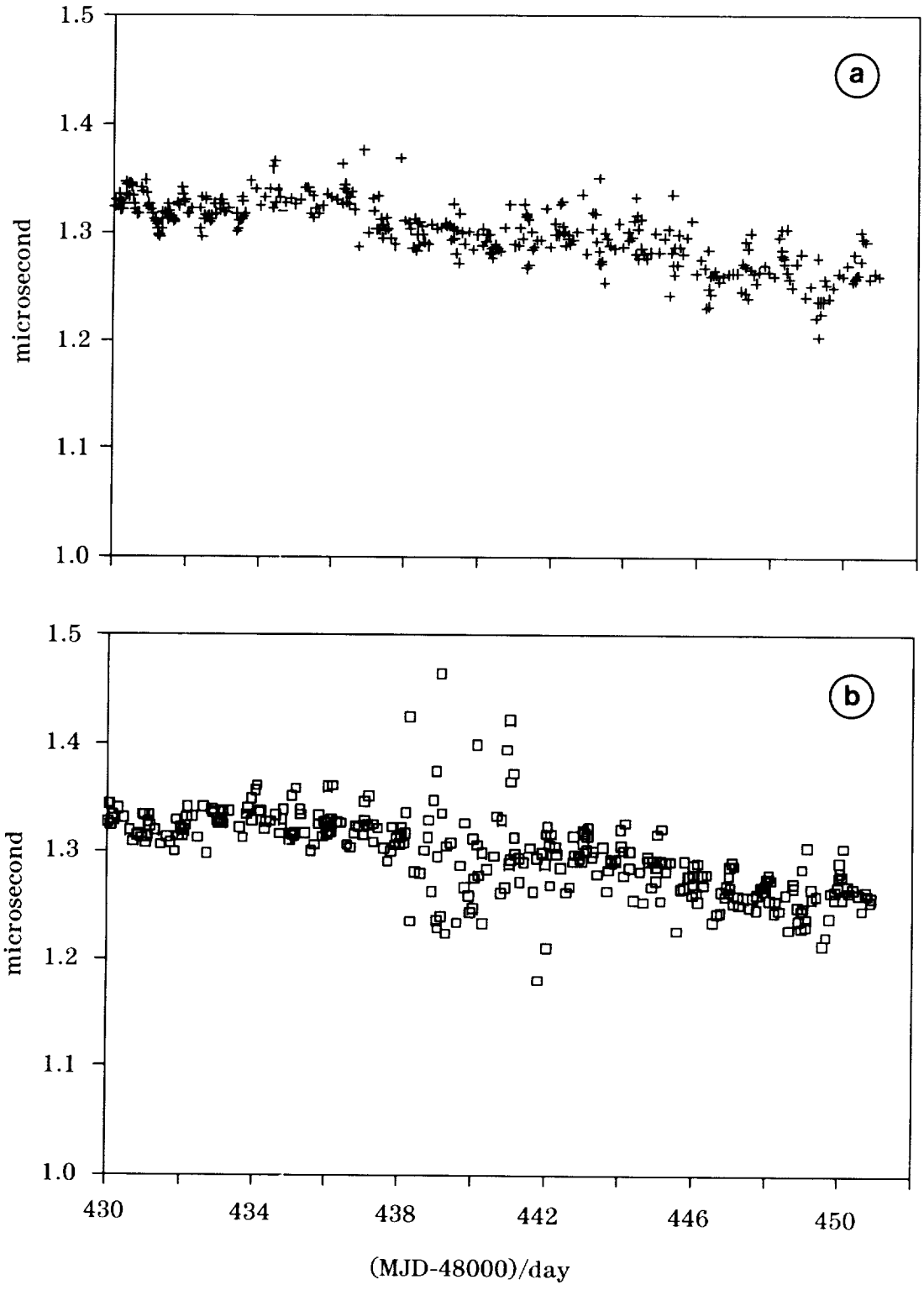

FIGURE 2. *Raw GPS data [UTC(OP) - GPS time] taken at Paris Observatory from 23 June to 14 July 1991,*
2-a. from Block I satellites only,
2-b. from a selection of Block II satellites.

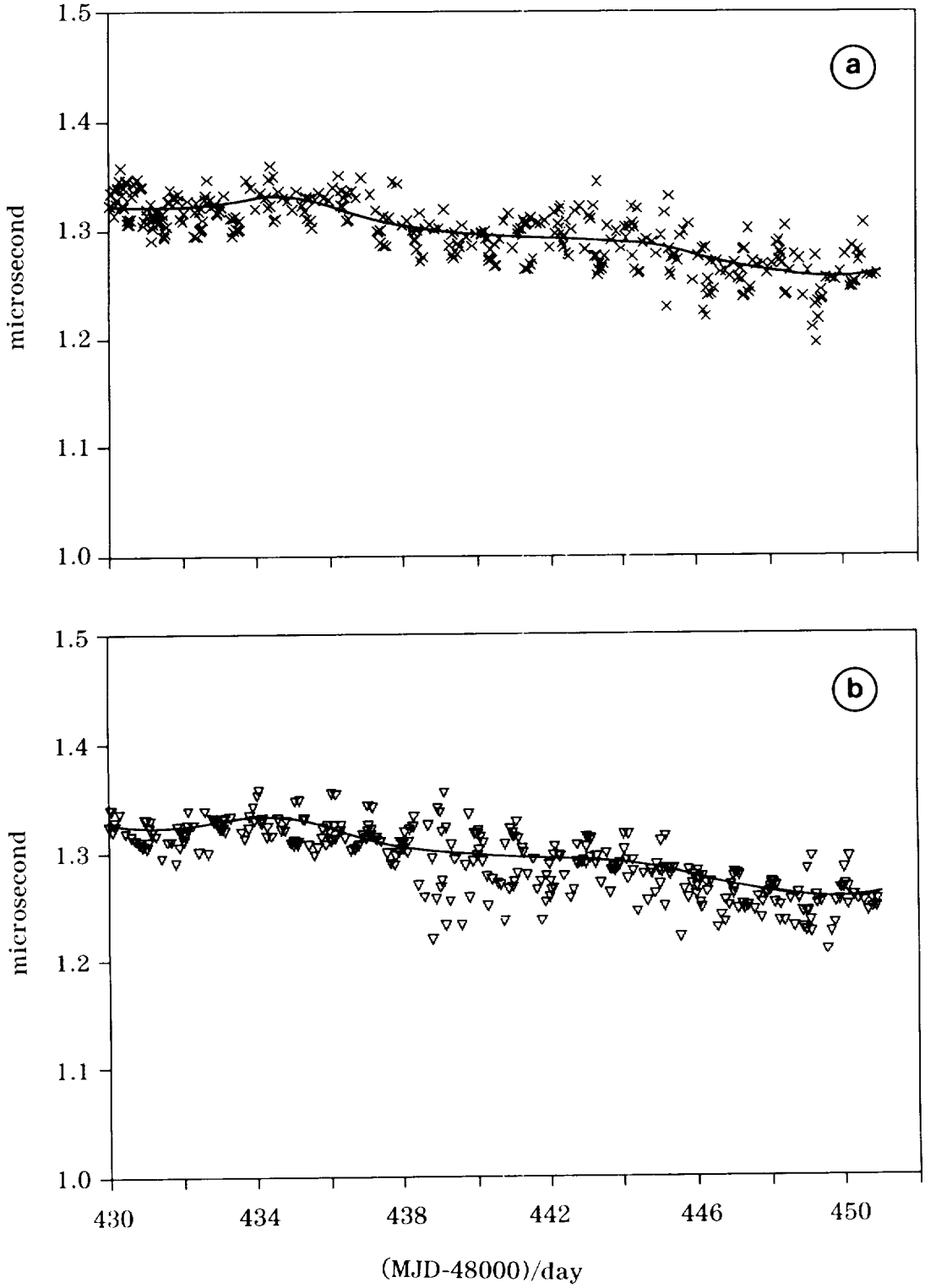

FIGURE 3. *GPS data [UTC(OP) - GPS time] taken at Paris Observatory from 23 June to 14 July 1991, after correction for precise ephemerides,*
3-a. from Block I satellites only,
3-b. from a selection of Block II satellites.
The continuous line represents the smoothed values [UTC(OP) - GPS time] obtained from Block I satellites only.

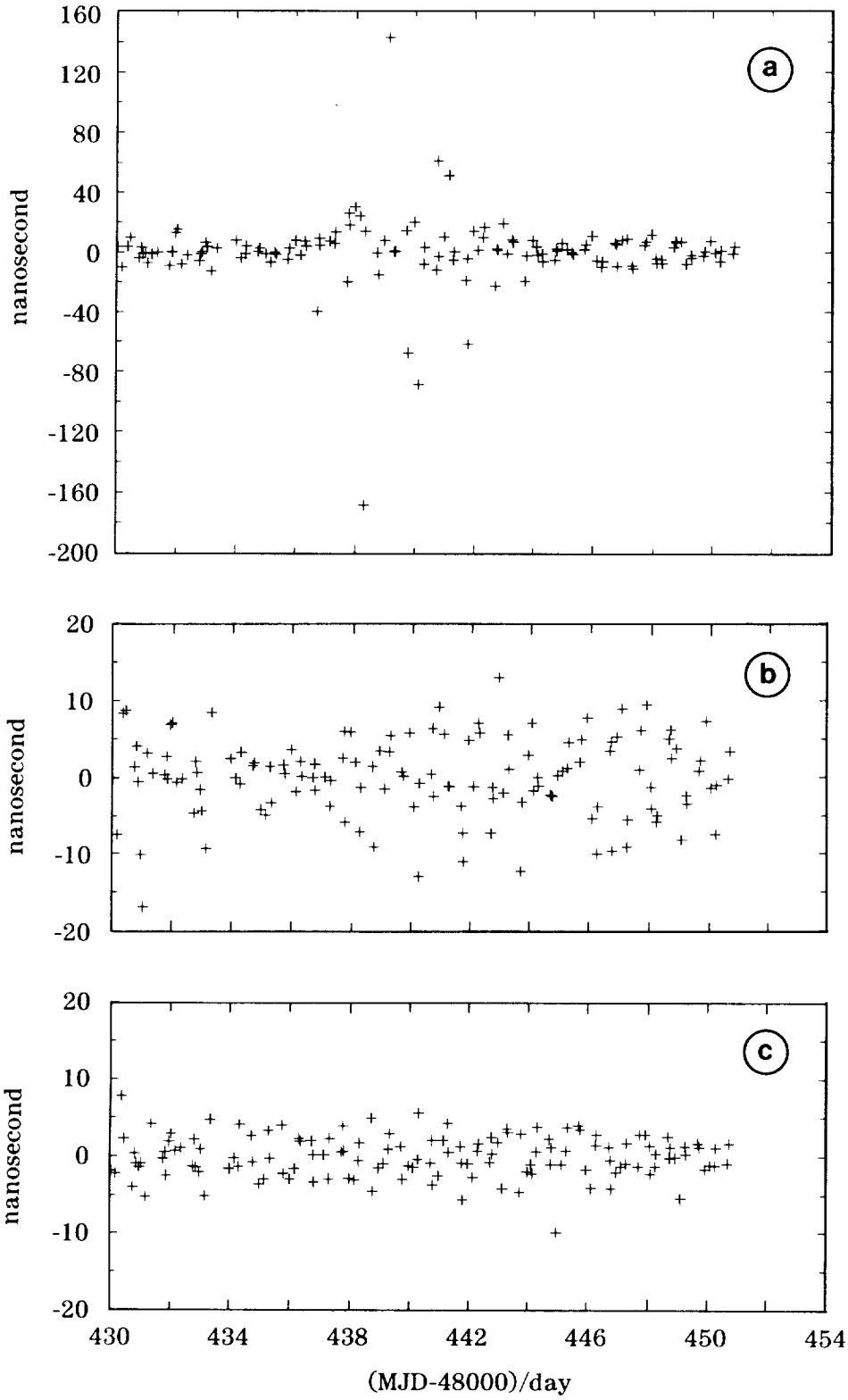

FIGURE 4. *Time link [UTC(OP) - UTC(NIST)] computed from strict common views,*
4-a. with raw GPS data,
4-b. with GPS data corrected for precise ephemerides,
4-c. with GPS data corrected for precise ephemerides and ionospheric measurements.

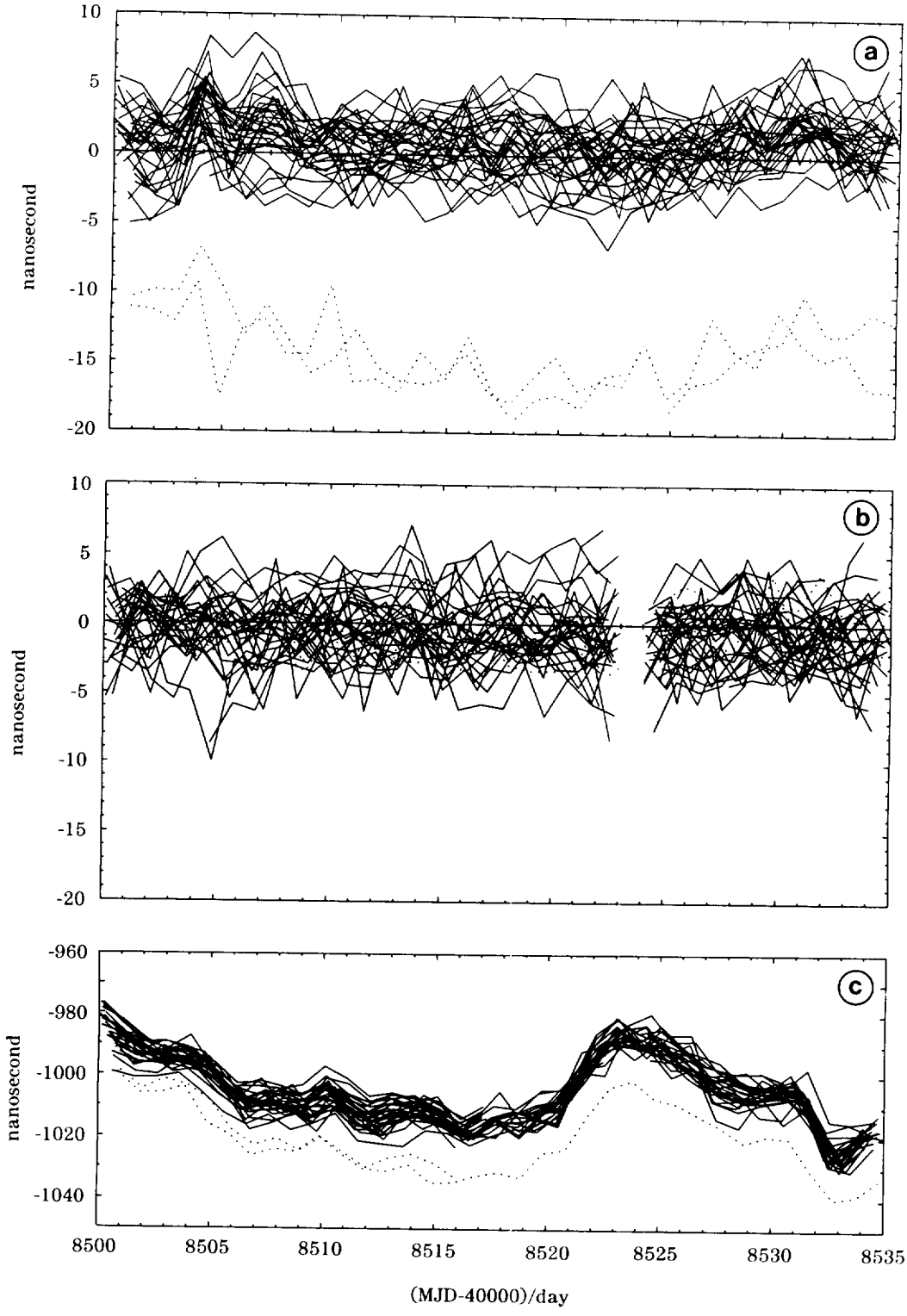

FIGURE 5. *GPS data taken by three different GPS time receivers (A-, B-, C-type) at two sites in France (Observatoire de Paris, Paris and Centre National d'Etudes Spatiales, Toulouse). Observations from satellite 19 are represented with a dash line.*

5-a. $[UTC(OP) - GPS\ time]_A - [UTC(OP) - GPS\ time]_B$,

5-b. $[UTC(OP) - GPS\ time]_C - [UTC(OP) - GPS\ time]_B$,

5-c. $[UTC(CNES) - GPS\ time]_A - [UTC(OP) - GPS\ time]_B$.

U.S. COAST GUARD GPS INFORMATION CENTER (GPSIC) AND ITS FUNCTION WITHIN THE CIVIL GPS SERVICE (CGS)*

Lieutenant Luann Barndt

Chief, Global Positioning System Information Center Branch
U.S. Coast Guard Omega Navigation System Center

Abstract

The Global Positioning System Information Center (GPSIC) was created to provide civil users of the Global Positioning System with timely system status and other GPS satellite information. The GPSIC began providing basic services on a test and evaluation basis in March 1990. Since then we have improved these services, formalized the information gathering processes, and expanded GPSIC operations to meet GPS user needs.

The GPSIC serves as a central point of contact for civil users to make their interests and needs known to the system operator, the Department of Defense (DOD) under the management of the U.S. Air Force. The GPSIC provides GPS information to civil users through Operational Advisory Broadcasts (OAB) containing GPS performance data. The OABs are disseminated through numerous sources including 24 hour access to a voice telephone recording and a computer bulletin board system (BBS). The GPSIC staff also responds to individual user inquiries, comments, or concerns about civil access to and use of the GPS during normal working hours.

This paper provides an overview of the Civil GPS Service as well as the details of the type of information and services that are available through the GPSIC and how they can be obtained. It will also address the future expansion of GPSIC responsibilities.

THE GLOBAL POSITIONING SYSTEM INFORMATION CENTER

The mission of the Global Positioning System Information Center (GPSIC) is to:

* gather,
* process, and
* disseminate

*The views expressed herein are those of the author and are not to be construed as official or reflecting the views of the Commandant or of the U.S. Coast Guard.

timely GPS status information to civil users of the global positioning satellite navigation system.

Specifically, the functions to be performed by the GPSIC include the following:

* Provide the Operational Advisory Broadcast Service (OAB)
* Answer questions by telephone or written correspondence
* Provide information to the public on the GPSIC services available
* Provide instruction on the access and use of the information services available
* Maintain tutorial, instructional and other relevant handbooks and material for distribution to users
* Maintain records of GPS broadcast information, GPS data bases or relevant data for reference purposes
* Maintain data bases of users by category, receiver manufacturers, providers of various services which use GPS, and other information sources
* Maintain bibliography of GPS publications
* Maintain and augment the computer and communications equipment as required
* Develop new user services as required

OVERVIEW OF THE CIVIL GPS SERVICE (CGS)

In 1987, the Department of Defense (DOD) formally requested the Department of Transportation (DOT) assume responsibility for establishing and providing an office that would respond to non-military user needs for GPS information, data, and assistance. In February 1989, the Coast Guard assumed the responsibility as the lead agency within DOT for this project. Three areas requiring interaction was were identified:

* Near real-time operational status reporting
* Distribution of the precise satellite ephemerides
* Civil use of the precise positioning service

In 1988, the U.S. Space Command (USSPACECOM) invited the U.S. Coast Guard to assist in the development of the DOD Operational Capability (OPSCAP) reporting system. Since that time, the U.S. Coast Guard Radionavigation Division has worked with USSPACECOM to develop requirements and implement a plan to provide the requested interface with the nonmilitary GPS community. Most of these civil GPS services are now in place; others are planned to be ready by the time GPS is fully operational.

As the Department of Transportation (DOT) operational agency, the U.S. Coast Guard is responsible for the oversight and management of the Civil GPS Service. The function is implemented by the following organizational elements:

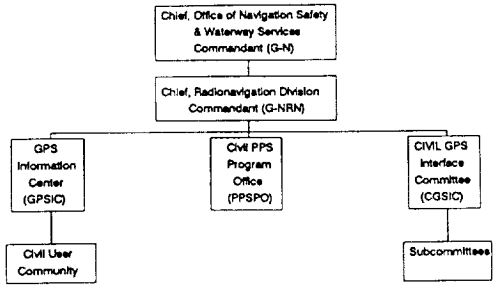

Chief, Office of Navigation Safety and Waterway Services (G-N), located at Coast Guard Headquarters, provides top-level oversight and management of the CGS program. The primary responsibility is the provision of broad, high-level policy guidance. This direction is provided in support of:

* DOT positions
* Congressional mandates
* Federal Radionavigation policies

This office is the focal point for information feedback from the Civil GPS Service Interface Committee. Members of this staff interface with the heads of other Federal agencies with an interest in the Civil GPS Service program.

Chief, Radionavigation Division (G-NRN), also located at Coast Guard Headquarters, is the program manager responsible for the activities of the PPSPO and the GPSIC operations. This office assists with the budgetary planning for for these services.

The Civil GPS Service consists of four main elements:

GPS Information Center (GPSIC) is the operational entity of the CGS which provides GPS status information to civilian users of the Global Positioning System based on input from the:

* GPS control segment
* Department of Defense (DOD)
* Other sources

PPS Program Office (PPSPO) is responsible for administering the program which will allow qualified civil users to have access to the Precise Positioning Service (PPS) signal. This program office is currently under development in the Radionavigation Division of the Office of Navigation Safety and Waterways Service (G-NRN-2) located at Coast Guard Headquarters in Washington, D.C.

Civil GPS Service Interface Committee (CGSIC) was established to identify civil GPS user technical information needs in support of the Civil GPS Service program. Its purpose and goal is of an information exchange nature only.

Differential GPS (DGPS) was established to develop an extension of GPS to enhance the Standard Positioning Service for civil users in the maritime regions of the United States.

The DOT Navigation Council and the DOT Radionavigation Working Group will continue in their traditional roles in the oversight of navigation including radionavigation.

Two other DOT agencies have Civil GPS Service functions:

The Federal Aviation Agency (FAA) handles aviation issues, including Notices to Airmen (NOTAM), the National Aviation Standard for GPS, and GPS integrity as it relates to aviation.

The Research and Special Programs Administration (RSPA) handles intermodal navigation issues and planning.

Although the DOT has assumed the principal oversight and management responsibilities for the Civil GPS Service, other federal agencies will play a role. The involvement of Federal agencies, other than those under DOT, will be particularly appropriate with regard to users outside of the navigation community.

THE GLOBAL POSITIONING SYSTEM INFORMATION CENTER (GPSIC)

The GPSIC began providing basic services on a test and evaluation basis in March 1990.

Since then, the GPSIC has improved these services, formalized the information gathering processes and expanded GPSIC operations to meet GPS user needs.

The GPSIC serves as a central point of contact for civil users to make their interests and needs known to the system operator, the Department of Defense, under the management of the U.S. Air Force.

Operated and maintained by the U.S. Coast Guard for the Department of Transportation, the GPSIC is a branch within the U.S. Coast Guard Omega Navigation System Center (ONSCEN) located in Alexandria, Virginia.

The development of the GPSIC is evolving as an extension of the Coast Guard's existing involvement in providing information on worldwide Radionavigation systems. The GPSIC will continue to be responsive to the needs of the user and remain flexible in its implementation plan to ensure that the user's needs are considered when implementing new services or changing existing ones.

The overall implementation effort consists of three phases:

Phase I has been completed: The GPSIC was established at ONSCEN and began operations on a test and evaluation basis in March 1990.

Phase II will coincide with the completion of working level agreements which detail the information passing responsibilities between ONSCEN and the Master Control Station (MCS). We expect to realize a sharp increase in users as the number of satellites increases. In anticipation of this, the GPSIC accomplished the following tasks:

* Obtained additional personnel
* Produced user documentation
* Developed and implemented the GPS Road Show

Phase III will occur when DOD declares the system operational. (Expected in 1993, refer to FRP for details). The increase in the number of satellites as well as users may increase the amount of available information and demand for it. If these major increases occur and we realize a worldwide GPS reference network/interface, the GPSIC may implement a second watch position in order to increase the hours personnel are available to provide real-time information.

The GPSIC is currently in a test and evaluation phase which means:

* Some services are not on line yet
* Details of information content and format have not been finalized
* Changes may be made without prior notice
* Operational standards have not yet been established for continuity of operation, and allowable time delays

Users of GPS are also cautioned that the Global Positioning System is not yet fully operational. Signal availability and accuracy are subject to change without warning due to an incomplete satellite constellation and operational test activities.

In general, the GPS Information Branch personnel are responsible for the day-to-day operations of

the GPSIC. This includes collecting the information and data required to create the Operational Advisory Broadcast (OAB) and then transforming this information and data into required formats for the various information services accessed by the GPSIC. The GPSIC branch consists of the following personnel:

* Branch Chief
* Operations Officer
* Navigation Information Specialist
* Telecommunications Specialist
* Navigation Information Clerk

GATHERING GPS INFORMATION

A Memorandum of Agreement (MOA) establishes policies and procedures for the exchange of GPS status information between the U.S. Space Command (USSPACECOM) and the Coast Guard. This agreement addresses relative roles and responsibilities of each organization. A similar MOA is being drafted between the Air Force and the Coast Guard.

The U.S. Air Force Second Satellite Control Squadron (2SCS), which operates the GPS Master Control Station (MCS) in Colorado Springs, provides the following GPS information for the GPSIC:

Notice Advisory to NAVSTAR Users (NANU) are near real-time operational status capability reports. NANUS are issued to notify users of future, current, or past satellite outages, system adjustments, or any condition which might adversely affect users. NANUS are generated by 2SCS as events occur.

GPS Status Message contains general information that is downloaded daily from the 2SCS's bulletin board. The message contains information about the satellite orbit (plane/slot), clocks, and current or recent NANUS. Status Messages are generated by 2SCS once a day Monday through Friday.

Almanacs contain the orbital information and clock data of all the satellites. The almanac for all satellites can be obtained from downloading the continuously transmitted data stream from any satellite.

In addition to receiving information from the MCS, the GPSIC works with representatives of National Geodetic Survey (NGS) to offer NGS computed precise GPS orbit data to the public via the GPSIC bulletin board.

NGS provides data products "SP3" (in ASCII format) and "EF18" (in binary format). In the past NGS distributed this information to some users on diskettes by mail.

Precise ephemeris data describes the orbit of each satellite as observed by numerous ground stations. It is useful in making a refined determination of where the satellites were at some time in the past. For more information about Precise Ephemeris Data contact:

National Geodetic Information Branch (N/CG174)
Charting and Geodetic Services
National Ocean Service
National Oceanic and Atmospheric Administration
Rockville, MD 20852
Telephone: (301) 443-8631

Features of the GPSIC services are created and improved in response to suggestions from our users. The GPSIC will continue to work with GPS organizations to ensure the continuation and development of the best possible user services. Specifically, the GPSIC will:

* Maintain liaison with other U.S. Government agencies as necessary to sustain GPS system status, technical information exchange and resource availability
* Maintain liaison with the Civil GPS Interface Committee and international civil GPS organizations to establish the requirements for GPS information exchange.

DISSEMINATING GPS INFORMATION

The GPSIC sends GPS status information to civil users through Operational Advisory Broadcasts (OAB). These broadcasts contain the following general categories of GPS performance data:

* Current constellation status
* Recent outages
* Scheduled outages
* Almanac data

The Operational Advisory Broadcast (OAB) consists of textual matter containing the GPS performance data listed above. Conditions that impair the GPS for navigational purposes receive special attention and wide distribution.

The Operational Advisory Broadcast is updated by the GPSIC staff at a minimum of once per day Monday through Friday except Federal Holidays. OAB's are updated more frequently if information on changes in the constellation are received prior to 4:00 p.m. EST. The following table outlines the update schedule for sources of GPS information received by the GPSIC:

SOURCE	UPDATE SCHEDULE
NANU	The GPS staff processes NANUS received during GPSIC working hours as soon as possible. NANUS received after hours or on weekends are processed immediately the next normal working morning.
STATUS MESSAGE	The GPSIC watchstanders access this information at 1300 EST Monday through Friday except Federal Holidays.
ALMANAC	The almanac is distributed once a week or when changes that appreciably affect system coverage occur.
NGS	NGS provides the precise ephemeris data to the GPSIC two weeks after the period it describes. Data will be updated weekly. Data sets from at least the last six weeks will be posted on the GPSIC BBS.

The Operational Advisory Broadcast is disseminated through the following media:

* GPSIC Computer Bulletin Board System (BBS)
* GPSIC 24-Hour Status Recording
* WWV/WWVH worldwide high-frequency radio broadcasts
* Coast Guard Marine Information Broadcasts (MIB)
* DMAHTC Broadcast Warnings
* DMAHTC Weekly Notice to Mariners
* DMA Navigation Information Network (NAVINFONET)
* NAVTEX Data Broadcast

Some of these services have limited time or space available for GPS information. The following paragraphs describe each service and the GPS information available.

GPSIC BULLETIN BOARD SYSTEM (BBS)

The GPSIC Bulletin Board System (BBS) provides information in data format via telephone modem. The only costs associated with the service are the fees charged by the user's phone company for the telephone call.

The GPSIC BBS connection information is contained in the following table:

PHONE NUMBER	SPEED	PROTOCOL	MODEM
(703) 866-3890	300	Bell 103	Supra-
	1200	Bell 212A	Modern
	2400	CCITT V.22bis	2400
(703) 866-3894	1200	CCITT V.22bis	Digicom
		CCITT V.22	Systems,
		Bell 212A	Inc.
	2400	CCITT V.22bis	9624
	4800	CCITT V.32	
	9600	CCITT V.32	

The main body of information within the bulletin board is contained in Subject Information Groups (SIGS). These are a collection of bulletins, some of which have attached files. They contain all of the GPSIC's information about GPS. The following table provides a description of the SIGS:

SIG	DESCRIPTION
HELLO	Short introduction to the SIGS, Plus background and miscellaneous information, CGSIC announcements, Road Show schedule.
SUMMARY	Summaries of recent events, outages.
NANU	Notice Advisory to NAVSTAR Users messages. 30 most recent NANUS messages maintained on BBS.
ALMANAC	Data describing the orbit of each satellite. Previous 3 months data maintained on BBS.
SEM	Almanacs formatted for use by the System Effectiveness Model (SEM) software V 3.5.
STATUS	Contains excerpts from Operational Control's stsus message.
OMEGA	U.S. Coast Guard weekly status summaries for the Omega radio-navigation system. (An independent system, not part of GPS.)
NGS	Precise ephemeris data from NGS. Contains 8 day segments.

The size of the GPSIC data files are as follows:

* NANU (batch of 10) 7K
* NANU (single) (estimated) 1K
* Status Message 2K
* Almanac (16 satellites) 10K
* Almanac (24 satellites) 15K
* SEM Almanac (16 satellites) 4K
* SEM Almanac (24 satellites) 6K
* Precise Ephemeris SP2 274K
* Precise Ephemeris SP3 371K
* Precise Ephemeris EF13 80K
* Precise Ephemeris EF18 110K

The GPSIC BBS has 8 incoming phone lines with the capability to expand up to 64. The BBS is also accessible via SprintNet. SprintNet is a major public data network (X.25) which enables high-speed, error-free data transfer to most major cities within the United States and a number of locations abroad. The GPSIC BBS net address is: 202 1328.

In order to use SprintNet, an account must be established with Sprint. This involves a connection charge and monthly billing for the service. To obtain more information about setting up an account:

Telephone: U.S. (800) 736-1130
International (913) 541-6876

An account with a similar network may be able to "gateway" over to SprintNet and access the GPSIC BBS without establishing an account with Sprint. Consult your network representative about how to use the gateway and resulting billing. The more complete gateway net address is: 311020201328.

Users may connect with the GPSIC BBS using the U.S. domestic telephone network or any other dial-up voice grade telephone system that interfaces with it. To connect with the GPSIC BBS, users need:

* Personal computer
* Modem
* Communications software package

The GPSIC BBS can accommodate baud rates from 300 to bits per second (bps). The user has the option of a modem rate setting of 300, 1200, 2400, 4800 or 9600 bps. Regardless of the baud rate selected, the modem should be configured as follows:

* Asynchronous communications
* 8 data bits
* 1 stop bit
* No parity
* Full duplex

First time bulletin board users can register on line. Users must provide their names and addresses and establish a user ID and password. The BBS also has a Page System Operator (SysOp) function which allows the user to page the system operator for on line assistance during normal working hours.

GPSIC 24-HOUR GPS STATUS RECORDING

The 24-hour status recording provides information in voice format. The amount of information is strictly limited since the maximum tape length is 92 seconds long.

The telephone number for the status recording is:

(703) 866-3826

The following information is available on the 24-hour status recording depending on the space available. The information is prioritized as listed below:

* Cautionary
* Current system status
* Forecast outages
* Historical outages
* Other changes in the GPS

OTHER DISTRIBUTION MEDIA

GPS information available from each of these additional sources is prepared and assembled at the GPSIC. These sources were chosen because they were already established to provide other types of information. Most of these service are already used by a portion of the GPS user community, primarily marine navigators. These services offer significant advantages in coverage and accessibility. The following section provides:

* Description of each information source
* Type of GPS information available
* How the user can obtain the GPS information

WWV/WWVH: Since 1923, the National Institute of Standards and Technology (NIST), formerly National Bureau of Standards, has provided a highly accurate time service to the national and

international time and frequency community. NIST currently broadcasts continuous signals from its high frequency radio stations. Services provided by WWV/WWVH include:

* Time announcements
* Standard time intervals
* Standard frequencies
* Geophysical alerts
* Marine storm warnings
* Omega Navigation System status reports
* Universal Time Coordinated (UTC) time corrections
* BCD time code
* GPS information

GPS information is broadcast in voice on WWV/WWVH at the following times and frequencies:

STATION	LOCATION	FREQUENCY	TIME
WWV	Fort Collins, Colorado	2.5, 5, 10 15, 20 MHz	Minutes 14 and 15
WWVH	Kauai, Hawaii	2.5, 5, 10 15 MHz	Minutes 43 and 44

The time for the WWV/WWVH GPS broadcast is strictly limited. Depending on the space available the GPS information is prioritized as listed below:

* Cautionary
* GPSIC operating hours and phone number
* Current system status
* Forecast outages
* Other changes in GPS Status

USCG AND DMA MIB: USCG Marine Information Broadcasts and DMA Broadcast Warnings are methods by which important maritime navigation information is disseminated in the most expedient manner. This system covers a variety of topics of interest to mariners including:

* Status of navigation aids
* Weather
* Search and Rescue (SAR) operations
* Military exercises
* Marine obstructions
* Ice reports
* Changes in channel conditions
* Important bridge information

Within the United States, the U.S. Coast Guard and the Defense Mapping Agency Hydrographic-Topographic Center (DMAHTC) are responsible for broadcasting navigation information described above. Each agency has a particular geographic area of responsibility:

AGENCY	AREA OF RESPONSIBILITY
USCG	Local and coastal navigation information broadcasts from sources within the U.S and its possessions.
DMAHTC	Long-range navigation broadcasts from countries within the NAVAREA IV and NAVAREA XII.

NAVAREA IV	Covers the Atalntic coast eastward to 35 degrees W.
NAVAREA XII	Covers the Pacific coast westward to 172 degrees E.

The Coast Guard provides vital maritime information in voice format via an established system of VHF and HF radio broadcasts. These Marine Information Broadcasts (MIB) include the following types of messages:

Urgent Messages concern the safety of a person, ship, aircraft or other vehicle.

Safety Messages contain important navigational or meteorological warnings that cannot be delayed because of hazardous conditions.

Scheduled Broadcasts include:

* Notice to Mariners (NTM)
* Hydrographic information
* Storm warnings
* Advisories
* Other important marine information
* Safety and urgent messages which remain in effect

Cancellation Messages are sent by the originator to cancel previous broadcast when action is no longer necessary.

USCG Marine Information Broadcasts are issued via voice and continuous wave (CW) transmissions. The following table outlines the MIB frequencies:

STATION	COVERAGE
VHF-FM Cha 16 Ch 22A	Information that applies to inland waters seaward to 25 nautical miles.
MF 2182 kHz 2670 kHz	Duplicate VHF-FM broadcasts and additionally covers waters out to 200 nautical miles.
HF-CW 500kHz	Info that applies for waters from the coastline to 200 nautical miles.

Broadcasts are scheduled several times a day depending on the location of the broadcasting site. Stations designated to make regularly scheduled broadcasts are listed in the *Coast Guard Radio Frequency Plan.* The length of messages broadcast is kept to a minimum.

DMAHTC is responsible for broadcasting navigation information concerning the "high seas" Information is provided in message format via an established system of message dissemination. DMA broadcasts are known as NAVAREA, HYDROLANT, or HYDROPAC and are generally geared to the deep draft mariner.

DMAHTC also publishes a weekly Notice to Mariners (NTM) containing USCG Marine Information Broadcasts and DMA Broadcast Warnings for a seven day period.

GPS status information is found in Section III of the Notice to Mariners, which summarizes voice or data broadcast warnings.

Additional information on the DMA Notice to Mariners Information is available from:

Director, Defense Mapping Agency
Hydrographic/Topographic Center
Attention: MCNM
6500 Brokes Lane
Washington, DC 20315-0030
Telephone: (301) 227-3126

DMA NAVINFONET: In carrying out its mission to produce Notices to Mariners, DMA has developed a data base called Automated Notice to Mariners System (ANMS). This data base contains information dealing with navigational safety. It is a supplemental source of up-to-date maritime information for the user. The software developed for this data base provides remote query capabilities which DMA makes available to the entire maritime community through the Navigation Information Network (NAVINFONET). NAVINFONET provides information in data format via telephone modem. Information includes:

* Chart Corrections
* Broadcast Warnings
* MARAD Advisories
* DMA List of Lights
* Anti-Shipping Activities Messages
* Oil Drill Rig locations
* Corrections to DMA Hydrographic Product Catalogs
* U.S. Coast Guard Light Lists & GPS

The following GPS information is available from the DMA NAVINFONET under item 8 in the bulletin board menu:

* Cautionary
* Current system status
* Forecast outages
* Historical outages
* Almanac data
* Civil GPS Service information

Users must register for the NAVINFONET bulletin board off-line before they will be granted access to the system. For a user ID and information book contact DMA at the address listed above:

Attention: MCN/NAVINFONET

Telephone: (301) 227-3296

NAVTEX: NAVTEX is a an internationally adopted radio telex system used to broadcast marine navigational warnings and other safety related information to ships. This system assures world-wide coverage by transmitting on an international frequency of 518 KHz. Vessels' NAVTEX receiver/teleprinters are permanently tuned to the worldwide frequency and remain on standby to receive and print out all the messages automatically. Navigation information broadcasted through NAVTEX includes:

* Notices to mariners
* Weather warnings and forecasts
* Ice warnings
* Other marine information

Coast Guard Atlantic and Pacific Area Commanders coordinate NAVTEX broadcasts transmitted by all Coast Guard Communications. NAVTEX messages are normally broadcasted four times a day which may be increased to six broadcasts with a maximum duration of 40 minutes.

NAVTEX messages are categorized by subject area. GPS status messages are currently available in NAVTEX category "K"; Other Electronic Navaid System messages. GPS information available from NAVTEX includes the following:

* Cautionary
* Current system status
* Forecast outages
* Other changes in GPS Status

ADDITIONAL GPSIC SERVICES

The GPSIC publishes documents which provide detailed information about GPS, other radionavigation systems, the GPS Information Center and how to obtain these services. The following table describes the GPSIC publications available:

PUBLICATION	DESCRIPTION
GPSIC BROCHURE	Describes information services provided by the GPSIC
GPSIC USERS' MANUAL	Provides detailed instruction on the access and use of the services available at the GPSIC
GPS/RA POSTCARDS	Lists publications available on a self addressed postcard
GPS FACTS & FIGURES	Describes the system, its concept, accuraccies and applications
OMEGA FACTS & FIGURES	Describes the Omega radionavigation system
LORAN-C FACTS & FIG	Describes LORAN-C
RADIOBEACON Facts & FIG	Describes Radiobeacons.

The GPSIC distributes documents provided by other GPS interested organizations. The following table describes other GPS publications available through the GPSIC:

PUBLICATION	PUBLISHER	DESCRIPTION
NAVSTAR GPS USER EQUIPMENT	JPO	Describes the system, equipment applications & capabilities
GPS NAVSTAR OVERVIEW	JPO	Provides general information about GPS
GPS A GUIDE TO THE NEXT UTILITY	Trimble Navigation	Describes what GPS is and how it works

The GPSIC no longer distributes copies of the ICD-200. The revised Public Release Version of this document is available through the GPS Joint Program Office. For more information contact:

CDR Dennis McLean, USCG
Space Division MZT
PO Box 92960 WPC
Los Angeles, CA 90009-2960
Phone: (213) 363-0354
Fax: (213) 363-2930

In an effort to make the public aware of the services offered by the GPSIC, the GPSIC sets up a GPS display at trade shows throughout the United States. The display includes a model of a satellite and rocket loaned by GE Astrospace and McDonnell Douglas respectively. The GPSIC staff distributes brochures and answers questions about GPS in order to educate users about the system.

The GPSIC responds to individual user inquiries, comments, and concerns about civil access to, and use of the GPS. The GPSIC fields requests for information Monday though Friday from 8:00 a.m. to 4:00 p.m. Eastern Standard Time. Most inquiries can be answered immediately over the phone. Some technical questions or requests are referred to a more authoritative source.

If you would like to comment on any of these services or ask questions about present or future services write to:

Commanding Officer (GPSIC)
US Coast Guard Omega Navigation System Center
7323 Telegraph Road
Alexandria, Virginia 22310-3998
Or call (703) 866-3806

An answering machine records messages after working hours. Messages are normally returned the following workday.

FUTURE PLANS FOR GPSIC

The Coast Guard plans to evaluate the possibility of expanding the GPS Information Center into a Radionavigation or Navigation Information Center. As such, the Information Center would provide navigation information on all navigation systems involving the Coast Guard both nationally and internationally.

Information concerning other radionavigation systems the Coast Guard is involved with would be posted on the BBS. As a first step in this direction, the GPSIC currently provides the Omega weekly status message on the BBS.

DIFFERENTIAL GPS (DGPS)

Consistent with its role as the civil interface for GPS, the U.S. Coast Guard has a research and development project to develop an extension of GPS, known as differential GPS (DGPS). This is an enhancement to the Standard Positioning Service which should achieve accuracies of 10 meters or better for civil users in the maritime regions of the United States.

Based on encouraging results of operational testing of a prototype reference station, a project has been initiated to implement DGPS in U.S. near-coastal areas to improve upon current harbor and harbor-approach navigation accuracy. Project plans are being formulated. Additional prototypes began operation during September/October 1991. If fully funded, an operational system is expected by the end of 1995.

For additional information on DGPS, contact:

Commandant (G-NRN)
U.S. Coast Guard
2100 2nd Street, S.W.
Washington, DC 20593
Telephone: (202) 267-0283
Fax: (202) 267-4427

PRECISE POSITIONING SERVICE PROGRAM OFFICE (PPSPO)

The Precise Positioning Service Program Office (PPSPO) will administer civil applications and collect fees for access to encoded PPS capabilities.

The Government will publish detailed guidance for users interested in requesting access to PPSPO once policy is established for the following:

* Submitting applications
* Granting approval for user access
* Establishing operational procedures and compliance requirements for accessing data from the GPS PPS

The Federal Radionavigation Plan (FRP) contains general criteria for qualified civil use of PPS.

Access determination will be made on a case by case basis. The following criteria may be refined as Government policy is developed:

* Access is in the U.S. national interest
* Security requirements can be met
* There are no other means reasonably available to the civil user to obtain a capability equivalent to that provided by the GPS PPS

For additional information on the PPSPO, contact Commandant (G-NRN) at the address listed above or call:

Telephone: (202) 267-0298

CIVIL GPS SERVICE INTERFACE COMMITTEE (CGSIC)

The roles of the Civil GPS Service Interface Committee (CGSIC) are to:

* Provide a forum for exchanging technical information in the civil GPS user community regarding GPS information needs
* Identify types of information and methods of distribution to the civil GPS user community
* Identify any issues that may need resolution by the CGS program office

The CGSIC will work with the following organizations:

* U.S. Coast Guard Office of Navigation Safety and Waterway Services (Civil GPS Program Office)
* DOT Navigation Working Group
* Joint DOD/DOT Radionavigation Working Group

The Civil GPS Service Interface Committee is comprised of representatives from relevant private, government, and industry user groups, both U.S. and international.

The CGSIC consists of:

* General Committee
* Five Subcommittees

The Committee is jointly chaired by the U.S. Coast Guard and the DOT Research and Special Programs Administration (RSPA). The joint chair is based on the USCG being DOT's lead agency for the civil GPS service which includes the government's interface with civil GPS users, and RSPA's responsibility to coordinate intermodal navigation planning with DOD.

The Civil GPS Service Interface Committee may create subcommittees to identify specific areas of civil GPS user information needs and facilitate technical information exchange as required. Standing subcommittees have been established for:

* Surveying and Positioning Information
* Timing Information
* International Information
* Reference Station, Technology, and Applications
* Real-time Carrier Phase Applications

The International Information Subcommittee (IISC) of the Civil GPS Service Interface Committee is investigating the feasibility of a regional international information media. The GPSIC would provide the OAB into an electronic mailbox designated, controlled, and financed by the IISC.

The Civil GPS Service Interface Committee meets as necessary to exchange technical information regarding civil GPS information needs.

For additional information on the CGSIC, contact:

Volpe National Transportation Systems Center (VNTSC)
55 Kendall Square
Cambridge, MA 02142-1093
Telephone: (617) 494-2432
Fax: (617) 494-2628

FEDERAL RADIONAVIGATION PLAN (FRP)

The Federal Radionavigation Plan contains the official statement of government policy on civil use of GPS. This plan covers other government operated radionavigation systems in addition to GPS. Information provided includes:

* Policy and plans for the future radionavigation systems mix
* GPS System description
* Table of SPS and PPS signal characteristics
* Various other topics

In order to obtain the user's perspective on Federal policies and future plans for U.S. Government provided radionavigation systems, the DOT conducts open meetings for all interested persons. Users are encouraged to attend FRP conferences to provide inputs for the 1992 edition. FRP Conferences are scheduled for Alexandria, Virginia in November and Seattle, Washington in December. For more information on these conferences, contact: Volpe National Transportation Systems Center (VNTSC) at the address listed above attention:

Conference Office (DTS-930)
Telephone: (617) 494-2307

Navigation systems that will be discussed at these conferences include:

* Loran-C
* Omega
* Transit
* Radiobeacons
* VOR/DME
* MLS/ILS
* GPS

ACKNOWLEDGMENTS

The author wishes to express appreciation to the GPSIC and Omega staff who helped in preparing and updating this manuscript. This paper has been updated as of 30 October 1991.

REFERENCES

Bennett, CDR Verne and David J. Pietraszewski, The U.S. Coast Guard Civil GPS Program, 1990.

Civil GPS Service Interface Committee, Charter For The Civil GPS Service Interface Committee (CGSIC), 1991.

Defense Mapping Agency Hydrographic/Topographic Center, Navigation Information Network Users Manual, 1990.

Defense Mapping Agency Hydrographic/Topographic Center, Notice to Mariners No. 32, 1991.

Department of Defense & Department of Transportation, Federal Radionavigation Plan, U.S. Government Printing Office, 1990.

Desilets, CWO Gary E., The U.S. Coast Guard's Role in the Civil GPS Service, Coast Guard Omega Navigation System Center, 1991.

Omega Navigation System Center, GPS Operations Manual, ONSCEN Instruction 16575, Coast Guard Omega Navigation System Center, 1991.

Radio Technical Commission For Maritime Services, Maritime Navigational Safety Information Sources, RTCM, 1991.

U.S. Coast Guard, Global Positioning System Program Plan Civil GPS Service, U.S. Coast Guard Printing Office, 1991.

U.S. Coast Guard GPSIC, GPS Information Center, U.S. Coast Guard Printing Office, 1990.

U.S. Coast Guard GPSIC, GPS Information Center Users Manual, U.S. Coast Guard Printing Office, 1990.

U.S. Coast Guard, Telecommunications Manual (TCM), COMDTINST M2000.3B, U.S. Coast Guard Printing Office, 1988.

U.S. Space Command, U.S. Coast Guard, Memorandum of Agreement: Distribution of NAVSTAR Global Positioning System (GPS) Status Information, 1990.

THE GPSIC QUICK REFERENCE OAB DISTRIBUTION

The GPS Information Center provides the Operational Advisory Broadcasts through the following services:

SERVICE	AVAILABILITY	INFO TYPE	CONTACT NUMBER
GYPSIC WATCHSTANDER WATCH- STANDER	8AM–4PM Monday through Friday	USER INQUIRIES	(703) 866-3806 FAX (713)866-3825
GYPSIC COMPUTER BULLETIN BOARD SERVICE	24 hours	STATUS FORE/HIST OUTAGES NGS DATA OMEGA/FRP MISC INFO	(703) 866-3890 300-2400 BAUD (703) 866-3894 UP TO 9600 BAUD Sprintnet (x.25) 202-1328
GYPSIC VOICE TAPE RECORDING	24 hours	STATUS FORECASTS HISTORIC	(703) 866-3826
WWV	Minutes 14 & 15	STATUS FORECASTS	2.5, 5, 10, 15 and 20 MHz
WWVH	Minutes 43 & 44	STATUS FORECASTS	2.5, 5, 10 15 MHz
USCG MIB MIB	When broadcasted	STATUS FORECASTS	VHF Radio, marine band
DMA BROADCAST WARNINGS BROADCAST WARNINGS	When broadcasted	STATUS FORECASTS OUTAGES	
DMA WEEKLY NOTICE TO MARINERS	Published & mailed weekly	STATUS FORECASTS OUTAGES	(301) 227-3126
DMA NAVINFONET AUTOMATED NOTICE TO MARINERS SYSTEM	24 hours	STATUS FORECASTS HISTORIC ALMANACS FOR MORE INFO CALL	(301) 227-3351 300 BAUD (301) 227-5925 1200 BAUD (301) 227-4360 2400 BAUD (301) 227-3296
NAVTEX DATA BROADCAST	When broadcasted 4–6 times/day	STATUS FORECAST OUTAGES	518 kHz

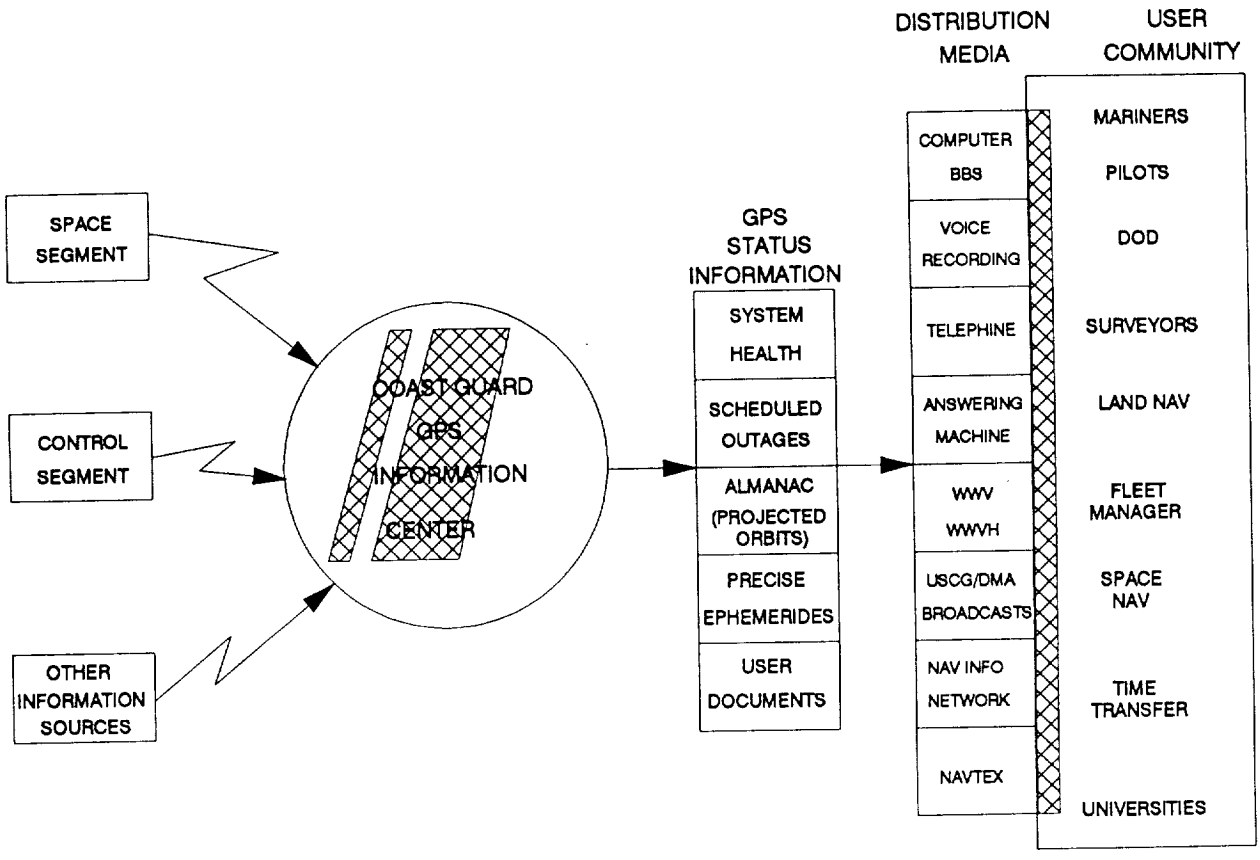
DISTRIBUTION MEDIA
USER COMMUNITY
SPACE SEGMENT
CONTROL SEGMENT
OTHER INFORMATION SOURCES
COAST GUARD GPS INFORMATION CENTER
GPS STATUS INFORMATION
SYSTEM HEALTH
SCHEDULED OUTAGES
ALMANAC (PROJECTED ORBITS)
PRECISE EPHEMERIDES
USER DOCUMENTS
COMPUTER BBS
VOICE RECORDING
TELEPHINE
ANSWERING MACHINE
WWV WWVH
USCG/DMA BROADCASTS
NAV INFO NETWORK
NAVTEX
MARINERS
PILOTS
DOD
SURVEYORS
LAND NAV
FLEET MANAGER
SPACE NAV
TIME TRANSFER
UNIVERSITIES

Evaluation of GPS/UTC Steering Performance

W. A. Feess, H. Holtz, A. L. Satin, C. H. Yinger
The Aerospace Corporation, El Segundo, CA

Abstract

The Global Positioning System (GPS) is required to maintain GPS time to UTC to an accuracy of one microsecond and broadcast to the user the offset between GPS and UTC to an accuracy of 100 nanoseconds (1 sigma). On June 25, 1990, an automatic steering algorithm was implemented to control GPS time to synchronize it with UTC. The description of the steering laws and predicted performance results were presented at the 1989 PTTI conference, while preliminary performance results were presented at the 1990 PTTI conference. The initial performance was not as predicted, resulting in an in-depth analysis of the observed performance and a more thorough sensitivity analysis. In addition, responses to anomalies were investigated. This paper will describe these analyses and results, and evaluate actual steering performance from June 1990 to November 1991. Although anomalies were observed during the initial phase of steering, recent experience is more in line with expectations.

1.0 Introduction

The Global Positioning System (GPS) is a Department of Defense space-based navigation and time dissemination system. When fully deployed it will consist of a constellation of 21 operational satellites (Blk II/IIA) plus three active spares. The current constellation consists of nine Blk II and two Blk IIA satellites. In addition, five Blk I development satellites are still functioning.

As a navigation system, each satellite is required to deliver to a user a timing signal and information relative to the satellite vehicle (SV) position and time offset with respect to system time (GPS time) to an accuracy of six meters (20 nanoseconds) one sigma. Given this accuracy of time signals to four SV's with appropriate geometry, an authorized dual frequency user can navigate in three dimensions to an accuracy of 16 m SEP. A user who knows his location in the reference coordinate system of GPS (WGS84), can synchronize his time to GPS time. The accuracy of this time transfer is also dependent on the user's ability to remove propagation effects (ionospheric and tropospheric) and when applicable the effects of selective availability (SA).

GPS is also required to synchronize GPS time to Universal Coordinated Time (UTC) maintained by the U.S. Naval Observatory (USNO) and to broadcast to the user the time difference between these two timing systems. The requirement is to synchronize to one microsecond (1000 ns) and to broadcast the difference to an accuracy of 100 nanoseconds (one sigma). This paper evaluates the performance of these functions.

2.0 Steering Performance

To meet these requirements, USNO is equipped with GPS receivers to monitor GPS time and the broadcasted GPS-UTC time difference. Reference 1 describes in detail the equipment and tracking schedules used to perform these functions. The data collected is processed by USNO and available for transmission to the Operational Control Segment (OCS) daily via secure telephone lines. The OCS operates with this data to control GPS time. This operation is pictorially and schematically presented in Figure 1. Early in the program, the control was manual in that the operator would observe the time history of the timing difference and periodically effect a magnitude and time duration command to steer the GPS time offset towards zero. The command is a frequency drift command (second derivative of time) whose magnitude is limited. The limit was set to protect the navigation user in the event the OCS was rendered inoperable due to hostile or natural causes. More recently (June of 1990) steering was automated to ease the operator function and to improve performance. Several control laws were considered for automation of the control function. Reference 2 described and analyzed these control laws, and presented predicted performance. In addition to steering, the GPS time reference was changed from a GPS master clock to a GPS clock ensemble configuration (composite clock). Reference 3 presented the preliminary performance of these changes after initial turn on. To put steering performance in prospective, Figure 2 shows the time history over the past five years.

The steering law implemented is that designed by the Control Segment contractor (IBM) which is described in Reference 2. It is a three state controller, i.e., plus, minus or zero command. The command rate is the limiter value of 2E−19 s/s^2 ($\approx$ 1.5 ns/day^2). The anticipated steady state performance after initial transients have subsided was 10 ns one sigma (Reference 2). Automatic steering was initiated June 25, 1990 (MJD=48067). Figure 3 presents the GPS/UTC time difference and steering command from turn on to November 1, 1991 (48561). The initial overshoot was expected, however the large undershoot was much larger than expected and the magnitude of the second overshoot was not anticipated at all. Concern was raised with the initial undershoot and analyses were initiated after the second overshoot. Automatic steering was turned off for 9 days following the initial undershoot (48120 to 48129) and turned off from 48160 to the end of 1990 (MJD 48256). Occasional manual steers were introduced during this later period.

The observed performance was of particular concern to us, because the concepts for steering here are being applied to a more difficult task for the Blk IIR SV's currently being designed. The task there will be to synchronize two GPS clock ensembles, the Blk IIR SVs ensemble operating in their autonomous navigation mode and the current OCS clock ensemble of all SV's and monitor stations. The GPS/UTC synchronization will also be required.

To investigate the situation, a set of OCS filter data covering the first 22 days of October, 1990 (MJD 48165 to 48187) were obtained and analyzed. At this point in time, it was not known whether the problem existed with the steering or the GPS clock ensemble since both were initiated about the same time. Prior to this analysis the steering algorithm was checked and found to be producing the correct steering commands for the phase and frequency offsets observed by USNO. Two major phenomenon were observed from the filter data. First, estimates of aging on two of the SV's with rubidium frequency standards (PRN's 3 and 16) had large estimation errors. Second, it was observed that Nav 16 had a large uncompensated frequency jump ($\Delta f/f \approx$ 4E-12) causing a change in frequency estimates of the other clocks in the ensemble of opposite polarity and about one fifteenth the size. During this period, the frequency standard at the Colorado Springs monitoring station was switched to the NRL's hardware ensemble (48167). Although the frequency of the two

standards were considerably different, the transition was handled correctly by the filter with no detectable changes in ensemble frequency.

Simulations of the steering loop to aging and frequency jumps led to the conclusion that the first undershoot problem was due to the filter mismodeled aging and the second overshoot was a combined effect of NAV 16 frequency jump and a change in aging. Based on these findings it was concluded that the problem was in the clock ensembling process and not in the steering loop design. It was therefore recommended that all SV rubiduim clocks and any other SV which was experiencing estimation problems of clock or ephemeris be removed from the GPS ensemble process. This was done in December and automatic steering was again initiated January 1, 1991.

The performance since January 1 still reflects spurious responses which can be associated with monitoring station clock problems. It should also be noted here that it is not necessary that SV rubiduim clocks be excluded from the GPS ensembling process; however, it is necessary that the filter be tuned properly to estimate the aging state.

3.0 Stability of GPS Time

The common measure of time stability is the Allan Variance of the sample function. This is presented in Figure 4 for the time history of the GPS time offset presented in Figure 3. This represents the composite of the GPS time ensemble and the steering function. When the steering command is integrated twice and removed from the sample function of Figure 3, a measure of the GPS ensemble time is obtained. This is also presented in Figure 4. These are rather complex functions to make any quantitative statements; however, certain qualitative observations can be made. The one day value ($\approx$ 2.8 E-14) is a reasonable assessment of the GPS ensemble time since its value is not affected by the contribution of steering. Also included in this number is the accuracy of the measuring system which includes the SV clocks, therefore it can be concluded the GPS ensemble is performing better than 2.8 E-14 at one day. In the interval of 1 to 100 days, the GPS time ensemble response suggests a significant component of aging noise. Beyond 25 days, the steering loop significantly removes the effects of this noise as evidence by the intersection of the open and closed loop curves.

4.0 Time Dissemination Performance

The time dissemination relates to how well a GPS user can determine his time offset with respect to UTC. USNO monitors this function by correcting the observed GPS time offset by the offset broadcast by GPS in subframe 4. The phase, computed frequency and reference time received from USNO for steering is also used at the OCS to prepare the subframe 4 data. USNO then uses what it receives in the message to arrive at the GPS (UTC) error. What is computed by USNO and presented here in Figure 5 is the daily mean and the one sigma value about the mean for the interval when steering was turned on to November 1, 1991. Observing Figure 5 it is seen that early in the steering interval, June to October 1990 (MJD 48067 to 48165), the pattern and magnitude of error was larger than the rest of the interval. Initially a three day least squares polynomial fit was done at the OCS using a subset of the total data collected by USNO. Problems associated with this procedure resulted in the change to the current procedure (see Section 5) and associated improved performance.

The RSS value of the mean and sigma is more the intent of the 100 ns requirement. Table I summarizes the performance of these quantities over the total interval and over the interval covering this year.

Table 1. Disseminated Time Accuracy RMS Statistics over each interval (ns)

Interval	Mean	Sigma	RSS	Max RSS
June 25 '90 to Nov 1 '91	8.3	11.8	14.5	52.6
Jan 1 '91 to Nov 1 '91	4.9	10.9	12.0	23.6

5.0 Sensitivity Study

Because of the anomalous performance initially experienced, a re-examination of the steering loop was initiated. The new simulation depicted more closely the USNO to OCS interface and the OCS to satellite interface system than was used in the original study (Reference 2). Figure 6 presents the new simulation diagram. As in the original study the OCS Ephemeris and Clock Kalman filter is represented as a simple two stage clock model. In the simulation, the steering command is integrated twice to reflect schematically the response while in the OCS the steering command is fed directly to the Kalman filter and the filter performs the integration. This schematic representation has the advantages that more realistic representations of the Kalman filter could be implemented without changing the steering diagram. The difference of these two outputs (filter and steering) represents GPS time and is used as the reference for uploads to the satellite system. Each SV in the constellation of N satellites is also modeled as a two stage clock with phase and frequency outputs being reset daily to represent the upload function. For most studies, N was set to 12 and the rotary switch would reset a different SV clock every two hours. On the other end of the SV simulation is another rotary switch sampling one of the SV's in the constellation every 15 min representing the operation at the USNO. Noise is added to these samples to represent errors in the USNO caused by receiver and correction errors. The current procedure since Oct 1990 has been for USNO to collect 38 hours of data (0 hrs GMT to 14 hrs the next day) and to perform a least squares linear fit on the data to produce a phase and frequency offset of GPS time to USNO time. The time tag for this data is 24 hour into the fit interval. For our simulation, an hour delay is incorporated to allow time for transmitting and entering the data into the OCS system. The OCS uses the first difference of the daily phase error data to represent frequency error. This output is fed daily to the steering law. The IBM steering law operates on this command every 15 minutes to determine an output steering command. The steering law is described in Reference 2 with a change to the TOL value (error tolerance from 1 to 10 ns) which was recommended by IBM. For comparison, the linear law of Reference 2 was also simulated where steering commands are computed once per day subject to the output limit.

The main inputs to this simulation for steady-state performance analysis are the performance parameters of the ground ensemble, the performance of the SV clocks, and the noise level of the measurement process. Figure 7 presents Allan Variance curves for the clock models and defines the nominal values used for stochastic parameters in this study. Other inputs of initial conditions, ensemble aging and/or frequency jumps, limiter level, data dropouts, number of SV clocks simulated, measurement filtering intervals, and delay variations were also investigated but not reported here.

One of the characteristics noted in this simulation was the non-repeatability of statistical results with changes in the seed to the random number generator. It was initially thought that simulation

intervals of 3 to 5 time constants (100 to 200 days) would be adequate to portray performance for a particular set of inputs. However, it was found that significant changes in results occur even for simulation intervals of 1000 days. Figure 8 is a typical example where the first 300 days exhibits large excursions (parasitic oscillations) with a significant change in apparent performance over the remainder of the interval. For the same input conditions (except for a change in the random number seed) a completely different response results. Similarly for the same seed, but a change in the magnitude of one of the input noise levels, results in a complete change in apparent performance over time. For this reason, it is difficult to conduct a sensitivity analysis on a non-linear controller. To a lesser extent, the linear controller also suffers when noise levels are sufficient to cause frequent limiting action. The nonlinearity violates laws of superposition and stationarity enjoyed by linear systems and makes the analysis for stochastic inputs more difficult to predict.

With this characteristic noted, a sensitivity study was run simulating both the current controller and a linear controller. Table II defines the parameters and values used and presents results in terms of RMS phase and frequency errors for each case. Figure 9 graphically summarizes the phase errors for each class of input and variation used.

It is seen from these results that the loop performance is most sensitive to the performance of the ground clock ensemble and relatively insensitive to measurement noise at USNO or to individual SV clock performance.

Table II Sensitivity Study Parameters and Results

	Input						RMS Results			
	Noise Seed	Ground Clock		SV Clocks		Meas. Noise (ns)	IBM		Linear	
Symbol	REP	W1E	W2E	W1S	W2S	MNZ	Phase (ns)	Freq (ns/day)	Phase (ns)	Freq (ns/day)
Nominal	3	3	1	9	3	10	22.1	4.6	14.7	3.3
Seed	1	"	"	"	"	"	15.9	4.0	12.7	3.0
	2	"	"	"	"	"	12.3	3.8	11.1	3.0
	4	"	"	"	"	"	15.5	3.7	14.5	3.1
	5	"	"	"	"	"	20.4	4.2	15.1	3.2
Grd Clk	3	6	"	"	"	"	36.1	6.0	27.1	4.9
	"	1.5	"	"	"	"	17.0	3.6	11.9	7.6
	"	3	2	"	"	"	56.8	7.1	53.2	6.8
	"	"	.5	"	"	"	10.2	3.1	9.8	2.5
SV Clk	"	"	1	27	"	"	20.0	4.3	19.8	3.8
	"	"	"	3	"	"	14.2	3.7	13.8	3.1
	"	"	"	9	9	"	21.8	4.5	14.9	3.3
	"	"	"	"	1.5	"	19.2	4.2	14.7	3.3
Meas. Noise	"	"	"	"	3	20	21.8	4.4	16.0	3.4
	"	"	"	"	"	5	18.8	4.3	14.4	3.2

6.0 Performance Improvements

Although the current performance (both in control of GPS time and dissemination of the GPS/UTC time difference) are well within required accuracies, improvements are always possible. The major perturbation to control accuracy is detection of and compensation for individual clock anomalies. To this end, an enhancement to the control segment software, called Performance Visibility, is currently in the design stage by IBM (Reference 4). This enhancement will examine the Kalman filter

products to automatically detect anomalous magnitudes, trends, etc. so that operator intervention and correction can be applied before anomalies spread into the GPS system and the constellation of satellites.

Currently, the clocks contributing to ensemble time are all equally weighted. The Colorado Springs monitor station has the NRL hardware ensemble as its reference and could be weighted so as to enhance stability of GPS time with corresponding improvement in control of GPS time. This requires no software changes. Converting to a linear controller in contrast to the IBM controller offers some improvement, particularly if the limits were increased so higher gains could be used.

Time dissemination improvement is harder to achieve. The accuracy is primarily dictated by the SV clock performance in prediction and the update rates involved. Update rates, e.g., twice a day could offer perhaps a factor of two improvement and perhaps would not be that difficult to implement. Relative to SV clocks, our experience with Blk II rubiduim clocks (NAV 16) is limited and its performance plagued with frequency jumps not necessarily inherent in the standard design. In the absence of frequency jumps and with proper modeling of aging in the Kalman filter, the stability of Nav 16 standard over one day was excellent. The Blk IIR rubiduim clocks could offer improved performance, while the autonomous navigation feature will offer enhanced accuracy of SV broadcast time.

7.0 Conclusions

Both control and dissemination of GPS time with respect to USNO time have been demonstrated to exceed performances requirements by at least an order of magnitude. The performance of the GPS Composite clock demonstrates an accuracy better than 3E-14 frequency stability at one day. Every indication is that this will improve with enhanced anomaly detection and filter tuning. The lesson learned is to evaluate system design under anomalous performance as well as nominal performance. Also, not all clocks perform equally and should not be weighted equally. For questionable clocks, zero weights are much preferred to equal weights. Finally, the techniques to evaluate performance are valid and should carry through to designs of the Blk IIR constellation synchronization and GPS/USNO control and dissemination. Anomaly studies of the Blk IIR has been an integral part of the design activity and experience here reinforces the need for anomaly analysis during the design phase.

References

1. M. Miranian and W. J. Klepczynski, *"Time Transfer Via GPS at USNO"*, ION GPS-91 ION Satellite Division's 4th International Technical Meeting, September, 1991.

2. C. H. McKenzie, et al., *"GPS-UTC Time Synchronization"*, Proceedings of the 21st Annual PTTI Applications and Planning Meeting, November 1989.

3. A. L. Satin, W. A. Feess, H. F. Fliegel, C. H. Yinger, *"GPS Composite Clock Software Performance"*, 22nd Annual Precise Time and Time Interval (PTTI) Applications and Planning Meeting, Vienna, Virginia, December 4-6, 1990.

4. K. R. Brown, *"Navigation Performance Visibility Study Report for the NAVSTAR Global Positioning System (GPS) Operational Control Segment (OCS) Residual Development"*, IBM, Gaithersburg, Maryland, July 8, 1991.

Figure 1. GPS/UTC Steering Diagram

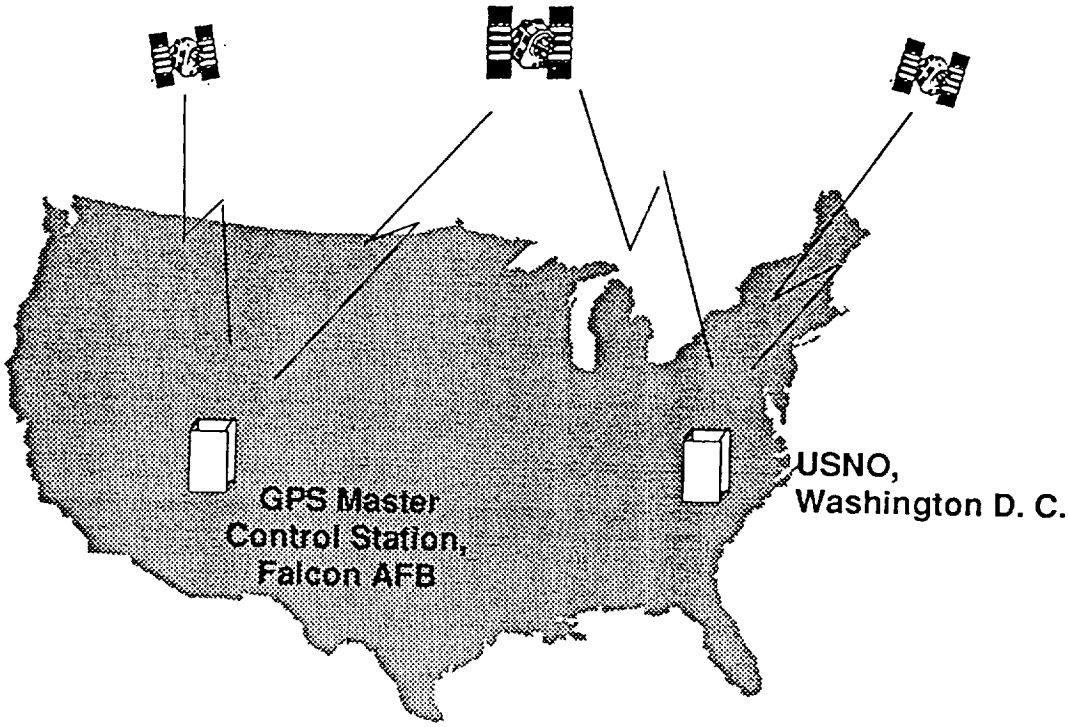

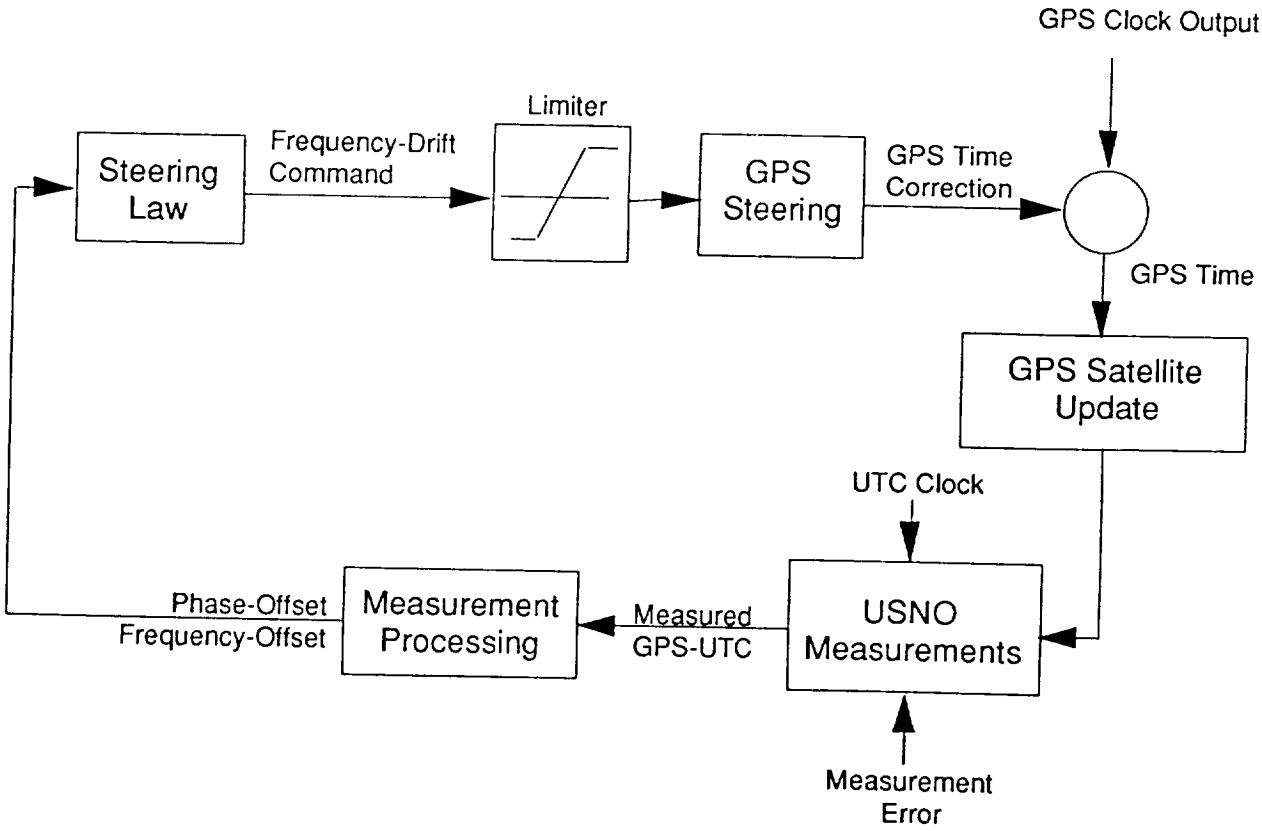

Figure 2. GPS-UTC Steering Performance

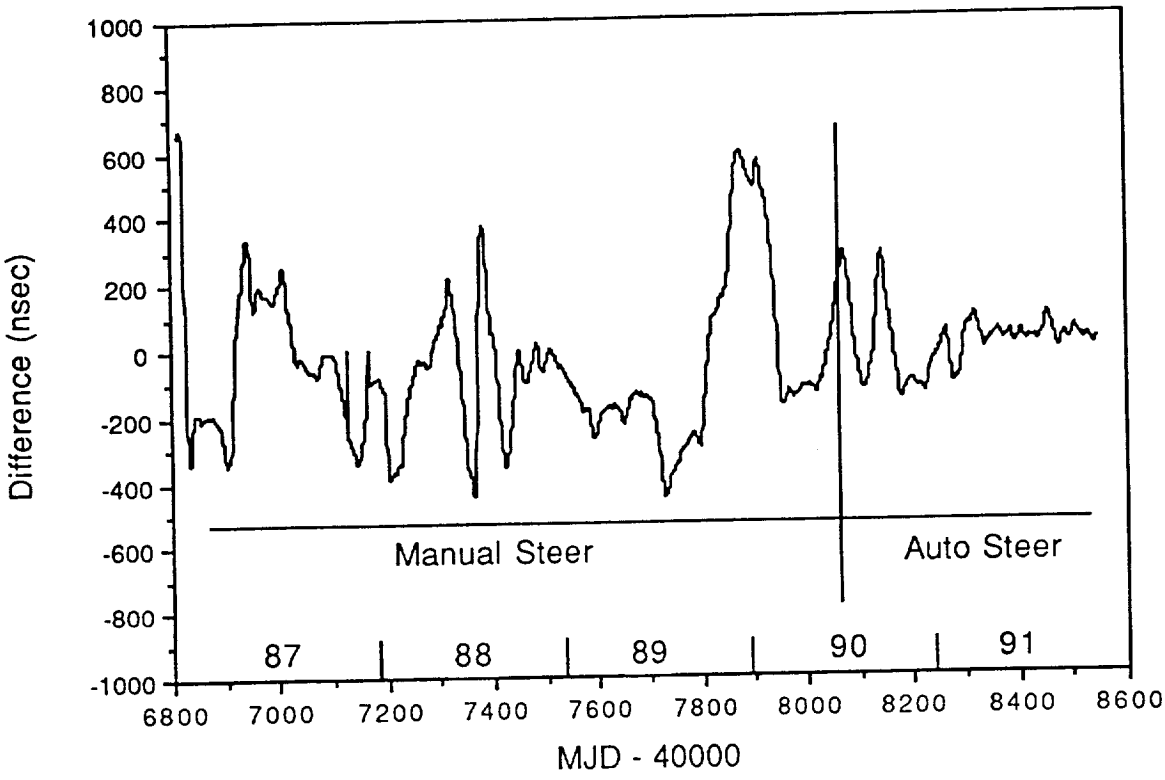

Figure 3. GPS-UTC Performance (Auto Steer)

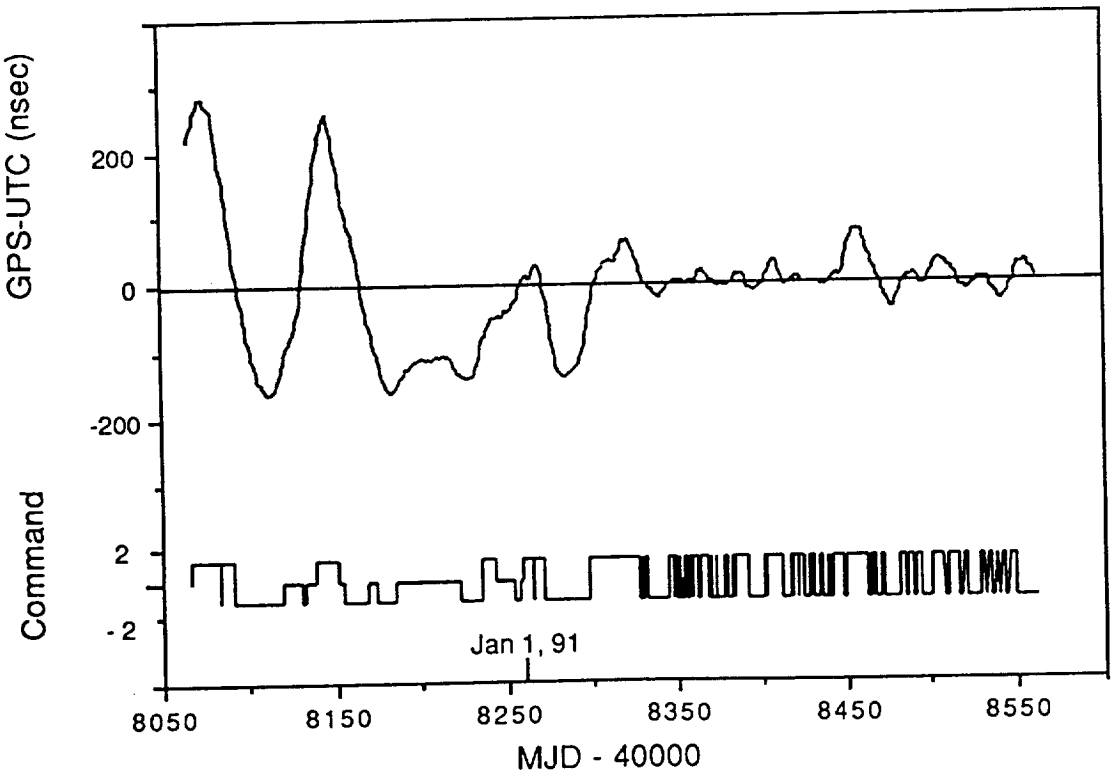

Figure 4. Allan Variance of GPS Time

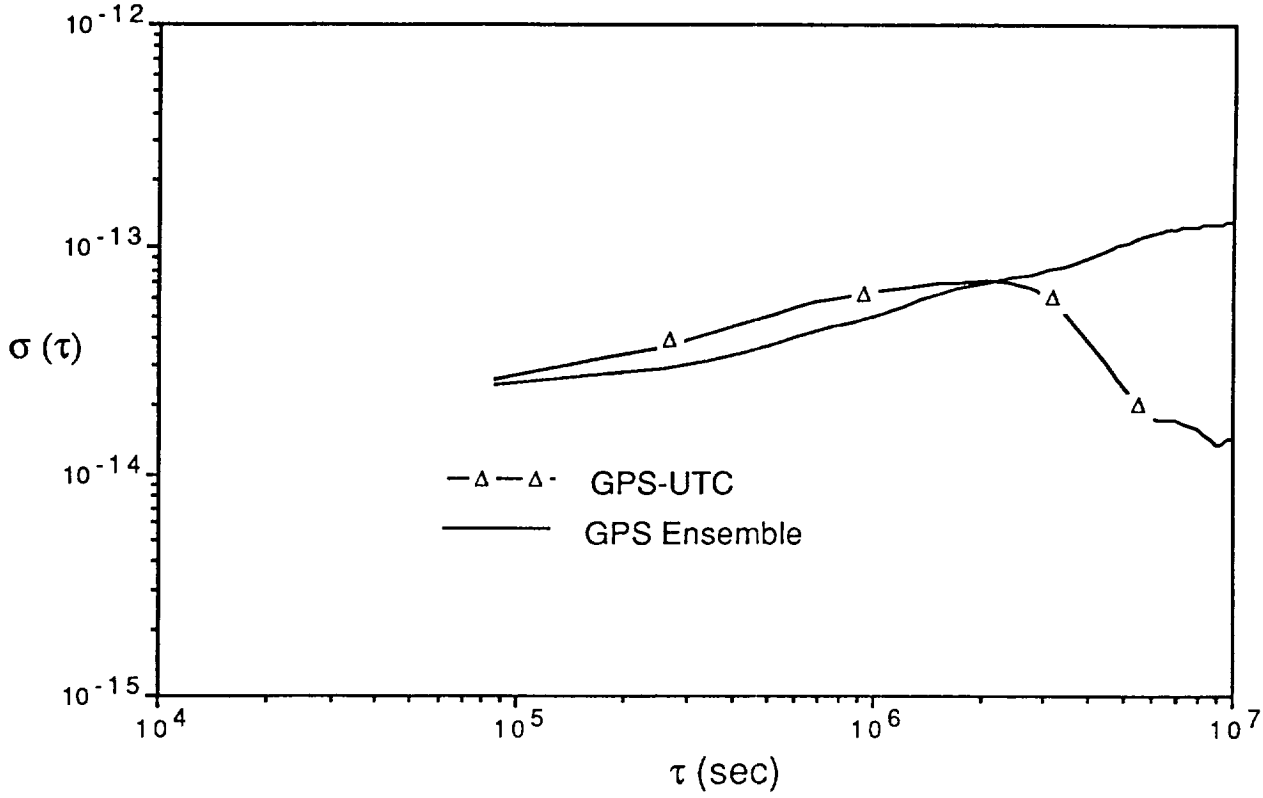

Figure 5. GPS (UTC) Performance

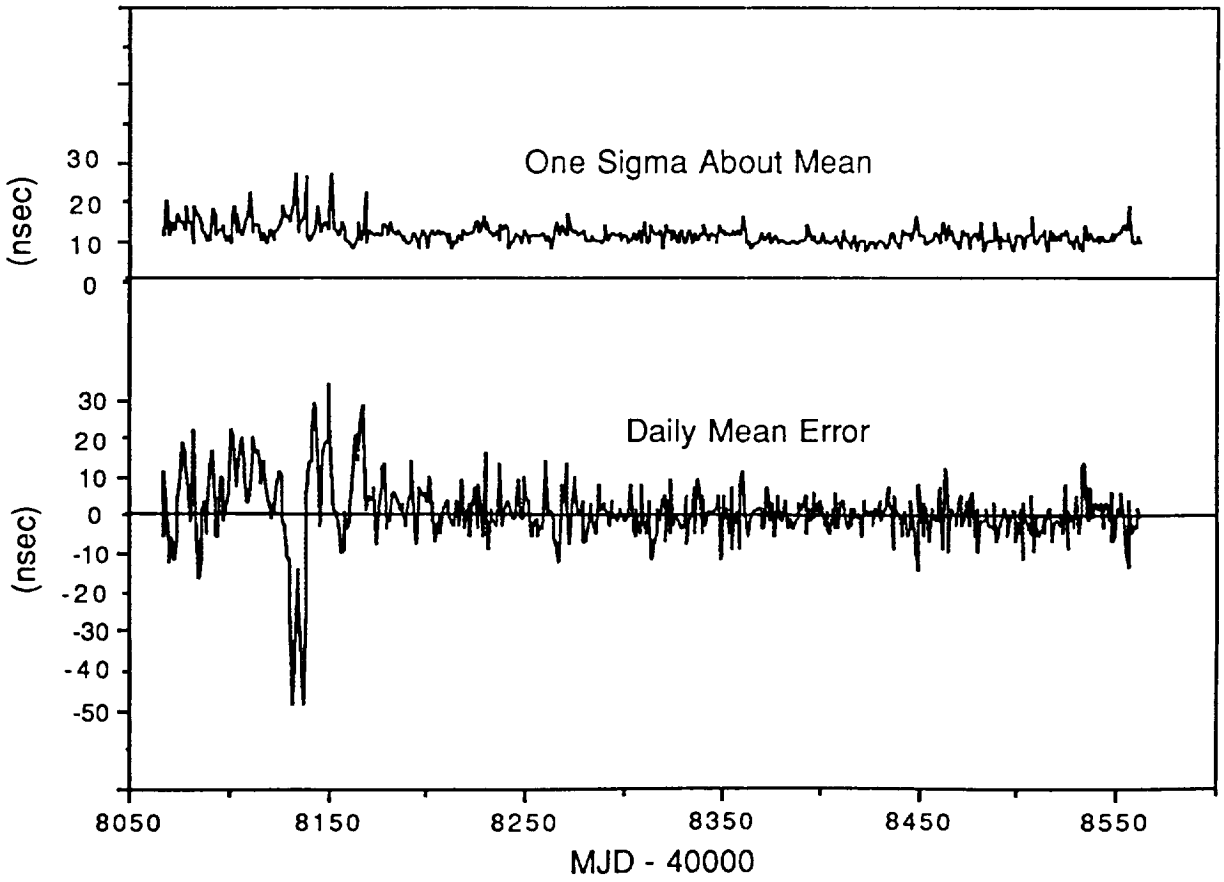

Figure 6. GPS-UTC Steering Model

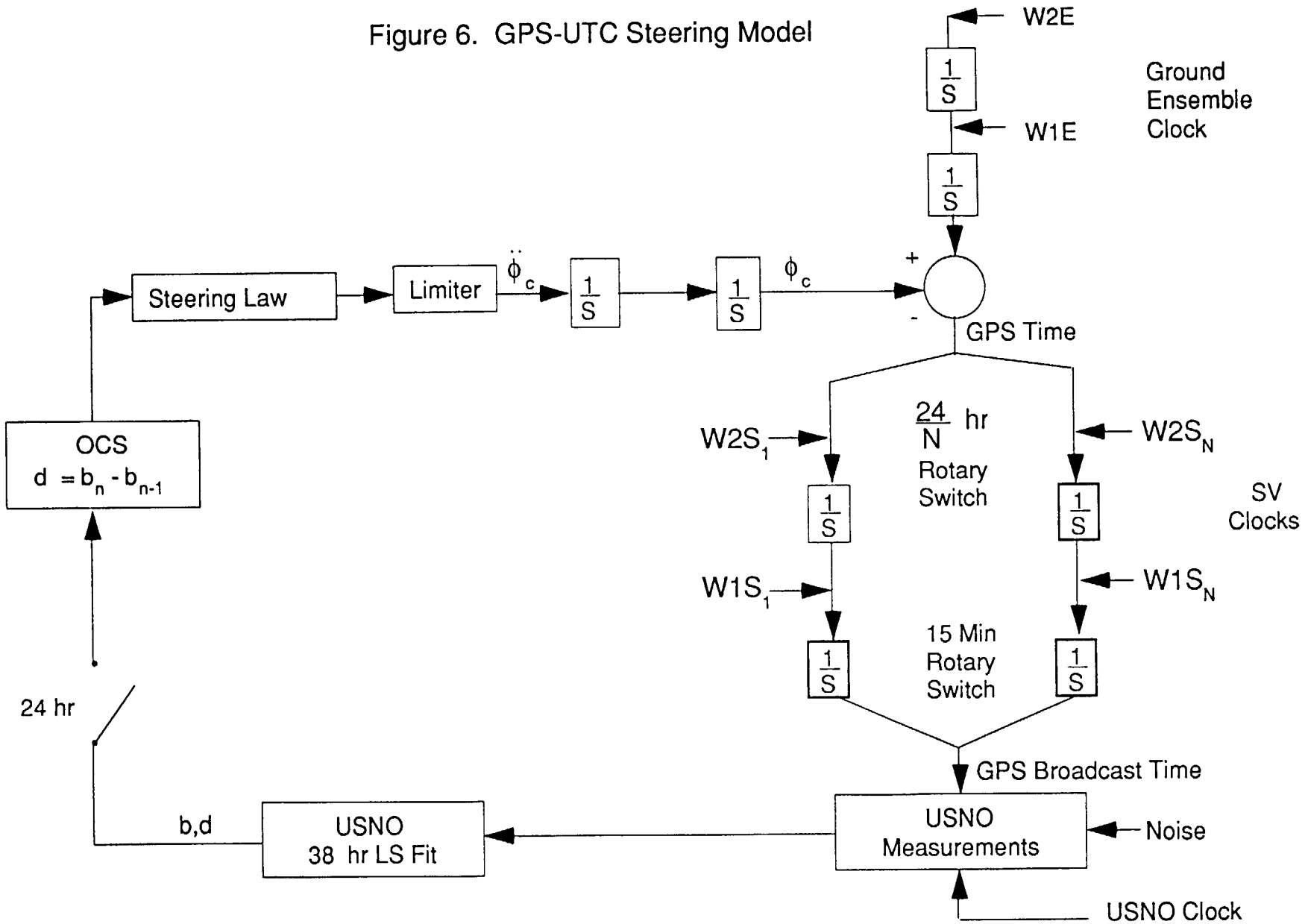

Figure 7. Allan Variance Clock Models

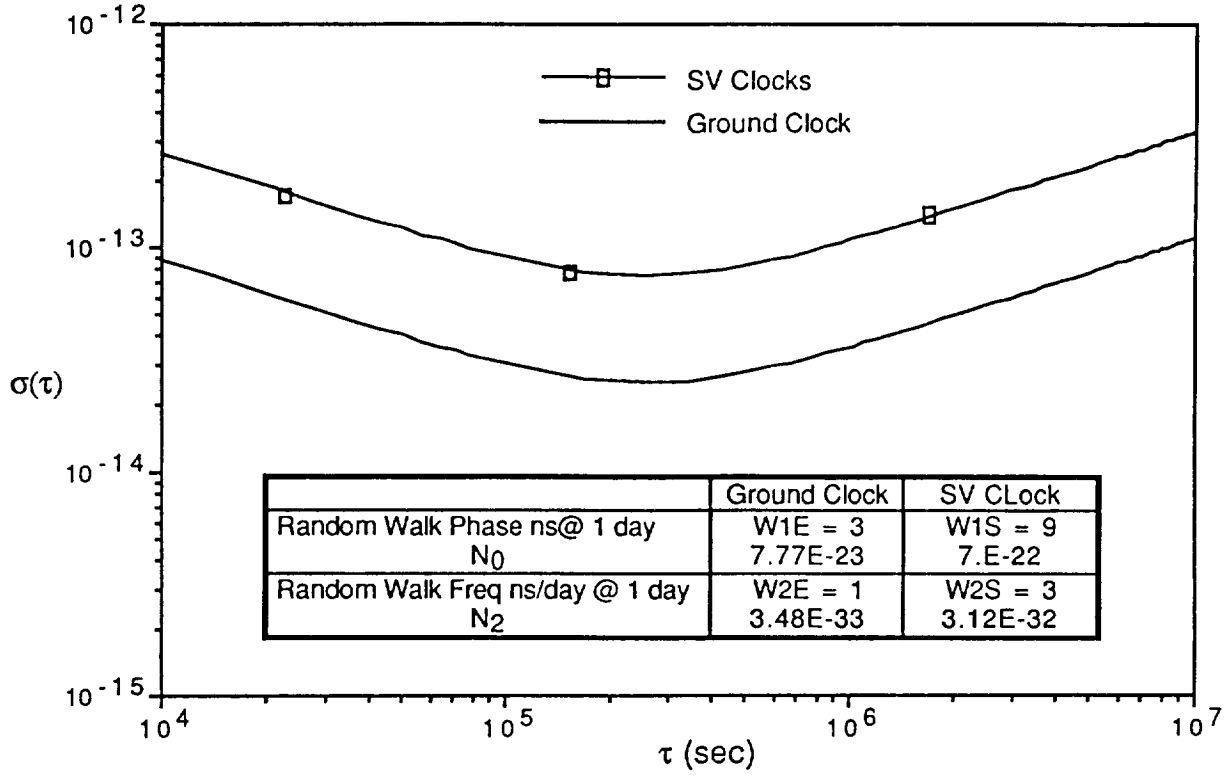

	Ground Clock	SV CLock
Random Walk Phase ns@ 1 day N_0	W1E = 3 7.77E-23	W1S = 9 7.E-22
Random Walk Freq ns/day @ 1 day N_2	W2E = 1 3.48E-33	W2S = 3 3.12E-32

Figure 8. Typical Simulated Sample Function

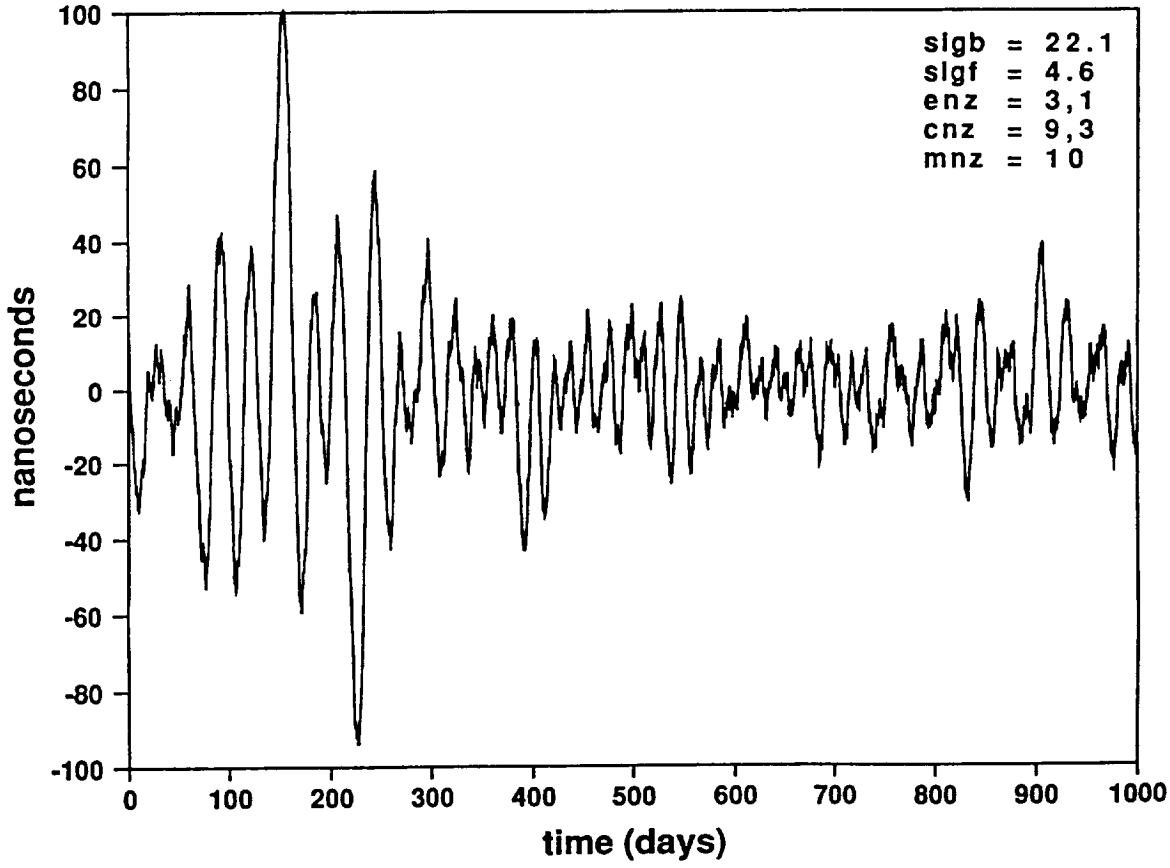

Figure 9. Sensitivity Study Summary

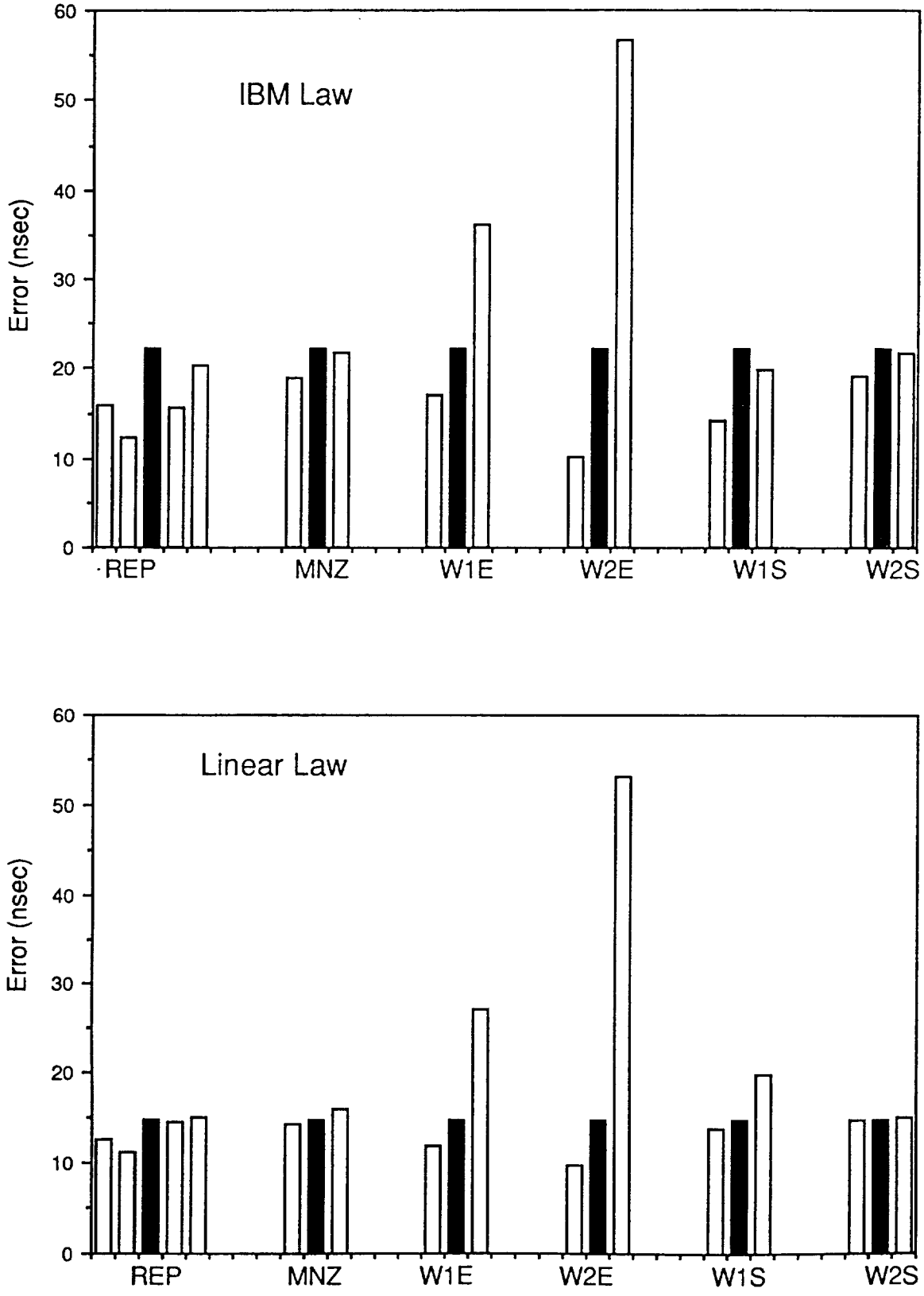

QUESTIONS AND ANSWERS

David Allan, NIST: In your previous chart, where you showed the state of the steering law, plus or minus or zero, during the period where it was operating well, it was almost never at zero. Where it was operating poorly, it was often at zero. Intuitively, one would say that, since it is almost never at zero during that last period, there could be something done to make it work even better, even though it is as good as you need. Statistics says that it should be often at zero, rather than always at the limit.

Mr. Feess: If the two are synchronized, and have no driving force, that is true. Simulation shows that it is usually in this state, unless you are responding to some transient. The system is essentially driven by random processes. It would be nice if we didn't have random processes, because then we would expect it to remain at zero.

Mr. Allan: Intuitively it seems that, with improved digital design, one could spend part of the states at zero, instead of at the hard limit.

Mr. Feess: That is the way that it is designed, to be either plus or minus. If you used a linear law, you would operate most often at one-half or one-quarter of this level, but never at zero during the active steering mode.

Dr. Gernot Winkler, USNO: I share David Allan's concern. In other words, we are constantly steering, and that is the consequence of the principal of bang-bang steering. A three-state control...

Mr. Feess: It is a three-state controller with zero, but it very seldom stays at the zero point.

Dr. Winkler: I think that this can be incorporated by allowing for a dead-band. Then, when you are in the dead-band, you are not steering. I have another comment; in your chart where you showed the assumed Allan Variance for the ground clocks as compared to the space clocks, the space clocks are about three dB above the ground clocks. My question is: is that a result of the Kalman filter which puts all sorts of errors into the clock states, which would, of course, be erroneous. Why are they higher by three dB?

Mr. Feess: The space clocks were assumed to be three dB higher than the ground clocks because the specifications are higher.

Dr. Winkler: Yes, but that is not necessarily realistic in terms of performance. David Allan has shown repeatedly that the satellite clocks are performing very well, and in fact may be better than the ground clocks.

Mr. Feess: The satellite clocks that we have assumed here are better than specification by a factor of two to four. We know that the clocks are performing better than specification. The specification on the ground clocks is better, but are they really performing to specification? We think that they are not, and probably are performing no better than the satellite clocks, except for the one at Colorado Springs. We have measures that indicate that it is performing much better, and we should weight that clock more if we really wanted to optimize the system.

David Allan, NIST: I think that one of the problems with the Kalman Queuing is that they have only one set of queues distributed uniformly across all clocks.

Mr. Feess: No, there is a separate queue for each clock in the system.

Mr. Allan: Appropriate to its performance?

Mr. Feess: No, it is set by an operator.

Mr. Allan: There is the problem because the statistics that we observe on the clocks are different than what is queued in.

Mr. Feess: Right. That is one of the things that could improve the performance. We could tune the clocks for better timing performance.

Mr. Allan: An ensemble would work much better.

Mr. Feess: The system is designed more for the NAV user than the timing user and there is some reluctance to change anything. If it ain't broke, don't fix it.

Dr. Claudine Thomas, BIPM: I would like to make one comment: what you are doing is steering on UTC(USNO) and not on UTC.

Mr. Feess: That is true. We regard USNO as UTC. That is our requirement. Whether Dr. Winkler agrees with that...

Dr. Winkler: Let me comment on that. You are absolutely correct. Of course, UTC(USNO) is steered, in very long term, with respect to UTC. At the moment the offset is somewhat like eight nanoseconds. It is our intent to keep that as small as possible within the constraints: the delay of 45 to 70 days to receive BIPM information, and additionally you do not want steering changes that exceed one part in 10^{14} maximum, you do not want to make changes frequently–there are a number of boundary conditions within which you want to follow the principle that, in the long run, the offset should be as small as possible. That is our policy and therefore we must take reference to one physical clock and in fact, it is also dictated by the regulations of the DoD, that that clock should be used as an operational reference. In the interest of international coordination, we have to be as close to BIPM as we can.

We do **not** have a bang-bang controller!

Mr. Feess: I am not recommending the bang-bang, in fact I would recommend not the bang-bang.

Dr. Henry Fliegel, Aerospace: We have long considered the effect of the bang-bang steering and have in fact discussed the possibility of introducing a dead-band. Obviously, there is a trade off between maintaining frequency stability and timing stability. As you can clearly see from Bill's graphs, what we have opted for is the smallest mean offset of GPS minus UTC in time. We realize that makes a very busy situation in frequency. The frequencies are continually going up and down. We would appreciate any response from actual users who may want more in the way of frequency stability even at the cost of having larger swings in the time domain. We are open for suggestions at this point, at least at Aerospace, and we will try to convince our Airforce colleagues accordingly.

GPS Orbit Determination at the National Geodetic Survey

Dr. M. S. Schenewerk
Ocean and Earth Sciences
NOAA, Rockville, MD 20852

Abstract

The National Geodetic Survey (NGS) independently generates precise ephemerides for all available Global Positioning System (GPS) satellites. Beginning in 1991, these ephemerides have been produced from double-differenced phase observations solely from the Cooperative International GPS Network (CIGNET) tracking sites. The double-difference technique combines simultaneous observations of two satellites from two ground stations effectively eliminating satellite and ground receiver clock errors, and the Selective Availability (S/A) signal degradation currently in effect. CIGNET is a global GPS tracking network whose primary purpose is to provide data for orbit production. The CIGNET data are collected daily at NGS and are available to the public. Each ephemeris covers a single week and is available within one month after the data were taken. Verification is by baseline repeatability and direct comparison with other ephemerides. Typically, an ephemeris is accurate at a few parts in 10^7. This corresponds to a 10 meter error in the reported satellite positions. NGS is actively investigating methods to improve the accuracy of its orbits, the ultimate goal being one part in 10^8 or better. The ephemerides are generally available to the public through the Coast Guard GPS Information Center or directly from NGS through the Geodetic Information Service. An overview of the techniques and software used in orbit generation will be given, the current status of CIGNET will be described, and a summary of the ephemeris verification results will be presented.

CIGNET

The Cooperative International GPS Network, or CIGNET, was created to make available reliable and continuous GPS tracking data from a global network of fiducial stations. The tracking site positions are defined in the International Earth Rotation Service (IERS) reference frame, and the sites are maintained for crustal motion studies and as a common starting point for GPS satellite ephemerides generation. The National Geodetic Survey (NGS) has been an active participant in CIGNET since its inception and serves as the CIGNET Information Center (CIC). Figure 1 shows the distribution of CIGNET tracking sites. Facilities at each site are provided and run by the sponsoring organizations. All sites are equipped with a personal or mini computer and power backup systems for automated routine operation. External frequency standards are available at most sites providing superior receiver clock performance. Data are taken continuously at 30 second intervals and surface meteorological measurements taken hourly. A minimum satellite observation elevation of 10 degrees is imposed. Many sites are equipped with high speed modems making possible remote receiver control. Table I contains a list of the CIGNET locations displayed in Figure 1 with their

Table 1: CIGNET DEVELOPMENT

STATION		INSTALLED	RECEIVER	SPONSOR
MOJAVE CA	USA	NOV 1986	MiniMac 2816AT	NATIONAL GEODETIC SURVEY (NGS)
YELLOWKNIFE	CANADA	JAN 1987	ROGUE	GEOLOGICAL SURVEY OF CANADA (GSC)/EMR
WETTZELL	GERMANY	NOV 1987	ROGUE	INSTITUT FUR ANGEWANDTE GEODASIE
TROMSO	NORWAY	DEC 1987	ROGUE	STATENS KARTWERK
ONSALA	SWEDEN	DEC 1987	ROGUE	ONSALA SPACE OBSERVATORY
RICHMOND FL	USA	FEB 1988	MiniMac 2816AT	U.S. NAVAL OBSERVATORY
KOKEE PARK HI	USA	APR 1988	TRIMBLE 4000SST	CDP/GSFC/NASA
TSUKUBA	JAPAN	JUL 1988	MiniMac 2816AT	GEOGRAPHICAL SURVEY INSTITUTE (GSI)
HOBART	AUSTRALIA	DEC 1989	MiniMac 2816AT	UNIVERSITY OF TASMANIA
WELLINGTON	NEW ZEALAND	JAN 1990	TRIMBLE 4000SST	DEPT. OF SURVEY AND LAND INFORMATION
TOWNSVILLE	AUSTRALIA	MAR 1990	TRIMBLE 4000SST	DIV. OF GEOGRAPHIC INF/DEPT. OF LANDS
HARTEBEESTHOCK	S. AFRICA	JAN 1991	ROGUE	CNES/IGN FRANCE
ANKARA	TURKEY	JAN 1991	MiniMac 2816AT	TURKEY ARMY
VICTORIA/PENTICTON	CANADA	APR 1991	ROGUE	PACIFIC GEOSCIENCE CENTRE/GSC/EMR
METSAHOVI	FINLAND	MAY 1991	ASHTECH	FINNISH GEODETIC INSTITUTE
TAI-SHI	TAIWAN	JUL 1991	MiniMac 2816AT	INSTITUTE OF EARTH SCIENCE
HERSTMONCEUX	GREAT BRITAIN	JUN 1991	ROGUE	UNIVERSITY OF NEWCASTLE UPON TYNE
KOOTWIJK	NETHERLANDS	JAN 1991	ROGUE	DELFT UNIVERSITY OF TECHNOLOGY
PLATTEVILLE CO	USA	AUG 1991	TRIMBLE 4000SST	UNAVCO
MATERA	ITALY	JAN 1991	ROGUE	ITALIAN SPACE AGENCY
ORRORAL	AUSTRALIA	JAN 1991	TRIMBLE 4000SST	AUSTRALIAN SURVEYING & LAND INFORMATION
FORTALEZA	BRAZIL	(FUTURE)	ROGUE/TRIMBLE	BRAZILIAN SPACE AGENCY
BRASILIA	BRAZIL	(FUTURE)	TRIMBLE	BRAZILIAN INS. OF GEOGRAPHY & STATISTICS
PORT HARCOURT	NIGERIA	(FUTURE)	TRIMBLE 4000SST	RIVERS STATE U. OF SCIENCE & TECHNOLOGY
BADARY	USSR	(FUTURE)	MiniMac 2816AT	USSR ACADEMY OF SCIENCES

dates of installation, current receivers, and sponsors. Four future sites, indicated with crosses in Figure 1, are also listed.

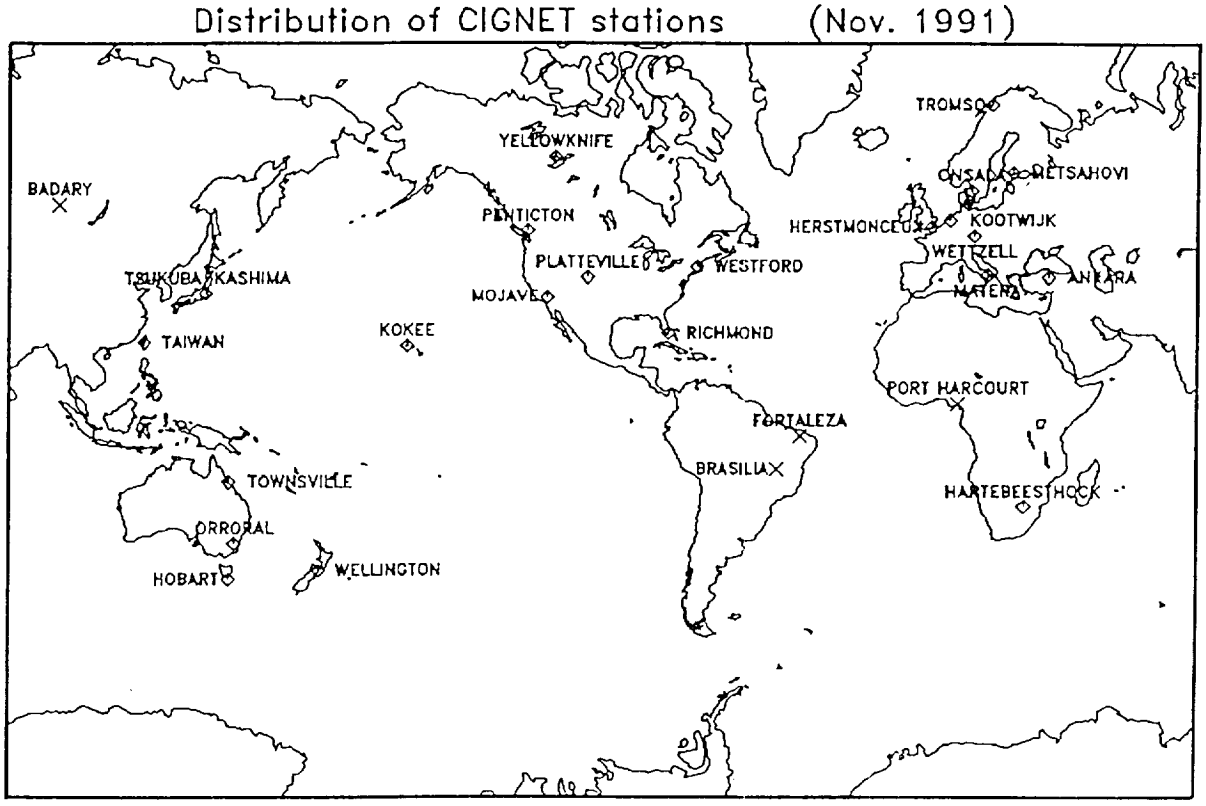

Figure 1

Data retrieval at the CIC is accomplished, where possible, via modem or computer network. Upon receipt, the raw data are converted into an ASCII exchange format. The reformatted data are then processed to provide receiver health, station clock health, satellite coverage, Selective Availability (S/A) status, cycle slip evaluation, and meteorological summary information. The entire operation is fully automated and completed each morning before 7:00 AM Eastern Time. The raw and reformatted data are archived on 9-track tape or magneto-optical disk. Occasionally, situations require the data to be copied onto floppy disks at each site and shipped to the CIC via express mail services. Upon receipt these data are processed manually and are typically available within one week.

The reformatted ASCII and raw data files are available through the CIC. The most recent data may be accessed directly through ARPAnet from an HP9000/825 computer with UNIX operating system. The network address is gracie.grdl.noaa.gov or 192.64.68.199; the system guest login name and password are anonymous. Individual data files are stored in subdirectories branching off /users/ftp/dist/cignet. The subdirectories are named d###a or d###b where ### is the day-of-year of the data. d###a contains the reformatted ASCII, and d###b, original binary files. Large quantities of data are transferred on 9-track, 6250 bpi tapes. Smaller requests may be sent via IBM compatible floppy disks or 9-track tape at the user's discretion. All users are urged to retrieve the data over the computer networks if possible. Requests, questions, or problems

can be directed to Miranda Chin, N/OES13, NOAA/NOS/OES, Room 418, 11400 Rockville Pike, Rockville, MD 20852, USA; phone: 301-443-8798 or 301-443-0139; FAX: 301-443-5714; ARPAnet: ernie@gracie.grdl.noaa.gov.

GPS SATELLITE EPHEMERIDES

The growing use of GPS has motivated NGS to take an active interest in the production GPS satellite ephemerides. In addition, NGS agreed in April 1990 to be responsible for providing GPS ephemerides through the Civil GPS Service. The participation in CIGNET has made possible an effort to produce these ephemerides at NGS. Typically, the NGS ephemerides are available one month after the data were taken. These ephemerides can be gotten, via modem and free of charge, through the Civil GPS Service Interface Committee (GPSIC) bulletin board operated by the United States Coast Guard. Only the most recent ephemerides will be available because of space limitations. The GPSIC bulletin board may be reached by dialing 703-866-3890 for 300 - 2400 bps modems, or 703-866-3894 for 9600 bps modems. The communication parameters are asynchronous, 8 data bits, 1 start bit, 1 stop bit, no parity, full duplex, and XON/XOFF. Both Bell And CCITT protocols are recognized. In addition to the GPSIC bulletin board, all NGS ephemerides are available through the NGS Geodetic Information Branch. There is a $50 (US) charge for each week requested plus a 25% surcharge for distribution outside the United States. For additional information, the Information Branch may be telephoned directly at 301-443-8631.

Production is composed of three primary tasks or stages: the creation of a priori ephemeris, data pre-processing, and orbit adjustment. The a priori ephemerides are created with ARC, an orbit integrator program, provided by the Massachusetts Institute of Technology. ARC employs an eleventh order Adams-Moulton predictor-corrector to produce satellite positions and partial derivatives to the initial conditions at 22.5 minute intervals. The constants used in the program were defined in the IERS standards (McCarthy, 1989) with an 8x8 gravity field taken from the GEM-T2 model (Marsh et al. 1989). A simplified ROCK4 model (Columbo, 1989) for the satellite radiation pressure, ad hoc Y-bias, and the related partial derivatives are currently in use. Conversion between inertial and Earth-centered fixed coordinates uses polar motion and UT1-UTC values determined from VLBI observations, and nutation values generated from IAU 1980 Theory of Nutation (Seidelmann, 1982; Wahr, 1981). In routine production, initial conditions taken from the previous week's adjusted ephemeris are used although any precise or broadcast ephemerides can provide these.

Pre-processing involves the creation of databases, and the identification and removal of cycle slips. Both tasks are accomplished with the OMNI software developed at NGS; however, human intervention is required to verify and complete the cycle slip removal. Cycle slip correction, being the most intensive and time consuming task, is the current limiting factor in ephemeris production.

The program PAGE2 combines the a priori ephemerides from ARC with the tracking data in a least-squares adjustment to produce the corrected ephemerides. Designed for background or batch operation, PAGE2 can process observations of 24 satellite from 20 sites. Dual frequency data are combined to produce an ionosphere-free, double-differenced observable. Double-differencing effectively removes all clock errors. S/A, which manifests itself a satellite clock error, is therefore also removed with this technique. A neutral atmosphere path length correction derived from the Saastamoinen dry atmosphere (Saastamoinen, 1972) plus the Chao wet atmosphere (Chao, 1972) zenith corrections combined with the Center for Astrophysics 2.2 mapping function (Davis et al., 1985), and an Earth tide correction (Melchion, 1978) for the tracking sites are applied. Data from

a GPS week plus one day before and after are used to create the weekly ephemerides. The two additional days are included to help smooth discontinuities between subsequent ephemerides. Typically, adjustments to all satellite positions and velocities, scale factors for the radiation pressures, Y-biases, and tropospheric delays, and phase bias values are determined. The site coordinates are not adjusted in normal operation. Currently, time and physical limitations allow only sub-networks in the U.S., Europe, and Australia to be processed for orbit determination. Planned software and hardware improvements, and the continued growth of CIGNET will allow other sites to be included in the near future.

Ephemeris verification is performed using two methods. The first is direct comparisons with independently produced ephemerides. Through the advent of continuous S/A in the Block II satellites, agreement between all sources has been at a few parts in 10^7. Although this method is valuable for long term improvement of the techniques and models used in the ephemerides adjustment, it does not satisfy the strict time constraints of routine production. To address the problem in a timely fashion, a repeatability study using tracking sites not included in the orbit solution was proposed. Three permanent tracking sites equipped with P-code receivers in southern California were used in the example shown here. The three sites, designated JPLMESA, PIN1, and SIO1, are part of the Permanent GPS Geodetic Array, a NASA pilot project operated by the Scripps Institution of Oceanography and the Jet Propulsion Lab with the assistance of the California Institute of Technology, the Massachusetts Institute of Technology, and the University of California at Los Angeles. The relative positions of these sites is shown if Figure 2. Data from August 18 through September 28, 1991 were processed. These data span GPS weeks 606 - 611, days-of-year 230 - 271. The position of SIO1 was held fix as the reference position. The variation of the estimated positions for the other two sites could then be used to judge the quality of the input ephemerides. The resulting baseline lengths were 171.2 km for JPLMESA to SIO1, and 110.9 km for PIN1 to SIO1. Consistency required that similar observing scenarios be used each day. If substantial data were missing from more than one site, the day was eliminated from consideration. Thus, days 236, 239, 257, 258, and 267 are not included in the subsequent discussion. In addition, PIN1 data were unavailable for most of GPS week 611. The week 611 results for PIN1 are included for completeness and should not be considered a reliable diagnostic for that ephemeris. Ionosphere-free, double difference phase measurements of the baselines were made using the OMNI software and NGS generated ephemerides. Hourly tropospheric path length scaling factors were estimated to minimize tropospheric modelling errors. The data were edited automatically, but only down to the few cycle level. Examination of randomly selected days revealed that several small cycle slips remained in the data after the editing. Undoubtedly cycle slips of this magnitude exist in each set of data. Although these cycle slips will worsen the repeatability, in essence giving a worst case evaluation, the slips are not large or frequent enough to prevent an evaluation of ephemeris quality. A single set of coordinates for all three sites were adopted to simplify comparisons.

Figures 3 through 6 show the estimated offsets from the a priori positions. Lines connect points that belong to the same GPS week. Table II summarizes the weekly and overall RMS deviations from the mean for these offsets. Two extreme cases appear in the weekly results. GPS week 608 shows a large variation in the east component for the PIN1 - SIO1 baseline. This variation is not seen in the JPLMESA - SIO1 baseline and probably results from missing or improperly edited data from the PIN1 site. GPS week 607 is more troubling. Both baselines show similar large variations. Again, missing or improperly edited data, this time from the common reference station SIO1, is the likely source. Although an ephemeris error can not be completely ruled out, the north components do not show a similar variation which implies a specific event rather than a more global ephemeris error. Weekly RMS variations are typically 1 - 3 cm in the horizontal, 4 - 6 cm in the vertical

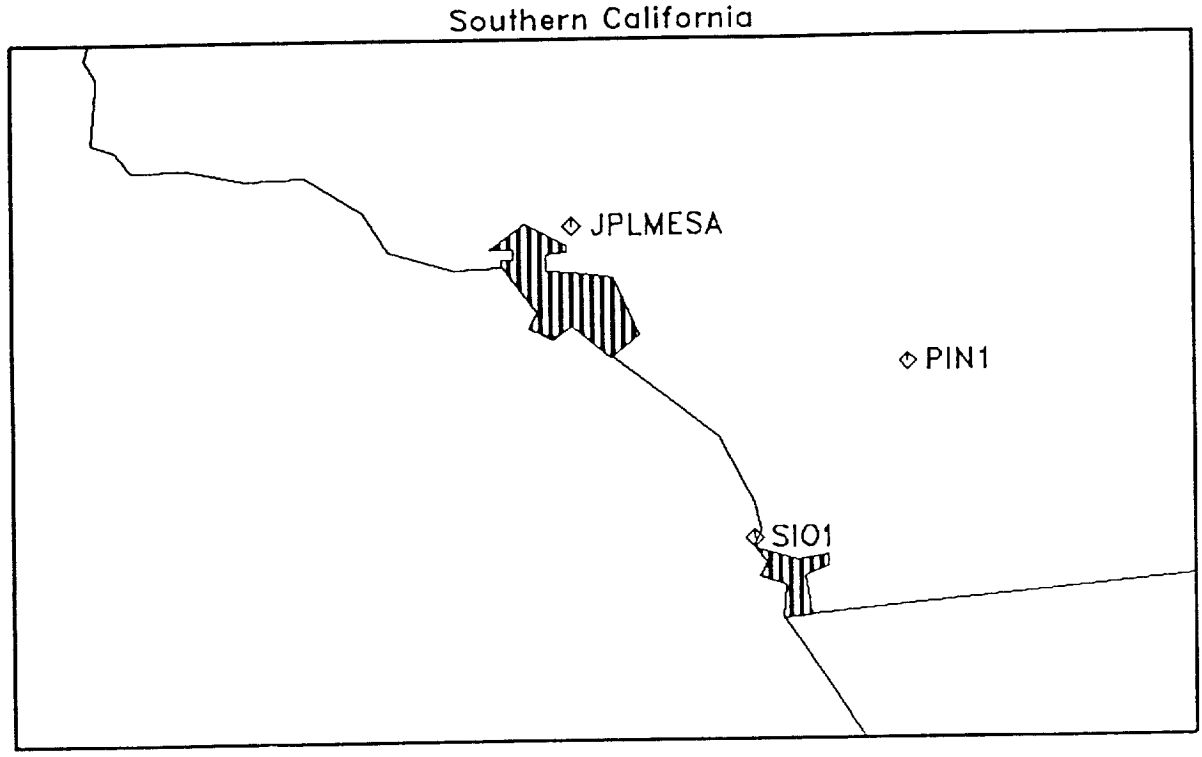

Figure 2: Relative location of sites used in the repeatability study.

components of the baselines. Limitations of satellite geometry and coverage, errors in tropospheric modelling, and signal multipathing generally manifest themselves most strongly as errors in the vertical component of a baseline solution. The weekly results are consistent with these effects. These results imply NGS ephemerides are internally consistent at 1 part in 10^7. The overall RMS values are significantly larger for the east and vertical components indicating possible week-to-week ephemeris variations. Such week-to-week variations are expected and efforts are taken to minimize them. The overall RMS values indicates the "worst case" accuracy of slightly better than 1 part in 10^6; however, the repeatability in the north component implies results an order of magnitude better.

Table II: RMS variations of the baseline components. All values are in meters.

	JPLMESA - SIO1			PIN1 - SIO1		
GPS WEEK	EAST	NORTH	UP	EAST	NORTH	UP
606	0.0184	0.0105	0.0252	0.0213	0.0090	0.0307
607	0.0861	0.0114	0.1345	0.0621	0.0259	0.1503
608	0.0435	0.0081	0.0345	0.1299	0.0099	0.0436
609	0.0278	0.0139	0.0534	0.0221	0.0122	0.0404
610	0.0081	0.0061	0.0460	0.0256	0.0104	0.0669
611	0.0160	0.0102	0.0308	0.1391	0.0148	0.0104
OVERALL	0.1350	0.0130	0.0910	0.0972	0.0183	0.0927

Conclusion

CIGNET is a global GPS tracking network whose data are generally available for geodetic and geophysical studies, and ephemeris generation. The data are retrieved and available through the CIGNET Information Center daily. In turn, these tracking data are used in GPS ephemeris generation at National Geodetic Survey. Each ephemeris covers a single GPS week and is available one month after the data were taken. Direct comparisons with independent sources and baseline repeatability studies indicate the accuracy of the NGS ephemerides to be roughly 1 part in 10^7.

REFERENCES

- Chao, C. C., 1972, *"A Model for Tropospheric Calibration from daily Surface and Radiosonde Balloon Measurements"*, Tech. Memo Calif. Inst. Technol. Jet Propul. Lab., 17.
- Columbo O., 1989, Private Communication.
- Davis, J. L., et al., *"Geodesy by radio interferometry: Effects of atmospheric modeling errors on estimates of baseline length"*, Radio Science, 20, 6, pp. 1593-1607.
- Marsh, J. G. et al., 1989, *"The GEM-T2 Gravitational Model"*, NASA Technical Memorandum 100746.
- McCarthy, D. D. et al., 1989, *"IERS Standards (1989)"*, IERS Technical Note 3.
- Melchion, P., 1978, *"The Tides of the Planet Earth"*, Pergamon Press, pp. 109-121.
- Saastamoinen, J., *"Atmospheric correction for the troposphere and stratosphere in radio ranging of satellites"*, The Use of Artificial Satellites for Geodesy, Geophys. Monogr. Ser., 15, ed. S. W. Henriksen et al., AGU, Washington, D. C., pp. 247-251.
- Seidelmann, P. K., *"Theory of the Rotation of the Rigid Earth"*, Celestial Mechanics, 15, pp. 277-326.
- Wahr, J. M., 1981, *"The Forced Nutations of an Elliptical Rotation Elastic, and Oceanless Earth"*, Geophys. J. Roy. Astron. Soc., 64, pp. 705-727.

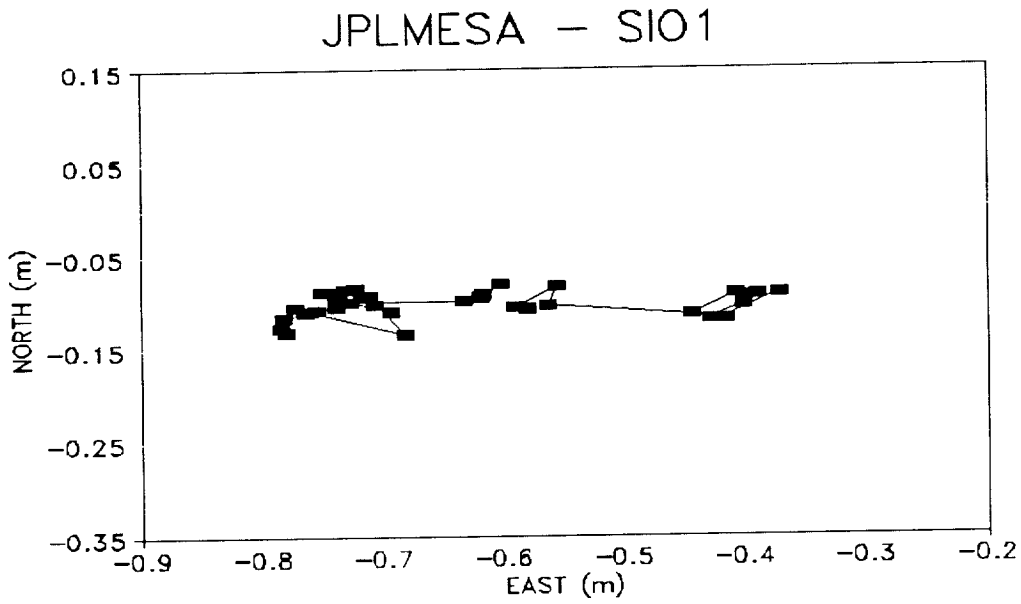

Figure 3: JPLMESA - SIO1 estimated daily horizontal offset from the a prior position.

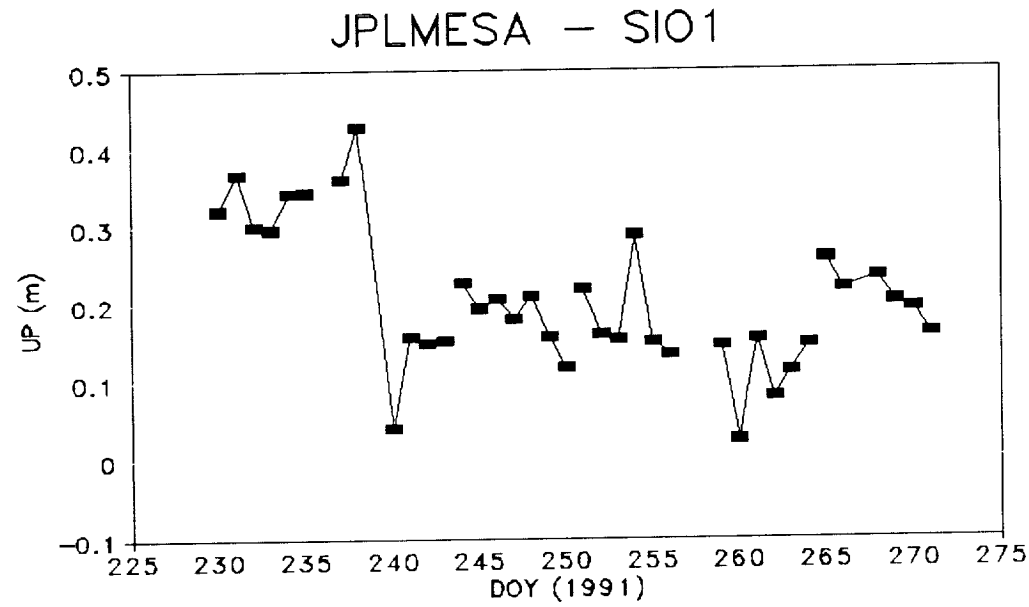

Figure 4: JPLMESA - SIO1 estimated daily vertical offset from the a priori position.

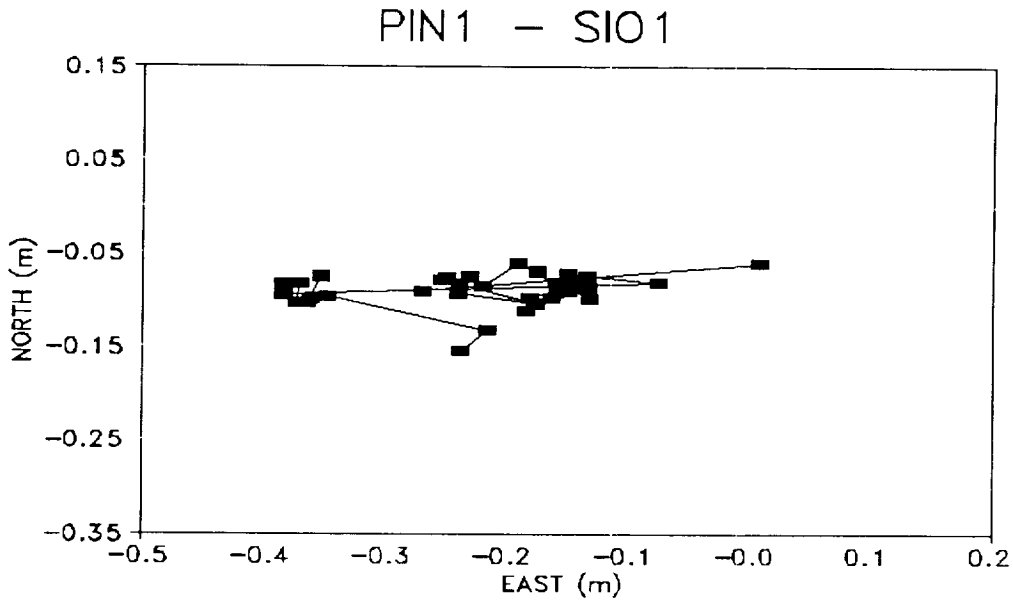

Figure 5: PIN1 - SIO1 estimated daily horizontal offset from the a priori position.

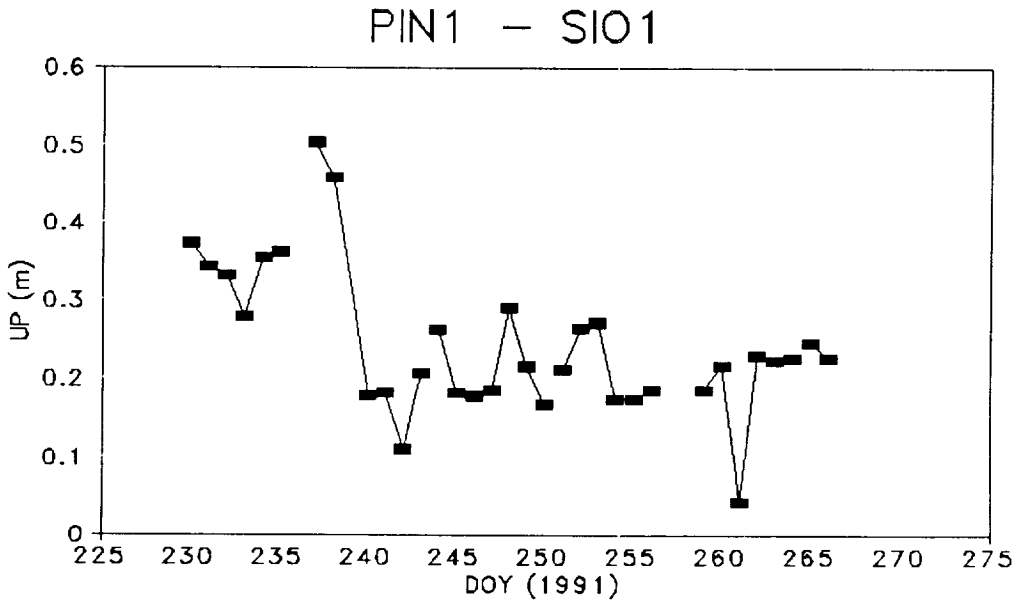

Figure 6: PIN1 - SIO1 estimated daily vertical offset from the a priori position.

QUESTIONS AND ANSWERS

G. Petit, BIPM: Is the processing to produce the ephemeris a global process? This means that all satellites are equivalent?

Mr. Schenewerk: At this point in time that is correct. I am sure that it is something that you can sympathize with and occasionally it is something that I am embarrassed about. A binding force in the universe is the establishment of a procedure for operations. We do have set procedures so that we have traceability of our ephemerides. We use equal weighting for all satellites and all stations that are involved. It varies of course from week to week depending on the availability of the data. Roughly, eight or ten stations, scattered around the globe, go into these ephemerides.

Mr. Petit: Did you get a chance to compare your three station network with the other positions? From VLBI or other?

Mr. Schenewerk: For this particular experiment, which is in actuality an attempt to establish a procedure for our verification project, all the sites, both in the orbit production and SIO for this experiment were held fixed. In other work that we have done, we have estimated the position of the tracking sites as well as the orbit when we do the solution. In those cases, we have fairly consistently got a correspondence with the VLBI and other locations at about one part in 10^8. Given the limitations of an incomplete constellation this is very good.

PRECISE GPS EPHEMERIDES FROM DMA AND NGS TESTED BY TIME TRANSFER

W. Lewandowski, G. Petit, C. Thomas
Bureau International des Poids et Mesures
Pavillon de Breteuil
92312 Sèvres Cedex, France

Abstract

It has already been shown that the use of DMA precise ephemerides brings a significant improvement to the accuracy of GPS time transfer. At present a new set of precise ephemerides produced by the NGS has been made available to the timing community. This study demonstrates that both types of precise ephemerides improve long-distance GPS time transfer and remove the effects of SA degradation of broadcast ephemerides. The issue of overcoming SA is also discussed in terms of the routine availability of precise ephemerides.

INTRODUCTION

Among the many challenges faced by the timing metrology community two of immediate concern are:

- improving the accuracy of routine intercontinental GPS time transfer from the 10-20ns level (a large part of which is due to broadcast ephemerides) to a few nanoseconds,
- overcoming the SA degradation of GPS broadcast ephemerides.

It appears that the best way to progress is to tackle both problems by correcting raw GPS data with post-processed precise ephemerides. Other improvements of GPS common-view time transfer [1], such as adoption of more accurate antenna coordinates, introduction of double-frequency ionospheric measurement systems, differential calibrations of receivers are progressively being introduced [2,3,4].

Previous papers showed the improvements brought about by use of the post-processed precise ephemerides produced by Defense Mapping Agency (DMA) [5,3]. At present the National Geodetic Survey (NGS) provides publicly available precise ephemerides. The purpose of this study is to test both types of ephemerides by long-distance GPS time transfer. Also removal of the effects of degradation of broadcast ephemerides, in case of Selective Availability (SA), is investigated. The issue of overcoming SA is also discussed in terms of the routine availability of precise ephemerides. We present here an experiment of 38 days duration in which three long-distance time links are

computed using both types of ephemerides. The precision of time links is estimated from the residuals of the smoothed common-view values. In addition we use the accuracy test of the closure around the world [3], which is the combination of these time links: the three independent time links should add to zero. The laboratories involved are the Paris Observatory (Paris, France), the National Institute of Standards and Technology (Boulder, Colorado, USA) and the Communications Research Laboratory (Tokyo, Japan). First we present briefly DMA and NGS precise ephemerides.

DMA PRECISE EPHEMERIDES

The United States Defense Mapping Agency (DMA) produces GPS precise ephemerides in support of its operational geodesy requirements [6]. From the beginning of 1986 until July 29, 1989 precise ephemerides were provided to the DMA by the Naval Surface Warfare Center (NSWC). Since July 30, 1989 they have been computed at the DMA. Since January 1990 Block II satellites have been included in the computations.

The pseudo-range measurements used for the computations of DMA precise ephemerides are performed at ten tracking stations. Five of the stations are operated by the United States Air Force and five by the DMA. The ten stations are quite evenly spread on the Earth surface.

The software system currently used, called OMNIS, includes a multisatellite Kalman filter/smoother that estimates a set of parameters including satellite orbits, satellite clocks, station clocks, and Earth orientation. Each precise ephemeris consists of the Earth-fixed position and velocity of the satellite center of mass at 15-minute intervals given in the WGS 84 reference frame. Estimates of the offsets between each satellite clock and GPS time and frequency at one-hour intervals are also generated. Over the years improvements have been made both to processing procedures and to the OMNIS software system with a view of improving the accuracy of the products and making them more compatible with the IERS standards within the framework of the WGS 84. Estimated uncertainty of the DMA precise ephemerides ranges from 1m to 5m. The DMA precise ephemerides are available for some research purposes with a delay of about 2 months.

NGS PRECISE EPHEMERIDES

The National Geodetic Survey (NGS) independently generates precise ephemerides for all available GPS satellites [7]. Beginning in 1991, these ephemerides have been produced from double-differenced phase observations solely from the Cooperative International GPS Network (CIGNET) tracking sites. The double-difference technique combines simultaneous observations of two satellites from two ground stations effectively eliminating satellite and ground receiver clock errors, and the Selective Availability signal degradation currently in effect.

CIGNET is a global GPS tracking network whose primary purpose is to provide orbit parameters. At present there are twenty- two CIGNET sites which are located mainly in the northern hemisphere. In addition, time and physical limitations allow only sub-networks in the United States, Europe, and Australia to be processed for orbit determination. Planned software and hardware improvements, and the continued growth of CIGNET will allow other sites to be included in the near future.

Each ephemeris covers a single week and is available within one month after the data were taken. Each is expressed in the ITRF reference frame. Checking is performed by baseline repeatability

and direct comparison with other ephemerides. The estimated uncertainty of NGS ephemerides is 10m.

The NGS is actively investigating methods to improve the accuracy of its orbits and to reduce the delay in availability [8]. The ephemerides have been available to the public since July 1, 1991 through the Coast Guard GPS Information Center or directly from NGS through the Geodetic Information Service.

THE EXPERIMENT

The three long-distance time transfers UTC(OP)–UTC(NIST), UTC(NIST)–UTC(CRL) and UTC(CRL)–UTC(OP) were computed by the common-view method [1] using both types of ephemerides. At the time of processing, the DMA and NGS precise ephemerides, made available to the BIPM, covered a 42-day period, from June 2, 1991 (MJD=48409) to July 13, 1991 (MJD=48450).

The GPS data taken at the three sites corresponds to the international schedules No 16 and 17, issued by the BIPM. These schedules include Block I and Block II satellites. For one part of the period under study (July 1 to 4, 1991), the intentional degradation of GPS signals, known as Selective Availability (SA), was turned on for Block II satellites. This application of SA consisted of phase jitter degrading the readings of satellite clocks, which can be removed by strict common views [9], and of broadcast ephemerides degradation by a bias which changes frequently. It should be noted that one Block II satellite, PRN18, was removed from the tests for the period of SA: both types of precise ephemerides failed to correct it.

In our experiment only common views with the same starting time and the same track length were kept. Time comparison values UTC(Lab1)-UTC(Lab2) were obtained for each observed satellite at the time T_{mid}, of the midpoint of the track. About 7 common views were available daily for each of the three time links.

The GPS receivers used at the OP and the NIST come from the same maker and use the same software to treat the short-term data. This enhances the symmetry of the experiment for the time link OP-NIST. This is not the case for the the NIST-CRL and CRL-OP links, the GPS receiver in regular operation at CRL coming from another maker.

For this experiment the measurements of ionospheric delays were used. They were provided at the OP and the NIST by similar dual-frequency GPS receivers of the NIST type [10] (NIST Ionospheric Measurement System) and at the CRL by another type of dual-frequency GPS receiver designed by the CRL [11] (Realtime TECmeter). Detailed procedures for the application of ionospheric measurements to GPS time transfer can be found in [3].

The antenna coordinates of the three laboratories involved are expressed in the ITRF88 reference frame with an uncertainty of 50cm for OP, 30cm for NIST and 10cm for CRL.

APPLICATION OF PRECISE EPHEMERIDES TO TIME TRANSFER

In practice, computations with precise ephemerides require knowledge of the broadcast ephemerides used, during the observation, by the receiver software in order to apply differential corrections

[5,3]. For our three time links which encircle the Earth we needed access to recorded broadcast ephemerides on at least two correctly situated sites. We have used the broadcast ephemerides recorded at the BIPM (Sèvres near Paris, France) and recorded by the NGS in Mojave (California, USA).

The precise ephemerides, $\mathbf{PE}_i$, are provided in cartesian coordinates (expressed in WGS 84 reference frame for DMA and in ITRF88 reference frame for NGS) at time $\mathbf{T}_j$ corresponding to round quarters of hours: 0h00 UTC, 0h15 UTC, 0h30 UTC etc. It is then necessary to compute, from the broadcast Keplerian elements of the observed satellite, its positions $\mathbf{BE}_1$, $\mathbf{BE}_2$ and $\mathbf{BE}_3$ at three times $\mathbf{T}_1$, $\mathbf{T}_2$ and $\mathbf{T}_3$, such that:

$$T_1 < T_{\mathbf{start}} < T_{\mathbf{stop}} < T_3$$

where $\mathbf{T}_{\mathbf{start}}$ and $\mathbf{T}_{\mathbf{stop}}$ are the starting time and the stopping time of the usual 13-minute tracking. The ephemerides corrections $\mathbf{PE}_i - \mathbf{BE}_i$ for i = 1,2,3, are transformed in a frame linked to the satellite (On-track, Radial, Cross-track) and a quadratic polynomial in time is computed to represent each component. A quadratic representation is also computed in the same frame for the vector satellite-station. The inner product of these quadratic representations provides the corrections to the GPS measurements each 15 seconds. A linear fit over 13 minutes on these short-term corrections gives the corrections at the middle-time, $\mathbf{T}_{mid}$, of the track.

CONDITIONS OF TESTING

To test the precise ephemerides we have analyzed the precision and accuracy of three long-distance time links with each of two available sets of precise ephemerides. We have considered three different cases for each time link and for the closure, which is the sum of the three links:

- non-corrected values.
- values corrected by DMA ephemerides and ionospheric measurements.
- values corrected by NGS ephemerides and ionospheric measurements.

For each case, a Vondrak smoothing [12] is performed on the values UTC(Lab1)-UTC(Lab2). The smoothing used acts as a low-pass filter with a cut-off period of about 4 days. For the closure, the smoothed values are interpolated for 0h UTC of each day and the interpolated values are simply added.

PRECISE EPHEMERIDES TESTED BY PRECISION OF TIME LINKS

For the estimation of the precision of the time links we have used the standard deviations of the residuals to the smoothed values. These standard deviations for the complete period of the study are given in Table 1.

TABLE 1. Standard deviation, in nanoseconds, of the residuals to the smoothed values UTC(OP)-UTC(NIST), UTC(NIST)-UTC(CRL) and UTC(CRL)-UTC(OP) for the period of the study with application or not of the corrections.

	OP-NIST (7388km)	NIST-CRL (8522km)	CRL-OP (8816km)
non-corrected	19.5	19.6	26.3
DMA ephem.+iono.	2.9	4.2	4.2
NGS ephem.+iono.	6.7	9.0	7.4

We observe a clear improvement of the precision of the time links for both types of precise ephemerides with, however, a better performance for DMA ephemerides. This improvement is linked to the length of the baselines involved. For such long baselines, common-view observations are mostly at low elevations and so are more sensitive to ionospheric effects and to satellite positions.

The improvements brought by the corrections of ephemerides and ionosphere are also illustrated by Figures 1 to 3. The figures represent individual common views without smoothing. Both, DMA and NGS precise ephemerides, perform very well, in particularly for the removal of the effects of the SA ephemerides degradation.

PRECISE EPHEMERIDES TESTED BY THE ACCURACY OF TIME TRANSFER

A test of accuracy for GPS time transfer can be performed by computing the closure around the world via OP, NIST and CRL. Daily values of UTC(OP)-UTC(NIST), UTC(NIST)-UTC(CRL) and UTC(CRL)-UTC(OP) were estimated from the smoothed data points. The resulting daily values of the deviation from closure, for the period under study, are shown in Figure 4. This test shows an evident gain in accuracy brought by DMA ephemerides. One can see an improvement for the NGS ephemerides in the last part of the experiment, although the period is too short for a definitive conclusion. Detailed studies of the closure around the world with the DMA ephemerides are provided by [3] and [13].

CONCLUSIONS

The DMA and NGS precise satellite ephemerides improve the precision and accuracy of long distance GPS time transfer. Further improvements of the quality of these ephemerides are expected, mainly for NGS after amelioration of the coverage of the globe by CIGNET stations.

Both types of precise ephemerides remove the SA degradation of GPS broadcast ephemerides.

Post-processed precise ephemerides can resolve the problem of SA degradation for TAI computation, provided that the BIPM has access to these ephemerides with a delay not exceeding two weeks.

ACKNOWLEDGMENTS

The authors gratefully thank Dr M.S. Schenewerk of the NGS and the staff of the DMA's Hydrographic/Topographic Center for providing the ephemeris data used in this study.

REFERENCES

[1] D. W. Allan, M. A. Weiss, *"Accurate Time and Frequency Transfer During Common-View of a GPS Satellite"*, in Proc. 34th Annual Symposium on Frequency Control, pp. 334-346, 1980.

[2] W. Lewandowski, C. Thomas, *"GPS time transfer"*, in Proc. of the IEEE, Special issue on Time and Frequency, pp. 991-1000, July 1991.

[3] W. Lewandowski, G. Petit, C. Thomas, *"GPS Time Closure Around the World Using Precise Ephemerides, Ionospheric Measurements and Accurate Antenna Coordinates"*, in Proc. 5th European Frequency and Time Forum, pp. 215-220, 1991.

[4] W. Lewandowski, G. Petit, C. Thomas, *"The Need for GPS Standardization"*, in these Proceedings.

[5] W. Lewandowski, M. Weiss, *"The use of precise ephemerides for GPS time transfer"*, in Proc. 21st Annual Precise Time and Time Interval (PTTI) Application and Planning Meeting, pp. 95-106, 1989.

[6] E.R. Swift, *"GPS Orbit/Clock Estimation Based on Smoothed Pseudorange Data from a Ten-Station Global Network"*, in Proc. IAG Symposium G2-Permanent Satellite Tracking Networks for Geodesy and Geodynamics, Vienna, August 1991, in press.

[7] M.S. Schenewerk, *"GPS Orbit Determination at the National Geodetic Survey"*, in these Proceedings.

[8] M.S. Schenewerk, personal communication,NGS.

[9] D.W. Allan, M. Granveaud, W.J. Klepczynski, W. Lewandowski, *"GPS time transfer with implementation of Selective Availability"*, in Proc. 22nd Annual Precise Time and Time Interval (PTTI) Application and Planning Meeting, pp. 145-156, 1990.

[10] D. Davis, M.A. Weiss, M. Vidmar, *"A codeless ionospheric calibrator for time transfer applications"*, in Proc. of the Institute of Navigation Satellite Division, 2nd International Technical Meeting, 1989.

[11] M. Imae, W. Lewandowski, C. Thomas, C. Miki, *"A dual-frequency GPS receiver measuring ionospheric effects without code demodulation and its application to time comparisons"*, in Proc. 20th Annual Precise Time and Time Interval Application and Planning Meeting, pp. 77-86, 1988.

[12] J. Vondrak, *"A Contribution to the Problem of Smoothing Observational Data,"* in Bull. Astron. Inst. Czechoslovakia, 20, pp. 349-355, 1969.

[13] W. Lewandowski, G. Petit, C. Thomas, *"Accuracy of GPS time Transfer Verified by Closure Around the World"*, in these Proceedings.

ACRONYMS

BIPM	Bureau International des Poids et Mesures, Sèvres, France
CIGNET	Cooperative International GPS Network
CRL	Communications Research Laboratory, Tokyo, Japan
DMA	Defense Mapping Agency
GPS	Global Positioning SSystem
IERS	International Earth Rotation Service
ITRF	IERS Terrestrial Reference Frame
NGS	National Geodetic Survey
NIST	National Institute of Standards and Technology
NSWC	Naval Surface Warfare Center
OP	Paris Observatory, Paris, France
TAI	International Atomic Time
SA	Selective Availability of GPS
UTC	Coordinated Universal Time
UTC(CRL)	Coordinated Universal Time as realized by the CRL
UTC(NIST)	Coordinated Universal Time as realized by the NIST
UTC(OP)	Coordinated Universal Time as realized by the OP
WGS	World Geodetic System

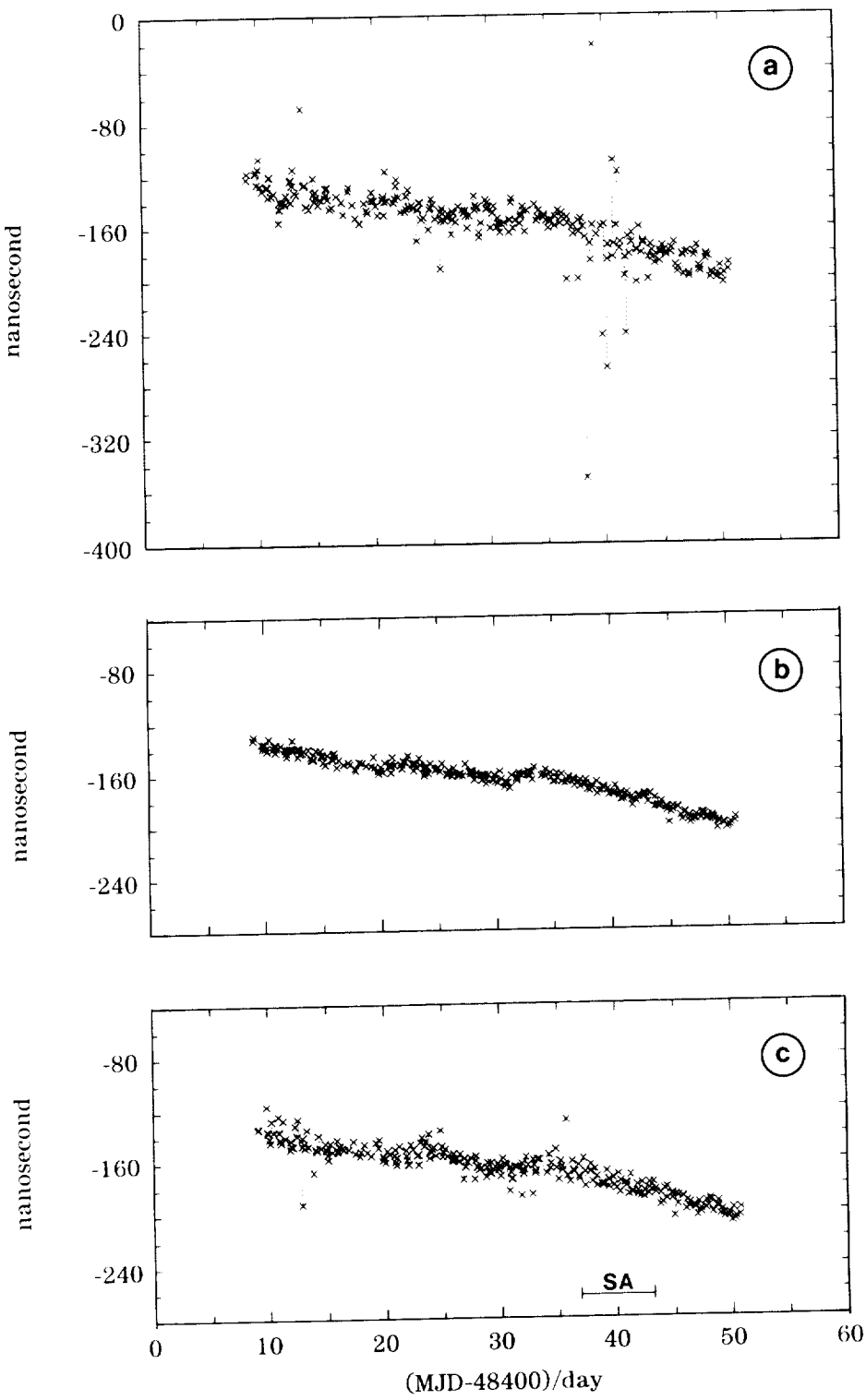

FIGURE 1. *GPS time link UTC(OP)-UTC(NIST) obtained with:*
1-a. non-corrected data,
1-b. data corrected for DMA ephemerides and measured ionospheric delays,
1-c. data corrected for NGS ephemerides and measured ionospheric delays.

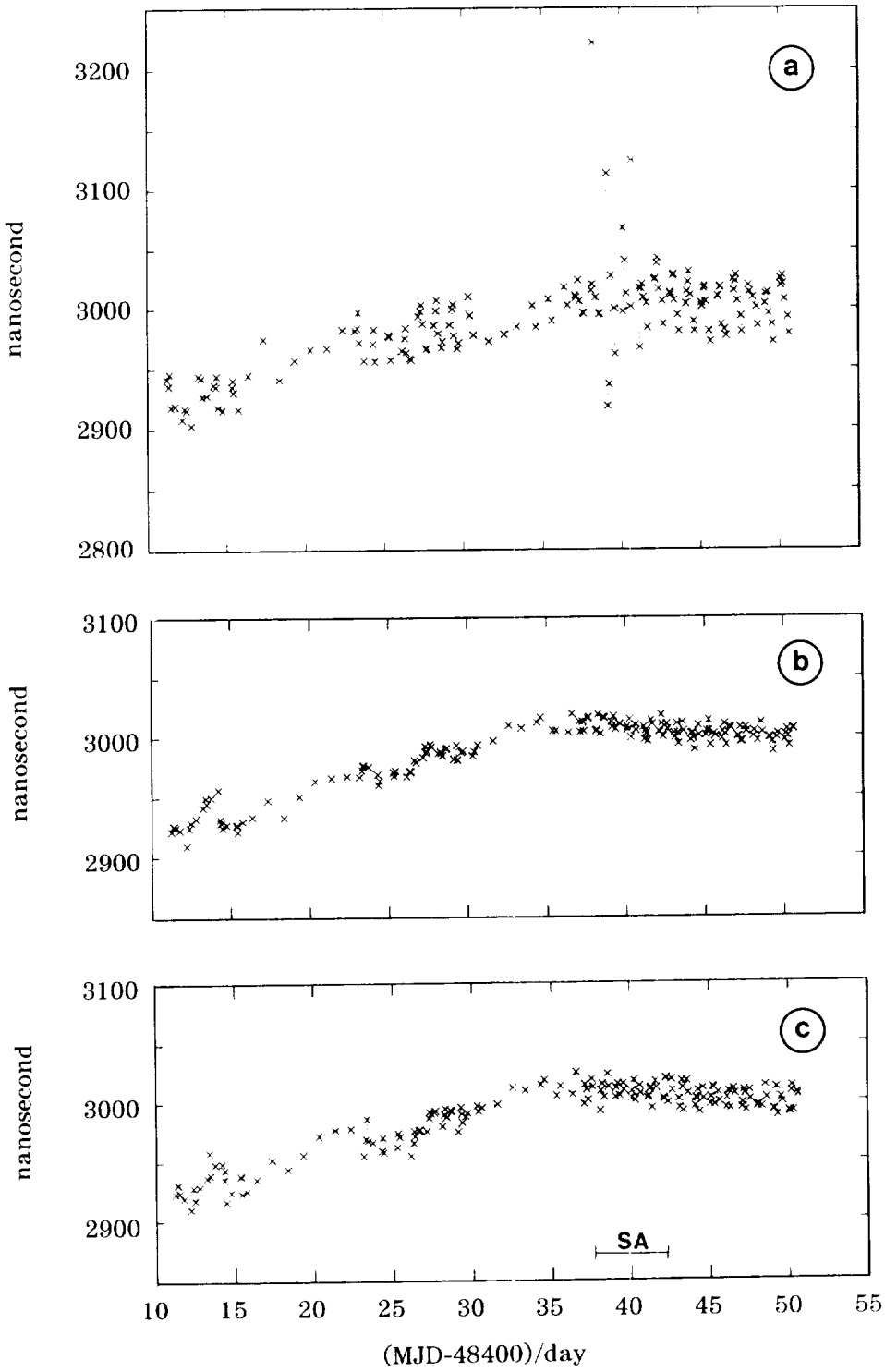

FIGURE 2. *GPS time link UTC(OP)-UTC(CRL) obtained with:*
2-a. non-corrected data,
2-b. data corrected for DMA ephemerides and measured ionospheric delays,
2-c. data corrected for NGS ephemerides and measured ionospheric delays.

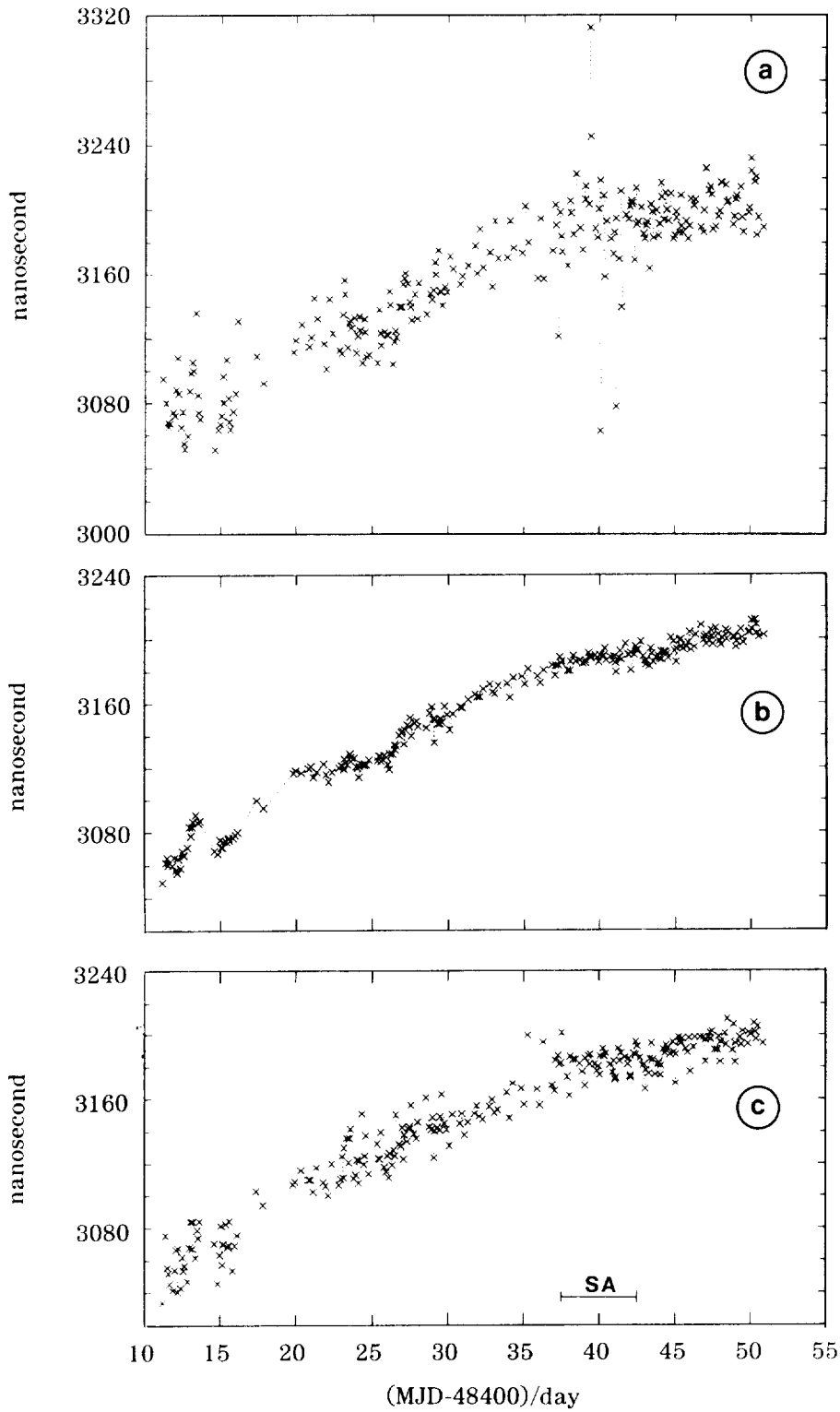

FIGURE 3. *GPS time link UTC(NIST)-UTC(CRL) obtained with:*
3-a. non-corrected data,
3-b. data corrected for DMA ephemerides and measured ionospheric delays,
3-c. data corrected for NGS ephemerides and measured ionospheric delays.

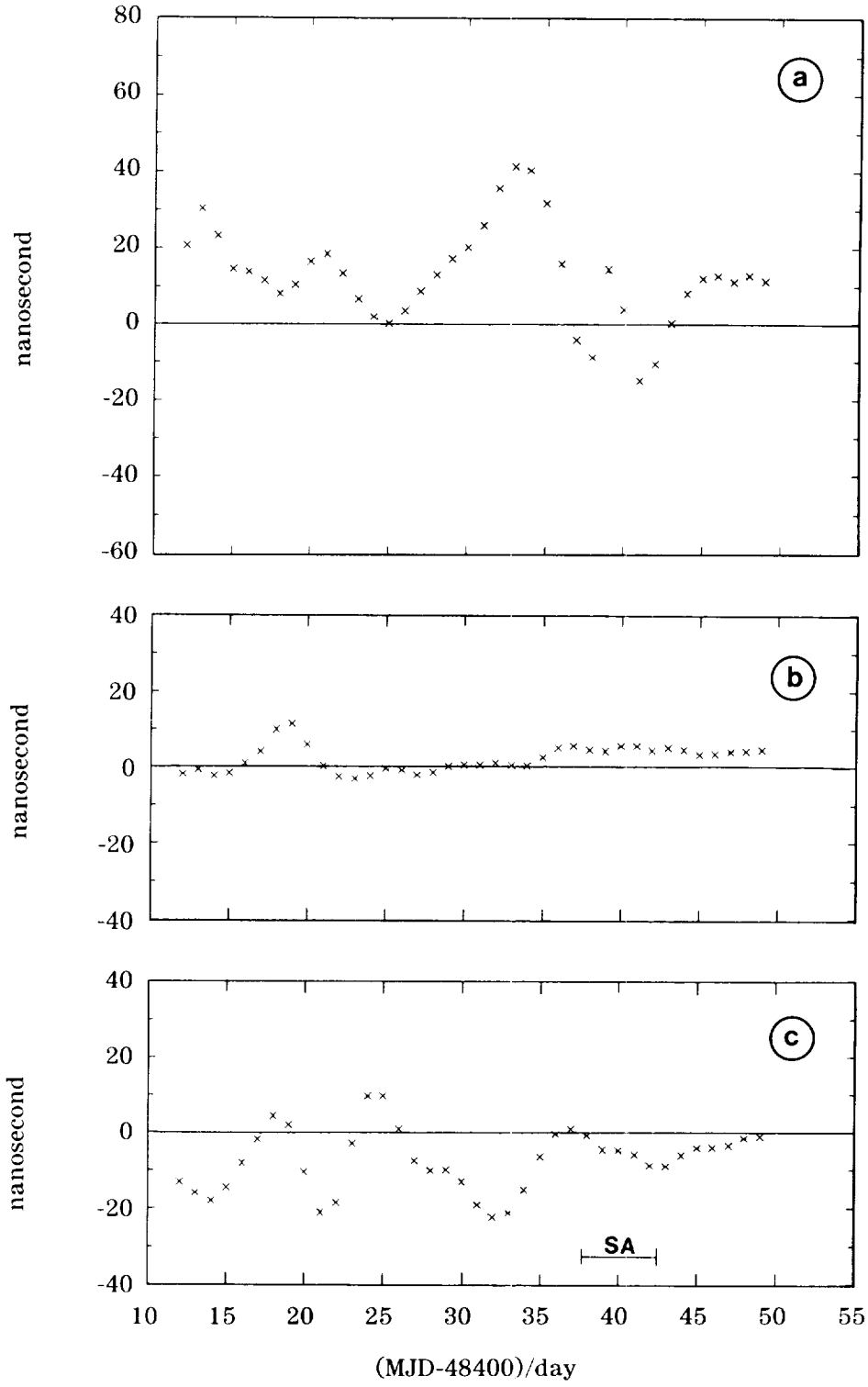

FIGURE 4. *Deviation from closure around the world via OP, NIST and CRL obtained with:*
4-a. non-corrected GPS data,
4-b. data corrected for DMA ephemerides and measured ionospheric delays,
4-c. data corrected for NGS ephemerides and measured ionospheric delays.

QUESTIONS AND ANSWERS

Professor Leschiutta, Politechnico Di Turino: Both DMA and NGS precise ephemeris correct for the ionospheric effects. Can you elaborate concerning a couple of questions? Do they use the same model, the same receiver, the same algorithm in order to correct for the ionospheric effects?

Mr. Lewandowski: I am not sure how they produce the corrections. I can only tell you what we are doing for the ionosphere. We use an ionosphere calibrator which was developed at the BIPM and is used also in Tokyo. NIST has produced another type which is used in Boulder. So, for this work, the same type of calibrators were used for all the data. Each of them should, theoretically, give a one nanosecond accuracy, but it is probably a few nanoseconds.

Samuel Ward, ex-JPL: Does that NGS offset that appears to be a bias occur because of a seasonal effect and the data span is too short?

Mr. Lewandowski: This is a short period so it is difficult to talk about seasonal effects. It is only a 38 day period. It *could* be, why not?

COMPARISON OF TWO-WAY SATELLITE TIME TRANSFER AND GPS COMMON-VIEW TIME TRANSFER BETWEEN OCA AND TUG

D. Kirchner and U. Thyr
Technical University Graz, Austria

H. Ressler and R. Robnik
Space Research Institute, Graz, Austria

P. Grudler, F. Baumont, and Ch. Veillet
Observatoire de la Côte d'Azur, Grasse, France

W. Lewandowski
Bureau International des Poids et Mesures, Paris, France

W. Hanson, A. Clements, J. Jespersen, D. Howe, and M. Lombardi
National Institute of Standards and Technology, Boulder, U.S.A.

W. Klepczynski, P. Wheeler, W. Powell, and A. Davis
U.S. Naval Observatory, Washington, U.S.A.

P. Uhrich, R. Tourde, and M. Granveaud
Laboratoire Primaire du Temps et des Fréquences, Paris, France

Abstract

For about one year the time scales UTC(OCA) and UTC(TUG) were compared by means of GPS and two-way satellite time transfer. At the end of the experiment both links were independently "calibrated" by measuring the differential delays of the GPS receivers and of the satellite earth stations by transportation of a GPS receiver and of one of the satellite terminals. The results obtained by both methods differ by about 3 ns, but reveal a seasonal variation of about 8 ns peak-to-peak which is likely the result of a temperature-dependence of the delays of the GPS receivers used. For the comparison of both methods the stabilities of the timescales are of great importance. Unfortunately during the last three months of the experiment a less stable clock had to be used for the generation of UTC(TUG).

INTRODUCTION

The GPS common-view technique presently provides the best operational means for comparing remote time scales with high precision and nanosecond accuracy [1]. In the future this will change with Selective Availability (SA) turned on. The degradation caused by SA can only be overcome by strict procedural standardization, and if necessary, the use of post-processed ephemerides. Of great

importance for the obtainable accuracy is the knowledge of the receiver delays. The differential delay of the receivers can be measured by receiver transportation.

Two-way time transfer via communication satellites using spread-spectrum techniques is capable of 100 ps precision but needs transmit and receive satellite terminals at both stations which have to work together in pairs [2]. Accuracies of nanosecond or even subnanosecond level are expected by calibration of the station delays by means of portable satellite terminals.

Through the cooperative efforts of several laboratories both methods have been implemented at the Observatoire de la Cote d'Azur (OCA), Grasse, France, and the Technical University Graz (TUG), Austria, allowing the comparison of these two state-of-the-art techniques over a period of nearly one year. Apart from other reasons OCA and TUG were chosen because at that time these stations were the only ones able to work with LASSO (Laser Synchronization from Stationary Orbit), the third technique capable of nanosecond accuracy. Due to various reasons no time transfer with that accuracy could be obtained despite successful LASSO sessions at both stations [3].

First results of the comparison between the GPS and two-way links have already been published [4]. The experiment was concluded by an independent "calibration" (measurement of the differential delays) of the GPS receivers and two-way stations by transportation of a GPS receiver and one of the satellite terminals. In the following the final results including the "calibration" will be given.

BASICS OF TWO-WAY

The two-way technique is used for point-to-point time transfer of highest precision and accuracy. Both laboratories need receive and transmit stations in order to exchange timing information via communication satellites employing pseudo noise (pn) coded signals and code division multiple access (CDMA). The measurement consists of simultaneous time interval measurements at both sites in which the one-pulse-per-second (1 PPS) generated by the local clock starts both the local time interval counter and, transmitted via the satellite, stops the remote time interval counter. The time difference T1 - T2 between the clocks of both stations is given by the following equation [2]:

$$\begin{aligned} T1 - T2 &= 1/2(C1 - C2) \\ &+ 1/2[(d1U + d2D) - (d2U + d1D)] \\ &+ 1/2(d12 - d21) \\ &+ dR \\ &+ 1/2[(d1TX - d1RX) - (d2TX - d2RX)] \end{aligned} \tag{1}$$

The first term of the right hand side of equation (1) is given by the difference of the counter readings of station 1 and 2 which have to be exchanged to compute the clock differences. The second term contains the differences of the sums of the signal delays in the uplink and downlink for both signal directions. Under the assumption of path reciprocity this term cancels out. This assumption is likely to hold to better than 100 ps for simultaneous transmissions at Ku-band frequencies [5]. The third term contains the difference of the transponder delays in both directions and is also zero when employing the same transponder in both signal directions. In the case of different transponders for both signal directions, the transponder delay difference has to be known. The fourth term is a correction for the path nonreciprocity caused by the earth rotation (Sagnac effect). It can be

computed from the positions of the earth stations and the satellite without requiring the knowledge of these positions with high accuracy. The last term is given by the difference of the differential delays of the transmit part and receive part (station delays) of earth station 1 and 2. The knowledge of these station delay differences mainly determines the accuracy of the time comparison.

The delay difference of both stations can be measured by means of a third station used as a transfer standard or by collocation of both stations involved. For the latter case one obtains [6]:

$$(d1TX - d1RX) - (d2TX - d2RX) = C2 - C1 \tag{2}$$

with the right hand side of equation (2) being the difference of the counter readings obtained during collocation of the stations.

EXPERIMENT CONFIGURATION AND EQUIPMENT

Each of the time scales UTC(OCA) and UTC(TUG) is generated by a single atomic clock. Fig. 1 shows the frequency and time distribution and measurement set-up at OCA and Figs. 2 and 3 present the same for TUG. UTC(OCA) has been generated by a HP 5061A opt. 004 (CS 560) using the internal clock module. UTC(TUG) was first generated by a HP 5061A opt. 004 (CS 1654) and after its sudden break-down (January 14, 1991) by a HP 5061A (CS 524) and using an external clock module (DDC 6459) for the generation of the 1 PPS.

The on-site GPS receiver at OCA has been an Allen Osborne TTR-5 SN053 and at TUG an original NBS receiver (NBS SN03) has been operated together with a Stanford Telecommunications Inc. TTS-502B SN04. At the beginning of the experiment TTR-5 and NBS 03 differed concerning the use of Block II satellites but this effect was removed by a software update which has been in use since December 12, 1990. An Allen Osborne TTR-6 SN0262 was used as a portable receiver in order to measure the differential delay of the on-site receivers, thus enabling an absolute comparison of UTC(OCA) and UTC(TUG) by means of GPS. For this purpose in both stations also the delay between UTC(Lab) and the 1 PPS used as time reference (1 PPS Ref) for the portable receiver has to be measured.

In the beginning the two-way measurements were carried out via the SMS (Satellite Multi-Service) transponder of the European communication satellite EUTELSAT I-F2 and since October 16, 1990 via the SMS transponder of EUTELSAT I-F4 both at a nominal position of 7°E.

The satellite earth stations used were the permanent station of TUG at the Observatory Lustbühel Graz and a temporary station at OCA of the VSAT type [6], which was then used as a portable station to measure the differential delay of the stations necessary for the absolute two-way comparison of UTC(OCA) and UTC(TUG). The main characteristics of both stations are given in Table 1.

To obtain a nominal carrier-to-noise power density ratio (C/N_o) of 55 dBHz at both stations, according to EUTELSAT link budget calculations OCA transmitted with its maximum EIRP and TUG with about 2 dB more than OCA to compensate for the smaller G/T of the OCA station. A block diagram of the two-way set-up employed at OCA and of that at TUG including the transported OCA station and thus also showing the configuration used for the measurement of the differential delay, is given in Figs. 1 and 3, respectively. Because of the allocated frequency of 14022.0 MHz for transmission and a frequency of 12522.0 MHz for reception resulting from the

nominal satellite translation frequency of 1500 MHz, which turned out to be very stable, no problem was caused by the limited frequency agility of the VSAT [6,7].

	TUG	OCA
Location	15° 30'E 47° 04'N 480 m MSL	06° 55'E 43° 45'N 1260 m MSL
Usage	various experiments	time transfer only
Antenna:		
Diameter	3 m	1.8 m
Mount	steerable	fixed
Max. EIRP	72 dBW	49 dBW
G/T	23 dB/K	21 dB/K
Frequency agility:		
Independence of up and down conversion	yes	no
Synthesizer step-size	100 Hz	1 MHz

Table 1 Main characteristics of the TUG and OCA earth stations.

At both stations MITREX modems [8,9] of the original type were used. The modems require 5 or 10 MHz as a reference frequency to internally generate the 1 PPS which is then modulated onto the pn-sequence (derived from the same reference frequency) for transmission. The internally generated 1 PPS (PPS TX) can be synchronized with the reference 1 PPS (1 PPS Ref) by an internal synchronization circuit or by employing an external device as done at TUG [10]. In contrast to the basic two-way procedure outlined in the previous chapter where the 1 PPS generated by the station clock starts the local counter and is transmitted to the remote station, in the actual set-up the local counter is started by a 1 PPS generated by the station clock the so-called reference 1 PPS (1 PPS Ref), but the transmitted pulse (PPS TX) is generated by the MITREX modem. Therefore in each station the delay between UTC(Lab) and the 1 PPS Ref and the delay between the 1 PPS Ref and the PPS TX have to be measured in addition to the actual time transfer measurements, during which the counter is started by the 1 PPS Ref and stopped by the received 1 PPS called PPS RX. Using this procedure the start input of the counter is always connected to the 1 PPS Ref and the stop input is connected to a PPS coming from the MITREX thus the configuration of each counter input can be set to best fit the employed signals and does not have to be changed. The stability of the 1 PPS Ref is given by the stability of the frequency standard, the clock and the time distribution system and that of the PPS TX by the stability of the frequency standard, the frequency distribution system and the divider and synchronization circuits of the MITREX. Both stations first used counters of the type HP 5370A, later (from March 20, 1991, on) a HP 5370B was used at OCA until the end of the experiment.

MEASUREMENTS

Two-way comparisons began on a regular basis on June 22, 1990, ended on October 10 and restarted on November 9 lasting to April 17, 1991. The interruption resulted from a break-down of the

receive part of the OCA station caused by humidity in the transmit reject filter oozing through an improperly sealed waveguide connection and required disassembly and reassembly of the driver unit.

A schedule of three sessions per week (Monday, Wednesday and Friday) each lasting from 12:00 to 12:30 UTC was used. Initially each session consisted of two measurement blocks of four minutes duration, each consisting of 240 individual measurements 1 s apart, starting at 12:15 and 12:20 UTC, respectively, and from July 30, 1990, of two minutes duration starting at the same times. Two minutes of data have been found sufficient in earlier experiments to obtain good average values of the time transfer [**11**]. Since November 9, 1990, a third two minutes block was performed starting at 12:27 UTC whereby the counter at OCA was started by the PPS TX instead of the 1 PPS Ref. In this measurement scheme the stability of the start pulse does not depend on the stability of the clock module, but on that of the MITREX divider and synchronization circuits. On the other hand it requires trigger level adjustment of the start input of the counter. This additional measurement was introduced because it turned out that the jitter of the clock module used to generate UTC(OCA) was rather large (700 ps). Before and after the time transfer measurements several measurements were carried out to determine the delay between 1 PPS Ref and PPS TX. Furthermore also the MITREX P-signal and Delta-f-meter readings were recorded giving an indication of changes in the received signal power and the deviation of the center frequency of the received signal from the nominal 70 MHz, respectively [**10**]. However no deviations were recorded which would cause a modem delay change exceeding 200 ps. In order to study the stability of the measurements over longer periods on August 20, 22 and 24, 1990 and March 27 and 29, 1991 only one block per session, but lasting about twenty minutes, was carried out [**4**]. The measurement of the differential delay of the stations was performed on April 23 and 24, 1991, with one measurement block (12:25 to 12:28 UTC) on the first day and on the second day three measurement blocks lasting four minutes and starting at 12:05, 12:10 and 12:15 UTC and a fourth block of 19 minutes duration beginning at 12:40 UTC.

The delay between UTC(Lab) and the 1 PPS Ref for the two-way measurements and the delay between UTC(Lab) and the 1 PPS Ref for the GPS measurements were measured at TUG at the beginning of the experiment and during the MITREX and GPS delay comparisons and at OCA the final measurements of these delays were carried out after the experiment.

At TUG the same trigger level was used for the start and stop channel of the counter throughout the experiment and also at OCA until September 19, 1990. Then OCA changed the start and stop trigger levels after using a different stop trigger level on September 21 and 24. During the third session both trigger levels were the same. During the collocation of the stations on April 23 and 24 the OCA counter was adjusted for the usual start and stop trigger levels, but for the last block another start trigger level was used.

GPS measurements have been carried out for years at OCA and TUG using the European common-view schedules issued by the Bureau International des Poids et Mesures (BIPM). Thus at the beginning of the experiment schedule No. 15 issued on June 12, 1990, was used. This schedule includes Block I and Block II satellites. The daily distribution of the 13 minutes tracks (32 per day) is shown in Fig. 4 revealing the changing and gradually degrading configuration of tracks around the two-way measurements. Therefore starting with December 19 for OCA and TUG a special schedule (48 tracks per day) including the European schedule No. 16 was introduced and used until the end of the experiment (see Fig. 5).

The delay comparisons between TTR-5 and NBS 03 by means of TTR-6 were carried out in the

time frame March 30 until May 21 starting (March 30 to April 8) and ending (May 16 to May 21) with comparisons between TTR-6 and the on-site receiver (TTR-5 SN051) of the Paris Observatory (OP). The comparisons at OCA were performed during the period April 11 to 19 and April 30 to May 15 and that at TUG during the period April 22 to 27.

DATA PROCESSING AND RESULTS

Nearly all GPS data were common-view data in the strict sense but also tracks with a maximum tolerance of 4 minutes were used. All time comparisons were referred to the midpoints of the tracks and restricted to tracks with elevation angles greater than 10° and a standard deviation below 20 ns. Furthermore all satellites reported as unusable by the U.S. Naval Observatory (USNO) including Block II satellites with SA [1] on were discarded and also all tracks between August 5, 7:22 and August 10, 8:06 were not used because they were not valid due to receiver problems at OCA. The average standard deviation of the 13 minutes tracks for OCA and TUG was about 5 ns and 4 ns, respectively.

In order to derive the two-way time differences UTC(TUG) - UTC(OCA), in a first step for each measurement block the expected value – referred to the midpoint of the block – of a linear regression through the second-to-second differences divided by two and the standard deviations were computed.

Fig. 6 depicts the standard deviations of all sessions including the sessions performed at TUG in order to measure the differential delay. The values which are higher than the usual ones (on average 0.8 ns until February) for a given period of time are caused by outliers in the measurements of OCA and TUG or in several cases of OCA only because of the rather large jitter of the 1 PPS Ref at OCA. This can be seen from the data of each station by computing a second order regression and studying the residuals and also from the generally smaller standard deviations of the third block (at OCA PPS TX starts the counter) until the change over from the high performance clock to the standard clock at TUG (dashed vertical line in Fig. 6). The larger standard deviations of all measurement blocks on December 10 are explained by the presence of an unknown carrier within the allocated two-way frequency band. The gradual increase of the standard deviations beginning with February is probably due to a degradation of the performance of the satellite link. For the data actually used outliers were eliminated from the two minutes sessions using a window of ±3 ns around the expected value. But using all data of a measurement block or only the data with outliers removed yielded at a maximum a difference of 0.16 ns for the expected value of the block.

The midpoint value was corrected by the differences (1 PPS Ref - PPS TX) measured in both stations. For each session a mean of the (1 PPS Ref - PPS TX) measurements each consisting of a block of hundred measurements 1 s apart was computed. The average standard deviation of these blocks of hundred measurements at TUG and OCA was 0.06 ns and 0.7 ns, respectively. The higher standard deviations at OCA results from the poor performance of the clock module used at OCA. For the first two blocks of a session this correction is given by 1/2[(1 PPS Ref - PPS TX)TUG - (1 PPS Ref - PPS TX)OCA] and for the third block (counter started by PPS TX at OCA) the correction is [1/2(1 PPS Ref - PPS TX)TUG - (1 PPS Ref - PPS TX)OCA]. No further correction for the third block is required because the cable which was used between the start input of the counter and the PPS TX of the modem was of the same length as that used between the stop input and the PPS RX.

Using the data thus obtained Fig. 7 shows the difference UTC(TUG) - UTC(OCA) obtained by GPS and two-way (without corrections for the GPS and two-way differential delays) after removing all time steps (OCA: Oct. 20, 20 μs; TUG: Dec. 19, 9 μ s and Jan. 14, 274 ns) and a slope of 117.88 ns per day before the clock change at TUG and a slope of 159.88 ns per day after the change. The dashed vertical lines in this and following figures indicate the change of the schedule and of the clock at TUG.

The result of the GPS receiver delay comparisons performed at OP, OCA and TUG is given in Table 2 **[12]**.

Laboratory	Date	No. of tracks	Mean[1] ns	Std. Dev. ns
OP	Mar. 30 - Apr. 7	292	-0.9	2.3
OCA	Apr. 12 - Apr. 15	154	17.6	2.0
TUG	Apr. 23 - Apr. 26	158	10.3	2.0
OCA	May 1 - May 12	452	15.7	1.6
OP	May 17 - May 20	147	-1.8	2.2

[1]This is the mean of [UTC(Lab) - GPS-time]TTR-6 - [UTC(Lab) - GPS-time]Lab given by the single tracks.

Table 2 Results of the differential delay measurements obtained by transportation of GPS receiver TTR-6.

According to the values given in Table 2 (using the mean of the data obtained at OCA) the difference UTC(TUG) - UTC(OCA) obtained from the uncorrected GPS data has to be corrected by -6.4 ns. The uncertainty estimated from the repeated comparisons at OP and OCA is 1.5 ns **[12]**.

The result of the delay comparison of the two-way stations performed at TUG is given in Table 3.

Date	No. of Measurements	Mean ns	Std. Dev. ns
Apr. 23	128	-81.37	1.2[1]
Apr. 24 (Block 1 - 3)	720	-81.04	1.0
Apr. 24 (Block 4)	1140	-81.41[2]	1.0

[1]VSAT not optimally pointed

[2]This value is already corrected for the different trigger levels used (see chapter MEASUREMENTS)

Table 3 Differential delay of the two-way stations obtained by station collocation at TUG. The overall mean is -81.3 ns.

In order to obtain UTC(TUG) - UTC(OCA) via two-way the data already corrected by (1 PPS Ref - PPS TX) have to be corrected further by the differential delay of the stations being -81.3 ns and by the difference (UTC(Lab) - 1 PPS Ref) of both stations being 307.7 ns. Finally the correction for the Earth rotation (Sagnac effect) amounting to -22.2 ns has to be applied. This results in a total two-way correction of 204.2 ns.

Considering the change of the trigger level of the counter at OCA (see chapter MEASUREMENTS) a correction of 1 ns has to be applied to the data of September 21 and 24 and one of 3 ns to the

data before September 21. Unfortunately these offsets caused by the change of the trigger levels were not measured but can be estimated from the shape of the pulses involved with an uncertainty of about 0.5 and 1 ns, respectively.

Fig. 8 shows UTC(TUG) - UTC(OCA) via GPS and via two-way for a period of five days after applying all of the above corrections. Evidently the GPS data have to be smoothed and interpolated to get GPS time transfer results concurrent with the two-way measurements.

In order to find the degree of smoothing to be applied to the GPS data to smooth the measurement noise without smoothing out the clock noise, Allan variances from the data shown in Fig. 7 were computed (see Fig. 9). The MITREX points with two minutes sampling time were computed from two minutes smoothed data obtained from the long measurement blocks performed in August 1990 and March 1991. Also shown in Fig. 9 are the Allan variances computed from the data presented in Fig. 11 (difference between [UTC(TUG) - UTC(OCA)] measured by two-way and GPS). The data were further analysed by computation of the modified Allan variance [13] revealing white-noise PM for the data marked by slope = -1. For the two-way minus GPS measurement results this applies to an averaging time of about 60 days. The smoothing time obtained for the period comparing the two high performance clocks (CS 1654 and CS 560) is about 8 hours and that for the period comparing the standard clock with the high performance clock is about 1 hour. For appropriate sections of the data different smoothing and interpolation techniques including Vondrak smoothing combined with Lagrange interpolation - routinely used at BIPM for GPS data processing - were applied, but gave about the same results. The problem is that before the change of the tracking schedule there were stable clocks, but for most of the time there was only a small number of GPS tracks near the time of the two-way measurements and that after the change very soon at TUG one had to switch over to a less stable clock. Thus only a short intermediate period represents the ideal situation of stable clocks and many GPS tracks near the time of the two-way measurements. Considering the facts given above the GPS data were smoothed by the computation of the means for the given smoothing periods of eight hours and one hour around the two-way measurements, using the data with the mean difference of the clock rates already removed. The result obtained for [UTC(TUG) - UTC(OCA)]MITREX - [UTC(TUG) - UTC(OCA)]GPS is given in Fig. 10. The lower trace in this figure indicates the number of tracks per smoothing period. The choice of the smoothing periods used was confirmed by using other smoothing periods which gave a larger scatter of the data especially for longer smoothing times during the period with the standard clock.

After the repair CS 1654 was reconnected to the measurement system on January 17, 1991. This means a comparison with the other TUG clocks every hour and at GPS measurement times and a continuous phase recording (0.5 ns resolution) with CS 524. It was thus possible to replace CS 524 by CS 1654 in the computations of the two-way and GPS differences. Using CS 1654 and eight hour smoothing (from January 22, 1991) instead of CS 524 and one hour smoothing shows the same long term behaviour of the data as in Fig. 10, but less scatter (see Fig. 11).

At TUG temperature, humidity and air pressure are recorded every hour and for all GPS measurements. The daily outside temperature at TUG for 12 UTC is shown in Fig. 12 and that at OCA for the days of two-way measurements is shown in Fig. 13. Also given (Fig. 14) is the differential delay of the two GPS receivers permanently operated at TUG.

ANALYSIS OF RESULTS AND CONCLUSION

The data presented in Figs. 10 and 11 show the agreement between UTC(TUG) - UTC(OCA) obtained by two-way and UTC(TUG) - UTC(OCA) obtained by GPS after having independently "calibrated" (measurement of the differential delays of the two-way and GPS equipment) both comparison methods at the end of the experiment.

Estimates of the time comparison accuracy obtained by GPS can be found in the literature [1]. For distances up to 1000 km and station coordinates known to better than 30 cm and no difference in receiver software one obtains for a single common-view track about 9 ns and for 10 common-view tracks (one day average) about 3.4 ns assuming an uncertainty of the relative receiver delay of 2 ns, but without considering contributions caused by the noise of the station clocks and the rise time of the reference pulses. The OCA-TUG baseline is about 800 km and the GPS antenna coordinates of both stations are known with an uncertainty of 10 cm in the ITRF-88 [14].

An attempt of an error budget for the two-way time transfer is given in Table 4.

UTC(Lab) - 1 PPS Ref	0.5 ns
Counter	0.5 ns
MITREX	1.0 ns
Earth station delay (relative)	1.2 ns
Transponder delay (relative)[1]	0.0 ns
Satellite link (Ku-band)	0.1 ns
Sagnac effect	0.1 ns
Total	1.7 ns

[1] The same frequency band of one transponder is used for both signal directions

Table 4 Error budget for the two-way time transfer (about 100 measurements 1 s apart). Possible contributions due to coherence among signals are not considered here [15].

Because the two-way minus GPS differences exhibit white-noise PM up to an averaging time of about 60 days (see chapter DATA PROCESSING AND RESULTS) the computation of the mean is justified for data intervals up to this length. The means of the last 28 and 56 days computed from the data shown in Figs. 10 and 11 are given in Table 5.

Data	Date	No. of Measurements	Mean ns	Std. Dev. ns
Fig. 10	Mar. 20 - Apr. 17	28	3.3	4.3
	Feb. 18 - Apr. 17	59	3.2	3.4
Fig. 11	Mar. 20 - Apr. 17	28	3.7	3.2
	Feb. 18 - Apr. 17	59	3.1	2.5

Table 5 Difference of [UTC(TUG) - UTC(OCA)] measured by two-way and GPS after having independently "calibrated" both links.

The result is in good agreement with the total uncertainty estimate of the GPS and two-way delay comparisons. The mean computed over the full data length is 3.6 ns for both data sets.

Comparing Figs. 10 and 11 with Figs. 12 and 13 reveals an obvious correlation between the long term behaviour of the difference of [UTC(TUG) - UTC(OCA)] obtained by two-way and GPS and the outside temperature recorded at TUG and OCA. For the duration of the experiment the data given in Figs. 10 and 11 can well be approximated by third order polynomials. The residuals from these polynomials fitted to the data (solid line) have a standard deviation of 3.3 ns (Fig. 10) and 2.6 ns (Fig. 11), respectively. The peak-to-peak variation is about 8 ns.

Different contributions causing the temperature-dependent behaviour are conceivable, but the main contribution is most likely explained by a different temperature behaviour of the GPS receivers used. This becomes even more evident from Fig. 14, which shows the differential delay of the two GPS receivers permanently operated at TUG. Using TTS-502B instead of NBS 03 for the time comparison between TUG and OCA reduces the temperature dependence by about 20 percent (see dashed line in Fig. 10).

The experiment allowed to compare the accuracies of the two most accurate time transfer methods nowadays in operation and demonstrated the feasibility of earth station delay comparison by means of a portable station. The main problem in the comparison of both methods resulted from the clock noise and therefore for future experiments addressing this question the most stable clocks and a well balanced GPS tracking schedule should be used. Furthermore all equipment employed should be checked carefully before the experiment to detect a possible systematic behaviour affecting the measurement accuracy. Concerning the temperature-dependence of the delays of the outdoor units (antenna, preamplifier/mixer, cable) of the GPS receivers this could be done in a temperature chamber using a GPS signal simulator. GPS receiver delay comparisons by receiver transport should be repeated in course of the experiment in order to check the consistency of the measurements and it would be advisable to operate more than one GPS receiver at each site. Also the delays of the two-way systems should be compared several times and the satellite terminals should preferably be adapted to detect delay variations by use of local means such as a satellite simulator. By selecting appropriate equipment and careful operation the first four contributions to the error budget given in Table 4 may be reduced by at least a factor of three leading to a two-way accuracy of about 0.5 ns. Similar accuracies are expected for GPS using geodetic receivers and ultra-precise ephemerides [1].

ACKNOWLEDGMENTS

The loan of a MITREX modem by Professor Ph. Hartl, University of Stuttgart, is deeply appreciated. The support of this experiment by EUTELSAT in providing three month of transponder time free of charge and the help of Mr. S. Fiedler and Mr. M. Chabrol (EUTELSAT) and Mr. J. Meunier and Mr. C. Bacot (France Telecom) and Mr. W. Schladofsky (ÖPTV) in administrative and technical matters are gratefully acknowledged. The work was supported by Bureau Nationale de Métrologie, France and the Austrian Academy of Sciences and the Jubilee Fund of the Austrian National Bank.

REFERENCES

[1] W. Lewandowski and C. Thomas, "*GPS time transfer*", Proc. IEEE, vol. 79, pp. 991-1000, 1991.

[2] D. Kirchner, "*Two-way satellite time transfer via communication satellites*", Proc. IEEE, vol. 79, pp. 983-990, 1991.

[3] C. Veillet et al., "*LASSO, two-way and GPS time comparisons: A (very) preliminary status report*", in Proc. 22nd Annual PTTI Meeting, 1990, pp. 575-582.

[4] P. Uhrich et al., "*Preliminary comparison of time transfer via Lasso, GPS and two-way satellite*", in Proc. 5th European Frequency and Time Forum, 1991, pp. 96-104.

[5] D.W. Hanson, "*Fundamentals of two-way time transfer by satellite*", in Proc. 43rd Annual Symp. on Frequency Control, 1989, pp. 174-178.

[6] D.A. Howe, "*Ku-Band satellite two-way timing using a very small aperture terminal (VSAT)*" in Proc. 41st Annual Symp. on Frequency Control, 1987, pp. 147-160.

[7] D. Kirchner, "*Design considerations for Ku-band two-way satellite time transfer terminals*", in Proc. 4th European Frequency and Time Forum, 1990, pp. 631-637.

[8] Ph. Hartl, N. Gieschen, K.M. Müssener, W. Schäfer, and C.M. Wende, "*High accuracy global time transfer via geosynchronous telecommunication satellites with MITREX*", Journ. of Flight Sciences and Space Research, vol. 7 (5), pp. 335-342, 1983.

[9] P. Hartl et al., "*MITREX 2500, a modem for microwave time and ranging experiments via telecommunication satellites*", Inst. of Navigation, Univ. Stuttgart, 1985.

[10] H. Ressler and D. Kirchner, "*Experience with the MITREX modem*", Technical Univ. Graz, Dept. of Comm. and Wave Prop., Int. Rep. INW 8501, 1985.

[11] W.J. Klepczynski, P.J. Wheeler, W. Powell, J. Jeffries, A. Myers, R.T. Clarke, W. Hanson, J. Jespersen, and D. Howe, "*Preliminary comparison between GPS and two-way satellite time transfer*", in Proc. 42nd Annual Symp. on Frequency Control, 1988, pp. 472-477.

[12] W. Lewandowski, "*Determination of differential time corrections between the GPS time receivers located at the Observatoire de Paris, the Observatoire de la Côte d'Azur and the Technical University of Graz*", Rapport BIPM-91/6, 1991.

[13] D.W. Allan, "*Time and frequency metrology: Current status and future considerations*", in Proc. 5th European Frequency and Time Forum, 1991, pp. 1-9.

[14] W. Lewandowski, "*High accuracy ground-antenna coordinates for GPS time transfer*", in Proc. IAG Symposium G2-Permanent Satellite Tracking Networks for Geodesy and Geodynamics, Vienna, August 1991, in press.

[15] D.A. Howe, "*Time tracking error in direct sequence spread-spectrum networks due to coherence among signals*", IEEE Trans. on Comm., vol. 38, pp. 2103-2105, 1990.

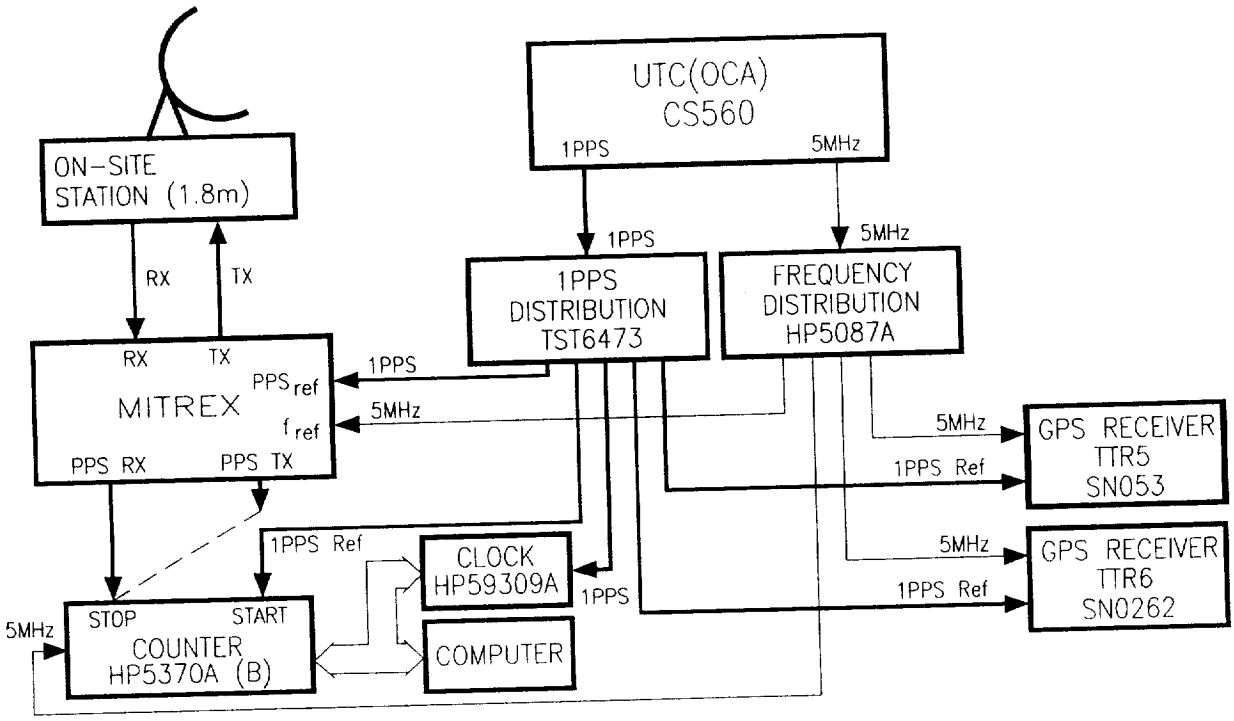

Fig. 1 Frequency and time distribution, as well as GPS and two-way set-up at OCA.

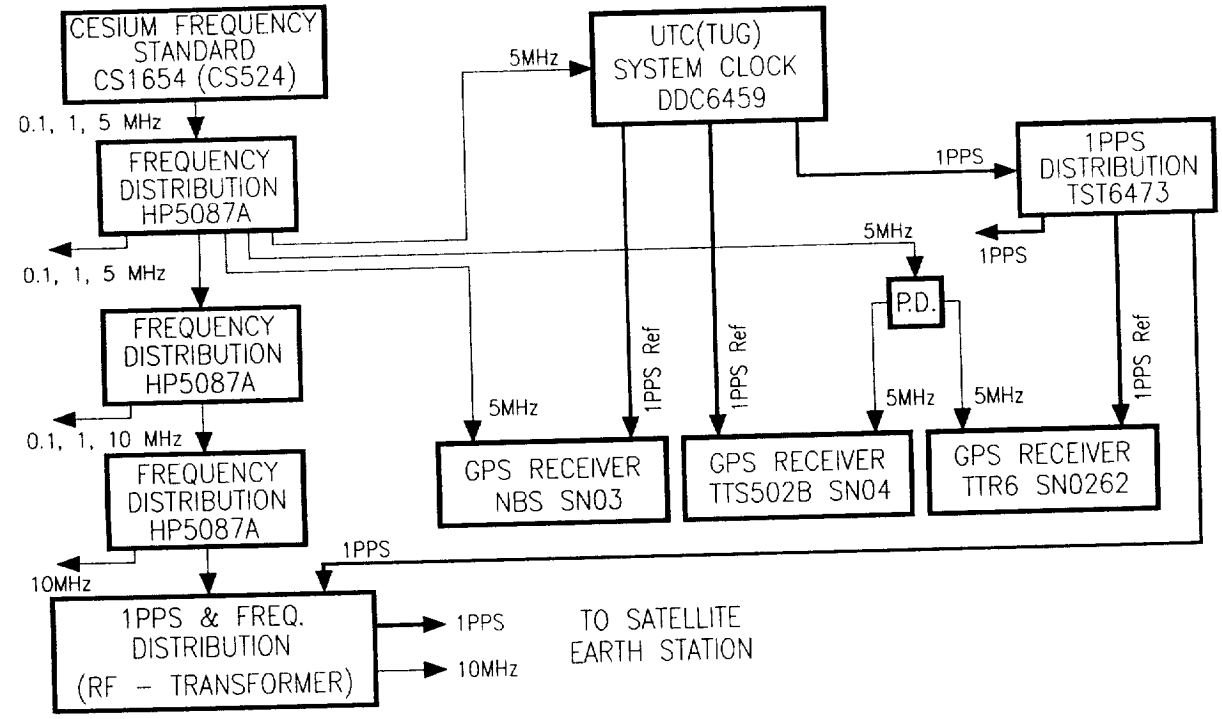

Fig. 2 Frequency and time distribution, as well as GPS set-up at TUG.

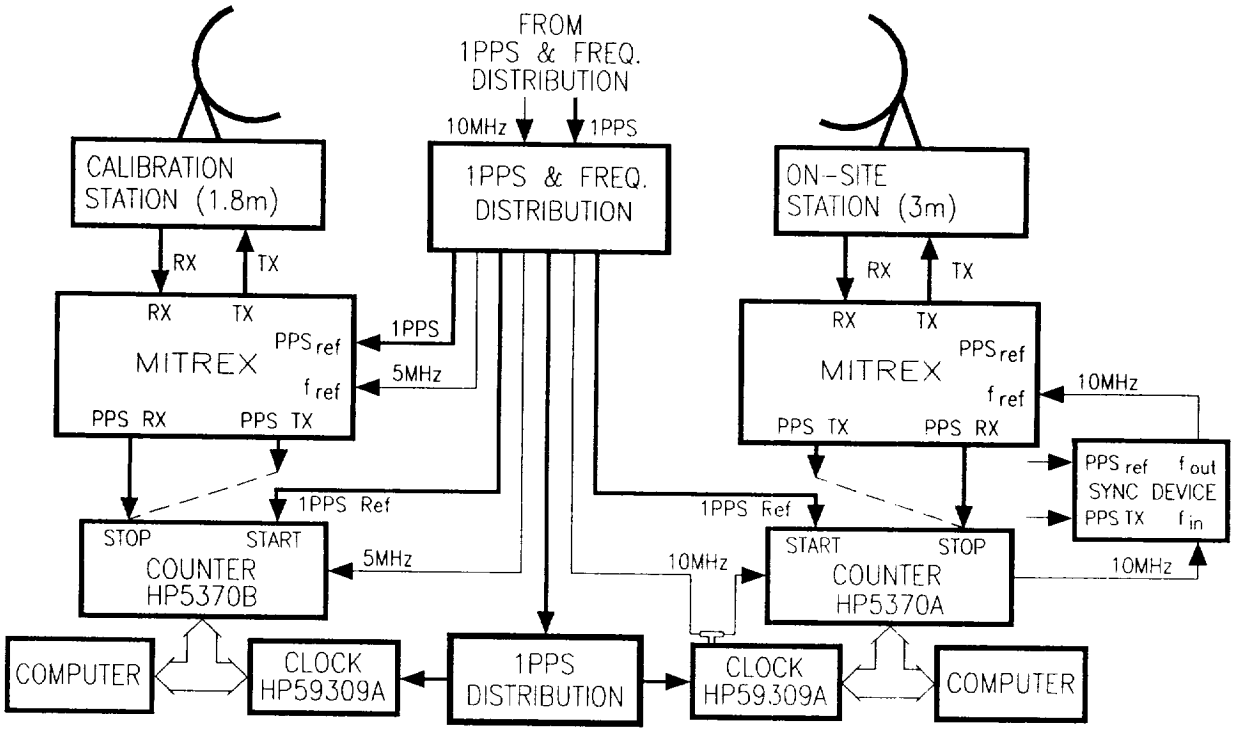

Fig. 3 Two-way set-up at TUG including the transported OCA station.

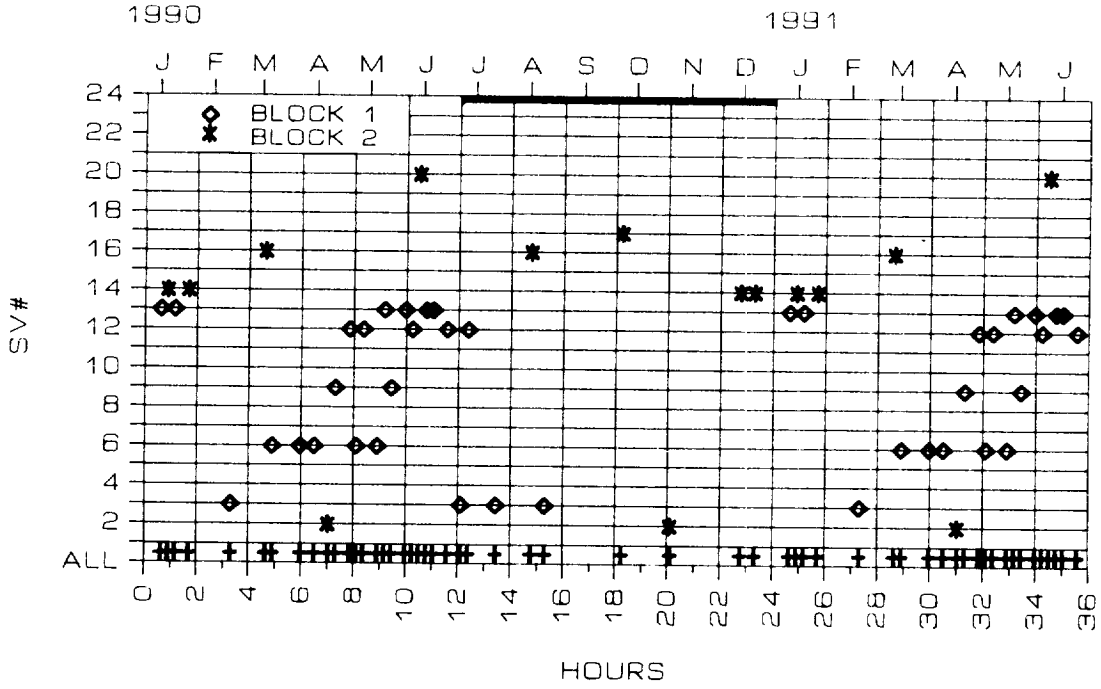

Fig. 4 European schedule No. 15. The ticks for the months given at the top are centered at the two-way measurement times.

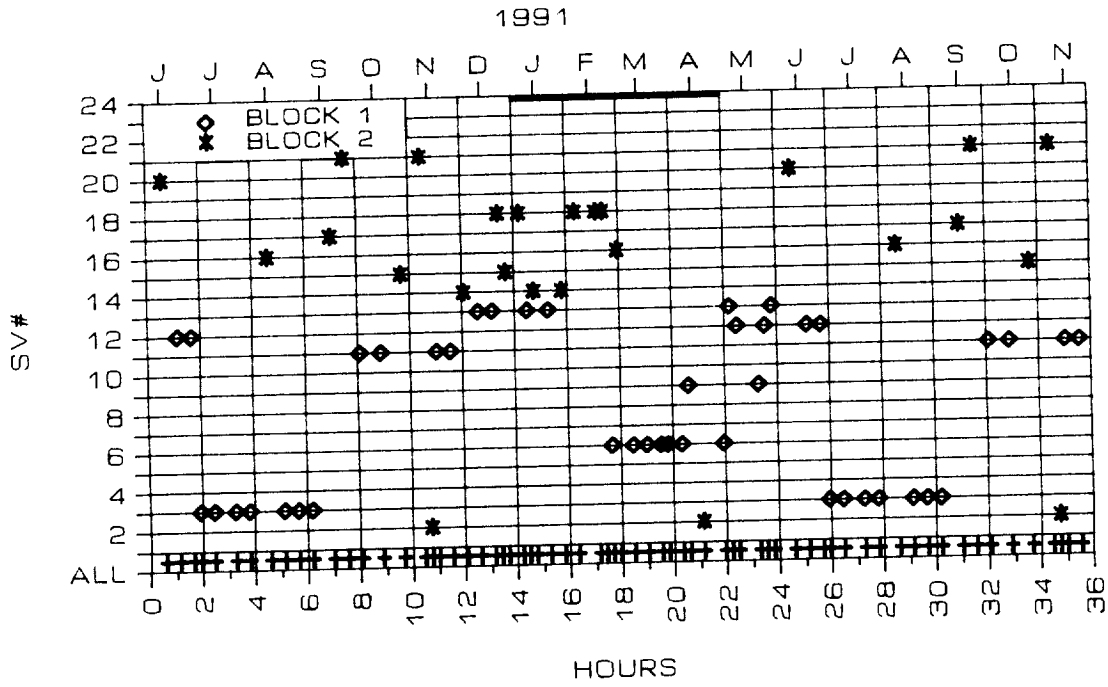

Fig. 5 Special OCA and TUG schedule including European schedule No. 16 valid since December 19, 1991.

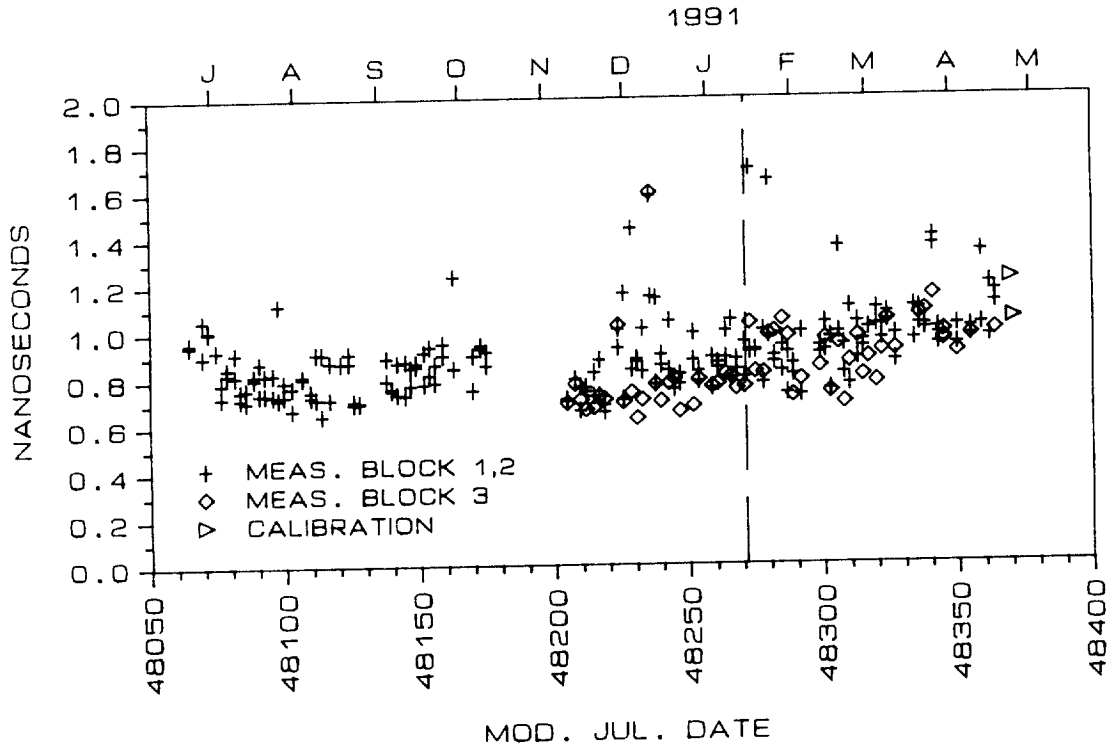

Fig. 6 Standard deviations of all two-way sessions including the sessions for delay comparison.

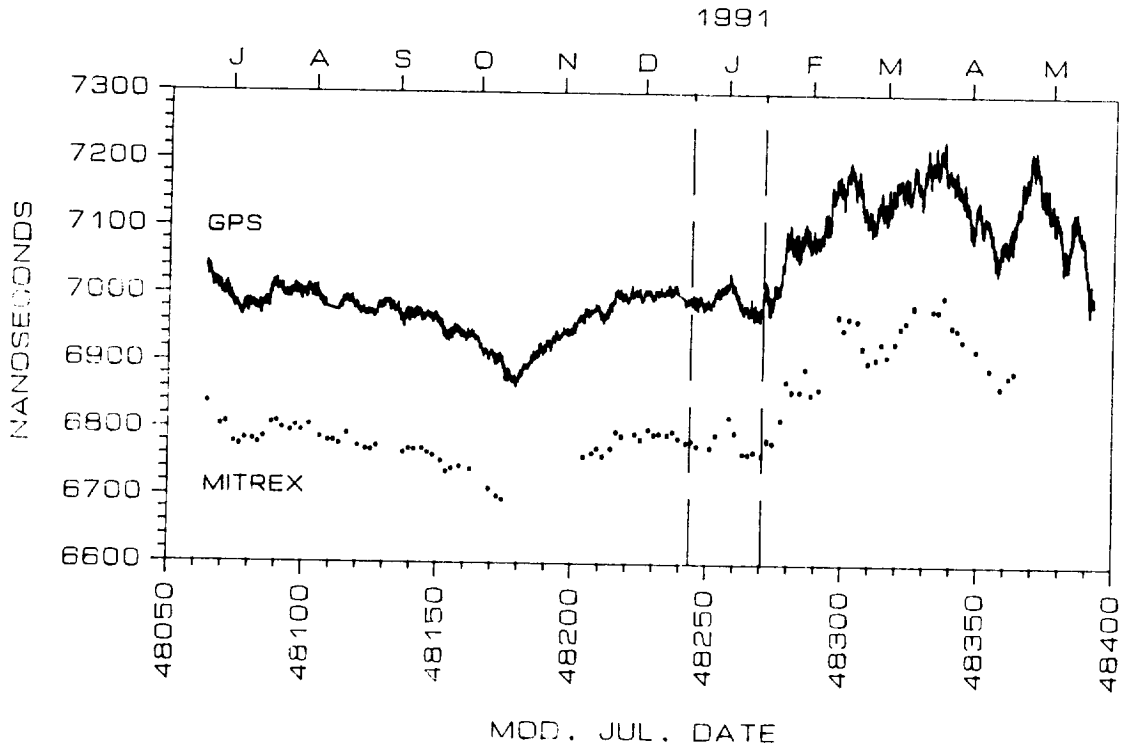

Fig. 7 UTC(TUG) - UTC(OCA) by GPS and two-way (corrected for 1 PPS Ref - PPS TX) after removal of all time steps and the mean difference of the clock rates.

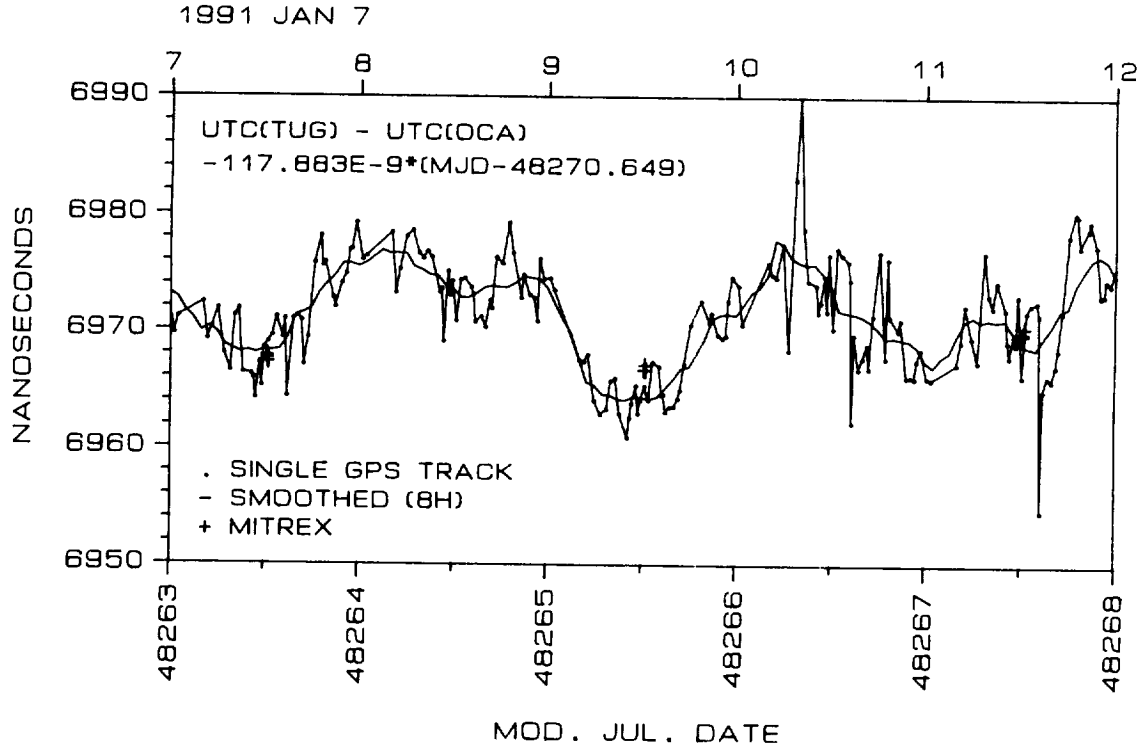

Fig. 8 GPS raw and smoothed data (eight hour mean) and two-way data for a period of five days (all corrections applied).

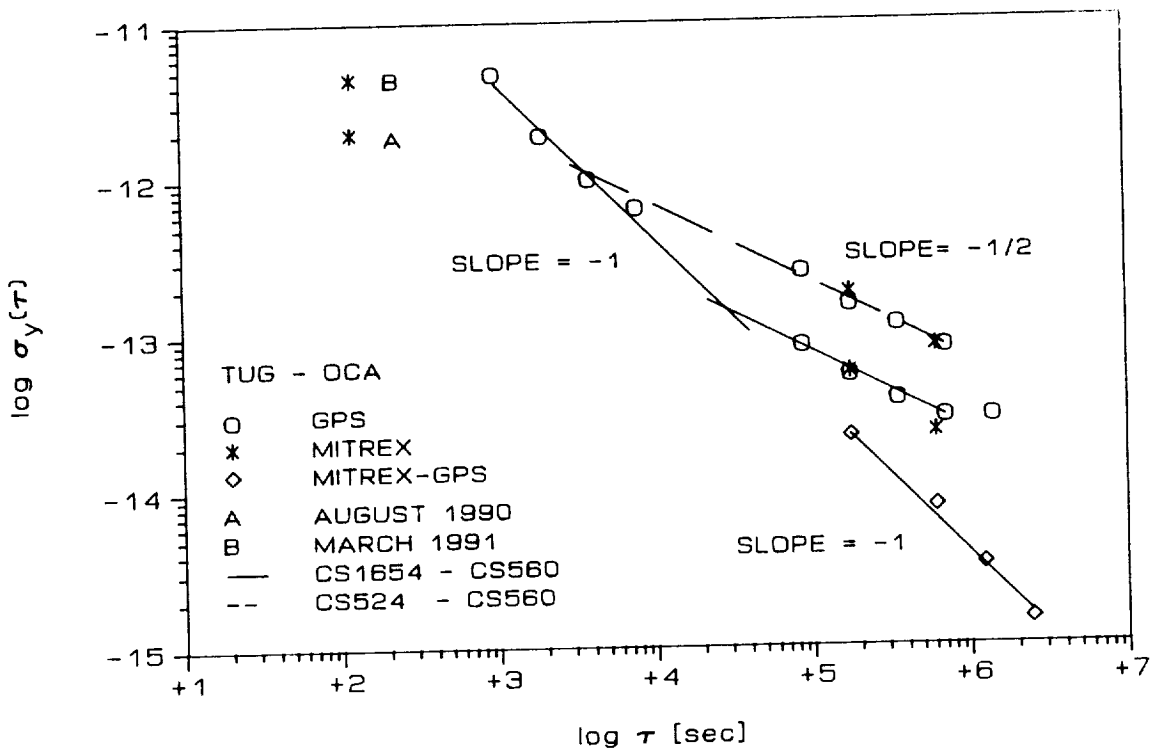

Fig. 9 Square root of the Allan variance of the GPS and two-way comparisons between UTC(TUG) and UTC(OCA).

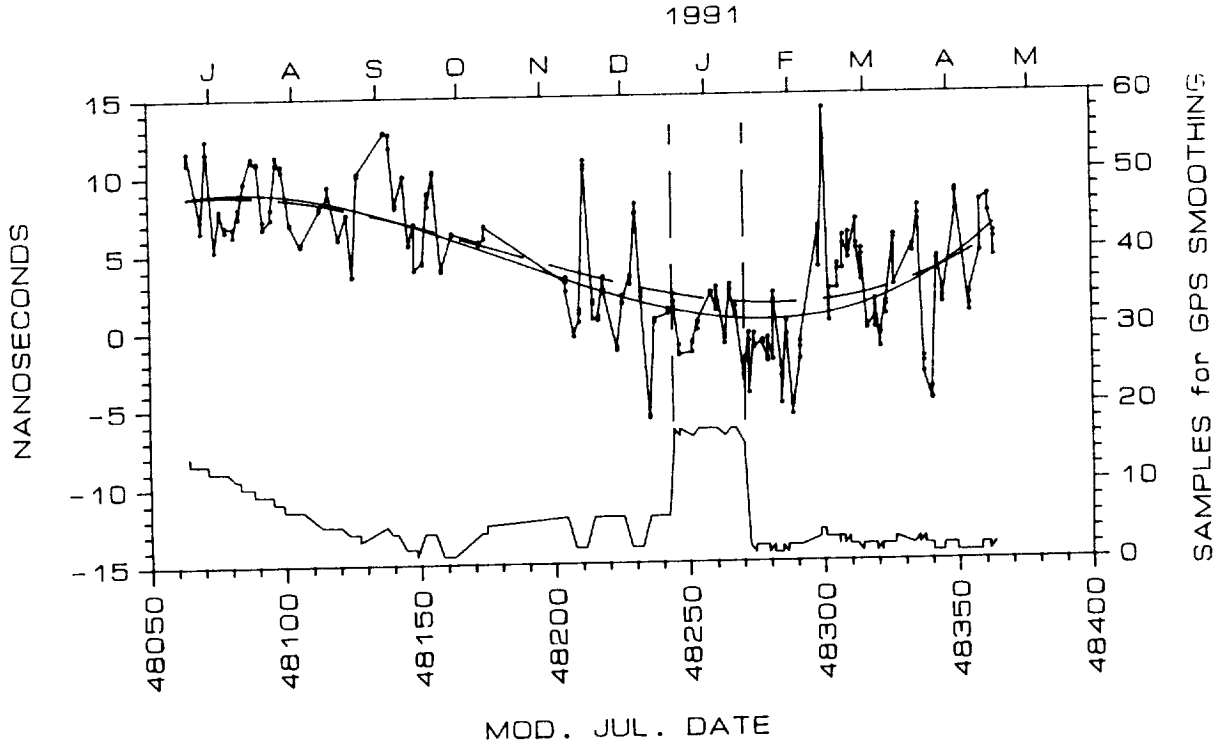

Fig. 10 Difference between [UTC(TUG) - UTC(OCA)] measured by two-way and GPS, and number of tracks per smoothing period.

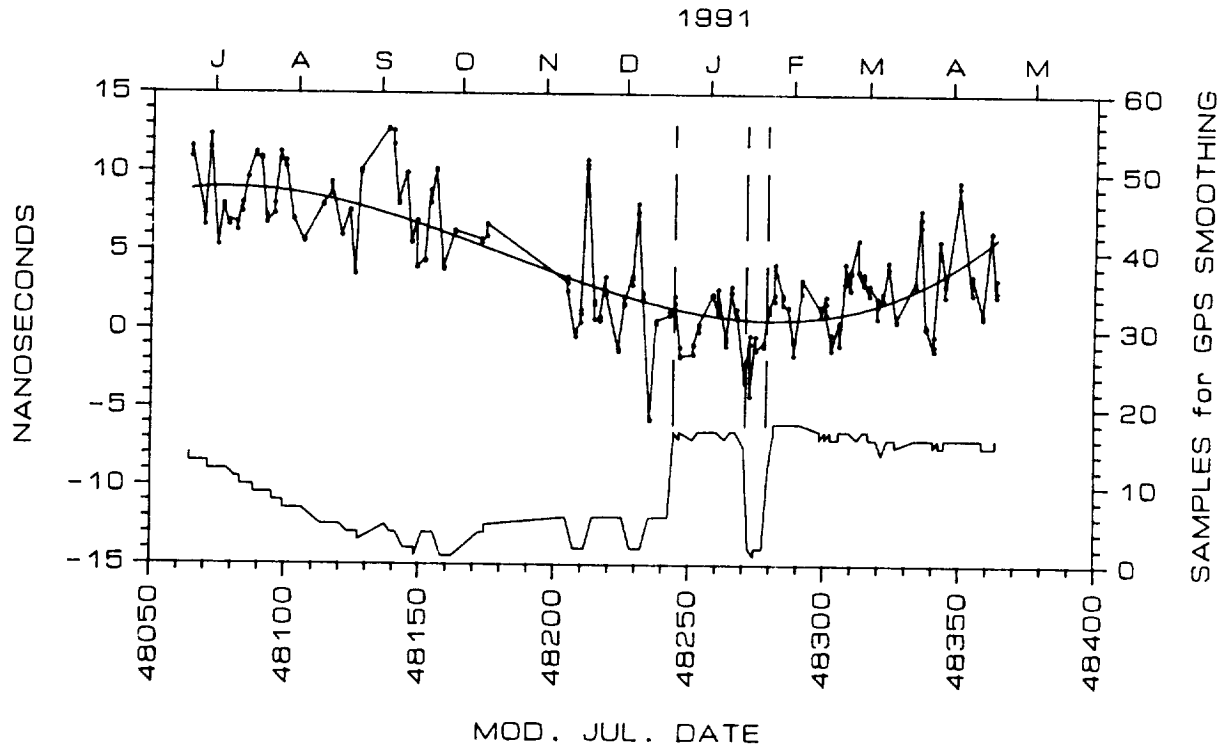

Fig. 11 Same as Fig. 10, but from January 22, 1991, on referred to CS 1654.

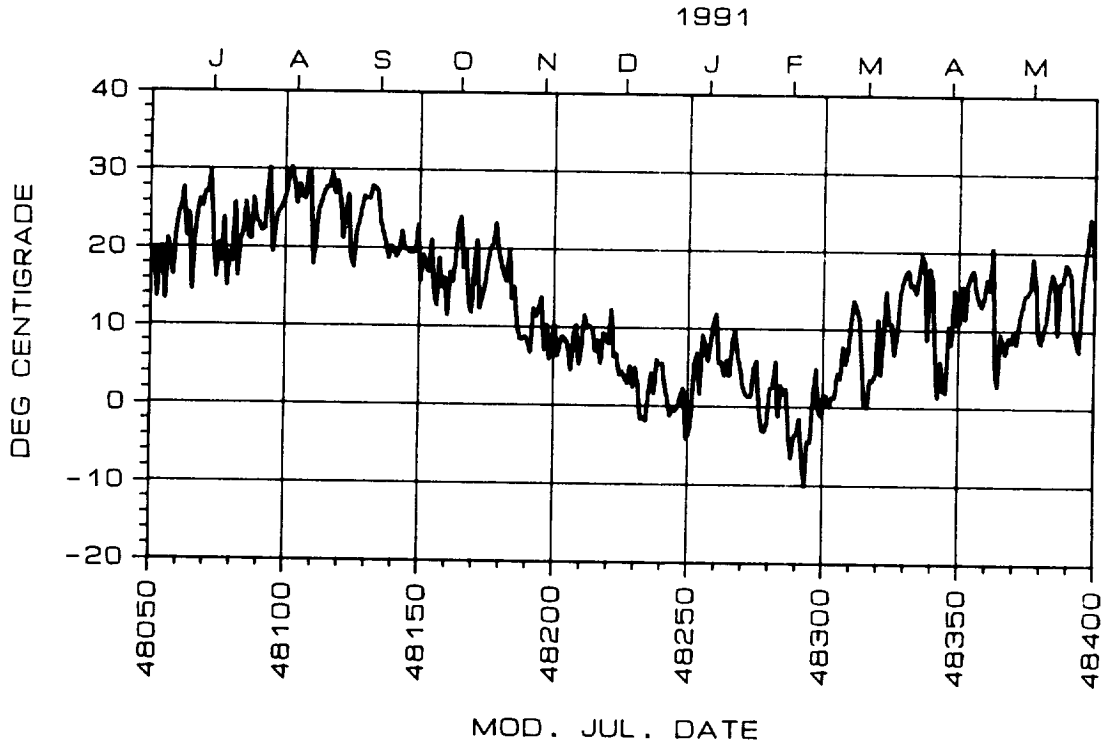

Fig. 12 Outside temperature at TUG (12 UTC).

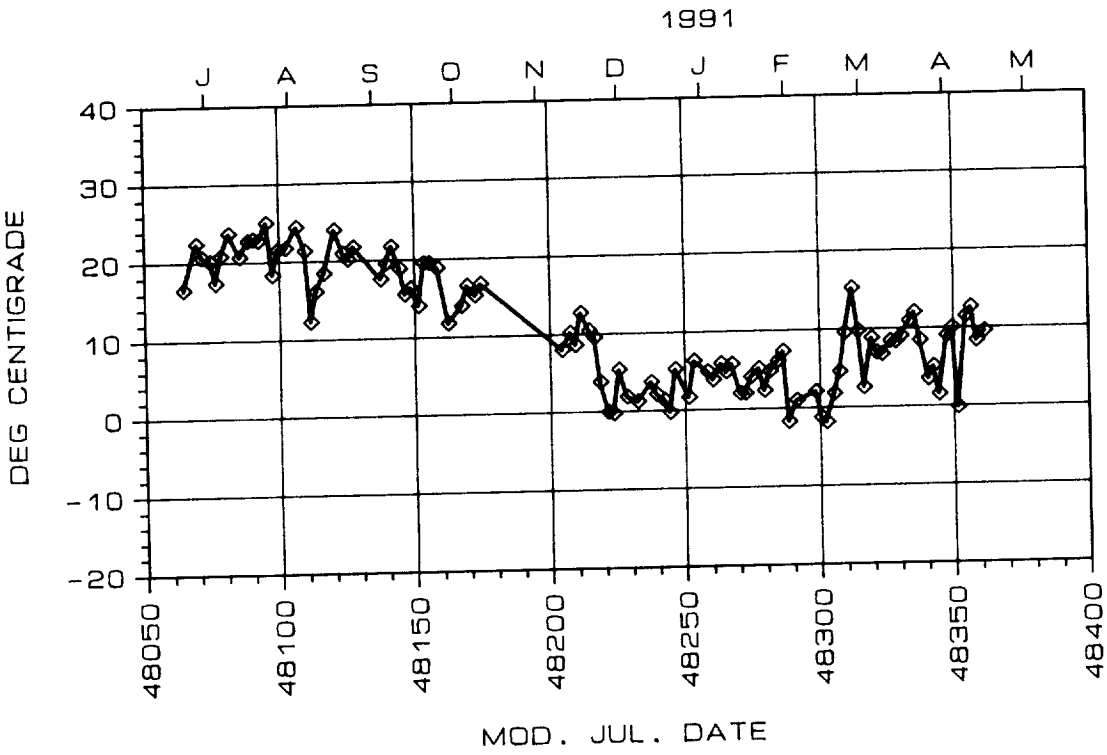

Fig. 13 Outside temperature at OCA (12 UTC).

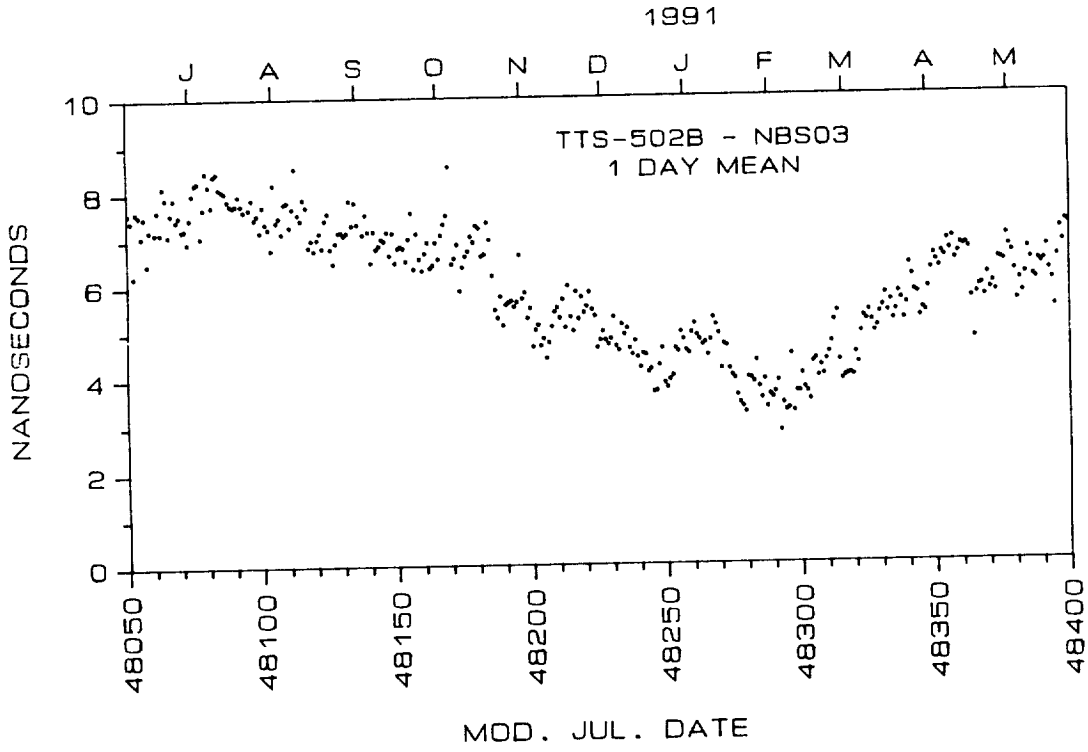

Fig. 14 Differential delay (daily mean) of TTS-502B and NBS 03.

57-70

N92-33357

Sub-Nanosecond Clock Synchronization* and Precision Deep Space Tracking

Charles Dunn, Stephen Lichten, David Jefferson and James S. Border
Jet Propulsion Laboratory
California Institute of Technology
4800 Oak Grove Dr. / MS 238-600
Pasadena, California 91109

Abstract

Interferometric spacecraft tracking is accomplished by the NASA Deep Space Network (DSN) by comparing the arrival time of electromagnetic spacecraft signals at ground antennas separated by baselines on the order of 8000 km. Clock synchronization errors within and between DSN stations directly impact the attainable tracking accuracy, with a 0.3 ns error in clock sync resulting in an 11 nrad angular position error . This level of synchronization is currently achieved by observing a quasar which is angularly close to the spacecraft just after the spacecraft observations. By determining the differential arrival times of the random quasar signal at the stations, clock synchronization and propagation delays within the atmosphere and within the DSN stations are calibrated. Recent developments in time transfer techniques may allow medium accuracy (50-100 nrad) spacecraft observations without near-simultaneous quasar-based calibrations. Solutions are presented for a global network of GPS receivers in which the formal errors in clock offset parameters are less than 0.5 ns. Comparisons of clock rate offsets derived from GPS measurements and from very long baseline interferometry and the examination of clock closure suggest that these formal errors are a realistic measure of GPS-based clock offset precision and accuracy.

Incorporating GPS-based clock synchronization measurements into a spacecraft differential ranging system would allow tracking without near-simultaneous quasar observations. The impact on individual spacecraft navigation error sources due to elimination of quasar-based calibrations is presented. System implementation, including calibration of station electronic delays, is discussed.

1. Introduction

NASA's Deep Space Network (DSN) supports spacecraft navigation for an international community of users. In order to complete most missions successfully, the location of the spacecraft must be determined with very high accuracy. This is done by comparing the arrival time of a signal broadcast by the spacecraft as it is received at two widely separated DSN stations. The delay observable thus formed provides some of the data from which the spacecraft's orbit is determined.

*The work described in this paper was carried out by the Jet Propulsion Laboratory, California Institute of Technology, under contract with the National Aeronautics and Space Administration.

Most of the observed time delay between two stations is due to the geometry of the spacecraft and receiving stations; however, delays due to solar plasma, the atmosphere of the earth, ground station instrumentation, and general relativity also play a role. This measurement technique is shown in Figure 1 and is called very long baseline interferometry (VLBI). In order to determine the angle, Θ, giving the direction to the spacecraft to an accuracy of $\delta\Theta$, the error in determining the delay, δt, can be no more than:

$$\delta t \leq \frac{D}{c}\delta\Theta \tag{1}$$

where D is the separation of the stations and c is the speed of light. Clearly, it is advantageous to use the longest baselines possible. Currently there are three DSN complexes at Goldstone, California; Madrid, Spain; and Canberra, Australia. Thus, a typical DSN baseline is 8000 km. A typical medium-accuracy tracking requirement is 50 nrad. Using equation (1) we arrive at a maximum error of 1.33 ns. In order to keep the total error in delay within this limit, the effective VLBI clock synchronization must be much better than 1 ns. Sub-nanosecond time transfer is a difficult problem, yet 50 nrad accuracy of spacecraft angular position in the radio reference frame is routinely obtained, and 5 nrad accuracy is achieved in special cases. This high level of performance is accomplished by using the signals from an extra-galactic radio source (quasar) to calibrate spacecraft observations. The radio signal from the quasar is essentially wide-band random noise, so when the recorded signals from the two stations are cross-correlated, significant correlation amplitude arises only when the quasar delay is precisely matched. This has the effect of measuring the station clock offset as well as differencing out many of the errors which are common to the quasar and spacecraft observations. The spacecraft signal spectrum contains tones which are used to measure a one-way range from the spacecraft to the earth station. An observable formed by subtracting the quasar delay from the spacecraft one way range, difference between stations, determines one component of the geocentric angle between the spacecraft and quasar. Measurements must be made on two baselines to determine both components of angular position.

An error budget for spacecraft-quasar differential VLBI delay measurements is given in Table 1. This error estimate is based on expected DSN receiver performance and calibration systems capabilities in the late 1990's. [4]. The root-sum-square error is 0.22 ns. By contrast, systems operating today provide an accuracy of about 0.67 ns. [3].

Error Source	Magnitude (ns)
Quasar SNR	0.11
Spacecraft SNR	0.033
Quasar Position	0.066
Clock Offset	0.030
Phase Ripple	0.10
Station Location	0.033
Earth Orientation	0.056
Troposphere	0.080
Ionosphere	0.010
Solar Plasma	0.017
RSS:	0.22

Table I: Spacecraft–Quasar differential VLBI error budget

Although this method provides accuracy sufficient to carry out deep space missions, it has some drawbacks. In order to be useful, the quasar observations must be made as close in time as possible to the spacecraft observations. In order to view the quasar, the antenna must be physically pointed at the quasar and is unable to receive signals from the spacecraft. As a result, the phase data from the spacecraft is not continuous, which results in a weaker orbit solution and a gap in spacecraft telemetry while the quasar is being observed.

Quasar observations also complicate the hardware otherwise required to track a spacecraft. The quasar is a wideband radio source, and so a wide bandwidth is required to record and process the quasar data. If the quasar could be dispensed with, only the phases of the received spacecraft signals at each time point would need to be recorded. In the quasar-less system proposed here, 50 nrad observables could be available in near-real-time. The number of bits resulting from spacecraft tracking would be reduced from 10^9 to 10^5.In this paper, we will examine medium-accuracy deep space tracking as an application of sub-nanosecond clock synchronization. We will begin by defining the requirements 50 nrad tracking accuracy places on the clock synchronization system. We will then discuss recent results obtained using the U. S. Global Positioning System (GPS) satellites for clock synchronization which indicate this level of accuracy may be possible on an operational basis. Finally, we will discuss the hurdles remaining before this technology can be implemented.

2. Clock Synchronization Requirements

Time-transfer aided spacecraft tracking will never be able to achieve the accuracy possible using quasar-based differential VLBI. This is because in differencing the quasar signals, many of the media errors affecting the signal are differenced out as well. Without quasar differencing, the errors due to station location, earth orientation, troposphere and ionosphere would increase by a factor of 2 to 4. The GPS solution from which the VLBI clock offset will be derived can also be used to provide calibrations for earth orientation and troposphere and ionosphere delays. We will assume that these errors increase by a factor of three compared to quasar calibrated VLBI. Of the remaining errors, those pertaining to quasar SNR and quasar location are eliminated with the elimination of the quasar. The errors due to spacecraft SNR, phase ripple, and solar plasma would remain unchanged. If GPS is used to estimate clock offsets every six minutes during the spacecraft pass, the clock instability error remains roughly the same. The RSS of all errors excluding the clock is 0.534 ns. This leaves 1.2 ns maximum allowable clock synchronization error, which includes instrumental errors incurred in tying GPS time to VLBI time. A reasonable system allocation is 0.5 ns for clock synchronization errors.

3. Achieving Sub-Nanosecond Clock Synchronization

Since the inception of the Global Positioning System in 1978, the possibility of using it for high accuracy clock synchronization has matured rapidly. The number of GPS satellites has recently reached 16, and, in addition, capable p-code receivers have proliferated. For this reason, the possibility of achieving ns and better clock synchronization using the GPS system has been studied **[5,1,9,16,6]**.

In order to investigate the feasibility of meeting the requirements posed in section 2, the authors investigated clock offset solutions for a global network of Rogue **[10]** GPS receivers which was assembled for the IERS GIG-'91 campaign in January and February of 1991 **[11]**. Clock offsets

were calculated for the three DSN sites and compared with clock data derived from VLBI quasar measurements. A closure measurement was made to verify the internal consistency of the method.

3a. Comparison With VLBI

The GIG-'91 data from the 21 global Rogue sites were processed with the Jet Propulsion Laboratory's GIPSY software. A general description of the square-root Kalman filtering algorithms used for determination of timing and geodynamical parameters simultaneously along with GPS orbits is described in detail by Lichten **[7,8, and references therein]**. Estimated parameters included: GPS positions and velocities, three solar pressure coefficients per satellite, GPS carrier phase biases, non-fiducial station coordinates, variations in Earth rotation (UT1-UTC), random walk zenith troposphere delays for each site, and white noise transmitter/receiver clocks. The only significant constraint imposed on the estimated parameters was the random walk constraint for the tropospheric delay, $1.2\text{cm}/\sqrt{hr}$ (the random walk model adds process noise to the system such that in the absence of data, the uncertainty for the parameter increases as the square-root of time). All other estimated parameters, including the clocks, were essentially unconstrained. The white noise **[8,2]** clock model for the station and satellite clocks corresponds to estimation of a new and independent clock offset for each receiver/transmitter (one ground clock was held fixed as reference for all the other clocks in the system) at each measurement time (every six minutes in this case). This approach is very conservative, since most of the GPS clocks and many of the receiver clocks were running off atomic standards (high quality hydrogen masers for the three Deep Space Network sites) and it would be quite reasonable to apply constraints based on known stable behavior of such clocks. However, we wished to test the capability of GPS to independently and completely characterize all the clocks in the system without *a priori* knowledge and therefore used the white noise model. Coordinates for two fiducial sites, Goldstone (California) and Kootwijk (Netherlands), were held fixed (not estimated) to their SV5 values. SV5 is a reference frame defined primarily by VLBI measurements of baselines and satellite laser ranging determination of the geocenter **[12]**. Three geocenter parameters were also estimated, representing a translation estimated from the GPS data for the Earth center of mass relative to the nominal SV5 origin. The GPS data were initially filtered in 24-hr increments, with new solutions for the orbits determined for each day. Since the computed formal errors for the estimated clock offsets appeared to be well below 1 ns (typically several tenths of ns), in some cases we used 12-hr solution arcs in order to shorten the processing time.

The nominal time series for both polar motion and UT1-UTC was from the International Earth Rotation Service (IERS) Bulletins B37 and B38, which contain a smoothed time series from VLBI measurements separated by 5 days. The GPS data were used to estimate variations in UT1-UTC twice per day relative to this nominal time series. These Earth rotation estimates had only an insignificant effect on the clock estimates. In order to tie GPS data to the DSN station clocks, the Rogue GPS receiver was fed a 5 MHz reference signal generated by the station hydrogen maser frequency standard. The time tags of the data are derived from this reference, subject to delays within the interconnection and the receiver. The highly digital nature of the Rogue receiver eliminates most of the delay variations which arise from variability of analog components **[14]**. The remaining receiver instrumental delays have been shown to remain constant on a day-to-day basis to within 0.7 ns **[17]**. This insures that the receiver clock and the station clock run at the same rate within $\sim$.7 ns/day.

Currently there exists no system to measure the offset between the station clock and the receiver clock. As a result, we assume a constant offset and compare clock rates derived from GPS with

those derived from VLBI. This problem will be discussed further in section 4.

For this experiment, GPS selective availability (SA) was not turned on. Because the measurements involve only differenced data involving many receivers and satellites with dynamically estimated orbits and spacecraft clocks, this technique is insensitive to SA. This statement is based on our limited experience from the past two years. When SA was active, the accuracy and precision of ground station position estimates were insensitive to SA. If the p-code is encrypted with anti-spoofing (AS), however, our results would be somewhat degraded. Because the Rogue receiver is able to extract ionospheric TEC by cross- correlating the P1 and P2 signals, however, even in the event of AS we expect to maintain sub-nanosecond clock synchronization.

Date (1991)	Baseline	VLBI (ns/day)		GPS (ns/day)	
Jan 23	Canberra-Goldstone	-10.0	±1.6	-9.0	±0.9
Jan 27	Madrid-Goldstone	-4.5	±2.2	-2.7	±0.5
Jan 30	Canberra-Goldstone	-7.9	±3.1	-9.1	±0.9
Feb 06	Canberra-Goldstone	46.6	±1.3	46.4	±1.9
Feb 10	Madrid-Goldstone	5.9	±1.8	2.8	±0.4

Table 2: Clock rate estimates

Table 2 presents a comparison of the GPS clock rates with VLBI clock rates on days when VLBI solutions were available (GPS solutions were available nearly continuously during the 3-week experiment). The column labelled "VLBI" presents the clock frequency offset between the specified DSN sites as determined by the DSN TEMPO [13] service. These measurements are made by observing a set of quasars over a three hour interval centered on the listed time tag. The column labelled "GPS" was produced by decimating clock estimates originally computed at a 6-min minute interval to a 60-min interval and then fitting six or seven of these points to a line. The hourly points are selected to be centered as closely as possible on the VLBI time tag. An example of one of these fits is shown in Graph 1. The typical RMS scatter in these GPS clock fits was 0.1- 0.3 ns.

VLBI is probably the most accurate established independent technique for measuring clock differences between tracking sites separated by intercontinental distances. Yet the formal errors for the GPS fits are similar, and in most cases, lower than the VLBI formal errors. The reduced χ^2 statistic for the GPS fits, which basically measures the ratio of the post-fit scatter to the formal clock estimate errors, was generally 0.5-1.0. The agreement between the GPS and VLBI clock rate estimates shown above in the table is at the $\sim$ ns/day level and can in all except one case be explained by the VLBI formal errors in estimating the clock rates (the one exception on Feb 10 shows a difference of about 1.5 VLBI standard deviations). Note that some aspects of our conservative GPS fitting procedure (decimation of data by a factor of 30, and fitting a line to the clock offset time series instead of solving explicitly for the rate parameter with the original data) tend to make the GPS formal errors (and presumably the actual errors) larger. A more aggressive analysis strategy could easily be devised to further reduce the GPS clock rate estimation errors. The results suggest, in any case, that the GPS observations can be straightforwardly used to faithfully track clock variations at time and frequency standards separated by thousands of km. Our comparison with the independent VLBI technique appears to be limited by the uncertainties in the VLBI data, not by uncertainties in the GPS data.

3b. Clock Closure

To investigate the internal consistency of our estimates, we chose a typical day (February 2) and estimated the clock offset between each pair of DSN stations with the data from the remaining station excluded for a twelve hour period. The sum of these numbers was then formed, which we refer to as the clock closure. If the receiver clocks have the same estimate in each of the runs, the clock closure will be zero. The clock closure is shown as a function of time in Graph 2. The formal errors presented are calculated assuming each of the six estimates has an independent random error, summed in quadrature, and are thus probably on the conservative side.

Removing the data from a single station should have a very small effect on the result. Non- zero clock closure is an indication of systematic errors in the calculation of the offset of the remaining two clocks. By examining the clock closure, we hope to identify error sources as well as verify that nothing is seriously wrong with our estimates.

The curve in Graph 2 has several interesting features. We believe the large, slow, variation in the clock closure result is due to errors in our estimated GPS satellite orbits. To test this, we initialized the orbital parameters with values estimated from data collected in the previous 24 hour period, including all stations. The resulting clock closure is shown in Graph 3. The large scale variation is absent, although it has been replaced with a 0.2 ns bias. This can be explained because the orbits are constrained by the previous 24 hours of data and therefore are less sensitive to data noise. On the other hand, systematic orbit errors due to dynamic models are more important for longer data arcs and may be causing the 0.2 ns bias.

Another of these features is the small (0.1 ns) jump occurring just before 2 am on Graph 2. We believe this is due to an abrupt change in the satellite geometry, with most satellites either rising or setting, as can be inferred from the change in size of the formal error bars. The step seen at 2 am is an indication of an error in clock determination due to poor sattelite geometry before 2 and the short data arcs resulting from sattelites setting. The jump near noon appears to be due to similar satellite geometry problems, as well as a short data outage.

The GPS constellation in early 1991 consisted of only 15 operational satellites. There are short periods of time when GPS visibility is poor from a given ground site, thus leading to high sensitivity to scheduling of observations and data gaps such as described above. We expect that in the future, with the fully operational 21-satellite constellation, such events would cause less error.

In another test for data consistency, we changed the reference clock. For Jan. 23, we compared the clock solutions with Goldstone the reference clock and with Kokee (Hawaii) the reference clock. Because both clocks were hydrogen masers, no appreciable difference in solutions should occur. The clock rate solutions differed by 0.03 ns/day and 0.01 ns/day respectively for the two cases, a statistically insignificant difference.

3c. Data Availability

Another important issue to be addressed is whether high quality GPS clock estimates can be produced reliably enough to be used operationally. During the IERS GIG-91 campaign, it was possible to form a clock offset with formal errors less than 1 ns for 74% of the hourly estimates on the Goldstone-Madrid baseline and 79% of the time on the Goldstone- Canberra baseline. This includes times in which there was insufficient common view to obtain an accurate clock offset, as well as periods in which one of the two receivers was not tracking satellites.

With the full 21-satellite GPS constellation and with data from approximately six to nine globally distributed stations in addition to the DSN stations, it should be possible to continuously provide sub-nanosecond clock offset estimates for the DSN complexes. It is currently possible to service such a network and provide one day turnaround of clock estimates [personal communication; G. Blewett]. With the development of forward-running Kalman filters and a real-time data-retrieval system, it would conceivably be possible to provide one ns, hydrogen maser, clock offsets in as little as 5 minutes. Somewhat better offsets could be provided within a few hours. More study is needed to determine the minimal configuration necessary to provide near-real-time clock estimates. Note that because the DSN stations are equipped with hydrogen masers, errors in estimated clock offsets grow gradually, so that short GPS data outages are more likely to result in degraded system performance rather than catastrophic system failure.

4. Implementation

In order to implement an operational GPS-aided VLBI system, the receiver clock synchronization discussed above must be transferred to the VLBI clock. This can be done by using a time interval counter (TIC) to measure the difference in the 1 pps signals generated by Rogue and VLBI time. It is not difficult to obtain time interval counters accurate to 100 psec, which would not severely impact our level of accuracy. This TIC would be machine readable to allow real-time calibration at a rate similar to the frequency of clock offset estimates available from the GPS solution.

The calculated clock offset between receiver time and GPS time includes the delays and phase shifts introduced by the analog electronics between the GPS antenna and the Rogue receiver. The only remaining uncalibrated delays are between internal receiver time and the resultant 1 pps signal, and the corresponding delay in the VLBI system. JPL experiments have shown that these combined delays in the receiver remain constant over four days period to within 0.3 to 0.7 ns [**17**]. These delays can be calibrated by making quasar VLBI observations and comparing the clock synchronizations determined by this method with GPS clock synchronization. Two-way satellite time transfer is also approaching the accuracy necessary to calibrate GPS instrumental errors. Quasar observations are currently performed weekly on each baseline to determine earth orientation and clock offsets and rates. If receiver delays can be held constant to within the 0.5 ns limit given in section 2, it appears that instrumental errors in GPS clock synchronization can be dealt with by weekly quasar calibration. If this is not possible, two-way satellite time transfers on a more frequent basis may be necessary.

5. Conclusion

A sub-nanosecond clock synchronization capability would be of great benefit to deep space tracking. This level of synchronization would allow spacecraft angular position to be instantaneously measured to an accuracy of 50 nrad by differential ranging at two widely separated tracking stations. Quasar-based differential VLBI, which is currently used for this purpose, might be reserved for only the most demanding navigation challenges. Clock offsets between DSN stations with formal errors of approximately 0.5 ns have been determined from GPS measurements. Comparisons of VLBI and GPS clock rates and analysis of clock closure suggest that these formal errors are a realistic measure of the precision of the GPS clock solutions. The calibration of absolute station instrumental delays and of the offset between VLBI time (used to time-tag differential spacecraft range measurements)

and GPS receiver time appear to be tractable implementation tasks.

Acknowledgment

We would like to thank Susan G. Finley, Susan Oliveau, Lawrence Young, Thomas Meehan and Ruth Neilan for their contributions to this work. The GIG'91 GPS data were collected by dozens of technical institutions worldwide and the participation of these collaborators was essential for the success of the experiment and the clock synchronization analysis presented here.

References:

1. Allen, D. W. and Weiss, M., *"Accurate time and frequency transfer during common-view of a GPS satellite"*, Proc. 34th Annual Sympossium on Frequecy Control, 1980.

2. Bierman, G. J., *"Factorized Methods for Discrete Sequential Estimation"*, Academic Press, New York (1977).

3. Border, J. S., *"Analysis of DDOR and DDOD Measurement Errors for Mars Observer Using the DSN Narrow Channel Bandwidth VLBI System"*, JPL Internal Document. (1990)

4. Border, J. S. and Kursinski, E. R., *"Deep Space Tracking and Frequency Standards"*, proceedings, 45th Annual Symposium on Frequency Control, Los Angeles, (1991).

5. Buennagel, L. A., Spitzmesser, D. J. and Young, L. E., *"One Nanosecond Time Synchronization Using Series and GPS"*, procedings of the 24th Annual Precise Time and Time Interval (PTTI), 1982. NASA Conf. Pub. 2265.

6. Kepczynski, W. J., et al, *"Comparison of Two-Way Satellite Time Transfers and GPS Common View Time Transfers"*, 43rd Annual Symposium on Frequency Control - 1989.

7. Lichten, S. M., *"Towards GPS Orbit Accuracy of Tens of Centimeters"*, Geophys. Res. Lett., 17, 215-218, 1990a.

8. Lichten, S. M., *"Estimation and Filtering for High-Precision GPS Positioning Applications"*, Manuscripta Geodaetica, 15, 159-176, 1990b.

9. Lewandowski, et al, *"The Use of Precise Ephemerides, Ionospheric Data and Corrected Antenna Coordinates in a Long-Distance GPS Time Transfer"*, procedings of the 22nd Annual Precise Time and Time Interval (PTTI) Applications and Planning Meeting, Vienna, VA. 1990. NASA Conf. Pub 3116.

10. Meehan, T. K., et al, *"ROGUE: A new high accuracy digital GPS receiver"*, paper presented at the 19th General Assembly, Int. Union of Geod. and Geophys., Vancouver, Canada, Aug. 9-22, 1987.

11. Melbourne, W. G., et al, *"The First GPS IERS and Geodynamics Experiment-1991"*, XX General Assembly International Union of Geodesy and Geophysics, Symposium G2.2 (International Association of Geodesy), Vienna, 1991 (In Press).

12. Murray, M. H., King, R. W., and Morgan, P. J., *"SV5: A Terrestrial Reference Frame for Monitoring Crustal Deformation with the Global Positioning System"*, 1990 Fall AGU Meeting, EOS Trans. AGU, 71, 1274, 1990.

13. Steppe, J. A., Oliveau, S. H. and Sovers, O. J., *"Earth Rotation Parameters from DSN VLBI: 1991"*, JPL Geodesy and Geophysics Preprint No. 210, April, 1991 (submitted to the International Earth Rotation Service Annual Report for 1991).

14. Thomas, J. B., it "Functional Description of Signal Processing in the Rogue GPS Receiver", JPL Publication 88-15 (1988).

15. Thompson, A. R., Moran, J. M., and Swenson, G. W., *"Interferometry and Synthesis in Radio Astronomy"*, Wiley-Interscience, New York (1986).

16. Veillet, C., et al, *"LASSO, Two-way and GPS Time Comparisons: A (Very) Preliminary Status Report"*, procedings of the 22nd Annual Precise Time and Time Interval (PTTI) Applications and Planning Meeting, Vienna, VA. 1990. NASA Conf. Pub 3116.

17. Young, L. E., *"Rogue Clock Synch Data; JPL Internal Document"*, January 28, 1991.

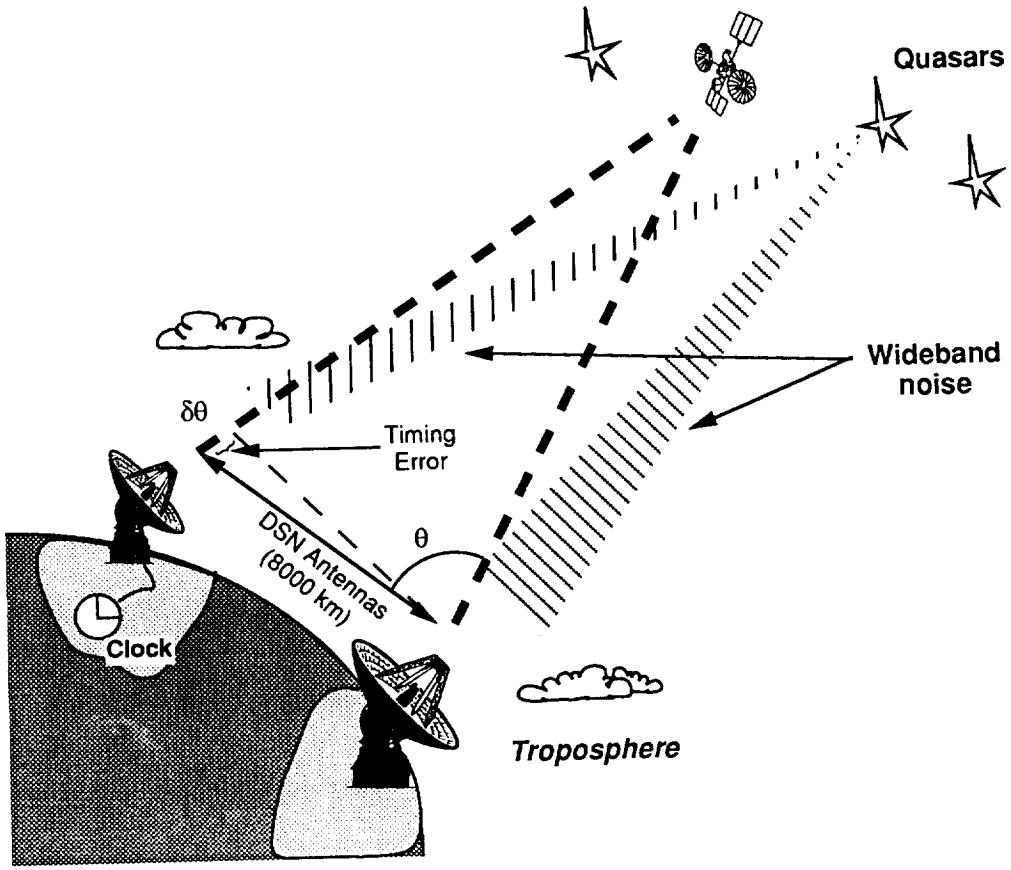

Figure 1: Quasar differenced VLBI spacecraft tracking.

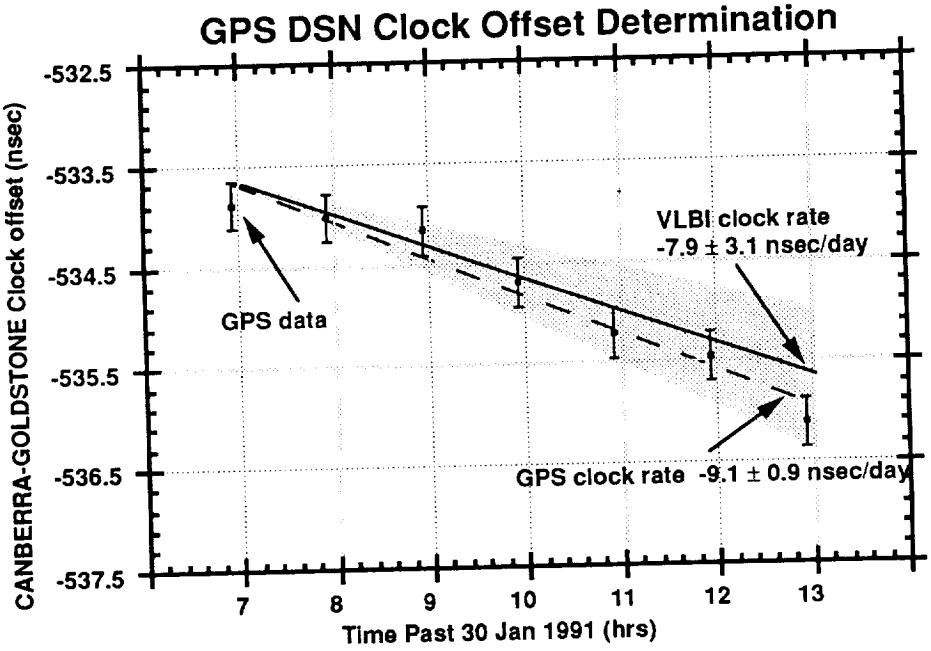

Graph 1: Comparison of GPS and VLBI derived clock offset estimates.

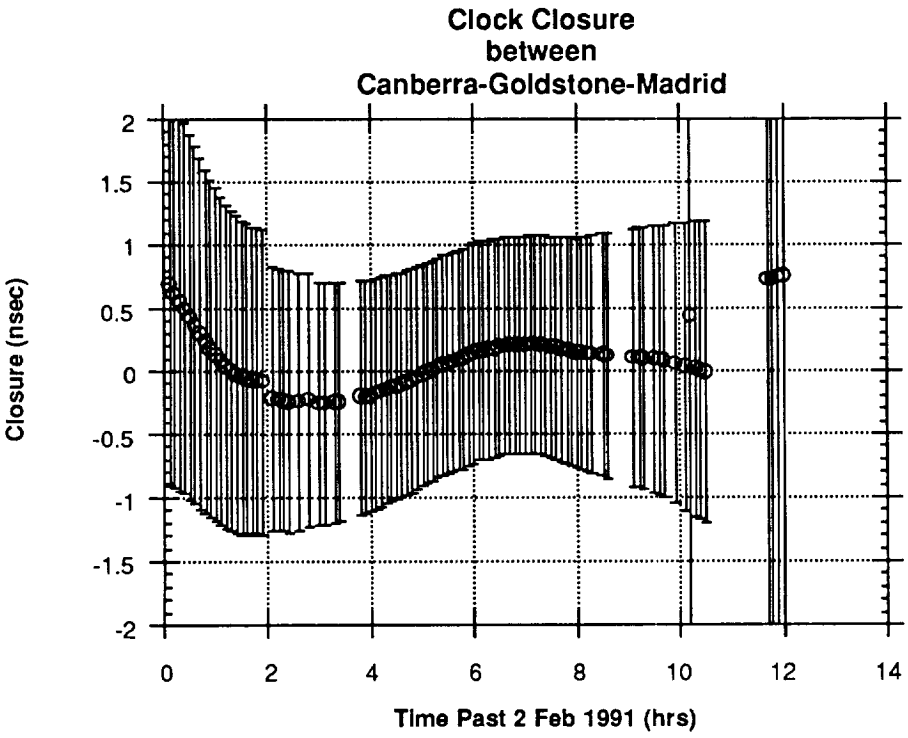

Graph 2: Clock closure with dynamically determined orbits.

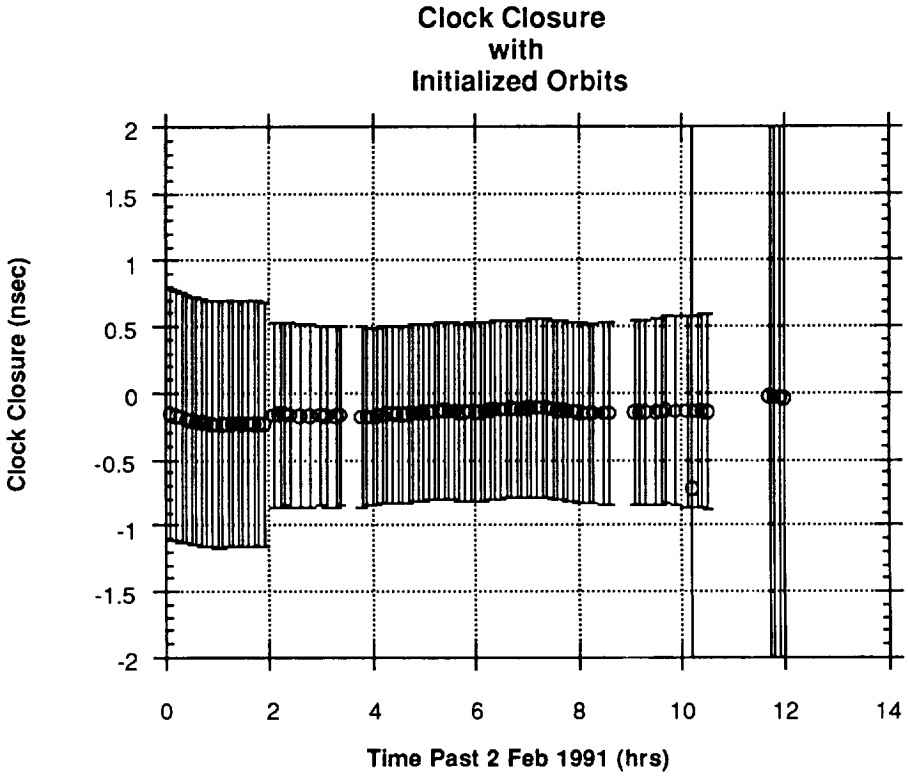

Graph 3: Clock closure with orbits initialized from previous day.

QUESTIONS AND ANSWERS

Dr. Gernot Winkler, USNO: Your results are outstanding. What is the reason for that. Your orbit determinations appear to be much better than anything else that I have seen. Have you had an opportunity to compare your orbits *ex post facto* with DMA or NGS orbits?

Mr. Border: I am not an expert on the orbits. If you care to talk to me afterwards, I can give you some names of people that could give you better information. I know that, within our section, we believe the orbits are good to 50 nanoseconds. That comes from comparing with baselines from VLBI, daily repeatabilities, and comparisons of our orbits with other peoples orbits.

Dr. Winkler: You must also have a better signal-to-noise in your receivers. Which antennas are you using?

Mr. Border: We are using ROGUE Receivers with Dorne-Margolin (sp?) antennas. The receivers are highly digital receivers, so they produce high quality data with very few cycle slips.

Mark Weiss, NIST: I am curious about the feasibility of using techniques like this for time transfer in a near-real-time mode. Even a week after fact would be useful. I am wondering about cycle slips, does the GYPSY software automatically detect and correct for cycle slips?

Mr. Border: GYPSY software automatically handles cycle slips and things like that. With ROGUE receivers, cycle slips are not generally a very significant problem. The strategy that I presented here was the standard estimation strategy used for geodetic measurements. GYPSY handles orbits, cycle slips and things like that. The other question that you asked was about near-real-time results. More software development will be needed to develop a forward-running filter, so that we can incorporate data as it arrives. Right now we have about a days turn around on our numbers. Reducing that is one of the future goals.

Mr. Weiss: So you are saying that we can do time transfer at the sub-nanosecond leave using ROGUE receivers, with a days turn-around.

Mr. Dunn: Yes, that is what I am saying.

Mr. Weiss: But we would have to have ROGUE receivers spread around the world to be able to do the orbits.

Mr. Dunn: Certainly to duplicate our results. We are using 21 receivers around the world, but we think that is overkill for doing time transfer. You would need a number of sites.

G. Petit, BIPM: Is your processing with the GYPSY software with all the satellites all the time?

Mr. Dunn: It is with all satellites, all the time. For a given estimate, the clocks necessarily close. In order to produce clock offset estimates that don't necessarily close, we remove the data from one of the DSN stations and produce a clock offset estimate for the remaining two. We do this three times, for the different stations, and sum the offsets. Because most of the stations are still in, we expect the errors to be highly correlated. As a result, this is probably an underestimate of our total error. This particular closure method is a good diagnostic tool in terms of seeing what magnitude of effect we can expect from orbit error. However, I would like to point out that, when people use broadcast ephemerides, they are essentially using correlated information, so those clock closure measurements have a very similar interpretation.

David Allan, NIST: I have two questions. First, on the same chart, do have any explanation about the steps in the data near the end, and second, what do you do about SA?

Mr. Dunn: There were a number of satellites that rose and set about the same time and also some of the equipment was turned off at that time. We aren't entirely sure what caused the step. The large errors near the ends of the run are due to the fact that, for this data set, we used 12 hour data arcs to reduce the processing time. When a satellite rises near the end of the arc or sets near the beginning of the arc, then you have fairly low data weight for that satellite. As a result, you can see that the formal errors blow up quite a bit. In routine processing this will be less of an issue, since there will be more satellites in the constellation and we will be able to run over longer periods. In geodetic work, we have found that we are fairly insensitive to SA. You can see the effect in the results, however it is very small. We believe that this is due to the fact that these measurements are essentially a differenced data type. We solve for all of the clocks at each epoch and so SA should tend to difference out. AS, on the other hand, could be a significant problem.

LORAN-C DATA REDUCTION AT THE U.S. NAVAL OBSERVATORY

N92-33358

Harold Chadsey
U.S. Naval Observatory
34th & Massachusetts Avenue, NW
Washington, DC 20392-5100

Abstract

As part of its mission and in cooperation with the U.S. Coast Guard, the U.S. Naval Observatory (USNO) monitors and reports the timing of the LORAN-C chains. The procedures for monitoring and processing the reported values have evolved with advances in monitoring equipment, computer interfaces and PCs. This paper discusses the current standardized procedures used by USNO to sort the raw data according to GRI rate; to fit and smooth the data points; and, for chains remotely monitored, to tie the values to the USNO Master Clock. The results of these procedures are the LORAN time of transmission values, as referenced to UTC(USNO) for all LORAN chains. This information is available to users via USNO publications and the USNO Automated Data Service (ADS).

Introduction

On 1 June 1961, the U.S. Naval Observatory (USNO) began monitoring the LORAN-C signal of the East Coast chain transmitting from Carolina Beach, North Carolina [1]. The time difference values were taken manually at 14:00 Local Standard Time (LST) (this particular time was chosen in view of the diurnal shift of the signal). A few years later, time corrections were needed for the West Coast and other LORAN chains. USNO in Washington, DC, is located outside the groundwave coverage of these LORAN chains; therefore, a need to develop remote monitoring stations was created. This also meant that methods to tie the remote reference clock to the USNO Master Clock (MC) had to be developed. In the beginning, the readings were taken manually. A portable clock from the Observatory visited each remote monitoring site to determine the difference between the station reference clock and the USNO MC.

With the advent of microcomputers, many of the manual operations could be done automatically. This included the taking of readings, sending data to USNO for analysis, and adjustment of local time standard to USNO Master Clock. These automated monitoring systems require little or no human intervention except in the cases of equipment failure or the encountering of an error that cannot be predicted, e.g., data corruption by noise on the phone line.

Data Collection Methods

The LORAN Time-of-Arrival data (TOA), from which the Time-of-Emission (TOE) information found in the USNO Series 4 Publication is derived, are collected by microcomputer-controlled Data Acquisition Systems (DAS) located at USNO and throughout the United States.

Figure 1 — Approximate location of LORAN transmitters (·) and USNO DASs (×) to monitor the LORAN timing signal.

USNO and most of these remote DAS units monitor both LORAN and GPS signals. The LORAN chains outside the U.S. are monitored and data analyses are performed using other methods not covered in this paper.

Each morning, HP1000 computers begin a scheduled sequence of events (see flowchart 1). Each of the remote DAS units receives a phone call from a computer. The LORAN and GPS data are downloaded into the HP1000 and the DAS starts collecting data again. Because of the amount of data collected at some locations, this data transfer can take several minutes to complete. The phone calls are made early in the morning because of the long data collection time slowing computer processes and the needs to have the completed results available by certain deadlines, to reduce telephone costs, and to obtain the highest data transmission quality possible. Once all the collectable DAS data are in the USNO HP1000 computers, it is transferred to a UNIX work station environment, where all data analysis is performed. The work station was chosen because it processes data more than 30 times faster then the HP1000. Its versatility allows for data collected in numerous ways to be centrally processed, and it provides an extra level of security. The software that is commercially available or is custom written at USNO allows the data, once they are entered, to remain in the same computer (albeit in different forms) until the final reports are created and sent out. The work station runs a single master set of data analysis programs rather than an individualized set for each DAS's data. This makes program maintenance and system operations considerably easier.

Data Analysis

The raw data are received from the HP1000 computers into the work station via inter-computer file transfers (USNO has DAS systems on two independently running HP1000 computers. This allows for increased reliability and system checks). Once the data are located in the work station's file system, a series of programs are executed by means of script files (similar to PC batch files). In many instances, one script file calls another, which in turn calls a third. By having the processes controlled by a series of script files, any segment or group of segments of the data reduction process can easily be reprocessed if necessary.

```
--------------------
48520.8333333
99600.5
.02665509
--------------------
48520.8750000
89700.1
.07449299
--------------------
48520.9166667
89700.3
.01639081
--------------------
48520.9583333
99600.1
.06952863
############
3   1991263235248   1991264000006   69    +2.80E-011   +186.516E-010   +15.4E-009   -15
12  1991264000306   1991264001300   100   +5.18E-012   +320.117E-010   +12.0E-010   -15
12  1991264001312   1991264002306   100   -5.58E-012   +314.471E-010   +12.4E-010   -15
12  1991264002318   1991264003312   100   +2.30E-011   +222.160E-010   +13.8E-010   -15
```

Figure 2-A sample of LORAN and GPS data as received at USNO from a DAS

The first program in the script files sorts and reformats the data. The data must be sorted because, at some locations, the LORAN data are in the same file as the GPS data (at other locations, the two data types are in separate files). Whether the data need to be segregated or not, this same program also reformats the data into a standardized form for the analysis programs and makes a copy for the history files (there is one master set of analysis programs requiring a standardized input data format).

These history files are used to reprocess data covering long periods of time. Once the LORAN and GPS data have been standardized in format and copies made for the record books, they can be reduced to more meaningful values.

The LORAN data-processing program analyzes all the data per block of time (usually 24 hours) during each pass through the input file. It will process the file as many times as needed to insure that all days with complete sets of data present are analyzed before terminating. As the data are read, the program sorts the data points into a large array according to the Group Repetition Interval (GRI) of the LORAN chains monitored at the particular site. The data points falling more than 750 nanoseconds away from the previous day's processed value are automatically disregarded. This filtering eliminates obviously bad values. After all data for the period in question have been entered into the array, all the GRI data points are linearly fit to a point of 01:00 local standard time. (The change from 14:00 LST to 01:00 LST was due to requirements of the U.S. Coast Guard for steering of the LORAN chains' TOE. It was also found that the data were much more reliable and consistent at this early morning hour.) While computing the linear fit, a sigma value of the fit is also calculated. One-and-a-half times this sigma value is then used as a filter for a second pass through the linear fit solution. This second result is then smoothed to remove the extreme effects from the environment and filed for later use. From previous research, it was found that no LORAN chain jumps more then 30 nanoseconds from one day to the next under normal circumstances. When a value does jump more than thirty nanoseconds from one day to the next, the filed value is the previous day's processed value plus half the jumped amount [2].

MJD TIME	8970-M	8970-X	9960_M	9960-Z
48500.250	-0.13	-0.15	-0.08	-0.11
48501.250	-0.15	-0.18	-0.13	-0.14
48502.250	-0.08	-0.10	-0.08	-0.11
48503.250	-0.04	-0.07	0.02	-0.01
48504.250	-0.04	-0.09	0.05	0.07
48505.250	-0.10	-0.14	0.02	0.05

Figure 3-Processed LORAN. A sample of LORAN data after linear fit processing for four LORAN stations.

Date MJD	USNO MC-GPS	Slope	RMS	N	DAS SC-GPS	Slope	RMS	N	USNO-DAS	Slope
48500.0	0.013	0.000	0.011	77	-0.004	-0.006	0.011	222	0.017	0.007
48501.0	0.023	0.012	0.009	74	0.010	0.012	0.012	223	0.014	0.000
48502.0	0.036	0.013	0.009	71	0.020	0.012	0.012	226	0.016	0.001
48503.0	0.041	0.004	0.010	75	0.027	0.010	0.010	224	0.013	0.001
48504.0	0.043	0.001	0.009	75	0.034	0.011	0.011	227	0.009	-0.007
48505.0	0.045	0.003	0.011	75	0.041	0.014	0.014	229	0.003	-0.004

Figure 4-A sample of GPS data after linear fit processing

The GPS data processing works much the same way as the LORAN data processing program. The data points from each monitoring site and USNO are entered into a large array. All data points outside a reasonable value are automatically disregarded. These data points are linearly fitted, two-times-sigma filtered, and linearly fitted a second time. These USNO versus monitoring site clock difference results are filed for later use. The present philosophy at USNO is to reduce all of the time values from the various satellites as though they were from one. This is referred to as the "melting pot" method of reduction. This linear fit method works well for a large number of data points or when only a very few data points are available from a consistent satellite from day to day.

In other cases, it is better to use the GPS common-view method. This method requires the monitoring site and USNO to be looking at the same satellite at exactly the same time in order to determine the reference clock time difference. As a result of the large number of variables present to perform the reduction of data, it is difficult to automate this process; therefore, it is only used at a few exceptional locations where automatic DAS units are impractical or unusable for technical reasons. In the case of remotely-monitored LORAN chains, the results from the LORAN data analysis are finally corrected to a value of USNO-MC minus the various chains by applying the GPS difference calculation. It is this corrected value from the remote DAS units and the values directly monitored at USNO that appear in the USNO Series 4 publication.

A separate program uses the reduced GPS values of the monitoring sites and the reported values for the various U.S. LORAN chains to calculate microstepper corrections. These corrections are applied to the remote station clocks and the LORAN transmitter units respectively. The monitoring site microstepper corrections keep each remote site's clock approximately set to the USNO MC. The LORAN microstepper settings assist the U.S. Coast Guard in meeting Public Law 100-223,

MJD TIME	*8970-M*	*8970-X*	*9960-M*	*9960-Z*
48500.250	*-0.07*	*-0.09*	*-0.02*	*-0.05*
48501.250	*-0.09*	*-0.12*	*-0.07*	*-0.08*
48502.250	*-0.02*	*-0.04*	*-0.02*	*-0.05*
48503.250	*0.02*	*-0.01*	*0.08*	*0.05*
48504.250	*0.02*	*-0.03*	*0.11*	*0.13*
48505.250	*-0.04*	*-0.08*	*0.08*	*0.11*

Figure 5-Results. A sample of the processed LORAN value after correction of station clock via GPS for four LORAN stations.

which states that "each master transmitter shall be synchronized to within approximately 100 nanoseconds of universal time" **[3]**. The accompanying graphs are examples of how well this data analysis and microstepper corrections provided to the LORAN transmitting sites are keeping the LORAN TOE values within tolerance.

Summary

By means of automated Data Acquisition Systems and time-scheduled data analysis programs, the U.S. Naval Observatory is disseminating UTC time via LORAN-C transmissions to a greater accuracy then ever before. USNO is continuing its efforts in researching new analytical methods. It will also be investigating various methods by which users can increase the accuracy of their timekeeping relative to UTC time via LORAN timing signals.

References

1) Charron, L. G., "*Evaluation of LORAN-C Timing Techniques*", Proceedings of Wild Goose Association Meeting, October 1983, Washington, DC.

2) Miranian, M. (USNO), private communication.

3) Vogt, G. (USCG), private communication, 5 December 1990.

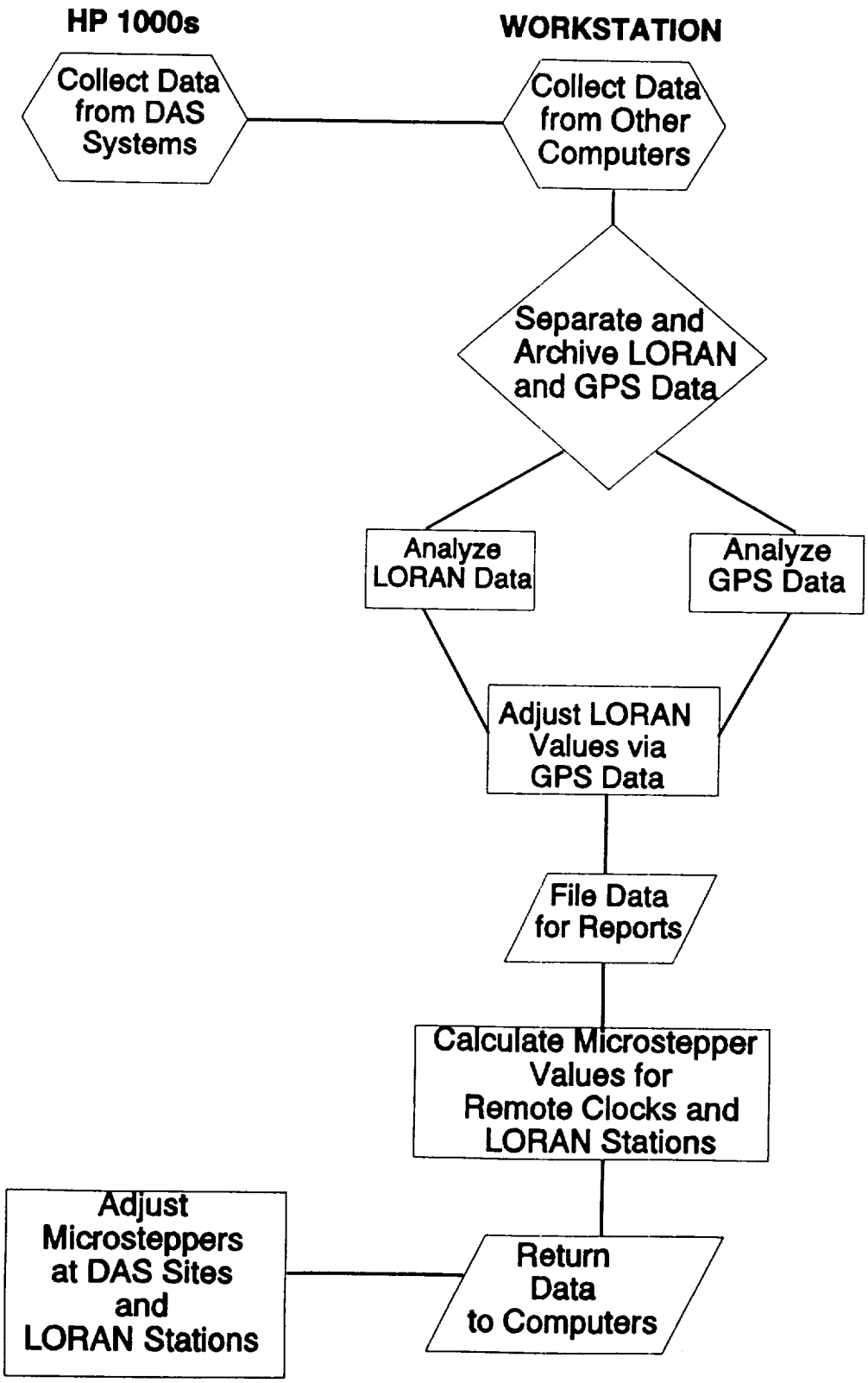

Flowchart 1-Flow diagram of LORAN and GPS data processing. The data for reports are found in the USNO Series 4 publication.

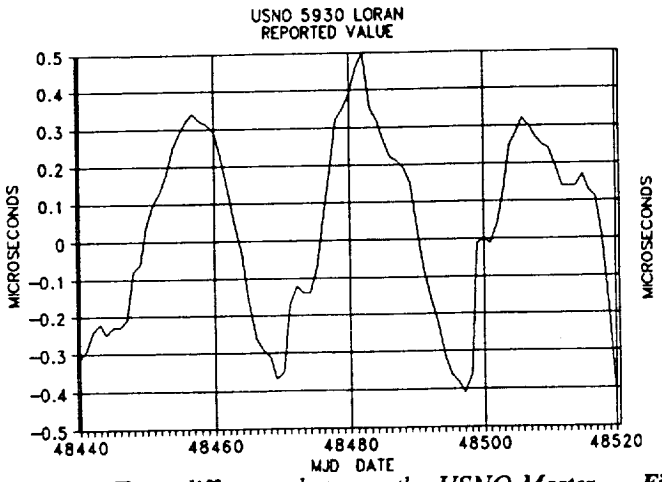

Figure 6-Time difference between the USNO Master Clock and the 5930 LORAN Chain.

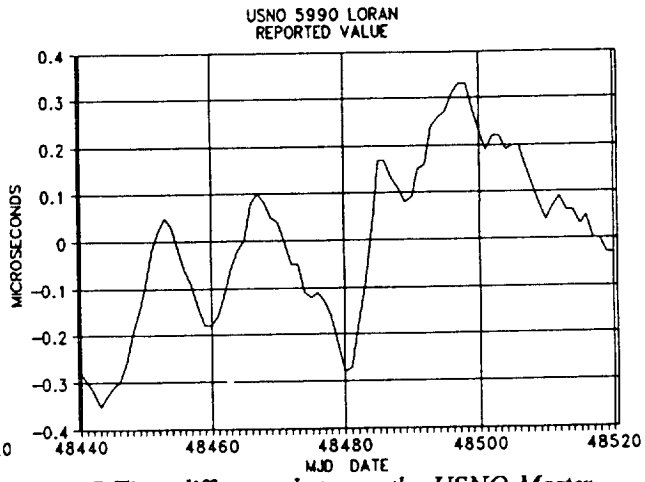

Figure 7-Time difference between the USNO Master Clock and the 5990 LORAN Chain.

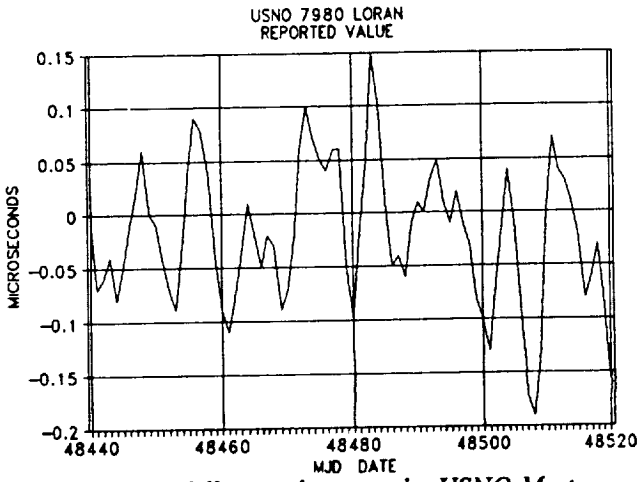

Figure 8-Time difference between the USNO Master Clock and the 7980 LORAN chain.

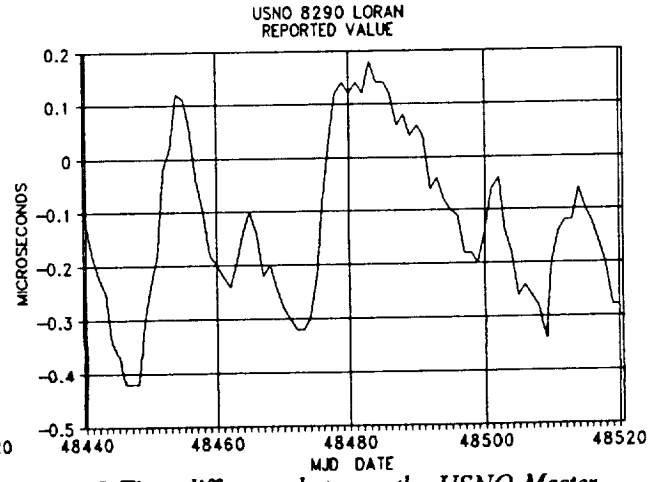

Figure 9-Time difference between the USNO Master Clock and the 8290 LORAN Chain.

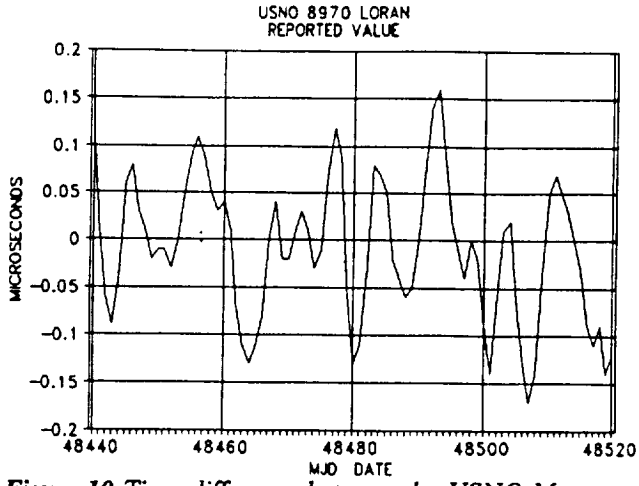

Figure 10-Time difference between the USNO Master Clock and the 8970 LORAN Chain.

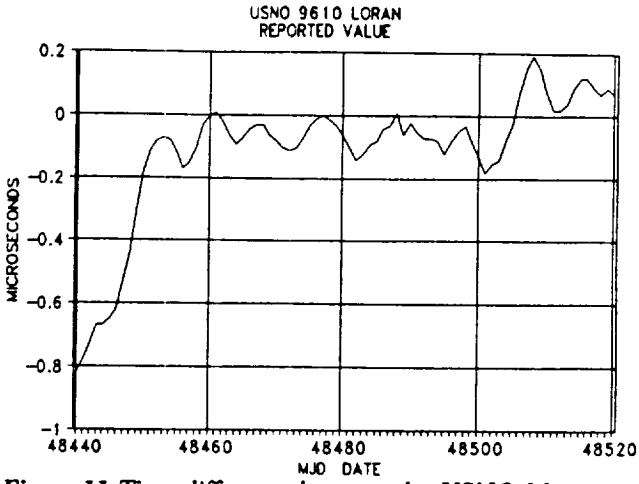

Figure 11-Time difference between the USNO Master Clock and the 9610 LORAN Chain. Note: USNO began providing steer corrections for 9610 on MJD 48440.

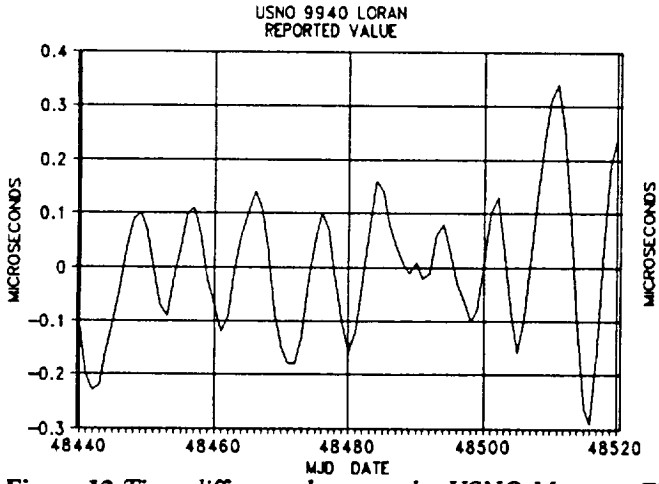

Figure 12-Time difference between the USNO Master Clock and the 9940 LORAN chain.

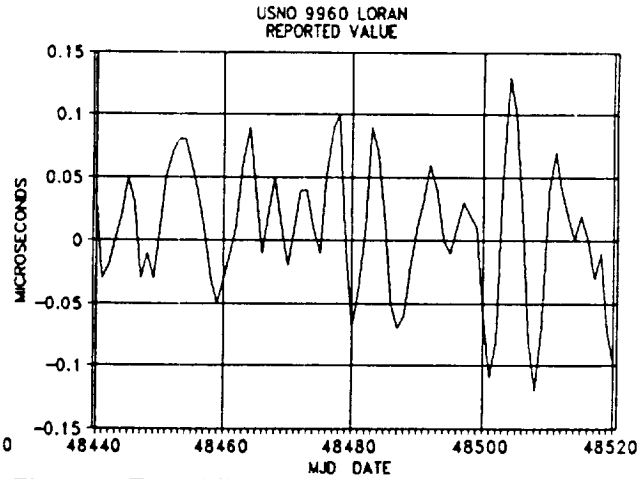

Figure 13-Time difference between the USNO Master Clock and the 9960 LORAN chain.

QUESTIONS AND ANSWERS

David Allan, NIST: Some work at NBS showed that you can look at the index of refraction as a ground wave, the gradient. One might be able to get some nominal weather data and do some modeling to see why these delay variations come, due to these storms and fronts, etc., and account for some of the variations that are causing you these tracking problems.

Mr. Chadsey: One of the things that we are looking at is the USNO is working on a project with the Coast Guard at the 9960 transmitting site at Seneca. We will be doing two-way time transfer with that transmitting site. Their clock will be set precisely to USNO, with a very small error. We will then monitor that *versus* received values, and plot that *versus* the various weather conditions that we can monitor, such as temperature, humidity, barometric pressure, etc. in order to try to model some of these effects. This will the first time that we can do it on a fairly accurate basis.

Mr. Allan: What I meant to say was that they said that the strongest effect was gradient, rather than the temperature itself. You might keep that in mind as work on the meddling.

Mr. Chadsey: That is one of the things that will have to come into this. As we do the weather plots, we will have to get weather, not only from the local receiver and transmitter sites, but also from points along the way and plot out the various lines.

The Role of Clocks in Operating Deep Space Missions*

S. W. Asmar and E. R. Kursinski
Jet Propulsion Laboratory
California Institute of Technology
Pasadena, California 91109

Abstract

Operation of deep space missions requires stable frequency references and clocks to perform several mission critical functions. These references are used in generating the telecommunication links to maintain communications between earth and spacecraft, in generating accurate doppler, range and VLBI observables for determining the spacecraft's time varying position, and to generate on-board timing information for clocking out timed commands and time tagging instrument data. In addition, science applications exist particularly those utilizing radio instrumentation which can require additional functions and levels of performance. The design necessary to support these functions affects both the spacecraft and the ground tracking stations. This paper provides a brief description of these functions and some of the key requirements needed to support them.

I. Introduction

The operation of deep space missions require the utilization of stable clocks and frequency references to perform several mission-critical functions both on-board the spacecraft as well as at the ground tracking stations. The telecommunications link needed to maintain communications between earth and the spacecraft is derived from these oscillators. They play a role in the following functions: on-board timing, telemetry, navigation, and science. Though there is potentially substantial overlap, these functions are typically supported by distinctly different clocks on-board the spacecraft. The design necessary to support these functions affects the ground tracking stations as well. Navigation data observables as well as certain radio science experiments require ground-based hydrogen maser clocks to provide superior stability (in terms of Allan deviation at longer integration times) over crystal oscillators.

II. On-Board Timing

As part of the spacecraft's command and data handling subsystem, the on-board clock has the function of generating timing information for clocking-out stored commands and time tagging payload data. The on-board timing clock provides timing signals needed to time tag events observed

*This work was carried out at the Jet Propulsion Laboratory, California Institute of Technology, under a contract with the National Aeronautics and Space Administration.

by the different spacecraft engineering subsystems and science instrument payload. The time-tagged data is either transmitted to earth in real-time or recorded on data storage units for telemetry transmission during some period following the flyby.

Typically based on redundant crystal oscillators operating at or near 5 MHz, the data handling clock is stable to 5×10^{-9} over any one minute. The oscillator signal is divided into clock frequencies ranging from 0.25 Hz to 640 kHz which are then distributed to engineering and scientific subsystem users. The clock provides a time code that is inserted in the data packets. The time code may contain 40 bits divided into a coarse and fine time segments and is transmitted once every second. The coarse time code, 32 bits, is a straight, continuous binary count of seconds with the LSB being 1 second. Its period is 2^{32} seconds, or 136 years. The fine time code, 8 bits, is a straight count of binary fractional subseconds with the LSB being 1/256 seconds.

Execution of complicated sets of stored commands is required to successfully operate a complicated planetary mission particularly in the outer solar system. As Voyager 2 approached Neptune, the time delay from command transmission to reception at the earth of the spacecraft command confirmation was more than eight hours. The magnitude of this delay was comparable to the entire close-up flyby period making autonomous spacecraft operation an absolute necessity. In general for planetary missions, the spacecraft must act as a robot executing a precisely timed series of preprogrammed command sequences by relying on an on-board clock to determine proper execution time. These commands are carefully designed on earth, up-linked and stored on-board the spacecraft as much as a year prior to the flyby (subsequent modifications are up-linked as necessary). During a close flyby, the required accuracy of command execution timing can be a fraction of a second. To achieve this precision during the long Voyager mission the clock was seldom corrected; instead, the clock drift was continually monitored during the months prior to each flyby, the offset estimated and the execution times of command sequences then shifted to compensate for the anticipated clock error.

The tightest requirements on execution time accuracy occur when the spacecraft flies very close to an object of interest causing the geometry to change very rapidly. In the case of the Voyager Neptune flyby, the tightest requirement was driven by the "limb-tracking" maneuver executed during the radio occultation observations of the planet's atmosphere. This maneuver is executed while the spacecraft flies behind Neptune as viewed from the earth. It maintains the spacecraft orientation such that the three meter telecommunications antenna is pointed at the location in the planet's atmosphere where the image of the earth appears in order that the spacecraft's signal can be received on earth throughout the occultation period. The narrowness of the spacecraft antenna beam and the rapidly changing geometry required an execution accuracy of approximately one second. The combination of the clock drift and navigation uncertainties required this command sequence to be updated about one week prior to the encounter.

III. Telemetry

In deep space communications, the design chosen to get science and engineering data from the spacecraft to the earth phase modulates the data onto a video frequency subcarrier which is modulated onto a microwave carrier signal [1]. This requires three oscillators: one to generate the carrier signal, one to drive the subcarrier signal, and the data rate clock. These oscillators are separate and independent of one another to avoid coherent spurious signals which can severely degrade the accuracy of the data recovered in the demodulation process. The oscillator from which the carrier

signal is derived is a crystal oscillator either free running or voltage controlled to maintain phase-lock with the up-link signal from earth. The free running type is either an auxiliary oscillator, provided as part of the spacecraft's standard transponder, or an "ultra-stable" oscillator (USO), which is available on certain deep space missions as instrumentation for radio science experiments and will be discussed further under the role of clocks in science. Free running oscillators are used when communication is in the "one-way" doppler mode where no uplink from the ground is either necessary or available. The voltage controlled oscillator (VCO) is used when the spacecraft is in two or three-way mode of communication with ground stations and the uplink signal is used as the phase reference for the downlink carrier signal. The one-way mode is simpler and more robust whereas the VCO mode is typically used when range and doppler navigation data is also required.

The second clock which drives the subcarrier is a free running crystal oscillator in the telemetry modulation unit. The third clock, the data rate clock is a crystal oscillator residing in the command and data handling subsystem discussed in the previous section.

From a telemetry standpoint, the primary requirement is that these oscillators be phase coherent over the time scales important to phase modulation and demodulation. This is required in order that the phase modulation be readily detected in the presence of the natural variability of the reference signal phase. Deep space data rates generally range from a few bits per second to hundreds of kilobits per second implying time scales ranging from microseconds up to a second. This type of requirement leads to frequency stability requirements on the order of 10^{-11} at 1 second for the carrier signal oscillator. In practice, the auxiliary oscillator, the telemetry modulation unit clock and the command and data handling clock are all of comparable stability.

IV. Navigation

Oscillators and clocks are used in navigation to generate accurate doppler, range, and very long baseline interferometry (VLBI) observables for determining the spacecraft's position as a function of time. Deep space missions are generally navigated via radio tracking where signals are typically referenced to ground-based clocks such as hydrogen masers in two or three-way coherent doppler modes. Optical navigation is used on some missions when the spacecraft is sufficiently close to an object that pictures are useful indetermining its position relative to the object.

There are three categories of radio navigation data types: range, range rate (doppler) and VLBI. Range and range rate are measurements of path length and change in path length along the line of sight between the earth and spacecraft. By observing the change in the path length as the earth rotates one can also determine the spacecraft angular position in the plane of the sky [2]. VLBI directly measures the spacecraft angular position and its rate of change. The range and VLBI type measurements are orthogonal and therefore complementary in determining spacecraft position.

Following the discussion of [2], a range observable is a measure of round trip light time (RTLT) as recorded by the station clock

$$r_k = ST(t_k) - ST(t_k - RTLT) \tag{1}$$

where $ST(t_k)$ is the time as kept by the station clock at true time t_k. A doppler measurement d_k is defined in terms of differenced range by:

$$d_k = \frac{r_{k-1} - r_k}{T_c} \tag{2}$$

where $T_c = t_{k+1} - t_k$ is the doppler count time.

It is clear from these simple expressions that two of the relevant time scales are the signal integration time (on the order of seconds to minutes) and the RTLT (minutes to hours). The duration of the station's tracking pass ($\approx$12 hours) is also important particularly for determining the angular position. With the present performance of hydrogen masers used in the DSN, the clock is generally not the limiting error source in two and three way doppler or range measurements. A more detailed description of the error budget in the navigation observables is given in [2].

One-way doppler measurements are seldom used at present because of the instability of spacecraft oscillators. However, as spacecraft oscillators continue to improve one-way doppler may be used more frequently. One obvious scenario is the case where a number of spacecraft are in orbit around a planet or residing on its surface. It would be desirable to have a navigation system which did not require separate stable uplink signals to each vehicle. If sufficiently stable oscillators could be placed on each vehicle, then all navigation could be done utilizing one-way links with a single ground tracking antenna dramatically reducing the complexity of the ground equipment requirements and operation.

In VLBI, the relative delay between the arrival of a signal received at a small set of widely spaced sites is measured. This delay is a function of the angular position of the spacecraft. Because the receive sites are so widely separated, independent clocks must be used at each site. Any clock errors cause an error in the measured delay creating an error in the inferred angular position. This would cause clocks to be a major error source in VLBI measurements except that a differential observational technique is used to remove many of the instrumental effects including that of the clocks. The technique is simply to sequentially observe the spacecraft and a natural radio source whose angular position is well established. In this way the spacecraft's angular position is measured relative to the radio source and many of the common mode error sources such as clocks simply cancel.

V. Science

Scientific experiments utilizing radio instrumentation have evolved largely out of the navigation capability and can require additional clock functions and levels of performance. These experiments can largely be broken into two classes. The first measures gravity and celestial mechanics related parameters. Two and three-way coherent doppler measurements are used to study gravity fields of planets as well as search for very low frequency gravitational waves. Two-way ranging measurements to the spacecraft as the spacecraft flies by the target body are used to derive a more accurate orbital ephemeris of that body .

The second class of observations measures the effects of media on the telecommunications signals as they propagate between the earth and spacecraft. The various media probed includes planetary atmospheres, ionospheres, magnetospheres and ring systems as well as interplanetary plasma generated by the sun. A particularly thorough overview and discussion of these propagation experiments is given in [3].

The different experiments each have their own desires and needs. [4] discusses three of the exper-

iments which have tended to drive the performance of the ground tracking station and spacecraft oscillator performance. The celestial mechanics experiments are typically operated in the two and three-way coherent doppler modes and utilize the station's clocks for frequency reference. Occultation and some relativity experiments are conducted in the one-way mode and utilize a USO on-board the spacecraft. The USO is used as a reliable frequency reference in the one-way mode when intervening media or solid bodies degrade or block the uplink to the spacecraft. The first such device was implemented on the two Voyager spacecraft and was very much responsible for many of the impressive set of results achieved by the Voyager radio science experiments.

The USO's implemented to date have consisted of a single quartz crystal oscillator operating near 5 MHz which is multiplied to the desired microwave signal frequency (e.g., X-band). The most recent USO's built for Mars Observer and TOPEX have demonstrated performance around one part in 10^{-13} from 1 up to 1000 seconds. These crystal USO's are highly sensitive to the ambient environment and are, as a result, contained in temperature controlled single or dual oven dewars; thermal coefficients can then reach 10^{-12} per degree centigrade. Depending on the mission some USOs must be radiation hardened and some must be shielded against stray magnetic fields generated by adjacent equipment on the spacecraft. Despite the environmental sensitivities, these oscillators are well suited to planetary missions. small, light weight and consume a small amount pf power (primarily for the oven) and have optimum performance (in terms of the Allan deviation) in the 1 to 1000 second regime which is the typical regime of interest for occultation type measurements. Unlike all the other oscillators on a deep space spacecraft, the USO is considered a science payload and is, therefore, designed to less stringent requirements in terms of reliability and redundancy.

REFERENCES:

[1] **Deep Space Telecommunications Systems Engineering**, J. H. Yuen, Ed., JPL Publication 82-76, April 1983

[2] J. S. Border and E. R. Kursinski, *"Deep Space Tracking and Frequency Standards"*, Proceedings of 45th Annual Symposium on Frequency Control, May 29-31 1991, pp. 594-607

[3] G. L. Tyler, *"Radio Propagation Experiments in the Outer Solar System with Voyager"*, IEEE Proc., Vol. 75, No. 10, Oct. 1987, pp. 1404-1431

[4] E. R. Kursinski, *"Application of High Stability Oscillators to Radio Science Experiments Using Deep Space Probes"*, Proc. of 22nd Annual Precise Time and Time Interval Planning Meeting (PTTI), Dec. 4-6, 1990, pp. 253-263

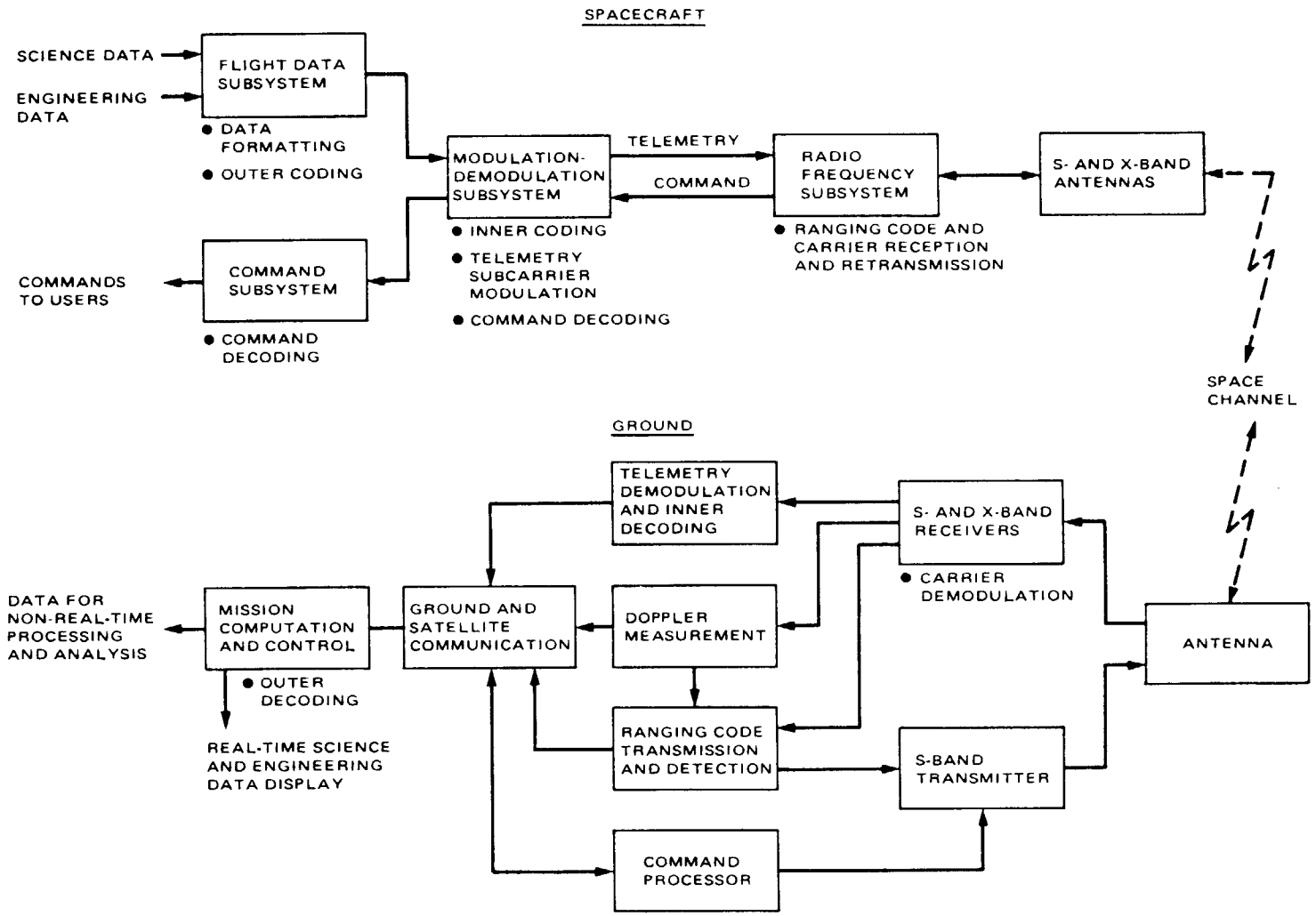

Figure 1: A typical deep space telecommunications system

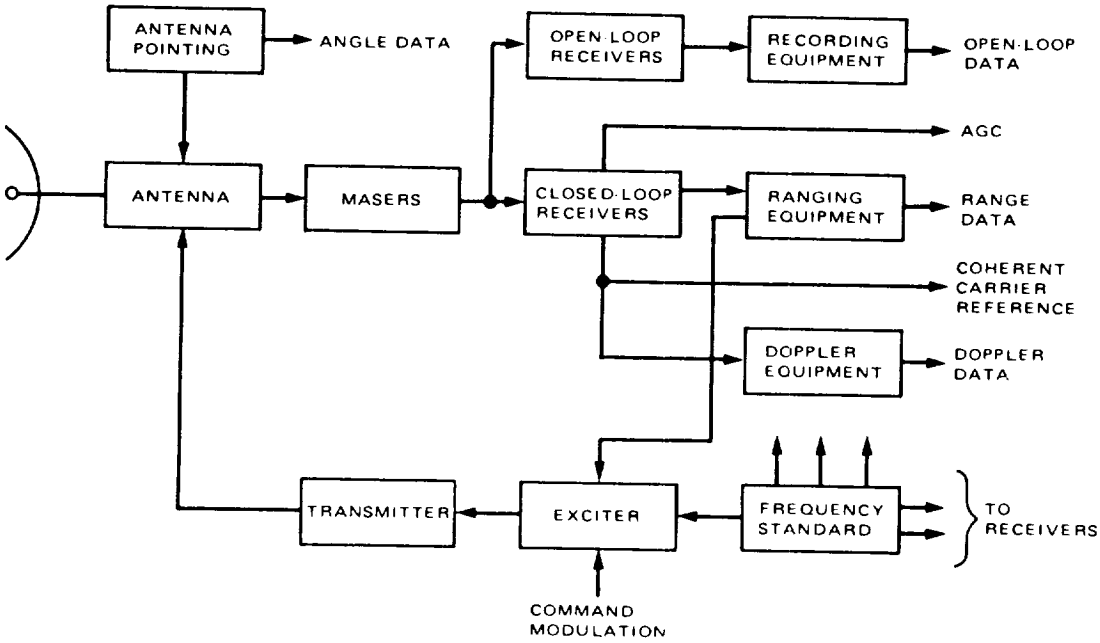

Figure 2: Ground tracking system block diagram

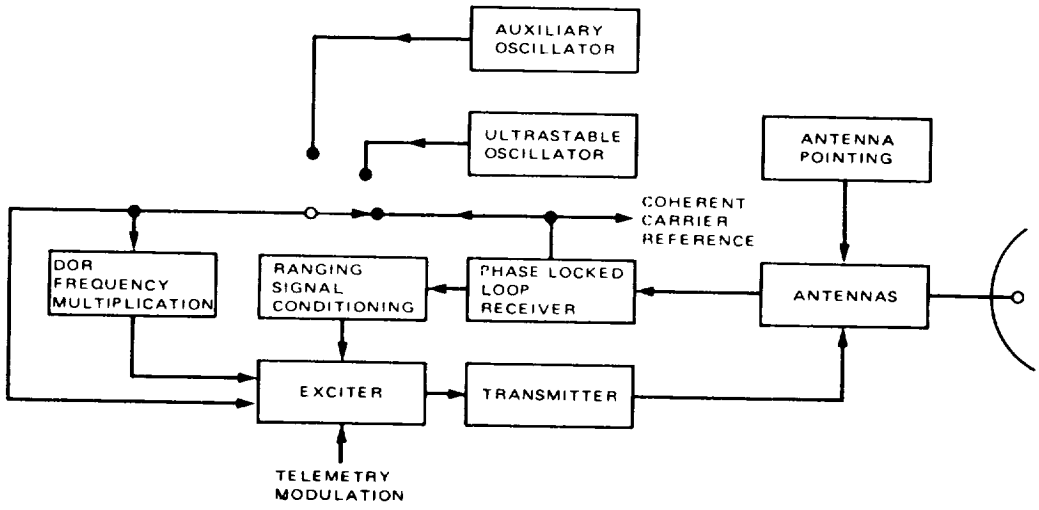

Figure 3: Spacecraft tracking system block diagram

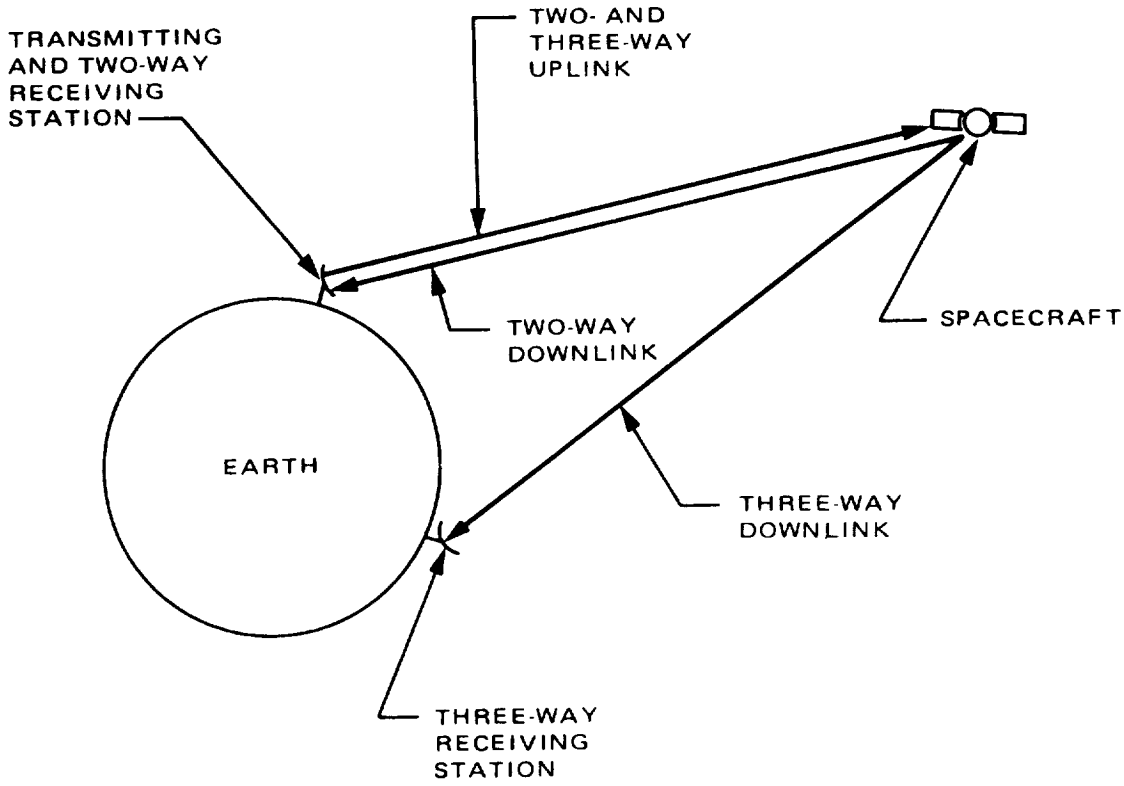

Figure 4: Transmitting and receiving configuration for two- and three-way data

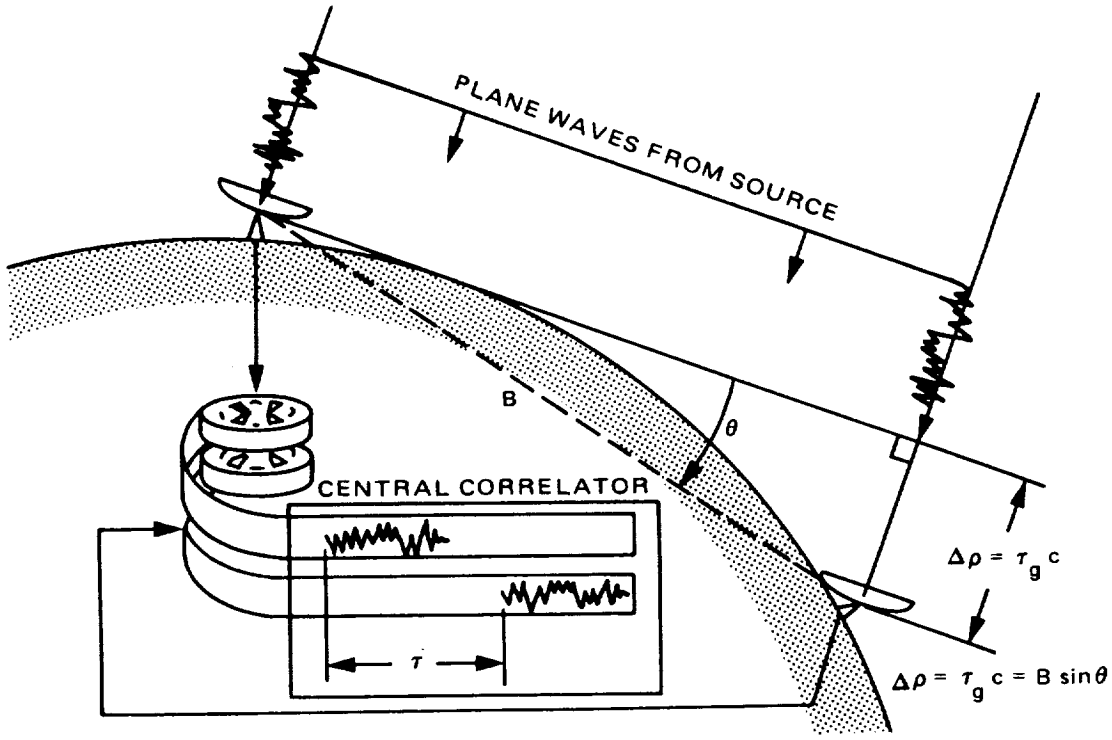

Figure 5: Measuring angular position with VLBI

TIMING SYSTEM FOR FIRING WIDELY SPACED TEST NUCLEAR DETONATIONS

Ralph E. Partridge
Los Alamos National Laboratory
P.O.Box 1663, M/S P947
Los Alamos, New Mexico 87545

The national nuclear weapons design laboratories (Los Alamos National Laboratory and Lawrence Livermore National Laboratory) test fire nuclear devices at the Nevada Test Site (NTS), which is spread over an area of over 1200 square miles (a bit larger than the state of Rhode Island). On each test there are hundreds of high time resolution recordings made of nuclear output waveforms and other phenomena. In order to synchronize these recordings with each other, with the nuclear device, and with offsite recordings, there is a requirement that the permanent command center and the outlying temporary firing sites be time tied to each other and to UTC to permit firing the shot at a predetermined time with an accuracy of about a microsecond. The system is so designed that this can be reduced to about 100 nanoseconds if it should prove necessary in the future.

New firing sites are created about every month. A year or so lead time is needed to drill and prepare each ground zero emplacement hole and its associated trailer park in the forward area. A few weeks before the nuclear device is brought in, the recording stations and trailers are emplaced in the trailer park and interconnected, and dry runs begin. By this time the trailer park timing station has been linked to the control room at the command center control point by fiber optics or microwaves. The timing station and the control room are synchronized by travelling clocks, by the communication links, and by GPS receivers. The control room can be linked simultaneously with up to four forward area sites in various stages of preparation.

Fig. 1 shows the location of the NTS and its relationship to other facilities of interest as seen from a GPS satellite. The layout of the NTS is illustrated in Fig. 2. Test area one is in the flat desert. Areas two and three are on the Pahute plateau, which is raised one to two thousand feet above the flats. In area two shots are fired in tunnels bored a mile or so northwest into the plateau. Area three is used for the larger yield shots that require greater depths of burial. Livermore fires shots in other test areas not marked on this map. In Fig. 3 we see some of the desert terrain and the results of thirty years of underground shooting. The depressions are subsidence craters where the earth has fallen in to fill the void left after a shot has vaporized and compressed the surrounding rock. Three trailer parks under construction can be seen in the background. In Fig. 4 are seen the connections between the primary facilities of the system. Timing signals are sent from the control point to the timing station by fiber optics or microwaves and thence signals are coupled to the "Red Shack" (where some of the nuclear device firing ciruits are located), many recording stations, and the downhole equipment rack by coaxial cables and fiber optics. Signal waveforms come back up from detectors in the rack to be recorded in the trailers.

A typical experiment rack is shown in Fig. 5. It is about six feet in diameter and 100 feet long. The canister containing the nuclear device will be attached at the lower end, which is facing us in

this picture. Note the large number of cables attached to the upper end. The largest cranes can lift 1,000,000 pounds (500 tons). Fig. 6 shows a typical trailer park. The tower in the background is where the rack is suspended while the detectors and nuclear device are being installed. Emanating from the tower is the loop of cables that eventually will go downhole. Next to the cables is a train of carts that carry the cables to the hole during the trip downhole. The timing station and red shack are on the right side, and the microwave antennas can be seen on the short white towers.

Currently the primary time reference for the test site is maintained in an EG&G laboratory in North Las Vegas. EG&G and we collaborate in developing the time system. The North Las Vegas location is now used only for historical reasons, and we plan to move it to the control point soon. Time is obtained from NIST by common view of GPS satellites and a modem connection. NIST provides us with a monthly record of our clock's performance with a resolution of about ten nanoseconds. This time is transferred by a portable rubidium clock from North Las Vegas to the control point about 85 miles northwest. Transfer is accomplished monthly, weekly, or daily, depending on the current level of activity at the NTS. A separate GPS receiver at the control point maintains an independent check. The control point clock and this receiver continuously monitor each other, and we watch this comparison by modem from Los Alamos when we are not at the NTS.

The major components of the system are diagrammed in Fig. 7. The master clock for the NTS resides in the control room. Time is transferred from there to the forward area trailer park timing station clock either by the portable rubidium clock or by the forward area clock synchronizer (FACS). The latter equipment sends the basic one pulse per second (1 pps) signal to the forward area over fiber optics or a microwave link and measures the time required for it to be returned from the timing station. Subsequent pulses are then advanced in time and are sent out early by half of the round trip delay time so that they arrive at the timing station on time. The resolution of the time advance is twenty nanoseconds when the signals are sent over fiber optics or baseband microwave, and about 800 nanoseconds when they are multiplexed with other signals on the microwave links. The portable clock can check the setting of the forward area clock with a resolution of twenty nanoseconds. A GPS receiver is sometimes used in the timing station for an independent check.

Two of the available 1 pps sources (clock, FACS, or GPS receiver) in the timing station are chosen to be redundant trains from which a single pulse will eventually be selected to fire the nuclear explosive. Currently GPS is in disfavor for this use because its system integrity is not sufficiently assured to inspire confidence that the pulse train will not experience sudden jumps. Such jumps have indeed been observed. When the system achieves an integrity level such that the FAA will approve it for terminal area aircraft navigation, it probably will become the source of choice. An alternative may be to use two receivers that look at different groups of satellites, with an oversight circuit that requires that the independent sources agree on the time to within a suitable tolerance. This approach may be feasible as soon as a few more satellites are in orbit. Microwave channel noise could cause the FACS to generate pulses at incorrect times. For the time being this possibility is being minimized by only opening a short time window in which pulses will be accepted. On the drawing board we have a flywheel circuit to be inserted between the microwave system and the FACS interface. Both rubidium and crystal oscillators are being investigated for use in the flywheel.

In the control room the 1 pps train and standard frequencies from the master clock are sent along with an IRIG-B time code to the master signal programmer. The programmer contains a series of electrically programmable read-only memory chips (EPROMs) into which have been burned the non time critical control signals that are to be sent out for this particular nuclear test. As the countdown progresses, the signals are encoded and multiplexed and sent over the fiber optic

or microwave channels to the timing station in the forward area, where they are demultiplexed, decoded, and converted to contact closures sent to the recording stations. A number of signals also go to the red shack and perform several preliminary operations that are needed to prepare the device for firing.

Near the end of the countdown the programmer sends the fire enable signal just before the second on which the device is to be fired. This closes a relay that lets the ORed 1 pps trains pass through to the device firing circuits, and the first immediately succeeding pulse fires the device. There is a plethora of precautions, procedures, and circuits to ensure that an inadvertent firing can not take place. In addition, there are a number of interlocks in series with the fire enable line to ensure that the firing circuits and a number of the more critical recording facilities are ready. There may be an additional arbitrary delay added between the 1 pps train and the actual firing pulse. This is somewhat analogous to the Selective Availability (SA) used by DoD on the GPS satellite signals to deny their full accuracy to unauthorized users.

The largest array of equipment is used to provide more accurate timing signals to those users who require them. One of the signals emanating from the signal programmer is a countdown time code. This contains a bit stream enumerating the countdown time at the last 1 pps tick and the time for the next tick. The starting time for the countdown can be anywhere from minus a few minutes to minus 99:59, depending on requirements of the test. This countdown time code is sent to the timing station over fibers or microwaves and there it is pulse width modulated on a one megahertz carrier along with other control signals and is distributed with the 1 pps via fiber optics to the recording stations.

In each station there is a "user box" that receives the code and into which the user enters up to eight desired times for events related to recording or downhole control to occur. Typical functions that a user might want to perform are opening of camera shutters, triggering of digitizers, turning on power supplies, starting a calibration sequence, or operating downhole vacuum valves. Fig. 8 shows the front panel of a prototype unit. The countdown time and status are displayed in the upper left corner for the convenience of the operators during dry runs. In the lower right portion of the panel is where the desired event times are entered. Above it the stored times can be displayed. An in station dry run can be performed using the controls in the lower left corner, without the need for a system-wide run.

The event times are stored in nonvolatile memory with a resolution of one microsecond. As the countdown reaches each of these preselected times, its associated channel generates a selectable-width pulse, a dc level shift, and a form C relay contact actuation. The user can reprogram his choices of times up until shortly before the final dry run, but a flag is sent back to the control room when he does so, in order that the test director and control room personnel know that there have been changes made. Any channel can be used to turn off the dc level shift and contact actuation from a previous channel. This provides a start-stop mode of control for experiments that need such a capability. The user can also decide whether or not a dc level shift or contact actuation should be dropped in the event of a hold in the countdown after that particular event time has occurred.

Offsite users who are not directly connected into the timing system use GPS receivers or independent clocks to keep time. They then have their equipment continuously subtract the predicted firing time from the current time to obtain countdown time. In the event of a hold, information to update the firing time can be transmitted as time offsets by VHF radio or modems, or by ordinary telephone conversations if the remote station is manned.

At Los Alamos we maintain a time laboratory that we use in developing systems for use at the NTS. There we keep two cesium oscillators, various rubidium and crystal oscillators, GPS receivers, a countdown signal programmer, and simulated multiplexed microwave and fiber optic links.

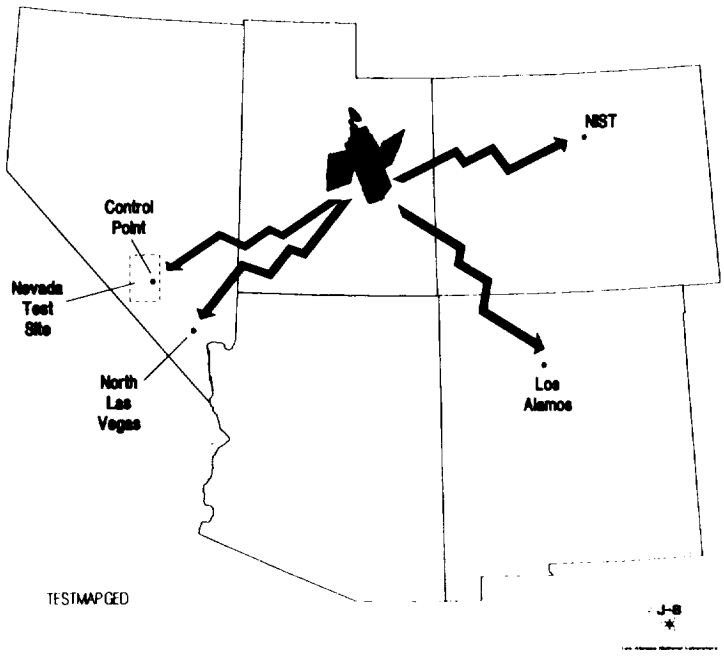

Fig. 1. Nevada Test Site and other facilities

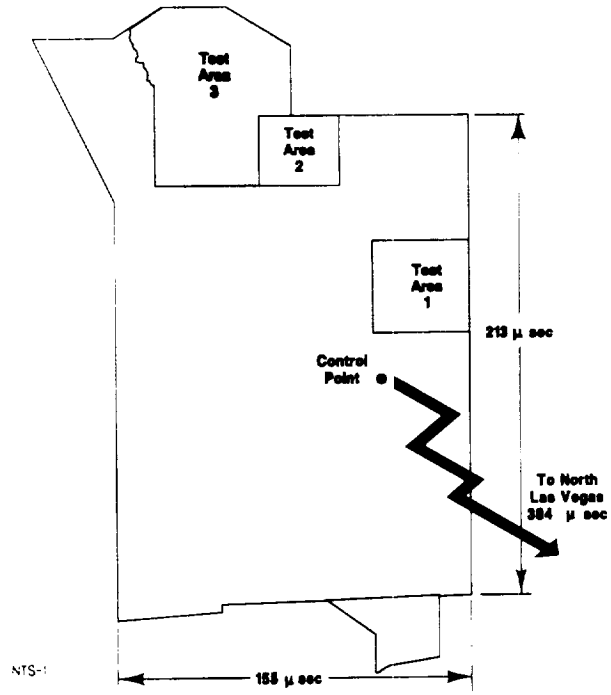

Fig. 2. Test Site layout

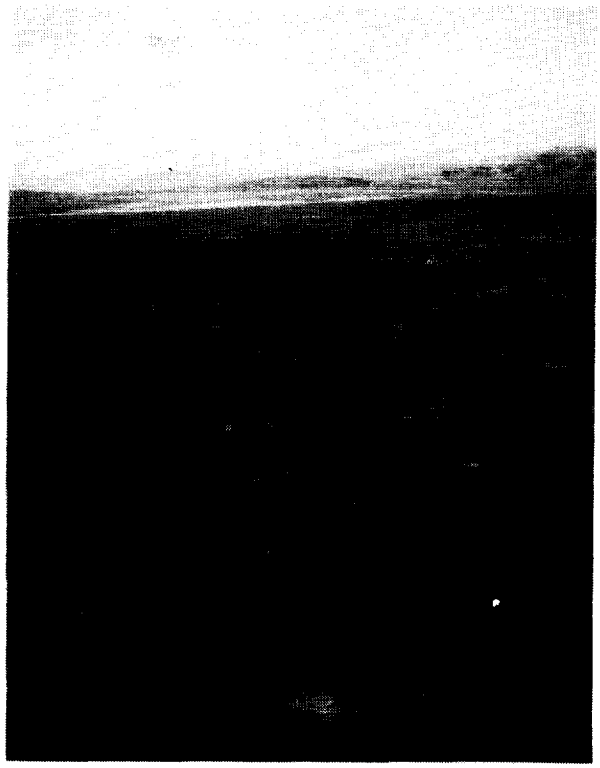

Fig. 3. Desert terrain with craters and trailer parks

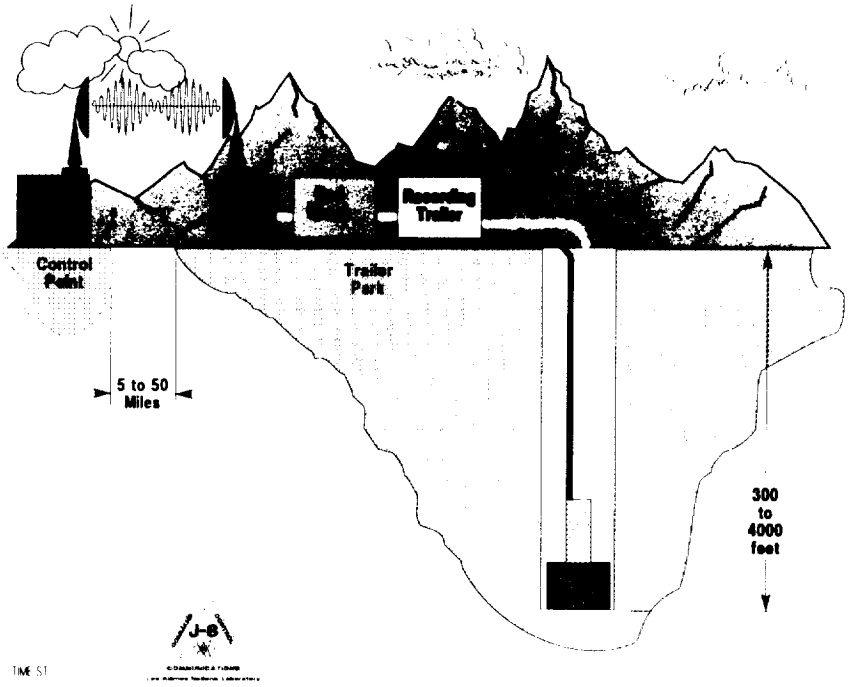

Fig. 4. Connections between primary facilities

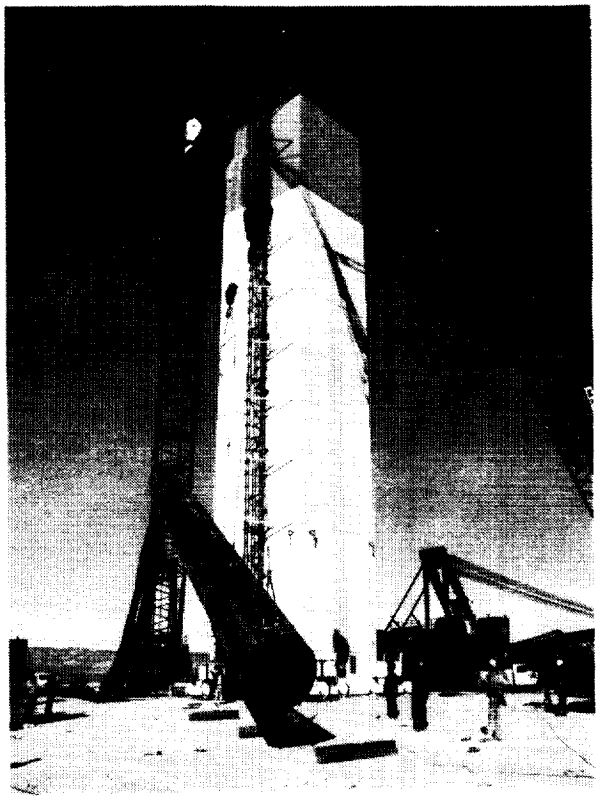

Fig. 5. Partially raised experiment rack

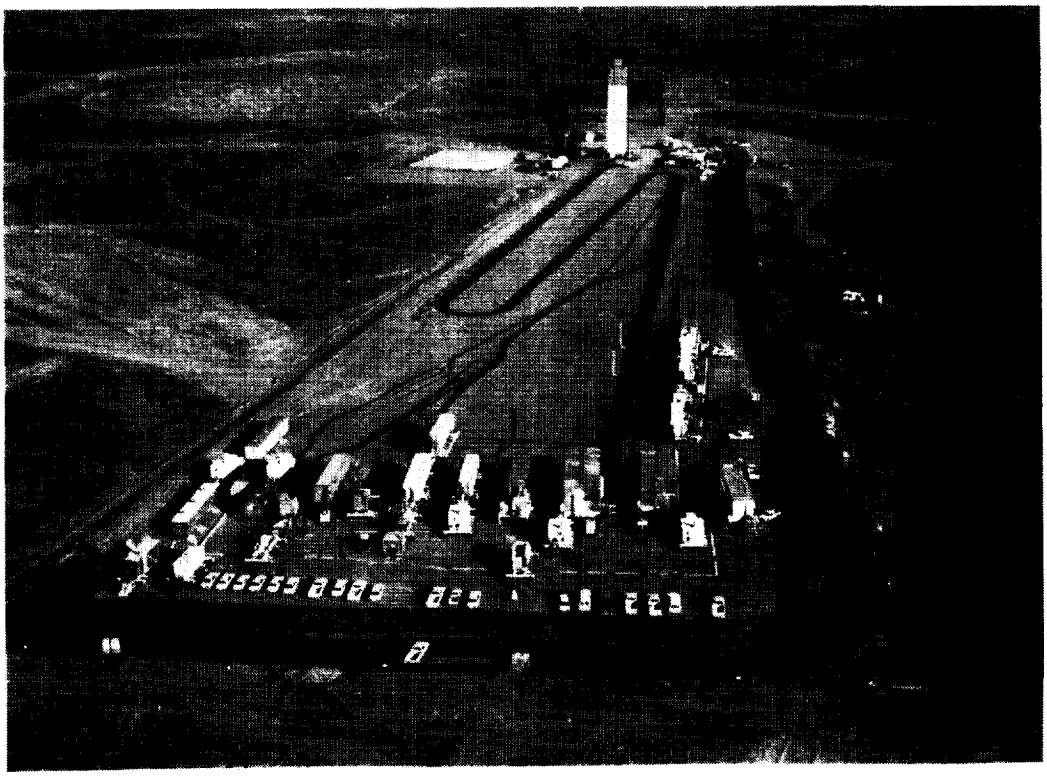

Fig. 6. Typical trailer park

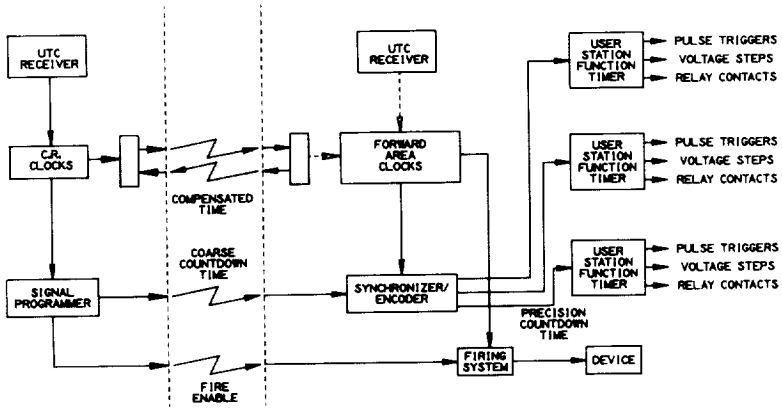

Fig. 7. Simplified system schematic

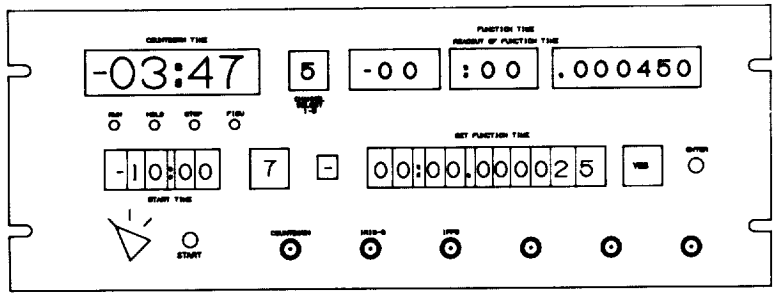

Fig. 8. Prototype user box panel

Naval Space Surveillance Center Uses of Time, Frequency and Phase

Carroll C. Hayden and Stephen H. Knowles
Naval Space Surveillance Center
Dahlgren, Va. 22448-5180

The Naval Space Surveillance Center (NAVSPASUR) is an operational naval command that has the mission of determining the location of all manmade objects in space and transmitting information on objects of interest to the fleet. NAVSPASUR operates a 217 MHz radar fence that has 9 transmitting and receiving stations deployed in a line across southern CONUS. This surveillance fence provides unalerted detection of all satellites overflying CONUS. NAVSPASUR also maintains a space catalog of all orbiting space objects, including payloads, rocket bodies and debris, and distributes information on satellite orbits to the fleet and other users by means of Navy tactical communication circuits and other means. NAVSPASUR plays an important role as operational alternate to the primary national Space Surveillance Center (SSC) and Space Defence Operations Center (SPADOC) located in Colorado Springs, Colorado. In executing these responsibilities, NAVSPASUR has need of precise and/or standardized time and frequency in a number of applications. These include maintenance of the radar fence references to specification, and coordination with other commands and agencies for data receipt and dissemination. Precise time and frequency must be maintained within each site to enable proper operation of the interferometry phasing technique used. Precise time-of-day clocking must exist between sites for proper intersite coordination. After 'time tags' are attached to the data at the receiver sites, proper referencing and standardization are necessary at the Dahlgren, Va. operations center to ensure proper data synchronization and communications with the fleet and other agencies.

Time as such is not required at the transmitters as presently configured because of the continuous wave (A0) modulation used. If possible plans to make the entire phase-coherent for VLBI operation are implemented, this requirement Time is required at the receiver sites with an accuracy at the millisecond level. The basic timing accuracy needed is controlled by satellite kinematics that result in a near-earth satellite velocity of about 7.5 kilometers per second. Planned sensor improvements are expected to result in an achievable sensor accuracy of about 50 meters. To avoid adding error the station timing should be at least 10X more precise. This results in a required timing accuracy of ± 0.5 millisecond for an equivalent position error of less than 5 meters. While this accuracy is well within the current state of the art, it is not achieved by the HF WWV receivers used at present. HF timing suffers from unreliable propagation and can have errors of several milliseconds. The planned installation of GPS timing will result in a timing accuracy more than sufficient for NAVSPASUR's needs.

Frequency is presently precisely controlled. Frequency at both transmitter sites (three) and receiver sites (six) is controlled by cesium beam frequency standards, which maintain the 216.980 MHz. carrier frequency and all local oscillators within ± 0.001 Hz. Spurious control on the transmitter emissions is -80 dBc or better.

Phase may be considered a derivative of time and frequency. Its control within each transmitter or receiver site is of great importance to NAVSPASUR because of the operation of the sensor as an interferometer system, with source direction angles as the primary observable. Determination of the angular position of a satellite is directly dependent on the accuracy with which the differential phase between spaced subarrays can be measured at each receiver site. Interferometer lobe width is about 11 arcminutes on the sky. The high signal to noise ratio for many satellites means that angular accuracies of 0.1 arcminutes or less can be achieved. This corresponds to a phase angle accuracy of about 2 degrees. Since one 217 MHz wavelength is equivalent to about 5 nanoseconds of time, a 2 degree phase accuracy requires about 25 picoseconds relative time control. Thus, NAVSPASUR has a requirement for very precise time control within the up to 2 mile confines of each site. If VLBI techniques are instituted in the future, between-sites phase control to this precision will also be necessary.

NAVSPASUR also attaches great importance to minimizing a quantity that may be called timeliness. Timeliness refers to the time interval required for processing and communication in analyzing and transmitting data to customers. While not customarily thought of as precise time, minimization of processing delays is of great importance to the utility of NAVSPASUR's perishable data product.

Figures 1 and 2 show simplified views of time/frequency/phase usage at NAVSPASUR receiver and transmitter sites. Installation of dual-frequency GPS receivers at all sites is planned. This will serve several purposes. It will eliminate the timing errors of up to 5 milliseconds that presently reduce accuracy on fence observations. It will allow better calibration and monitoring of the performance of our cesium beam frequency standards. It will allow a direct correction for the effect of the ionosphere, which causes a significant uncalibrateable refraction error in our measured direction angles at present.

Another important application of innovative technology is in the use of fiber-optics cables to provide within-site phase calibration. As mentioned above, NAVSPASUR requires maintenance of carrier phase to within ±25 picoseconds throughout each site over a wide variety of environmental conditions. The current technique, implemented when the radar system was first constructed 30+ years ago, uses air-dielectric coaxial calibration cables, and has proven unsatisfactory because of well-known coaxial cable stability deficiencies. This problem is especially crucial at our main Lake Kickapoo, Texas transmitter site, so a fiber optics calibration design was developed for installation there [1]. Although use of fiber optics for digital data transmission is well developed, phase-stable distribution of an analog signal required development of state- of-the-art techniques. The basic configuration of the fiber optics system is shown in Figure 3. The physical layout of the Kickapoo transmitter consists of a two-mile long array of dipoles, each with its own power amplifier. For control purposes, this array is divided into 18 bays. The phase calibration is applied at the bay level. The basic requirement for the fiber optics system is that it maintain a phase stability within ±2 degrees across all bays, over the expected range of environmental variations at this north Texas site. It must be reliable, easily maintainable and have an expected service life of at least 15 years. Several operating modes were considered, including active (closed loop phase compensation) and passive (open loop operator adjusted) and comparison at the central site or at each bay. The passive central site approach was chosen as providing adequate performance at minimum cost. It will utilize existing phase monitor and control equipment and software. A loose-tube single mode optical fiber manufactured by Siecor was chosen. Transmitters at each bay are temperature-controlled to minimize variations with temperature.

The above two projects are two items being undertaken as part of a comprehensive effort being undertaken under the direction of the Commanding Officer, Capt. H.W. Turner IV, to optimize the performance of our sensor . Figure 4 shows the overall plan. Emphasis is placed on utilizing in-house capability to the maximum extent possible. The overall plan includes emphases in improved communications with other sensor sites and users, on improved sensor electronics and on improved reliability/maintainability. Areas of particular importance to precision time/frequency/phase include improved use of time/frequency standards and improved site phase control. There are also several new initiatives being undertaken in the central operations center software that are of importance. These include optimization of the software used to reduce observations, compensation for the space environment, improvement of the propagator used for observation comparison, and an improved sensor performance monitoring system.

The present complex routine used to determine angular position, known as ADR, is being rewritten to provide proper time synchronization between sites used to form a triangulated position. This will eliminate a differential timing error that could result in the worst case in up to 50 milliseconds misalignment between observations. In addition, this rewrite will result in an optimized extraction of all possible information from each pass, and should result for the first time in significant single-pass capability for NAVSPASUR. Increased attention is also being paid to calibration of the system phases via software. We are using certain precision orbits that are seen by the fence on a regular basis to calibrate system constants including antenna separations and station parameters.

The ionosphere perturbs the apparent direction of arrival, especially near the horizon, by up to several arcminutes in a way that cannot be modeled well a priori. Use of dual-frequency GPS receivers should greatly reduce errors from this source. Use of calibration satellites with accurately known positions can also provide a somewhat less effective alternative.

The largest single error source for most low-altitude satellite orbits is the uncertainty in the atmospheric drag. NAVSPASUR is implementing a procedure using a Kalman filter sequential estimator technique for real-time measurement and compensation of this effect. This should result in significantly better performance and fewer lost satellites (UCTs), especially under worst case or solar storm conditions.

A final area of improvement is in the propagator used. NAVSPASUR presently uses an orbital propagator developed by Dirk Brouwer in 1959. This propagator has an expected accuracy of only about 500 meters for near-earth orbit. An improved propagator when installed should result in a significantly improved accuracy. Standardization of the propagators is an equally important issue. The surveillance community has suffered from the existence of different software at different installations that, while each capable of providing an adequate representation of the motion of a body, produce discordant results when using another group's elements. The United States Space Command (USSPACECOM) is presently undertaking an initiative to standardize these astrodynamic codes and constants, in which NAVSPASUR is participating. This work when completed should have significant impact on the precision GPS orbits used in much PTTI work.

These initiatives when fully implemented should result in an improvement in our observational accuracy from the present 400 meters nominal to a goal of between 50 and 100 meters.

In summary, time and frequency referencing will play a critical role in NAVSPASUR's meeting future operational requirements. NAVSPASUR is working together with other DoD organizations, including USSPACECOM, our parent Naval Space Command, SPAWAR, the Naval Observatory, the Naval Research Laboratory and other naval commands, as well as with such non-DoD groups

as NASA and the AIAA, to ensure optimum use of time, frequency and phase in engineering our system.

References

1. J. Webber and D.L. Thacker, *"Phase Distribution on Fiber Optic Cable"*, Proc. 21st Ann. P.T.T.I. meeting, 11/28-30/1989, Redondo Beach, Ca., p. 139

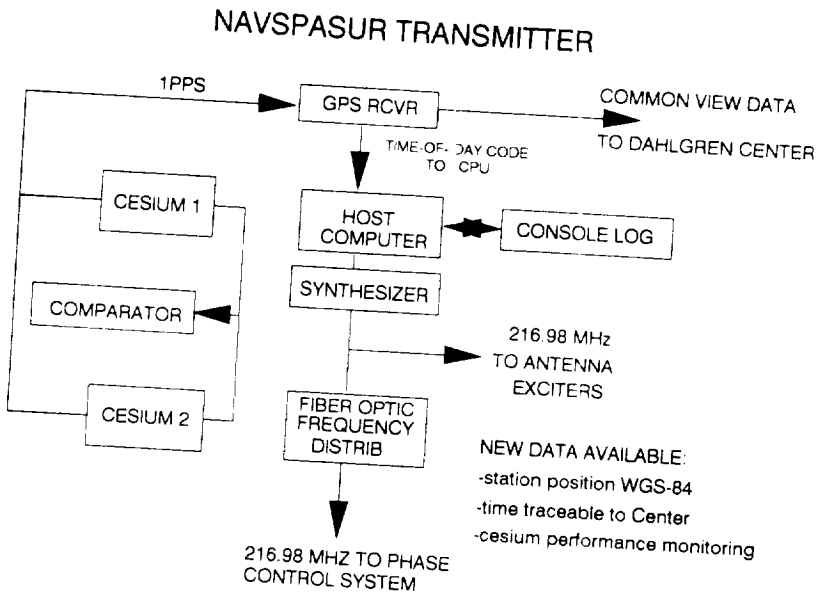

1 - Transmitter block diagram

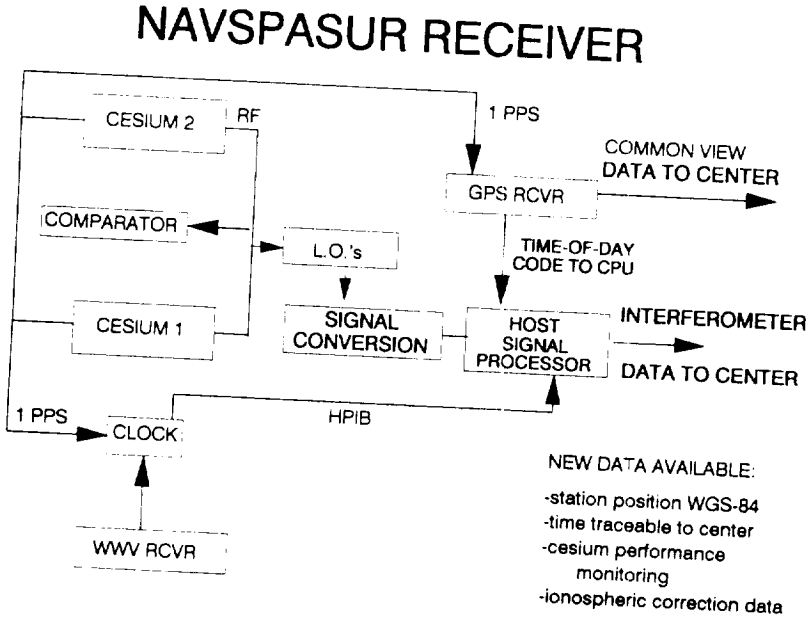

2 - Receiver block diagram

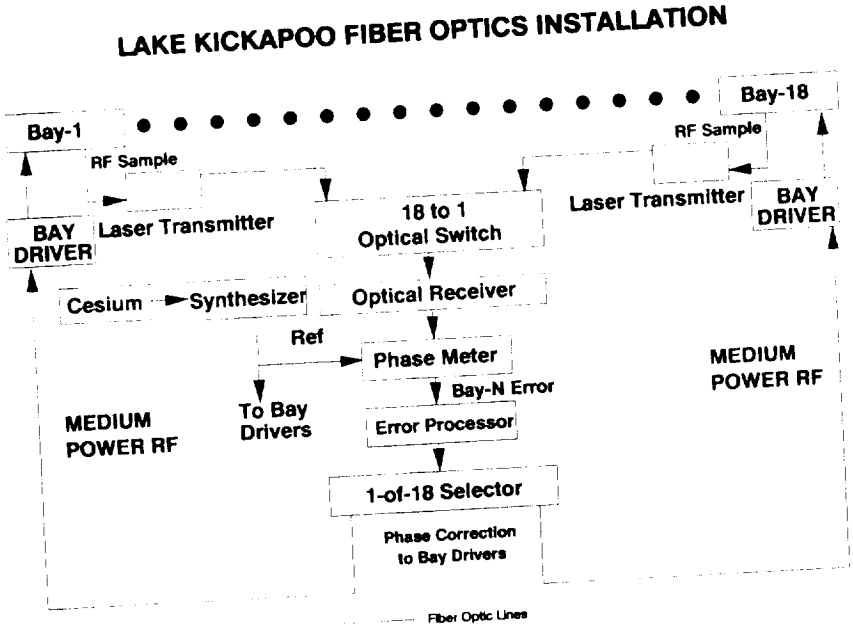

3 - Fiber optics block diagram

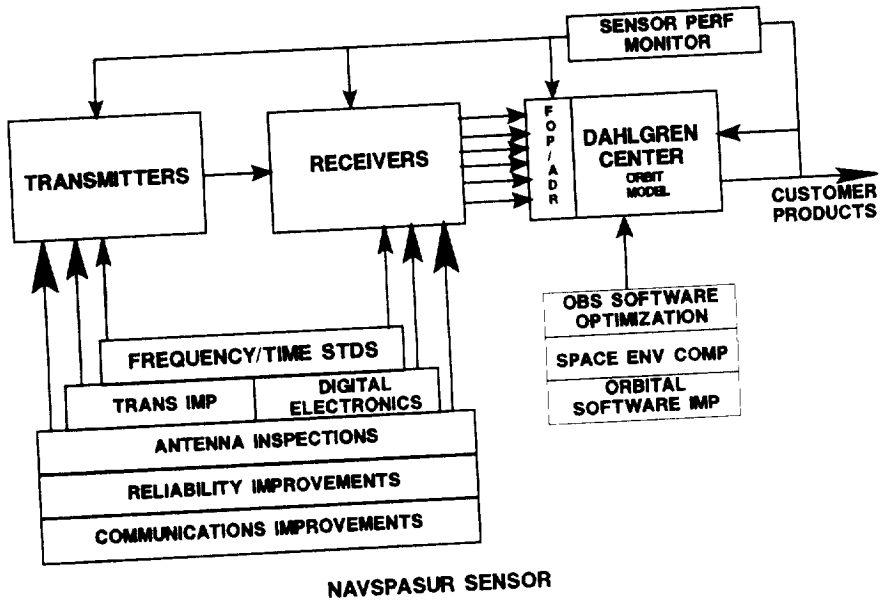

4 - NAVSPASUR sensor development plan

Precise Time and Time Interval Applications to Electric Power Systems

Robert E. Wilson
Department of Electrical Engineering University of Idaho Moscow, Idaho

Abstract

There are many applications of precise time and time interval (frequency) in operating modern electric power systems. Many generators and customer loads are operated in parallel. The reliable transfer of electrical power to the consumer partly depends on measuring power system frequency consistently in many locations. The internal oscillators in the widely dispersed frequency measuring units must be syntonized.

Elaborate protection and control systems guard the high voltage equipment from short and open circuits. For the highest reliability of electric service, engineers need to study all control system operations. Precise timekeeping networks aid in the analysis of power system operations by synchronizing the clocks on recording instruments. Utility engineers want to reproduce events that caused loss of service to customers. Precise timekeeping networks can synchronize protective relay test-sets.

For dependable electrical service, all generators and large motors must remain close to speed synchronism. The stable response of a power system to perturbations is critical to continuity of electrical service. Research shows that measure- ment of the power system state vector can aid in the monitoring and control of system stability.

If power system operators know that a lightning storm is approaching a critical transmission line or transformer, they can modify operating strategies. Knowledge of the location of a short circuit fault can speed the re-energizing of a transmission line. One fault location technique requires clocks synchronized to one microsecond (μs). Current research seeks to find out if one microsecond timekeeping can aid and improve power system control and operation.

I. INTRODUCTION

At previous meetings of this and other conferences, engineers and scientists have discussed precise time and time interval (PTTI) applications to electric power systems [1,2,3,4]. One application was the time synchronizing of recording instruments. The accuracy was 1 millisecond (ms) accuracy with respect to Coordinated Universal Time (UTC). One millisecond was the design goal because a recording instrument called a sequential events recorder (SER) had 1 ms resolution. Moderately priced "range timing" equipment developed for missile tracking was used without extensive changes [1,3].

Frequency plays an important role in power systems operations. Alternating current (AC) circuits transmit most of our electrical energy. There are two basic requirements for the successful operation of AC systems:

1. Large generators and (synchronous) motors must remain in close speed synchronism,
2. Voltages must be kept near their rated values [5].

A power system is a dynamic non-linear structure that uses feedback control to maintain these requirements. For example, a feedback loop regulates generator voltage by varying the voltage on the field winding [6]. A feedback technique called "net interchange tie line bias control" controls the balance between generation and consumption (load) over a utilities service area.

A closely related concept is the idea of power system stability. A power system is stable if, after a disturbance, the response is dampened and the system settles to a new operating condition in finite time [7]. Instability is when some generators lose speed synchronism and go "out-of-step." We will discuss this idea in a later section.

The electric power system of the United States, Canada and northern Baja California, Mexico is divided into nine regional reliability councils. Examples are the Electric Reliability Council of Texas (ERCOT) and the Western Systems Coordinating Council (WSCC). Through the North American Electric Reliability Council (NERC) these councils coordinate policy issues. One issue is the reliable operation of generation and transmission facilities and the adequacy and security of member electric systems [8].

A large interconnected power system is divided into many "control areas." Usually one utility operates a control area that serves a particular geographical region. During emergencies control areas share on-line standby generation (called "spinning reserve") [9]. The larger structure is called an inter-connection or grid. A disadvantage of an inter-connection is stability is harder to maintain [10].

The word "synchronize" has different meanings in different parts of this paper. Synchronous generators produce most electrical power and energy. Here synchronous refers to a particular type of electrical machinery. When we say generators must remain in synchronism for successful operation, we mean speed synchronism. Many applications discussed in this paper require accurate clock synchronizations. In this instance, we mean time synchronism.

II. MORE INFORMATION FOR POWER SYSTEM OPERATORS

Modern electric power systems use very high voltage to send large blocks of power over long distances. A lightning strike to an energized conductor causes a voltage impulse that usually jumps across the electrical insulation. Faulted pieces of equipment or transmission lines must be quickly isolated from all sources of power.

A protective relay is specialized equipment designed to detect short-circuit faults. When a relay detects a fault, it sends a signal to a power circuit breaker. A relay may be inactive for several years before having to respond to a power system fault. A transmission line relay may have to estimate the distance to a fault and decide if the fault is internal or external to the transmission line [11]. The time interval from fault inception to the opening of the PCB may have to be one or two electrical cycles to maintain system stability.

The protection system may mis-operate occasionally. These improper responses significantly affect

system operations and can lead to power system instability. Years could pass before engineers find errors in relay applications or settings. Records kept by NERC show that relay mis-operations play a large role in the major power system disturbances and blackouts [12].

The number of faults on a typical transmission line ranges from 1 every few years to 15 per year. Light beam or digital oscillographs record selected voltage and current waveshapes for later analysis [13]. Some protective relays can produce time synchronized event reports [14]. A millisecond timekeeping network can turn isolated recorders and relays into a system-wide analysis tool. Many utilities have wisely synchronized to UTC so any recorded event can be related to any other time-tagged event.

Information from a digital oscillograph, a SER, and relays in some cases can be remotely retrieved and processed in a "master station" [15]. It is my experience that the master stations do not synchronize the recording instruments. Recording systems need a separate timekeeping network.

Information about lightning activity can aid system operation. If a lightning storm is raging near a critical transmission line or substation, the system operators may start contingency measures. The amount of power transported along a key transmission line may be decreased. Say a lightning strike was detected near a transmission line at about the same time the protection system de-energized the line. With this information the control system or power system operator could quickly reenergize this line (see the section on fault location).

One commercial lightning detection network uses a time of arrival technique. Time synchronization is presently by LORAN-C. The network may use GPS in the future [16]. Orville and Songster [17] discuss a lightning detection network developed by the State University of New York at Buffalo.

III. POWER SYSTEMS OPERATIONS

The measurement of power system frequency plays an important role in the operation of an inter-connected system. At the 1986 PTTI meeting Dr. Giles Missout pointed out that electric utilities operate the largest frequency dissemination system. As shown on Table 1 the accuracy of this frequency has been decreasing. The reason for this is economic. When the power system frequency can vary within wider bounds, the power output of large generators do not have to changed as often. Steady power output is the most efficient operating mode for thermal generation plants.

System frequency is a sensitive indicator of the health of the power system. Frequency reflects the balance between real (active) power generation and consumption [6]. Frequency measurements between different control areas need to be accurate and syntonized.

An instrument called a power system time and frequency monitor measures four quantities: standard frequency, standard time (UTC), power system frequency, and power system time. Time error is the difference between UTC and power system time. To standardize measurements the historical source of standard time and frequency synchronization has been low frequency radio station WWVB [18]. A utility can now purchase equipment that uses WWVB, GOES, OMEGA or GPS for synchronization.

Operators control the frequency of the power grid to roughly ± 0.05 Hz of the nominal frequency. Beyond good operating practice, there is no formal requirement on frequency deviation. Operators monitor time error, the integral of frequency deviation and corrected over a longer period. Table 1 lists acceptable time errors within three different North American inter-connections [19].

TABLE 1. Time Error Correction Practices.

Time Error	Time of Day	Initiation			Termination		
SLOW	0000-0400	-4	-2	-3	0	±0.5	±0.5
	0400-2000	-8	-2	-3	-4	±0.5	±0.5
	2000-2400	-4	-2	-3	0	±0.5	±0.5
FAST	0000-0400	+8	+4	+3	+4	±0.5	±0.5
	0400-1200	+4	+2	+3	0	±0.5	±0.5
	1200-1700	+8	+2	+3	+4	±0.5	±0.5
	1700-2000	+4	+2	+3	0	±0.5	±0.5
	2000-2400	+8	+2	+3	+4	±0.5	±0.5

Note: The entries refer to Eastern US, Western US and Texas

Within an interconnection one control area acts as timekeeper. Periodically the timekeeper transmits its measured time error so other control areas can reset their measurements. When the time error exceeds the listed amount the timekeeper directs all members of the interconnection to raise or lower the "scheduled" system frequency. The entire interconnection is then operated at this higher or lower frequency. System frequency is returned to 60 Hz when the time error is reduced to the values shown on Table 1.

IV. POWER SYSTEM CONTROL

Many power systems are operated in an "open loop" manner. For an example, assume that lightning strikes a transmission line that is not automatically reclosed. The protective relays will detect the fault and trip the power circuit breakers. These events are displayed at a centralized control center. If there is no sign of trouble, a power system operator closes the power circuit breakers to return the line to service. The time interval is typically one-half to two minutes. This procedure has worked well for slowly changing system events.

Present power system protection is divided into discrete and slightly overlapping domains of measurement and control called zones of protection. Equipment assigned to one zone of protection is mostly unaware of events outside that zone. The state of the power system can change, but preprogrammed settings fix the response of most relays. Changing the settings on an electromechanical relay is a multi-hour task.

Modern microprocessor based relays offer new possibilities. Through communications ports, relays can have their settings changed in response to changes in the high voltage system. This is called "adaptive" relaying **[20,21]**. Nested in the idea of adaptive relaying is the move toward a hierarchy of control and protection equipment. The digital relay communicates with computers that monitor and control the entire substation. In turn, the substation computer communicates with another computer at the dispatch or control center.

Stability The thermal capacity of the conductors is usually not the limiting factor for the power that can be sent over a transmission line. Often the limiting factor is power system stability. Above a certain level, any additional transmitted power causes some generators to loose speed synchronism and go "out of step." Protective equipment would remove these generators from service, possibly

causing an imbalance between generation and consumption. Loss of generation in one control area could cause an overload on a transmission line or transformer. Soon the relays may remove this equipment from service possibly leading to a blackout [22].

There is a limit to the dynamic performance of an isolated protective relay that uses local information only. Hansen and Dalpiaz point out:

> ...it seemed that with each new line installation, the task of coordinating the OOS (out-of-step) relays grew more difficult. This difficulty was eventually found to stem from a fundamental problem: OOS relaying (or any other impedance based relaying) is not always the best tool for instability protection, but it is usually the most convenient. Often OOS relaying is adequate, but as a power system grows more complex, OOS relaying's weakness is revealed. This weakness is that, being impedance based, OOS relaying is "line oriented" rather than "system oriented". And instability problems in a power system are really system problems. [23]

These researchers found that the fastest and most global indicators of imminent power system instability are: voltage phase angles, power flow through key lines or units, voltage magnitude, network status, and time [24]. We will discuss voltage phase angles shortly.

In addition to the work just discussed, other researchers are using PTTI techniques for stability enhancement. An out-of-step relaying system that uses the utility's digital communications system for synchronizing voltage sampling has recently been reported [25]. The level of synchronization is that of the digital communications system, 50 μs. At the recent Power Engineering Society Summer Power Meeting several engineers from France discussed a new loss of synchronism system. As with similar systems, the objective is to isolate the fault and prevent propagation of the disturbance. They built several "phasemeters" synchronized by a GPS receivers. The system is presently experimental with the first portion going into service in 1994 [26]. There are reports of similar work in mainland China and the island of Taiwan.

State Vectors and Estimators A state vector shows the actual condition or state of a system. The complex voltages of all substation busses are the state vectors of the power system. Complex voltage means the magnitude and the relative phase angle of that voltage with respect to a system-wide reference. The present practice in many control centers is to calculate the voltage angles from other measurements. This is called state estimation. The purpose of state estimation is primarily to detect, identify, and correct gross measurement errors and to compute a good estimate of the voltage angles. Knowledge of the state vector helps in evaluating power system security. The disadvantage to state estimation is the time interval required to compute the phase angles. The state vector is not available in "real-time."

Measuring voltage magnitude is routine but measuring the voltage phase angle is more difficult [27]. The phase angle is measured by comparing the zero crossings of the voltage waveform with a system-wide reference time marker. See Figure 1 for a conceptual explanation. A better method is to measure the positive sequence voltage [28]. One electrical degree of the 60 Hertz waveform equals about 46 μs. Across short transmission lines (less than 50 km), measurements may need to be made to 0.1 electrical degree. This translates to a clock synchronization of roughly 5 μs [29].

Fault Location Operators can use knowledge of the relative location of transmission line short circuit faults to improve system control. Most line faults are temporary and rapid circuit breaker reclosing usually can help maintain system stability. However, rapid circuit breaker reclosing presents a risk to stability and fault location techniques can lower this risk.

Immediately after a fault some generators may be oscillating relative to a 60 (or 50) Hz frame of reference. Reclosing a breaker into a nearby permanent fault may further perturb some generators and lead to instability. Generally the risk of instability decreases as the distance between generation and the fault increases. If the location of the fault is accurately known, the control system or the operator can make better re-closing decisions. If the fault is permanent, line maintenance crews can go to the exact location.

Either "time domain" or impedance techniques can locate transmission line faults [**30,31**]. As discussed by M. Street at the 1990 PTTI meeting, time domain techniques need microsecond clock synchronizations [**32**]. Please see Figure 2. Fault-induced waves travel at the speed of light, 300 meters per microsecond. By time-tagging the arrival of fault-induced pulses at each end of the transmission line to within one microsecond, the fault can be located to within 300 meters. Three hundred meters is the typical tower spacing on a high voltage transmission line. Time domain techniques must be used on lines with series compensation. On the other hand, impedance techniques are accurate to about 1 or 2 % of the length of a line or roughly one kilometer, whichever is larger [**30**]. This is true for 90% of all faults.

Protective Relay Testing It has long been the relay engineer's desire to test the protection system under conditions that are as close to actual conditions as possible. When a critical transmission line falsely trips, engineers need to find the reasons for this mis-operation. A good method of analysis would be to retest the whole protection scheme with a recorded reenactment of the fault or disturbance that produced the problem. Field testing based on either a recording or a computer generated simulation requires a means to synchronize the test signals. In this application, the needed synchronization may be 10 μs [**33**].

V. WHAT T&F SERVICES DO UTILITIES USE?

Radio station WWVB has been a popular source of time and frequency information at the utility control center. Receiver specifications of 1 ms on equipment suggests that WWVB would be a good source for oscillograph and SER synchronization at the substations. Wright reported on one utility in Colorado successfully constructing a disturbance recorder synchronization system using WWVB [**34**]. WWVB receivers were less expensive than other alternatives and worked well in substations and power plants.

Other utilities have experienced difficulties receiving WWVB. Burnett reported reception problems in the state of Georgia [**1**] where the receiver lost the signal twice daily at local sunrise and sunset. Corona and other substation generated noise made reception difficult. Missout experienced similar difficulties in Quebec, Canada [**35**]. In some cases United Kingdom station MSF, which also transmits on 60 kilohertz, produces interference.

LORAN-C promises microsecond timekeeping. Burnett reported unsatisfactory reception by a portable automatic receiver in a 500 kilo-volt substation. On the other hand, he used LORAN-C at the utility control center [**1**]. Missout temporarily used LORAN-C for manually synchronizing a phase angle measuring system [**36**]. An informal survey has produced no known LORAN-C substation usage.

In 1981 Missout experimented with using the GOES system in a phase angle measurement system. The requirement was for clock synchronization of 40 μs [37] but the GOES system proved unsatisfactory [**38**].

Burnett used a centralized approach to timekeeping for most of his timekeeping needs [1]. In this approach, UTC is received at the control center then a serial time code is broadcast over a utility voice-grade microwave radio channel. At the substations, time code generators correct for propagation delay. Where a utility microwave radio channel was not available, GOES clocks were installed. The difference between a GOES clock and a substation time code generator recorder was at most 500 μs [39]. I constructed a similar system [3].

For their work on stability assessment and global relaying, Hansen and Dalpiaz initially selected the GOES system for synchronization [40]. Here the required level of synchronization between clocks was one electrical degree of 60 Hz (46 μs). Clocks were synchronized via the "common view" mode. GPS clocks will replace the GOES equipment for the substation encoders. For time tagging of disturbances, the centrally located master decoder was synchronized to UTC via GOES equipment.

Arun Phadke, who spoke at the 1990 PTTI meting, is using GPS clocks to synchronize digital sampling between different sites [41]. Two measurement systems under development were tested in a laboratory experiment [42]. The Bonneville Power Administration, U.S. Department of Energy, has installed several GPS clocks for phase angle measurement using a encoding system developed by Phadke. Data are telemetered back from several substations to the control center for project evaluation. Please refer to the paper by Ken Martin in these Proceedings.

VII. CONCLUSIONS

The accuracy requirements of the power industry are relatively modest when compared with other applications. An important consideration is the continuity and availability of any time and frequency broadcast service. For power system operations all components must be available always.

Table 2 Summary of Applications

Application	Accuracy	Source
Time & Frequency Monitor	1 ms & 1 E 5	WWVB, GOES, GPS
Recording Instruments SERs & Oscillographs	1 ms	GOES or utility system
Relay Test-Sets	10-20 μ	GPS
Phase Angles & Phasemeter	4.6-46 μs	GPS
Short-Circuit Fault Location	1.0 μs	GPS or custom

A major advantage to satellite based timekeeping is saving of limited bandwidth on the utility microwave radio communications network. The communications network will be needed for moving data between the control centers and the substations. If the timekeeping network or the communications fails, the control system must revert to a secure operating mode. Some of the futuristic concepts discussed here are for the very high voltage transmission systems that are the "super highways" of our power systems. It is unlikely that you will see GPS synchronized measuring units in lower voltage substations.

Standardized frequency measurements and millisecond time-keeping is a proven and accepted part of operating many electric utilities. Fault location is gaining acceptance as a valuable tool. At

the present, the estimated distance to the fault is displayed but not programmed into automatic control schemes.

Think Green! That was one message I took away from the IEEE Power Engineering Society (PES) Summer Meeting. The message was the health of our planet is becoming more important to the consuming public. At the Student-Faculty-Industry Luncheon Mr. Bernie Palk of the Los Angeles Department of Water and Power pointed out that:

> "The dominant mind-set of our industry for the previous three decades has been growth-oriented. How much new (generator and transmission line) capacity will we need, and when will we need it? Today the question is more likely to be, how can we stretch the capacity we've got?"

Valid environmental, financial and biological concerns, make new high voltage transmission lines difficult to build. On the other hand, society is demanding more electrical energy. One possibility is that the advanced control techniques discussed here will allow heavier usage of the existing transmission system. An issue is whether this can be done without any real loss of reliability. If there is an incremental loss in reliability, will the utility industry and society accept this loss of reliability in exchange for fewer new transmission lines?

REFERENCES

1. R.O. Burnett, Jr. *"Field Experience With Absolute Time Synchronization Between Remotely Located Fault Recorders and Sequence of Events Recorders,"* IEEE Trans. on Power Apparatus and Systems, vol. PAS-103, July 1984, pp. 1739-1742.

2. G. Missout, J. Bèland, G. Bèdard, P. Bussières, *"Study of Time Dissemination Methods Used on an Electric Power System With Particular Reference to Hydro-Quebec,"* IEEE Trans. on PAS, Vol. PAS-102, No. 4, April 1984, pp. 861-868.

3. R.E. Wilson, *"Uses of Precise Time and Frequency in Power Systems,"* IEEE Special Issue on Time and Frequency, Vol. 79, No. 7, July 1991, pp. 1009-1018.

4. P. Bonanomi, *"Phase Angle Measurements with Synchronized Clocks - Principle and Applications,"* IEEE Transactions on Power Apparatus and Systems, vol. PAS-100, No. 12, December 1981, pp. 5036-5043

5. T.J.E. Miller, *"The Theory of Steady State Reactive Power Control in Electric Transmission Systems,"* in Reactive Power Control in Electric Systems, T.J.E.Miller, Ed., New York, NY; Wiley-InterScience, 1982, pp. 52-54.

6. O.I. Elgerd, Electric Energy Systems Theory: An Introduction, New York, NY; McGraw-Hill, 1971, pp. 57-64.

7. P.M. Anderson, A.A. Fouad, Power System Control and Stability, Ames, IA; Iowa State University Press, 1977, pp.5-7.

8. North American Electric Reliability Council, 1989 System Disturbances, Princeton, NJ, August 1990.

9. N. Cohn, Control of Generation and Power Flow on Interconnected Power Systems, New York, NY; J. Wiley & Sons, 1961, p.3.

10. R.T. Byerly, E.W. Kimbark, Eds., Stability of Large Electric Power Systems, New York, NY; IEEE Press, p. 2.

11. J.L. Blackburn, Protective Relaying - Principle and Applications, New York, NY; Marcel Dekker, 1987.

12. North American Electric Reliability Council, 1983, 1984, 1985, 1989 System Disturbances, Princeton, NJ; 1984, 1985, 1986, 1990 (four reports).

13. E.A. Taylor, *"Fault Recorders and Power System Transients - Some Case Studies,"* Utility Fault and Disturbance Analysis Conference, Denver, CO, October 8-9, 1989.

14. J. Roberts, E.O. Schweitzer, III, *"Analysis of Event Reports,"* Western Protective Relay Conference, Spokane, WA, October 24-26, 1989.

15. L.E. Smith, *"The Remote Acquisition and Analyzation of Power System Disturbance Data,"* Utility Fault and Disturbance Analysis Conference, Denver, Colorado, October 30-31, 1986.

16. Atmospheric Research Systems, Inc., *"Accurate National Lightning Information,"* Palm Bay, FL, 1991.

17. R. Orville, H. Songster, *"The East Coast Lightning Detection Network,"* IEEE Trans. on Power Delivery, Vol. PWRD-2, No. 3, July 1987, pp. 899-907.

18. N. Cohn, *"Power Systems-Time and Frequency,"* Leeds and Northrup Technical Journal, No. 7, Fall 1969, pp. 3-11.

19. North American Electric Reliability Council, *"Appendix to Operating Guide 1.C.-Time Error Correction Procedures,"* Princeton, NJ, February 1, 1990.

20. A.G. Phadke, J.S. Thorp, S.H. Horowitz, *"Impact of Adaptive Protection on Power System Control,"* Proceedings of the Ninth Power System Computation Conference, Lisbon, Portugal, August 1987.

21. G.D. Rockefeller, C.L. Wagner, J.R. Linders, K.L. Hicks, D.T. Rizy, *"Adaptive Transmission Relaying Concepts for Improved Performance,"* IEEE Trans. on Power Delivery, vol. 3, no. 4, October 1988, pp. 1446-1458.

22. L.M. Olmstead, W.D. Brown, J. Bleiweis, *"The Blackout: It All Happened in 12 Minutes,"* Electrical World, January 24, 1966, pp.67-73.

23. D.J. Hansen, *"Real Time Digital Encoding and Telemetry of Key Power System Transient Quantities,"* Western Protective Relay Conference, Spokane, WA, October 23-25, 1984.

24. D.J. Hansen, *"Recent Progress on Stability Margin Measurement,"* Second Conference on Precise Time and Frequency in Power Systems, Fort Collins, Colorado, September 28-29, 1987.

25. Y. Ohura, et. al., *"A Predictive Out-Of-Step Protection System Based on Observation of the Phase Difference Between Substations,"* IEEE Trans. on Power Delivery, Vol. 5, No. 4, November 1990, pp. 1695-1704.

26. Ph. Denys, C. Counan, L. Hossenlopp, C. Holweck, *"Measurement of Voltage Phase for the French Future Defense Plan Against Loss of Synchronism,"* IEEE PES Summer Meeting, San Diego, CA, July 28-August 1, 1991, paper 91 SM 353-3 PWRD.

27. G. Missout, J. Bèland, G. Bèdard, Y. Lafleur, *"Dynamic Measurement of the Absolute Voltage Angle on Long Transmission Lines,"* IEEE Trans. on Power Apparatus and Systems, Vol. PAS-100, No. 11, November 1981, pp. 4428-4434.

28. J.S. Thorp, A.G. Phadke, S.H. Horowitz, M.M. Begovic, *"Some Applications of Phasor Measurements to Adaptive Protection"*, IEEE Trans. on Power Systems, vol. 3, No. 2, pp. 791-798, May 1988.

29. R.E. Wilson, *"Timing Within the Western Area Power Administration,"* Eighteenth Annual Precise Time and Time Interval (PTTI) Applications and Planning Meeting, Washington, DC, December 2-4, 1986.

30. E.O. Schweitzer, III, *"A Review of Impedance Based Fault Locating Experience,"* Western Protective Relay Conference, Spokane, WA, October 25-27, 1988.

31. T.W. Stringfield, D.J. Marihart, R.F. Stevens, *"Fault Location Methods for Overhead Lines,"* AIEE Trans. Paper No. 57- 160, August 1957.

32. M.A. Street, *"Delivery and Applications of Precise Timing for a Traveling Wave Powerline Fault Locator System,"* 22md Annual Precise Time and Time Interval (PTTI) Applications and Planning Meeting, Vienna, VA, December 4-6, 1990, pp. 355-360.

33. J.A. Jodice, *"Time Synchronous End-to End Relay Testing,"* Second Conference on Precise Time and Frequency in Power Systems, Fort Collins, CO, September 28-29, 1987.

34. K. Wright, *"Synchronization Work at Public Service Company of Colorado,"* Second Conference on Precise Time and Frequency in Power Systems, Fort Collins, CO, September 28-29, 1987.

35. G. Missout, *"PTTI Applications in Power Utilities,"* Eighteenth Annual Precise Time and Time Interval Applications and Planning Meeting, Washington, DC, December 2-4, 1986.

36. G. Missout, P. Girard, *"Measurement of Bus Voltage Angle Between Montreal and Sept-Iles,"* IEEE Trans. on PAS, Vol. PAS-99, No. 2, March/April 1980, pp. 536-539.

37. G. Missout, J. Bèland, G. Bèdard, Y. Lafleur, *"Dynamic Measurement of the Absolute Voltage Angle on Long Transmission Lines,"* IEEE Trans. on PAS, Vol. PAS-100, No. 11, November 1981, pp. 4428-4434.

38. G. Missout, J. Bèland, P. Lebel, G. Bèdard, P. Bussières, *"Time Transfer by IRIG-B Time Code Via Dedicated Telephone Link,"* Thirteenth Annual Precise Time and Time Interval (PTTI) Applica- tions and Planning Meeting, Greenbelt, MD, December 2-4, 1980.

39. R.O. Burnett, Jr. *"Additional Developments With the Georgia Power Time Synchronizing Project for Fault Recorders and Sequence of Events Recorders,"* Second Conference on Precise Time and Frequency in Power Systems, Fort Collins, CO, September 28-29, 1987.

40. C.P. Dalpiaz, D. J. Hansen, *"High Rate Telemetry of System Voltage Phase Angle and Other Stability Related Quantities,"* IEEE Trans. on Power Systems, Vol. PWRS-1, No. 3, August 1986, pp. 202-206.

41. A.G. Phadke, M.M. Begovic, V.A. Centemo, V. Phamiraj, *"Clock Synchronization For Improved Monitoring, Protection and Control,"* Proc. High Technology in the Power Industry International Symposium, Scottsdale, AZ, March 1-4, 1988, pp. 9-13.

42. A.G. Phadke, *"Precise Synchronization of Phasor Measurements in Electric Power Systems,"* Twenty-Second Annual Precise Time and Time Interval (PTTI) Applications and Planning Meeting, Washington, DC, December 5-7, 1990.

Figure 1. Voltage Phase Angles

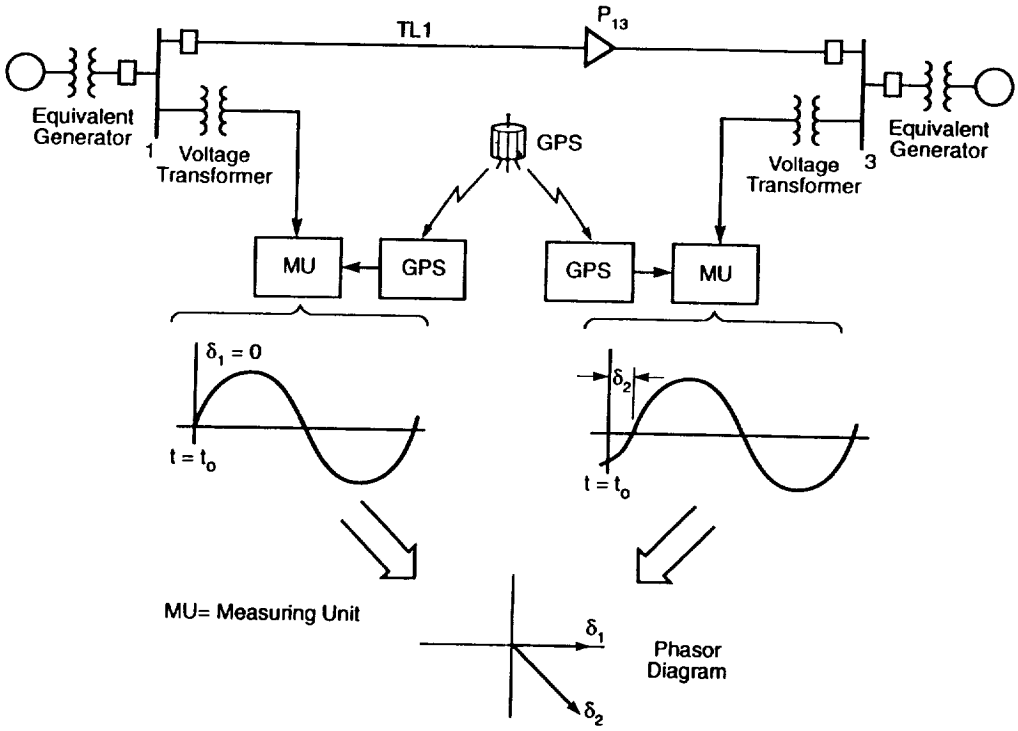

Figure 2. Fault Location

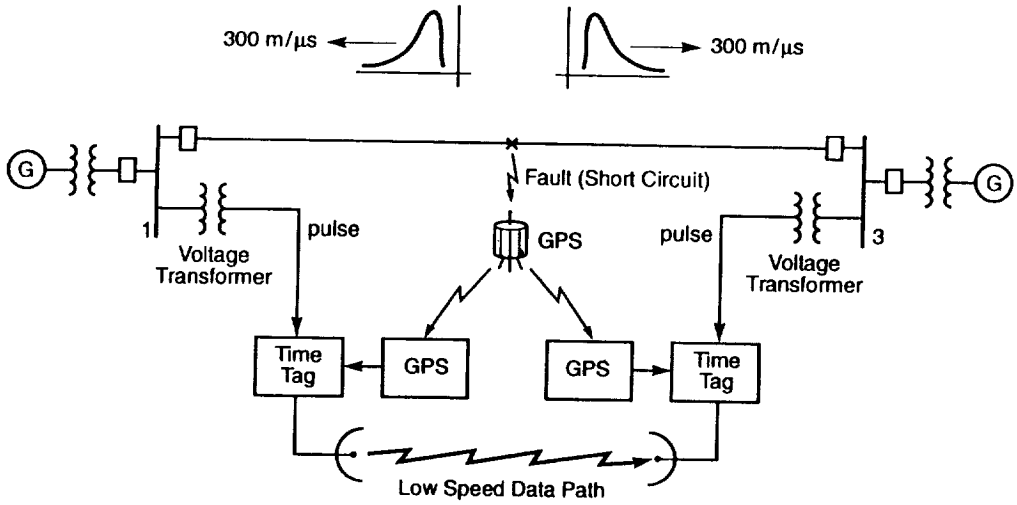

QUESTIONS AND ANSWERS

David Allan, NIST: If it would be of help, the Department of Transportation has a real time output of all lightning strikes across the United States.

Mr. Wilson: More and more utilities are seeing the usefulness of this data. It varies with region.

PRECISE TIME DISSEMINATION AND APPLICATIONS DEVELOPMENT ON THE BONNEVILLE POWER ADMINISTRATION SYSTEM

K.E.Martin and J.Esztergalyos
U.S.Department of Energy - Bonneville Power Administration
Division of Laboratories, PO Box 491
Vancouver, Washington 98666

Abstract

The Bonneville Power Administration (BPA) uses IRIG-B transmitted over microwave as its primary system time dissemination. Problems with accuracy and reliability have led to ongoing research into better methods. BPA has also developed and deployed a unique fault locator which uses precise clocks synchronized by a pulse over microwave. It automatically transmits the data to a central computer for analysis. A proposed system could combine fault location timing and time dissemination into a Global Position System (GPS) timing receiver and close the verification loop through a master station at the Dittmer Control Center. Such a system would have many advantages, including lower cost, higher reliability and wider industry support. Test results indicate GPS has sufficient accuracy and reliability for this and other current timing requirements including synchronous phase angle measurements. A phasor measurement system which provides phase angle has recently been tested with excellent results. Phase angle is a key parameter in power system control applications including dynamic braking, DC modulation, remedial action schemes, and system state estimation. Further research is required to determine the applications which can most effectively use real-time phase angle measurements and the best method to apply them.

Introduction

Electric power systems have evolved from a few generators connected to a load in a nearby city to vast interconnected networks with hundreds of generators and loads spanning half the country. Commensurately time synchronization has evolved from locally set ac clocks with second accuracy to microwave pulse and satellite signals with microsecond accuracy. Modern power systems require increasingly complex controls to maintain stability. Recent developments in time dissemination provide an opportunity for major advancements in power system control, protection, and operation. Precise time distributed over a large power system allows synchronous sampling of voltage and current for real-time power and phase measurements as well as accurate event recording and fault location. Precise time and phase angle will enhance the development of regional real-time control systems.

Time Dissemination

Early power system controls were based on power, current, and voltage measured at a terminal. Scheduling was handled by demand, and disturbances were localized enough that time synchronization was not required for analysis. As systems grew they became more complex and interconnected. Timing was required to coordinate scheduling and to compare disturbance recordings made across the system. Locally set ac clocks were adequate for the task in most cases, but created problems where distant clocks had been set several seconds apart.

In 1974, Bonneville Power Administration (BPA) commissioned the Dittmer Control Center in Vancouver, Washington, as the main dispatching and control center for the BPA system. A primary feature of the control center was the SCADA computer system to allow most of the system monitoring, switching, and control functions to be operated remotely. The Central Time System (CTS) synchronized to WWVB was installed as BPA's primary time source. Over the next decade time dissemination was extended throughout the system using IRIG-B over dedicated microwave channels.

The IRIG-B signal synchronized time throughout the system to at least tenths of a second 99 percent of the time. However, it was found phase slips in multiplex equipment and channel frequency response could cause enough distortion to make IRIG-B difficult to read, and noise could cause momentary interruptions. When recorded directly on an oscillograph, these impairments didn't cause much problem, but they played havoc with automatic decoding equipment. They caused time miscues that could be days off and take hours to resynchronize. In some locations automatic alarm recording equipment recorded pages of time errors. In addition, there were several BPA substations which didn't have direct microwave communications and needed accurate time.

GOES satellite receivers were installed at several sites in an attempt to solve both problems. Success was limited. They had trouble synchronizing, suffered from radio interference, and needed occasional antenna repointing. Time accuracy was no better than IRIG-B over the microwave although they did not need the millisecond delay corrections required for microwave transmission.

BPA has experimented with phase modulated IRIG-B and found it to be much more resistant to microwave impairments than the standard amplitude modulation. Since it is not available commercially and requires special encoding and decoding hardware, it has not been implemented. Consideration is being given to the whole spectrum of BPA's timing needs before developing a specialized system.

BPA is in the process of specifying a new CTS system for the Dittmer Control Center. GPS rather than WWVB will be used to acquire UTC time in order to achieve microsecond level synchronization. The system will employ triple redundant time generation for automatic switching and higher reliability. It will have an independent rubidium based clock for local verifiability and better local timekeeping in the event of GPS signal loss. The system will upgrade the central timekeeping capabilities to support all BPA system and Western region timing requirements for the foreseeable future.

Time Domain Fault Location

BPA has pioneered a unique system for locating power line faults (short circuits) using precise timing. When a fault occurs, the instantaneous change in potential creates a voltage wave that travels along the power line at nearly the speed of light. By precisely timing the arrival of the traveling waves at each end of a power line section, a simple formula yields the distance to fault from the end of the line **[1,2,3]**.

The original system, called Type B, had a master with a counter and several slaves that would relay the fault pulses to the master via microwave. The system was reasonably reliable, but could only be calibrated by known faults and needed to be interpolated by experienced personnel using information from past readings. The present version, called FLAR for Fault Location Acquisition Reporter, employs remote timetagging units with stable clocks at a number of substations [1]. The clocks are synchronized every 100 seconds by a phase shift keyed 2.3 MHz tone sent over the microwave. The remote units communicate over an automated data net with a master computer which retrieves these timetags, calculates the fault distances, and reports to system dispatching. This system has proven to be reliable and accurate for sites which can be linked by high frequency microwave communication. It is easy to use and is being improved with software to sort out good readings from the many generated by noise during a fault.

In 1989 the FLAR system was extended beyond the BPA microwave system by synchronizing the master with a GPS receiver. A GPS receiver installed at a substation can provide sync in place of the microwave transmitted pulse. The extension has worked well so far.

Requirements for a Combined System

The Western Systems Coordinating Council (WSCC) is a regional electric utility group which consists of 61 interconnected utilities west of the great plains from central British Columbia to Mexico. It has set a goal of 8 millisecond timing accuracy throughout the region. BPA has set its current requirement for 5 milliseconds maximum throughout its system, and 1 millisecond synchronization for all systems within a station.

Time domain fault location requires 1 microsecond synchronization throughout at least every area which might be reporting the same fault. Several other uses which have not been discussed yet are relaying, transient stability control, and state estimator. Relaying, which detects power line faults and controls the large power circuit breakers, optimally must be able to detect fault distance within 1000 meters to function correctly. Stability control and state estimation operate relative to the 60 Hz cycle which is 46 microseconds/electrical degree. These requirements are summarized in Table 1.

System Function	Measurement	Optimum Accuracy
Fault Locator	300 meters	1 microsecond
Relaying	1000 meters	3 microseconds
Transient Stability control	±1 degre	46 microseconds
State Estimator	±1 degree	46 microseconds
Oscillograph		1 millisecond
Event Recorder		1 millisecond

Table 1. Electrical Power System Precise Time Requirements

The most stringent accuracy requirement is fault location; any timing system with microsecond accuracy throughout the region will satisfy all the needs. Less obvious is the requirement for reliability and availability. Power systems are expected to operate all the time. Any control, protection, or monitoring system must be ready to operate reliably at any time. A timing system that operates reliably or produces the required accuracy 98 percent of the time is not acceptable. BPA currently

requires its control and communication systems to demonstrate a 99.986 percent availability for full performance operation. Any system with required outage times that cannot be scheduled into maintenance intervals (i.e., will fail occasionally at random times) is not acceptable. When systems fail the results can be dramatic–New York blackout of 1965–and destroy equipment worth millions of dollars.

IRIG-B sent over the microwave could achieve the 1 millisecond requirement using the phase modulation technique. Tests have demonstrated that it will never achieve 1 microsecond reliably, even with a steered oscillator. A Cesium oscillator at each station would achieve the required accuracy, but the necessary calibration and costs would be prohibitive.

GOES satellite receivers have proven to be not much better than IRIG-B sent over microwave. Radio signals such as WWVB do not give the required accuracy. Loran C is powerful in the Northwest and accurate but does not easily yield time.

The FLAR system has the accuracy and high reliability but only provides synchronization, not time of day. Incorporating time of day will require a major redesign of the hardware and software of the remote unit, an expensive and time consuming proposition. An additional shortcoming is its reliance on a direct high frequency microwave link which isn't available to all sites where BPA would like accurate time of day. It also is not available to neighboring utilities where synchronization may be desirable.

The GPS system can provide the 1 microsecond accuracy throughout the system. It is relatively new and has unproven reliability as far as BPA is concerned. However because it does offer such a great potential, BPA has purchased several receivers and has done extensive testing over the last 4 years. The advantages include good manufacturer support, less expensive, inherent delay compensation, no high frequency microwave requirement, better coordination with neighboring utilities, and an excellent system failure tolerance. The disadvantages are an imperfect receiver performance record to date, lack of knowledge of how the system will perform in a substation environment, and the uncertainty of Department of Defense policy. However recent results from GPS receiver testing have been excellent. That and policy statements by the Department of Defense have given enough confidence in the GPS system to propose a combined timing/fault locator system based on GPS.

Closed Loop Precise Time System

It has been proposed to install at each substation a GPS receiver with an IRIG-B output, a timetag option, and software that would allow it to communicate with the FLAR master. The receiver would provide precise time locally to the substation, timetag faults, and report times to the FLAR master. The master would additionally check the remote GPS time and operation. This system would eliminate the need for the high frequency microwave channel and several voice grade channels presently used to disseminate IRIG-B. It would replace the time code generator and FLAR remote unit with a single GPS receiver. Further advantages include:

a. **Manufacturer Support** The current FLAR system is BPA designed and supported. A proposed phase shift key modulated IRIG-B would also need to be designed for BPA. The proposed system would add only two options a basic GPS receiver produced by several manufacturers. The options are likely be used by many utilities, potentially making the configuration a standard piece of equipment.

b. **Less Expensive** At today's prices, the GPS receiver unit is competitive with the two remote units it would replace. With quantity production, and as GPS receiver technology improves, the cost would be less. Additional savings are realized by microwave capacity not used.

c. **Inherent Delay Compensation** The broadcast delay from the CTS to each substation has to be calculated and entered in each remote unit. BPA is in the process of implementing an alternate control center from which time code could alternately be broadcast, creating two different delays for each remote. Alternate path routing for catastrophic microwave system problems further complicate the problem. A GPS receiver outputs time corrected for its location.

d. **Closed Loop Verification** The present broadcast IRIG-B has no verification that the time is correct and the remote equipment is operating. FLAR is a closed loop system, reporting every 100 seconds any events and remote status. The proposed system would report GPS receiver health, oscillator status, and tracking information if required. It would also report local time to verify timekeeping within a millisecond. An additional timetag input can be added to receive broadcast FLAR sync pulses to verify timing to a microsecond. The master could also set the remote for daylight time changes and tracking schedules if needed. Verification of remote operation should remove much of the uncertainty of relying on a remote clock that receives its signals from tiny dots in space.

e. **Improved Inter-utility Synchronization** Even a precise central system can drift from a common reference (UTC); when it does, all nodes drift with it. If each substation is directly synchronized to the same source as all other utilities, the systems on the average will remain better synchronized at all times.

f. **Improved Systematic Reliability** While the centralized system broadcasts from a redundant CTS on a microwave system of very high reliability, there are common power sources, single wire interconnections, and combined signal paths. Any interruption of this long linked chain or error in time generation can cause multiple remote outages. GPS relies on multiple satellites, each individually timed with extensive built in redundancy. Incorrect control signals to the satellites could cause errors, but not likely with all satellites at once. Since several satellites are in view at all times, receivers can be designed with logic to ignore signals from a satellite with sudden changes or with excessive variance from the others in view. The GPS receiver itself uses an internal oscillator which is slaved and compared with the satellite signal. If the RF input fails for any reason, the internal time generation can carry the output accurately for some period of time. If the internal timekeeping generates an error, it can be corrected from the GPS signal. Communication failure interrupts fault reporting and verification, not time. Catastrophic failure of any station does not affect the timing at any other station.

A test program is planned to deploy several units with the required software and three timetag inputs, one for faults, one to mark the operation of the station oscillograph and the other to time the arrival of the sync pulse. The oscillograph will typically only trigger on significant disturbances, so the FLAR master uses its trigger to sort possible faults from the many timetags due to noise and switching. Timing the sync pulse will allow long term monitoring of performance to the highest accuracy level. The test program will allow BPA to develop a longer term performance and reliability record.

Precise Time and Phase Measurement R & D at BPA

GPS Receiver Testing

In conjunction with the Phasor R & D program, BPA has tested GPS receivers for use in timing on the BPA system. Since continuous accuracy is the main concern, testing has focused on long term monitoring of the output. In most GPS receivers a 1 Pulse Per Second (1 PPS) signal provides internal sync for all other timekeeping signals, so it provides a simple reference for monitoring overall performance. The 1 PPS output was compared against a 1 PPS signal generated locally by a Cesium reference standard. Originally only the average between the two sources was measured and computed periodically. It was found that unlike an oscillator, the GPS derived signal could make sudden jumps to another value for one to many seconds and then snap back. Testing was expanded to monitor the 1 PPS signal every second for jumps as well as take 100 second averages every 15 minutes. A 100 second average provides reasonable noise smoothing that fits in well with the 15 minute interval, though it may not provide the best sigma tau variance.

In the last 6 years we have seen receivers improve from units that kept time within several microseconds only 95 percent of the time to units that typically keep tenths of microsecond accuracy 99.9 percent of the time with less than 3 microsecond deviation at any time. The improvement is partly due to better satellite coverage but mostly due to receiver technology development. Performance at the present level is quite acceptable to BPA. Figure 1 is a 2 week plot of the 100 second averages comparing GPS with Cesium. The drift of 1.6E-12 of the Cesium standard relative to UTC is left in the plot so the curves for each week don't overlap.

We have also compared a GPS receiver installed at the Malin Substation with the FLAR sync pulse received at that site. Malin is in southern Oregon on the California border and about 260 air miles from the Dittmer Control Center. The sync pulse delay time was measured by transmitting the signal from Dittmer, re-transmitting it back, and measuring the round trip time. An average of 400 measurements was divided by two to estimate a one way transit time of 1689.3 microseconds. Since the FLAR master at Dittmer is now synchronized by GPS, it is easy test the one way transit time with a GPS receiver at Malin. The transit time averaged over 15 minute intervals is around 1691.3 microseconds, very close to the previously calculated time (Figure 2). The 2 microsecond difference was constant over the 5 month monitoring interval and has not been investigated, but is probably due to additional cable and transmitter equipment at Dittmer and differences in microwave system filter tuning. The effects of the microwave system and GPS receivers cannot be separated in this data, but even combined they are within an acceptable performance level for the FLAR system.

While the averaged data only varied around 300 nanoseconds from the mean, of greater concern is the worst case performance. Figure 3 is a plot of the span between the maximum and minimum measured during the interval. The time interval counter used in this test only has a 100 nanosecond resolution so the plots appear rather quantized. The fact the difference is always less than 1.5 microseconds is amazing, considering the plot combines the effects of two GPS receivers 260 miles apart and the microwave communications in between.

Synchronous Phase Angle Measurements R & D Program

BPA installed a prototype Synchronous Phasor Measurement System developed by the Department of Electrical Engineering at Virginia Polytechnic Institute and State University in Blacksburg, Virginia on BPA's 500 kVAC Pacific Northwest-Southwest (PNW-SW) Intertie. The system consists of a remote terminal installed at John Day and Malin Substations (about 250 miles apart) and a master terminal

at the BPA Laboratories in Vancouver, Washington. The two remote terminals are synchronized by GPS receivers.

A remote unit is a microcomputer with a A/D and serial interfaces. Three phase power line waveforms are synchronously digitized at a 720 sample/second rate, clocked directly by a precisely timed signal from the GPS receiver. After each sample, the latest 12 samples are filtered with a Fourier transform to extract the 60 Hz component and converted with the symmetrical component transformation to yield the complex positive sequence phasor. This phasor represents the magnitude and phase of a balanced three phase system and is a good representation of the state of a real power system in all but extreme fault conditions. Since each phasor is computed with 12 samples, it gives a true 60 Hz response to changes. The precise timing makes data comparable for accurate phase angle determination over a region of any size [7,8].

In addition to calculating phasors, the remote also computes frequency and rate of change of frequency. It monitors the computed data for sudden changes and flags any that go beyond preset limits. It will communicate these values to the master terminal on demand either as a stored table or a real time data flow.

In this test, data was gathered from the real time data flow using 4800 BPS modems over the BPA microwave system. Data was transmitted at 12 Hz (every 60th sample) in order to fit into the protocol and data rate. The master monitored the disturbance flags and saved a 3 minute table of raw data (including 30 seconds of preflag data) whenever a flag was detected. The master also computed continuous statistics from the data and recorded it every 15 minutes. The test system diagram is shown in Figure 4.

Phasor System Test Results

The purpose of the test program was both to evaluate the phasor measurement system and to provide operational information on the GPS receivers used for the precise time source. The system has been fully operational since September, 1990, and 8 months of continuous data has been recorded for analysis.

The system has performed very well. In 2 years of field of deployment there has only been one hard failure in a GPS receiver and none in the phasor remote units. Data communications has less than a 1 percent error rate. The phasor data appears to have a better response with greater accuracy and less noise than comparable analog telemetered data. The final test results are now being analyzed with a report to follow in 1992.

A sample disturbance records a bus fault at the WNP-2 plant near Richland, Washington, followed by a loss of 1094 MW of generation at 10:10:55 on December 7, 1990. A sharp voltage dip is seen at both John Day and Malin during the fault (about 30 milliseconds duration). It is followed by a voltage rise and decrease in phase angle between John Day and Malin which accompanies the drop in power transfer. The frequency traces from the two stations are nearly identical; the squared appearance is due to the algorithm being used at the time which takes longer averages to improve accuracy near 60 Hz. The system gradually approaches its old operating point during the 2 minutes following the fault.

Future Applications of Precise Time and Phase Angle Measurements

Precise timing enables implementation of event time-tagging, fault location, and the synchronous measurements of key transient stability indicators such as voltage phase angle in near real time. These measurement techniques enable the development of new protection and control schemes, some of which are described in the following paragraphs.

Stability Control Schemes

The aim of stability control schemes is to prevent unnecessary shutdown of generators, loss of load, separation of the power grid, and avoid blackouts and damage to power system equipment. Control schemes accomplish this by a graduated response to system disturbances which only take effect when the disturbance is significant enough to endanger overall system stability. When a disturbance is great enough to cause generators to go out-of-step, the frequency to become unstable, or the voltage to collapse, controls respond with appropriate remedial measures such as dynamic braking, generator dropping, load shedding, and finally controlled islanding.

Existing control schemes within the WSCC service area are Type A high speed actions based on a worst case scenario and Type B which takes slower corrective action after an event. Type A controls tend to take excessive action and can only respond to preprogrammed events. Type B tend to be too little or too late to prevent system problems to propagate as they would with no control action.

Future stability control systems based on digital phase measurement can offer significant advantages over the systems currently employed. Phase measurements could be combined with Type A high-speed control logic to compute an appropriate proportional response and be substituted for Type B for longer term control actions. During a major system disturbance, control computers can sort and process synchronous field data to compute a response appropriate to the current system operating conditions. Within a few cycles from the beginning of the disturbance, they can provide an output response to the disturbance. If this initial high-speed action doesn't stabilize the system, further Type B actions could be taken to taken to correct it. Considerable long range R & D is required to assess the feasibility of such systems and develop and verify the necessary strategies, hardware, and software.

HVDC Modulation

HVDC systems are powerful tools for improving the transient and dynamic stability of AC power systems. In contrast to an AC line, the power transfer over a DC link does not depend on the voltage phase-angle between the ends of the line and can be quickly changed independently from other system parameters. The control may be continuous in nature, using feedback variables, or it may be discrete, consisting of predetermined changes in DC power. Voltage phase angle between stations in the AC system are powerful input parameters for this type of control. The first swing (transient) stability can be improved by using a voltage phase angle measurement on an AC line to modulate the parallel HVDC link. Damping of oscillations in the AC grid can also be achieved by using the rate of change of voltage phase angle as an input to the DC Link control.

Dynamic Braking

When a power line fault occurs, the current is shorted back to the generator bypassing the load. Since power system equipment is mostly inductive rather than resistive, it absorbs little energy, so the driving force tends to accelerate the generators. In North-central Washington BPA has a 1400 MW resistor which serves as a dynamic brake for the many large hydro generators in the area. It is used to prevent AC system separation by burning up excess kinetic energy from system generators. At present, the beginning of braking is usually triggered by the detection of a disturbance such as a multi-phase fault or intertie separation. The brake is applied once for 30 cycles to stabilize the initial swing. A single application may be too little or too much to stabilize the system for a particular incident. Voltage phase angle could integrated into a dynamic control that could apply the brake to maintain phase within a maximum limit using up to six, consecutive 30 cycle applications.

Subsynchronous Resonance

In a multi-machine power system the controls on the various generators will at certain operating points with certain power grid configurations oscillate at a low frequency and amplitude, threatening operating stability and putting undue stress on generation equipment. This subsynchronous resonance is a well known and generally controlled phenomena, but hard to eliminate entirely due to many possible operating configurations in a large power grid. The ability to measure voltage phase angle between key generating units would provide a means of avoiding or damping out some of these oscillations.

System State Estimation

System State Estimation is a mathematical technique that has evolved for determining stability of a power system based on its characteristic equations. The major input requirement is knowledge of the complex voltages at the power system busses throughout the system [8].

The present State Estimator uses a least squares algorithm to compute the complex voltages from raw power system data like voltage magnitudes and power flows. Thus the voltage phase-angles are derived in the estimation process rather than obtained by direct field measurement. The slow response time (seconds to minutes) renders the system usable only for static analysis. In addition, it requires consistent and complete sets of measurements to accurately implement the algorithm. When the data is inconsistent or missing, system phase angles are abnormally large, or the system is in an oscillatory condition the solutions may not converge. Line flow measurements are needed for any bus to be included, so the contribution of neighboring power systems may be impossible to compute even though they contribute to system stability.

A State Estimator that uses direct phase angle information measured by precise time synchronous sampling would avoid most of these problems. The system would be fast (in the order of a few cycles) since the complex voltages used in the algorithm would be measured rather than computed. If a reading was in error or missing only estimations surrounding a particular bus would be thrown out. Abnormal phase angles and system oscillations would not affect the process. State estimation could be incorporated into dynamic control schemes.

Monitoring Power Flow.

The power flow across a line is equal to the product of the two terminal voltages and the sine of the phase angle across the line divided by the line impedance [4]. The terminal voltages are normally

closely regulated to a fixed value and the transmission line is usually constant. Thus, the power flow is basically determined by the voltage phase-angle difference between the busses. A maximum phase angle can be determined based on the line and bus-generator characteristics, above which the generators will not stay in sync. This stability limit then determines the maximum power that can be transmitted across the power line.

Monitoring voltage phase angles rather than line loading for power system security assessment may be a more reliable method. Generally speaking, in multi-machine systems small angles between the regions or buses is "relatively secure" and angles approaching 90 degrees is unstable. If bus voltage phase angles along with stability margins were displayed for system dispatchers on the power system diagrams, the load flow and stability situation could be verified at a glance.

Monitoring Reactive Power Requirements

The reactive power injections which are required for controlling voltage magnitudes in the power system depend basically on two factors: the load characteristics and the reactive losses in the network. Phase-angles are important quantities in this respect because they influence the reactive losses in transmission lines, especially for large angles.

This relationship was a major factor in the voltage collapse and subsequent blackout in France in 1978 and the blackout in the SW region of California in 1982. Abnormally large angles produced large power transfers. These, in turn, increased the demand for large reactive compensation and the system became unstable when it was not available.

High speed phase measurements will allow real-time monitoring of the reactive power requirements of the of the system or a region. Following a system disturbance it is fast enough to initiate high-speed reactive compensation, such as shunt capacitor switching to control voltage.

Reduction of Losses

From precise synchronous field data it is possible to construct a precise computer model of the system. By using this model, computer studies could be run to match a specific load demand at minimum losses. Security considerations permitting, savings could be realized for example, by opening some lines which carry essentially no load at a specific time of the day or season.

System Restoration

Following a major blackout, generating plants or regions can be reclosed rapidly if they are in phase with one another. With remote voltage phase-angle measurements at key points, it would be possible to synchronize and restore remote substations reliably and securely. This should make system restoration faster and more versatile.

Summary

BPA is continuing research on precise timing systems and applications development for operation and control of its electric power system. It has developed and employed an accurate and reliable fault locator system and the precise timing network that enables it to operate. GPS is being used to extend the range of that system beyond BPA's network. Investigation also continues of better

methods to dissemination system time. A demonstration R & D project is being initiated to combine time dissemination and fault location timing into a GPS receiver.

Research in system wide phase angle measurements is also continuing. The first test phase of a phasor measurement system has been completed. A GPS receiver provides the precise timing required for the synchronous sampling used to compute voltage and current phasors. Results have been very good, and consequently new system deployment is being investigated.

A successful phase angle measurement system will have many applications. These include a new generation of controls including remedial action schemes, dynamic brake and capacitor insertion, DC system modulation, and system state estimation. As power system loading and interconnection increase, new and more automated controls will need to be developed. High speed, real-time phase angle measurement may prove to be a key to the next generation of controls.

References

[1] M. Street, *"Delivery and Application of Precise timing for a Traveling Wave Fault Detector System,"* Proceedings of 22nd Annual Precise Time and Time Interval Applications and Planning Meeting, 1990, NASA Publication 3116 (1991).

[2] D. C. Erickson and J. Andres, *"Automatic Fault Location Using MICROTIME,"* BPA Document No. AFL-100-01, May 25, 1982.

[3] J. Esztergalyos, D. C. Erickson and J. Andres, *"The Application of Synchronous Clocks for Power System Fault Location, Control, and Protection,"* Western Protective Relay Conference, October 23, 1984.

[4] Westinghouse Electric Corporation, Electrical Transmission and Distribution Reference Book, Chapter 13, *"Power System Stability - Theory and Applications"*

[5] D. J. Hansen and C. P. Dalpiaz, *"Real-time Digital Encoding and Telemetry of Key Power System Transient Quantities,"* Western Protective Relay Conference, October 23, 1984.

[6] G. Missout, J. Beland, G. Bedard and Y. Lafleur, *"Dynamic Measurement of the Absolute Voltage Angle on Long Transmission Lines,"* IEEE Trans. PAS, November 1981.

[7] A. G. Phadke, J. S. Thorpe and M. G. Adamiac, *"A New Measurement Technique of Tracking Voltage Phasors, Local System Frequency and Rate of Change of Frequency,"* IEEE Transactions on Power Apparatus and Systems, Vol. PAS-102, No. 5, May 1983.

[8] A. G. Phadke, *"Precise Synchronization of Phasor Measurements in Electric Power Systems,"* Proceedings of 22nd Annual Precise Time and Time Interval Applications and Planning Meeting, 1990, NASA Publication 3116 (1991).

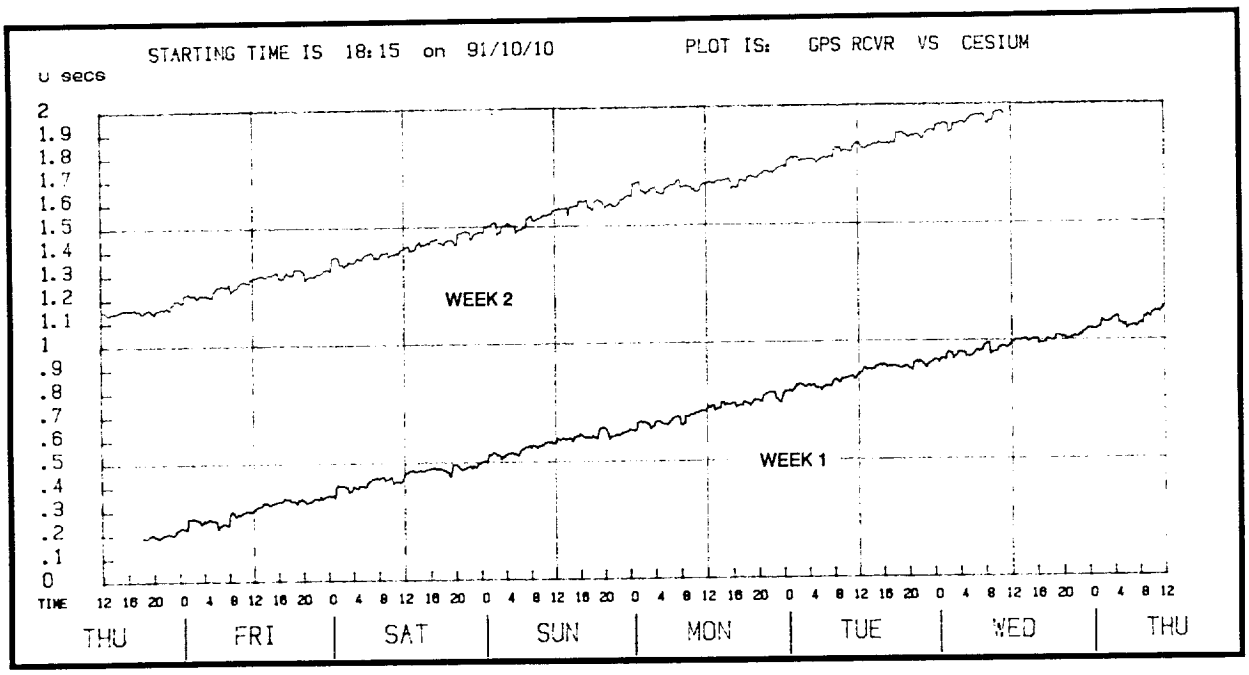

Figure 1. Typical GPS receiver performance versus a Cesium Standard.

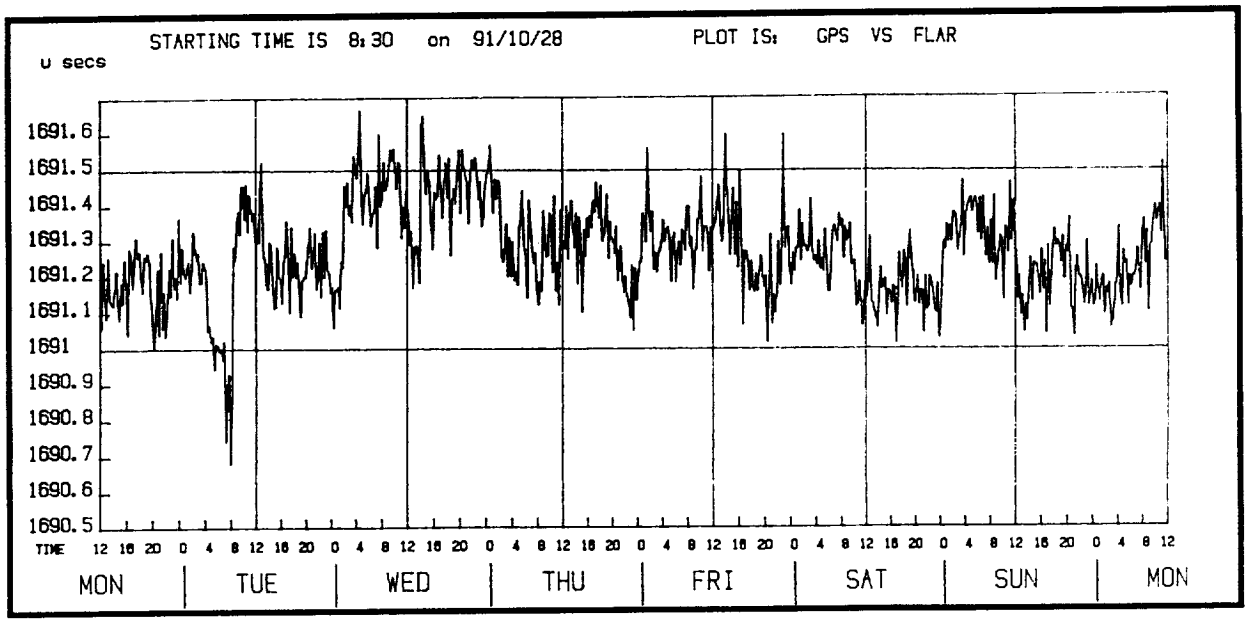

Figure 2. Average of FLAR versus GPS timing.

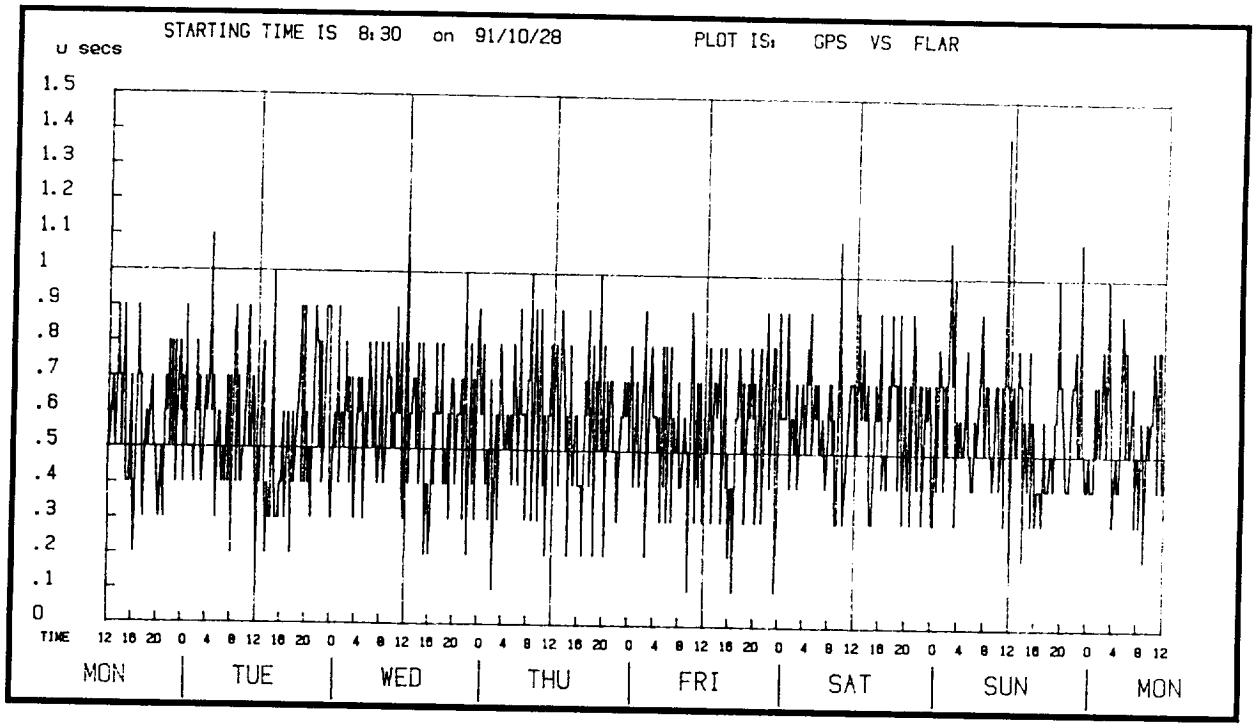

Figure 3. Worst Case of FLAR versus GPS timing (Span or Maximum-Minimum).

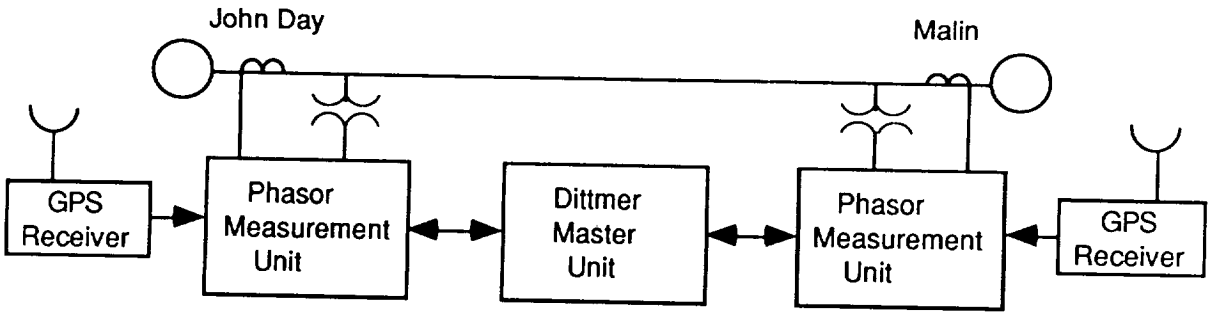

Figure 4. Synchronous Phasor Measurement System One line Diagram

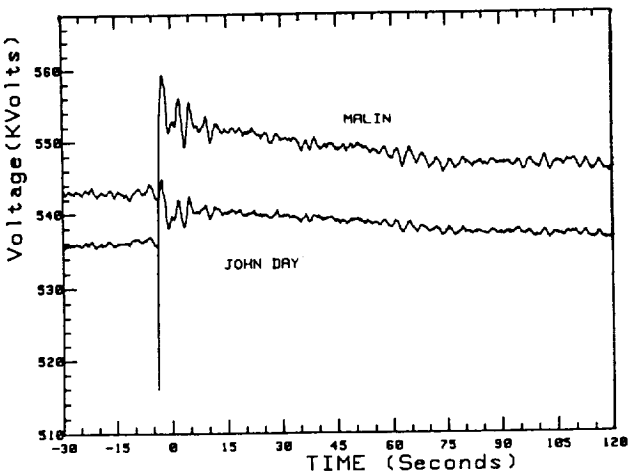

Figure 5. Voltage Magnitude at John Day and Malin Substations

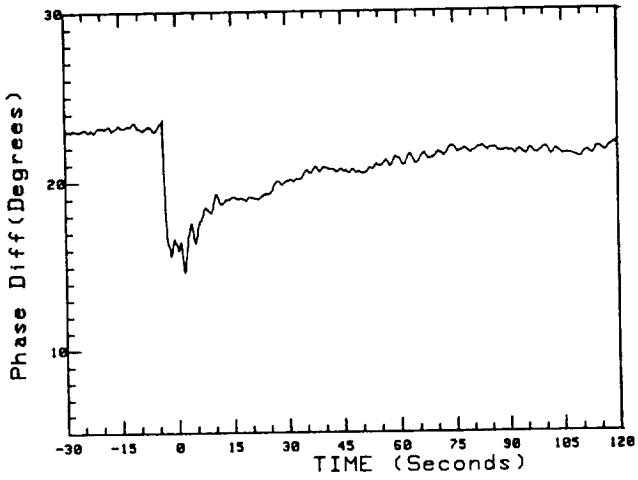

Figure 6. Voltage Phase-Angle between John Day and Malin Substations

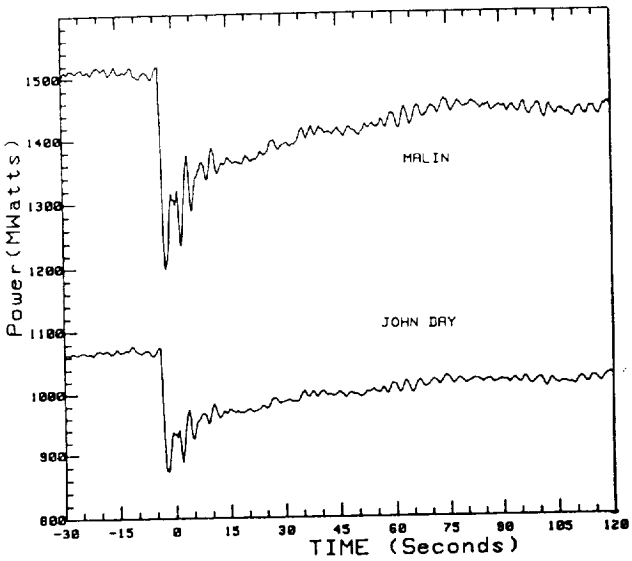

Figure 7. MW Power flow on Line 1 at John Day and Malin Substations

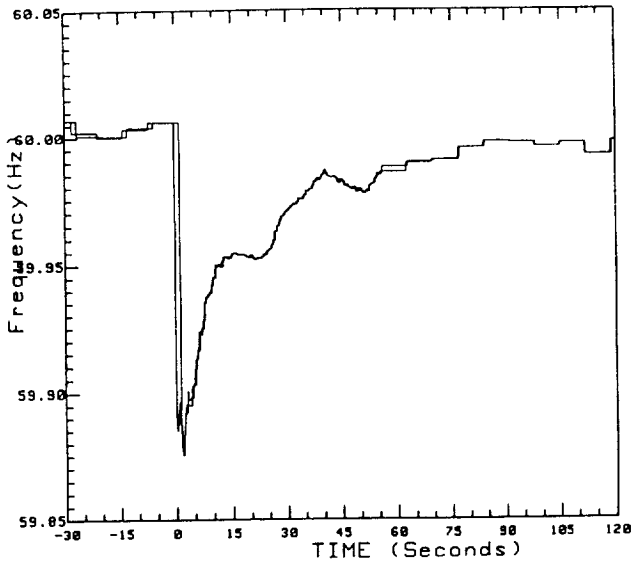

Figure 8. Frequency at John Day and Malin Substations

A HYDROGEN MASER WITH CAVITY AUTO-TUNER FOR TIMEKEEPING

C. F. Lin, J. W. He, and Z. C. Zhai
Shanghai Observatory
Academia Sinica

Abstract

A hydrogen maser frequency standard for timekeeping has been worked at Shanghai Observatory. The maser employs a fast cavity auto-tuner, which can detect and compensate the frequency drift of the high-Q resonant cavity with a short time constant by means of a signal injection method, so the long term frequency stability of the maser standard was greatly improved. This paper describes the cavity auto-tuning system and some maser data obtained from the atomic time comparison.

INTRODUCTION

Shanghai Observatory has very strict requirements for precise frequency and time. These requirements arise from the need of atomic time scale keeping as well as a variety of radio astronomical experiments such as VLBI. At the present time, the hydrogen maser standards developed by Shanghai Observatory have been used for timekeeping and VLBI stations in China. The frequency stability of the standards is to parts in 10^{-15} at 1,000 seconds averaging period of time, but this stability degrades at longer averaging intervals due to the influences of environment and cavity aging. This long term stability leads to time and frequency errors which requires frequency correction to maintain clock accuracy.

To greatly reduce the requirement for frequency adjustment and tuning to compensate for long term cavity drift and/or environmental changes, a continuous cavity auto- tuner for the hydrogen maser was developed at Shanghai Observatory with good success. The auto-tuner has been installed in a hydrogen maser and proved a successful method which can provide such continuous tuning without much perturbing the maser short term stability.

GENERAL DESCRIPTION

The hydrogen maser frequency standard with the auto-tuner is an active oscillator. Fig. 1 is a picture of the maser and Fig. 2 is a line drawing illustrating the maser structure. One of the unique and important features of the maser is the incorporation of a cavity auto-tuner to maintain the cavity at a constant frequency relative to the hydrogen

emission line. The auto-tuner is a stand-alone system and does not require periodic source pressure changes or a separate frequency reference as used in the traditional spin-exchange method of cavity tuning. Besides, the present design of all the maser standard paid more attention to the compact configuration, so that the maser has a rugged, reliable and transportable feature〔1〕,〔2〕.

CAVITY AUTO-TUNER

The principle of the cavity auto-tuner is described in Fig. 3〔3〕,〔4〕.when a frequency modulated microwave signal f(t) is transmitted through the cavity, an amplitude response signal A(t) is obtained in the output signal, then applied to varactor coupled to the microwave cavity by a lock-in amplifier, so that the cavity resonant frequency response is maintained to the desired solid curve throughout. A schematic diagram of the cavity auto-tuner for the maser is shown in Fig. 4.

1. 1Hz Sequarewave Generator

The block diagram of the generator is shown in Fig. 5. The generator has two outputs. The one is applied to the $20.405 \pm f_m$MHz switched synthesizer to modulate the frequency, the other one is applied to a synchronous detector circuit where an "up" or "down" error signal is generated. The phase shifter is adjusted to ensure that the cavity auto-tuner is a negative feedback system.

2. $20.405 \pm f_m$MHz switched synthesizer

As we knew, the $20.405 \pm f_m$MHz signal which is mixed with 1,400MHz signal generates a $1,420.405 \pm f_m$MHz frequency modulated signal. To prevent interference with the maser operation, the nearly complete carrier suppression in the injected microwave signal must be required. At the same time, the power of the injected signal in $1,420.405+ f_m$MHz, and one of the signal in $1,420.405-f_m$MHz must be equal, where f_m=0.015MHz. Fig.6 is the block diagram of the $20.405 \pm f_m$MHz switched synthesizer, where using PLL is to improve the frequency spectrum of the output signal. Fig.7 (a) and (b) are the pictures of $20.405 \pm f_m$MHz and $1,420.405 \pm f_m$MHz signals, which are measured by HP8566A frequency spectrum analyzer.

3. Lock-in Amplifier

The lock-in amplifier is described in Fig.8.The amplitude response signal is amplified, rectified and sent to a synchronous detector, and then an "up" or "down" signal is given.

After filted and integrated, the signal by a bias is added to the varactor in the cavity.

4. Phase-locked receiver

Some improvements were made in the phase-locked receiver. First, a narrow crystal filter (BW=2KHz), which suppresses the injected signal, is inserted to prevent it from interfering the phase-locked loop operation. However, all circuits before the crystal filter must have a wide operating frequency band to transmit the injected signal to lock-in amplifier without phase and amplitude loss. Second, the 405KHz digital synthesizer adopted a new digit direct-dividing and combining technique and avoided the adjusting complexity of the phase-locked loop combination.

TEST RESULTS

The first series of tests were made to determine the operating characteristics of the maser with and without the auto-tuner. Allan variance data plots, turning on and off the cavity auto-tuner, are contained Fig. 9, and clearly show that there is only minimal degration of the maser short term stability with the introduction of the injected signal of the cavity auto-tuner. However, the long term stability of the maser has greatly been improved.

These tests have been made under normal working laboratory conditions in an area where the temperature is held to approximately 23℃±1℃. The reference maser is H_7 [1], [2].

In addition, the maser has been working continuously for atomic timekeeping at Shanghai Observatory since June, 1991. Fig. 10 shows the comparison data measured between the maser clock and UTC by means of GPS receiver. The data illustrates the maser frequency standards with cavity auto-tuner can be used for time keeping.

Much more stability data will be taken under different condition of operation and for longer times. The maser is still being tested and adjusted to optimize the maser parameters, however, the present data is quite encouraging.

ACKNOWLEDGEMENTS

We are very much obliged to thank Dr. Nakagiri and Dr. Onta at CRL, Japan for offering the first author the opportunity to work in CRL. We also greatfully wish to thank our colleagues for supporting this work.

REFERENCES

[1]. Z.C.Zhai, etc, Proc.of 41st annual symposium on Frequency Control.1987
[2]. Z.C.Zhai, etc, Proc. of international symposium on Electromagnetic Metrology,1989
[3]. C. Audion, Rev.Phys. Appl., 16(1981)
[4]. C.F.Lin, etc. Joural of CRL, Japan, No., 1989
[5]. J.W.He, etc. Annuals of Shanghai Observatory, Academia Sinica,1990

ORIGINAL PAGE
BLACK AND WHITE PHOTOGRAPH

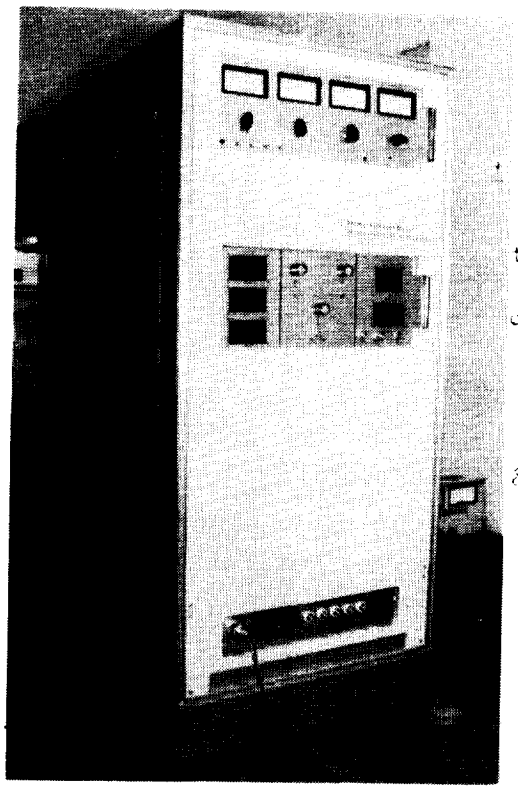

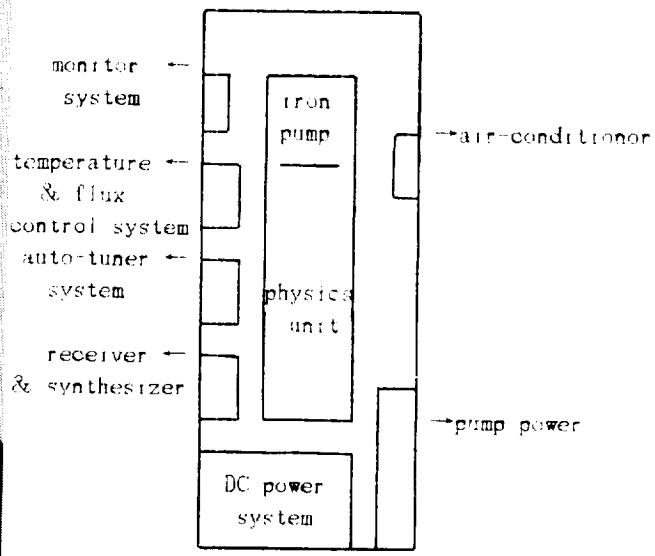

Fig. 2. The Maser Structure

Fig. 1. The Hydrogen Maser with Auto-Tuner for Time Keeping

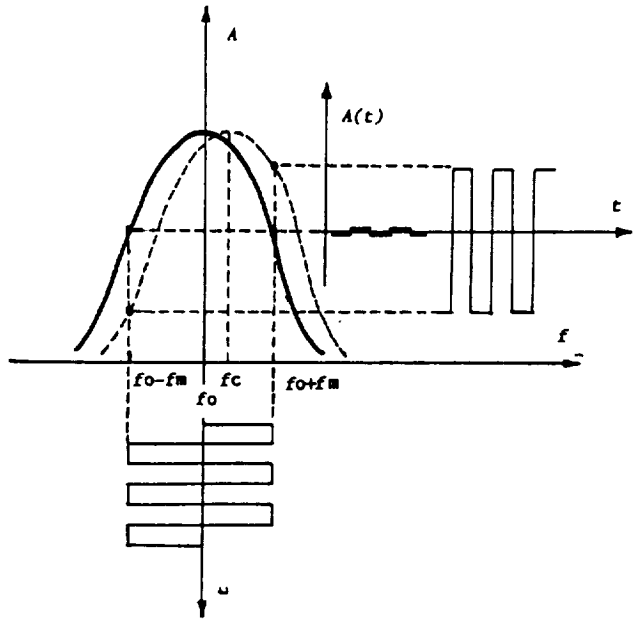

Fig. 3. Response of Cavity to Frequency Modulated Signal

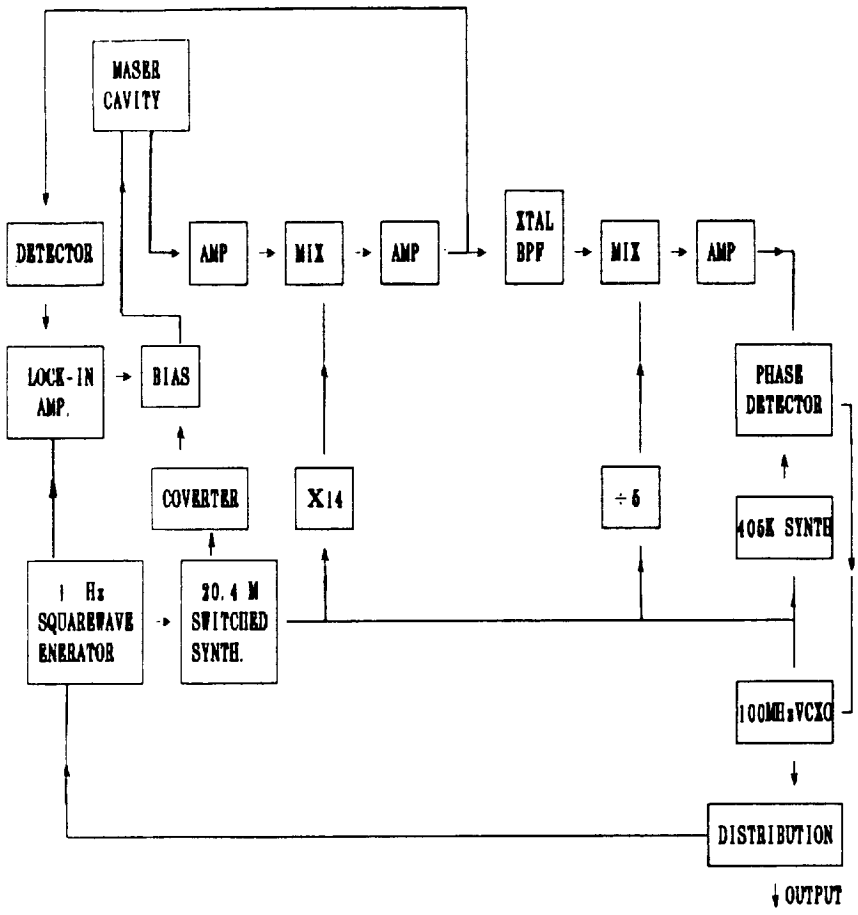

Fig. 4. Cavity Auto-Tuner System

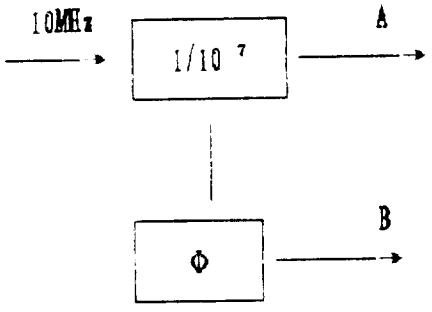

Fig. 5. 1Hz Squarewave Generator

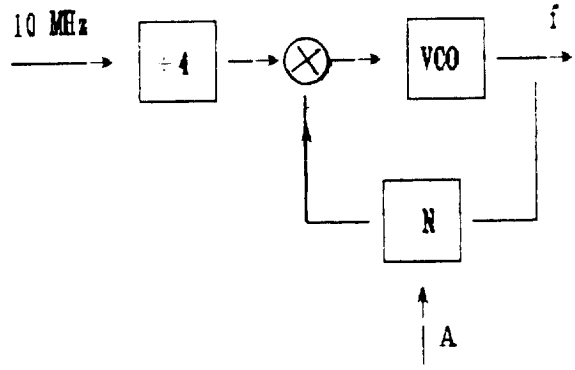

Fig. 6. 20.405± f_MHz Switchod Synthesizer

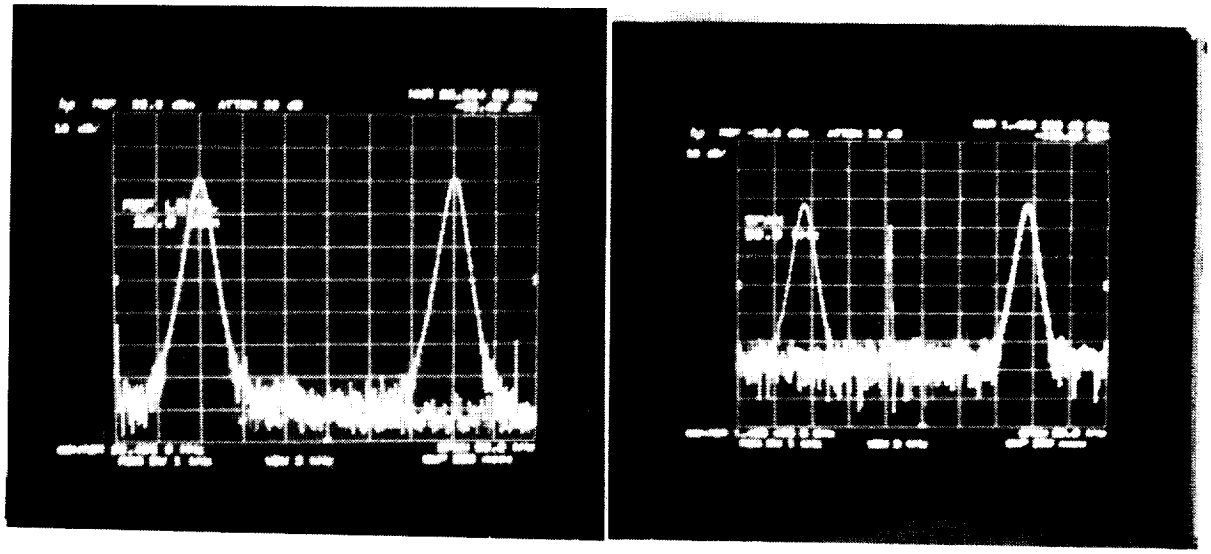

(a) (b)

Fig. 7. Frequency Spectrum of $20.405 \pm f_m$MHz and $1,420.405 \pm f_m$MHz signals

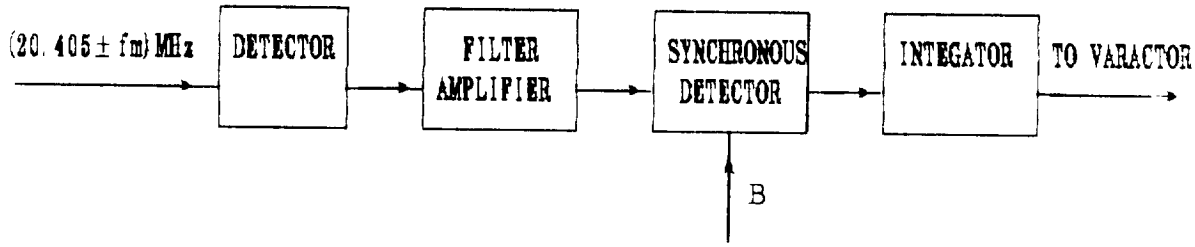

Fig. 8. Lock-in Amplifier

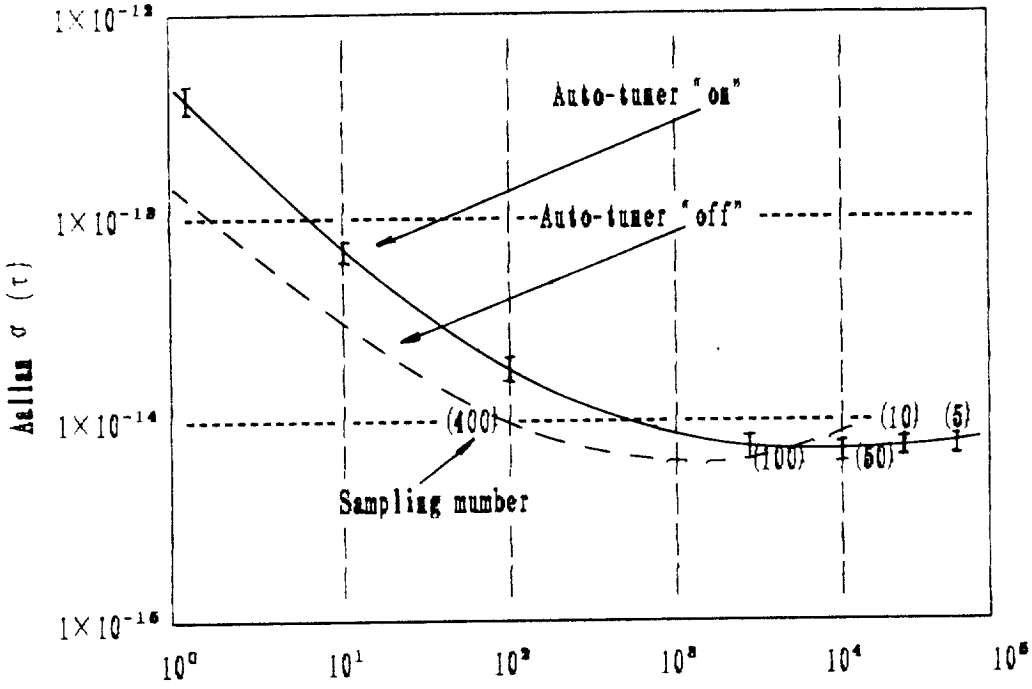

Fig. 9. Allan variance

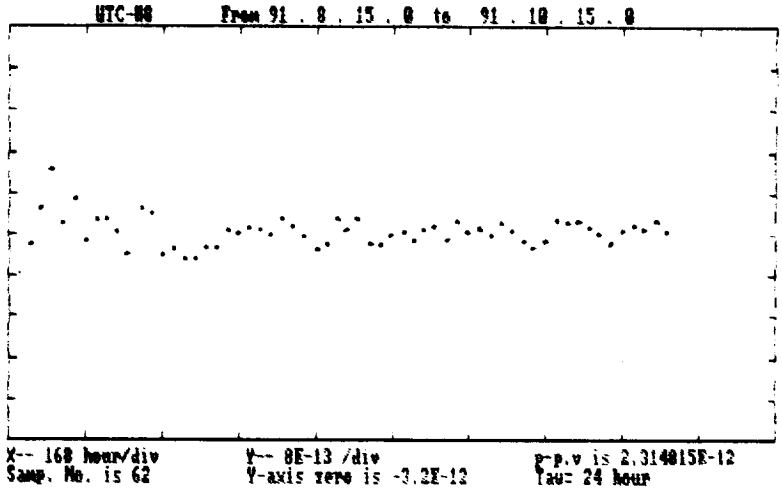

Fig. 10. Maser Clock and UTC compared data

A KIND OF SMALL HYDROGEN MASER FOR TIME-KEEPING

Z. C. Zhai, C. F. Lin, J. W. He, H. X. Huang, J. F. Lü
Shanghai Observatory
Academia Sinica

ABSTRACT

A kind of small hydrogen maser standard for timekeeping is being developed at Shanghai Observatory. The maser employs a cylindrical capacitively loaded cavity construction, resulting in significant size and weight reduction compared to a traditional hydrogen maser. The Q of the compact cavity is electronically enhanced by a suitable positive feedback into the cavity to enable sustained maser oscillation. The long-term stability of the maser is improved by a cavity frequency stabilization servo system. This paper describes the design and development of the maser, as well as photographs of the new maser system during the construction phase.

INTRODUCTION

After the success of the first Chinese hydrogen Maser made at Shanghai Observatory in 1972, 5 more hydrogen Masers with several improvements to the maser design were made at Shanghai Observatory for VLBI observations and for time-keeping. These hydrogen Masers are conventional laboratory standards. [1]

To equip chinese VLBI network, a new generation of hydrogen maser, a integrated, rugged and easily transportable maser, was developed successfully in 1987. [2, 3] And so far 5 this kind of hydrogen masers have been put to use in chinese VLBI network and in military [4, 5]

At present, Shanghai Observatory meanwhile is developing the third generation of hydrogen maser, a Q-enhanced maser, which employs a compact cavity design, resulting in significant size and weight reductions compared to a conventional maser. The long-term stability for this kind of maser is improved by a cavity frequency stabilization servo system. This paper describes the design and development of the Q-enhanced hydrogen maser, as well as photographs during the construction phase.

C-3

OPERATION PRINCIPLE [8]

The operation principle of a Q-enhanced maser oscillator is shown in Figure 1. Similar to a conventional maser, a state-selected beam of hydrogen atoms is focused into a storage bulb placed inside a compact cavity tuned to the hyperfine transition frequency of ground-state hydrogen atoms. The interaction of the atoms with the cavity electromagnetic field causes the atoms to radiate. The losses in the compact cavity are such that the maser oscillation condition is difficult to satisfy. This limitation is overcome by positive feedback, as shown in Fig 1. A portion of the externally amplified maser output is fed back into the cavity. The attenuation in the feedback loop determines the amount of feedback, while the phase shifter adjusts propagation delays to ensure that the feedback signal is in phase with the electromagnetic field in the cavity. Thus, the cavity losses are effectively reduced or cavity Q-enhanced and sustained maser oscillation can be obtained.

However, the cavity in a Q-enhanced oscillator is not an isolated component as in a conventional maser. The cavity resonance frequency is sensitive to phase shift in the feedback loop. In fact, the cavity and the feedback loop form a resonant system that is susceptible to environmental perturbations. It is therefore essential to have a cavity frequency stabilization servo system.

MASER OSCILLATOR SYSTEM

The physics unit of the Q-enhanced maser is shown in Fig 2. The mechanical structure except for the cavity is similar to a conventional maser. The vacuum chamber is made of aluminum and is connected to the source manifold by a titanium tube which provides mechanical support with low thermal leakage to the cavity interaction region. Vacuum maintenance is provided by 70 l /s ion pump, as shown in Fig 3. The source of the state-selected atomic hydrogen beam, consisting of an rf dissociator and a hexapole magnet, is fabricated as the conventional design. The solenoid is made of multi-layer printed circuit design, allows very complete cancellation of spurious magnetic field and provides a rugged, close-fitting, and simple coil system which is equipped with two end field gradient correction coils driven from the same current source as the main coil. Magnetic shielding is provided by four layers of concentric cylindrical shields with conical end caps as shown in Fig 4.

The cavity consists of a section of 15cm O.D. × 5mm wall × 15cm long aluminum tubing with aluminum end plates. Input and output coupling loops as well as a varactor reactance tuner are mounted on the bottom end plate. For tuning the frequency of the cavity, a big mechanical piston inside the cavity is mounted on the top end plate. The storage bulb, 10cm O.D. × 11cm long, provides mechanical support for the cylindrical loading capacitor. The

capacitor consists of four equally spaced electrodes fabricated from 0.5mm thick ×6cm wide×11cm long copper shims and attached to the bulb by epoxy. The bulb is coated on the inside surface with F46 Teflon by standard techniques. The loaded carity Q is about 5000. Fig 5 shows the cavity-storage bulb subassembly

Separate temperature controls are provided at the done, cyinder, and base sections of the vacuum chamber as well as at outoven aluminum cylinder located the outside of the second layer of the magnetic shields To minimize DC stray fields, double bifilar heater windings and DC heater currents are used Fig 6 shows under assembling of the maser oscillator

ELECTRONICS SYSTEM

As mentioned above, the cavity and the feedback loop form a resonant system that is susceptible to environmental perturbations It is therefore essential to have a cavity frequency stabilization servo system. As shown in Fig 7, if the desired cavity frequency is fo, then two test signals of equal amplitude at frequencies f_1 and f_2 symmetrically situated with respect to fo and at half-power points of the cavity response will be alternately injected into the cavity by square wave modulating the test signal source. If the cavity response is represented by the solid curve in Fig 7, then the rectified test signals have the same amplitude and there would be no error signal at the modullating frequency. On the other hand, if the cavity has drifted so that the response is represented by the dotted curve, cavity transmissions at frequency f_1 and f_2 are quite different. The rectified test signals produce a square wave at the modulating frequency. This error signal is synchronously detected and additional gain is provided by a smoothing integrator, the output of which is used to bias the varactor reactance tuner so that the cavity response is slewed back to the desired solid curve.

A functional block diagram of Q-enhanced maser signal-processing system is shown in Fig 8. The cavity Q enhancement and frequency stabilization servo are located, respectively, in the central portion and in the left side of the diagram. The front end microwave electronics is common to both systems After the first conversion, the signal is divided into two channels by a power-divider. In one channel, a narrow crystal band pass filter (3W=3KHZ) passes maser oscillation signal to the clock signal processing circuits. In the other channel, the signals are rectifed and synchronously detected for the cavity stabilization servo system To minimize interference with radiating atoms due to switching sidebands, the test signal synthesizer is switched to generate alternately the two test frequencies at a relatively low rate of 1HZ. The spacing of the frequencies f_1 and f_2 is selected to be 30KHz since strong maser oscillation could be obtained with an enhanced cavity width of that magnitude.

What we should mention is that except for the front-end components, the signal-processing electronics is housed in a rack seperate from the physics unit. A thermal control unit is used to regulate the temperature of an aluminum box in which the front-end microwave electronic components are mounted These components include the feedback loops and the integrator that drives the reactance tuner The box location is chosen to minimize the length of the transmission line used in maser input-outgoing coupling. Fig 9 shows the maser electronics system including the cavity stabilization servo. [7]

THE LAST WORD

In the sections above, we described the design and development of a small oscillating compact hydrogen maser at Shanghai Observatory, as well as some photographs during the construction phase At present, the maser is under assembling and testing. Hopefully we can obtain some data at the beginning of the next year.

REFERENCES

[1] Z C. Zhai, Shanghai Observatory's hydrogen masers, JIETE Vol 27, 11, 1981.

[2] Z C. Zhai etc, A kind of applied hydrogen maser, "Progress in Astronomy", Vol. 6, No 3, 1988.

[3] Z.C. Zhai, C.F. Lin etc, Performance evaluation of the Shanghai Observatory's new H-maser, "Electromagnetic Metrology", International Academia publishers, 1989.

[4] Z.C. Zhai, C.F. Lin etc, A new H-maser time and Frequency standard at Sheshan VLBI station of Shanghai Observatory, proc of 21st PTTI meeting, 1989.

[5] J Y Liao, and Z.C. Zhai, A report on the hydrogen maser to be used for GPS time comparison, proc of PTTD, 1990.

[6] H.T.M. Wang, An oscillating compact hydrogen maser, proc of 34th Annua symposium on Frequency control, 1980.

[7] C.F. Lin J.W. He etc, A hydrogen maser with cavity auto-tuner for time keeping, to be published in the proc of 23rd PTTI meeting, 1991.

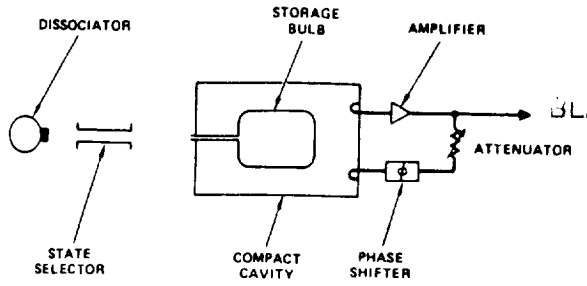

Fig. 1 Schematic of a Q-enhanced maser oscillator

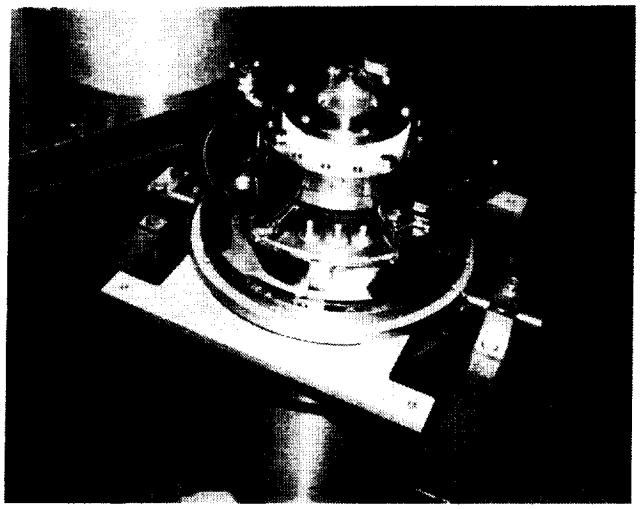

Fig. 2 The photograph of a Q-enhanced maser oscillator system

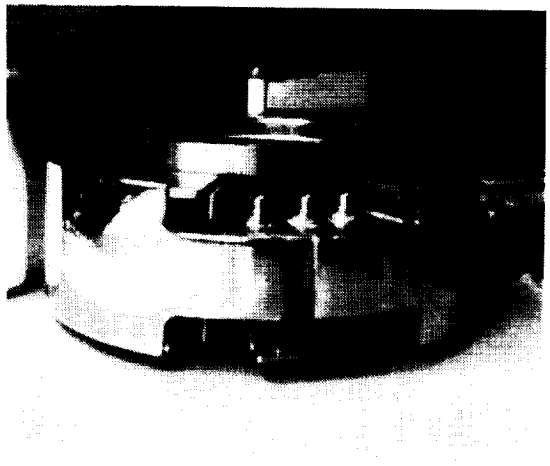

Fig. 3 The photograph of a small size Ion pump

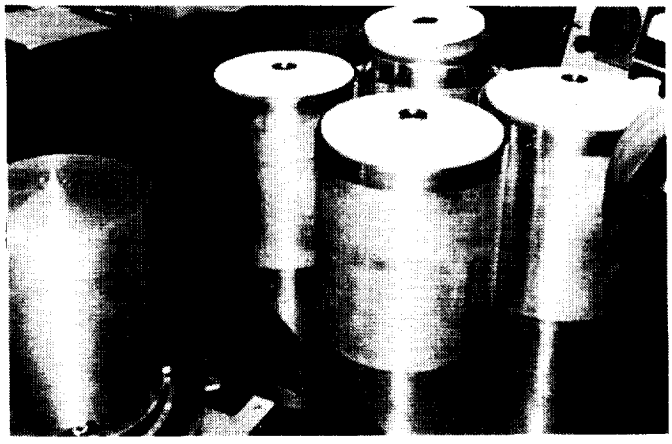

Fig 4 The photograph of magnetic shielding with conical end caps.

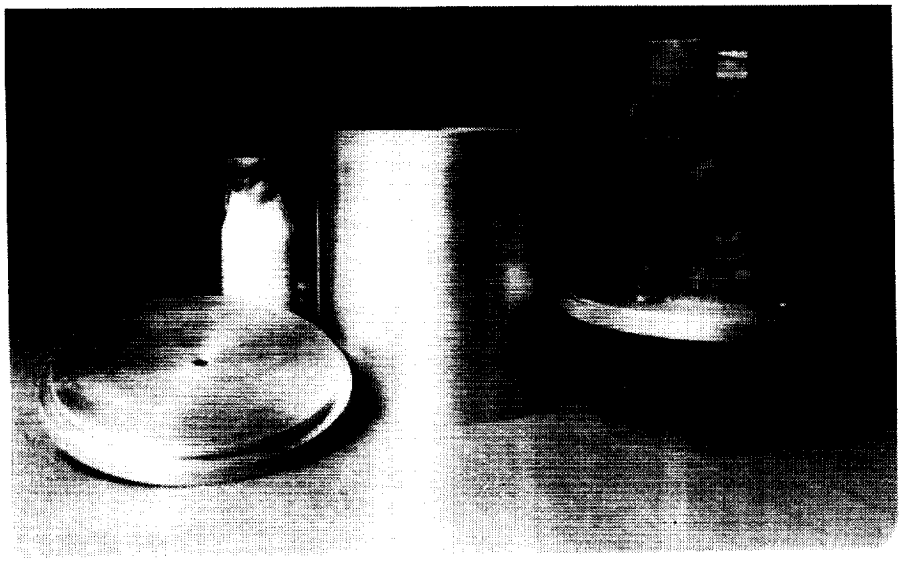

Fig 5 The photograph of compact cavity-bulb structure

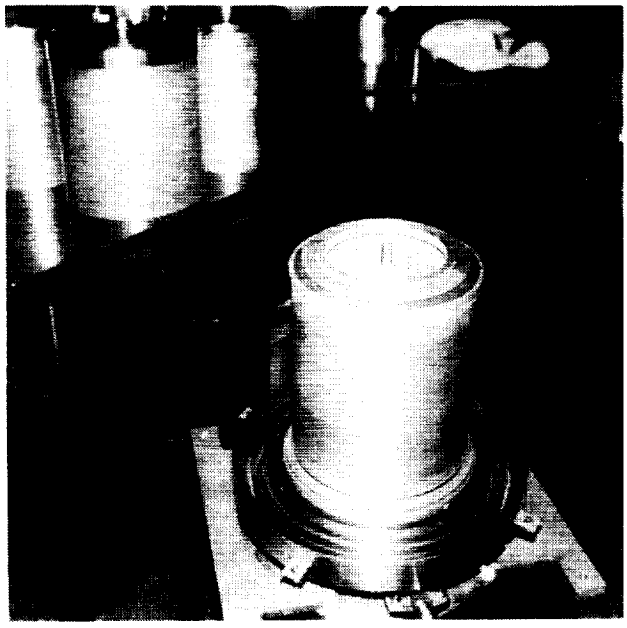

Fig 6 The maser oscillator system under assembling

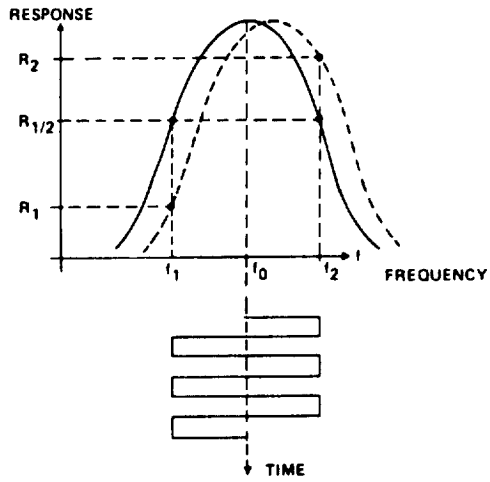

Fig 7 concept for cavity freguency stabilization servo system

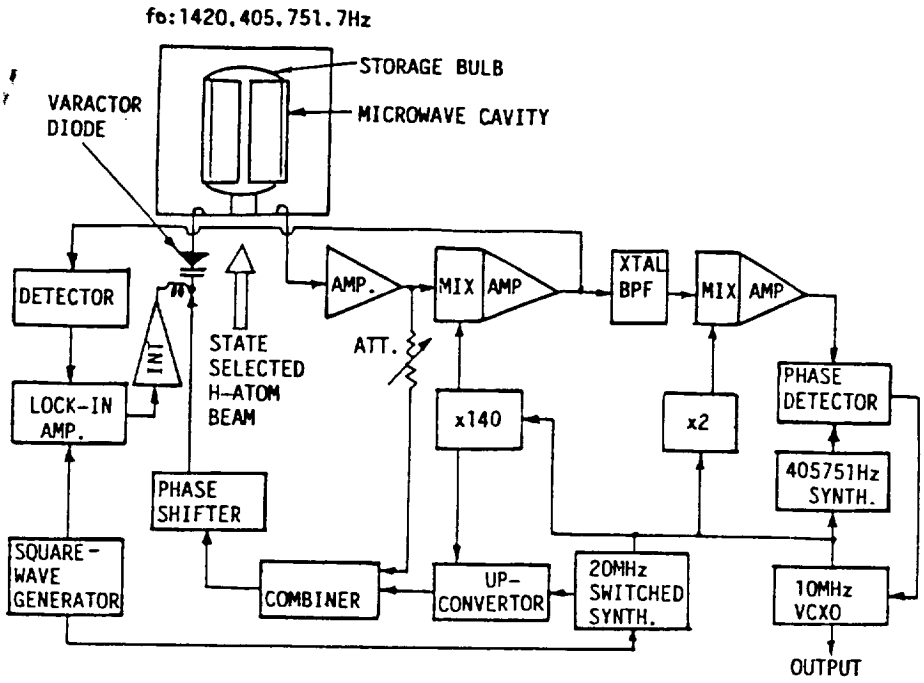

Fig 8 Functional block diagram of Q-enhanced maser oscillator with cavity stabilization servo system

Fig.9 The photograph of Q-enhanced maser electronics system

UNIVERSAL, COMPUTER FACILITATED, STEADY STATE OSCILLATOR, CLOSED LOOP ANALYSIS THEORY AND SOME APPLICATIONS TO PRECISION OSCILLATORS

Benjamin Parzen
consulting engineer
3634 Seventh Avenue
San Diego, CA 92103

Abstract

The theory of oscillator analysis in the immittance domain was presented in Ref 1 which should be read in conjunction with the additional theory in this paper. The combined theory enables the computer simulation of the steady state oscillator. The simulation makes practical the calculation of the oscillator total steady state performance, including noise at all oscillator locations. Some specific precision oscillators are analyzed.

PART 1 THEORY

1. INTRODUCTION

The theory consists of all the material in Ref 1 plus the material of Sections 3.12 through 3.14 presented in this paper.

3. THE REAL OSCILLATOR

3.12 The circuit noise transformation function, $CTRm\ (f)$, in the ZN configuration of Fig 2 of Reference 1

Eq 20, repeated here for convenience,

$$\underset{\mathcal{L}_m(f)}{<term\ 0>} = \underset{\mathcal{L}_{Vn}(f)}{<term\ 1>} \bullet \underset{|\ RT/(Zt(f)\ |^2}{<term\ 2>} \tag{20}$$

may be considered a special case of general Eq 25

$$\underset{\mathcal{L}_m(f)}{<term\ 0>} = \underset{\mathcal{L}_R(f)}{<term\ 1>} \bullet \underset{CTRm(f)}{<term\ 2>} \tag{25}$$

In Eq 25, *term* 0 is the oscillator phase noise at location m, where, in Eq 20, $m = Ix$. Term 1 is called the residual phase noise [6] of the active or other device. Term 2 is called the circuit transformation of residual noise function at location m.

The importance of the residual noise lies in the fact that it can be measured independently of the oscillator. Then, one needs only to compute the applicable $CTRm(f)$ and then, using Eq 25, determine the oscillator noise, at any and every location.

Since it is stipulated that the noise is due to Vn, then

$$\mathcal{L} = PS - V_n(f)/[V_{in}(0)]^2 \tag{26}$$

$$= \mathcal{L}_{Vn}(f) \bullet [V_s(0)/V_{in}(0)]^2, \tag{27}$$

where V_{in} is the carrier input voltage at which the residual phase noise is measured and V_s is defined in Fig 2 (in Ref 1) and used in Eq 21.

3.12.1 The computation of CTRm(f)

From Eq 23;

$$\mathcal{L}_m = PS_m(f)/PS_m(0) \tag{28}$$

From Eq 12a;

$$PS_m(f) = CF_{mVn}(f) \bullet PS_{Vn}(f) \tag{29}$$

$$= CF_{mVn}(f) \bullet \mathcal{L}_{Vn}(f) \bullet [V_s(0)]^2 \tag{30}$$

From Eq 21

$$= CF_{mVn}(f) \bullet \mathcal{L}_R(f) \bullet (V_{in})^2 \tag{31}$$

From Eq 27

$$RO_m = PS(0)/PS_{V_in}(0) \tag{32}$$

Let

$$= PS_m(0)/(V_{in})^2 \tag{32a}$$

Then

$$PS_m(0) = (V_{in})^2 \bullet RO_m \tag{32b}$$

Combining Eqs 28, 31 and 32b, we obtain;

$$\mathcal{L}_m(f) = \mathcal{L}_R(f) \bullet CF_{mVn}(f)/R0_m \tag{33}$$

Comparing Eq 33 with Eq 25, we see that:

$$CTR_m(f) = CF_{mVn}(f)/R)_m \tag{34}$$

CF_{mVn} is calculated as in Sect. 3.9.

3.12.2 The calculation of $R0_m$ with the BPT program.

(Note that $R0_m$ is independent of Vn and dR)

a. Enter the applicable ZN configuration of the oscillator.

b. Set $F = f_o$ and $dR = 1E-9$ ohm.

c. Make Vn a VW component (white noise voltage source) of convenient magnitude.

d. Execute Option C and note the magnitudes Vm, at locations m and V_in.

Then

$$RO_M = (V_m/V_{in})^2 \tag{35}$$

or in dB using the DB option,

$$R)_m(dB) = V_m \text{ referred to } V_{in} \tag{35a}$$

3.12.3 Notes for Sect 3.12

a. Validity of this section – The reader is reminded that, for flicker noise, this section is valid only for Fourier frequencies, f, at which $X_t(f) >> R_t(f)$ as stipulated in Sect 3.11

b. Figure of merit – $CTR_m(f)$ is a very useful figure of merit of the transformation of device residual noise into oscillator noise at all locations.

c. If it is desired to ascertain the magnitudes of the voltages and currents at all locations at $f = 0$, then

1. Make dR a value such as that of Step 3.12.2.b.
2. Set the Magnitude of Vn in step 3.12.2.c so that $V_{in}(osc)$ becomes equal to V_in (residual measurement input V) by means of Option E.
3. Execute Option C and record the data.

3.13 The oscillator $Q_{opm}(f)$

Q_{op}, the oscillator operating Q, is generally defined by

$$Q_{op} = (dx/df)_{f\to 0} \bullet f_0/2RT \tag{36}$$

It is seen that Q_{op} applies only to low f.

It is proposed that Eq 36 be extended to be

$$Q_{opm}(f) = (dx/df) \bullet f_0/2RT \tag{37}$$

(which includes Q_{op})
as it will yield more information.
It can be shown that

$$Q_{opm}(f) \approx f_0 \bullet (V_{in}/V_x)/\{2 \bullet SQR[CTR_m(f) \bullet f\} \tag{38}$$

Both Q_{opm} and CTR_m will become more important with the expanded use of oscillators, with more complicated resonators, for which Leeson's noise model **[1],[5]** may not apply.

3.14 Oscillator circuit configs.

Thus far the Z and N configurations have been described. There are additional useful configurations which are considered in detail in Ref 9. Some of these are

3.14.1 N config – This is the raw complete oscillator circuit It is assigned node numbers and then entered into the computer.

3.14.1.1 ZN config – This is the N config set up by means of the Z config. The N config of Fig 2 of Ref 1 is a ZN config.

3.14.2 Y config –This is the Y dual of the Z config and has dG, GV, and BV instead of dR, RV, and XV.

3.14.3 YN config –This is the N config. set up by means of the Y config. In addition, it has a jumper to enable Z measurements.

3.14.4 ZYN config –This is the ZN configuration which has also been provided with BV, GV, and dG.

Y and YN configurations have the important advantage of having fewer nodes.

The Z configuration is preferred over the Y configuration because of its much greater frequency capture range.

There are also many more possible Y, YN, and ZYN configurations since tuning elements can be connected between any 2 nodes. nodes. Choosing the optimum node pair is difficult.

PART 2 SOME APPLICATIONS TO PRECISION OSCILLATORS

7. INTRODUCTION

This part describes some applications to the precision oscillators likely to be found in PTTI systems.

The data was obtained with program BPT as directed by the user guided by the above theory. The circuit is entered into the computer as a NETLIST via a file or the keyboard. The computer translates the netlist into a PARTS LIST which is readily understood by any user. The user then interactively directs the computer to generate the desired data.

The program is basically an elaborate laboratory simulator with extensive stockroom, fabrication, instrument room, measurement, housekeeping, and recordkeeping facilities, unmatchable in any real laboratory. At present, the program is available for the IBM PC, AT etc. and compatible computers. The user proceeds, controls and operates the program as if he or she were constructing, testing, and then modifying the "simulated breadboard circuit", as directed by the user and the program, in exactly the same manner as in a real laboratory, but much more expeditiously, accurately, thoroughly. and with much greater understanding. The important difference is that the simulated breadboard includes only the information as directed by the user but the real breadboard also includes intrinsic information, unknown to the user, such as parasitic components and frequencies. This difference signifies that only about 90% of the real laboratory testing can be eliminated by the computer simulation.

From this program description, is seen that the general analysis and design modification procedures consists of the following 5 steps all performed within the program environment.

1. Construction of the oscillator.
2. Trimming this oscillator to the desired operating frequency.
3. Analyzing and evaluating the oscillator performance with the aid of the extensive measurement facilities within the program.
4. Modifying the oscillator to improve the performance.
5. Repeating steps 3 and 4 until the desired performance is obtained.
6. The analysis is then confirmed by constructing and testing the real oscillator to check the correct entrance of the parts and layout data into the computer and to be alerted of important omissions in the data.

It will be noted that above steps 1 to 5 are exactly those followed in the real laboratory but slightly modified for use with the above described theory. The effort and time required to perform these steps will be a small fraction of those for step 6.

The main difference between the this method of analysis and the customary present methods are

1. The circuit of the device being analyzed is that of the full real oscillator and not a possibly poor approximation incapable of producing all the important and correct data.
2. The type of data obtained closely resembles that for the real oscillator and, in addition, types, practically, unobtainable in the real laboratory.

The difference is primarily due to the closed loop analysis and the noise source, amplifier and filter oscillator model, made possible by the computer and the above theory, as contrasted with the customary open loop analysis . It should be remembered that the real oscillator operates closed, and not open, loop.

The applications are:

1. A 10 MHz 1 resonator oscillator.
2. A 10 MHz 2 resonator oscillator.

Application 1 has been and is being manufactured in very large quantities and it is difficult to appreciate the value of a detailed analysis at this stage in its design history. However, the analysis is still useful, at this time, in the following respects:

1. It provides a greater understanding of the oscillator operation.
2. It clearly demonstrates the validity of the complete design basis including the optimum noise performance.

3. It serves as a production control tool for quickly determining the effect of changes in part characteristics upon the total oscillator performance and thus providing information as to the permissibility of substituting parts with these changes. Such changes are very often found necessary during production.

Application 2 is an example of the use of the theory and program as a research and development tool. This oscillator has never been built and it is advisable to conduct a preliminary computer study to explore its behavior and desirability prior to more intensive computer studies and expensive experimental efforts.

The data for these applications are presented in the form of simplified schematics, a typical netlist, a typical parts list, and plots of the more important, and infrequently or not previously published, operating characteristics. Comments on the data are also included.

The oscillator plots are for 2 quantities versus the Fourier frequency, f.

The circuit transformation of residual noise at location m, $CTR_m(f)$. The magnitude of the closed loop impedance, $Z_{in}(f)$, at the input terminals of the active device.

The CTR_m function is described in Sect 3.12

If the noise performance of the oscillator, $\mathcal{L}_m(f)$, has been experimentally determined and $CTR_m(f)$ has been calculated, then the residual noise can then be calculated from Eq 25.

The Z_{in} quantity determines the contribution of the active device input noise current, I_n, to the oscillator noise as it produces a noise voltage, $E_n = I_n \bullet Z_{in}$, across the active device input terminals. It is therefore very important, when measuring the device residual noise, that the device be terminated to simulate the impedances present in the closed loop oscillator.

In this connection, the noise currents may be determined by measuring the residual noises at the calculated terminations and then calculating the corresponding noise currents (see Sect 3.12.3c).

8. 10 MHz 1 RESONATOR OSCILLATOR

Fig 4 is the schematic diagram of this oscillator, called **OSC1**.

It is the familiar Colpitts type with an SC cut 3rd overtone crystal resonator, XL, having R1 = 70 Ohms, C1 = 2.1E-16 Farad and Qx = 1.083E6.

There are 5 additional components which are critical and therefore must be carefully controlled; CA, LA, CN, LN, and C'L. CA and LA make up the resonator mode selector network, X1 (see Ref 3). CN and LN make up the resonator overtone selector network, X2. It is possible to combine the overtone and mode selector functions into 1 three element network, either in X1 or X2. However, in production, the control of the elements becomes very difficult.

C'L is the tuning element of the resonator. It may be a capacitance, inductance, or a network including a tuning diode.

The use of elements consuming RF power has been minimized so that the calculated oscillator Q_{op}, 1.080E6, is very close to Q_x. This is true only when RL is 1 Megohm. For RL = 10 Kilohms, Q_{op} becomes 9.605E5 and for RL = 1 Kilohm, Q_{op} = 4.885E5 and quickly decreases with further reductions in RL.

Fig 4 shows both V_{in} and V_s (see Sect 3.12) defined as if RE were an integral part of the transistor

Q1. This is done to ensure that the measurement of the residual noise, $\mathcal{L}R(f)$, in Q1 includes the, well known, marked reduction in flicker noise due to RE. . Fig 5 shows CTR_m and Z_{in} plotted versus f.

CTR data is presented for 2 locations, RL and I_x. RL is the normal output location. However, the curves indicate that the I_x noise performance is superior past $f = 10$ Hz and much superior at high values of f. Therefore consideration should be given to extracting the output from I_x. One method of doing this without significant deterioration in Q_{op} and the low frequency noise performance is described in Ref 8.

The curves include data for both the upper and lower sidebands, $+f$ and $-f$, of the spectrum since they may not be symmetrical. symmetrical. The asymmetry is caused by the fact that the signal, at the location being observed, is the sum of at least 2 signals arriving via different paths. If there is only 1 major llator noise source then the signals are correlated and must be combined as phasors.

The relative phase varies with the frequency f, and at $f = f_a$ the signals will be in phase in one sideband and out of phase in the other sideband. The out of phase signals causes dips in the CTR function in the region of f_a. The value of f_a has a strong dependence upon Q_{op}, being closer to f_o the greater the Q_{op}, because the phase shifts more rapidly.

The magnitude of the dip is a function of the equality of the magnitudes of the 2 signals. Curve B of Fig 5 shows a dip of about 20 db at about 20 Hz below the carrier. There is no conspicuous dip in the resonator current, I_x, noise because of the resonator filtering action. This effect may be of great importance in systems which require an usually low noise signal in a relatively narrow f region close to the carrier.

A strong dip also exists in curve G, the curve for $Z_{in} - f$, at a somewhat higher magnitude f_a.

The Z_{in} plots show an increase of over X 100 as f varies from 100 to .1 Hz.

9. 10 MHz 2 RESONATOR OSCILLATOR

The following reports on the result of a preliminary computer study to determine whether it merits additional computer and experimental studies.

Fig 6 is the working but unoptimized schematic diagram of the ac circuits of this oscillator, called **OSC2**.

It is a modified Pierce type with 2 resonators, XL1 and XL2, identical to XL1 of Fig 4, capacitively coupled by Cc.

The oscillator parts list in shown in Fig 7 and the netlist is that in Fig 8.

For simplicity, the mode selector and overtone selector networks are not included but they can be similar to those of **OSC1**. It is interesting to observe that their omission is tolerable in the computer oscillator but may be disastrous in the real oscillator.

C'L1 and C'L2 are the tuning adjustments for their respective resonators. These adjustments also serve to set the oscillator frequency, f_o, and to shape the oscillator phase noise curve at low Fourier frequencies.

A +1 Hz shift in the effective f_s of XL1 corresponds to +.43 Hz shift in the oscillator f_o.

A +1 Hz shift in the effective f_s of XL2 corresponds to +.55 Hz shift in the oscillator f_o. This data

shows that the resonators are almost equally important in determining the oscillator long term frequency stability.

Q_{op} = 1.47E6 which is about 40—because of the 2 resonators.

At $f < 8$ Hz the noise is identical at all locations and equal to those of **OSC1** except for the 3 dB improvement due to the higher Q_{op}.

At $f > 20$ Hz the noise performance may be much superior to that of **OSC1**. The best performance, that at location C2, is also plotted on Fig 5 to facilitate the comparison of the noise performance of the 2 oscillators. It will be seen, from that figure, that at 10 KHz, the OSC2 performance is potentially better by about 60 dB.

The Z_{in} plots are appreciably better than those of **OSC1**.

The following carrier signal levels were calculated by BPT after setting dR so that I_x of XL1 = 1 mA, corresponding to dR =1.36E-5 ohm :

I_x of XL2 = 0.17 mA
V of C1 = 0.099 V., V of Cc = 0.015 V., V of C2 = 0.026 V.
The calculated Idc of Q1, is, assuming ALC limiting, 0.75 mA.

10. ADDITIONAL NOISE SOURCES

A large part of the just reported very good noise performance of **OSC1** and the even better performance of **OSC2** may be nullified by the following important additional noise sources:

Resonator noise (See Section 3.3)- Resonator noise, which is mainly flicker frequency noise, produces f^{-3} phase noise which, in good circuit designs, swamps the circuit flicker noise and thus effectively determines the total oscillator phase noise, at low f.

Additive noise- Noises, produced by passive component thermal and other noise sources and noises generated in active devices such as buffer and output amplifiers, set effective limits to the total oscillator noise floors.

Those readers, not used to the CTR_m and residual noise concepts but are familiar with the customary $\mathcal{L}(f)$ noise data, are reminded that, since $\mathcal{L}(1E4)$ of a good active device is better than -140 dBc, the 10 KHz point on curve E of Fig 9 corresponds to a highly improbable $\mathcal{L}_{C2}(1E4)$ of (-140 -125) = -265 dBc.

11. CONCLUSIONS for PART 2

In spite of its relatively complex circuit, requiring 2 high performance resonators, the following conclusion are reached:

In view of its potentially excellent noise performance, the 2 resonator oscillator merits further computer and experimental study including the possibility of also using the 2 resonators as part of a vibration noise cancellation system.

Much additional effort is desirable to decrease the effect of the noise sources described in Sect 10.

12. REFERENCES

[1] B.Parzen, *"Steady State Oscillator Analysis in the Immittance Domain"*, Proc. 21st Annual Precise Time and Time Interval Applications and Planning Meeting, pp 161-168, Nov. Nov. 1989

[2] D.B. Leeson, *"A Simple Model of Feedback Oscillator Noise Spectrum"*, Proc. I.E.E.E, vol 54, pp. 329-330, Feb. 1966.

[3] B. Parzen, Design of Crystal and Other Harmonic Oscillators. Oscillators. New York:Wiley, 1983.

[4] W.P. Robins, Phase Noise in Signal Sources. London:Peter Peregrinus Ltd, 1982.

[5] B. Parzen, *"Universal, Computer Facilitated, Steady State Oscillator Analysis Theory and Some UHF and Microwave Applications"*, Proc. 45th Annual Frequency Control Symposium, pp. 368-383. May 1991.

[6] B. Parzen, *"Clarification and a Generalized Restatement of Leeson's Oscillator Noise Model"*, Proc. 42nd Annual Frequency Control Symposium, pp. 348-351, June 1988.

[7] G. Montrose et al., *"Residual Noise Measurements of VHF, UHF, and Microwave Components"*, Proc. 43rd Annual Frequency Control Symposium, pp. 349-359, May 1989.

[8] R. Burgoon and H. l. Wilson, *"Design Aspects of an Oscillator Using the SC Cut Crystal"* Proc. 23rd Annual Frequency Control Symposium, pp. 411-416, 1979.

[9] B. Parzen, Oscillator and Stability Analysis in the Immittance Domain. In preparation.

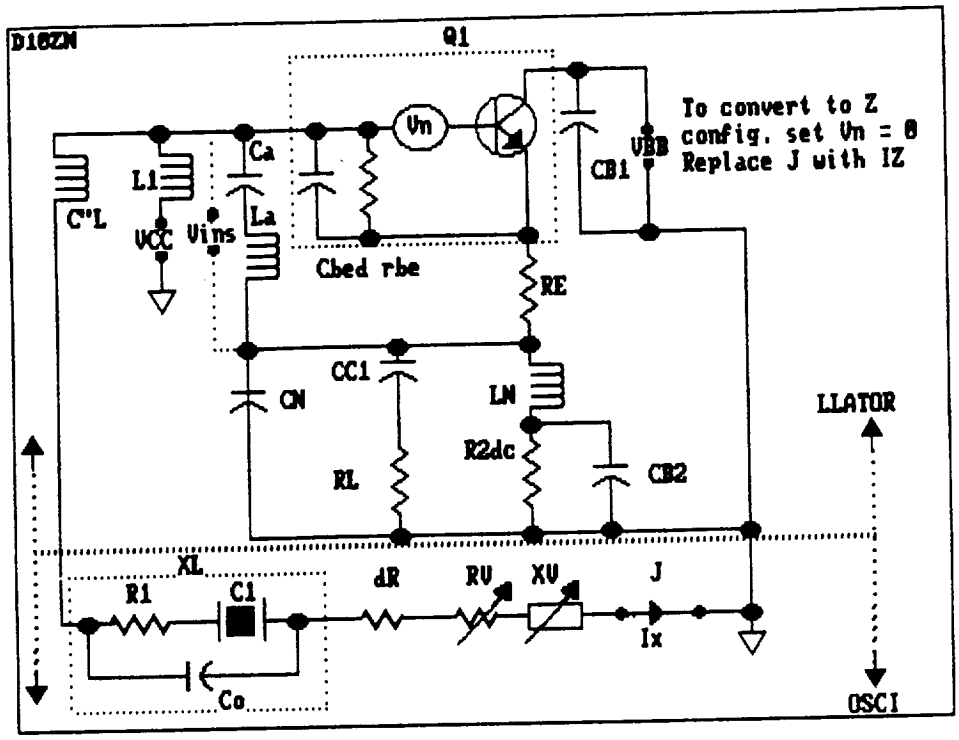

FIG 4 10 MHz 1 XTAL OSCILLATOR
ZN CONFIG

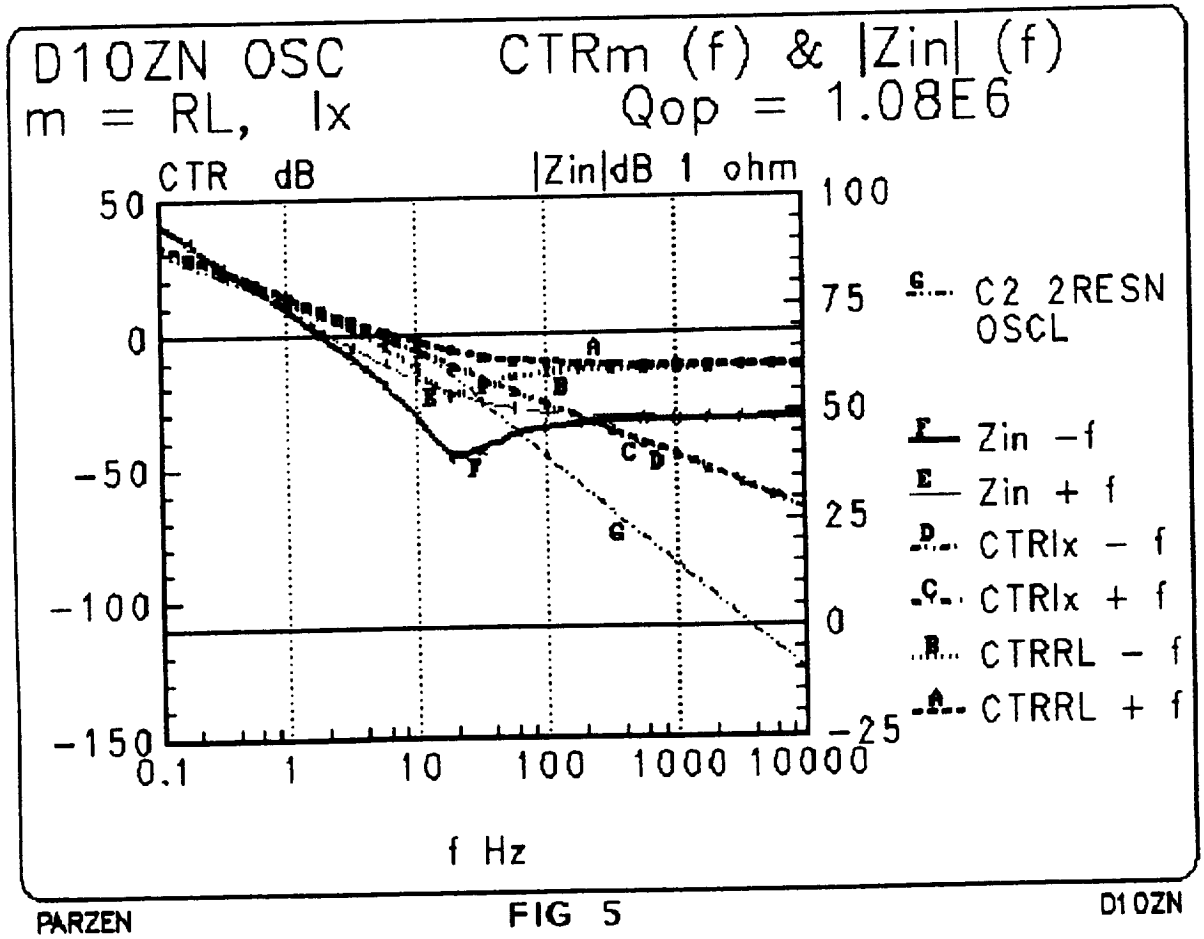

FIG 5

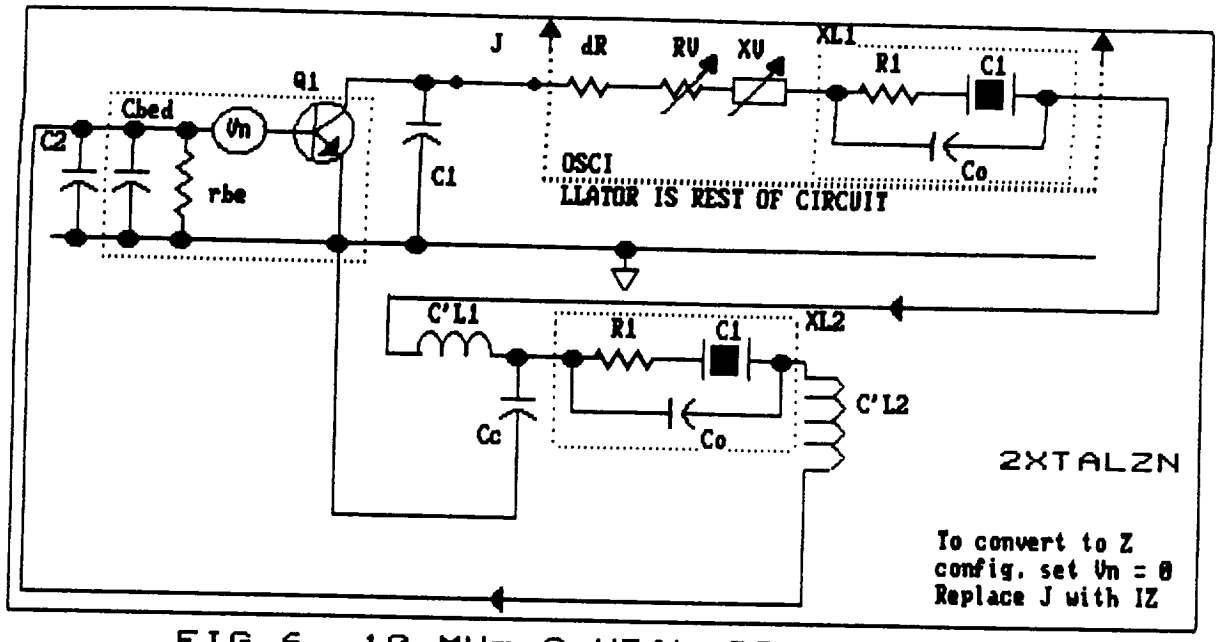

FIG 6 10 MHz 2 XTAL OSCILLATOR
ZN CONFIG

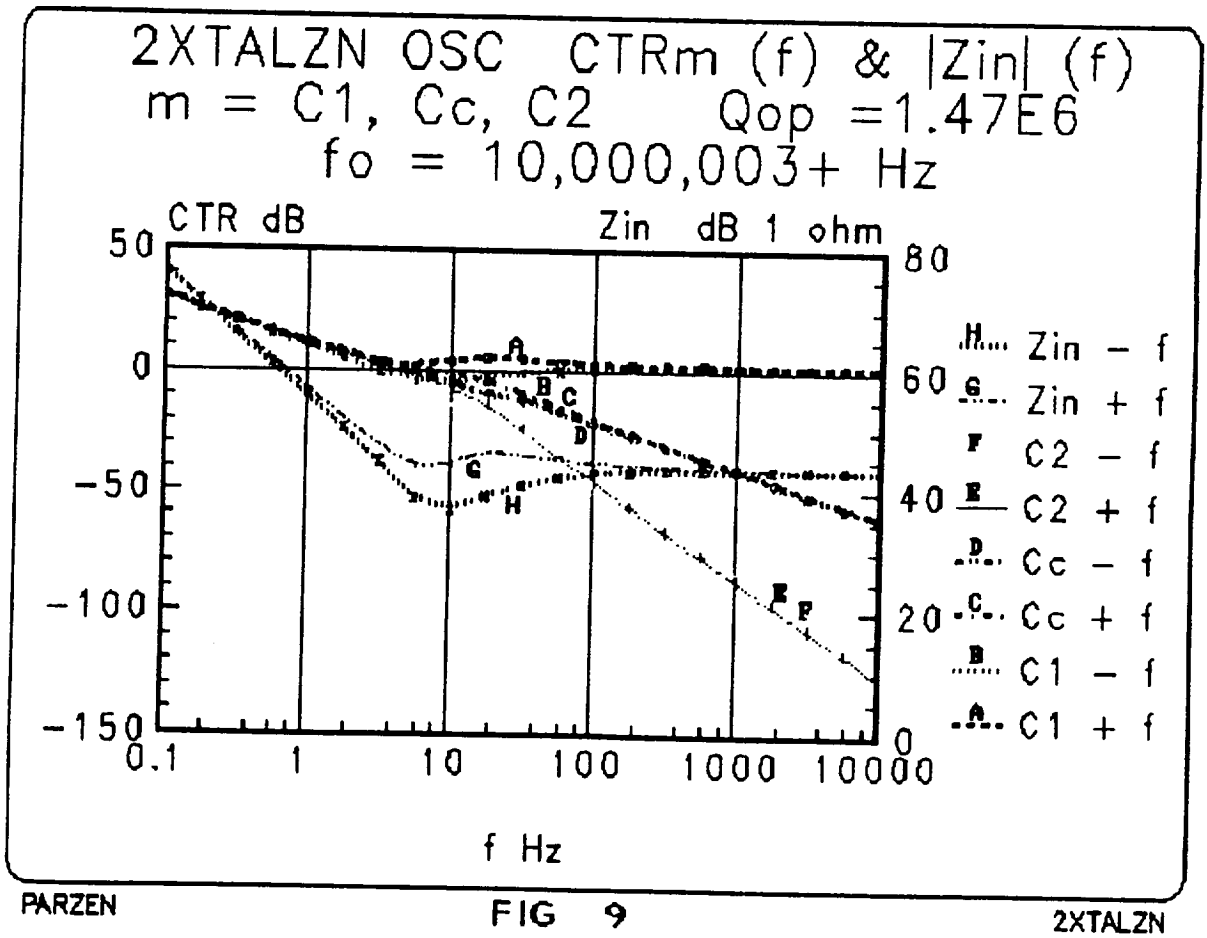

FIG 9

```
11-18-1991    09:48:26
# OF COMPONENTS =  20   HIGHEST NODE # =  13    # OF VOLTAGE SOURCES =  1
2XTALDRZ                          FREQUENCY= 10000003.14865001
CIRCUIT NOTE :  10 mhz 2xtal osc z config
  COMPNT. CONNECTED TO NODE
 #   SYB   N1-   +N2      TYPE         VALUE          PHASE ANGLE
 1   c1      1 - 0        CAPACITOR     1E-010
 2   {J}     1 - 10       JUMPER,     R =  9.999999999999999E-021
 3   {dR}    10 - 11      RESISTOR      1.36E-005
 4   {RV}    11 - 12      RESISTOR     -3.917113507084587E-002
 5   {XV}    12 - 13      X, REACTANCE      -1.876242564109969E-007
 6   (R1)XL1 13 - 2       RESISTOR      70                              PO XL
 7   (C1)    2 - 3        XTAL RSN'TOR  C1= 2.1E-016  fs= 10000000
 8   (Co)    1 - 3        CAPACITOR     1E-050                          PO XL
 9   C'L1    3 - 4        INDUCTOR      5.386228087475492E-007
 10  Cc      4 - 0        CAPACITOR     1E-009
 11  (R1)XL2 4 - 5        RESISTOR      70                              PO XL
 12  (C1)    5 - 6        XTAL RSN'TOR  C1= 2E-016    fs= 10000000
 13  (Co)    4 - 6        CAPACITOR     1E-050                          PO XL
 14  C'L2    6 - 7        INDUCTOR      1E-006
 15  C2      7 - 0        CAPACITOR     1E-010
 16  mm      B= 9 E= 0 C= 1        N, NPN BIP TRANSISTOR
                    gmo= 2.859460045734375E-002   BETA= 100   FT (MHz)= 1000
 17  (rbe)   0 - 7        RESISTOR      3497.163744224225               PO BIP
 18  (Cbed)  0 - 7        CAPACITOR     4.550972008524029E-012          PO BIP
 19  Vn      7 - 9        VW, WH NS V   3E-009                          PO BIP
 20  Vins    0 - 7        TESTPOINT SET,   R =  1E+020
```

FIG 7 PARTS LIST
2 RESONATOR OSCILLATOR

```
10 mhz 2xtal osc z config, 1
c1,C, 1 , 0 , 1E-010 , 0 , 0 , 0
{IZ},I, 1 , 10 , 1 , 0 , 0 , 0
{dR},R, 10 , 11 , 1.36E-005 , 0 , 0 , 0
{RV},R, 11 , 12 ,-3.917113507084587E-002 , 0 , 1 , 0
{XV},X, 12 , 13 ,-1.876242564109969E-007 , 0 , 0 , 0
(R1)XL1,R, 13 , 2 , 70 , 0 , 9 , 0
(C1),C, 2 , 3 , 2.1E-016 , 0 , 9 , 10000000
(Co),C, 1 , 3 , 1E-050 , 0 , 9 , 0
C'L1,L, 3 , 4 , 5.386228087475492E-007 , 0 , 1 , 0
Cc,C, 4 , 0 , 1E-009 , 0 , 0 , 0
(R1)XL2,R, 4 , 5 , 70 , 0 , 9 , 0
(C1),C, 5 , 6 , 2E-016 , 0 , 9 , 10000000
(Co),C, 4 , 6 , 1E-050 , 0 , 9 , 0
C'L2,L, 6 , 7 , 1E-006 , 0 , 1 , 0
C2,C, 7 , 0 , 1E-010 , 0 , 0 , 0
mm,N, 9 , 0 , 1 , 2.859460045734375E-002 , 100 , 1000
(rbe),R, 0 , 7 , 3497.163744224224 , 0 , 7 , 0
(Cbed),C, 0 , 7 , 4.550972008524029E-012 , 0 , 7 , 0
Vn,VW, 7 , 9 , 0 , 0 , 0 , 0
Vins,TP, 0 , 7 , 1E+020 , 0 , 0 , 0
```

FIG 8 NETLIST
2 RESONATOR OSCILLATOR

MEASUREMENT OF PRECISION OSCILLATOR PHASE NOISE USING THE TWO-OSCILLATOR COHERENT DOWN-CONVERSION TECHNIQUE

Christopher J. Pagnanelli and William F. Cashin
Ball Corporation, Efratom Division
Irvine, CA

Abstract

This paper addresses the characterization of precision frequency standard phase noise and spurious outputs using the two-oscillator coherent downconversion technique. This paper focuses on techniques for making accurate measurements of phase noise and spurious outputs within 100 KHz of a carrier. Significant sources of measurement error related to hardware design problems and inadequate measurement procedures are discussed, such as: measurement errors resulting from system noise sources, phase-locked loop effects, and system bandwidth limitations. In addition, methods and design considerations for minimizing the effects of such errors are presented. Analytic discussions and results are supplemented with actual test data and measurements made using measurement hardware developed at Ball Corporation, Efratom Division.

THEORY OF OPERATION

Two-oscillator coherent downconversion is a process by which the noise fluctuations and spurious outputs of a test oscillator are converted to equivalent baseband voltage fluctuations. As shown in Figure 1a, the basic ideal system consists of a test oscillator, a noiseless reference oscillator, an ideal mixer, a noiseless amplifier, and a spectrum analyzer. The spectrum analyzer is used to measure the power of the voltage fluctuations at the output of the coherent downconverter. Although this technique is commonly used at Efratom to make phase noise and spurious outputs measurements on precision frequency standards having output frequencies of 5 MHz or 10 MHz, coherent downconversion is a suitable technique for making noise measurements at any test oscillator frequency.

Random voltage fluctuations, at the output of the coherent downconverter, are produced by test oscillator phase noise and are expressed in terms of spectral density (dBc/Hz or dBV/Hz). However, making noise power measurements in a 1 Hz bandwidth can be inconvenient. For this reason, random noise power is typically measured in some known bandwidth and is then converted to an equivalent spectral density under the assumption that the voltage fluctuations approximate white noise within the measurement bandwidth. The conversion from noise power to noise spectral density can be realized by adding a correction factor equal to 10log(1/BW) to the measured noise power.

The term BW is noise bandwidth and is approximately equal to the resolution bandwidth of the spectrum analyzer used during the measurement. Most modern low frequency, digital spectrum analyzers can be configured to display measurements as spectral densities. Voltage-relative spectral densities, in units of dBV/Hz, can be converted to carrier power-relative spectral densities, in units of dBc/Hz, by taking into account the carrier power of the test oscillator.

Deterministic voltage fluctuations, at the output of the coherent downconverter, are produced by test oscillator spurious outputs. Deterministic voltage fluctuations are narrowband and are, therefore, expressed in terms of spectral power (dBc or dBV). Spurious outputs are generally measured in units of dBV and are then converted to more meaningful carrier power-relative units of dBc by taking into account the carrier power of the test oscillator.

Since, in the ideal case, the reference oscillator has no phase noise, its output $v_r(t)$ can be represented by a pure sinusoid;

$$v_r(t) = A_r \sin[2\pi(f_r)t]. \tag{1}$$

The output of the test oscillator differs from a pure sinusoid in that it is modulated in amplitude, frequency, and/or phase by random and deterministic noise. Although all these modulation components contribute to the overall spectral density of the test oscillator output, treatment of each is beyond the scope of this paper. Therefore, for simplicity the effects of frequency modulation and amplitude modulation will be ignored. The resulting output of the test oscillator, $v_0(t)$, is given by

$$v_0(t) = A_0 \sin[2\pi(f_0)t] = \Phi(t). \tag{2}$$

The term $\Phi(t)$ accounts for both random and deterministic phase fluctuations, which are typically referred to as phase noise. The output, $m(t)$, of the ideal mixer is the product of the reference and test oscillator outputs and is given by

$$m(t) = [(A_r/2)K_a A_0]\{\sin[2\pi(f_r - f_0)t + \Phi(t)] + \sin[2\pi(f_r + f_0)t - \Phi(t)]\}. \tag{3}$$

The term K_a is the low noise amplifier gain and the term $A_r/2$ can be thought of as the conversion gain/loss of the ideal mixer. Assuming that the reference oscillator and test oscillator are stable enough that they can be set to the same output frequency (i.e. $f_r = f_0$) and can be maintained in a quadrature phase relationship, then the output of the ideal mixer is given by

$$m(t) = [(A_r/2)K_a A_0]\{\sin[\Phi(t)] + \sin[2\pi(2f_0)t - \Phi(t)]\}. \tag{4}$$

The sum term is filtered away via a discrete filter, or via the bandwidth limitations of the low noise amplifier and/or spectrum analyzer, leaving only the difference frequency term. If a small signal approximation is made for $\Phi(t)$, then

$$\sin[\Phi(t)] \sim [\Phi(t)] \tag{5}$$

and the filtered output, $m_f(t)$, of the ideal coherent downconverter is approximately given by

$$m_f(t) = [(A_r/2)K_a A_0]\Phi(t). \tag{6}$$

As equation 6 indicates, the output of the ideal coherent downconverter is a baseband signal having voltage fluctuations which are proportional to the phase noise fluctuations of the test oscillator.

Practical implementations of the coherent downconverter usually differ from the ideal implementation in several respects. One difference is that the ideal mixer is generally implemented as a double-balanced diode mixer to provide inherent input/output isolation, and to provide AM rejection and rejection of some spurious outputs applied to the non-linear (LO) port. Modern double-balanced mixers use schottky diodes which have an exponential voltage versus current response. The output of the double-balanced schottky diode mixer is, therefore, a highly nonlinear function containing many high-order terms. In addition to sum and difference frequency products, the mixer generates harmonic intermodulation products at frequencies equal to $[\pm M f_r \pm N f_0]$, where M and N are integers. Although double balancing serves to suppress products formed by even values of M and N, even products are nonetheless present.

In addition to producing harmonic intermodulation products, a double-balanced diode mixer has only one linear input port (the RF port) and its conversion gain/loss is a nonlinear function of the drive level applied to the nonlinear port (the LO port). Ignoring all but the first-order mixer products, and assuming that the reference oscillator output drives the nonlinear mixer port, then the filtered coherent downconverter output for a double-balanced mixer takes the form

$$m_f(t) = [G_m(A_r) K_a A_0] \sin[2\pi(f_r - f_0)t]. \tag{7}$$

In equation 7, the nonlinear function $G_m(A_r)$ replaces the term $A_r/2$ in equation 6 as the conversion loss of the of the double-balanced mixer.

Although Gilbert cell mixers, such as modern active FET mixers, are a better approximation of the ideal mixer (having a square law relationship of voltage versus current response), the noise performance of such mixers has in the past been inferior to that of schottky diode mixers. It is also more difficult to implement double-balanced mixers with FETs than with schottky diodes, which is probably why the schottky diode mixers are used more frequently despite their lack of conversion gain. References 3 and 4 are useful sources of more information on the subject of mixers.

A second difference between the ideal and non-ideal system is that the frequency coherence and quadrature relationship between the reference and test oscillators is difficult to maintain manually. For this reason, servo electronics are typically employed. Since the double-balanced mixer acts as a phase detector, it includes an implicit integration (converting the oscillator frequency into phase). Therefore, a second integrator is usually the only additional circuitry required to implement a phase-locked servo loop. This is conveniently realized using an active lag-lead filter as shown in Figure 1b. If the frequency of the reference oscillator is not electronically controllable, than additional hardware may also be required to provide this feature.

Ideal and non-ideal systems also differ in that reference oscillator phase noise and low noise amplifier voltage noise contribute to the overall voltage fluctuations at the output of the coherent downconverter in practical systems. Although in some cases the noise contributions of the reference oscillator and low noise amplifier are insignificant, with regard to the measurement of precision oscillator phase noise this is generally not the case. Obtaining lower noise reference oscillators was essential for upgrading Efratom's phase noise test equipment to provide for more accurate, repeatable measurements.

Advantages/Disadvantages of the Coherent Downconversion Technique

When using the coherent downconversion technique, it is possible to make accurate measurements of precision oscillator phase noise and spurious outputs at small carrier offset frequencies. Such

measurements are difficult or impossible with some of the other phase noise measurement techniques. Direct spectrum analyzer measurements of phase noise and spurious outputs, for example, are limited by the resolution bandwidth and dynamic range of the spectrum analyzer. The noise power within the resolution bandwidth of the measurement must be large enough to overcome the dynamic range constraints of the spectrum analyzer. Thus, wide resolution bandwidths are required for making low level noise density measurements using the direct spectrum analyzer technique. However, it is difficult to make measurements at carrier offset frequencies much less than several times the measurement resolution bandwidth. Therefore, measurement of phase noise at low carrier offset frequencies requires use of a narrow resolution bandwidth. When narrow resolution bandwidths are employed, the noise power within the resolution bandwidth may be too low to overcome the dynamic range constraints of the spectrum analyzer. These measurement limitations, which are imposed by the frequency resolution and dynamic range constraints of spectrum analyzers, are avoided by using the coherent downconversion technique.

High-frequency commercial spectrum analyzers have frequency resolutions which are typically no better than 10 Hz and have dynamic ranges on the order of 80 dB. The 10 Hz resolution bandwidth limitation makes direct spectrum analyzer measurements difficult for carrier offsets much less than 100 Hz. Although suppressing the carrier in direct spectrum analyzer measurements with a calibrated narrow band notch filter can enhance measurement dynamic range by as much as 30 dB, this is generally insufficient improvement for making close-in phase noise measurements on precision oscillators. At offsets of 100 Hz, precision oscillator phase noise specifications can be better than -155 dBc/Hz. Assuming a measurement dynamic range of 110 dB and a frequency resolution of 10 Hz, the lower limit of direct spectrum analyzer noise measurements is -120 dBc/Hz. In comparison, coherent downconverter systems may have measurement capability which is better than -160 dBc/Hz at 100 Hz carrier offsets.

The graphs in Figure 2 are plots of the noise floor of the Efratom 5 MHz Phase Noise Tester, and demonstrate the low-noise measurement capability of coherent downconversion systems. The data was generated using two low noise 5 MHz oscillators. For each graph, output voltage fluctuations, in units of dBV/Hz, are plotted versus carrier offset frequency in Hz. The dBV/Hz readings are converted to dBc/Hz readings by subtracting 36 dB to take into account the power of the carrier at the output of the coherent downconverter. Therefore, according to Figure 2, phase noise measurements to nearly -160 dBc/Hz are possible at carrier offsets of 100 Hz and measurements to nearly -170 dBc/Hz are possible at carrier offsets of 10 KHz.

Phase noise and spurious outputs measurements using the coherent downconversion technique have several disadvantages, however. One disadvantage is the inability to distinguish lower sideband noise from upper sideband noise. Since coherent downconverter measurements are double-sideband measurements, the voltage fluctuations which appear at the output of the coherent downconverter are due to the combined effects of upper and lower sideband noise. Thus, measurement errors can result if an invalid assumption of sideband symmetry is made in converting double-sideband measurements to single-sideband measurements. Another disadvantage is that coherent downconverter systems are more complex and require significantly more hardware than direct measurement systems. This added complexity introduces various error sources which must be accounted for if accurate measurements are to be made. These disadvantages, however, are generally outweighed by the ability to make very low phase noise measurements close to the carrier using the coherent downconversion technique.

Conversion From Units of dBV to Units of dBc

In order to convert voltage-relative spectrum analyzer measurements to more useful carrier power-relative measurements, the amplitude of the test oscillator at the output of the coherent downconverter must be determined. Carrier amplitude can be accurately measured by producing a frequency offset between the test and reference oscillators and measuring the slope of the resultant beat note. If the test and reference oscillators are not at the same frequency and if the sum frequency and noise terms are ignored, then the coherent downconverter output, given by equation 3, becomes

$$m(t) = [G_m(A_r)K_a A_0]\sin[2\pi(f_r - f_0)t]. \tag{8}$$

This output beat note is usually severely clipped because of the voltage swing limitations of the low noise amplifier. Therefore, it is not possible to measure the peak voltage of the beat note directly. Measurement of beat note amplitude can be measured indirectly, however, by observing the slope of the rising and/or falling edges of the clipped waveform. It can be shown that the peak amplitude of the beat note is given by

$$[G_m(A_r)K_a A_0] = \frac{m(t_2) - m(t_1)}{\sin[2\pi(f_r - f_0)t_2] - \sin[2\pi(f_r - f_0)t_1]}. \tag{9}$$

Since only points on the beat note near the zero crossing are observed, the small signal approximation for a sinusoid is valid and equation 9 becomes

$$[G_m(A_r)K_a A_0] = \frac{m(t_2) - m(t_1)}{2\pi(f_r - f_0)(t_2 - t_1)} \tag{10}$$

$$= \frac{m(t_2) - m(t_1)}{t_2 - t_1} \times \frac{T}{2\pi}. \tag{11}$$

where T is the period of the beat note equal to $\frac{1}{f_r - f_0}$. Since voltage fluctuations are measured in units of dBV/Hz, beat note power P is usually expressed in units of dBV,

$$P\{[G_m(A_r)K_a A_0]\} = 20\log[\frac{m(t_2) - m(t_1)}{t_2 - t_1} \times \frac{T}{2\pi}] + 3 \text{ dB}. \tag{12}$$

The beat note/carrier power is commonly referred to as the "gain" of the coherent downconverter.

The 3 dB correction factor in equation 12 accounts for conversion from double-sideband to single-sideband in phase noise measurements (by convention, phase noise $\mathcal{L}(f)$ is defined as an upper sideband measurement) and conversion from peak to RMS in spurious outputs measurement. An additional 3 dB correction factor for conversion from double-sideband to single-sideband is sometimes included in spurious outputs measurement, resulting in an overall correction factor of 6 dB. However, the extra 3 dB for spurious outputs is valid only if the lower sideband spur is equal in amplitude and phase to the upper sideband spur. It is possible that the lower sideband spur amplitude is significantly different from that of the upper sideband spur. Therefore, the accepted method is to assume that one sideband does not contribute to the measured spur amplitude so that the same 3 dB correction factor is applied to both phase noise, $\mathcal{L}(f)$, and spurious outputs measurements.

SOURCES OF ERROR IN PHASE NOISE/SPURIOUS OUTPUTS MEASUREMENT

The limitations imposed by practical realizations of the ideal coherent downconverter result in error sources which must be accounted for in order to make accurate phase noise measurements. Usually, it is not difficult to eliminate and/or to compensate for these sources of error.

Reference Oscillator Noise

With regard to the phase noise measurement of precision frequency standards, the contribution made to coherent downconverter output voltage fluctuations by the reference oscillator noise cannot be neglected. If reference oscillator noise contributes significantly to the output voltage fluctuations of the coherent downconverter, then the reference oscillator output cannot be represented as a pure sinusoid. The output of a noisy reference oscillator is given by

$$v_r(t) = A_r \sin[2\pi(f_r)t - \Theta(t)], \tag{13}$$

where $\Phi(t)$ is the phase noise of the reference oscillator and, for illustration, frequency and amplitude noise have been ignored. Assuming that the reference oscillator drives the mixer nonlinear port and that the reference oscillator and test oscillator output frequencies are equal and in quadrature, then the coherent downconverter output is given by

$$m(t) = [G_m(A_r)K_a A_0][\Phi(t) + \Theta(t)], \tag{14}$$

neglecting all but the first-order difference term.

Equation 14 implies that the significance of reference oscillator noise depends on its power relative to the test oscillator noise. Reference oscillator noise relative to reference oscillator carrier power is less important due to the nonlinear operation of the mixer which causes test set gain to be relatively independent of reference oscillator carrier power. Reference oscillator noise is summed with the test oscillator noise to produce voltage fluctuations at the coherent downconverter output. The degree to which output voltage fluctuations increase as a function of reference oscillator noise power relative to test oscillator noise power is given in Table 1. As the table indicates, reference oscillator phase noise becomes significant when its power is greater than approximately -10 dB relative to test oscillator phase noise power. For these reasons, the effects of reference oscillator phase noise are minimized when the mixer LO nonlinear port is driven with the reference oscillator output at as low a level as possible to ensure on/off switching of the mixer diodes and the mixer linear port is driven with the test oscillator output at as high a level as high as possible without nearing the breakdown region of the mixer diodes.

Note that this approach contradicts the normal procedure of driving the LO port as hard as possible and the RF port as low as possible to get minimum intermodulation products (see references 1, 5, and 6). The actual optimal drive levels will be a compromise between the requirements for minimizing reference oscillator noise and for minimizing intermodulation products. These levels will depend on the noise contributions of the mixer/low pass filter, the test oscillator, and the reference oscillator. Note when testing units with a range of output amplitudes, low noise, variable-gain amplifiers may be employed to optimize mixer drive levels to achieve the best overall system performance.

To this point, it has been assumed that either the LO nonlinear port of the double-balanced mixer is driven with the reference oscillator output or that the reference oscillator and test oscillator output amplitudes are equal. The first is generally a good practice because noise and spurious outputs measurements made on a test oscillator are most meaningful to system designers when they are expressed relative to test oscillator carrier power. As mentioned previously, to convert voltage-relative measurements (in units of dBV) to carrier power-relative measurements (in units of dBc) the carrier power at the output of the coherent downconverter must be determined. The gain of the coherent downconverter is a measure of test oscillator carrier power only when the test oscillator drives the linear port of the mixer. This is because the nonlinear (LO) port of the mixer approximates a hard-limiter when it is driven hard to minimize unwanted intermodulation products. For this condition, mixer output power is approximately independent of nonlinear port drive level. Thus, if the test oscillator output drives the mixer nonlinear port, then coherent downconverter gain becomes a measure of reference oscillator carrier power. In this case, conversion of measurements from dBV/Hz to dBc/Hz results in the phase noise of the test oscillator being expressed relative to reference oscillator carrier power. Therefore, driving the mixer nonlinear port with the test oscillator output will result in measurement errors unless the reference oscillator carrier power is exactly equal to the test oscillator carrier power, or unless the oscillator power levels are accurately measured and the difference is taken into account. Ensuring such a condition may not be practical in a high volume production environment without expensive automated testing equipment and development.

Although driving the mixer nonlinear port with the test oscillator output will result in measurement errors when the amplitudes of the test and reference oscillator differ significantly, a potential advantage of this scheme is the suppression of test oscillator amplitude noise. Amplitude noise and angle noise are indistinguishable at the coherent downconverter output. If the amplitude noise of the reference oscillator is negligible, then driving the mixer nonlinear port with the test oscillator output provides a means of isolating test oscillator angle noise from test oscillator amplitude noise (see references 1 and 5).

Although reference oscillator noise is typically a significant error source in the measurement of precision oscillator phase noise, its effects can be accounted for in the phase noise measurement of a test oscillator if a third oscillator is available. As equation 14 indicates, output voltage fluctuations at the coherent downconverter output are approximately a linear function of the sum of reference oscillator and test oscillator phase noise fluctuations. Therefore, noise measurements made on each pair of three oscillators results in three independent linear equations which can be solved to determine the phase noise of the reference oscillator (keeping in mind the stochastic nature of the signals). Once reference oscillator phase noise is known, it can be subtracted from future phase noise measurements of test oscillators. This technique is sometimes referred to as a three-corner hat measurement [reference 1; Walls, *et al.*].

Low Noise Amplifier Effects

In addition to reference oscillator noise, low noise amplifier noise is another significant noise source with regard to the measurement of precision oscillator phase noise. The noise floor of the coherent downconverter system is a function of reference oscillator noise, mixer conversion loss and low noise amplifier noise. Therefore, careful attention should be given to the design or selection of the low noise amplifier.

PLL Tracking Effects

Servo electronics are typically employed in order to maintain the frequency coherence and quadrature phase relationship between the test and reference oscillators in coherent downconverter systems. Phase-locked loop (PLL) tracking effects, however, produce attenuation of test oscillator noise at frequencies significantly below the natural frequency of the loop and can, therefore, result in measurement errors. By examination of the block diagram in Figure 1b, the closed-loop transfer function from the coherent downconverter input to the coherent downconverter output can be written:

$$H(s) = \frac{\Phi_{out}}{\Phi_{in}} = \frac{2G_m(A_r)K_aA_0}{\pi} = \frac{s^2}{s^2 + s2\zeta W_n + W_n^2}, \tag{15}$$

where $W_n = \sqrt{\{4K_vG_m(A_r)K_aA_0/R_sC_f\}}$ and $\zeta = R_fC_fW_n/2$. The term K_v is the modulation sensitivity of the reference oscillator in units of hertz per volt. Equation 15 is the transfer function of a damped two-pole high-pass filter with a pole frequency at W_n. From equation 15 it is apparent that at frequencies much greater than W_n, phase noise fluctuations are amplified and at frequencies much below W_n, phase noise fluctuations are attenuated. The criteria for selection of the PLL filter is covered in many standard texts on phase-locked loops; reference 5 also includes a discussion.

Figure 3 contains plots of the measured spectral density of an Efratom commercial rubidium frequency standard (model FRS-C). Figure 3a is a plot of spectral noise at carrier offset frequencies ranging from 0 Hz to 5 Hz, measured using PLLs with three different natural frequencies. The results given in Figure 3a clearly demonstrate the effects of PLL tracking and their relation to loop natural frequency. Note that testing at low offset frequencies with a fast PLL loop can lead to significant errors in phase noise readings; over 18 dB at 1 Hz and 31 dB at 0.5 Hz for the measured FRS.

Because of PLL tracking effects, the bandwidth of coherent downconverter loops are generally very narrow (i.e., W_n is a low frequency). Not only does the use of narrow band loops minimize the errors associated with PLL tracking effects, but a secondary benefit is realized in that the noise contributions of the loop filter are minimized. Again, by examination of the block diagram in Figure 1b, the closed-loop transfer function from the loop filter input to the coherent downconverter output can be written

$$H(s) = \frac{e_n\text{out}}{e_n\text{in}} = \frac{2\zeta W_n + W_n^2}{s^2 + s2\zeta W_n + W_n^2}. \tag{16}$$

Equation 16 is a single-pole low pass filter response with a pole frequency at W_n]. Therefore, the input voltage noise associated with the loop filter is attenuated at frequencies greater than W_n.

A disadvantage of narrow band servo loops is that they acquire very slowly. If the frequency offset between the test oscillator and the reference oscillator is large compared to the loop bandwidth, acquisition may require hours. This problem is typically overcome by incorporating variable bandwidth capability into the coherent downconverter servo loop design. Acquisition is achieved quickly with a wide loop bandwidth and measurements are made in a narrow band mode. Measurement systems at Efratom have successfully employed variable-bandwidth phase-locked loop designs.

System Bandwidth Limitations

While PLL effects cause low frequency noise measurement errors, system bandwidth limitations result in the attenuation of high frequency noise, and therefore, produce measurement errors at high

frequency. The availability of wide band, low-noise amplifiers reduces the severity of this problem, and generally, it is not difficult to design low noise measurement systems with bandwidths in excess of a few hundred kilohertz. For example, the latest measurement systems at Efratom typically exhibit only fractions of a dB of amplitude variation to frequencies of 100 KHz, as shown by the flat noise floor performance to 100 KHz in Figures 2d, 3d, and 4d. The phase noise measurement system at Efratom uses a Hewlett Packard model HP3561A spectrum analyzer, which has a maximum frequency span of 100 KHz. A 100 KHz frequency span is typical of fast-fourier real time spectrum analyzers, although Tektronix has recently introduced a 200 KHz model (model 2642).

The usable bandwidth of a coherent downconverter system can be extended by measuring the amplitude response of the system versus frequency, and incorporating frequency dependent calibration factors into the equation for system gain. This compensates for the high frequency attenuation imposed by system bandwidth limitations. The amplitude response of a coherent downconverter can be determined using two synchronized signal generators in place of the test and reference oscillators.

Frequency Conversion Effects

Unlike an ideal mixer, a double-balanced mixer produces harmonic intermodulation products. For this reason, spurious outputs which are far from the test oscillator carrier, and are outside the measurement bandwidth of the coherent downconverter, can be translated to frequencies which are within the measurement bandwidth of the system. Although harmonic intermodulation products are typically many decibels below the desired first-order mixer products, high-order spurious conversion products which fall within the system bandwidth are indistinguishable from spurious outputs which are close to the carrier. One key to minimizing these effects is to properly terminate the output (IF) port of the mixer. This issue is discussed in detail in reference 4.

Accurate measurement of spurious outputs using coherent downconversion requires that high frequency spurious outputs first be identified and measured using a direct spectrum analyzer technique. An analysis of mixer spurious outputs, which takes into account the specified harmonic intermodulation performance of the mixer, can then be performed to predict the location and level of high-order spurious conversion products. However, such an analysis is generally not practical in a large-scale production environment, and the source of spurious outputs is usually of little concern as long as they are within specified performance limits.

Frequency conversion effects become more significant when, instead of a sinusoid, the test oscillator output is a square wave which is rich in harmonic content. Harmonic intermodulation effects resulting from square wave inputs can be minimized by inserting low pass filters between square wave oscillator outputs and coherent downconverter inputs. This technique was utilized in the measurements of the FRS-C TTL-compatible output of Figure 3.

60-cycle Interference and the Use of Batteries

Sixty-cycle interference and its harmonics couple onto system power supplies and appear in the output frequency spectrum of the coherent downconverter. Although 60-cycle spurs are easily identified according to frequency, 60-cycle interference can camouflage actual spurious outputs performance. Through careful system design, 60-cycle interference can be minimized, however. Careful attention to grounding and the use of battery supplies can virtually eliminate 60-cycle interference from the output spectrum of the coherent downconverter.

The use of magnetic shielding around the sensitive front end of the downconverter may also be

required, along with shielding the control voltage to the reference oscillator, in order to minimize 60-cycle interference. The use of separate batteries for the phase noise tester, the reference voltage-controlled oscillator, and the test oscillator can prevent ground loops that cause unusual spurious results.

A side effect of using batteries is that performance anomalies may occur as the batteries become deeply discharged, depending on the sensitivity of the measurement system to supply voltage levels. Battery voltage monitors and associated disconnect relays can be employed to prevent this.

FFT Windowing Effects

Because of their superior frequency resolution, digital spectrum analyzers are generally used to measure voltage fluctuations at the output of the coherent downconverter. The choice of the windowing function used with fast-fourier transform (FFT)-based spectrum analyzers, however, can affect measurement accuracy. Phase noise measurements are most accurately made using the Hanning windowing function. The Hanning window has a narrow passband and very low sidebands, providing better measurement resolution for analyzing broadband signals like noise. Spurious outputs are most accurately measured using a flat top windowing function. Although the flat top window has higher sideband energy, its broad passband makes it better suited for measurement of narrow band, deterministic signals. Errors which result from incorrect window choice are typically less than 1 dB. Reference 8 goes into more detail on this subject.

Vibration Effects

Precision oscillators are frequently designed using quartz crystal resonators to achieve superior phase noise and short-term frequency stability performance. The phase noise of crystal oscillators is affected by vibration, however. The "G sensitivity" of a precision crystal is typically on the order of parts in $10^{-10}[df/f]/G$ to parts in $10^{-9}[df/f]/G$; this translates into phase noise and spurs by well established formulas. The Efratom "Time and Frequency Handbook" of reference 13 goes into this and other related subjects in more detail. References 11, 14, 15, and 16 present a broad overview of vibration and other effects on phase noise.

Because of vibration sensitivities, it is important to shield and dampen both the reference oscillator and the test oscillator from shock and vibration in order to obtain accurate quiescent phase noise readings. Otherwise, the ambient vibration levels of the test building or test table can increase the apparent phase noise floor of the oscillator.

In addition, the capacitance of the coaxial cable often changes with vibration. This can again result in an apparently degraded phase noise floor performance of a test oscillator due to the cable-induced loading effects related to ambient vibration levels.

When it is necessary to measure the vibration performance of an oscillator, a number of factors must be considered. Mechanical resonances in the fixture holding the test oscillator to the shaker can give errors, as can the type of coaxial cable used to connect the test oscillator to the phase noise tester. Electromagnetic interference (EMI) induced from the shaker head and the controller can also result in measurement errors, often requiring either shielding or separation of the measurement equipment from the shaker.

Miscellaneous Error Sources

A number of additional error sources may be encountered in the measurement of precision oscillator phase noise and spurious outputs. Although not exhaustive, these error sources include: poor grounding and intermittent grounding; inadvertent conversion of deterministic signal power measurements from dBV to dBc/Hz; injection locking of the test and reference oscillators due to inadequate EMI shielding; magnetic and electrostatic susceptibility and emissions of the test oscillator and/or reference oscillator; and failure to account for cable losses in high frequency measurements.

TEST DATA

Phase noise test performance was measured for two Efratom rubidium oscillator products for this paper. Rubidium oscillators frequency lock a voltage-controlled crystal oscillator to the long-term stability of the hyperfine atomic energy state transitions of the Rb^{87} atom. They are utilized to provide excellent long term frequency stability (on the order of parts in 10^{11}/month with excellent phase noise and spurious outputs performances.

The phase noise behavior expected from crystal oscillators is described in reference 7. The presence of a rubidium control loop will modify the ideal oscillator behavior in a number of ways depending on the relative phase noise of the rubidium physics package and the crystal oscillator. The rubidium loop crossover frequency controls the hand-off between the two; an improvement in phase noise or a lower slope below this frequency implies a good physics package phase noise relative to the crystal oscillator used.

The first unit evaluated was a model FRS-C; a stock, economical, commercial 10 MHz TTL-compatible rubidium oscillator. The FRS-C is specified for a phase noise of -110 dBc/Hz at 100 Hz carrier offset and -130 dBc/Hz at 1000 Hz offset. Non-harmonic spurious outputs are specified at -65 dBc. The second unit evaluated was a stock, commercial 10 MHz sine output low noise unit (model FRK-LN). The FRK-LN is specified for a phase noise of -120 dBc/Hz at a 10 Hz carrier offset and -147 dBc/Hz at 100 Hz and 1000 Hz offsets. Non-harmonic spurious outputs are specified at -70 dBc. Although units with better phase noise performance are available at Efratom, these two products are representative.

Test data for the FRS-C is given in Figure 3 and for the FRK-LN data in Figure 4. The phase noise test system used to make these measurements is an upgrade to that formerly used at Efratom, and is in a final phase of development. Because the development of the system is not yet complete, the final grounding and shielding configurations were not implemented, leaving some residual problems in the spurious outputs performance of the system.

The HP3561A spectrum analyzer, used to make the measurements which are displayed in Figures 2 through 4, was configured to provide for automatic conversion from noise power to noise spectral density. Thus, chart readings are displayed in units of dBV/Hz. The coherent downconverter gain was measured to be roughly 30 dB for both units, including the necessary correction factors for double-sideband to single-sideband conversion and for peak to RMS conversion. Therefore, the chart measurements should be adjusted by -30 dB to give phase noise performance in dBc/Hz. Since spurious outputs must be expressed in terms of power rather than spectral density, it is necessary to convert the displayed spurious output levels from units of dBV/Hz to units of dBV. This is done by adding a conversion factor equal to 10log(BW), where BW is the resolution bandwidth of the measurement displayed at the bottom of each graph. Spurious output levels, in units of dBV,

should then be adjusted by an additional -30 dB to give spurious outputs performance in units of dBc.

Figure 3a gives three plots of FRS-C phase noise performance within 5 Hz of the carrier. The different PLL natural frequencies are clearly shown for each plot. The rubidium servo loop crossover frequency is at roughly 35 or 40 Hz for this unit, as shown by the spectral leveling which occurs in Figure 3b. Spurious outputs at the modulation frequency of the rubidium control loop are evident in Figure 3c; the 127 Hz rubidium loop modulation spurious output is roughly -80 dBc, after applying a correction factor of +6 dBc to convert from spectral density to power.

The noise floor of this unit is measured to be roughly -140 dBc, as shown in Figure 3d. Two plots have been superimposed in Figure 3d. One plot drives the coherent downconverter directly with the square wave output of the test oscillator. In the second plot, the test oscillator drives the coherent downconverter through a 10.5 MHz low pass filter, which removes harmonic frequency components. Note the addition of the filter changes the level and frequency of the spurious outputs, indicating they may not be produced directly by the test oscillator. It is possible these spurious outputs are related to grounding and/or shielding effects; this will be verified with the final version of the Efratom phase noise tester being developed. Although the source of these relatively high-frequency spurious outputs is not known, the largest shown in Figure 3d occurs at an offset frequency of about 78 KHz. Its level, using the output low pass filter, is -98 dBc after applying a correction factor of + 26 dBc to convert from spectral density to power. This is well below the -65 dBc spurious outputs specification of the unit.

Figure 4 gives similar performance curves for the model FRK-LN, 10 MHz unit. The rubidium servo loop crossover frequency occurs at about 2 Hz, as indicated by the spectral leveling shown in Figure 4a. Figure 4b gives phase noise performance to a carrier offset frequency of 100 Hz, while Figure 4c gives performance to an offset frequency of 1000 Hz. A spurious output at the modulation frequency of the rubidium control loop is shown in Figure 4c; the level of the 127 Hz spurious output is roughly -117 dBc, after correcting for carrier power and converting from spectral density to power. Figure 4d gives phase noise performance to an offset frequency of 100 KHz; the noise floor is shown to be roughly -157 dBc/Hz. Note that the noise floor is flat to the 100 KHz range of the spectrum analyzer.

CONCLUSION

The limitations imposed by practical realizations of the ideal coherent downconverter result in error sources which can result in inaccuracies in the measurement of precision oscillator phase noise and spurious outputs. Phase-locked loop tracking effects, system bandwidth limitations, and system noise can be significant sources of error. Most significant sources of error, however, can be eliminated and/or controlled through careful system design and calibration. The measurement system developed at Efratom has attempted to strike a balance between overall accuracy and volume testing in a production environment; the accuracy and repeatability for the production measurements performed at Efratom are on the order of 1 to 3 dB with an upgraded test measurement system and upgraded test procedure.

ACKNOWLEDGMENTS

The underlying principles of phase noise testing described in this paper are not new. The general subject has been covered in a number of papers and tutorial sessions, from both government sources (including the National Institute for Science and Technology, or NIST, at Boulder, Colorado and the US Army Laboratory Command at Fort Monmouth) and industry sources (Hewlett Packard, Raytheon, and others). Hopefully, this paper brings out new material with practical suggestions on designing and using phase noise testers that supplements the earlier work.

Dr. Fred Walls, Dave Allan, and David Howe and others at NIST (the National Institute for Science and Technology at Boulder, Colorado) have been of considerable help in broadening our understanding of phase noise measurement. They have developed techniques to accurately measure phase noise with 1 dB of accuracy for analysis bandwidths up to 10% of a carrier frequency up to a 1 GHz carrier, using a calibrated phase modulation technique and careful design [Walls, *et al.*]. These techniques have only been partially implemented in our current production phase noise test equipment at Efratom for two reasons; because of the need for inexpensive equipment used in a volume production environment, and because of our relatively narrow analysis bandwidth and low carrier frequencies tested (10 KHz to 100 KHz maximum bandwidths, and 5 MHz or 10 MHz carrier frequencies). However, the insights provided on error sources have been invaluable. Anyone new to the field wishing to gain a broad overview of time and frequency is well advised to attend the annual week long seminar provided by NIST.

Hewlett Packard has also been instrumental in providing a series of seminars, application notes and papers on phase noise measurement techniques (see references 9, 10). Their free seminars are well worth attending as well.

In addition, publications by John Vig and the US Army Laboratory Command have also provided valuable insight into the subject of precision oscillator phase noise performance in general.

References

[1] Walls, F.L. and Felton, C.M., Clements, A.J.D., " *Accuracy model for phase noise measurements,*" National Institute of Standards and Technology

[2] Allan, David, *et. al.*, *"Standard terminology for fundamental frequency and time metrology,"*

[3] Hayward, W., **"Introduction to Radio Frequency Design,"** Prentice Hall, 1982

[4] Maas, S., **"Microwave mixers,"** Artech House, 1986

[5] Wall, *et. al., "Design considerations in state-of-the-art signal processing and phase noise measuring systems,"* Frequency Stability: Fundamentals and Measurement, IEEE Press, 1983

[6] Howe, David, *"Frequency domain stability measurements: a tutorial introduction,"* NBS Technical Note 679, March 1976

[7] Moulton, G., *"Dig for the roots of oscillator noise,"* Microwaves & RF, April 1986

[8] Benson, D., *"Techniques for Signal and System Analysis,"* Tektronix, Inc., 1991

[9] Scherer, D., *"The 'art' of phase noise measurement,"* RF & Microwave Mesurement Symposium and Exhibition, Hewlett Packard, August 1985

[10] " *Understanding and measuring phase noise in the frequency domain,"* Hewlett Packard, Application Note 207

[11] Parker, T. and Montress, G., *"Introduction to phase noise measurements,"* Tutorial Presented at: 45th Annual Symposium on Frequency Control, 28 May 1991

[12] Goldman, S., *"Phase noise leakage through a mixer,"* MSN & CT, November 1987, pp 88-96

[13] **"Precision Time and Frequency Handbook,"** Ball Efratom Division, 8th Edition, 1991

[14] Camhi, Alfred and Shniper, Sam, *"Predict source phase noise under vibration,"* Microwaves and RF, April 1991, pp. 83-86

[15] Filler, Raymond L., *"The effects of vibration on frequency standards and clocks,"* Proceedings 35th Annual Frequency Control Symposium, Fort Monmouth, NJ: US Army Electronics Command, May 1981, pp. 31-39

[16] Vig, John, *et. al., "The effects of acceleration on precision frequency sources,"* Research and Development Technical Report SLCET-TR-91-3, Fort Monmouth, NJ: US Army Laboratory Command, March 1991

Table I. Increase in Measured Noise Versus Reference Oscillator Noise Relative to Test Oscillator Noise

Relative Amplitude of Ref Osc Phase Noise to Test Osc Phase Noise	Increase in Voltage Fluctuations at Coherent Downconverter Output
-20 dB	0.04 dB
-10 dB	0.42 dB
- 6 dB	0.97 dB
- 3 dB	1.76 dB
- 2 dB	2.12 dB
- 1 dB	2.54 dB
0 dB	3.01 dB
1 dB	3.54 dB
2 dB	4.12 dB
+3 dB	4.77 dB
+6 dB	6.99 dB

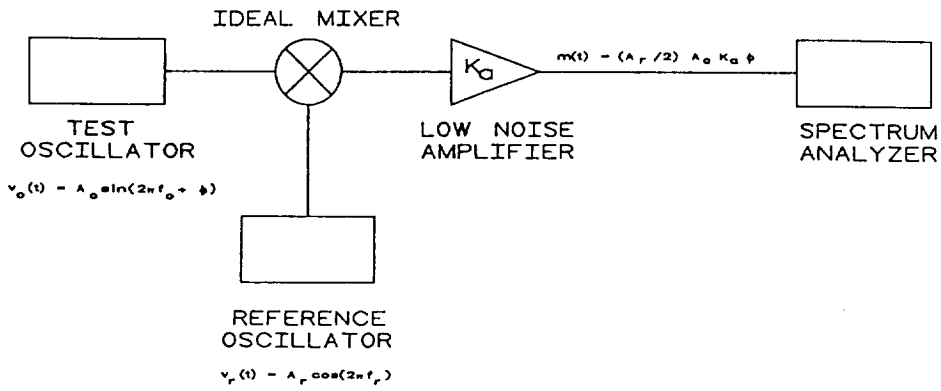

Figure 1a: Ideal Coherent Downconverter

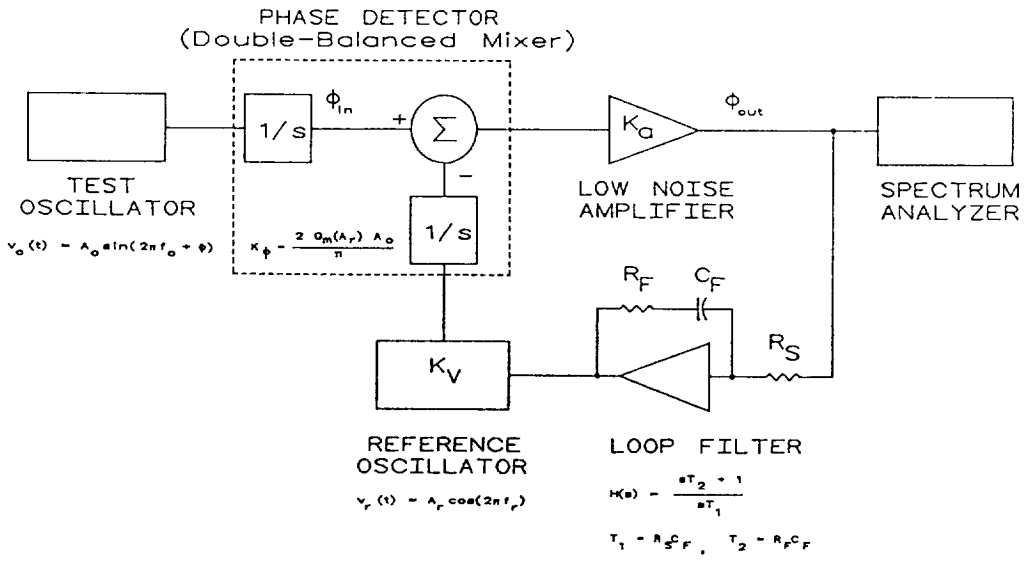

Figure 1b: Practical Implementation of Ideal Coherent Downconverter

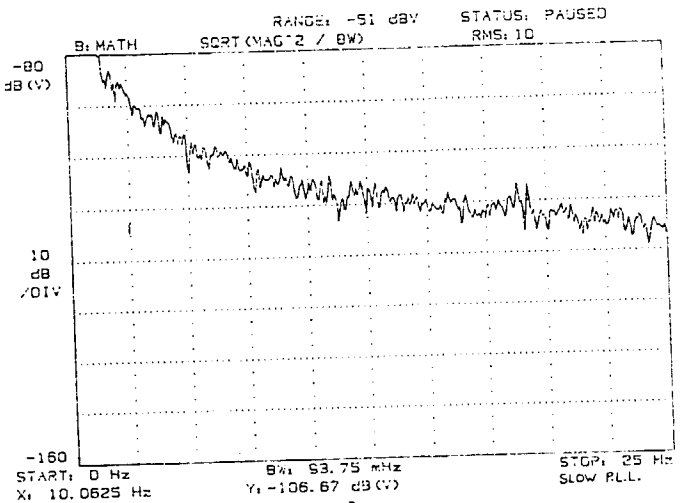

Figure 2a

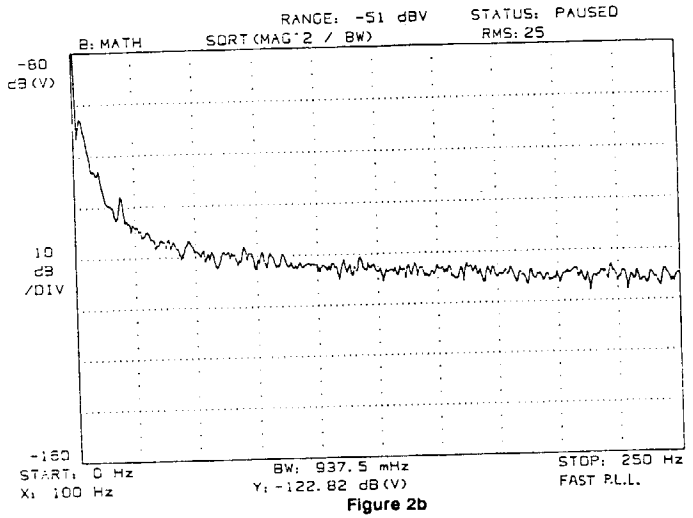

Figure 2b

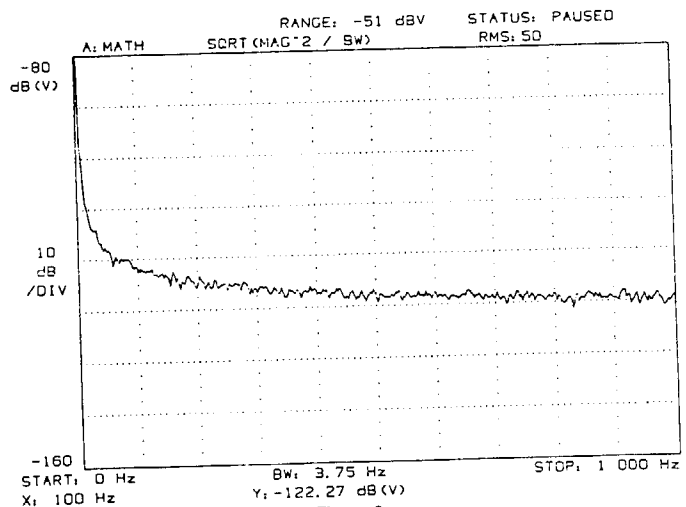

Figure 2c

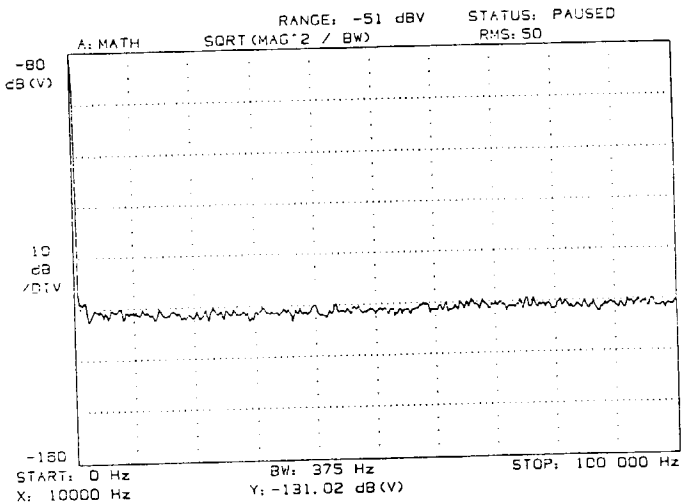

Figure 2d

(Test Set Gain ~ 33 dB)

Figure 2. 5 MHz LN Wensil Oscillators in Phase Noise Tester

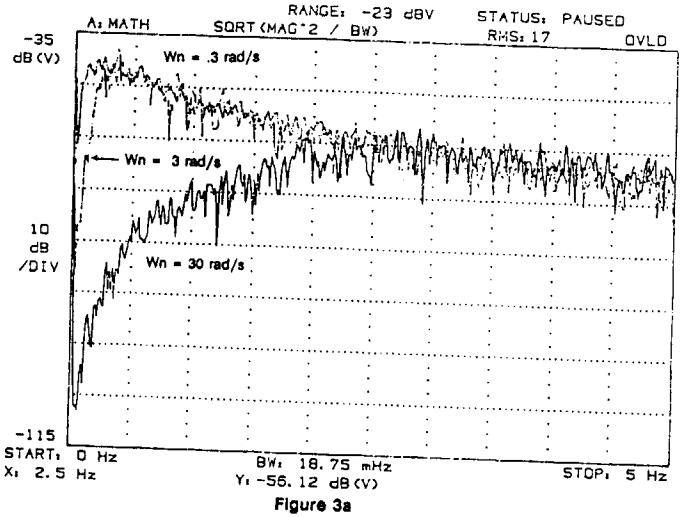

Figure 3a

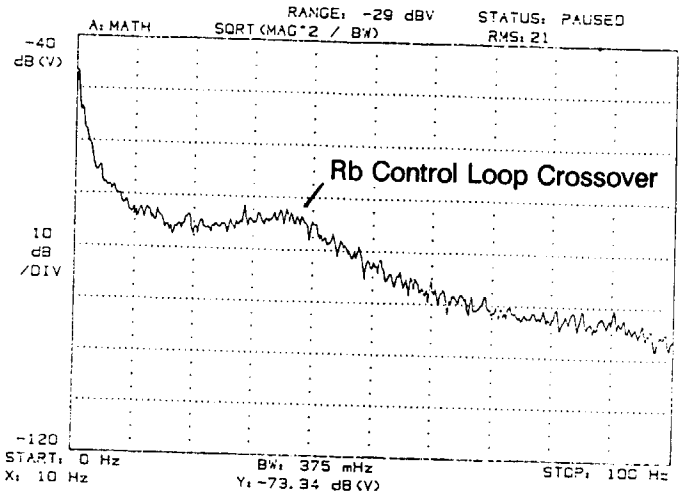

Figure 3b

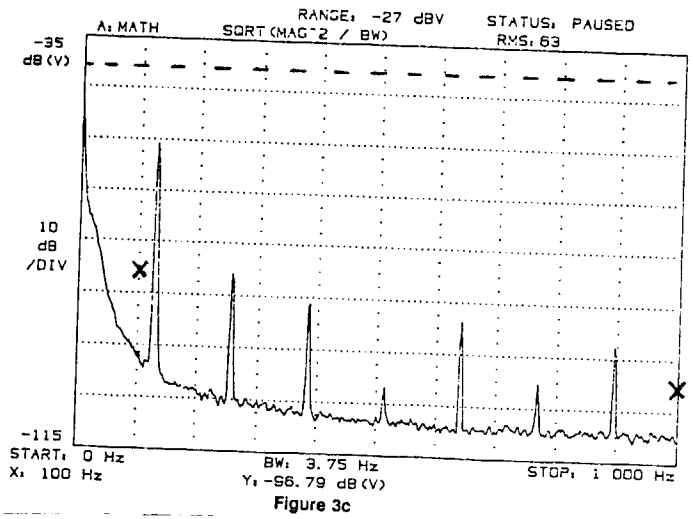

Figure 3c

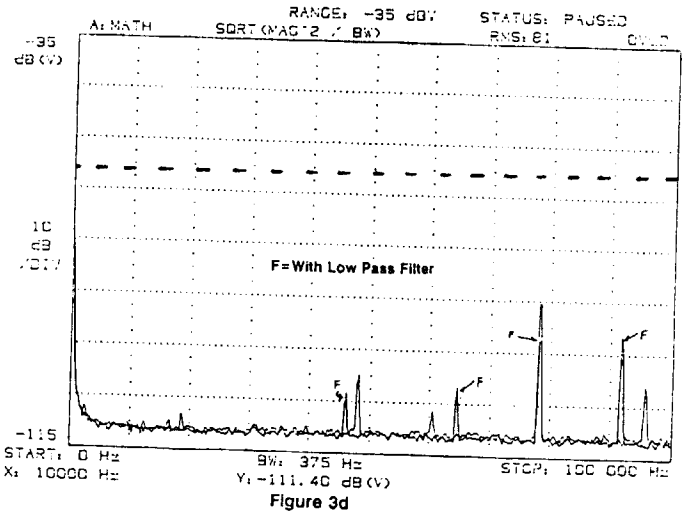

Figure 3d

Test Set Gain ~ 30 dB

--- Spur spec.
X Phase noise spec.

Figure 3. 10 MHz FRS-C Phase Noise Measurements (TTL Output)

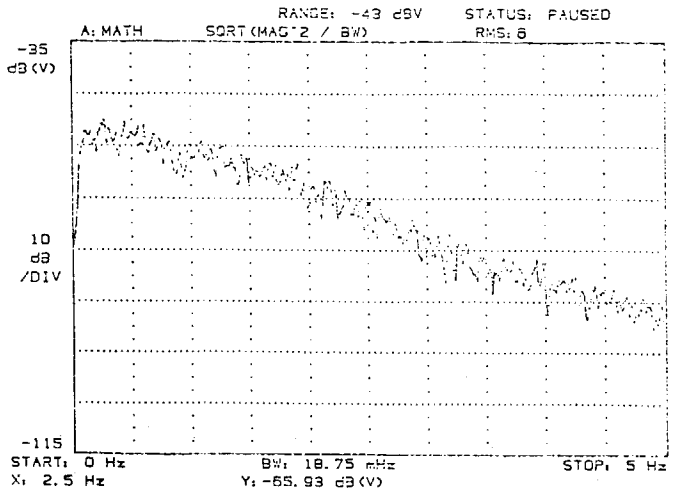

Figure 4a

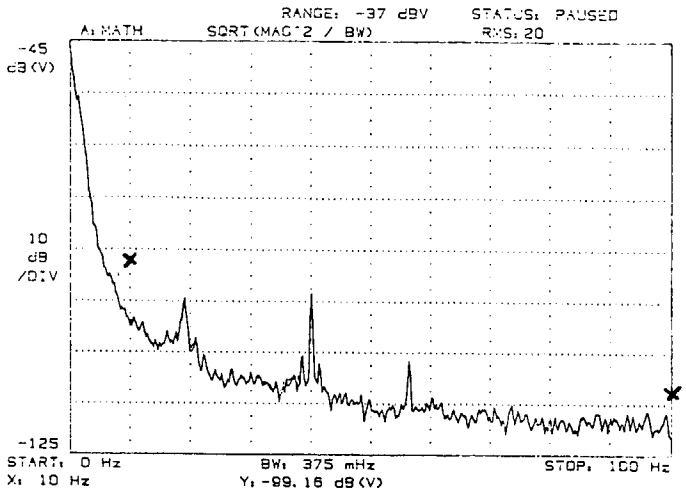

Figure 4b

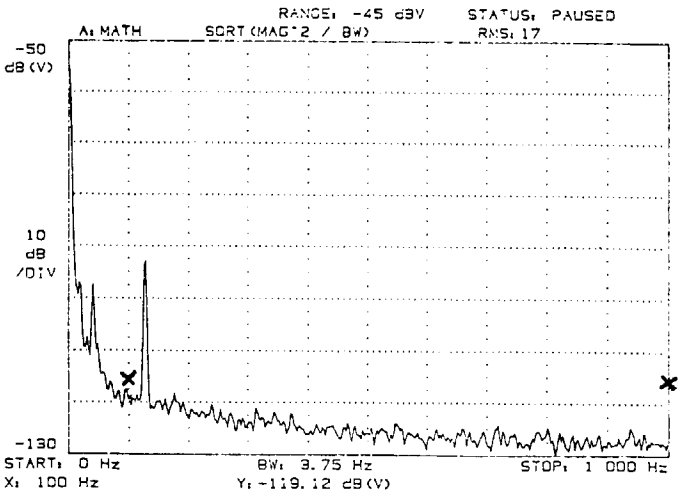

Figure 4c

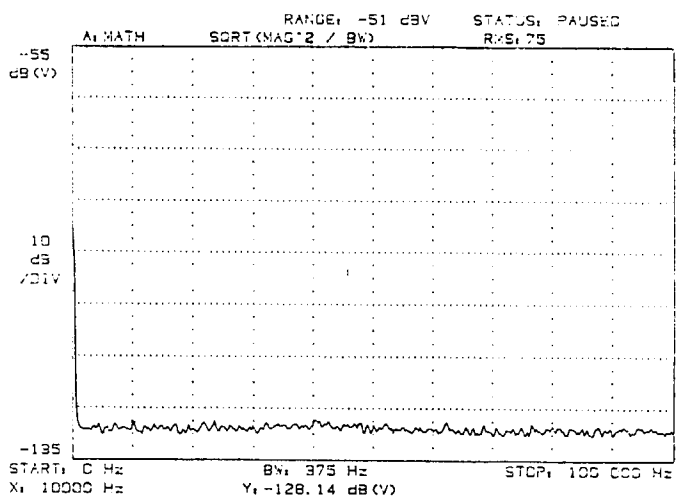

Figure 4d

Test Gain ~ 30 dB

X Phase noise spec.
Spur spec. off chart

Figure 4. 10 MHz FRK-LN Phase Noise Measurement

AN IMPROVED OFFSET GENERATOR DEVELOPED FOR ALLAN DEVIATION MEASUREMENT OF ULTRA STABLE FREQUENCY STANDARDS*

R. L. Hamell, P. F. Kuhnle, R. L. Sydnor
California Institute of Technology
Jet Propulsion Laboratory
4800 Oak Grove Drive
Pasadena, California 91109

Abstract

Measuring the performance of ultra stable frequency standards such as the Superconducting Cavity Maser Oscillator (SCMO) will necessitate improvement of some test instrumentation. The frequency stability test equipment used at JPL includes a 1 Hz Offset Generator to generate a beat frequency between a pair of 100 MHz signals that are being compared. The noise floor of the measurement system using the current Offset Generator (1.7×10^{-14} at 1 second tau and 6.2×10^{-17} at 1000 seconds), is adequate to characterize stability of hydrogen masers, but will not be for the SCMO. A new Offset Generator with improved stability has been designed and tested at JPL. With this Offset Generator, and a new Zero Crossing Detector recently developed at JPL, the measurement floor has been reduced by a factor of 5.5 at 1 second tau, 3.0 at 1000 seconds, and 9.4 at 10000 seconds, compared against the previous design. In addition to the new circuit designs of the Offset Generator and Zero Crossing Detector, tighter control of the measurement equipment environment has been required to achieve this improvement. The design of this new Offset Generator will be described, along with details of the environment control methods used.

INTRODUCTION

Allan Deviation measurements made at the Jet Propulsion Laboratories Frequency Standards Laboratory require an offset generator to test some types of equipment. The offset generator is used, for example, to test a frequency source when neither the measurement device or the frequency reference can be offset to obtain a 1 Hz beat for the zero crossing detector [1]. It is also used to test 2-port devices. A single 100 MHz reference carrier is split into two paths, with one path to the zero crossing detector containing the 2-port device in test, and the other path containing the offset generator to develop the 1 Hz beat signal for the zero crossing detector. Figure 1 shows the instrumentation used to perform these tests.

*This work was carried out at the Jet Propulsion Laboratory, California Institute of Technology, under a contract with the National Aeronautics and Space Administration.

OFFSET GENERATOR DESIGN

A block diagram of the offset generator is shown in Figure 2. The 1 Hz offset is generated in two steps, using divide and mix direct frequency synthesis to first develop a -10 Khz offset in the input stage, then a +9.999 KHz offset in the output stage. The input stage translates the input frequency by a factor of $1-10^{-4}$, and the output stage by a factor of $1+10^{-4}$ so that $F(out) = F(in) \times (1 - 10^{-4}) \times (1 + 10^{-4}) = 99.999999$ MHz. The output of each stage is taken from a phase locked crystal VCO acting as a narrow band output filter to minimize the spurious frequency products in the offset generator output.

OFFSET GENERATOR PERFORMANCE

Performance of the present day offset generator is adequate to measure stability of frequency standards in current use in the NASA/JPL Deep Space Network. Stability of the offset generator is compared against a hydrogen maser stability in Figure 3. Future requirements for the Deep Space Network specify tighter frequency stability limits than these present frequency standards can supply [2]. To test to these tighter standards in the future, and the very high stability fiber optic reference signal transportation links in current use by the Deep Space Network, some design changes have been made in the test instrumentation. A recent redesign of the zero crossing detector has improved it's stability [3]. At the same time, a fiber optic interface to the frequency counter and computer has been added to eliminate ground loops, and reduce crosstalk between channels in the measurement system.

OFFSET GENERATOR NOISE

During static environmental conditions, the primary elements that establish frequency stability of the offset generator are the local oscillator VCO and PLL elements, and the frequency dividers. At frequencies within the phase lock loop bandwidth, the VCO tracks the signal in test, canceling VCO phase instability, but not amplitude instability. AM to PM noise conversion that occurs in the zero crossing detector mixer [4],[5] will generate an additive phase instability in the measurement system.

The measured power spectral density of AM and PM noise of the 100 MHz VCO are plotted in Figure 4a. The calculated closed loop phase noise with a 100 Hz loop bandwidth, and the AM to PM converted noise generated in a mixer with a -30 dB AM to PM conversion coefficient are also shown on the same figure. The AM to PM converted noise is shown to predominate over closed loop VCO PM noise at offset frequencies below 4 Hz. Oscillator AM noise therefore appears to be a major factor in establishing long term stability of the offset generator.

1. Oscillator Redesign

In the redesign, the original oscillator has been replaced with a low noise 5 MHz BVA crystal oscillator followed by a X20 frequency multiplier. The plot of Figure 4b shows the measured and calculated noise performance improvement of this new oscillator/multiplier tested under the same conditions, and using the same loop bandwidth as for Figure 4a. At 1 Hz offset frequency, AM noise and PM noise have been reduced 20 dB and 40 dB respectively, below the original oscillator.

The oscillator/multiplier for the output frequency conversion is offset 0.05 Hz from nominal at 5 MHz, allowing use of an available, production 5 MHz VCO. The input frequency conversion requires a 500 Hz offset at 5 MHz, well beyond the pulling range of any available high precision 5 MHz VCO.

2. Single Sideband Mixer

To avoid a custom design for the input converter VCO, a single sideband mixer is used to suppress the input carrier in place of using a phase locked VCO. The unwanted sideband and input carrier are attenuated more than 45 dB below the output by adjusting amplitude and phase balance of the low frequency input to the mixers. The phase lock loop of the output conversion section further attenuates these unwanted frequency components to more than 110 dB below the output carrier of the offset generator. Figure 5 shows the basic design of the single sideband mixer.

3. Frequency Dividers

The frequency dividers are of conventional design, using an ECL divide-by 40 for the first divider, followed by HC74 series TTL dividers for the remaining lower frequency division of 250.

4. Environmental controls

At long measurement times where the stability approaches parts in 10^{-18}, the offset generator is affected by temperature variations, vibration, and relative humidity that can mask any improvements made in the electronics. The offset generator and zero crossing detector are both installed in a thermoelectric temperature controlled enclosure to reduce this sensitivity. The temperature control is set at 25 Celsius, and a thermal gain of 20 has been realized. The electronics are on a 1/2 inch thick aluminum coldplate coupled to the thermoelectric elements for heat transfer. The large mass of the coldplate serves also to reduce the mechanical resonant frequency of the assembly, which reduces sensitivity to shock and vibration. Further investigation is required to determine the best approach to reduce sensitivity to humidity.

5. Test Results

Allan Deviation of the original, and the revised designs of offset generator and zero crossing detector are compared in Figure 6. The new offset generator and zero crossing detector reduces the measurement noise floor by a factor of 5.5 at a tau of 1 second, 3.0 at 1000 seconds, and 9.4 at 10000 seconds.

CONCLUSIONS

Improvements have been made in the measurement floor of the Allan Deviation test equipment by replacing the crystal VCOs used in the offset generator with a lower noise 5 MHz crystal VCO and X20 frequency multiplier for one stage of the offset generator, and a single sideband mixer in place of a phase locked VCO to reduce spurious outputs in the other stage. Adding a thermoelectric temperature controller to the electronics has further improved stability by reducing temperature variations of the electronics by a factor of 20.

REFERENCES

[1] *"Environmental Testing at the Jet Propulsion Laboratory's Frequency Standards Laboratory,"* Richard L. Sydnor, 43rd Annual Symposium on Frequency Control-1989.

[2] *"NASA/JPL Deep Space Network Frequency and Timing,"* Paul F. Kuhnle, Proceedings of the 21st Annual Precise Time and Time Interval (PTTI) Applications and Planning Meeting 1989.

[3] *"Zero-Crossing Detector with Sub-Microsecond Jitter and Crosstalk,"* G. J. Dick, P. F. Kuhnle, and R. L. Sydnor, Proceedings, 22nd Annual Precise Time and Time Interval (PTTI) Applications and Planning Meeting-1990.

[4] *"RF and Microwave Phase Noise Measurement Seminar,"* Hewlett Packard, Jan.1987.

[5] *"Frequency Synthesizer Theory and Design,"*, Third Edition," Vadim Manassewitsch, John Wiley & Sons, Inc. 1987.

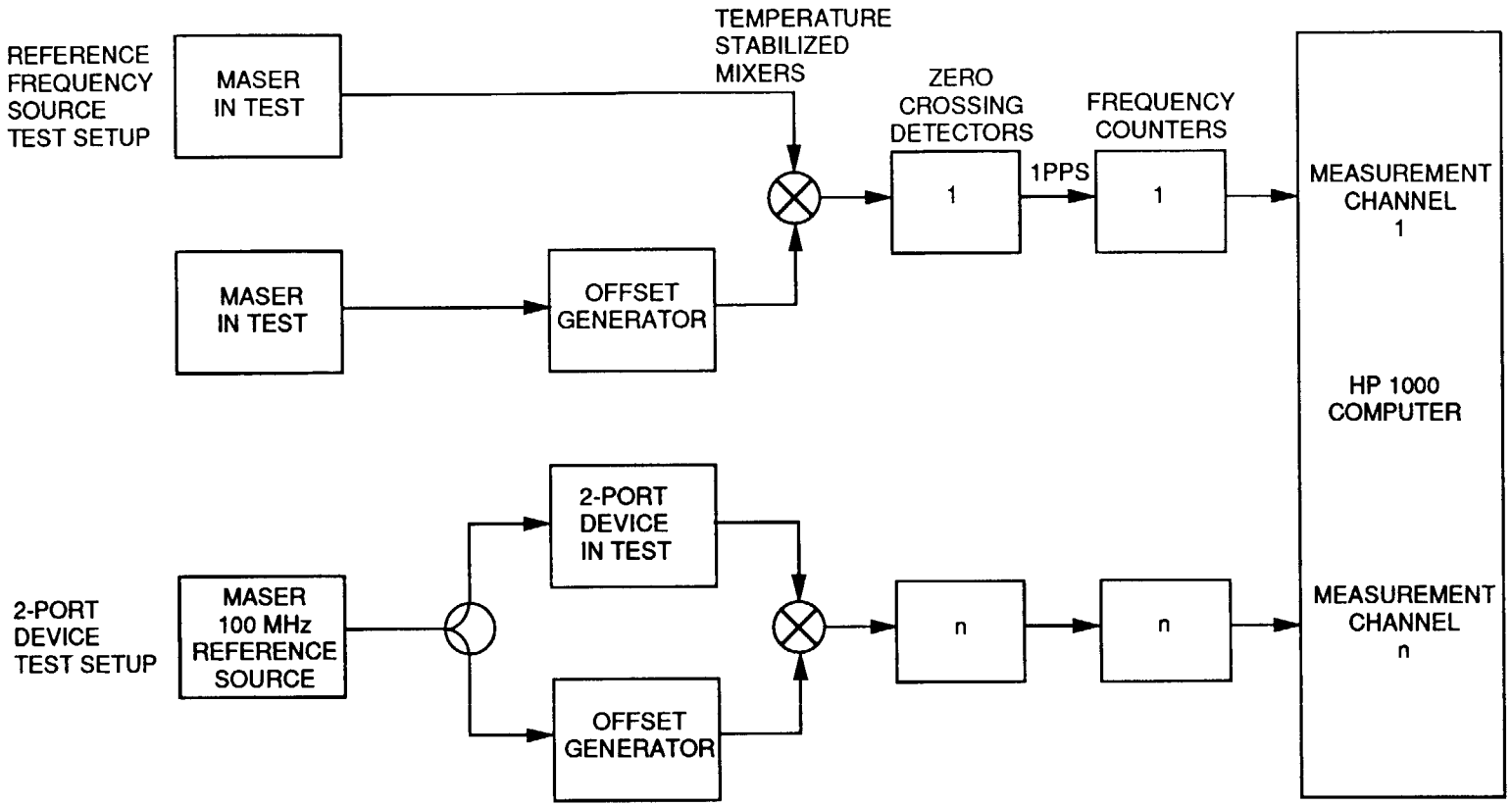

FIGURE 1

ALLAN DEVIATION TEST INSTRUMENTATION

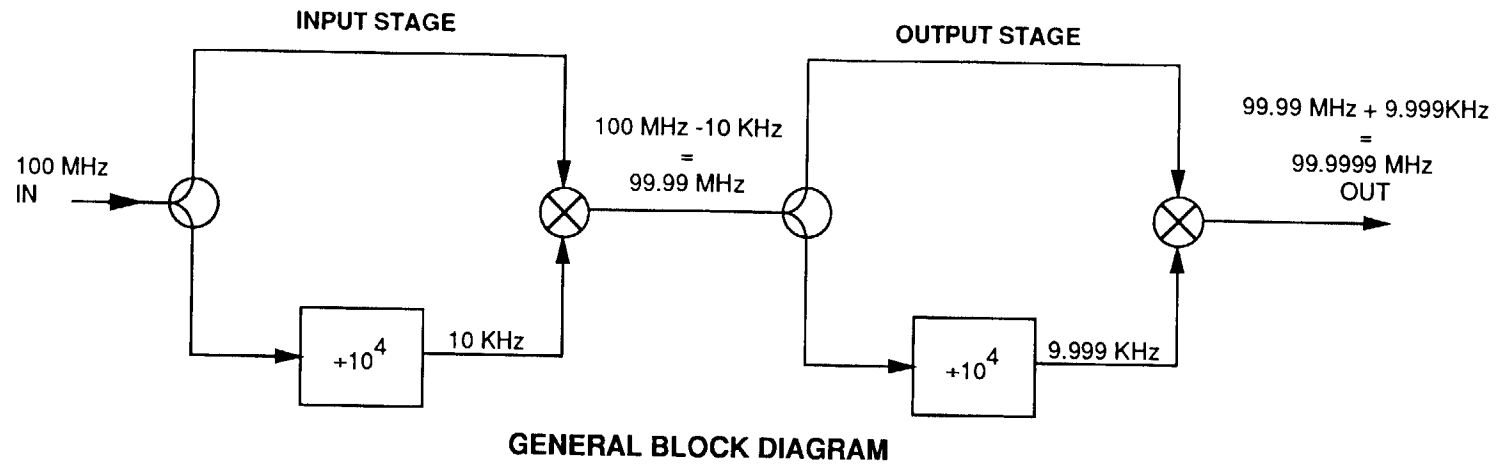

GENERAL BLOCK DIAGRAM

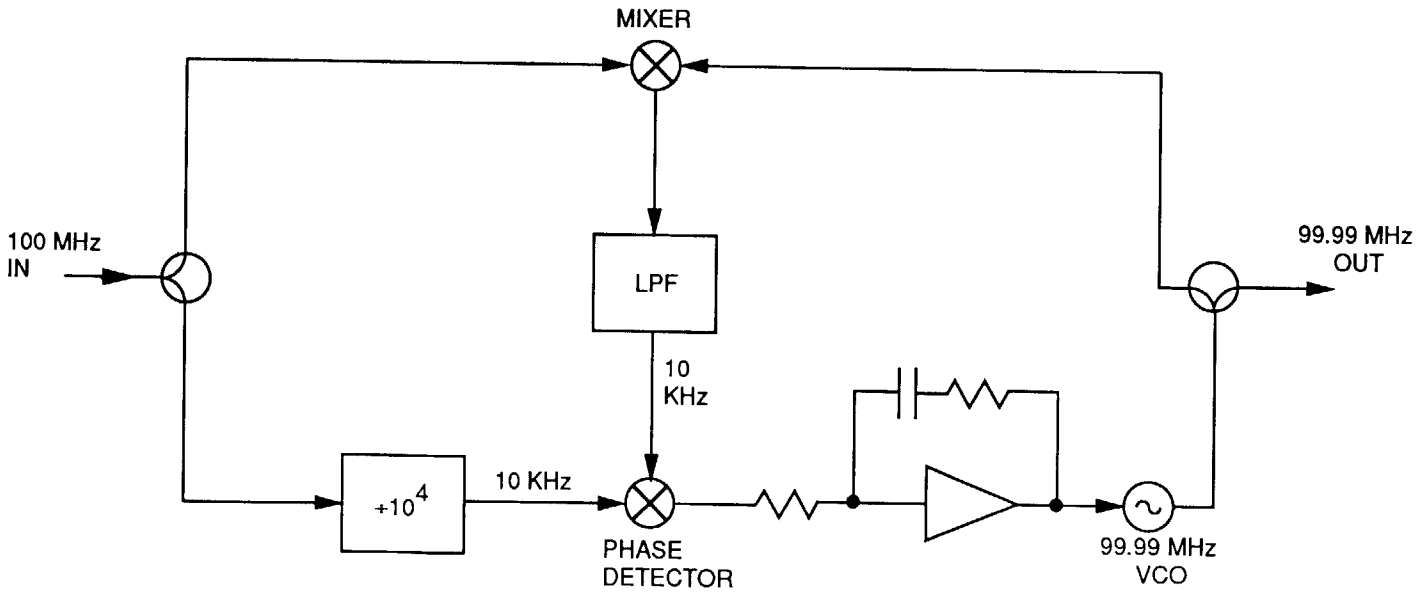

INPUT STAGE DETAILED DIAGRAM

FIGURE 2

OFFSET GENERATOR BLOCK DIAGRAM

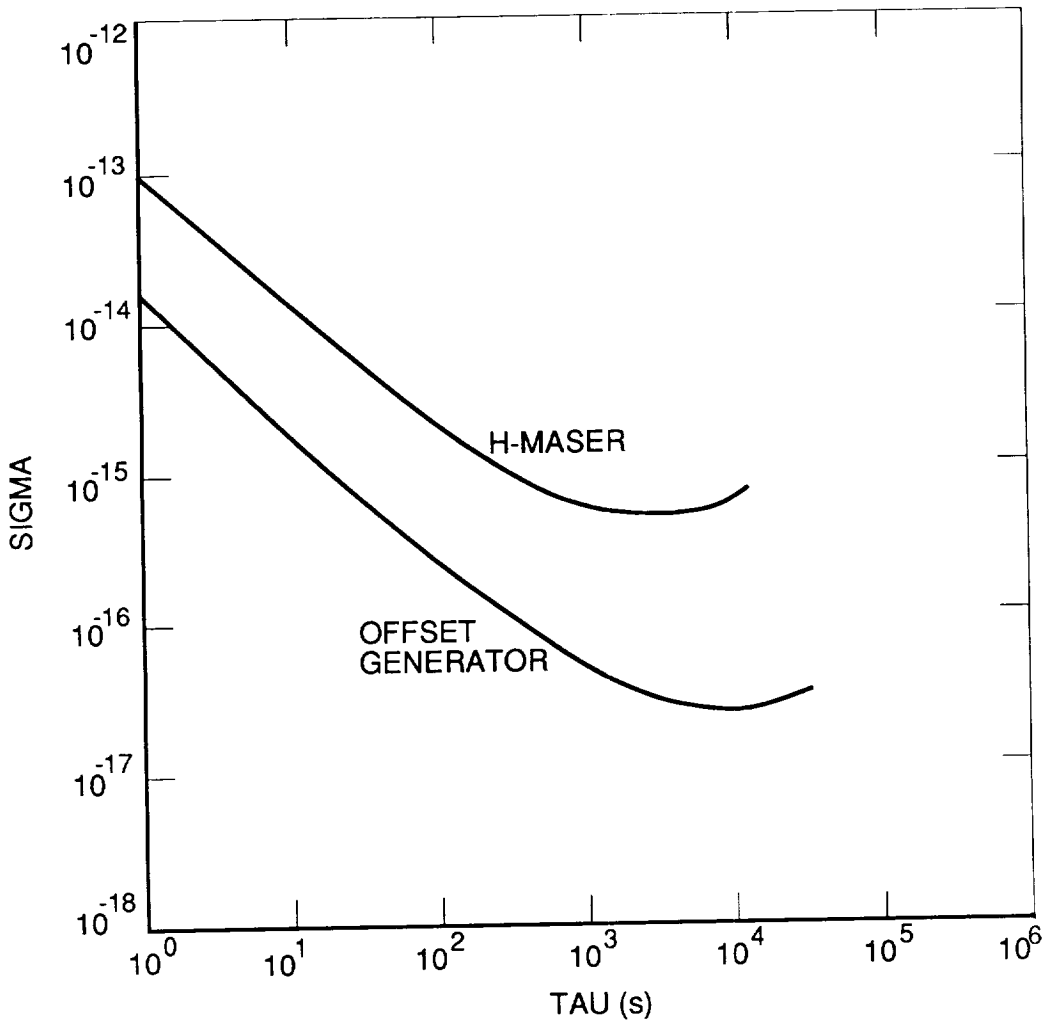

FIGURE 3

ALLAN DEVIATION
HYDROGEN MASER
AND
ORIGINAL OFFSET GENERATOR

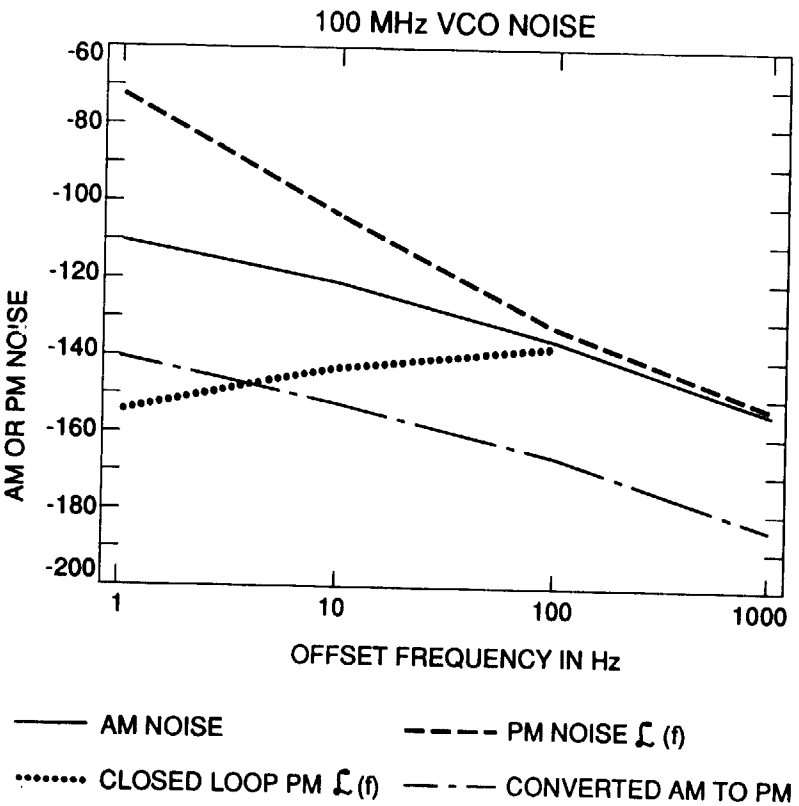

FIGURE 4a

AM AND PM NOISE
100 MHz VCO

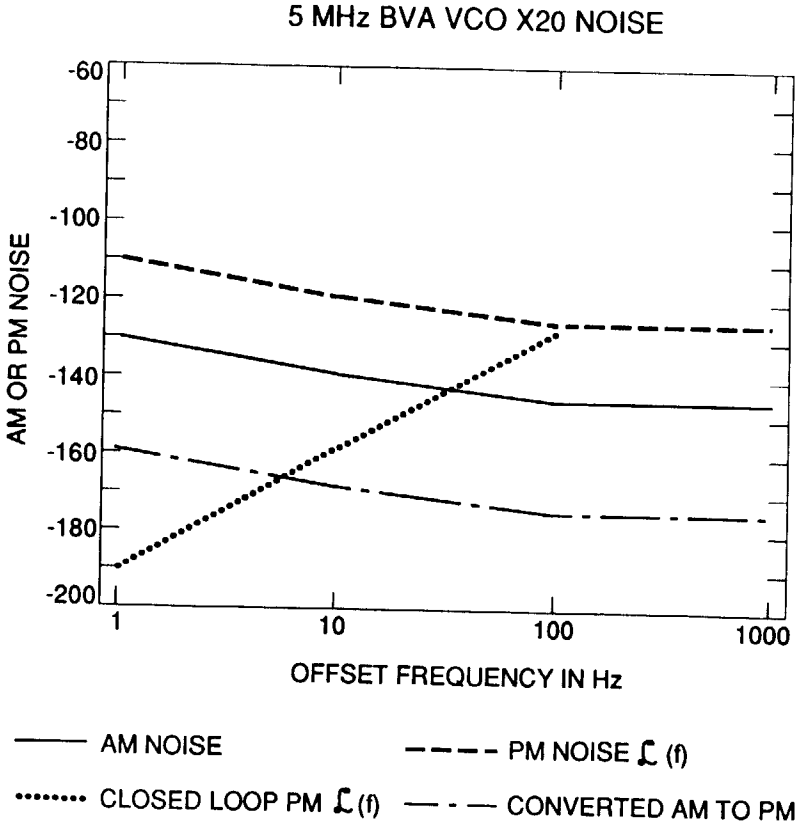

FIGURE 4b

AM AND PM NOISE
5 MHz BVA VCO/x20 MULT.

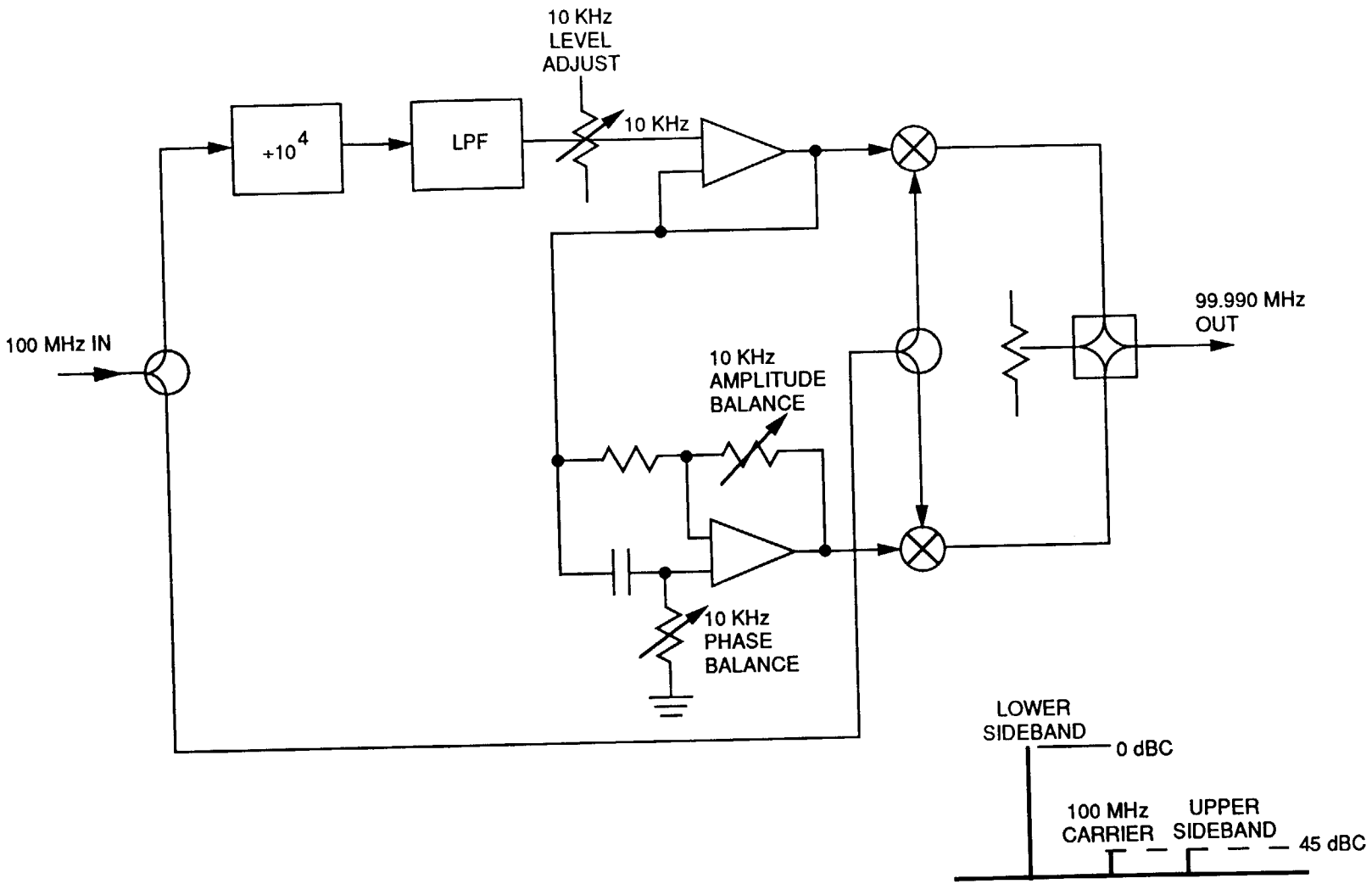

FIGURE 5
SINGLE SIDEBAND MIXER BLOCK DIAGRAM

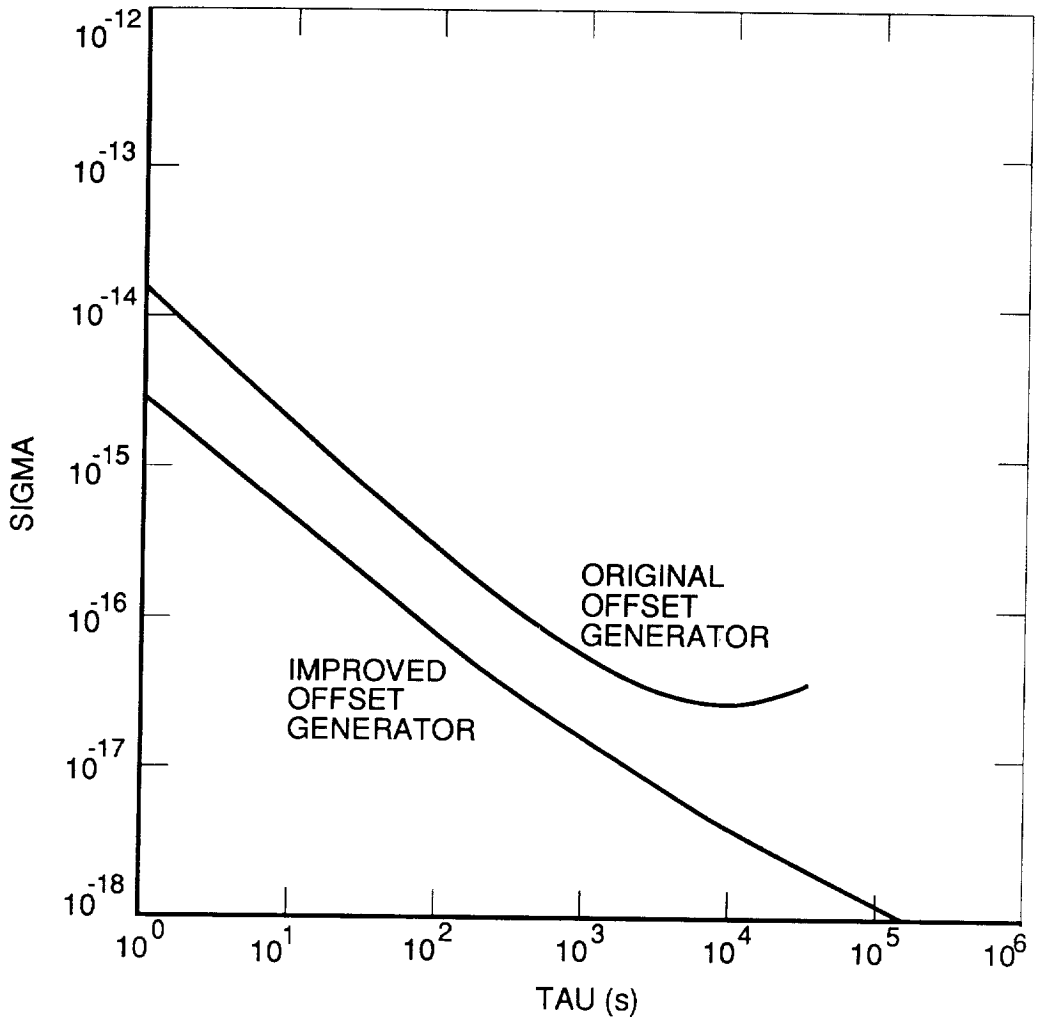

FIGURE 6

ALLAN DEVIATION ORIGINAL
vs IMPROVED OFFSET GENERATOR

THE MEASUREMENT SYSTEM OF PULSE MODULATED CARRIER FREQUENCY STABILITY AND TIMING JITTER

Li Cheng - Fu
Beijing Institute of Radio Metrology and Measurement
P.O. Box: 3920 Beijing, China

Abstract

This paper describes the definition of pulse modulated carrier frequency stability and timing jitter as well as the configuration and synchronous acquisition measurement method of its measurement system.

Frequency stability of pulse modulated carrier is measured with discrimination technique. The pulse modulated carrier under test is mixed with a reference frequency synthesizer. A delay line is used to convert the frequency fluctuation mixed IF signal to the voltage fluctuation. The system has the capability to make the phase noise measurement of two port devices on pulsed carrier using phase bridge.

The noise voltage mentioned above is applied to the data acquisition and processing unit by pc to realize stability measurement. The data acquisition is in the form of pulse synchronization so that the measurement system accuracy is increased. The pulse width is more than 0.3 μs. The phase fluctuation variance σ is less than 0.017.

The time interval measuring system with high resolution is used to make interpulse timing and pulse width jitters automatic measurement. The pulse width is less than 0.2 ns. The resolution is 0.1 ns. The system is successfully applied to radar measurement.

INTRODUCTION

The frequency stability is one of the important qualifications of signal source.

Characterization and measurement of CW frequency stability already have been matured and united. But there is still no unanimity in characterization of the carrier frequency stability on pulsed wave for the time being. An application of pulse wave to the radar on the other hand is urgently needed.

The duty cycle of pulse modulated wave is smaller in general. The signal frequency spectrum is more complex. This causes difficulty on characterization and measurement.

The CW method has been used to measure pulse modulated carrier frequency stability.

Measurement and characterization of pulse modulated carrier frequency stability using this method can cause the following problems. At first, the general pulse repeat frequency rate is lower. The RF pulse sideband spectrum line is a lot and dense. Pulse noise sophistication resulting from these factors stated above makes Fourier band noise be band is $\frac{f_p}{2}$.

Because of the same cases, Allan variance does not fit to characterize frequency stability in time domain.

The other question is to acquire very small video frequency impulse train of duty cycle. By CW acquisition, forming a lot of acquired data is useless.

The acquired data in the pulse width only is useful, and acquisition can also leak. The smaller the duty cycle, the greater the leakage rate. The confidence of measured results is degraded.

It is only adapted to measurement under the condition of higher duty cycle. The duty cycle required in general $\frac{\tau}{T}$ is larger than 5% (to test source), $\frac{\tau}{T} > 1\%$ (to test dual-port devices) [6].
Using the synchronization data acquisition technique proposed in this paper, we have solved the measurement problem of lower duty cycle.

This system has the capability to make frequency stability measurement of dual-port device on pulse modulated carrier. The microwave mixed IF discrimination technique is used to test pulse modulated carrier frequency stability.

Measurement of interpulse timing jitter is accomplished with analog interpolation and precision time measurement technique.

I. CHARACTERIZATION FOR FREQUENCY STABILITY ON PULSE MODULATED CARRIER

To measure pulse modulated carrier frequency stability may use for reference of CW characterization and measurement method in principle.

Our proposed methods are: to characterize frequency stability in time domain using interpulse variance, and to characterize phase noise sophistication efforts according to difference and practical necessary requirement between CW band pulse modulated wave.

1. Characterization of Pulse Modulated Carrier Frequency Stability in Time Domain

Change in the statistical rate of pulse modulated carrier series adjacent in pulse modulated carrier described by interpulse variance may be written as:

$$\sigma^2 = <(F_1 - F_2)^2> \tag{1}$$

When we determined with the measurement system in Figure 1, A/D converter output is a form of pulse repeat frequency at a rate as a separate digital time series, can be written as

$$\sigma^2(N.T.\tau) = \frac{1}{N-1}\sum_{i=1}^{N}[\Delta f(i) - \Delta f(i-1)]^2 \tag{2}$$

Where T = Pulse period

τ = Pulse width

N = Measurement number of each group

$f\Delta(i)$ = Average value of frequency fluctuation is 1th pulse.

2. Characterization of Pulse Modulated Carrier Frequency Stability in Frequency Domain

Assume,

unmodulated carrier $f_1(t) = A\cos\omega_c t$ (3)

pulsed waveform $f_2(t) = \frac{\tau}{T}\left(1 + \sum_{i=1}^{\infty}\frac{\sin n\omega_p\frac{\tau}{2}}{n\omega_p\frac{\tau}{2}}\right)$ (4)

pulse modulated signal $f_3(t) = f_1(t) \times f_2(t)$ (5)

$$f_3(t) = A\cdot\frac{\tau}{T}\cos\omega ct + A\cdot\frac{\tau}{T}\sum_{n=1}^{\infty}\frac{\sin\omega_p\frac{\tau}{2}}{n\omega_p\frac{\tau}{2}}[\cos(\omega_c + n\omega_p)t + \cos(\omega_c - n\omega_p)t] \tag{6}$$

the spectrum corresponding with equation (6) is shown in Figure 5.

The corresponding spectral density of phase fluctuation may be expressed as

$$S_\phi'(f) = A\frac{\tau}{T}S_\phi(f) + A\frac{\tau}{T}\sum_{n=1}^{\infty}\frac{\sin n\omega_p\frac{\tau}{2}}{\omega_p\frac{\tau}{2}}[S_\phi(f+nf_p) + S_\phi(f-nf_p)] \tag{7}$$

When ignoring the effect of the sample function, the equation (7) may be simplified as

$$S_\phi'(f) = A\frac{\tau}{T}\sum_{n=\infty}^{\infty}S_\phi(f+nf_p) \tag{8}$$

the influence of spectrum superimpose to $S_\phi(f)$ is calculated to $S_\phi'(f)$ in equation (8).

The magnitude of the superimposition phase noise is corresponding with the following:

(a) When τ is fixed, the spectral density and supimposition of phase noise are increased with a decrease of f_p.

(b) When f_p is fixed, the superimposition of phase noise is becoming worse, with the narrow of τ.

(c) If $S_\varphi(f)$ is composed of a broken line, $S_\varphi(f)$ will become the level line. If $S'_\varphi(f)$ is a monotone increasing or decreasing curve, $S'_\varphi(f)$ is level line approximately. [5]

II. SYSTEM CONSTRUCTION AND OPERATION PRINCIPLE

1. Additive Phase Noise Measurement

The measurement of pulse modulated Carrier phase fluctuation can be realized by using the measurement principle of microwave phase bridge shown in Figure 1. The CW signal is divided into two path signals through a power splitter. The signals form a pulse modulated carrier wave throughout the PIN modulator, respectively.

One of them passed device under test is applied to RF port of the phase detector; another passed the phase shifter is applied to the LO port of the phase detector.

We can make a dual-channel signal to quadrature by means of adjusting the phase shifter. When the electronic length of two path signals is equal, the phase noise of the source is cancelled, because of the correlation act while the DUT phase noise is detected.

When the phase detector shown in Figure 1 is in quadrature, the output voltage of the phase detector is:

$$\Delta V(t) = K_\Phi \sin\omega_p(t) \tag{9}$$

When $\Delta\Phi_{mix} \ll 1$ rad,

$$\Delta V(t) = K_\Phi \cdot \Delta\Phi(t) \tag{10}$$

where K_Φ = sensitivity of phase detection.

Thus, phase fluctuation under test of device is converted to voltage fluctuation $\Delta V(t)$. In measurement of phase fluctuation $\Delta\Phi(t)$ in time domain,

$$\Delta\Phi(t) = \frac{\Delta V(t)}{K_\Phi} \quad ,$$

RF pulse series, interpulse variance σ_p is given by data acquisition system as in Figure 4, and we can get $S'_\Phi(f)$ or $\pounds(f)$ through FFT.

The common source having lower phase noise is required in order to assure the measurement of the system having low phase noise bottom, at the same time the correlation of the measurement system is required in order to reduce the contribution of common source to output noise.

2. Interpulse Frequency Fluctuation Measurement

The measurement principle of interpulse frequency fluctuation is shown in Figure 2. Operation models of the system are single - channel and dual channel.

At first, IF is mixed up microwave signal. When using operation model of dual-channel, we can use IF quadrature dual-channel discrimination frequency system with a delayer as the frequency discriminator to measure pulsed carrier frequency fluctuation. It is fitted in with the source (transmitter) to measure large

frequency fluctuation. When using single channel operation model, the two path signals are applied to Q phase detector,

$$V_L(t) = A_1\cos[\omega_0 t + \varphi_1 + \varphi(t)] \tag{11}$$

$$V_R(t) = A_2\cos[\omega_0(t-\tau_1) + \Phi(t-\tau_1)] \tag{12}$$

Where, τ_1 = delay time, Φ_1 = shift of phase shifter, when two signals phase applied to phase detector are quadrature, detector output is

$$\Delta V(t) = \frac{1}{2} A_1 A_2 K \sin(\Phi(t) - \Phi(t-\tau_1)] \tag{13}$$

average frequency fluctuation in $(t, t-\tau_1)$

$$\Delta\omega = \frac{1}{\tau_1}\int_{t-\tau_1}^{t} \Phi'(t)dt = \frac{\Phi(t)-\Phi(t-\tau_1)}{\tau_1} = \Delta\omega = 2\pi\Delta f \tag{14}$$

when $\Delta\Phi(t) = \Phi(t) - \Phi(t-\tau_1) \ll 1$ rad, (14) fournula is substituted for (13) we can get:

$$\Delta V(t) = K_\Phi \cdot 2\pi\tau_1 \cdot \Delta f = Kd \cdot \Delta f \tag{15}$$

where $K_d = 2\pi\tau_1 K_\Phi$ as frequency discriminator constant.

3. Data Acquisition and Processing Unit

Figure 4 is a block diagram of a data acquisition and processing unit.

The output signal of phase fluctuation $\Delta\Phi(t)$, frequency fluctuation $\Delta f(\tau)$ is shown in Figure 1. Figure 2 is converted to discrete digital signal with a high speed A/D converter.

It works by a pulse controlled under test. In interpulse, high speed acquisition is carried to receive useful information.

The disadvantage of continuous sample is overcome. The system is controlled by a computer through STD bus.

4. Time Fluctuation Measurement

The measurement of pulse width and timing jitter is accomplished by a counting unit with the analog interpolation under computer-control. The system has high accuracry and resolution. The measurement principle is shown in Figure 3.

III. MEASUREMENT RESULTS

The pulse width of system measurement can be narrowed down to 0.3μs, interpulse phase fluctuation variance value σ is less than 0.017. Frequency fluctuation σ is less than 50 Hz, timing jitter variance is less than 0.2 ns, the resolution is 0.1 ns. This system has an application in measurement of radar transmitting. The measured pattern is shown in Figure 6 and Figure 7.

REFERENCES

[1] "Characterization of Frequency Stability" IEEE. Trans. on IM Vol. 1. 20, No. 2, May 1971.

[2] Stanley, J. Goldamn, "Phase Noise Analysis in Radar System Using Personal Computers", 1990.

[3] A. P. Rodis, "Phase Noise, Post and Telecommunication, 1988, Beijing.

[4] John M. Milan, "Test Set for the Measurement of Transmitter Stability Parameters", Pro. 29th Annual Frequency Control Symposium, 1975.

[5] Guo Yan Yin, "Frequency Stability of Modern Electronic Equipment" Astronautic Publishing House, 1989, Beijing.

[6] "Pulse Carrier Phase Noise Measurement Using the HP3048A Phase Noise Measurement System", Hewlett-Packard Company, Feb 6, 1990.

[7] Liu Xiafan and Mao Ruida, "An Automatic Measurement System for RF Pulse Stability Parameters", 20th PTTI, 1988.

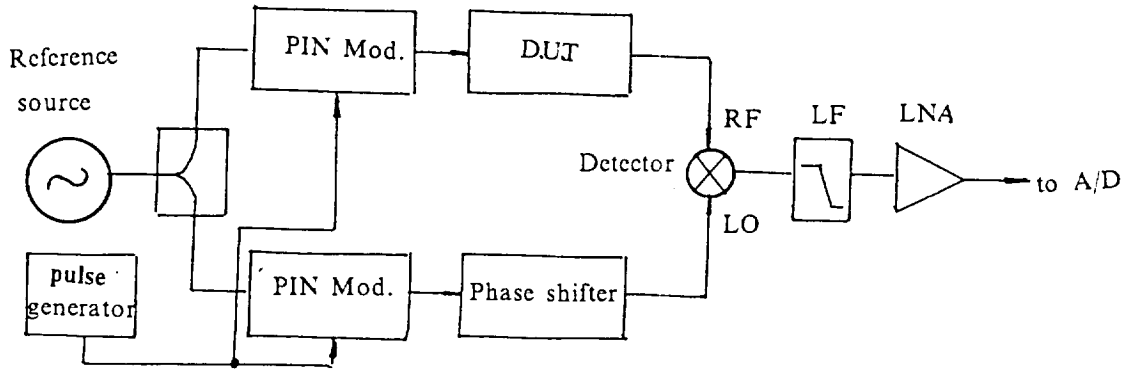

Fig.1 Additive phase noise measurement

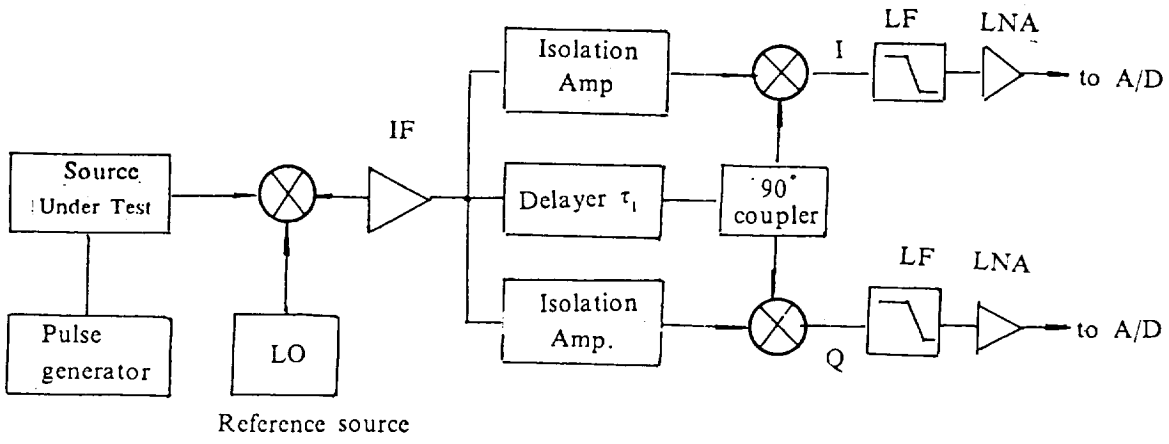

Fig.2 Measurment principle of frequency fluctuation

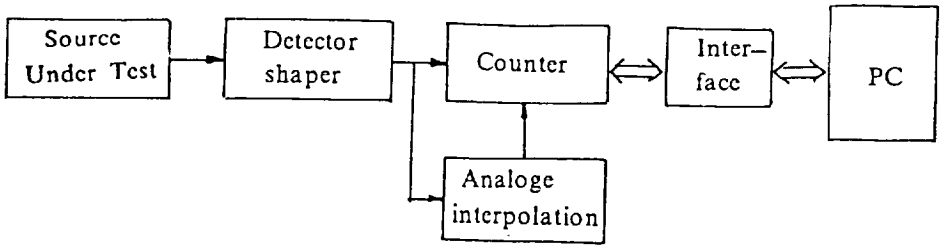

Fig.3 Time interval measurment

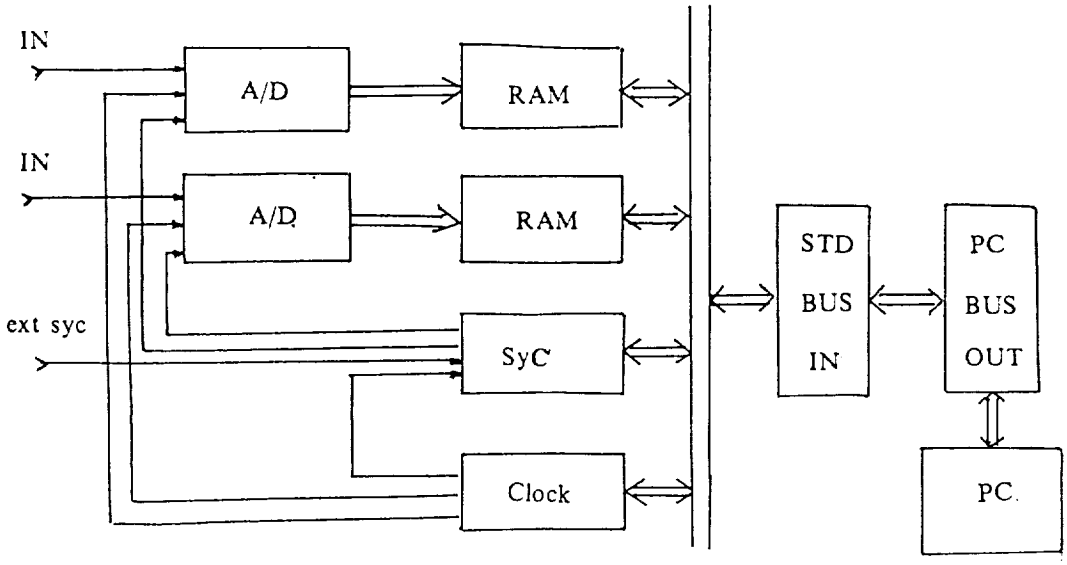

Fig.4 Data acquisition and processing unit

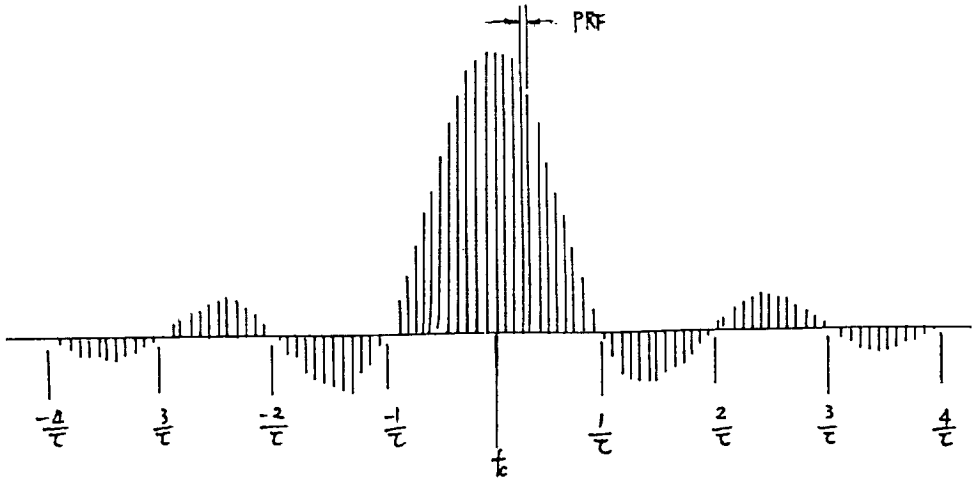

Fig.5 Frequency spectrum of pulse modulation carrier

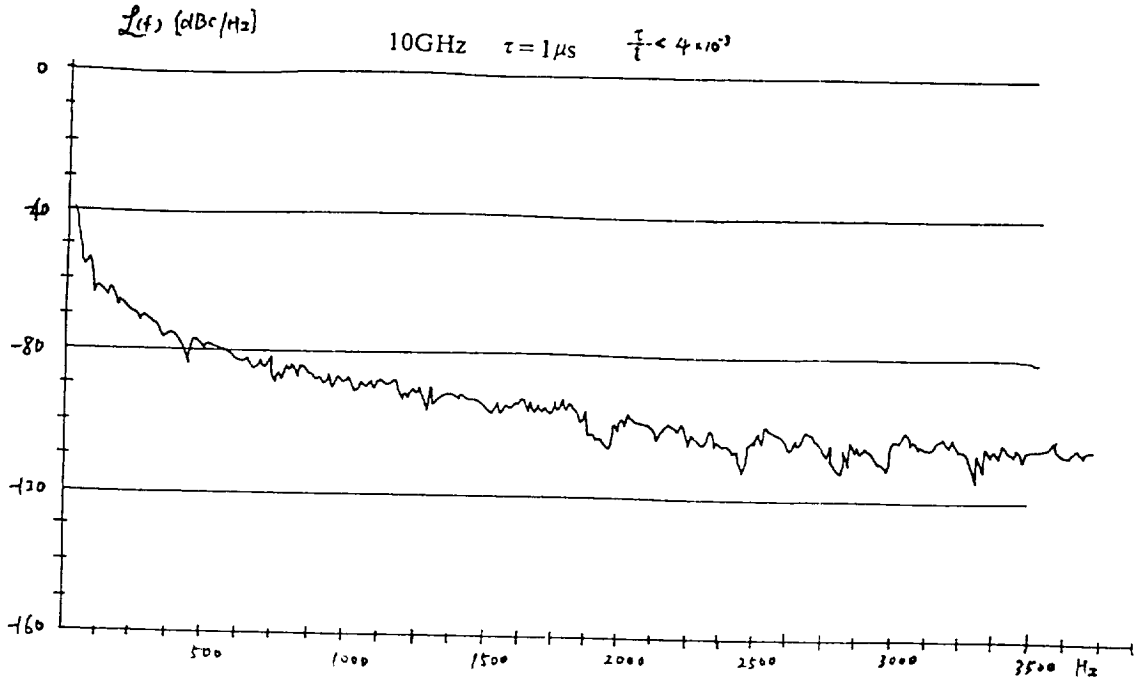

Fig.6 Radar TWT Amp. phase noise

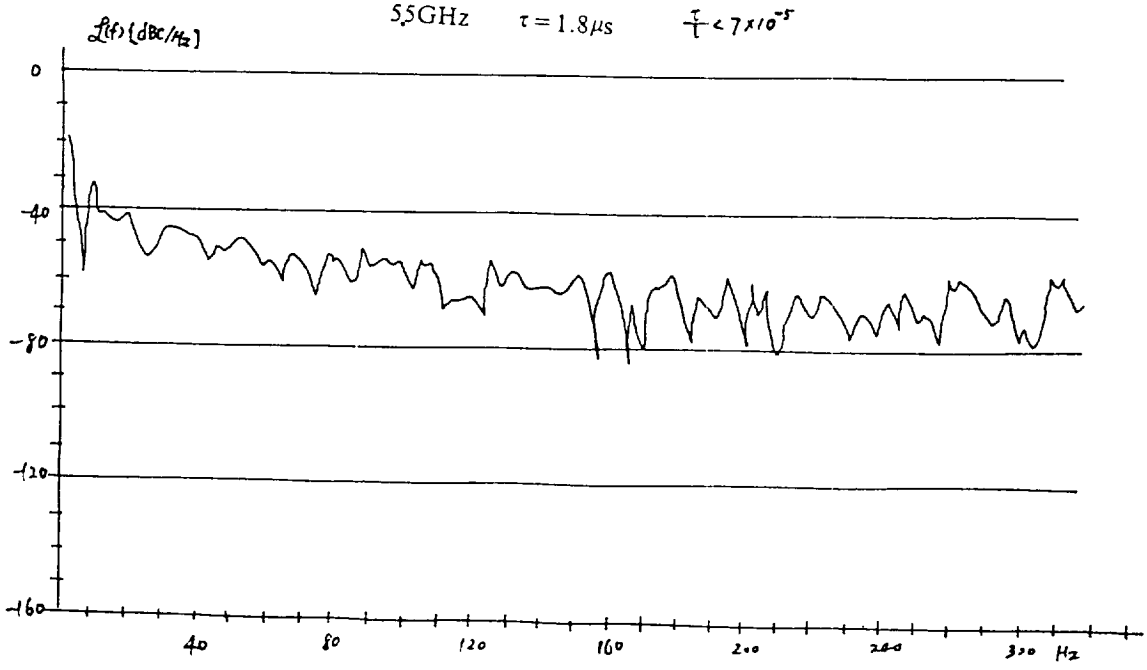

Fig.7 Radar transmitter source phase noise

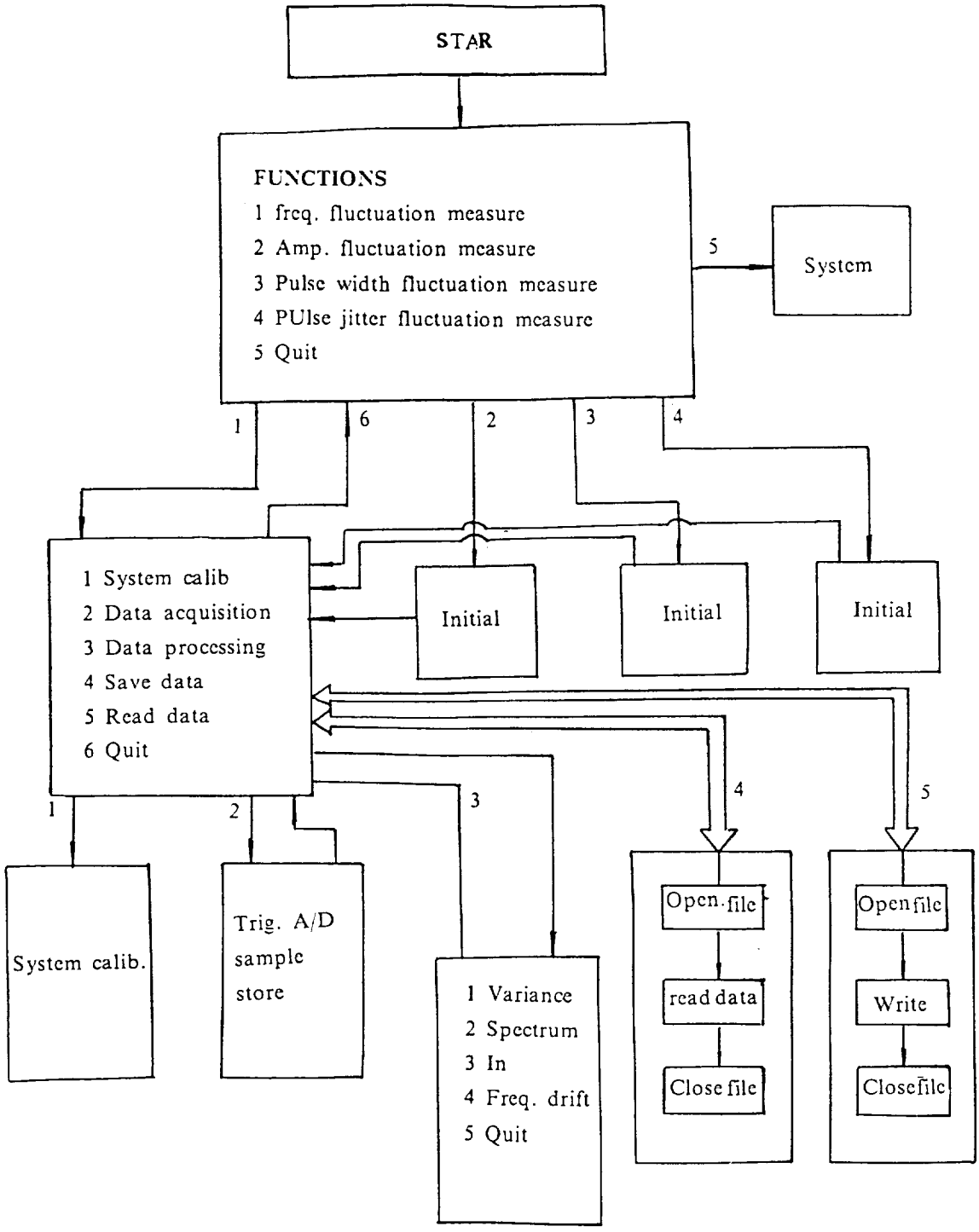

Fig.8 Flow chart of program

Measuring Frequency Changes due to Microwave Power Variations as a Function of C-field Setting in a Rubidium Frequency Standard

E. B. Sarosy, Maj, USAF
Space Systems Division, Air Force Systems Command
Los Angeles Air Force Base
P.O. Box 92960, Los Angeles, CA 90009-2960

vspace-.1in W. A. Johnson, S. K. Karuza, and F. J. Voit
Communications Electronics Department
The Aerospace Corporation
P.O. Box 92957, Los Angeles, CA 90009-2957

Abstract

It has been shown in previous studies that in some cesium frequency standards there exist certain C-field settings that minimize frequency changes that are due to variations in microwave power. In order to determine whether similar results could be obtained with rubidium (Rb) frequency standards (clocks), we performed a similar study, using a completely automated measurement system, on a commercial Rb standard. From our measurements we found that changing the microwave power to the filter cell resulted in significant changes in frequency, and that the magnitude of these frequency changes at low C-field levels went to zero and decreased as the C-field was increased.

Introduction

Since the passive Rb87 gas-cell frequency standard (or clock) is the most commonly used type of atomic frequency standard, there is interest in quantifying and understanding all the factors that affect the stability of the standard's output frequency. Earlier work by Risley [**1,2**] identified the mechanisms whereby changes in microwave power cause changes in frequency. Risley concluded that the major cause of this frequency shift was the line inhomogeneity, which is a combination of the relatively immobile Rb87 atoms (immobilized by the use of the buffer gas in the absorption cell) and a frequency gradient across the absorption cell; this frequency gradient is in turn affected by the light-shift mechanism and the C-field. The Rb line inhomogeneity results in a frequency dependence upon changes in microwave power. The frequency changes that we measure will also include any small cavity-tuning effects that might be present as a result of any slight cavity mistuning.

Measurements

The C-field experiment was performed in our laboratory on a commercial double-cell Rb frequency standard. This standard was modified to allow access to the C-field coil wires and the microwave power source. Figure 1 is a block diagram of the complete automated measurement system. Both of the parameters that are varied, namely the C-field current and the microwave power, are computer controlled; the current is set by a precision constant-current generator, while the microwave power is changed by using an electronic switch to change the resistance of a bias resistor on the step-recovery diode. The bias resistors were chosen to change the microwave power by +1.3, -1.1, -2.2, and -4.0 dB with reference to the nominal, factory-set power level P_0. The 6.834-GHz microwave power to the cell was sampled by coupling with a two-turn coil on the 6.834-GHz coaxial signal line. The bias resistors were chosen by using a Hewlett-Packard (H-P) model 8566 spectrum analyzer to observe the change in microwave power on this coupled signal.

The entire measurement system is controlled by an H-P series 300 computer, which also acquires and processes the data. Figure 2 is a block diagram of the frequency measurement system. The frequency reference for both the Fluke synthesizer and the H-P counter is an H-P model 5061A-004 cesium (Cs) frequency standard. A typical data-taking sequence consisted of the following steps:

1. Set the C-field current at some low value (typically 2 to 6 mA) and the microwave power at some value (e.g. at the nominal value P_0).
2. Measure the beat frequency over some long averaging time T (typically 1000 sec).
3. Change the microwave power level [e.g. to (P_0 - 1.1 dB)].
4. Measure the beat frequency over T again.
5. Increase the C-field current by some programmed amount (typically 0.5 mA).
6. Measure the beat frequency over T again.
7. Change the microwave power back to the initial value.
8. Repeat steps 2 through 7 until the final C-field current (typically 14 to 20 mA) is reached.

To determine the functional relationship between the C-field current and the Zeeman frequency, the microwave frequency is swept over approximately 1 MHz, centered about the main Rb resonance line. The output of the standard's dc-coupled current-to-voltage converter is then plotted as a function of frequency. Figure 3, for a C-field current of 4.5 mA, is a typical plot. This plot shows the main Rb transition state, as well as the four sigma transitions and the two pi transitions (the pi transitions are used to define the Zeeman frequency f_Z). We should note that the 0-to-39.53-mV ordinate in Figure 3 rides on top of a ~5 V bias, which we buck out with a precision low-noise floating voltage source. The Zeeman frequency is read from the plot in Figure 3. The measurement is then repeated for different C-field currents. For this particular standard, the Zeeman frequency is about 42.5 kHz per mA of C-field current.

Figure 4 is a plot of the signal at the absorption peak as a function of microwave power. The data, which are similar to those obtained by Risley [1], demonstrate that the manufacturer's drive-level power P_0 results in a maximum signal.

Measurement Results

Figure 5 shows the results of measurements made on the commercial Rb standard for changes in the microwave power level of +1.3, -1.1, -2.2, and -4.0 dB. Each data point, which represents the difference between two 1000-sec averages, is calculated as the difference in output frequency between the frequency at the higher power and that at the lower power, both powers being normalized to the nominal output. In other words,

$$\text{ordinate} = (\bar{f}_H - \bar{f}_L)/10 \text{ MHz}$$

where $\bar{f}_H$ is the average output frequency for the higher microwave power and $\bar{f}_L$ is the average output frequency for the lower microwave power. From Figure 5 we see that the maximum frequency change for the +1.3 and -1.1 dB data is about 3×10^{-11}, that for the -2.2 dB data is about 6×10^{-11}, and that for the -4.0 dB data is about 1.4×10^{-10}. As a function of the change in microwave power, the maximum frequency change is about 2.6×10^{-11}/dB.

The three curves have a similar shape, namely one that is fairly flat for Zeeman frequencies between 100 and 300 kHz, then decreasing monotonically for Zeeman frequencies between 300 and 850 kHz. In separate tests, data were obtained for the region of low Zeeman frequency. Figure 6 shows the results of those tests for the same microwave power changes as in Figure 5. From the curves in Figure 6 it is seen that there are zero crossings at about 20 and 80 kHz. The operation of the clock at one of these points would result in zero sensitivity of the clock frequency to microwave power changes and may result in improved long-term clock stability, as had been observed by De Marchi [3] in his investigations of Cs frequency standards. The manufacturer's C-field current setting for this clock was 4.5 mA, which gave a Zeeman frequency of about 191 kHz. Operating the clock at lower C-fields would also have the advantage of decreasing clock sensitivity to C-field current; i.e., a change in C-field current results in a smaller change in output frequency when the C-field current is small.

We suspect that the zero crossing at 80 kHz may be explained by the mechanisms discussed by Risley [2]. He states that this point may be interpreted in terms of (1) the opposing effect of the spacially inhomogeneous light shift and (2) the C-field gradient; the light shift produces a positive frequency shift, while the C-field gradient produces a negative frequency shift.

A comparison of the results in Figure 3 with similar results for Cs standards [3,4] shows that at the C-field setting that results in the maximum frequency change, the Rb standard is about ten times more sensitive to power changes than is the Cs standard. This result points out the need for a more stable microwave power source for Rb standards than for Cs standards. Most commercial Rb standards do not employ a microwave-power leveling circuit. This particular commercial Rb standard, however, did level the power into the final step-recovery-diode multiplier.

Conclusions

We have presented experimental results regarding the interaction of the C-field and the microwave power on the output frequency of a commercial Rb standard. These results showed that in this particular Rb standard, the maximum frequency change due to microwave power variations was about 2.6×10^{-11} per dB of power change. At this C-field setting an standard deviation of 0.01 dB in the microwave power would result in an Allan standard deviation in the frequency of 2.6×10^{-13} from the power changes alone. This illustrates the need for a very stable microwave power source.

It was also observed that for a particular C-field setting, the frequency change goes to zero. The frequency sensitivity of this Rb standard to changes in microwave power was about ten times higher than that of a Cs standard.

Acknowledgments

The authors are grateful to A. Leong and G. G. Berry for their technical assistance, and to M. T. Meyer for editing and preparing this paper.

References

[1] A. Risley, *"Effect of Line Inhomogeneity on the Frequency of Passive Rb87 Frequency Standards,,"* Proc. 32nd Symposium on Frequency Control (1978), pp. 506-513.

[2] A. Risley and S. Jarvis, Jr., *"The Dependence of Frequency upon Microwave Power of Wall-Coated and Buffer-Gas-Filled Gas Cell Rb87 Frequency Standards,,"* J. Appl. Phys. 51 [9], 4571-4576 (September 1980).

[3] A. De Marchi, *"New Insights into Causes and Cures of Frequency Instabilities (Drift and Long-Term Noise) in Cesium Beam Frequency Standards,,"* Proc. 41st Symposium on Frequency Control , Philadelphia, Pa. (1987), pp. 54-58.

[4] S. K. Karuza, W. A. Johnson, J. P. Hurrell, and F. J. Voit, *"Determining Optimum C-field Settings that Minimize Output Frequency Variations in Cesium Atomic Frequency Standards,,"* 21st Annual Precise Time and Time Interval Applications and Planning Meeting, Redondo Beach, Calif. (30 November 1989).

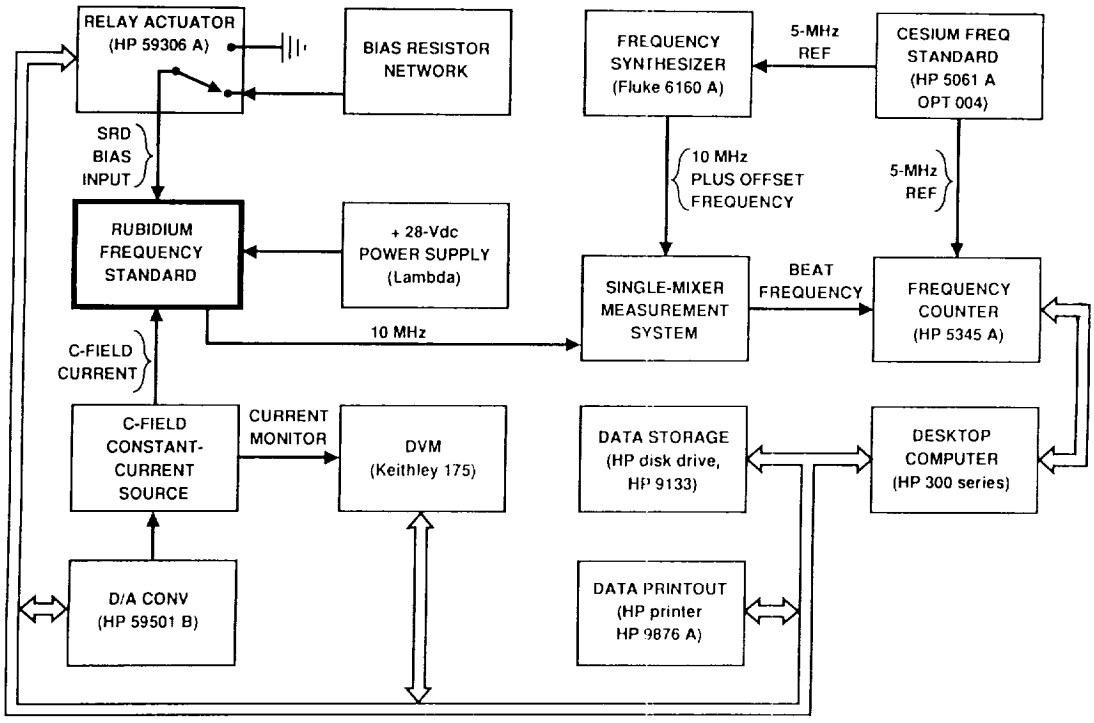

Figure 1. Block Diagram of the C-field Measurement System for a Rb Frequency Standard

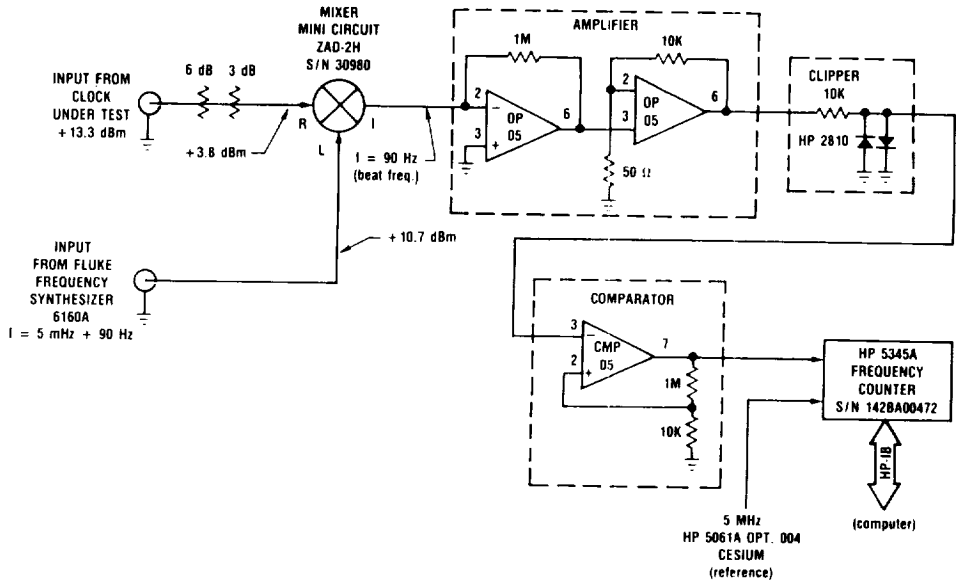

Figure 2. Circuit Diagram of the Single-Mixer Frequency-Measurement System Used to Determine the Fractional Frequency Changes at Different C-field Settings

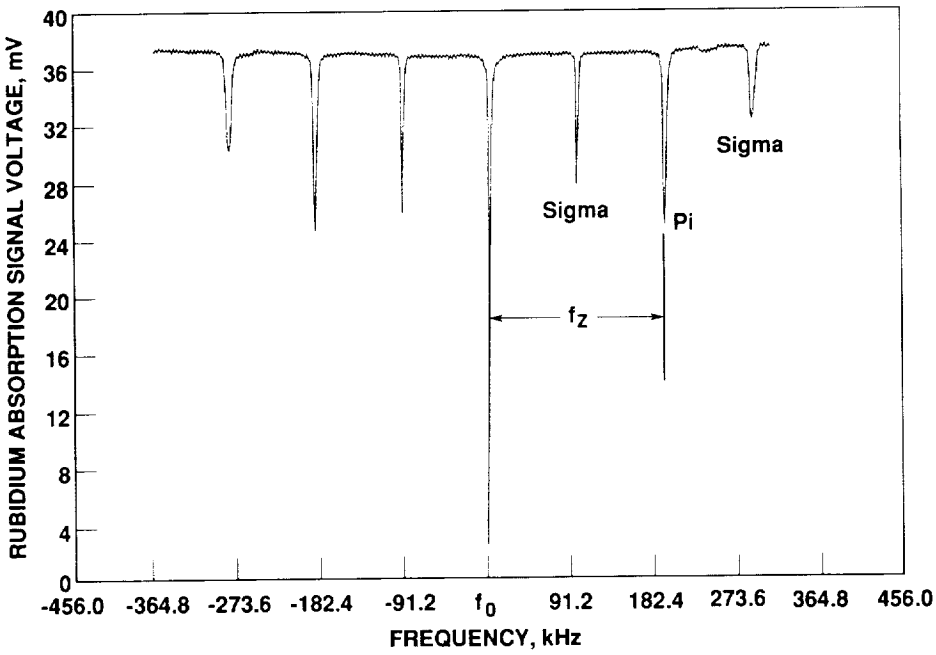

Figure 3. The CW Rb Resonance Patterns of the Seven Zeeman Transitions in a Rb Frequency Standard

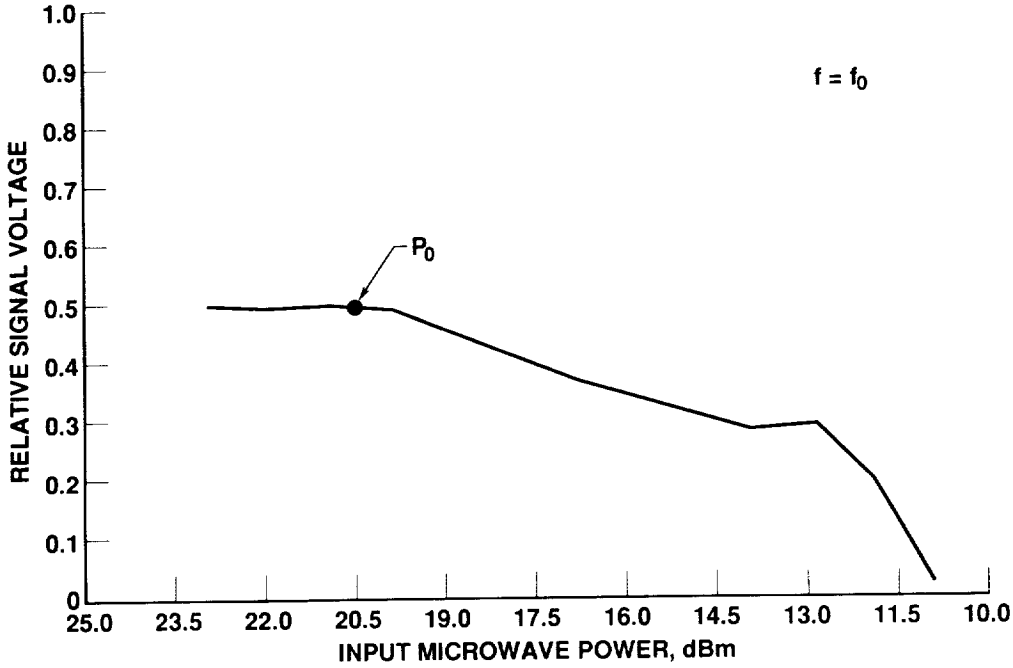

Figure 4. Plot of the Rb Resonance Signal Voltage vs. the Input Microwave Power of the Rb Frequency Standard with the Standard Tuned to f_0

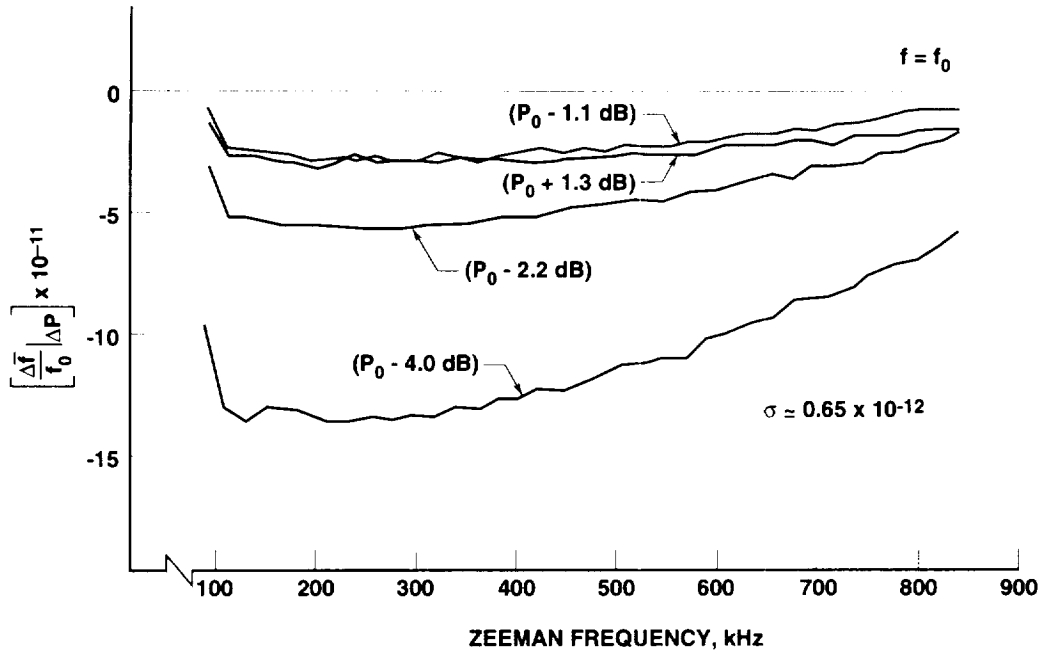

Figure 5. Average of the Final Data on the Rb Frequency Standard, Showing the Difference of the Average Frequencies as a Function of C-field for Microwave Power Changes of +1.3, -1.1, -2.2, and -4.0 dB with Respect to the Nominal Power Level P_0

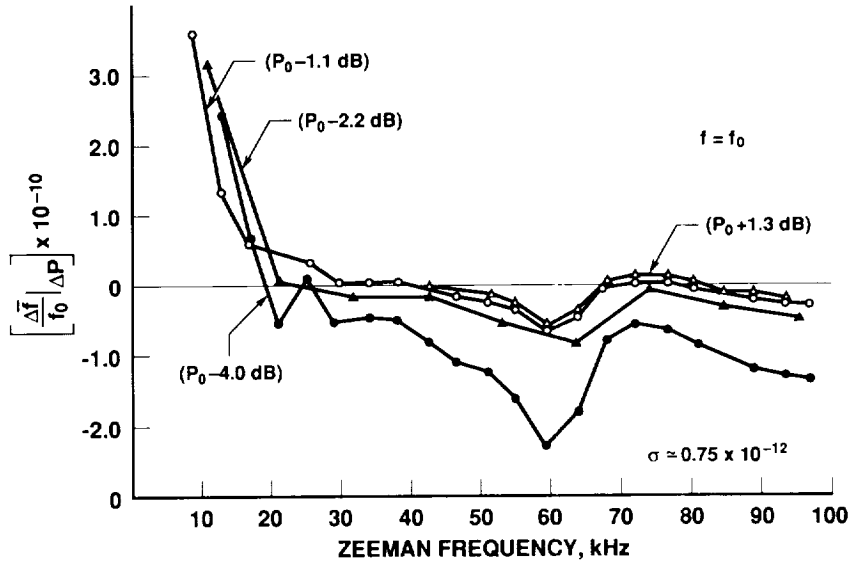

Figure 6. Plot of the Difference of the Average Frequencies of the Rb Standard as a Function of Low C-field for Microwave Power Changes of +1.3, -1.1, -2.2, and -4.0 dB with Respect to the Nominal Power Level P_0

Development of an Optically-pumped Cesium Standard at the Aerospace Corporation

Dr. Yat C. Chan
Electronics Technology Center
The Aerospace Corporation
Los Angeles, CA

Abstract

We have initiated a research program to study the performance of compact optically-pumped cesium (Cs) frequency standards, which have potential for future timekeeping applications in space. A Cs beam clock apparatus has been assembled. Basic functions of the frequency standard have been demonstrated. Clock signals are observed with optical pumping schemes using one or two lasers. With two-laser pumping, we are able to selectively place up to 80% of the atomic population into one of the clock transition states. The observed pattern of the microwave clock signal indicates that the velocity distribution of the Cs atoms contributing to the microwave signal is beam-Maxwellian. Thus, in the optically-pumped Cs frequency standards, the entire Cs population in the atomic beam could be utilized to generate the clock signals. This is in contrast to the conventional Cs beam standards where only ~1% of the atoms in the beam are used. More efficient Cs consumption can lead to improved reliability and increased useful lifetime of the clock. Our preliminary results are summarized in this paper.

INTRODUCTION

There has been considerable interest in the use of optical methods for state preparation and clock signal detection in the Cs frequency [1],[2],[3] Elimination of the state selection magnets in the frequency standard could significantly reduce the frequency biases which are magnetic dependent such as those due to the Majorana transitions and the distributed cavity phase-shifts. Reductions of the magnitudes of these effects can lead to a clock in which the stability and the accuracy are greatly improved over current designs. Potentially, an accuracy of 1 part in 10^{14} is achievable in optically-pumped Cs beam frequency [4].

In a conventional Cs beam clock, the state selection magnets select only a small group of Cs atoms with a narrow velocity spread and an appropriate hyperfine energy state, such that only ~1% of the total atoms in the beam contributes to the observed clock signal. Such inefficient use of the Cs has adverse effects on the lifetime of the beam clock, since the major cause of failures in the compact Cs beam clocks is due to the exhaustion of Cs in the oven. Optical excitation with the laser beam perpendicular to the atomic beam is insensitive to the velocity of Cs atoms along the atomic beam axis. Additionally, optical pumping schemes using two lasers can concentrate nearly the entire Cs population into one of the clock transition states. Thus, all of the Cs atoms in the beam could be utilized. This could translate into a larger clock signal and more efficient Cs consumption resulting in increased reliability and useful lifetime of the clock.

We have initiated a research program to gain familiarity with the optical pumping techniques in Cs frequency standards. In particular, we are interested in studying the stability and reliability of compact frequency standards which have potential for future timekeeping applications in space. Hopefully, these investigations will lead to improved performance in compact optically pumped Cs standards (OPCS). Our preliminary observations are summarized in this paper.

EXPERIMENTAL SECTION

A schematic diagram for our experimental setup is presented in Fig. 1. Our Cs beam apparatus consists of four main sections: a Cs source, a pumping chamber, a microwave region and a detection chamber. Separations between the Cs oven and the pumping and detection regions are 64 and 132 cm, respectively. The vacuum chamber is evacuated to $\sim 10^{-7}$ Torr by a 120 l/s ion pump. In the pumping chamber and the detection chamber, three optical windows are mounted perpendicular to the atomic beam providing access for the laser beams and for the detection of emission signals. Effusion of Cs atoms from the Cs oven through a 2.4 mm diameter opening into the vacuum chamber forms an atomic beam. The temperature of the Cs oven is maintained at 120 °C during the experiment. A graphite diaphragm with a 2.5 mm diameter aperture is placed 7.5 cm from the oven to reduce the beam divergence and the Cs background.

A single layer of 1.5 mm thick mu-metal provides shielding against interferences from ambient magnetic fields. Stray magnetic fields inside the chamber are less than 2.5 mG. A dc magnetic field (C-field), perpendicular to the atomic beam, is produced inside the magnetic-shielding chamber by four current-carrying copper rods placed 4 cm apart. Inhomogeneity of the C-field is less than 5 mG across the cross section of the atomic beam. A compact Ramsey-type microwave cavity of commercial design is mounted in the microwave chamber. Separation between the two, 1 cm long arms of the U-shaped microwave cavity is 12 cm. The cross sectional area of the cavity is ~ 15 mm^2 allowing approximately 2×10^{10} atoms/s to be interrogated by the microwave field. The output of a temperature stabilized VCXO, operating at 143 MHz, is multiplied 64 times to provide the required microwave radiation.

Diode lasers are used for both optical pumping and state detection. The lasers are tuned to the Cs D_2 transition frequencies by controlling both the laser heat-sink temperatures and the laser injection currents. In order to keep the laser frequency on resonance with the Cs atomic transitions throughout the experiment, the laser frequencies are locked onto the selected atomic transitions through an electronic feedback technique using the fluorescence signals provided by a photodiode detector in the pumping region. As a part of the electrical feedback technique, the injection currents of the lasers are modulated by small ac signals oscillating at 700 or 1000 Hz. The modulations increase the effective linewidths of the lasers to $\sim$80 MHz. Depending on the individual laser, laser powers available vary from 2 to 8 mW.

Fluorescence signals in the detection region are detected by a cooled GaAs photomultiplier tube. The signals are amplified by an electrometer with $\sim$1 s time constant.

RESULTS

(A) Hyperfine Pumping

An energy level diagram for the Cs D_2 transitions is given in Figure 2. Selection rules for the optical transitions are $\Delta F = 0$ or ± 1, (F is the total angular momentum of a state, nuclear plus electronic) such that six optical transitions between the ground $6^2S_{1/2}$ state and the excited $6^2P_{3/2}$ state are permitted. The selection rules also depend on the polarization of the excitation source. When the polarization of the laser is perpendicular to the magnetic field, σ-excitations will be induced, such that the allowed optical transitions are $\Delta M = \pm 1$ (M describes the projection of F onto the direction of the magnetic field). For the π-excitations, polarization of the laser is aligned parallel with the C-field, and the allowed transitions are $\Delta M = 0$, with the exception that $M = 0 \rightarrow M' = 0$ (primes indicate the angular momentum of the excited state) is forbidden when $\Delta F = 0$.

Transitions including: $F = 4 \rightarrow F' = 4$; $F = 4 \rightarrow F' = 3$; $F = 0 \rightarrow F' = 3$; $F = 30 \rightarrow F' = 4$ are known as the pumping transitions. With these pumping excitations, Cs population may be transferred from one of the ground electronic state hyperfine levels into the other, consequently give rise to the hyperfine pumping. For the cycling transitions, $F = 4 \rightarrow F' = 5$ and $F = 3 \rightarrow F' = 5$, the only decay pathway for the excited atoms upon excitation is returning to their original ground hyperfine levels, therefore they are not useful for optical pumping. Fig. 3a shows a fluorescence spectrum collected at the detection chamber when the frequency of a probe laser was scanned over the d_2 transitions of Cs around 852 nm. All six allowed optical transitions were observed. Fig. 3b shows a similar emission spectrum, when a second laser was tuned to the $F = 3 \rightarrow F' = 3$ transition and intersected the atomic beam in the pumping region. Emission signals corresponding to the $F = 3 \rightarrow F' = 2$, 3, 4 transitions disappeared completely. This is due to the complete removal of the $F = 3$ population by hyperfine pumping in the pumping region. Similar hyperfine pumping effects were observed with the other pumping excitations. These observations confirm that near complete population transfer from one hyperfine state into the other can be achieved by optical pumping using diode lasers.

(B) Optical Pumping with One Laser

In our one-laser experiment, the main laser beam was used for optical pumping in the pumping chamber. A fraction of the laser beam was diverted into the detection chamber for state detection. Hyperfine pumping was induced by tuning the laser onto one of the pumping transitions. When the microwave source fed to the Ramsey-cavity was off, emission signals observed in the detection region consisted mainly of scattered laser light and a small fluorescence signal from the unpumped Cs atoms. When the microwave frequency matched the Cs hyperfine transition frequencies, transitions between the two hyperfine states would be induced among the Cs atoms passing through the microwave cavity. This resulted in a change in the emission signals observed in the detection chamber. Fig. 4a shows the microwave spectrum with the $F = 3 \rightarrow F' = 3$ σ pumping scheme (3-3 σ), where the notation σ (or π) describes the polarization of the pumping laser with respect to the C-field as discussed in the previous section. The microwave spectrum consists of seven transitions. The (0-0) 'clock' transition, which couples the F=3, M=0 and F=4, M=0 states, shows the characteristic interference structures. The halfwidth of the central Ramsey peak is approximately 1 KHz. Such interference structures, however, were not observed in the other microwave transitions. This could be due to the fact that interference structures on these magnetic sensitive transitions were washed out by the inhomogeneity of the C-field. This result suggests that an improvement in the uniformity of the C-field is desirable.

State preparation involving 3–3 π and 4–4 π pumping are important components of the two-laser pumping techniques for putting all of the Cs atoms into one of the clock transition states. Fig. 4b shows the microwave spectrum when the 3–3 π pumping scheme is employed. By rotating the laser polarization 90 degrees, 3–3 σ excitation can be used for detection. Due to the selection rules, the $M = 0 \leftrightarrow M' = 0$ transition is forbidden in the 3–3 π excitation, such that population in the F=3, M=0 level will not undergo excitation. The unpumped Cs atoms contributed to a large background signal and an increased noise level in the spectrum. Figure 4c gives the microwave spectrum observed when the 4–4 σ pumping scheme is used.

Figure 4d compares the measured relative intensities of the microwave transitions resulting from the 3–3 σ excitation scheme of Fig. 4a with the calculated values. The calculated values are obtained from the matrix elements for the seven hyperfine transitions, assuming that the populations of the magnetic sublevels in the unpumped hyperfine state are equal and the pumped hyperfine state is completely depopulated. Excellent agreement between the experimental results and the calculated values indicates that the seven sublevels ($M = 0, \pm1, \pm2, \pm3$) in the F=4 hyperfine state are indeed equally populated. In certain pumping schemes, due to the selection rules and the differences in the transition probabilities for the D_2 lines among the Zeeman sublevels, alignment of the atomic population (i.e. nonuniform population of Zeeman sublevels) could be created. Relative intensities of the microwave signals in Fig. 4b and 4c are compared with the calculated values in Fig. 4e and 4f, respectively. It is clear that levels with the high magnetic quantum numbers, M, are favored when 3–3 π pumping is employed. In the case of the 4–4 σ scheme, levels with $M = \pm2$ are preferred.

(C) Two-Laser Experiment

In this experiment, two lasers are used in an attempt to concentrate all of the Cs population into one of the two clock transition Zeeman sublevels by using both the hyperfine and Zeeman optical pumping techniques. Experimental arrangements were similar to those used in the one-laser experiment with the exception that an additional pumping laser was used for Zeeman pumping. Fig. 5a shows the microwave spectrum with 4–4 π and 3–3 σ pumping, and 3–3 σ detecting. Signal for the (0–0) 'clock' transition was greatly increased compared to the one-laser pumping experiment at the expense of the other microwave transitions. With this arrangement, we were able to concentrate ~80% of the atomic population into the F=4 M=0 level. Fig. 5b shows the atomic population distribution among the magnetic sublevels of the F=4 hyperfine states. About 7% atomic population remained in the F=3 state, which contributed to the increased noise figure in the spectrum. With 4–4 σ and 3–3 π pumping, ~70% Cs atoms were concentrated into the F=3, M=0 level.

At low values of magnetic field strength, optical pumping efficiencies involving s-transitions will be reduced. This is due to the creation of $\Delta M = \pm2$ Zeeman coherences in the Cs ground state [5]. Thus, it would be undesirable to use σ-transitions in optically pumped frequency standards when a low C-field is needed. Figure 6 shows the result of our measurements of the % population concentrated in the F=3, M=0 clock state using the 3–3 σ and 4–4 π two-laser pumping scheme. Below 70 mG, the neighboring microwave transitions interfered with the clock signal, thus no measurement was conducted below that value of magnetic field. No evidence for the reduction of pumping efficiency was observed over the C-field range of 70 to 1500 mG.

(D) Velocity Distribution in the Atomic Beam

Figure 6 shows the Ramsey-Rabi signal of the (0–0) 'clock' transition obtained in an one-laser experiment. 3–3 σ excitation was used for both pumping and detecting. Calculated values of the clock signal, assuming that the velocity distribution in the Cs beam is beam-Maxwellian, are plotted as circles in the figure. Agreement between the experimental and the calculated values is satisfactory. This indicates that the velocity distribution of atoms contributing to the microwave signal is beam-Maxwellian, with a temperature consistent with that of the oven source.

CONCLUSIONS

We have established a facility for studying compact optically pumped Cs frequency standards. Basic functions of the atomic clock system have been demonstrated. In the two-laser experiment, we are able to concentrate ~80% of the atomic population in one of the 'clock' transition states. The velocity distribution of the Cs atoms in the atomic beam are found to be approximately beam-Maxwellian, which indicates that the optical state preparation and detection methods used in the OPCS are insensitive to the velocity of Cs atoms along the atomic beam. Thus in contrast to the magnetic state selection techniques used in conventional Cs clocks, optical state preparation and detection techniques allow much more efficient uses of the atomic beam flux, which can lead to improved reliability and increased useful lifetime of the clock.

ACKNOWLEDGEMENTS

The author would like to thank Dr R. Frueholz for his many helpful discussions and encouragements. This research was sponsored by the U.S. Air Force Space Systems Division under Contract No. F04701-88-C-0089.

REFERENCES

[1] N. Dimarcq, V. Giordano, G. Theobald and P. Cerez, J. Appl. Phys. 69, 1158 (91).

[2] S. Ohshima, Y. Nakadan, T. Ikegami, Y. Koga, R. Drullinger and L. Hollberg, IEEE Trans. Instrum. Meas. IM-38, 533 (89).

[3] P. Tremblay and C. Jacques, Phys. Rev. A, 41, 4989 (1980).

[4] R. E. Drullinger, Proc. 44th Annual Symposium on Frequncy Control 76 (1990).

[5] V. Giordano, A. Hamel, P. Petit, G. Theobald, N. Dimarcq, P. Cerez and C. Audoin, Proc. 43rd Annual Symposium on Frequency Control, 130 (1989).

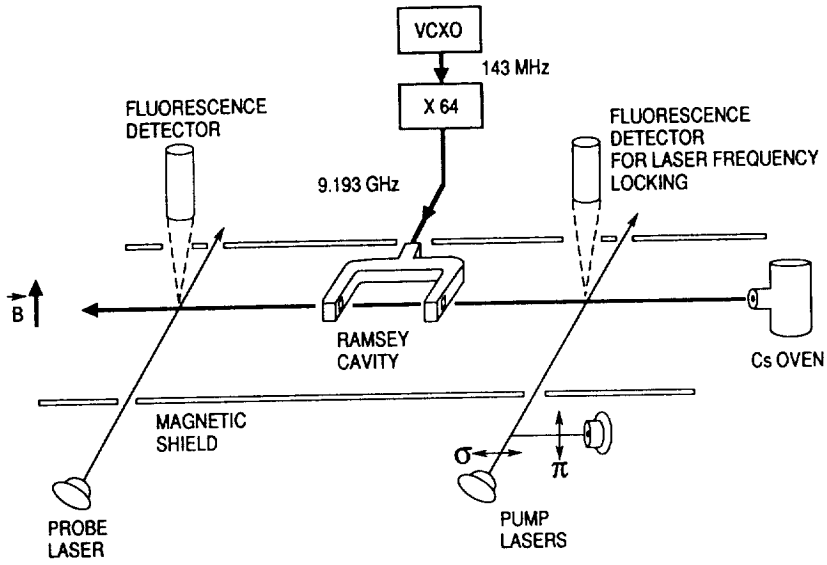

Fig. 1. Schematic representation of the optically pumped Cs frequency standard apparatus.

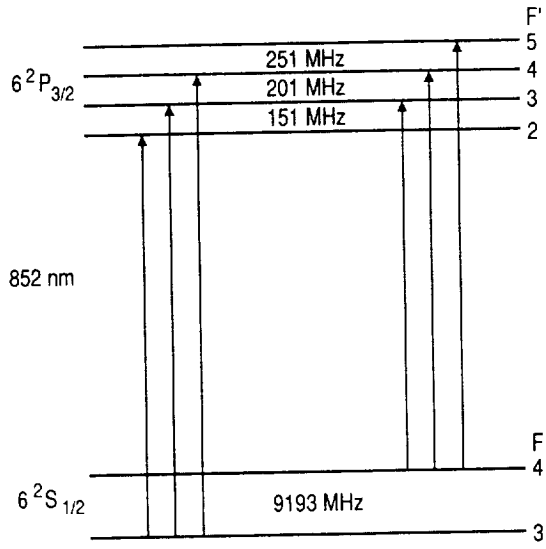

Fig. 2. Energy-level diagram for the D_2 transitions of Cs.

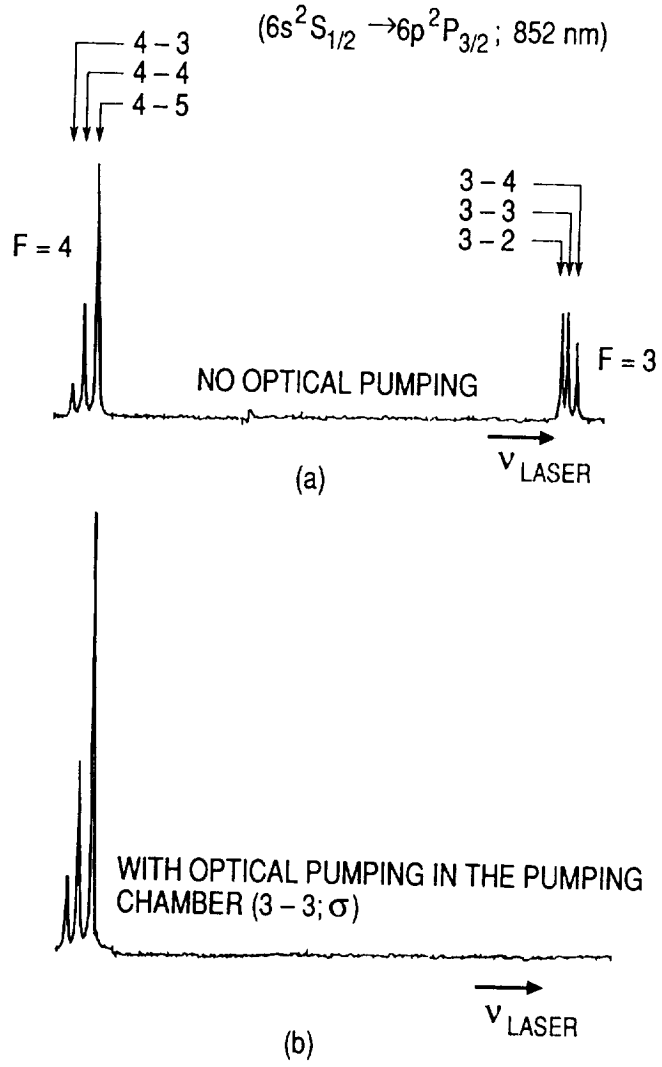

Fig. 3. Laser-induced fluorescence spectrum of the D_2 transitions of Cs at the detection chamber: (a) no optical pumping; (b) with 3-3 σ pumping in the pumping chamber.

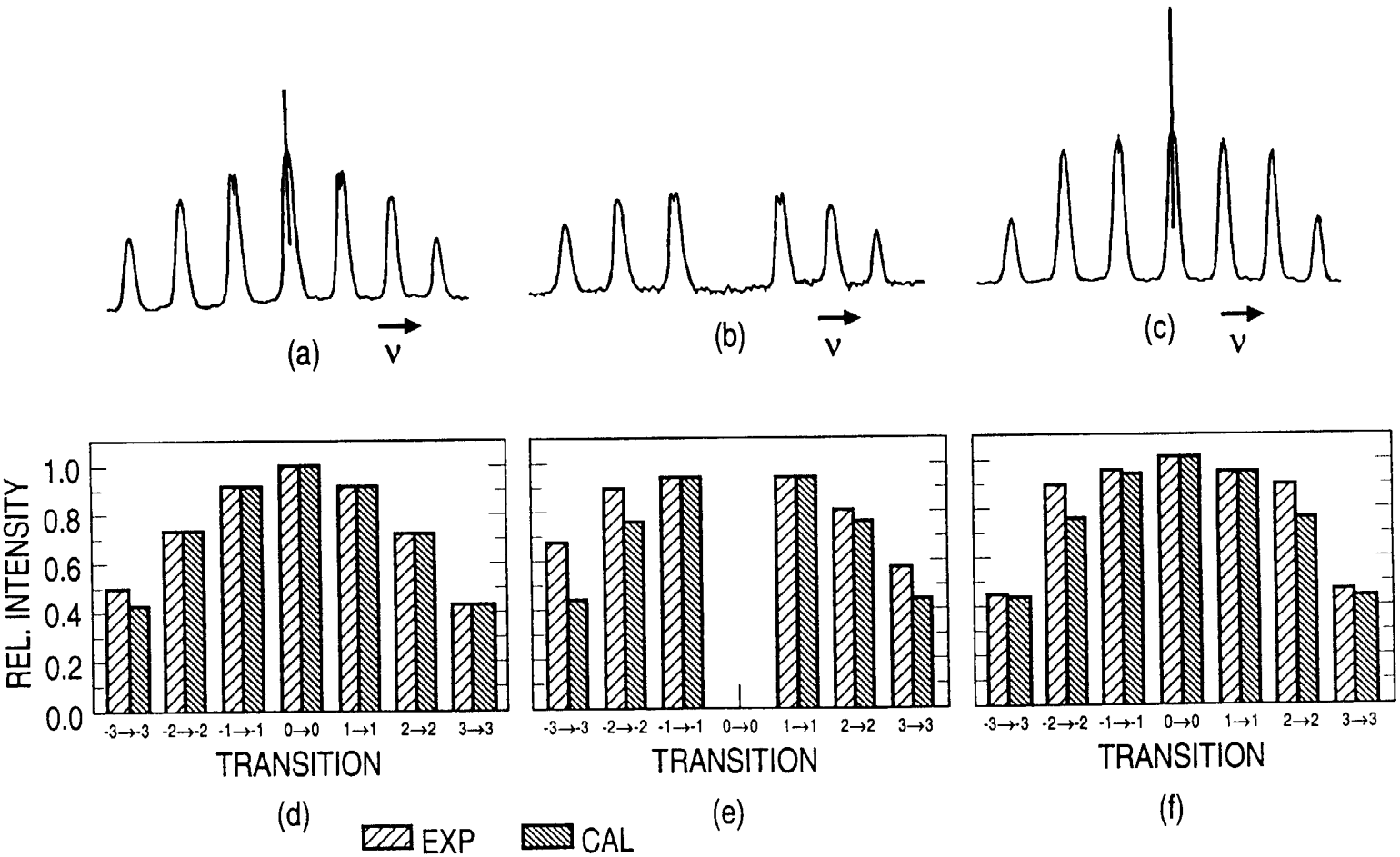

Fig. 4. (a), (b), (c) Microwave spectra of the OPCS pumped with one laser. Experimental conditions: (a) 3-3 σ pumping and detecting; (b) 3-3 π pumping and 3-3 σ detecting; (c) 4-4 σ pumping and detecting. Relative intensities of the microwave signals in (a), (b) and (c) are compared with the calculated values in (d), (e) and (f), respectively.

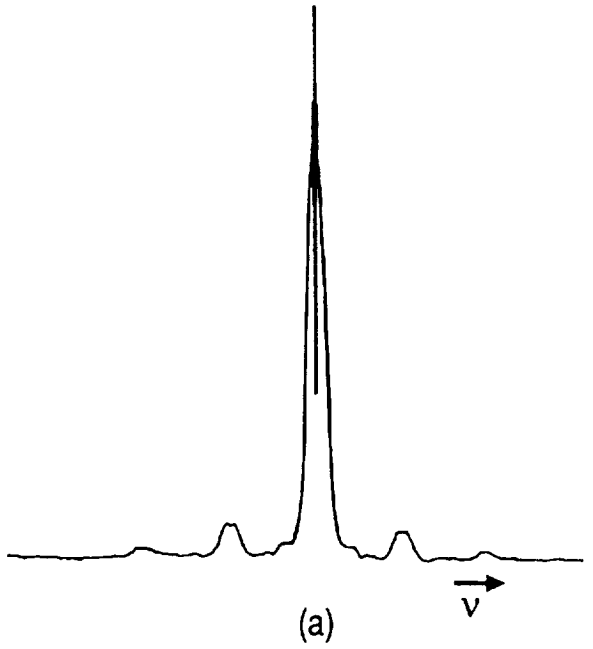

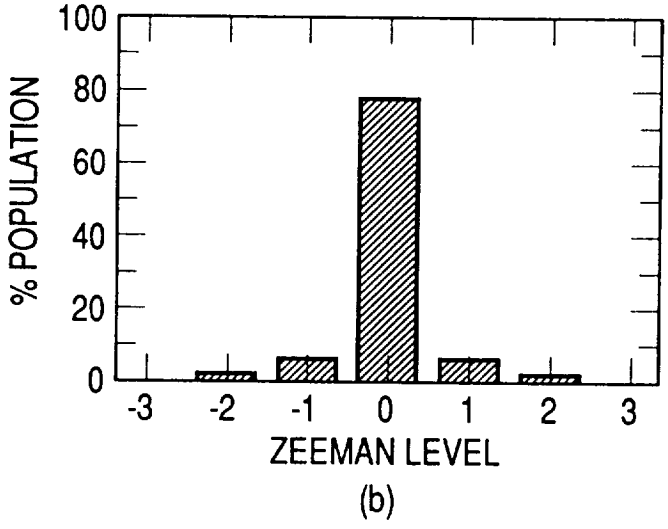

Fig. 5. (a) Microwave spectrum of the OPCS with the 4-4 π, and 3-3 σ pumping scheme and detected with the 3-3 σ transition. (b) Atomic population distributions among the Zeeman levels in F=4 level, as a result of the two laser pumping.

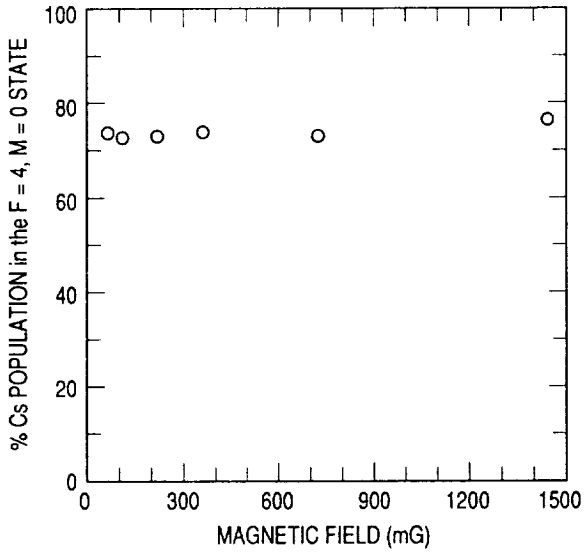

Fig. 6. Percent of atomic population concentrated in the F=4, M=0 level with two-laser pumping plotted as a function of the magnetic field. Pumping scheme is 3-3 σ and 4-4 π with 3-3 σ detecting.

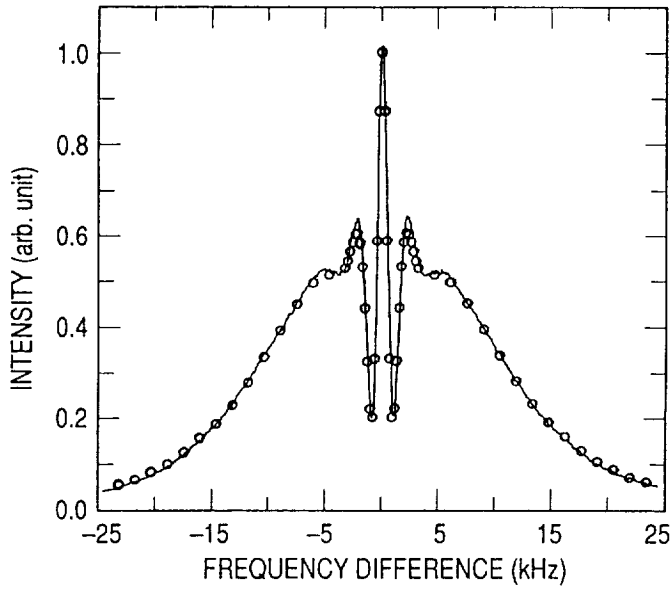

Fig. 7. Comparison of the experimental and the calculated Ramsey-Rabi structure of the (0-0) 'clock' transition. Experimental data and the calculated values are represented by the solid line and the circles, respectively.

A NEW TWO-WAY TIME TRANSFER MODEM

G.P. Landis, I.J. Galysh, G. Gifford
Naval Research Laboratory
4555 Overlook Ave. Southwest
Washington D.C. 20375-5000
and

Allen "Skip" Osborne III

Allen Osborne Associates, Inc.
756 Lakefield Road, BLDG J
Westlake Village, CA 91361-2624

Abstract

The use of commercial communication satellites for precise time transfer has been performed with a variety of techniques for a number of years. Military communications systems can also provide this function in a few deployed systems. This paper will demonstrate a new design of a time transfer modem that can be produced at a reasonable cost and enable users to make direct comparisons with the Naval Observatory with nanosecond precision. A flexible all-digital design is being implemented that will enable a variety of different codes to be employed. The design and operating modes of this equipment are demonstrated.

Introduction

Papers have been presented at the 1989 and 1990 PTTI meetings describing the hardware and the digital signal processing design of the NRL-USNO Two-Way Time Transfer Modem. This paper is intended to show the present status and preliminary results.

TWO-WAY TIME TRANSFER MODEM SOFTWARE OPERATION

The software for the Two-Way Time Transfer Modem allows for autonomous operation of the system. It handles the scheduling of time transfers, storage of the data, and post processing of the data. What will be described in this section is the operation of the software and how data is moved around.

The modem is controlled with a PC/AT type computer. The computer handles the user interface, scheduling of time transfers, and post processing of the data. The PC/AT is equipped with a VGA type display, a floppy disk drive, a hard drive, and keyboard. The modem consists of a digital

signal processing card, a digital modem card, and an analog interface as shown in figure one. The PC/AT computer and digital signal processing card communicate to each other through dual port memory.

Operation of the modem is controlled by the PC/AT through the dual port memory. Various locations of the dual port memory are allocated to specific functions. Some memory locations store the parameters of the modem such as carrier frequency, code rates, and code sizes. This allows easy reconfiguration of the modem without changing the software. About three-fourths of the dual port memory is allocated to data being transmitted and received.

There are two memory locations that control the operating modes of the modem. One location is called 'modem control.' The other location is called 'modem mode.' 'Modem control' is controlled by the PC/AT. The PC/AT puts a number in this location to control the operating mode of the modem. 'Modem mode' is a memory location that is set by the digital signal processor showing what mode it is presently in. The operating modes are setup in a way that the PC/AT can set the 'mode control' to the desired operating mode and the digital signal processor will increment through all of the modes until it reaches the desired operating mode. There are eleven operating modes defined to this point and more will come as the software matures. The operating modes are defined in table one.

Table 1. Operating Modes

0	Power up mode, DSP waits for PC/AT program to boot.
1	Initialize transmitter and synchronize the internal lock system timing with an external clock source.
2	Idle mode, stay off air and keep system time.
3	Initialize receiver section of modem, adjust the receiver attenuator so the A/D is not saturated.
4	Search for signal in frequency and time.
5	Verify search by trying to find the signal peak again.
6	Adjust the carrier NCO to the signal frequency.
7	Track carrier and code.
8	Search for data sync block and track carrier and code.
9	Search for station ID, do one-way time transfer.
10	Perform two-way time transfer.

The first operating mode is '0.' The digital signal processor sets the 'modem control' and 'modem mode' to zero so that it can wait for the PC/AT to initialize itself. When the system powers up, the PC/AT first loads the digital signal processor software and starts up the digital signal processor. It then loads the modem control software. In the mean time, the digital signal processor is executing its software and has accomplished preliminary initialization. Before the PC/AT has loaded its software, the digital signal processor is waiting for the PC/AT to set the operating mode. If the PC/AT hasn't set the operating mode, the 'modem control' memory location has an undefined number in it and can cause the digital signal processor to step through the operating modes prematurely. That is why the digital signal processor sets the memory locations to zero. After that, the 'modem control' memory location is set only by the PC/AT.

Mode one is used to initialize the transmitter section of the modem. The transmitter section is synchronized to the 1 PPS source once and then generates its own 1 PPS. It is assumed that the

clock providing the 1 PPS is also providing a coherent 5 MHz signal. The 5 MHz signal is multiplied to 25 MHz in the analog hardware. The phase of the 5 MHz signal is adjusted so that the positive edge of the 25 MHz matches the edge of the input 1 PPS. The 25 MHz provides the system timing. Once the transmitter is synchronized to the 1 PPS, the external 1 PPS signal is not required. After the transmitter circuit has been started, even though it is not transmitting to the satellite yet, the time of day can be kept.

The next mode, mode two, is the idle mode. The modem only keeps track of time and waits for a new mode. This mode is used only when a time transfer is not scheduled.

Mode three initializes the receiver section of the modem. The receiver NCO is set to about 2.5 MHz, and the code generator is loaded. The input to the receiver circuit is turned on so any signal received by the VSAT is sent to the analog to digital converter (ADC). The ADC has a bit to signal when it is saturated. The digital signal processor adjusts the receiver attenuator while monitoring the saturation bit. The modem is then ready to move on to the next mode.

Searching for a signal is done in mode four. The search is performed in a two-dimensional space through frequency and time. It performs a frequency search by way of an FFT operation. The search through time is by shifting its reference code against the incoming signal. An FFT is performed on each shift of the code. The code is shifted about one and a half code lengths. The maximum peak found is recorded for verification.

Mode five performs another search for the signal. This mode is the verification mode. Instead of searching for one and a half code lengths, the search stops when a peak in the signal is found that is equivalent to the peak found in mode four. The carrier offset found in the search is passed to the next mode. When the reference code matches the incoming signal code, the modem goes to the next mode.

In mode six, the carrier NCO is set to the incoming signal's carrier frequency to within 304 Hz. The digital signal processor acquires samples of the signal and makes a finer adjustment of the carrier NCO to a small offset.

Mode seven is another type of idle mode except that it runs the carrier tracking loop and the code tracking loop. Remember that while all of these operations have been going on, the modem is still keeping track of time.

In mode eight, the modem searches for a sync word in the data message. The word is a unique combination of ones and zeros. The hexadecimal representation of the sync word is FFFF0000h. This places a restriction on the rest of the data in that the data cannot in any way or combination appear as the sync pulse. This is overcome by aligning the data in thirty-two bit blocks. ASCII formatted data is aligned in eight bit characters and grouped in multiples of four characters. Data such as a time tag or time of arrival measurement are sent as binary integers. The integers or combination of integers can appear as a sync pulse. This is taken care of by determining the maximum number of bits required by the data and limiting the data to that size and adding an offset that only uses the unused bits of the thirty-two bit data integer. If the digital signal processor cannot find the sync pulse in five seconds, it starts over at mode four to reacquire the signal.

After the sync pulse is found, the modem can move up to mode nine. In this mode, the digital signal processor extracts the station identification information from the data and determines if it is the correct ID. If the incorrect ID is being received, the modem will keep extracting the ID from the data until the correct station ID is received. Then the next mode will be executed. While the

modem is waiting for the proper station ID, it will be performing time of arrival measurements.

Finally in mode ten, a complete two way time transfer can proceed. The modem will continue making time of arrival measurements and transmit its result to the other site. At the same time it will record the other sites data transmissions along with its own transmission for post processing. The modem remains in mode ten for three hundred seconds and then returns to mode two until the next time transfer is scheduled.

A two- way time transfer requires that one modem have control over the communications of the other modems. Assuming USNO is a master site for the two-way time transfer, USNO will be performing the time transfer with more than one other site. This requires control over which sites may transmit. Only one site may transmit with the master station at one time. This is the reason for station IDs. What will be described is the operation of a time transfer between the master site and two target sites. The operating modes of both modems will be modified slightly from what was described earlier.

TIME TRANSFER OPERATION

Assuming that all of the modems have been powered up and initialized, they will be idle in mode two. The transmitter output is turned off so the target sites will not transmit a signal to the satellite. At some time, the target site PC/ATs will determine that it is time for a time transfer. The target site PC/ATs will set the 'modem control' memory location to mode ten, a full two-way time transfer. The digital signal processor cards will detect the change in memory and proceeds to mode three and then mode four. It will stay at mode four until a signal from the master site has been detected. The transmitter signal is still off.

In the mean time, the master station is sitting idle at mode two. It's transmitter output is turned off. When the master station PC/AT determines it is time for a time transfer, it will turn on the transmitter and select the target site to do the time transfer with by transmitting the target's ID. The master station moves to mode three and then four. It will keep searching until the selected target starts transmitting.

Now that the master station is transmitting, the target stations will eventually find the master station signal and start tracking it. The target stations will find the sync word and start looking for the ID in the master data being transmitted. When the one target station recognizes its station ID, it will move to mode ten. At mode ten, the target will start transmitting back to the station. The other target stations do not transmit and stay in mode nine.

Now that the target station has started transmitting, the master station tries to acquire the target's signal. Eventually the master station will reach mode nine. In mode nine, instead of looking for its own ID, the master station looks for the targets ID. The transmitting target station must transmit its own ID. If the master station determines that the wrong target is transmitting, it will shut off its transmitter. This will cause the target station to lose signal lock and drop down to mode four. This mode change makes the target station to shut off its transmitter. The whole process will then start over.

When both sites are at mode ten, they will perform a two-way time transfer. This will last for 300 seconds. The two sites will only transmit data when both are at mode ten. There is a 32 bit word in the data message that indicates when the site is ready to receive data. When handshaking indicates that one of the sites is not at mode ten, the only information that is updated in the data

message is the seconds of the day time tag and the status word. All of the other information is not updated.

When the time transfer is completed, the master station will simply change the station ID to select another target. The previously selected target will notice the ID change and immediately drop to mode nine and shut off its transmitter output. The newly selected site will then begin transmitting and perform the time transfer.

Eventually the site's PC/AT will determine that time has elapsed and set the modem to mode two. At this point each site can proceed to process its data.

TRANSMITTING AND RECEIVING DATA

The data to be transmitted and received are placed in dual port memory. There is enough dual port memory allocated for fifty seconds of data transmission. Twenty-five seconds of data is available for receiving. This is obviously not enough for a 300 second time transfer. A technique called a circular buffer has been implemented with the memory.

The memory for transmitting data is preloaded with auxiliary data. The digital signal processor, when in mode ten, transmits the data over and over. The preloaded data is repeatedly transmitted every fifty seconds. Various preallocated locations in the data message are updated with measurements and a time tag every second.

On the receiving side, the data being stored is written over every twenty-five seconds. Since each second brings a new measurement, the data has to be saved before it is overwritten, The PC/AT monitors the receive data buffer and saves the data every twenty-five seconds. During the time transfer, the PC/AT saves the data in its memory. After the time transfer, the data is saved to disk.

Testing

Preliminary tests on the modem have been conducted but have not been completely analyzed. These tests were both bench and satellite tests. Additional tests are planned to investigate known problems and to study temperature, signal level and cross correlation problems.

The bench test used four different configurations of clocks and cabling. Stability and range rate sensitivity were investigated by using common or separate clocks. The 70 MHz cabling between the modem on the bench used both common and independent connections to investigate the cross correlation effects of the two signals. All bench test were done with very strong signal levels to look at systematic effects. Refer to Tables two and three.

Preliminary satellite tests were conducted with two modems and one VSAT to ease coordinate problems. The test used a common clock.

The data from each modem and the combined modem data was examined for residual noise by performing a least squares linear fit. The residual noise was calculated and plotted.

Results

In the single oscillator bench test, the residual plots showed a clean straight line without a slope. The rms modem noise was less than 100 picoseconds. (Figures 1, 2, and 3).

In the dual clock test, the modems have their own oscillator. The resulting plot showed the noise was not white. The use of two cables for modem communication did not change the data. The level of this problem was about 1 nanosecond peak to peak and about the same on both modems. It is not known if this is a hardware or software problem. (Figures 4, 5, and 6).

Data from the satellite test showed a parabola on both modems, this showed the presence of an acceleration term in the range and did not appear in the combined data. The satellite test showed an anomaly only in the data from the right modem. This anomaly is not a cross correlation problem because the code was generated by the same clock and the path is delayed by the same varying amount. Without this anomaly the quality of the time transfers was about 300 picoseconds rms. (Figures 7, 8, and 9).

Table 2.

TEST #	CLOCKS	PATH	FILE NAME
1	ONE	ONE WIRE	11111511
2	ONE	TWO WIRES	12131411
3	TWO	ONE WIRE	21081511
4	TWO	ONE WIRE	21091511
5	TWO	TWO WIRES	22141411
6	ONE	SATELLITE	11112511
7	ONE	SATELLITE	11122511

Table 3.
MODEM NOISE IN SECONDS

TEST	LEFT MODEM		RIGHT MODEM		COMBINATION		
#	LINEAR FIT	PARABOLA FIT	LINEAR FIT	PARABOLA FIT	LINEAR FIT	PARABOLA FIT	OSCILLATOR OFFSET
1	9.8E-11	9.8E-11	1.5E-10	1.5E-10	9.0E-11	8.9E-11	0.
2	9.3E-11	9.2E-11	9.9E-12	8.9E-12	4.7E-11	4.6E-11	0.
3	2.6E-10	2.6E-10	2.4E-10	2.4E-10	2.6E-10	2.4E-10	1.1E-10
4	2.8E-10	2.4E-10	2.8E-10	2.7E-10	1.9E-10	1.9E-10	2.2E-10
5	2.9E-10	2.1E-10	2.0E-10	2.0E-10	2.7E-10	1.4E-10	2.8E-10
6	5.3E-10	2.2E-10	6.9E-10	4.5E-10	2.6E-10	2.6E-10	2.7E-9*
7	5.5E-10	2.2E-10	7.9E-10	5.5E-10	3.1E-10	3.1E-10	2.6E-9*

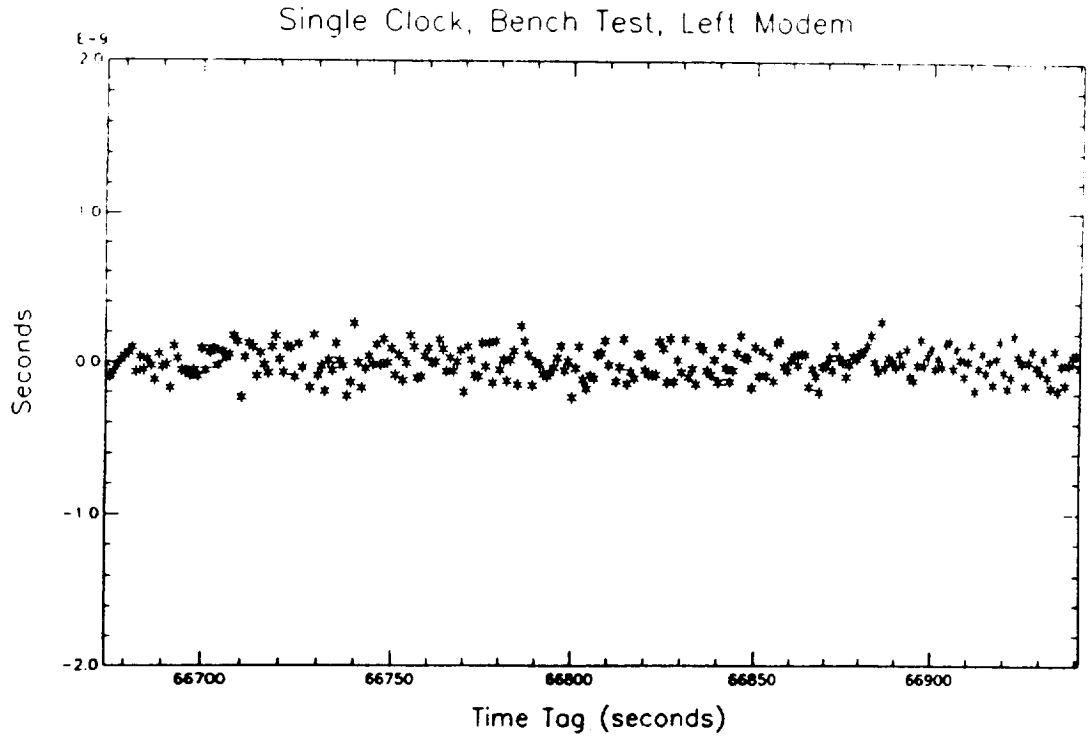

Figure 1

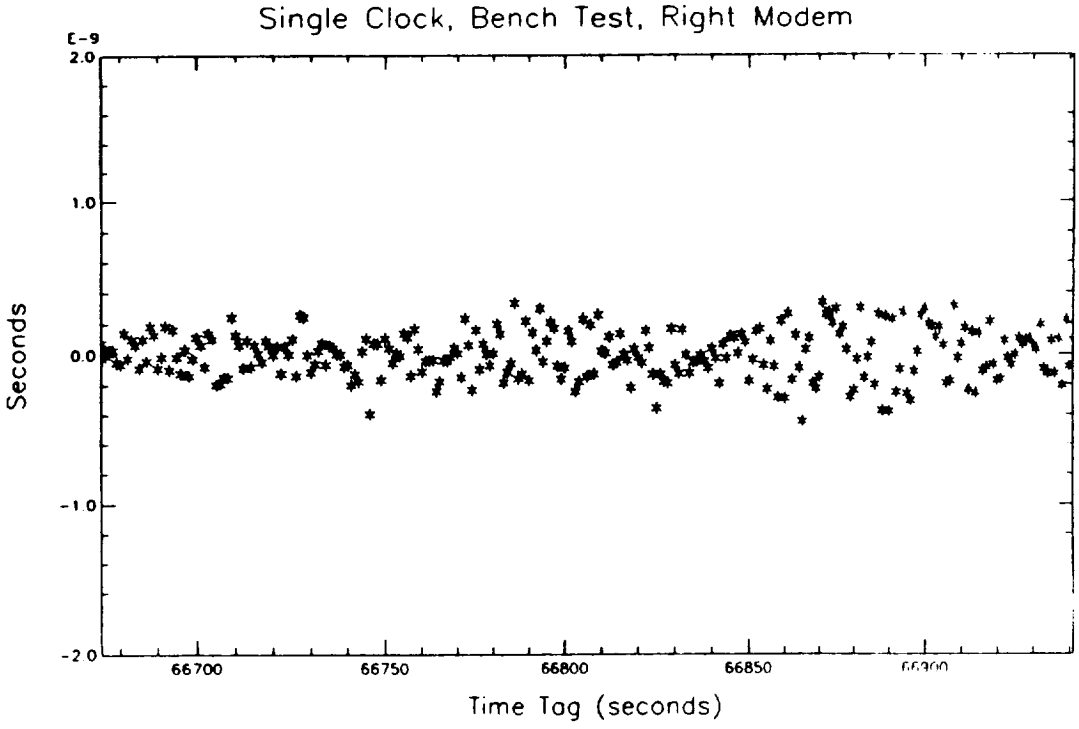

Figure 2

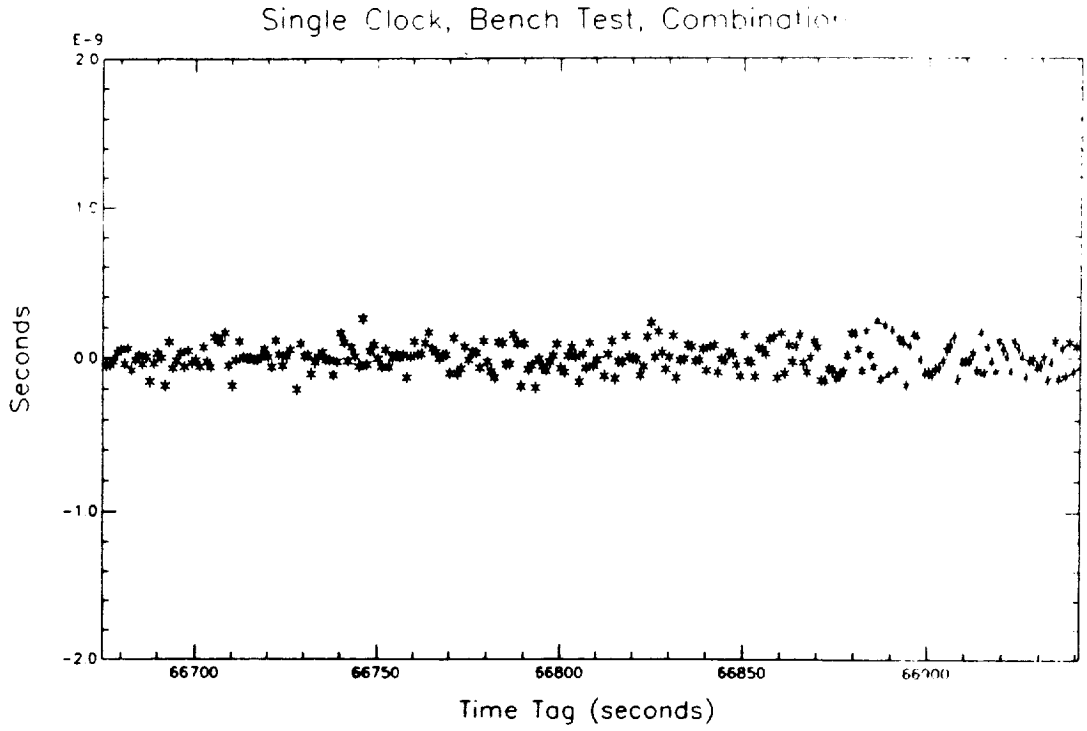

Figure 3

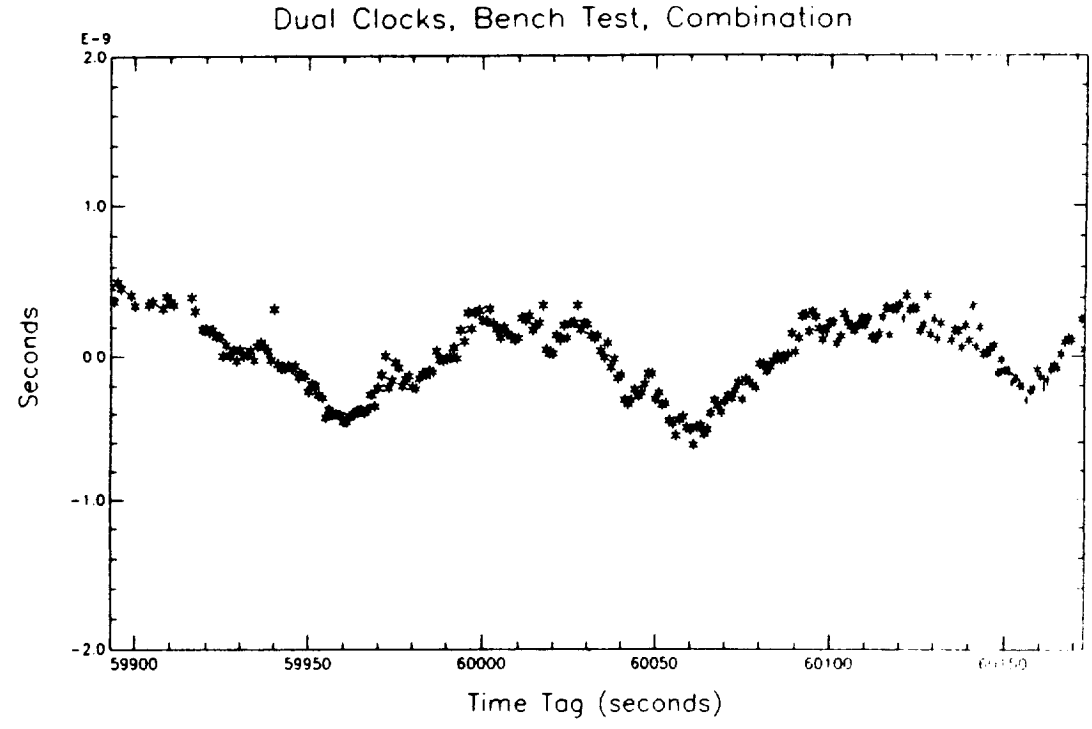

Figure 4

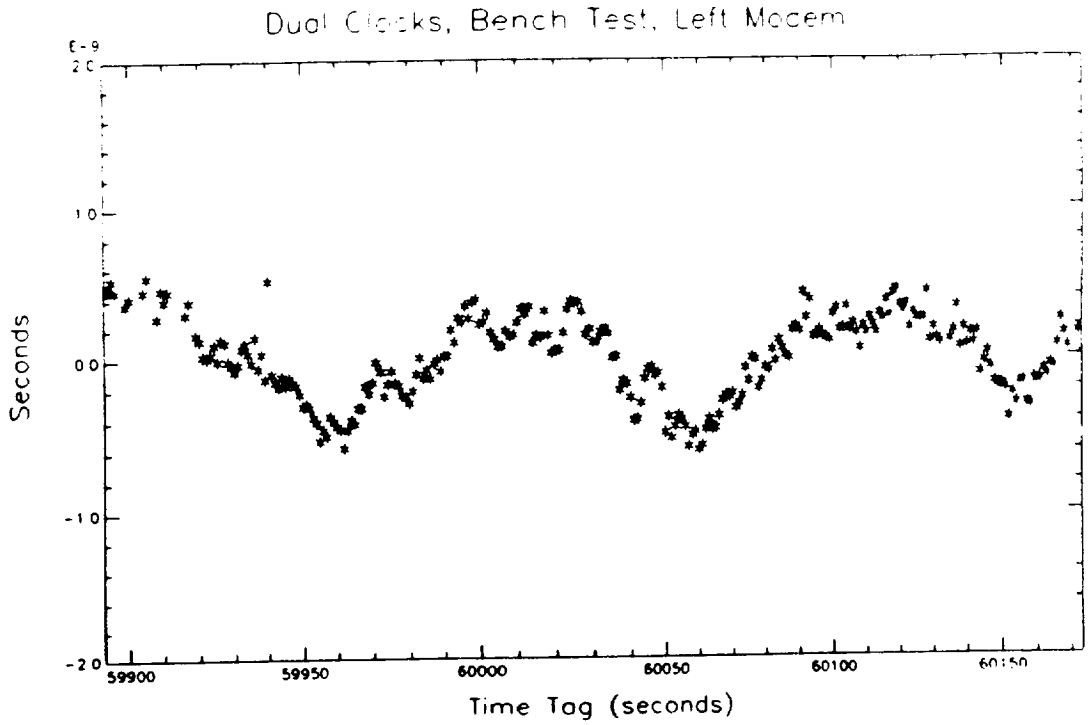

Figure 5

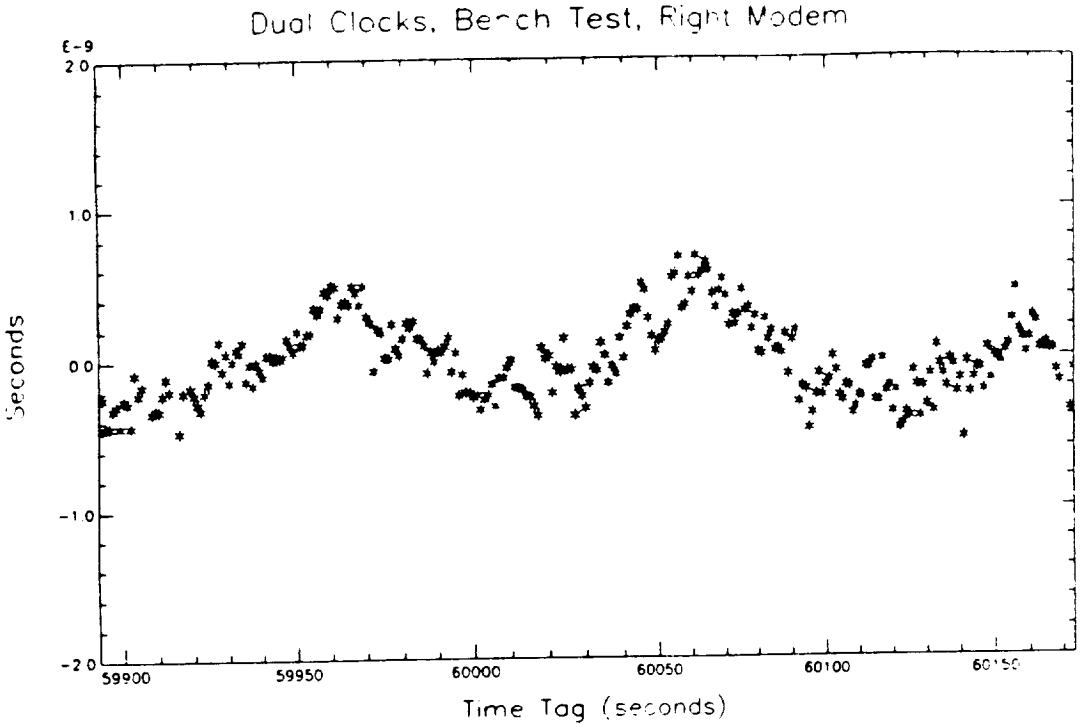

Figure 6

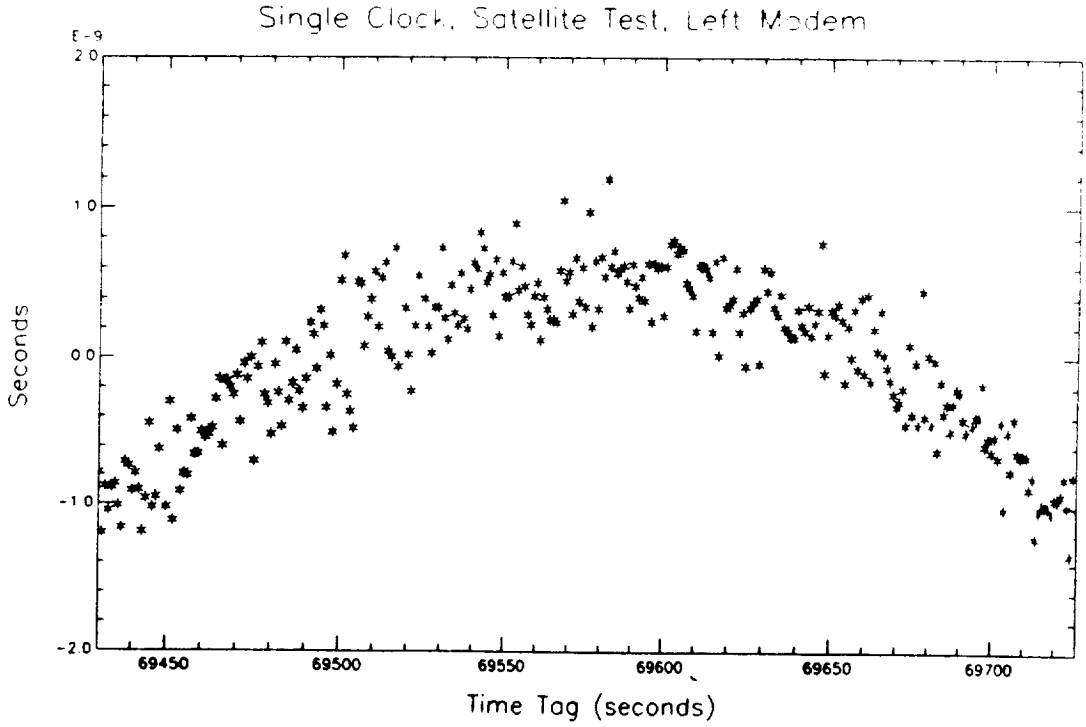

Figure 7

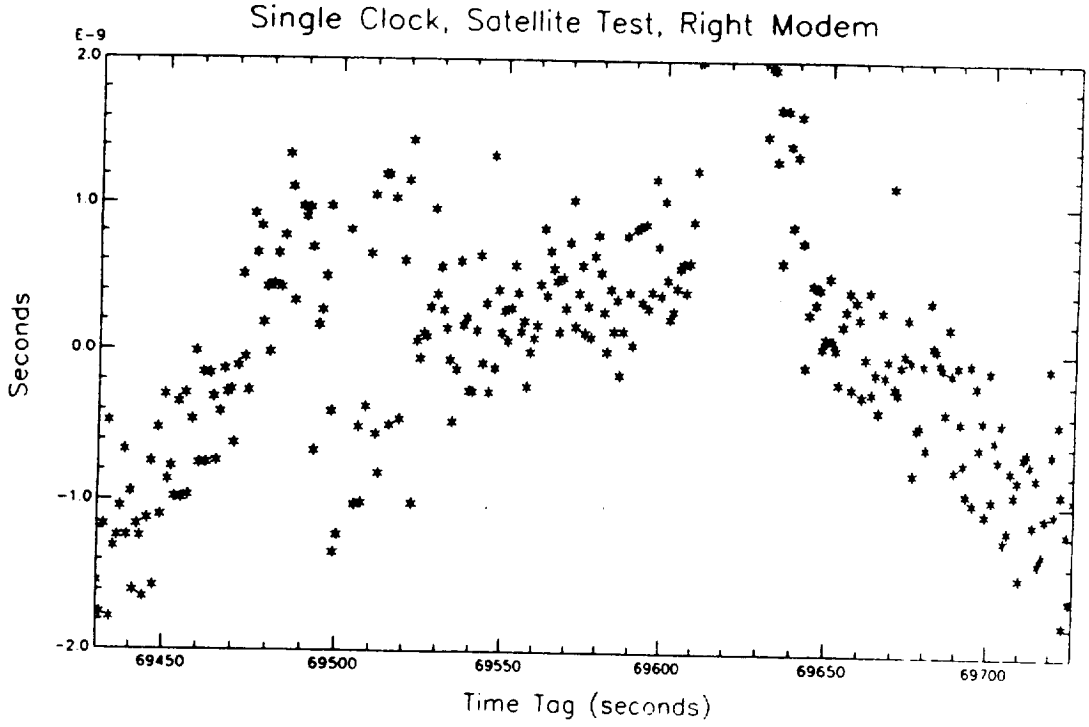

Figure 8

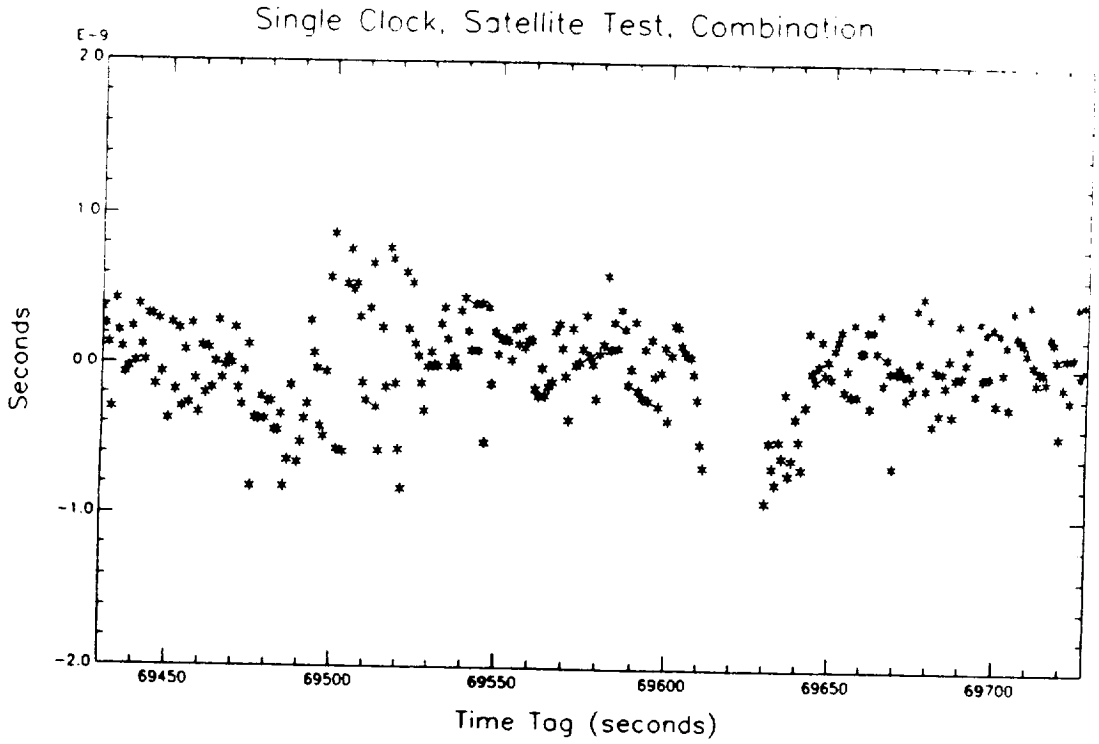
Single Clock, Satellite Test, Combination
E-9
2.0
1.0
0.0
-1.0
-2.0
Seconds
69450
69500
69550
69600
69650
69700
Time Tag (seconds)

Figure 9

Noninertial Coordinate Time: A New Concept Affecting Time Standards, Time Transfers and Clock Synchronization

Steven D. Deines

Abstract

Relativity compensations must be made in precise and accurate measurements whenever an observer is accelerated. Although many believe the Earth-centered frame is sufficiently inertial, accelerations of the Earth, as evidenced by the tides, prove that it is technically a noninertial system for even an Earth-based observer. Dr. Einstein introduced the concept that time was essentially a fourth component that could be added to any three-dimensional position. Using the constant speed of light, a set of fixed remote clocks in an inertial frame can be synchronized to a fixed master clock transmitting its time in that frame. The time on the remote clock defines the coordinate time at that coordinate position. However, the synchronization procedure for an accelerated frame is affected, because the distance between the master and remote clocks is altered due to the acceleration of the remote clock toward or away from the master clock during the transmission interval.

An exact metric that converts observations from noninertial frames to inertial frames was recently derived. Using this metric with other physical relationships, a new concept of noninertial coordinate time is defined. This noninertial coordinate time includes all relativity compensations. This new definition raises several timekeeping issues, such as proper time standards, time transfer processes, and clock synchronizations, all in the noninertial frame such as Earth.

Background

Relativity compensations must be made in precise and accurate measurements whenever an observer is accelerated. Noninertial reference frames are ones that experience accelerations, which include rotations. A reference frame centered on the Earth would appear to be inertial, but the observation of the tides demonstrates the existence of a force acting on the oceans. This force is the product of mass and acceleration, which proves that the mass of the Earth is being accelerated. The existence of the tides proves that any Earth-centered frame is not sufficiently inertial.

Dr. Albert Einstein accurately assumed that the speed of light (i.e. any electromagnetic radiation) in a vacuum is always the same constant for all inertial frames. He accurately predicted that a moving clock would appear to run slower than an identical, but stationary, clock. Dr. Einstein developed the concept that time was a relative quantity that essentially is a fourth coordinate associated with any three-dimensional position of a chosen reference frame. This resulted in the definition of coordinate time unique to every reference frame.

Conversion of position and time coordinates between inertial frames was accomplished by Dr. Einstein through the Lorentz transformation. The current practice in relativity science is

to use comoving inertial reference frames to match a noninertial reference frame and then apply the Lorentz transformation to convert observations from one inertial frame to another.

Only recently, an *exact* transformation which converts observations from noninertial frames to inertial frames was derived[1]. This was developed by Dr. Robert Nelson, and this transformation will be designated as the Nelson transformation to eliminate confusion. The metric for an accelerated, rotating frame has been derived as:

$$\begin{aligned} \mathbf{g_{00}} &= -\left[1+\frac{\bar{A}\cdot\bar{\rho}}{c^2}\right]^2+\left[\frac{\bar{\omega}\times\bar{\rho}}{c^2}\right]^2 \\ \mathbf{g_{oj}} &= \frac{1}{c}(\bar{\omega}\times\bar{\rho})_j) \\ \mathbf{g_{ij}} &= \delta_{ij} \end{aligned}$$

Definition of Noninertial Coordinate Time: A New Concept

The Nelson metric was modified in the g_{oo} term to include gravity effects[2] from the post-Newtonian approximation as follows:

$$\mathbf{g_{00}} = -1+\overset{2}{\mathbf{g}}_{\mathbf{00}}+\overset{4}{\mathbf{g}}_{\mathbf{00}}+\ldots=-\mathbf{1}-\mathbf{2\Phi}+\ldots \tag{1}$$

One fundamental property that remains invariant in relativity regardless of the reference frame is "proper time,"denoted here as τ. The proper time of an object is defined as the time measured by an ideal clock attached to the moving object[3]. An invariant equation relates coordinate time (t) and coordinate position ($\bar{X}$) with proper time (τ).

$$(c\ d\tau)^2=(c\ dt)^2-dx^2-dy^2-dz^2 \tag{2}$$

To facilitate the use of the relativity equations, the modified Nelson metric and the proper time used in Equation 2 have been converted from Einstein's repeating Roman index notation to the more familiar vector notation. The modified Nelson metric (Equation 1) was inserted into the invariant equation (Equation 2). Equation 3 was completely derived[4] using Equations 1 and 2.

$$d\tau=\sqrt{\left[1+\frac{\bar{A}\cdot\bar{\rho}}{c^2}\right]^2+\frac{2\Phi}{c^2}-\left[\frac{\bar{v}-\bar{V}}{c}\right]^2}\ \ dt \tag{3}$$

where

- Φ = the sum total of each gravitational potential at the remote clock's location as contributed by each measurable mass source. For locations near or on the Earth's surface, $\Phi = g(\phi)h$ as defined below.
- τ = the proper time of the noninertial Earth at the geoid.
- $\bar{A}$ = the acceleration vector of the remote clock in the chosen inertial reference frame.
- $\bar{V}$ = the velocity vector of the remote clock in the chosen inertial reference frame.
- $\bar{v}$ = the velocity vector of the master clock in the chosen inertial reference frame.

ϕ = the remote clock's geodetic latitude relative to Earth's geoid if that clock is near or on the Earth's surface.

$g(\phi)$ = the perpendicular gravity constant at the remote clock at the Earth's surface, which is a function of the geodetic latitude ϕ of the remote clock's location.

h = the altitude of the remote clock above the Earth's geoid for applications when that clock is on or near the Earth's surface.

c = the speed of light (i.e. any electromagnetic radiation) in a vacuum of an inertial frame.

$\bar{\rho}$ = the range vector from the remote clock to the master clock in the inertial reference frame.

t = the noninertial coordinate time of the remote clock at reception.

Noninertial coordinate time is therefore defined as a function of proper time of the remote clock in the noninertial frame. The square root term in Equation 3 includes the relativity contributions for nongravitational accelerations $\frac{\bar{A}\cdot\bar{\rho}}{c^2}$, gravity $\frac{2\Phi}{c^2}$, and velocity $\left[\frac{\bar{v}-\bar{V}}{c}\right]$. This square root term is the time dilation factor that will always exceed the value of one for a noninertial frame. So, division of this factor into proper time yields the noninertial coordinate time interval, which is always smaller than the proper time interval.

Noninertial coordinate time is the time given by a fixed remote clock in a noninertial reference frame synchronized to a fixed master clock in that frame, which includes all relativity compensations. Even the theorization of all the relativity compensations in a noninertial frame was not possible before the advent of the Nelson metric, and only assumptions and approximations for these relativity compensations have been previously available.

Conclusions

Based on the new definition of noninertial coordinate time, a reexamination of several timekeeping issues is warranted. A few of these issues include the proper time standard, the time transfer process and the clock synchronization procedure, all in a noninertial frame (e.g. the Earth).

Inertial coordinate time standards (e.g. TAI), which are based on time calibrations in an inertial frame, beat faster than a moving proper time standard, which undergoes time dilations in its noninertial reference frame. Theoretically, the leap second between TAI and UT1 standards may be the result of this difference. Work is ongoing to quantify what portion of the leap second is due to differences between inertial and noninertial coordinate times. It is recommended that a study be initiated to determine whether the current atomic time standard, which is correctly defined for an inertial reference frame, is appropriate in Earth's noninertial frame.

Time transfers are currently done between two remote precise time stations that simultaneously observe a satellite time transmission. Time transfers determine the time differences between stations A and B without having to transport physical clocks for comparison. Global Positioning System (GPS) time transfers use a GPS time receiver to get a coordinate time at reception. The time transfer equation is [A-t_A] - [B-t_B] = A - B when $t_A = t_B$ at equivalent time marks. The local proper times of the atomic clocks are A and B, respectively, and t_A and t_B are the noninertial coordinate reception times from GPS receivers.

Time transfers are also affected by Earth's rotation. The Earth's geoid is a theoretical construct where all ideal clocks will beat at the same rate. However, even on the geoid, the nongravitational

relativity effects have first and second order dependence on the velocity of the local clocks in the noninertial local frame. The time transfer relationship between a satellite clock (e.g. GPS) and the fixed local clocks not on the geoid of the rotating Earth, has been derived. The Earth's gravity, the rotational acceleration and tangential velocity were inserted into Equation 3 to yield:

$$t_{GPS} = \left[1 + \frac{g(\phi)h}{c^2} + \frac{(\bar{\omega} \times \bar{R})^2 - (\bar{\omega} \times \bar{R}_{\text{geoid}})^2}{2c^2}\right] \mathrm{t} + \frac{\bar{\omega} \times \bar{R} \cdot \bar{\rho}}{c^2} \tag{4}$$

where $\bar{R}_{\text{geoid}}$ is the position vector where receiver would be on the geoid if the receiver had no altitude.

Equation 4 is used to compute the noninertial coordinate times t for the two remote stations for t_A and t_B. The transmission time from the GPS satellite is t_{GPS}, and t is the noninertial coordinate time at reception for the local clock. When the noninertial coordinate time t_A equals t_B, the time transfer algorithm correctly gives the difference in proper times of A and B of the two clocks.

The last term in Equation 4 is equivalent to the Sagnac effect, which corrects for the first order change in the geometric range as the clock moves toward or away from the satellite during the time interval of transmission. Two new relativity compensations in Equation 4, which were not previously included in GPS time transfers, affect the noninertial coordinate time t. The gravitational effect, $\frac{g(\phi)h}{c^2}$, is due to the additional change in gravity due to the altitude h as compared to the expected gravity in GPS at the Earth's geoid. The nongravitational effect, $\frac{1}{2}\left[\frac{\bar{\omega}\times\bar{R}}{c}\right]^2 - \frac{1}{2}\left[\frac{\bar{\omega}\times\bar{R}_{\text{geoid}}}{c}\right]^2$, is difference in the expected tangential velocity due to Earth's rotation as compared to the expected tangential velocity in GPS at the Earth's geoid..

It is assumed that the current GPS receivers correct for the geometric range, which is the last term in Equation 4. The additional gravitational effect for an atomic clock 2000 meters above the Earth's geoid, would result in a drift rate of 2.18 x 10^{-13} s/s or 18.8 ns/day. The nongravitational drift rate for an atomic clock affected by Earth's rotation when elevated 2000 meters above the geoid at the equator would be 7.55 x 10^{-16} s/s or 0.06 ns/day. Such offsets in frequency contributions may currently be attributed to mechanical errors in the clocks rather than these uncompensated relativity effects.

Clock synchronization is simple to perform in an inertial frame, and all stationary clocks will beat the same for both proper and coordinate time. Clock synchronization in an inertial frame is simply accomplished by :

$$t_{\text{remote}} = t_{\text{transmitted master time}} + \frac{\text{distance between remote and master}}{\text{speed of light}}$$

However, with a noninertial frame, clock synchronization between a master clock and a remote clock at rest must be accomplished differently. The distance that the master clock transmission must travel to the remote clock varies, because the remote clock can be accelerated toward or away from the master clock during the transmission interval. In general, the noninertial master clock beats will fluctuate differently from the noninertial remote clock rate, compared to the steady beat of any synchronized inertial clock. To perform clock synchronizations in a noninertial frame, Equation 3 must be used to convert proper time of a remote noninertial clock to its noninertial coordinate time. Only then will the remote noninertial clocks be synchronized to the noninertial master clock in that frame.

In summary, noninertial coordinate time includes all the relativity compensations required with a noninertial reference frame. Since the Earth-centered frame is not sufficiently inertial, the potential applications for noninertial coordinate time are far-ranging. Timekeepers concerned with optimium accuracies would achieve substantial improvements by using this concept.

References

[1] Robert A. Nelson, *"Generalized Lorentz Transformation for an Accelerated, Rotating Frame of Reference,"* Journal of Mathematical Physics, 28, No. 10 (October 1987), pp. 2379-2383.

[2] Steven Weinberg, **Gravitation and Cosmology**, John Wiley & Sons, 1972, pp. 194-201.

[3] Arthur I. Miller, **Albert Einstein's Special Theory of Relativity**, Addison-Wesley, 1981, p. 271.

[4] Steven D. Deines, *"Missing Relativity Terms in GPS,"* Navigation, Spring 1992.

CHARACTERIZATION OF FREQUENCY STANDARD INSTABILITY BY ESTIMATION OF THEIR COVARIANCE MATRIX

Patrizia Tavella
Istituto Elettrotecnico Nazionale G. Ferraris
Strada delle Cacce, 91
10135, Torino, Italy

and

Amedeo Premoli
Dip. di Elettrotecnica, Elettronica ed Informatica
Universita' di Trieste
Via A. Valerio, 10
34127, Trieste, Italy

Abstract

The popular 3-cornered hat method used for evaluating the noise contributions of individual frequency standards is revisited. This method is used in several cases, but sometimes the results are not consistent because one or more estimated clock variances turn out to be negative. Different causes of this unacceptable result have been conjectured: among them one regards the hypothesis of uncorrelated clocks, essential in this method. Since recently realistic cases of correlation between clocks, mainly due to the environmental conditions, have been observed, this paper proposes an entirely revisited version of the 3-cornered hat method which permits to evaluate the individual variances and also the possible covariances between clocks, by relaxing the hypothesis of uncorrelation. The uncertainty and the lack of contemporaneity of the measurement series are assumed to be negligible. The lack of the uncorrelation hypothesis calls for a more general mathematical model leading to an underdetermined linear system. The estimates of the (co)variances of the measurement series as well as those of the individual clocks are introduced by means of the scalar product of the related time series and arranged in the respective covariance matrices S *and* R. *Since covariance matrix is positive definite by definition, the problem consists in estimating the unknown* R, *subject to the constraint of positive definiteness, from the known* S. *Unfortunately, this constraint is not sufficient to estimate* R. *Therefore a suitable optimization criterion is proposed, which assures the positive definiteness of* R *and, at the same time, minimizes the global correlation among clocks. Examples of frequency instability measurements processed by the "classical" 3-cornered hat method and the here-revisited method are presented showing that the solutions are identical only when the uncorrelation hypothesis doesn't violate the positive definiteness of* R.

1 INTRODUCTION

The evaluation of frequency standards is performed by comparing two or more of them and measuring differences in their signals. Results depend on the simultaneous contributions of all the standards and it is often desirable to estimate the noise contributions of the single units. In the past years, this problem has been considered in several papers, which introduced the popular "3-cornered hat" method [1], successively extended to N clocks [2,3,4] and further investigated in [5,6]. *In all the above papers, a basic hypothesis consists in considering all the clocks uncorrelated.*

In the classical 3-cornered hat method, three clocks are considered, three series of time differences between all the possible pairs are measured, and their variances are estimated. Three linear equations are then written, which tie the three unknown variances of the single clocks to the known variances of the time differences. In this way, a uniquely solvable system is obtained [1]. If more than three clocks are compared, such a system becomes overdetermined because the number of possible pairs exceeds the number of clocks. In this case, it has been suggested either to deal with different triads of clocks and then combine the results in a (weighted) average [1], or to utilize the N clocks together with a least squares technique [2,3].

Independently of the number of clocks, a more crucial problem arises: the estimated clock variances can turn out to be negative. In such a case it has been suggested to use the absolute value [2] or to consider vanishing a variance that should turn negative. However these tricks are not justified by any theoretical consideration.

Several questions related to the statistical processing of these measurements and the causes of negative estimated variances are still open:

1. **Uncertainty in the measured time differences.**
   If the noise of the measuring device is not negligible, it adds a term in the variance of the measured time differences and the linear system is not longer deterministically solvable [4,5]. To the authors' knowledge, this uncertainty is negligible in most cases, particularly in high resolution measurements. The case can be different if the clocks are compared at a distance, through a synchronization link, but the synchronization noise, usually corresponding to a white phase noise, can often be suitably modeled and filtered.

2. **Lack of contemporaneity of measurements.**
   In this case, the contribution of each clock cannot be considered the same in each difference measurement [5,6]. However, the lack of contemporaneity of the different measurements is negligible when the integration times over which the stability is to be estimated are far longer (days) than the shift in time of the beginning of the different measurements (seconds).

3. **Low number of measured samples.**
   In this case, a statistically significant characterization of the involved noises is not ensured [5,10]. The low number of statistical samples remains an open question because it gives a low confidence on the estimates and particular care is to be paid.

4. **Correlation between clocks.**
   In recent years cases of correlation between clocks, mainly due to the environmental conditions, have been detected [8-18]. Different methods have been used to evidence correlation between clocks and the discussion is still lively also in understanding which is the clock component responsible for the effect but, in each case, an appreciable presence of correlation between clock data has been pointed out.

To the authors' knowledge, cases of negative estimated variances appear even when there are several measured samples and causes 1) and 2) above are certainly to be excluded. Usually, the problem appears over long integration times (months) where correlated noise can become significant but, in the same time, not easy to be modeled and previously depurated [18].

This work lifts the assumption of uncorrelation, all in considering negligible the causes indicated in points 1 and 2 above, and proposes a new method which formulates an underdetermined but consistent system of equations involving variances and covariances (jointly denoted as (co)variances) between individual clocks. In order to estimate clock (co)variances, the (co)variances of the measure series are also introduced and arranged in positive definite covariance matrices, implicitly assuring the positiveness of the variances. With 3 clocks the uncorrelation hypothesis leads to a uniquely solvable linear system, while the lack of this hypothesis leads to an underdetermined linear system of three equations in six unknowns. A method to solve this underdetermined system, subject to the constraint of positive definiteness of the clock covariance matrix, is proposed.

2 STATEMENT OF THE PROBLEM

The statistical tool useful to characterize stability is the variance estimated by means of the available measured data. Let us denote x^i the signal of the i-th clock and $x^i_k (k = 1, 2, \ldots, M)$ its samples at the time instants t_1, t_2, ..., t_M. The M samples can be represented as the vector $\bar{\mathbf{x}}^i = [x^i_1\ x^i_2\ \ldots x^i_M]^T$, where superscript T denotes transposition. The estimate of the expected value of x^i is

$$\bar{x}^i = \mathcal{E}[x^i] = (1/M) \sum_{k=1}^{M} x^i_k \tag{1}$$

which is arranged into a vector of M coincident elements $\mathbf{x}^i = [\bar{x}^i \bar{x}^i \ldots \bar{x}^i]^T$. With these notations the estimated (co)variances r_{ij} of x^i and x^j are:

$$r_{ij} = \mathcal{E}[(x^i - \bar{x}^i)(x^j - \bar{x}^j)] = [1/(M-1)](\mathbf{x}^i - \bar{\mathbf{x}}^i)^T(\mathbf{x}^j - \bar{\mathbf{x}}^j) \qquad i, j = 1,\ 2,\ 3 \tag{2}$$

When $i = j$, r_{ij} represents the variance of the i-th signal, otherwise, it represents the covariance between the i-th and j-th signals.

In the case of frequency standards, measured data are often filtered, for instance, introducing the Allan-variance. In the following, the general case of a signal x^i will be dealt with, whatever may have been its previous filtering, in order to obtain a procedure applicable in all cases.

In clock stability characterization, the physical quantities involved in $\mathbf{x}^i$ are time deviations of the i-th clock. Since they are not directly measurable, the clock (co)variances r_{ij} play the role of the unknowns to be evaluated. The available measured quantities are differences between the signals of pairs of clocks: $y^{ij} = x^i - x^j$. When one of the three clocks, for instance clock #3, is chosen as the reference and it is compared at M different instants with clocks #1 and #2, two distinct measure vectors $\mathbf{y}^{13} = \mathbf{x}^1 - \mathbf{x}^3$ and $\mathbf{y}^{23} = \mathbf{x}^2 - \mathbf{x}^3$ are obtained.

The novelty here is that not only the variances of the signals y^{13} and y^{23} are estimated but also their covariance. This covariance was already suggested in [4,5]; however, full advantage of it could

not be taken in that work, because of the uncorrelation hypothesis. The estimates of the above measure (co)variances are:

$$s_{ij} = [1/(M-1)][(\mathbf{y}^{i3} - \bar{\mathbf{y}}^{i3})^T(\mathbf{y}^{j3} - \bar{\mathbf{y}}^{j3})] \quad i,j = 1,\ 2 \tag{3}$$

where the index 3 of the reference clock has been dropped in s_{ij} Sinc s_{ij} $(j = 1,\ 2)$ and r_{ij} $(i = 1,\ 2,\ 3)$ represent estimates of variances and they are sums of squares, they are necessarily positive. On the contrary, s_{ij} and $r_{ij}(i = 1,\ 2,\ 3)0$ may be either positive or negative, being estimates of covariances.

In case of noiseless measurements, when the covariance s_{12} is taken into account, the other possible difference measure vector $\mathbf{y}^{12} = \mathbf{x}^1 - \mathbf{x}^2$ and the related (co)variances don't add any information because they all can be obtained as linear combinations of s_{11}, s_{22} and s_{12}. In the 3-cornered hat method, the vector $\mathbf{y}^{12}$ and the related variance is used instead of the covariance $\mathbf{y}^{12}$, but, in this context, the use of s_{12} is more appropriate.

The 2x2 covariance matrix $\mathbf{S}$ and the 3x3 covariance matrix $\mathbf{R}$ are defined as follows:

$$\begin{bmatrix} s_{11} & s_{12} \\ s_{12} & s_{22} \end{bmatrix} \tag{4}$$

$$\begin{bmatrix} r_{11} & r_{12} & r_{13} \\ r_{12} & r_{22} & r_{23} \\ r_{13} & r_{23} & r_{33} \end{bmatrix} \tag{5}$$

Substituting the definition $\mathbf{y}^{i3} = \mathbf{x}^i - \mathbf{x}^3$ $(i = 1,\ 2)$ in (3) leads to the following relationship between $\mathbf{S}$ and $\mathbf{R}$:

$$\begin{bmatrix} s_{11} & s_{12} \\ s_{12} & s_{22} \end{bmatrix} = \begin{bmatrix} r_{11} + r_{33} - 2r_{13} & r_{12} + r_{33} - r_{13} - r_{23} \\ r_{12} + r_{33} - r_{13} - r_{23} & r_{22} + r_{33} - 2r_{23} \end{bmatrix}. \tag{6}$$

From measure vectors $\mathbf{y}^{13}$ and $\mathbf{y}^{23}$, three independent estimated (co)variances, s_{11}, s_{22} and s_{12} are calculated and, according to (6), they tie the six unknowns r_{11}, r_{12}, r_{13}, r_{22}, r_{23} and r_{33} in three independent equations.

Under the hypothesis of uncorrelated clocks, (6) simplifies to:

$$\begin{bmatrix} s_{11} & s_{12} \\ s_{12} & s_{22} \end{bmatrix} = \begin{bmatrix} r_{11} + r_{33} & r_{33} \\ r_{33} & r_{22} + r_{33} \end{bmatrix} \tag{7}$$

By inspection of (7), it can be seen that the uncorrelation hypothesis is acceptable only if matrix $\mathbf{S}$ verifies the following conditions ensuring the positiveness of the estimated variances r_{11}, r_{22} and r_{33}.

$$\begin{aligned} s_{12} &> 0 \\ s_{12} &< s_{11} \\ s_{12} &< s_{22} \end{aligned} \tag{8}$$

In such a case, the solution of (7), formally different but equivalent to that of the classical 3-cornered hat method [1], is:

$$\begin{aligned} r_{33} &= s_{12} \\ r_{11} &= s_{11} - s_{12} \\ r_{22} &= s_{22} - s_{12} \end{aligned} \tag{9}$$

Moreover, (7) reveals that if the third (reference) clock is "quasi-ideal" ($r_{33} \ll r_{11}$ and $r_{33} \ll r_{22}$, then $s_{12} \ll s_{11}$ and $s_{12} \ll s_{22}$ and **S**, as well as **R**, can be considered diagonal. So, if **S** is almost diagonal, the reference clock is of high quality and by changing reference clock we can get an idea of which of the clock is less noisy because it will result in a matrix **S** with minimum off-diagonal terms. On the contrary, when the values of s_{11}, s_{22} and s_{12} are clos, the variance r_{33} is dominant with respect to the other variances of **R**.

Conditions (8) do not assure the uncorrelation of all the clocks, because many different matrices **R** can be associated to the same matrix **s** and only one of them is diagonal. In any case, (8) suggest that the uncorrelation assumption is reasonable. If one of (8) is violated, the classical 3-cornered hat method cannot be applied and the complete (non-diagonal) matrix **R** must be taken into account.

As stated above, the matricial equation (6) is underdetermined. Some more reasonable requests are to be added in such a way as to fix the extra parameters and obtain estimates for the unknown elements of **R**. Supposing to know somehow the three (co)variances r_{13}, r_{23} and r_{33} involving the reference clock, the other (co)variances r_{11}, r_{22} and r_{12} can be uniquely calculated. In fact, from (6), the following expressions are obtained:

$$\begin{aligned} r_{11} &= s_{11} - r_{33} + 2r_{13} \\ r_{12} &= s_{12} - r_{33} + r_{13} + r_{23} \\ r_{22} &= s_{22} - r_{33} + 2r_{23} \end{aligned} \tag{10}$$

In order to fix the values of the free parameters r_{13}, r_{23} and r_{33} an appropriate criterion ought to be formulated but there is an important constraint which bounds the solution domain and which guarantees a significant result: *the estimated covariance matrix* **R** *must be positive definite.*

In fact, by means of their definitions both **S** and **R** as any covariance matrix are positive definite. Such a property does not depend on the number M of samples used in the estimation of the covariance matrix and it is shared by all the matrices defined as the product of a matrix times its transpose. For this reason the treatment here exposed is independent of the particular statistical tool used to estimate stability, it holds either for the variance as in (2) or for a different process as the commonly used two-sample variance. The positive definiteness of the covariance matrix implies, as a particular case, the positiveness of its diagonal elements, i.e. the variances.

The scalar conditions ensuring positive definite matrices regard the positiveness of the leading minors but, since matrices **R** and **S** are linked by (6), the positive definiteness of the unknown matrix **R** is ensured by a unique scalar condition according to the following property:

Property 1: The 3x3 matrix **R**, with arbitrary r_{13}, r_{23}, r_{33} and with r_{11}, r_{22}, r_{12} obtained from

the positive definite 2x2 matrix **S** according to (10), is positive definite if and only if the determinant of the matrix **R**, denoted $|\mathbf{R}|$, is positive, i.e.:

$$|\mathbf{R}| = r_{11}r_{22}r_{33} + 2r_{12}r_{23}r_{13} - r_{13}^2 r_{22} - r_{12}^2 r_{33} - r_{23}^2 r_{11} > 0 \qquad (11)$$

The proof is reported in **[19]**. It is also interesting to note **[19]** that the condition (11) would allow $r_{12} = r_{13} = r_{23} = 0$ only if the same conditions (8) above are satisfied.

The positive definiteness of matrix **R** can be geometrically interpreted. To begin with, let's regard r_{33} as a known parameter; the necessary and sufficient condition (11) can be rearranged as:

$$s_{22}(r_{13} - r_{33})^2 - 2s_{12}(r_{13} - r_{33})(r_{23} - r_{33}) + s_{11}(r_{23} - r_{33})^2 < r_{33}|\mathbf{S}| \qquad (12)$$

where the (co)variances r_{11}, r_{22}, r_{12} have been substituted by (10). This expression describes the area inside an ellipse in the plane r_{13}, r_{23}. The center is in the point of coordinates (r_{33}, r_{33}). The direction of the principal axes depends only on **S** and does not depend on r_{33}, because the coefficients of the quadratic terms are independent of r_{33}. The positive definiteness of **R** is then fulfilled when the choice of the parameters (r_{13}, r_{23} corresponds to a point inside this ellipse (for a given value of r_{33}). Fig. 1 illustrates several ellipses depending on different values of r_{33} for a given matrix **S**. The geometrical dimensions of the ellipse grow and the position departs from the origin for increasing values of r_{33}.

3 CHOICE OF FREE (CO)VARIANCES

In the previous section it was shown that the choice of the free parameters r_{13}, r_{23} and r_{33} must always fulfil the positive definiteness of **R**. Setting $H(r_{13}, r_{23}, r_{33}) = |\mathbf{R}|$, such a condition characterizes the domain of acceptable solutions in the space of free (co)variances r_{13}, r_{23} and r_{33} (see (12)):

$$H(r_{13}, r_{23}, r_{33}) = r_{33}|\mathbf{S}| - s_{22}(r_{13} - r_{33})^2 + 2s_{12}(r_{13} - r_{33})(r_{23} - r_{33}) - s_{11}(r_{23} - r_{33})^2 > 0 \qquad (13)$$

However, this condition is not sufficient to determine a unique solution for **R** and further requirements are therefore necessary.

The leading idea in defining an optimum choice for the free (co)variances is the hypothesis that no information is available about the possible covariances between different clocks, but they are supposed to be low. This is the same hypothesis of the "classical" method, but instead of forcing the solution of completely uncorrelated clocks, the solution of minimum correlation, compatible with the positive definiteness of **R**, is sought. Therefore the here-proposed solution should coincide with the "classical" one (9), when the positive definiteness of **R** (11) is safeguarded.

To this aim, the quadratic mean covariance $\sqrt{(r_{12}^2 + r_{13}^2 + r_{23}^2)/3}$ is defined as a measure of the global covariance among clocks. According to (10), it can be expressed as a function of r_{13}, r_{23} and r_{33}:

$$[G(r_{13}, r_{23}, r_{33})]^2 = (r_{12}^2 + r_{13}^2 + r_{33}^2)/3 \qquad (14)$$

$$
\begin{aligned}
= \; & [2(r_{13} - r_{33})^2 + 2(r_{13} - r_{33})^2 + 2r_{13} - r_{33}(r_{23} - r_{33}) + 2(r_{23} - r_{33})^2 \\
& + 2(2r_{33} + s_{12})(r_{13} - r_{33}) + 2(2r_{33} + s_{12})(r_{23} - r_{33}) + 2r_{33}^2 \\
& + (s_{12} + r_{33})^2]/3
\end{aligned}
$$

From experience, it can be assumed that the global covariance can be different from zero but, on the other hand, not too high. In fact a full correlation between two clocks would imply that their signals are coincident, apart from a multiplicative factor, and this fact is to be excluded.

To combine the request of positive definiteness of the estimated matrix $\mathbf{R}$ (13) and the minimization of the global covariance (14), let us introduce the objective function $F(r_{13},\ r_{23},\ r_{33})$:

$$
F(r_{13},\ r_{23},\ r_{33}) = \frac{3\sqrt{|\,\mathbf{S}\,|}[G(r_{13},\ r_{23},\ r_{33})]^2}{H(r_{13},\ r_{23},\ r_{33})} \tag{15}
$$

where the fixed factor $3\sqrt{|\,\mathbf{S}\,|}$ has been introduced for the sake of adimensionality.

In the solution domain $F(r_{13},\ r_{23},\ r_{33})$ represents a sort of squared global correlation and it is always positive or zero; it is zero when $G(r_{13},\ r_{23},\ r_{33})$ is zero, in the case of full uncorrelation. The minimization of $F(r_{13},\ r_{23},\ r_{33})$ leads to a solution of minimum global correlation safeguarding the positive definiteness of the resulting matrix $\mathbf{R}$. The quantity $H(r_{13},\ r_{23},\ r_{33})$, in the denominator of the objective function (15), prevents the choice of the free (co)variances from falling on the boundary of the feasible domain defined by (13). Such occurrence would yield a matrix $\mathbf{R}$ only positive semidefinite with a disequilibrium in the estimated covariance terms. Since no information is supposed to be available about the possible covariance between clocks, the solution with estimated covariance terms of similar amount is here preferred.

Such features have led to the choice of this objective function among the several ones investigated at the early stages of this work.

One and only one global minimum of $F(r_{13},\ r_{23},\ r_{33})$ exists inside the solution domain, while $F(r_{13},\ r_{23},\ r_{33})$ goes to infinity on its boundary. In fact, three-dimensional surfaces $F(r_{13},\ r_{23},\ r_{33}) = f$ (with F a positive constant) are associated to decreasing values of F going inward from the surface $H(r_{13},\ r_{23},\ r_{33}) = 0$ (corresponding to $f = \infty$, until they collapse to a single point corresponding to the global minimum. By the study of these surfaces [**19**], the minimization of $F(r_{13},\ r_{23},\ r_{33})$ can be performed in a analytical way supplying, as a result, the coordinates $r_{13}^{\min}$, $r_{23}^{\min}$ and $r_{33}^{\min}$ of the minimum. The provided solution coincides with the "classical" one (see (9)) of uncorrelated clocks, when conditions (8) are verified.

As a final remark it should be added that this definition of the objective function $f(r_{13},\ r_{23},\ r_{33})$ can be useful when the clocks are to be considered of the same quality level and when there is no information about their possible correlation. Otherwise $F(r_{13},\ r_{23},\ r_{33})$ could be defined by introducing a weighting factor for each covariance term in (14), if some reasons for two clocks to be less correlated than the others were known. The less correlated pair can have a larger weight factor multiplying its covariance term in (14), so that the search of the minimum will attribute a smaller correlation coefficient to that pair of clocks. Similarly, if the clock variances are expected to be different, (for instance, when clocks of different types are compared), also weighs for the variances r_{ii} can be introduced in the minimandum function (15).

4 EXPERIMENTAL RESULTS

In order to illustrate the effective capabilities of the method here-proposed, the data of three commercial cesium beam frequency standards maintained at IEN, Torino, Italy during the whole year 1987 are considered. The three clocks, designated by the serial numbers 12 303, 14 1230, 14 893, are considered as the first, second and third clock hereafter. The time difference of the clock signals are measured once a day and arranged in vectors $\mathbf{y}^{13}$ and $\mathbf{y}^{23}$. The measured samples are processed according to the Allan variance with overlapping samples for the integration times 1, 2, 5, 10, 30, 60, 100 days.

For each integration time the matrix $\mathbf{S}$ is calculated (second column of Table 1). The corresponding matrix $\mathbf{R}$, evaluated according to the here-revisited method, is reported in the third column and the (necessarily diagonal) matrix $\mathbf{R}$ calculated according to the classical 3-cornered hat method, is reported in the last column.

For short integration times (1, 2, 5, and 10 days) the results supplied by both methods coincide. In fact the matrix $\mathbf{S}$ doesn't violate conditions (8) allowing the uncorrelated solution and the minimization of the proposed function leads to the minimum allowed global correlation.

For longer integration times, the uncorrelated solution is not allowed and the matrix $\mathbf{R}$ estimated by the new method is not yet diagonal but gives information also about the covariance between clocks. The application of the classical method to these cases results in one negative estimated variance. By definition, the proposed minimandum function (15) leads to a solution with covariance terms of similar amount because no weight are inserted in (15). This is the simplest hypothesis when there is no information about the different clocks and their noises.

5 CONCLUSIONS

This paper reports a revisited version of the popular 3-cornered hat method suitable for estimating the individual clock variances and covariances, by lifting the too restrictive hypothesis of uncorrelated clocks. This formulation requires the introduction of covariances of measured data and of clocks arranged in positive definite covariance matrices and leads to a underdetermined system of equation. The underdeterminess has been resolved by considering a suitable objective function, whose minimization supplies an unique solution. Examples of the application of the proposed method to data of clocks maintained at IEN, Torino, Italy are presented: the obtained results show that, in this case, for long integration times the uncorrelation hypothesis doesn't hold and the revisited 3-cornered hat method provides a consistent solution of minimum allowed global correlation.

REFERENCES

[1] J. E. Gray, D. W. Allan, *"A method for estimating the frequency stability of an individual oscillator,"* in Proc. 28th Frequency Control Symposium, 1974, pp. 243-246.

[2] J. A. Barnes, *"Time scale algorithms using Kalman filters - Insights from simulation,"* presented at the 2nd Atomic Time Scale Algorithm Symposium, Boulder, CO, 1982.

[3] C. A. Greenhall, *"Likelihood and least-squares approaches to the M-cornered hat,"* in Proc. Precise Time and Time Interval Planning Meeting, 1987, pp. 219-225.

[4] J. Groslambert, D. Fest, M. Olivier, J. J. Gagnepain, *"Characterization of frequency fluctuations by crosscorrelations and by using three or more oscillators,"* in Proc. 35th Frequency Control Symposium, 1981, pp. 458-463.

[5] D. Fest, J. Groslambert, J. J. Gagnepain, *"Individual characterization of an oscillator by means of cross-correlation or cross-variance method,"* IEEE Trans. Instrum. Meas., vol. 32, n. 3, pp. 447-450, Sept. 1983.

[6] J. Groslambert, *"Méthodes expèrimentales de caractérisation des oscillateurs dans les domaines spectral et temporel,"* Bulletin du Bureau National de Métrologie, vol. 17, n. 63-64, pp. 7-15, Jan-Apr. 1986.

[7] S. R. Stein, *"Frequency and time measurement,"* in E.A.Gerber, A.Ballato, ed. **Precision Frequency Control**, Academic Press, 1985, section 12, pp. 216-217.

[8] S. Iijima, K. Fujiwara, H. Kobayashi, T. Kato, *"Effect of environmental conditions on the rate of a cesium clock,"* Annals of the Tokio Astronomical Observatory, Second Series, vol. 18, n. 1, pp. 50-67, 1978.

[9] G. Becker, *"Zeitskalenprobleme: jahreszeitliche gangschwankungen von atomuhren,"* PTB Mitteilungen 92 2/82, pp. 105-113, Phys. Tech. Bundesanst. Braunsweig, Germany, 1982.

[10] A. De Marchi, *"Understanding environmental sensitivity and ageing of cesium beam frequency standards,"* in Proc. 1st European Frequency and Time Forum, 1987, pp. 288-293.

[11] E. Bava, F. Cordara, V. Pettiti, P. Tavella, *"Analysis of the seasonal effects on cesium clocks to improve the long term stability of a time scale,"* in Proc. Precise Time and Time Interval Planning Meeting, 1987, pp. 185-202.

[12] L. A. Breakiron, *"The effects of ambient conditions on cesium clock rates,"* in Proc. Precise Time and Time Interval Planning Meeting, 1987, pp. 175-184.

[13] L. A. Breakiron, *"The effects of data processing and environmental conditions on the accuracy of the USNO time scale,"* in Proc. Precise Time and Time Interval Planning Meeting, 1988, pp. 221-236.

[14] J. E. Gray, H. E. Machlan, D. W. Allan, *"The effect of humidity on commercial cesium beam atomic clocks,"* in Proc. 42th Frequency Control Symposium, 1988, pp. 514-518.

[15] H. Hellwig, *"Environmental sensitivities of precision frequency sources,"* IEEE Trans. Instrum. Meas. vol. 39, n. 2, pp. 301-306, April 1990.

[16] A. De Marchi, E. Rubiola, *"Environmental sensitivity and long term stability limitations induced by C-field variations in commercial cesium beam frequency standards,"* in Proc. 5th European Frequency and Time Forum, 1991, pp.237-242.

[17] P. Tavella, C. Thomas, *"Study of the correlations among the frequency changes of the contributing clocks to TAI,"* in Proc. 4th European Frequency and Time Forum, 1990, pp. 527-541.

[18] C. Thomas, P. Tavella, *"Report on correlations in frequency changes among the clocks contributing to TAI,"* Rapport BIPM-91/4, Bureau International des Poids et Mesures, Sevres, France, 1991.

[19] A. Premoli, P. Tavella, *"A revisited 3-cornered hat method for estimating frequency standard instability,"* submitted for publication.

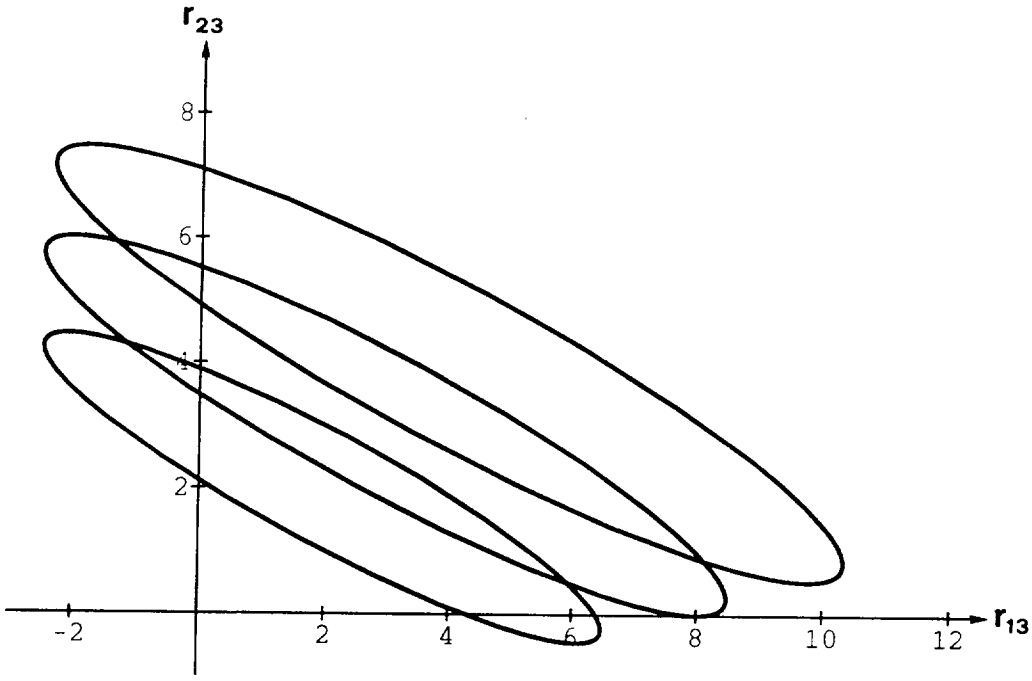

Fig. 1: Elliptical regions yielding the positive definiteness of **R** on the plane (r_{13},r_{23}) for a given matrix **S** (s_{11} = 10, s_{22} = 3, s_{12} = -5) and different values of r_{33} (r_{33} = 2,3,4).

τ [days]	measured difference covariance matrix $\begin{bmatrix} s_{11} & s_{12} \\ s_{12} & s_{22} \end{bmatrix}$	clock covariance matrix by the here-revisited method $\begin{bmatrix} r_{11} & r_{12} & r_{13} \\ r_{12} & r_{22} & r_{23} \\ r_{13} & r_{23} & r_{33} \end{bmatrix}$	clock variances by the classical method $\begin{bmatrix} r_{11} & & \\ & r_{22} & \\ & & r_{33} \end{bmatrix}$
1	$\begin{bmatrix} 412 & 128 \\ 128 & 161 \end{bmatrix}$	$\begin{bmatrix} 284 & 0 & 0 \\ 0 & 33 & 0 \\ 0 & 0 & 128 \end{bmatrix}$	$\begin{bmatrix} 284 & & \\ & 33 & \\ & & 128 \end{bmatrix}$
2	$\begin{bmatrix} 247 & 101 \\ 101 & 106 \end{bmatrix}$	$\begin{bmatrix} 146 & 0 & 0 \\ 0 & 5 & 0 \\ 0 & 0 & 101 \end{bmatrix}$	$\begin{bmatrix} 146 & & \\ & 5 & \\ & & 101 \end{bmatrix}$
5	$\begin{bmatrix} 115 & 48.6 \\ 48.6 & 53.3 \end{bmatrix}$	$\begin{bmatrix} 66.4 & 0 & 0 \\ 0 & 4.7 & 0 \\ 0 & 0 & 48.6 \end{bmatrix}$	$\begin{bmatrix} 66.4 & & \\ & 4.7 & \\ & & 48.6 \end{bmatrix}$
10	$\begin{bmatrix} 80.6 & 30.5 \\ 30.5 & 56 \end{bmatrix}$	$\begin{bmatrix} 50.1 & 0 & 0 \\ 0 & 25.5 & 0 \\ 0 & 0 & 30.5 \end{bmatrix}$	$\begin{bmatrix} 50.1 & & \\ & 25.5 & \\ & & 30.5 \end{bmatrix}$
30	$\begin{bmatrix} 39.5 & -28.3 \\ -28.3 & 109 \end{bmatrix}$	$\begin{bmatrix} 55.21 & -14.05 & 17.78 \\ -14.05 & 121.8 & 16.32 \\ 17.78 & 16.32 & 19.85 \end{bmatrix}$	$\begin{bmatrix} 67.8 & & \\ & 137.3 & \\ & & -28.3 \end{bmatrix}$
60	$\begin{bmatrix} 55.2 & -99.1 \\ -99.1 & 211 \end{bmatrix}$	$\begin{bmatrix} 117.0 & -43.23 & 60.64 \\ -43.23 & 260.9 & 54.67 \\ 60.64 & 54.67 & 59.44 \end{bmatrix}$	$\begin{bmatrix} 154.3 & & \\ & 310.1 & \\ & & -99.1 \end{bmatrix}$
100	$\begin{bmatrix} 72.3 & -102 \\ -102 & 181 \end{bmatrix}$	$\begin{bmatrix} 134.2 & -44.39 & 61.46 \\ -44.39 & 234.3 & 57.15 \\ 61.46 & 57.15 & 60.99 \end{bmatrix}$	$\begin{bmatrix} 174.3 & & \\ & 283 & \\ & & -102 \end{bmatrix}$

Table 1: Estimated variances and covariances for different integration times of three clocks maintained at IEN, Torino,Italy during 1987. The matrix elements are in unit of 10^{-28}.

COMPACT MICROWAVE CAVITY FOR HYDROGEN ATOMIC CLOCK

N92-33375

Zhang Dejun, Zhang Yan, Fu Yigen and Zhang Yanjun
Beijing Institute of Radio Metrology & Measurements
P.O.Box 3930 Beijing, China

Abstract

This paper gives a summary introduction to the compact microwave cavity used in the hydrogen atomic clock. Special emphasis is put on derivation of theoretical calculating equations of main parameters of the microwave cavity. A brief description is given of several methods for discriminating the oscillating modes. Experimental data and respective calculated values are also presented.

INTRODUCTION

The volume of the microwave cavity must be reduced so as to reduce the volume and weight of the hydrogen atomic clock. Nowadays, there are two methods to reach the goal. The first one is to fill the cavity with material of high dielectric constant and low loss. The second one is to adhere several electrodes outside the quartz storage bulb. This method provides more adaptability in reducing volume, meanwhile, it can reduce cost of the microwave cavity.

Since the microwave cavity adopting the second method has a more complicated structure it's very difficult to make out the accurate solution by wave equation, so no strict solution can be derived for its electromagnetic field distribution up to now. However, upon some reasonable hypotheses, it' s possible to derive the approximate expressions which show relations of resonant frequency and Q-factor to dimensions of the cavity. This paper describes a derivative method of the expressions in detail, and gives out essential derivation procedure.

We have manufactured a microwave cavity by the second method. Its resonant frequency meets the requirement of the hydrogen atomic clock, and its Q-factor is about 7000.

I Structure of the Cavity

We have manufactured an experimental compact cavity. Its structure is shown in Fig.1.

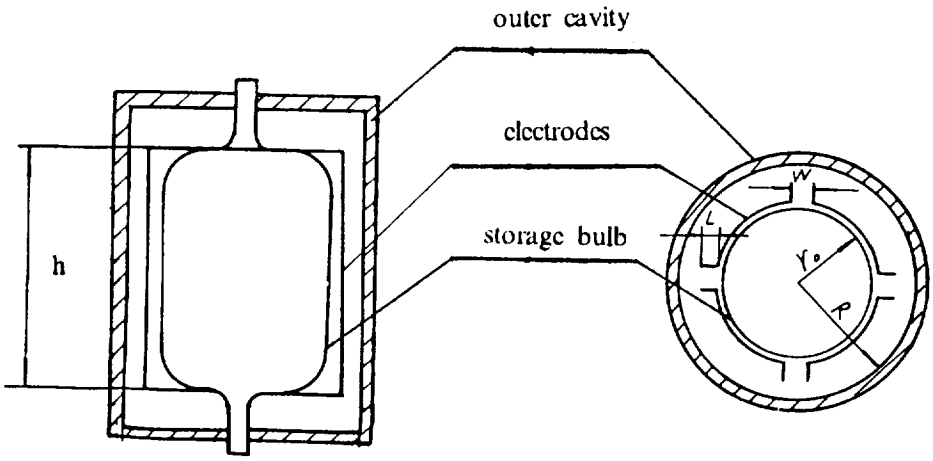

Figure 1. Structure of the Resonant Cavity

The outer cavity made of copper or aluminum is designed mainly to shield electromagnetic field of the electrodes. There is a quartz bulb in the outer cavity. It serves as a container of hydrogen atoms and a supporter of the electrodes as well. Usually four electrodes (two or three also allowed) are used, which are adhered on the quartz bulb by epoxy resin.

The resonant frequency of the cavity depends on the dimensions of the cavity and in particular on the adhered electrodes. The Q-factor is related to dimensions of the cavity, the metal material used and energy loss of the glue.

There is a piston on the top cover of the cavity (not shown in Fig.1). Its function is to coarsely adjust the resonant frequency of the cavity. Three holes in the bottom plate are for two coupling rings and a varactor diode respectively.

II Basic Parameters of the Resonant Cavity

In the microwave cavity shown in Figure 1, there are many wave modes. The electromagnetic field structure shown in Figure 2 is similar to TE_{011} mode, and it is the right mode required by the hydrogen atomic clock. Now we derive the estimate formulas for the basic parameters of the resonant cavity using the distribution of the electromagnetic field shown in Figure 2.

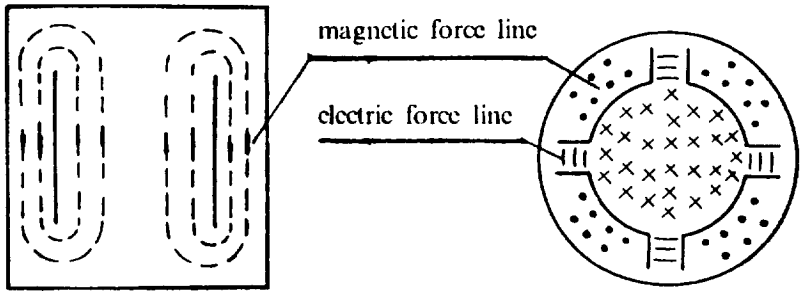

Figure 2. Distribution of the Electromagnetic Field

Assume that the electric field is distributed uniformly only between parallel parts of each pair of electrodes. Considering symmetry of the cavity, only the electromagnetic field distribution both outside and in one region is shwon in Figure 3. $\vec{E}$ represents electric field vector, and can be written as

$$\vec{E} = \vec{i}_y \, E_0 \sin\omega t \qquad (1)$$

where E_0 is amplitude, ω is angular frequency, t is time, and $\vec{i}_y$ is unit vector of y axis.

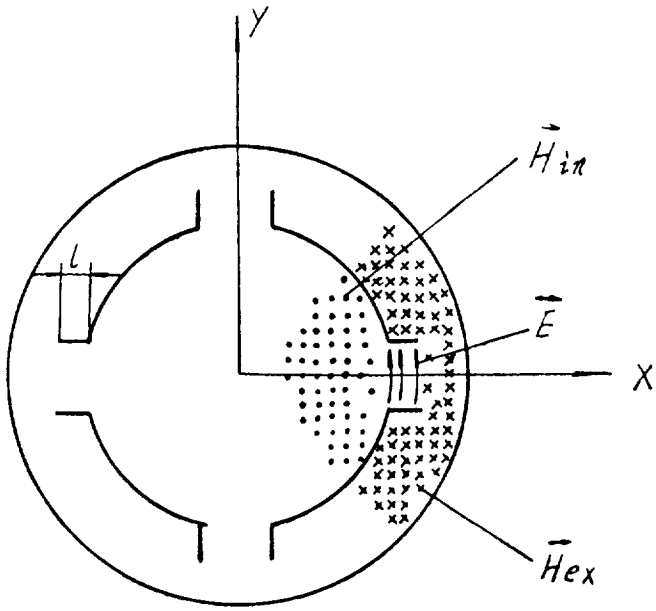

Figure 3. Electromagnetic Field Distribution near the Parallel Parts of two Electrodes

Let $\vec{H}_{in}$ represent magnetic density in area between the electrodes, let $\vec{H}_{ex}$ represent magnetic intensity in area between the electrodes and the outer cavity, and both them are regarded as uniformly distributed in their respective areas. Let $A_1 = \pi r_0^2$, $A_2 = \pi (R^2 - r_0^2)$. According to closed characteristic of the magnetic field line, we have

$$A_1 \vec{H}_{in} = -A_2 \vec{H}_{ex} \tag{2a}$$

$$\vec{H}_{in} = \vec{i}_z \; H_0 \cos\omega t \tag{2b}$$

$$\vec{H}_{ex} = -\vec{i}_z \frac{A_1}{A_2} \; H_0 \cos\omega t \tag{2c}$$

a. Resonant Frequency

When the microwave cavity resonates, there exist the following relations [1]

$$W_0 = W_e(t) + W_m(t) = W_{e,max} = \frac{\varepsilon_0}{2} \int |\vec{E}|^2 dv$$
$$= W_{m,max} = \frac{\mu_0}{2} \int_{V_{in}} |\vec{H}_{in}|^2 dv + \frac{\mu_0}{2} \int_{V_{ex}} |\vec{H}_{ex}|^2 \, dv \tag{3}$$

where W_0 is the total energy stored in the resonating cavity, W_e and W_m are electric energy and magnetic energy in the cavity respectively, ε_0 and μ_0 are dielectric constant and magnetic inductivity respectively, V represents the volume of the region between parallel parts of electrodes, V_{in} is the volume of the cylinder enclosed by the electrodes, V_{ex} is the volume of the region between the electrodes and the outer cavity.

Referring to Figure 1, expression (3) can be changed into the following expressions

$$W_{e,max} = \frac{1}{2} \varepsilon_0 N \omega l h E_0^2 \tag{4}$$

$$W_{m,max} = \frac{1}{2} \mu_0 A_1 h(1 + \frac{A_1}{A_2}) H_0^2 \tag{5}$$

where N is the number of electrodes.

Substituting expressions (4) and (5) into expression (3), we get the expression of E_0

$$E_0 = \sqrt{\frac{\mu_0 A_1 (1 + \frac{A_1}{A_2})}{\varepsilon_0 N \omega l}} \cdot H_0 \tag{6}$$

As shown in Figure 3, in the X−axis direction, the magnetic intensity $\vec{H}_{in}$ transits to $\vec{H}_{ex}$ in the region between parallel parts of two electrodes. In this transitional region, magnetic density is a function of x axis, and recorded as $\vec{H} = \vec{i}_z H(x)$. According to differential form of Maxwell's equations and expression (1), we have

$$\nabla \times \vec{H} = \varepsilon_0 \frac{\partial \vec{E}}{\partial t} = \vec{i}_y \omega_0 E_0 \varepsilon_0 \cos\omega t \qquad (7)$$

where ω_0 is the angular frequency when the cavity is resonating.

In the transitional region shown in Figure 3, if the magnetic density is regarded as linearly changing, and the length of the transiting region is $\frac{3}{2} l$, then

$$\begin{aligned} \nabla \times \vec{H} &= -\vec{i}_y \frac{\partial H(x)}{\partial x} \\ &= -\vec{i}_y \frac{H(x_{ex}) - H_{(x_{in})}}{\frac{3}{2} l} \\ &= \vec{i}_y \frac{2}{3l} H_0 (1 + \frac{A_1}{A_2}) \cos\omega t \end{aligned} \qquad (8)$$

By using expressions (7) and (8), we can get

$$E_0 = \frac{2}{3} \frac{(1 + \frac{A_1}{A_2}) H_0}{\varepsilon_0 \omega_0 l} \qquad (9)$$

substituting expression (9) into expression (6) and having $A_1 = \pi r_0^2$, we can get

$$\omega_0 = \frac{2c}{3r_0} \sqrt{(1 + \frac{A_1}{A_2}) \frac{NW}{\pi l}} \qquad (10)$$

where $C = \frac{1}{\sqrt{\mu_0 \varepsilon_0}}$ is the light velocity in free space.

b. Q−factor

According to the definition of Q−factor of the cavity, we have

$$Q = \frac{\omega_0 W_0}{P_0} \tag{11}$$

where P_0 is the power loss in the resonating cavity. The energy loss in the cavity mainly refers to the loss on the metal surfaces. If the medium loss can be neglected, we can get the approximate formula to calculate P_0 as follows[1]

$$P_0 = \frac{R_s}{2} \int_s |\vec{H}_t|^2 \, ds \tag{12}$$

where $\vec{H}_t$ represents the tangential component of the magnetic density on the metal surfaces in the cavity, S is the total area of metal surface in the cavity, R_S is expressed by the following formula

$$R_S = \frac{\delta}{2} \omega_0 \mu_0 \tag{13}$$

where δ is the skin effect depth of electromagnetic field in the metal wall. We suppose that the skin effect depths are the same in all the metal surfaces, i.e., all R_S are regarded as the same value when calculating the energy loss on the metal surfaces.

When calculating the energy loss on the electrodes surfaces, we also deal with the N pieces of electrodes as a cylinder tube aproximately. Let S_1 represent the inner surface area of the outer cavity, S_2 and S_3 the outer and inner surface areas of the cylinder tube respectively, S_4 the inner surface area of top cover and bottom plate of the outer cavity. By using expression (12) we get

$$P_0 = \frac{R_S}{2} \left(\int_{S_1} |\vec{H}_{ex}|^2 \, ds_1 + \int_{S_2} |\vec{H}_{ex}|^2 \, ds_2 + \int_{S_3} |\vec{H}_{in}|^2 \, ds_3 + \int_{S_4} |\vec{H}_{ex}|^2 \, ds_4 \right) \tag{14}$$

Substituting expression (2) into expression (4) and having $S_4 = 2\pi R^2$, we get

$$P_0 = \pi R_S h H_0^2 \left[r_0 + (r_0 + R + \frac{R^2}{h}) \left(\frac{A_1}{A_2} \right)^2 \right] \tag{15}$$

By using expressions (3) , (5), (15) and (11), we can get

$$Q_0 = \frac{r_0\omega_0\mu_0}{2R_s} \frac{1+\frac{A_1}{A_2}}{1+(1+\frac{R}{r_0}+\frac{R^2}{hr_0})(\frac{A_1}{A_2})^2}$$

Then substituting expression (13) into this one, we can get the final expression of Q_0

$$Q_0 = \frac{r_0}{\delta} \frac{1+\frac{A_1}{A_2}}{1+(1+\frac{R}{r_0}+\frac{R^2}{hr_0})(\frac{A_1}{A_2})^2} \qquad (16)$$

Ⅲ Judgement of the Oscillation Mode

Besides the oscillation mode shown in Figure 2, there are many other unnecessary modes in the resonant cavity. No wonder that identification of oscillation modes is of great importance. For this purpose, two methods are described hereafter.

a. Turning the Direction of the Coupling Ring

As seen from Figure 2, the magnetic density is radial near the bottom plate. One of the two coupling rings on the bottom plate is fixed for excitation, the other one can be turned in direction for coupling. For the field distribution shown in Figure 2, the energy output of coupling will be the largest when the turnable ring is made perpendicular to the radial direction.

b. Using the Perturbation Theory

From the perturbation theory[2], we know that the frequency rises when a small piece of conductor is placed on the point where the magnetic field is dominant. The frequency falls when a small piece of conductor is placed on the point where the electric field is dominant. The frequency change in accordance with perturbation theory can be got by placing copper block into the electric field region and the magnetic field region.

In addition to the above-mentioned methods, other methods can also be used to identify the oscillation mode of the resonant cavity. For example, the theory of resonant cavity indicates that Q is the highest when the oscillation mode is TE_{011}. The field structure shown in Figure 2 is similar to TE_{011} mode, so the Q-factor is high, too.

CONCLUSION

We have processed a resonant cavity according to the cavity structure shown in Figure 1. Its geometric dimensions (in millimeters) are as follows:

$r_0 = 50$, $R = 75$, $l = 7$ $W = 23$

Substituting these data into expressions (10) and (16) and considering that $\delta = 2.2 \times 10^{-3}$, we get the following results:

$\gamma_0 = 1.7\text{GHz}$ $(\omega_0 = 2\pi\gamma_0)$

$Q_0 = 13270$

The test results of this cavity are

Resonance frequency: 1.4GHz

Q－factor: 7000

An atomic clock of model CHYMNS－1 with a resonant cavity of such dimensions has been developed by Hughes Research Laboratories (HRL), U.S.A. The results measured are [3]

Resonance frequency: 1.4GHz

Q－factor: 9400

They have developed a smaller resonant cavity, whose dimensions are $r_0 = 25$, $R = 38$, $l = 5.3$, $W = 7.4$ (the last two are estimated data).

The results measured are [4]

Resonance frequency: 1.4GHz

Q－factor: 4600

Substituting the dimensions of the cavity into expressions (10)and (16), we get

$\gamma_0 = 1.6\text{GHz}$

$Q_0 = 6900$

By comparing the measured values with calculated values, we find that the resonance frequency tallies well, the Q－factor not so well. This is because that only the energy loss on the metal surfaces is calculated when deriving the Q－facotr formula, but the loss on the expoxy resin is not taken into account. We can consider the Q value calculated by the expression (16) is the highest value for this type of resonant cavity. The Q value of the cavity of American HRL, however, is higher than ours, which indicates that fineness of metal they processed is higher than ours, and the glue they used to adhere the electrodes may be better in the respect of energy loss.

Based on the data comparison, we can take expressions (10) and (16) as basis of designing this type of resonant cavity, so as to greatly reduce the blindness in designing.

References

[1] Shen Zhiyuan, "Microwave Technology", P204.

[2] Shen Zhiyuan, "Microwave Technology", P239, P240.

[3] H.T.M.Wang, "An Oscillating Compact Hydrogen Maser", Proc. 34th Ann. Sym on Frequency Control, 366, 1980.

[4] R.R.Hayes and H.T.M.Wang, "Design for A Subcompact Q-enhanced Active Maser", Proc. 38th Ann Symp. on Frequency Control, (1985)

A Correlational Analysis of the Effects of Changing Environmental Conditions on the NR Atomic Hydrogen Maser

R.A. Dragonette and J.J Suter
Johns Hopkins University
Applied Physics Laboratory
Laurel, Maryland 20723

Abstract

An extensive statistical analysis has been undertaken to determine if a correlation exists between changes in an NR atomic hydrogen maser's frequency offset and changes in environmental conditions. Data have been acquired over the past 20 months by recording the frequency offset of three NR atomic hydrogen masers along with the relative and absolute humidity, barometric pressure, and ambient temperature of the laboratory in which the masers are maintained.

Correlational analyses have been performed comparing barometric pressure, humidity, and temperature with maser frequency offset as functions of time for periods ranging from 5.5 to 17 days. Semi partial correlation coefficients as large as -0.9 have been found between barometric pressure and maser frequency offset for data covering periods as long as a week. Maser frequency offset and barometric pressure were consistently found to change simultaneously. The correlation between humidity and frequency offset is less predictable, and the resulting semi partial correlation coefficients were usually small when compared with those derived from the relationship between pressure and frequency offset. The time delay between changes in humidity and correlated changes in maser frequency offset was found to vary extensively with no predictable pattern. Analysis of temperature data indicates that, in the most current design, temperature does not significantly affect maser frequency offset in the laboratory environment.

Thus, the results of the analyses disclose a significant statistical correlation between changes in maser frequency offset and changes in barometric pressure. The statistics also reveal some correlation between humidity and frequency offset, but for reasons to be discussed, the effects of humidity should be considered secondary to the effects of changing barometric pressure.

INTRODUCTION

The NR atomic hydrogen maser has proven to be one of the most accurate time and frequency references available for use in the laboratory and in the field. The NR maser derives its stable frequency reference from electronic observation of the hyperfine transition of atomic hydrogen, which occurs at a frequency of 1.4204057518 GHz[1]. The narrow microwave resonance line characteristic of the hyperfine transition is observed using an electromagnetic resonant cavity operating in the TE_{011} mode. The resonant cavity consists of a metallic cylinder with adjustable top and bottom endplates. The movable endplates are used to adjust the cavity length for coarse tuning of the

resonant frequency. The cavity resonant frequency is fine tuned by controlling the temperature of the cavity walls within 10^{-6} K.

Using superheterodyne techniques, a 5 MHz crystal oscillator is phase locked to the signal coupled from the resonant cavity. The oscillator output reflects the long-term stability (greater than 100 s) of the maser as determined by its large atomic line Q (1.33×10^9). Under optimal conditions, the NR maser typically exhibits a frequency offset of a few parts in 10^{15} over a 24-hour period.

One would expect changing environmental conditions to affect the performance of any complex electronic system adversely. The hydrogen maser is no exception. Humidity and temperature changes affect the electronic circuitry used to tune the microwave resonant cavity to the hydrogen hyperfine transition frequency. Barometric pressure changes alter the compressive forces exerted on the resonant cavity, changing its resonant frequency.

To gain a better quantitative understanding of these environmental effects, a statistical analysis of the relationship between the frequency offset of the NR hydrogen maser and the surrounding environmental conditions was undertaken. In addition to other results, two important conclusions were derived from the analysis: (1) a strong correlation exists between barometric pressure and the NR maser's frequency offset, and (2) a change in the construction of the NR maser's resonant cavity has eliminated temperature fluctuations as a critical concern in the laboratory.

EXPERIMENTAL DATA

In previous generations of NR masers, the cylindrical microwave resonant cavity was constructed entirely from aluminum. The NR maser was later improved by enclosing the resonant cavity in a cylindrical quartz sleeve. In the present design, the resonant cavity consists of a coating of conductive silver ink on the inside of a thick quartz cylinder. This arrangement gives the resonant cavity the thermal expansion coefficient of a thick quartz tube as opposed to that of the thin aluminum cylinder used in the previous design. This change reduced the thermal sensitivity of the cavity's resonant frequency from 30 KHz/°C to 3 KHz/°C.

For the past 20 months the data acquisition system described in [2] has continuously recorded the environmental conditions and the frequency offset of three NR hydrogen masers. The system calculates maser frequency offset at five-minute intervals with an accuracy of parts in 10^{15}. Ambient air temperature, relative humidity, dew point temperature, and barometric pressure are simultaneously recorded by National Institute of Standards and Technology (NIST) traceable thermometers, hygrometers, dew point sensors, and barometers with single measurement accuracies of 0.1 °C, 2%, 0.5°C, 0.01 inch Hg, respectively. The repeatability of the humidity sensors is 0.5% for the relative humidity sensor and 0.05 °C for the dew point sensor. Repeatability is a better measure of how well these instruments track humidity changes.

Figures 1A through 6A show the maser frequency offset and the offset barometric pressure over time for periods ranging from 5.5 to 17 days. The offset barometric pressure was calculated by subtracting the measured value of the barometric pressure, in inches of mercury, from 30. This offset has the effect of inverting the barometric pressure curve, making the inverse relationship between pressure and frequency offset visually clear. From the similarity of the curves in Figures 1A through 6A, a significant correlation is apparent between barometric pressure and maser frequency offset.

Figures 1B through 6B show the maser frequency offset and humidity for the time periods considered in Figures 1A through 6A. The frequency offset data in Figure 1B have been delayed by 48 hours

with respect to the humidity curve. Similarly, the frequency offset has been delayed 24 hours in Figure 5B. These time delays were incorporated to demonstrate that the humidity shows a stronger similarity to the frequency offset if one allows for a time delay between changes in humidity and changes in frequency offset.

The data collected during the past 20 months have been analyzed statistically to gain a quantitative understanding of the effects seen in the graphical data. The statistics software package CSS:Statistica by Statsoft, Inc. was used to perform all statistical calculations. Semi partial correlation coefficients between the temperature and frequency offset, the pressure and frequency offset, and the humidity and frequency offset were calculated (see [**3**]). The calculations were made on blocks of data collected over periods ranging from 5.5 to 17 days. The square of the magnitude of the semi partial correlation coefficient between a dependent variable (frequency offset) and an independent variable (any one of the temperature, pressure, or humidity) gives the percentage of the total variation in the dependent variable uniquely accounted for by the independent variable with the effects of the remaining independent variables taken into account.

Temperature, humidity, and barometric pressure can be interrelated, so semi partial correlation coefficients were calculated to reduce the effects of this interrelation on the magnitude of the calculated coefficients. To allow for the potential existence of a time delay between a change in temperature or humidity and the resulting change in maser frequency offset, the semi partial correlation coefficients were calculated three times. Semi partial correlation coefficient calculations were performed using the frequency offset as it was measured and were then repeated incorporating time delays of 12 and 24 hours in the frequency offset data. For one data set containing 17 days' worth of data, a time delay of 48 hours was used.

EXPERIMENTAL RESULTS

The results of the calculations for nine sets of data are summarized in Table 1. The first data column shows the Mean Julian Date (MJD) of the first day that data were recorded for that set of coefficients. The number of days of data used in the calculations is indicated in parentheses underneath the MJD. A minimum of 100 data samples were used to calculate each of the coefficients presented in the table. Each data set consists of twenty-four equally spaced samples per day for every day considered. The next three columns are the semi partial correlation coefficients between frequency offset and temperature, pressure, and humidity, respectively.

Each block of coefficients in Table 1 consists of three rows of data displaying the semi partial correlation coefficients with time delays of 12 and 24 hours added to most of the the frequency offset data. A 48-hour time delay was added to the data set for MJD 47973. The data for MJD 48189 do not include time delay calculations because the humidity, barometric pressure, and frequency offset curves are nearly identical as measured.

The temperature in the laboratory where the masers were operated was maintained at 23±2°C throughout this investigation. This is a level of control easily accomplished with a computer room air conditioning system. Intimately surrounding the NR maser's resonant cavity with the thermally isolating quartz sleeve has reduced temperature-induced frequency offsets to a second order effect (at least in a laboratory environment), and examination of the coefficients in the temperature column of Table 1 is all that is necessary to convince oneself that ambient temperature fluctuations had no significant effect on the performance of the NR masers in this investigation. It is the interrelation of the barometric pressure and humidity with the frequency offset that is interesting.

As is visible in Table 1, both the humidity and pressure can be strongly correlational with maser frequency offset, but there are critical differences between the two correlations. The humidity does not consistently show significant correlation to the frequency offset; moreover, whenever the correlation seems significant, a time delay of up to 48 hours has been added to the frequency offset data to maximize the coefficients. The optimal time delay is not fixed. In the MJD 47973 data set, a 48-hour delay maximizes the correlation coefficient. Similarly, a time delay of 24 hours in the MJD 48314 data set maximizes the semi partial correlation coefficients between humidity and frequency offset.

One would expect that if humidity changes were significantly affecting maser frequency offset, the relation between the cause and effect would be more consistent. In many of the data sets presented in Table 1, the semi partial correlation coefficient between humidity and frequency offset is insignificant in comparison with that between the barometric pressure and frequency offset irrespective of the time delay used. It seems probable, therefore, that the occasional correspondence between humidity and frequency offset is being caused by a third variable influencing both the humidity and frequency offset.

In all observed cases where the humidity shows significant correlation with the frequency offset, the barometric pressure is also strongly interrelated with the frequency offset. A meteorological relationship exists between the barometric pressure and ambient humidity. It is this relationship that could account for the observed correlation between the humidity and frequency offset. Because of the inconsistency and unpredictability of the correlation between humidity and frequency offset, it seems apparent that what is being seen in the data is the often unpredictable correlation of humidity and barometric pressure in East Coast weather.

In sharp contrast to the humidity-frequency offset relationship, the observed barometric pressure-frequency offset correlation exhibits consistency. The changes in pressure and frequency offset are always observed to occur simultaneously. In addition to the data presented here, correlational analyses were performed on other data sets in which the environmental conditions and frequency offset were sampled at 5-minute intervals. Even in these cases, the semi partial correlation coefficients were maximized without adding time delays to the frequency offset.

The calculated semi partial correlation coefficients between barometric pressure and frequency offset presented in Table 1 are consistently on the order of -0.7. Correlation coefficients of this magnitude are seen for all sorts of barometric pressure patterns, including large, rapidly moving low-pressure fronts as depicted by Figure 1A; gradually increasing or decreasing pressures such as illustrated in Figures 3A and 5A; and semisinusoidal patterns as shown in Figure 4A.

Semi partial correlation coefficients near -0.7 are seen when the variation in the pressure is large (typically a variation $\geq$ 0.3 inch over a few days). The coefficients become smaller, and the relationship less linear, for smaller pressure fluctuations. This occurs because NR maser performance in stable conditions is one or two parts in 10^{15} over a 24-hour period, and this is the magnitude of the frequency offset effect one would expect to see from such small pressure variations. In Figure 1A, for example, it is clear that the barometric pressure is associated with frequency offsets as large as 9 parts in 10^{14} in response to the strong pressure front. During the first few days presented in Figure 1A, where the pressure variations are small, the frequency offset remains in the small parts in 10^{15} range.

Although correlational analysis cannot prove cause and effect, the findings that the semi partial correlation coefficients between pressure and frequency offset are consistently stronger than -0.7

and that the pressure and frequency offset change simultaneously give good reason to suspect a causal relationship between pressure and NR hydrogen maser frequency offset.

CONCLUSION

Since March 1990, the frequency offset of three NR hydrogen masers has been recorded synchronously with the environmental conditions in the laboratory enclosing the masers. Using these data, semi partial correlation coefficients were calculated between maser frequency offset and various environmental conditions (temperature, barometric pressure, and humidity). The statistical analysis revealed a strong correlation between large changes in the barometric pressure and changes in maser frequency offset.

Large variations in barometric pressure are consistently associated with changes in NR maser frequency offset as large as 9 parts in 10^{14}. The correlation is a negative one, so decreasing pressure is associated with a positive change in the frequency offset, and vice versa. When the barometric pressure variation is greater than approximately ± 0.3 inch of mercury over a few days, the calculated semi partial correlation coefficients are consistently near -0.7.

REFERENCES

[1] H. Helwig, **Precision Frequency Control**, Vol. 2, E. A. Gerber and A. Ballato, Eds. Orlando, FL: Academic Press, 1985, p. 159.

[2] R. A. Dragonette and J. J. Suter, *"Barometric Pressure-Induced Frequency Offsets in Hydrogen Masers"* Proc. 45th Annu. Symp. Freq. Control, 1991, p. 586.

[3] D. Harnett and A. Soni, **Statistical Methods for Business and Economics**, 4th ed. Reading, MA: Addison-Wesley, Inc., 1991.

TABLE 1
Semi Partial Correlation Coefficients Between The Temperature, Pressure And Humidity, And The Frequency Offset

	Mean Julian Date	Semi Partial Correlation Coefficients		
	(# DAYS)	Temperature	Pressure	Humidity
	47973			
Frequency Offset	(17)	.11	-.75	-.16
Frequency Offset (12h)		.12	-.64	.02
Frequency Offset (24h)		.12	-.51	.21
Frequency Offset (48h)		.19	-.22	.47
	48076			
Frequency Offset	(7)	-.01	-.86	-.08
Frequency Offset (12h)		-.24	-.77	-.07
Frequency Offset (24h)		-.33	-.41	0
	48094			
Frequency Offset	(6.5)	.10	-.66	.20
Frequency Offset (12h)		-.22	-.36	.19
Frequency Offset (24h)		-.02	-.03	.34
	48189			
Frequency Offset	(6.5)	-.20	-.49	.30
	48280			
Frequency Offset	(6)	.08	-.88	-.10
Frequency Offset (12h)		-.18	-.49	-.41
Frequency Offset (24h)		-.19	-.09	-.48
	48314			
Frequency Offset	(5.5)	-.01	-.61	-.22
Frequency Offset (12h)		.03	-.31	.10
Frequency Offset (24h)		.20	.00	.45
	48438			
Frequency Offset	(6)	-.07	-.61	-.17
Frequency Offset (12h)		-.08	-.33	-.22
Frequency Offset (24h)		-.03	.08	-.34
	48540			
Frequency Offset	(7)	.01	-.83	-.41
Frequency Offset (12h)		-.17	-.61	-.13
Frequency Offset (24h)		-.29	-.28	-.29
	48550			
Frequency Offset	(7)	.03	-.76	.07
Frequency Offset (12h)		-.32	-.25	-.13
Frequency Offset (24h)		-.56	.13	-.07

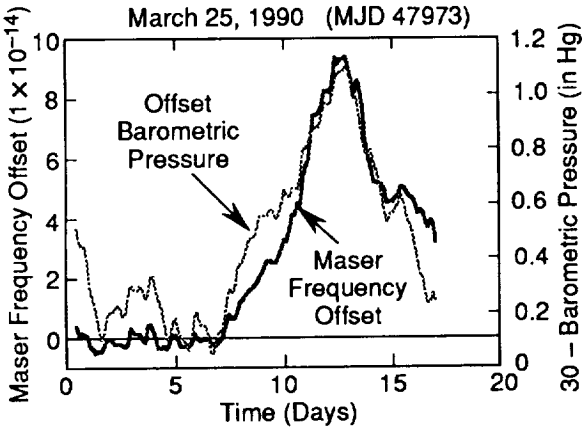

Figure 1A. Maser Frequency Offset and Offset Barometric Pressure Versus Time.

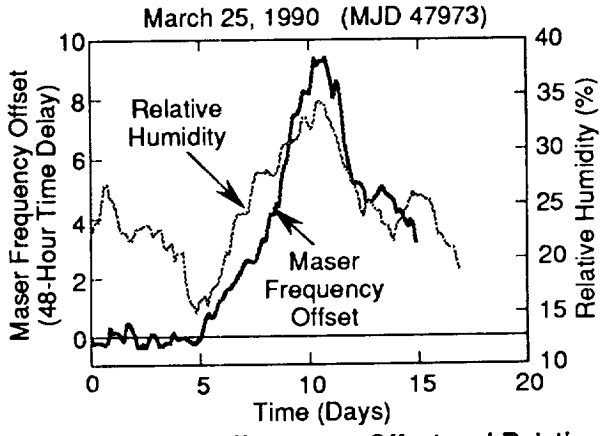

Figure 1B. Maser Frequency Offset and Relative Humidity Versus Time. (Note: The frequency offset curve has been delayed by 48 hours with respect to the relative humidity curve.)

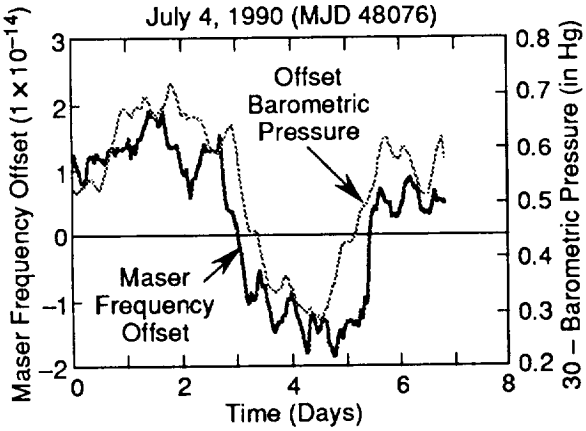

Figure 2A. Maser Frequency Offset and Offset Barometric Pressure Versus Time.

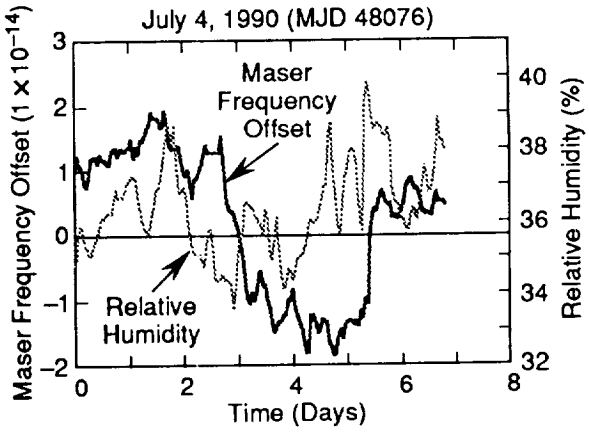

Figure 2B. Maser Frequency Offset and Relative Humidity Versus Time.

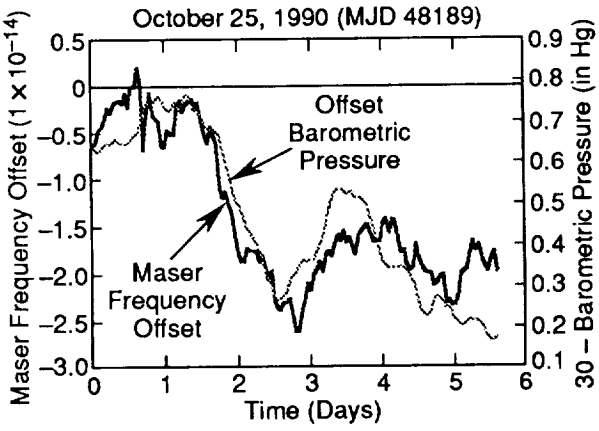

Figure 3A. Maser Frequency Offset and Offset Barometric Pressure Versus Time.

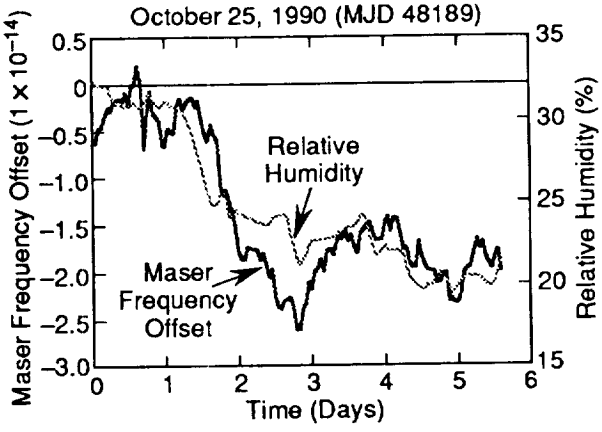

Figure 3B. Maser Frequency Offset and Relative Humidity Versus Time.

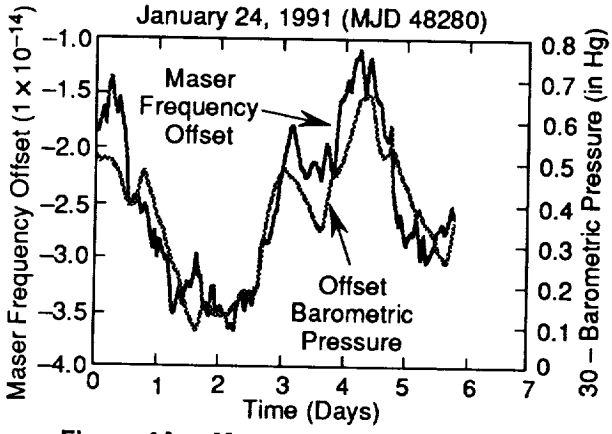

Figure 4A. Maser Frequency Offset and Offset Barometric Pressure Versus Time.

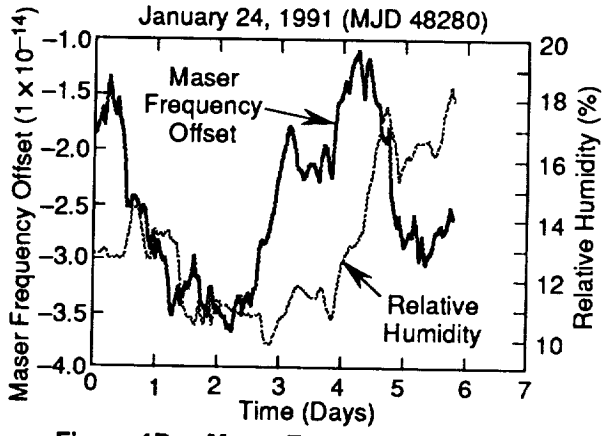

Figure 4B. Maser Frequency Offset and Relative Humidity Versus Time.

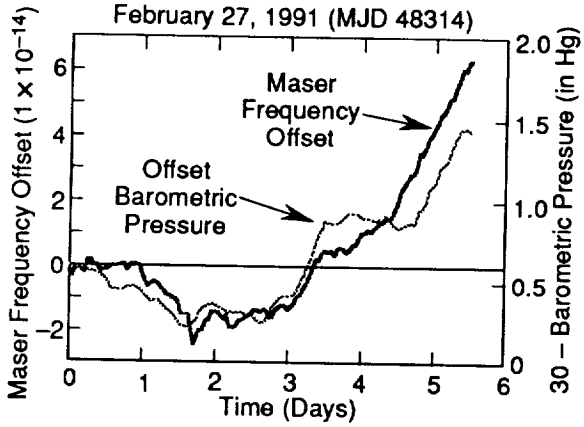

Figure 5A. Maser Frequency Offset and Offset Barometric Pressure Versus Time.

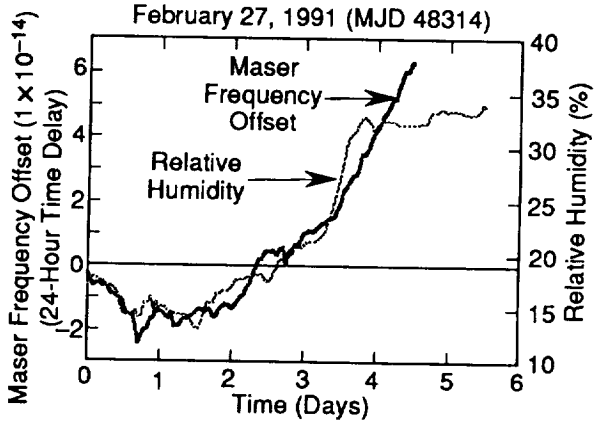

Figure 5B. Maser Frequency Offset and Relative Humidity Versus Time. (Note: The frequency offset curve has been delayed by 24 hours with respect to the relative humidity curve.)

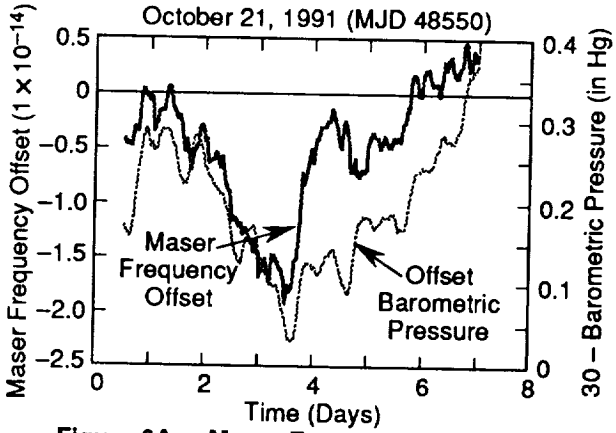

Figure 6A. Maser Frequency Offset and Offset Barometric Pressure Versus Time.

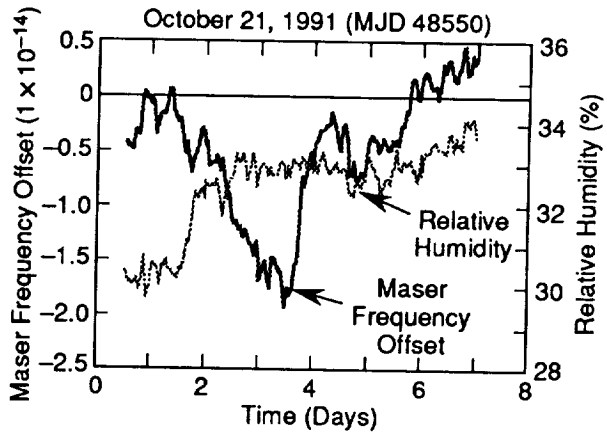

Figure 6B. Maser Frequency Offset and Relative Humidity Versus Time.

QUESTIONS AND ANSWERS

Harry Peters, Sigma Tau: I think that it is only fair to point out that what you are seeing is probably cavity frequency variations. This would not necessarily be characteristic of a maser which uses autotuning. That is, frequency variations due to atmospheric pressure variations would be eliminated in a maser which uses cavity autotuning, so this is not necessarily characteristic of all hydrogen masers.

N92-33877

TIMESCALE ALGORITHMS COMBINING CESIUM CLOCKS AND HYDROGEN MASERS

Lee A. Breakiron
U.S. Naval Observatory
Washington, DC 20392

Abstract

The USNO atomic timescale, formerly based on an ensemble of cesium clocks, is now produced by an ensemble of cesium clocks and hydrogen masers. In order to optimize stability and reliability, equal clock weighting has been replaced by a procedure reflecting the relative, time-varying noise characteristics of the two different types of clocks. Correction of frequency drift is required, and residual drift is avoided by the eventual complete deweighting of the masers.

INTRODUCTION

At timing laboratories, readings from an ensemble of clocks are combined mathematically by some sort of algorithm to produce a mean timescale in order to average down both random and systematic errors, thereby increasing overall stability and accuracy, respectively. Also, reliability is improved because individual clocks can be added as they become available or removed when they fail or need adjustment. In order to have a time signal continuously available, at least one "master clock" at USNO is steered in frequency so that its time approximates that of the mean "paper" timescale.

The optimum algorithm is not obvious and, indeed, depends on the needs of the user, which may favor stability over accuracy, for example. Algorithms can differ in their definition of mean timescale, in their clock weighting, in their use of filters to reduce measurement noise, and in their methods of predicting and steering clock frequencies. These aspects may depend on the type of clocks involved, since different clock types have different noise characteristics.

OLD AND NEW TIMESCALE ALGORITHMS

The atomic timescale at USNO has until recently been based entirely on an ensemble of commercial (nearly all Hewlett-Packard) cesium frequency standards whose frequencies have been averaged by a linear algorithm and equal clock weighting. Weighting by inverse Allan variances was not found to improve stability or accuracy significantly 1. The algorithm employed was the following:

$$z_t = z_{t-T} + \sum_i W_t(i)[x_t(i) - x_{t-T}(i) + Tr_t(i)] \qquad (1)$$

where z_t is the difference between the readings of the Master Clock and the mean timescale, $x_t(i)$ the difference between the readings of the Master Clock and clock i, $W_t(i)$ is the weight of clock i,

and $r_t(i)$ is the rate (frequency in time gained per time interval T) of clock i relative to the mean timescale, all at time t [2]. r_t was determined by least-squares using 5-day bins of hourly data, since over a span of 5 days oscillator noise can be well modelled by a combination of white FM noise and FM random walk [3].

The new algorithm mentioned in [2], based on ARIMA prediction modelling, was never implemented. Indeed, ARIMA modelling was found to yield a timescale no better than, and often significantly inferior to, that generated by Eq. (1), in spite of ancillary robust features, apparently because of model variations [1]. The apparent inferiority of the NIST algorithm on the short-term [1] may have been due to ignorance of an unpublished rate-change detector and upper weight limit [4].

Use of Eq. (1) assumes constant clock rates, aside from discrete changes that are monitored in real time and corrected for during postprocessing. This leads to a very occasional rejection of an otherwise satisfactory cesium clock because of a small frequency drift. More important, this algorithm would not be appropriate for an ensemble containing hydrogen masers in view of their significant, characteristic, and generally positive frequency drifts.

While Eq. (1) could be modified to incorporate a drift term, simultaneous solutions for rate and drift of comparable accuracy to previous solutions for rate alone would require data lengths greater than 5 days. Since solutions for rate alone are quite adequate for cesium clocks and because we have found (second-order) solutions for maser drifts to be insufficiently stable, we have chosen to retain first-order solutions and to derive drifts from long-term changes in the rates.

In the presence of a frequency drift $d_t(i)$, we have the following:

$$r_t(i) = r_{t-T}(i) + T d_{t-T}(i) \tag{2}$$

$$x_t(i) = x_{t-T}(i) + T r_{t-T} + 1/2\ T^2 d_{t-T}(i) \tag{3}$$

and:

$$z_t = z_{t-T} + \sum_i W_t(i)[x_t(i) - x_{t-T}(i) + T r_{t-T}(i) + 1/2\ T^2 d_{t-T}(i) \tag{4}$$

Solving Eq. (2) for r_{t-T} and substituting in Eq. (4), we get:

$$z_t = z_{t_T} + \sum_i W_t(i)[x_t(i) - x_{t_T}(i) + T r_t(i) - 1/2 T^2 d_{t-T}(i) \tag{5}$$

which replaces Eq. (1) as the USNO timescale algorithm.

Another restriction of the old USNO algorithm is its assumption of a homogeneous ensemble with regard to clock types. While equal clock weighting may be satisfactory for an ensemble of cesium clocks, it would not be appropriate for an ensemble of both cesium clocks and hydrogen masers, due to the significantly greater short-term stability of the masers compared to the cesiums and the significantly greater long-term stability of the cesiums compared to the masers.

STABILITY OF THE MEAN TIMESCALE

Over the past 21 months, the USNO ensemble has averaged 22 ±1 equally weighted cesiums. Since MJD 47842, between 3 and 7 masers have been added, at first with equal weight, each maser being retroactively unweighted 60 days in the past so as not to introduce a long-term frequency drift. Our six SAO masers have drifts relative to TAI of from +0.3 to +3.4 parts in 10^{15}/day and our four Sigma Tau masers have drifts of from +0.1 to +1.3 parts in 10^{15}/day [**5**]. Still, such a procedure does not minimize the noise because it overweights the cesiums relative to the masers in the short term.

One could construct a timescale based entirely on masers, determining and correcting their rates and drifts relative to another, pure cesium timescale. However, the small number of masers would make its operational reliability questionable, and the drifts would be difficult to determine relative to the noisier cesium timescale.

Optimal use of a given number of clocks in a mixed ensemble would be possible if the weight of a given maser, relative to a given cesium, were allowed to vary with time inversely as their relative Allan variances vary with sampling time. This would require that the entire mean timescale be retroactively recomputed every hourly time step, rather than a few times a week as before. Cesiums would be phased out with time (up to the present) while the masers would be phased in. All rates and drifts would be determined from a comparison with a combined timescale whose long-term trend would be determined by the cesiums and whose near-realtime stability would be determined by the masers.

In order to determine the weighting function, sigma-tau curves were constructed for our masers and an equal number of good cesiums. The intersection of a typical maser curve with a typical cesium curve, i.e. when their Allan deviations were equal, was found to occur at a sampling time of 7.5 days. Fitting second-order curves to the data, we obtained:

$$\log \sigma_{\rm cs} = 0.219x^2 - 0.432x - 13.608 \quad (6)$$

$$\log \sigma_{\rm HM} = 0.460x^2 + 0.049x - 13.917 \quad (7)$$

where $\sigma_{\rm CS}$ is the Allan deviation of a typical cesium, $\sigma_{\rm HM}$ is the Allan deviation of a typical maser, $x = \log t - 5.3$, and t is the time difference in seconds between a given hour's measurement and the most recent hour. At $t = 0$, x is arbitrarily set to x at $t = -1$. The weight of a maser relative to a cesium is taken to be the following:

$$w_{\rm HM}/w_{\rm CS} = \sigma_{\rm CS}^2/\sigma_{\rm HM}^2 \quad (8)$$

The relative weights change from 10:1 around the current hour to 1:10 around 25 days in the past (see Fig. 1). Accordingly, in practice, only the last 25 days of the timescale, rather than its entirety, are recomputed every hourly time step. Also, the masers are completely unweighted after 60 days to prevent the accumulation of any long-term drift.

Allan deviations were determined for a range of sampling times using 370 days of clock data and two of our masers as references. A three-cornered-hat analysis yielded the results in Fig. 2. The stability of the old algorithm was only slightly improved by the introduction of masers (at equal weight with the cesiums), but the new algorithm is significantly more stable for sampling times shorter than 11.5 days. The noise at shorter sampling times is mostly due to the old measurement

system. This noise will be reduced from 100 to 10 ps when transition is made to our new Erbtec measurement system currently under test 6. The weighting Eqs. (6) and (7) will then have to be reevaluated.

A by-product of this analysis is the sigma-tau plot for the reference masers in Fig. 3. Similar results at long sampling times were obtained by Powers et al. [5] using Erbtec data.

REALTIME STABILITY AND ACCURACY

The next question is how well this increased stability in the mean timescale translates into realtime stability on the part of a Master Clock (MC). MC #1 is a maser that is steered daily by an internal frequency synthesizer toward a linear prediction based on a least-squares solution of the past 24 hours of data, but with a 10-day damping time for time offsets and a maximum frequency change of 300 ns/day^2; both restrictions are due to user requirements for strict frequency stability and their exact values are currently under evaluation. A sigma-tau plot for MC #1 is given in Fig. 4, which shows a significant improvement using both the old and new mean timescales, when masers are incorporated, over use of the old mean timescale composed of cesiums alone. Only if the steering can be improved will full advantage be taken of the new algorithm; this possibility will be investigated.

While one measures and corrects for the relative rates and drifts of the masers and cesiums, some residual drift may affect the timescale, as will the rate and drift in common to all the clocks. It is of interest to compare the old and new means incorporating masers (never completely deweighting them) with the old, pure-cesium mean. Such a comparison is shown in Fig. 5. The old and new means incorporating masers drift about -11 ns and -35 ns, respectively, over 300 days. One would expect the new mean to drift more because of the greater weight of the masers. In practice, this drift never accumulates to this level in the USNO timescale because of the retroactive unweighting of the masers after 60 days. If this unweighting is not done, such a drift would presumably be a risk for any timescale that incorporates masers (e.g. TAI).

The USNO time signal actually derives from Master Clock #2, a maser that was formerly steered to the old mean. Recently it has been steered (by an internal frequency synthesizer) to TAI, or more specifically, to an extrapolation thereof based on the best performing USNO masers. This was done to synchronize UTC (USNO) with UTC (BIPM) within the limits required by NATO and other users. That being nearly accomplished, MC #2 will hereafter be steered toward the new mean, with occasional corrections to keep it within 200 ns (or perhaps less) of TAI (as is also done to MCs #1 and #3), with the same dampening factor (10 days) and limit on the steering (300 ns/day^2) that are being used and evaluated for MC #1. MC #3, a maser steered daily by a phase microstepper heretofore to MC #2, will also be steered similarly. These duplicative systems provide extra reliability. The maser of each MC is not weighted as a clock unless its unsteered signal is available (as it is if a microstepper is used) or its signal is corrected for steering.

Fig. 6 depicts the drifts of MCs #1 and #2 relative to TAI. MC #1 has some extra noise around a sampling time of 10 days as the result of its being steered toward our mean timescale; for the following sampling times, MCs #1 and #2 had the logarithmic Allan deviations listed below:

Tau (days)	MC #1	MC #2
10	-13.638	-13.867
20	-13.667	-13.700
30	-13.713	-13.543

Still, steering MC #2 to the mean has the advantage of greater statistical independence from TAI, which in turn would dampen the influence of fluctuations in TAI.

Aside from checks for large time and rate deviations, our clock measurements are not filtered, in order to have a near-realtime measure of accuracy and environmental response. However, the performance obtained by this and the other procedures described above will be compared with that obtained by a Kalman-filter algorithm developed by Stein 7,8 as part of continuing effort to improve the accuracy and stability of UTC (USNO).

ACKNOWLEDGMENTS

The inspiration for this work derived from discussions with Randolph T. Clarke, III of USNO. The author also acknowledges the help of summer assistant Blaine Bell.

REFERENCES

[1] Breakiron, L. A., *"The effects of data processing and environmental conditions on the accuracy of the USNO timescale,"* Proceedings of the 20th Annual Precise Time and Time Interval (PTTI) Applications and Planning Meeting, 29 November-1 December, 1988, Vienna, VA, pp. 221-236.

[2] Percival, D. B., *"The U.S. Naval Observatory clock time scales,"* IEEE Transactions on Instrumentation and Measurement, vol. IM-27, 1978, pp. 376-385.

[3] Percival, D. B., *"A heuristic model of long-term atomic clock behavior,"* Proceedings of the 30th Annual Symposium on Frequency Control, 2-4 June, 1976, Atlantic City, NJ, pp. 414-419.

[4] Allan, D. W., private communication, 1989.

[5] Powers, E., Gifford, A., and Wheeler, P., *"Hydrogen maser performance at the United States Naval Observatory and the Naval Research Laboratory,"* Proceedings of the 45th Annual Symposium on Frequency Control, 29-31 May 1991, Los Angeles, CA, pp. 582-585.

[6] Gifford, G. A. and Wheeler, P., *"Report on the Master Clock upgrade at USNO,"* Proceedings of the 43rd Annual Symposium on Frequency Control, 31 May-2 June 1989, Denver, CO, pp. 158-161.

[7] Stein, S. R., Gifford, G. A., and Breakiron, L. A., *"Report on the timescale algorithm test bed at USNO,"* Proceedings of the 21st Annual Precise Time and Time Interval (PTTI) Applications and Planning Meeting, 28-30 November 1989, Redondo Beach, CA, pp. 269-288.

[8] Stein, S. R. and Evans, J., *"The application of Kalman filters and ARIMA models to the study of time prediction errors of clocks for use in the Defense Communication System (DCS),"* Proceedings of the 44th Annual Symposium on Frequency Control, 23-25 May, 1990, pp. 631-635.

CORRIGENDA TO PREVIOUS PAPER

The following typographical errors should be corrected in [1]:

p. 223, l. 1, for "τ" read "σ" p. 223, l. 19, for "passive" read "active"

Table 5, 1st entry, for " ± 65.3 ± 39.9" read "± 65.3 ± 39.9"

Also, a list of figure captions was not published. The figures, however, are self-explanatory, except for the fact that the filled squares in Fig. 1 represent clocks whose beam tubes were replaced before the start of the data set in 1986.

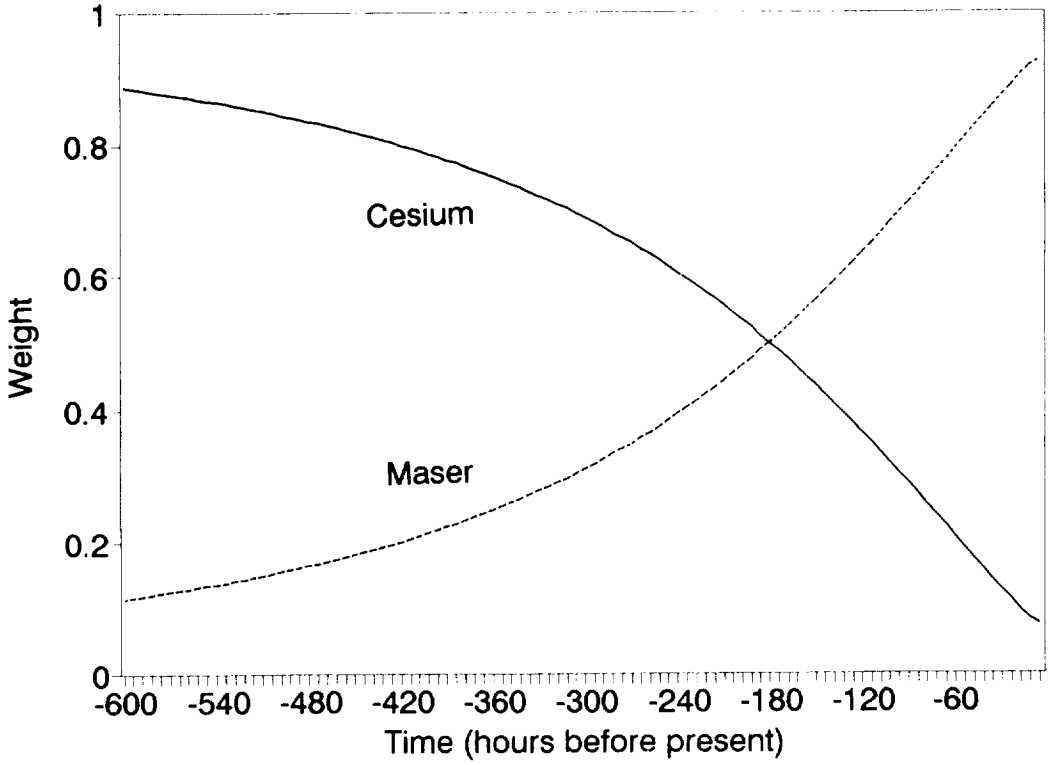

Fig. 1. The weight of a cesium clock and a hydrogen maser as functions of time in the new mean timescale algorithm.

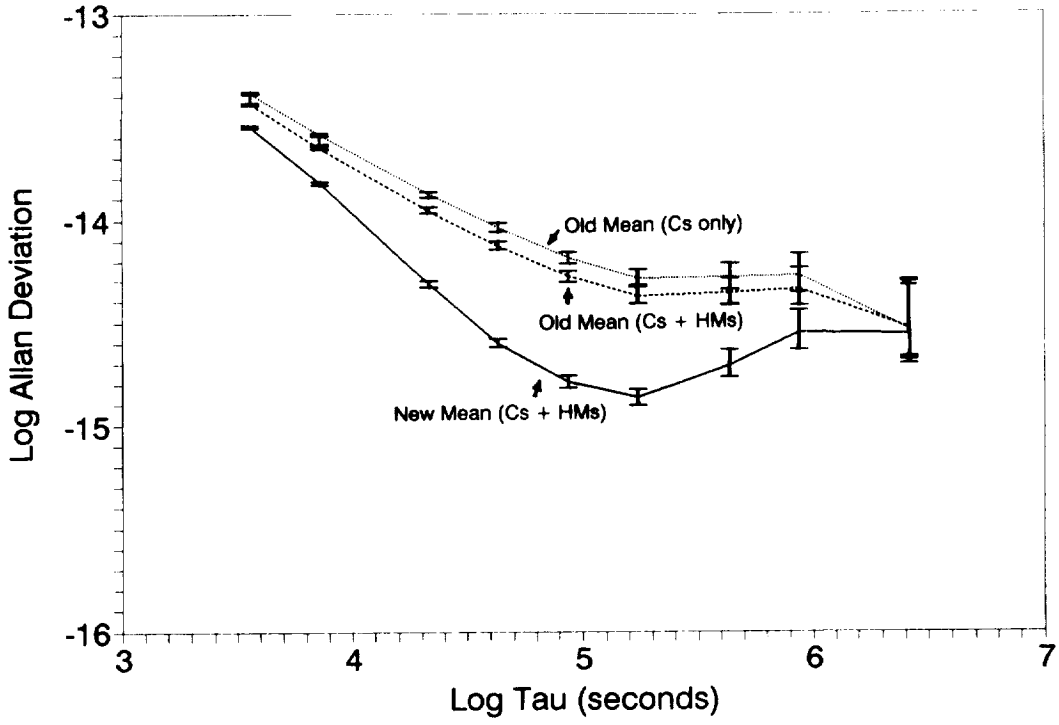

Fig. 2. The frequency stability of the old mean timescale (with and without masers) and the new mean timescale as a function of sampling time (tau). The error bars correspond to a confidence level of 90%.

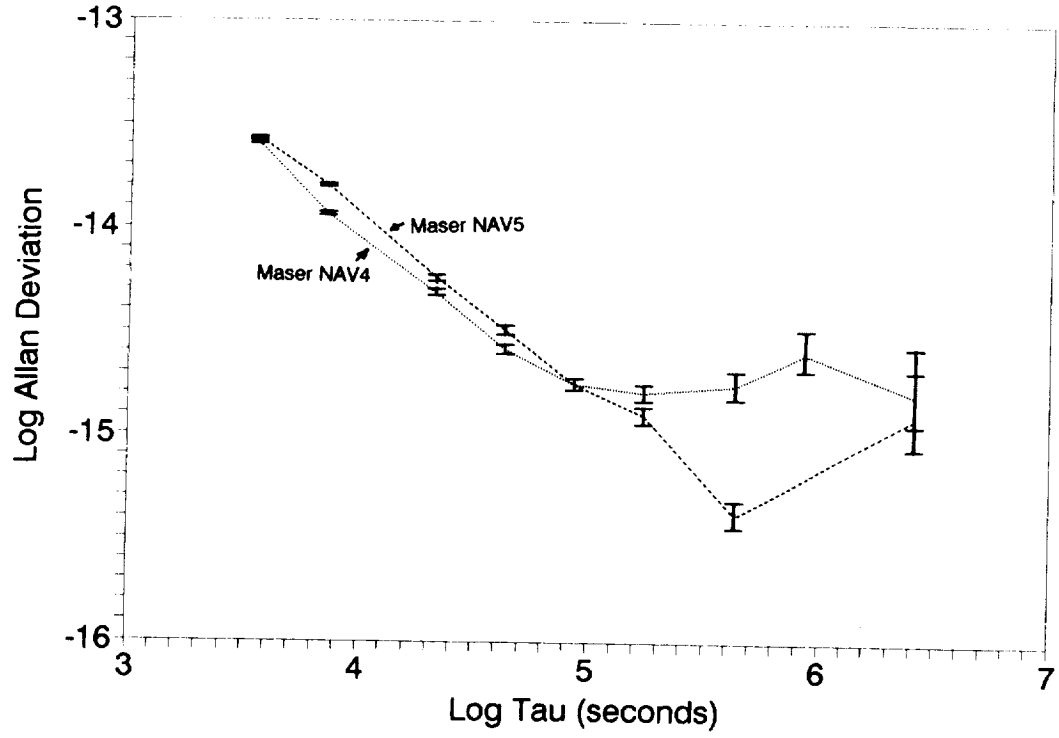

Fig. 3. The frequency stability of the two reference masers.

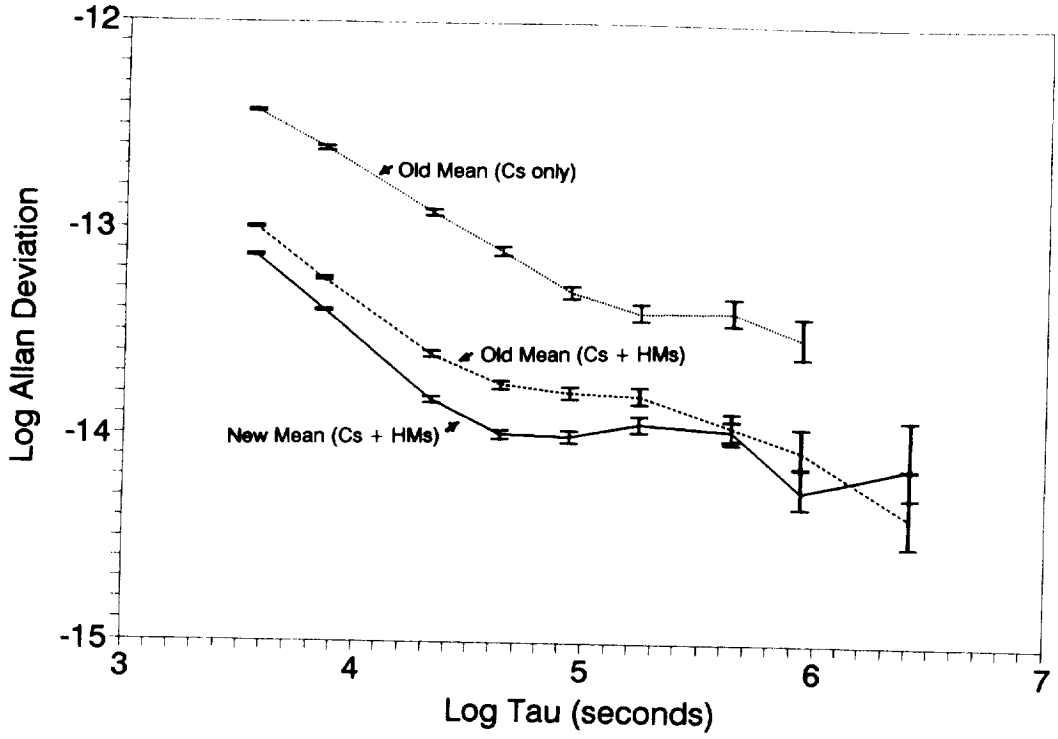

Fig. 4. The frequency stability of Master Clock #1 while being steered toward the old mean timescale (with and without masers) and toward the new mean timescale.

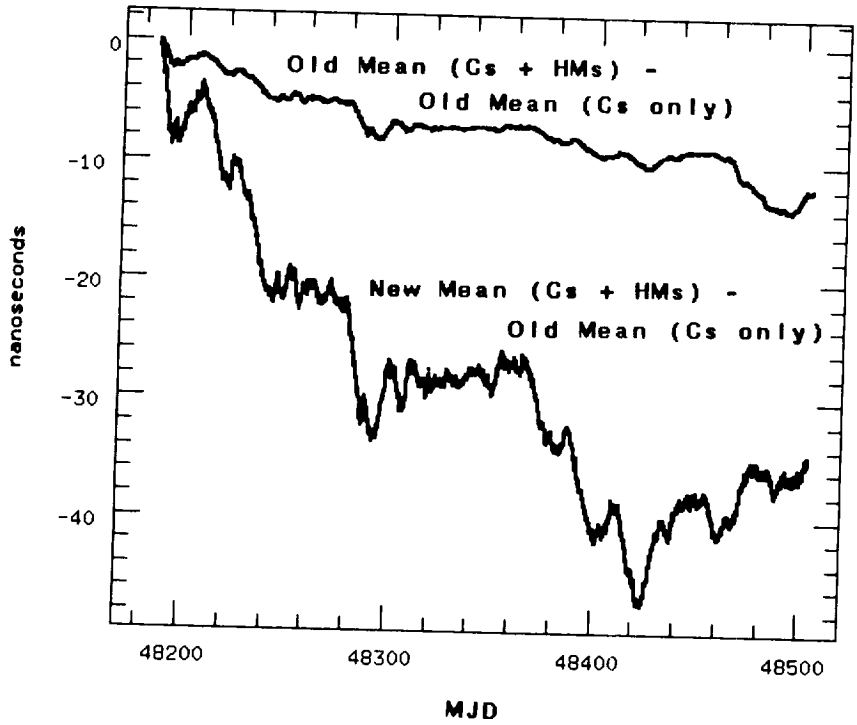

Fig. 5. The time drift, starting from an arbitrary point of enforced synchronism, of the old and new mean timescales incorporating masers, relative to the old mean timescale based on cesiums only, when the masers are never completely deweighted.

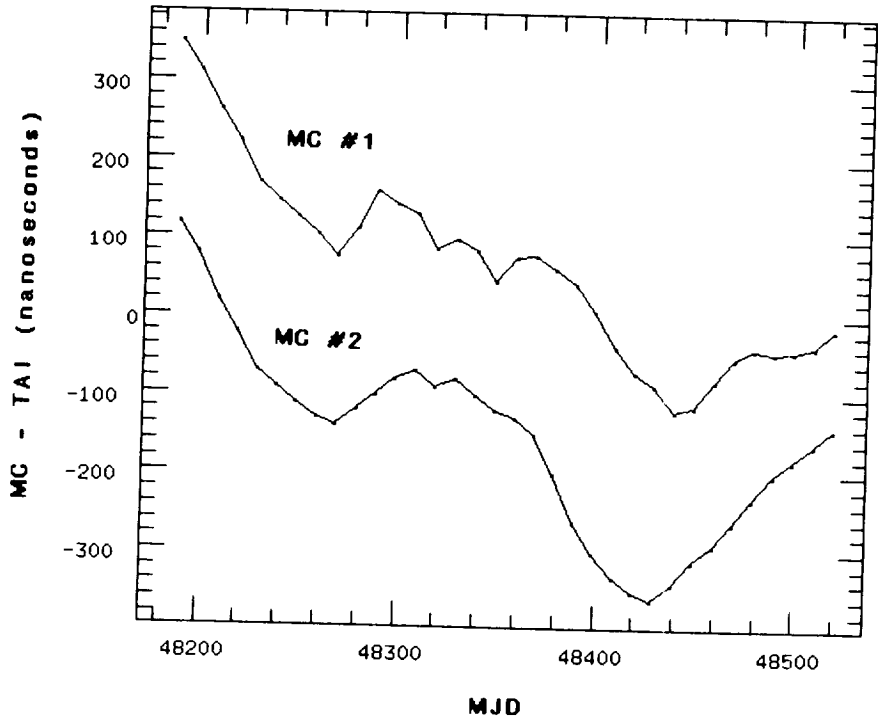

Fig. 6. The time drift of Master Clocks #1 and #2 relative to TAI.

FREQUENCY STABILITY OF GPS NAVSTAR BLOCK I AND BLOCK II ON-ORBIT CLOCKS

Thomas B. McCaskill
Wilson G. Reid
James A. Buisson
U.S. Naval Research Laboratory
Washington, D.C., 20375

and
Hugh E. Warren
Sachs Freeman Associates, Inc.

Abstract

Analysis of the frequency stability of on-orbit NAVSTAR clocks is performed by the Naval Research Laboratory.This work was sponsored by the GPS Joint Program Office. The frequency stability is presented for sample times of one day to 30 days. Composite frequency-stability profiles are presented for the Block I and Block II NAVSTAR clocks. Several NAVSTAR cesium clocks show frequency stabilities of a few parts in 10^{14} for long sample times. Time-domain noise-process analysis shows the dominant noise type to be white frequency noise for sample times of one to ten days. The non-stationary stochastic behavior of one of the cesium clocks, illustrated by its frequency-stability history, shows that the frequency stability is not always time-invariant.

INTRODUCTION

The Naval Research Laboratory determines on-orbit NAVSTAR clock performance using the process depicted in Figure 1. The analysis includes frequency and aging histories, frequency-stability profiles, time-prediction uncertainty profiles, time-domain noise process profiles, spectral analysis, and anomaly detection. Events that perturb the normal clock performance are of particular interest.

The results of the on-orbit analysis represent the behavior of the NAVSTAR clock with system errors superimposed. The influence of the system may enhance but usually degrades the observed performance of the clock. Therefore, deviations from nominal performance are analyzed in an attempt to identify the cause.

The Block I data was collected by the U.S. Naval Observatory using a single-frequency, time-transfer receiver with ionospheric corrections obtained from the model of the ionosphere broadcast in the navigation message. The Block II data was collected using a dual-frequency, authorized-user, time-transfer receiver which measures the ionospheric delay and automatically corrects for selected

availability (S/A). In both cases, the broadcast ephemeris is used by the receiver in computing the theoretical range from the monitor site to the space vehicle at the time of measurement. Table 1 summarizes the data used in the analysis.

Table 1
DATABASE
GPS BLOCK I AND BLOCK II CLOCKS
U.S. Naval Observatory Monitor Site

NAVSTAR Number	SV Number	Block Number	Clock Serial	Clock Type	Time Span mjd	mjd	days
3	6	I-3	20	Rb	8439–8571		133
8	11	I-8	2	Cs	6569–8571		2003
9	13	I-9	4	Cs	5894–8571		2678
10	12	I-10	5	Cs	5984–8571		2588
11	3	I-11	12	Rb	6369–8571		2203
14	14	II-1	8	Cs	7705–8571		867
13	2	II-2	14	Cs	7719–8571		853
16	16	II-3	11	Cs	8266–8571		306
19	19	II-4	27	Cs	7852–8571		720
17	17	II-5	25	Cs	7900–8571		672
18	18	II-6	31	Cs	7936–8571		636
20	20	II-7	30	Cs	8009–8571		562
21	21	II-8	6	Cs	8126–8400		275
15	15	II-9	37	Cs	8180–8571		392
23	23	II-10	36	Cs	8263–8571		309
24	24	II-11	52	Cs	8482–8571		90

The Block I space vehicles included in this analysis were not equipped with selective availability. Therefore, the data collected from these space vehicles by the single-frequency receiver was unaffected when S/A was implemented.

The clock offset is measured using a sequence of pseudorange measurements and the predicted range obtained from the space-vehicle orbital elements broadcast in the navigation message. The clock offset measurements are then smoothed over each non-overlapping 13-minute interval. The measurement representing a pass is the 13-minute measurement nearest the time of closest approach, or the one having the highest elevation angle, which minimizes the effect of the ionosphere on the measurement.

Time and frequency inputs to the time-transfer receiver were derived from the Observatory master clock which is a physical realization of the time scale generated by the Observatory from an ensemble of several types of atomic frequency standards. Since the stability of the time-scale is significantly better than that of an individual NAVSTAR clock, the measurements made by the Observatory reflect primarily the behavior of the NAVSTAR clocks.

The frequency stability of the Block I NAVSTAR clocks was computed using sample times from one day to a maximum of 30 days. In all cases the length of the database is a factor of ten, or more, greater than the maximum sample time evaluated. A long-term aging correction was determined

for each NAVSTAR clock and was removed from the data before computing the frequency stability.

BLOCK I NAVSTAR CLOCK PERFORMANCE

Figure 2 presents the frequency offset as a function of time for the NAVSTAR 3 rubidium clock. This is the second NAVSTAR 3 rubidium clock to be activated—the first having been activated in 1978 and having operated successfully for 13 years. The eclipse seasons are depicted by the shaded regions that repeat at a nominal rate of once every six months. The data shows large frequency fluctuations that appear to be related to the eclipse season. Previous analysis by the Naval Research Laboratory determined that the frequency offset of the first rubidium clock was sensitive to temperature and exhibited a temperature coefficient of $1.96 \times 10^{-12}/°C$. It is expected that the current rubidium clock will exhibit a similar temperature coefficient. It should be noted that beginning with NAVSTAR 8 all rubidium clocks had additional thermal control which appears to have isolated the clock from seasonal temperature variations.

Figure 3 presents the frequency offset for the NAVSTAR 8 cesium clock for a period of almost six years while Figures 4 and 5 present the frequency offset for the NAVSTAR 9 and NAVSTAR 10 cesium clocks for a period of more than seven years. The frequency offset for the clock on NAVSTAR 10 shows two knees in the data where the aging abruptly increased.

Figure 6 presents the frequency offset for the NAVSTAR 11 rubidium clock for a period of three years. The vertical scale has been expanded by plotting the residuals to a linear fit of the data. The sensitivity to temperature is evident in the wide seasonal swings in the frequency offset—similar to those seen previously on the first NAVSTAR 3 rubidium clock—with a fundamental period of nominally one year, although eclipse seasons occur every six months. Unlike that clock, however, the NAVSTAR 11 rubidium clock exhibits a negative temperature coefficient.

A composite of the frequency-stability profiles for all Block I NAVSTAR clocks operating on 11 November 1991 is presented in Figure 7. Of the five NAVSTAR clocks currently operating, two are rubidium and three are cesium. During 1991 all but NAVSTAR 10 had frequency stabilities less than 2×10^{-13} for a one-day sample time. The other two cesium clocks demonstrated excellent performance for all sample times that were evaluated. The stability varied from 1.8×10^{-13} at one day to 3.8×10^{-14} at 30 days. The NAVSTAR 10 cesium clock is well past its design life of five years during which time it performed within the specification of 2.0×10^{-13}. This can be seen from the frequency-stability history in Figure 8 which corresponds to the output of a 20-day moving average filter operating on the sequence of squared first differences of the one-day frequency offset measurements shown in Figure 5. The frequency stability of the two NAVSTAR rubidium clocks for an increasing sample time suffers from the wide swings in the frequency due to the seasonal temperature variations.

BLOCK II NAVSTAR CLOCK PERFORMANCE

Figure 9 presents the corrected frequency offset for the NAVSTAR 14 cesium clock over a two-year time span. The corrected frequency offset had a measured aging coefficient of $-3.2 \times 10^{-16}/day$ during the two-year span. Note a small change in the behavior of the frequency offset beginning near mjd 8150 (16 September 1990). After this date the frequency offset showed a change from white noise (uncorrelated) to slow fluctuations in the data. The presence of these fluctuations in

the data degrade the stability at larger sample times as will be seen from the frequency-stability profile.

Figure 10 presents the corrected frequency offset for the NAVSTAR 13 cesium clock. The frequency offset is well behaved with an aging coefficient of $-1.79 \times 10^{-15}/day$.

Figure 11 presents the corrected frequency offset for the NAVSTAR 16 cesium clock. The frequency offset shows slow fluctuations in the data that persist throughout 1991. The average aging during this eleven-month time span was $-2.61 \times 10^{-15}/day$. The phase offset for the first portion of the data was compared to that obtained using the precise ephemeris computed by the Defense Mapping Agency. The precise ephemeris yielded the same behavior which indicates that the accuracy of the broadcast ephemeris is not responsible for the observed behavior which is not characteristic of ground-based cesium clocks and has not been observed in the Block I cesium clocks.

Figure 12 presents the frequency offset for the NAVSTAR 19 cesium clock from shortly after initial turn-on to 11 November 1991. Anomalies in the form of sharp decreases in the frequency offset by as much as $-7pp10^{13}$ repeated at intervals of between 35 to 54 days began about 9 May 1989. Prior to occurrence of the first anomaly and during the subsequent intervals between the periodic breaks the clock exhibited an aging of about 1.63 $pp10^{14}/day$ which is rather high for a cesium clock. The aging exhibited during the initial period after turn-on and during the first twelve cycles appears to have changed appreciably at the beginning of the last cycle to approximately 5.0 $pp10^{14}/day$. The frequency stability was computed for the first 200 days and for the entire time span. The stability for the first segment is included in a composite stability plot. The stability for the entire time span marginally meets the Block II specification of 2×10^{-13} for sample times of one to ten days.

Figure 13 presents the corrected frequency offset for the NAVSTAR 17 cesium clock. The frequency offset from mjd 7900 to mjd 8068 was well behaved. An abrupt decrease in frequency on mjd 8068 was followed by a partial recovery. Then again on mjd 8195 the frequency appears to have further recovered. A comparison of the frequency stability for the period prior to mjd 8068 and again for the period after mjd 8195 showed a small degradation in the frequency stability for a one-day sample time following the frequency anomaly. The aging that occurred in the data during 1991 was $-1.40 \times 10^{-15}/day$.

Figure 14 presents the corrected frequency offset for the NAVSTAR 18 cesium clock. The frequency offset shows a small positive excursion beginning at mjd 8195—that correlates with the same behavior on the NAVSTAR 17 cesium clock. The data subsequent to this time appears to be noticeably quieter. The aging during 1991 for the NAVSTAR 18 cesium clock was $-5.00 \times 10^{-17}/day$.

Figure 15 presents the corrected frequency offset for the NAVSTAR 20 cesium clock. The frequency offset exhibits a small positive aging from initial operation and appears to have a small negative rate of change of aging. Except for the small apparent change in aging the data appears to be well behaved. The average aging during 1991 was $1.39 \times 10^{-15}/day$.

Figure 16 presents the corrected frequency offset for the NAVSTAR 21 cesium clock. Two frequency shifts, followed by recovery to the nominal frequency offset occurred on mjd 8451 and on mjd 8504. The cause of these unexpected shifts in the frequency is being investigated. The average aging before the shifts was $-1.74 \times 10^{-15}/day$. The frequency stability presented later in the composite plot of frequency stability was computed for the data before the shifts in frequency.

Figure 17 presents the corrected frequency offset for the NAVSTAR 15 cesium clock. The frequency appears well behaved and exhibited an aging during 1991 of $-2.8 \times 10^{-16}/day$.

Figure 18 presents the corrected frequency offset for the NAVSTAR 23 cesium clock. The frequency offset is well behaved and exhibited an aging during 1991 of $2.7 \times 10^{-16}/day$. Noteworthy is the fact that this is the first of the Block II-A NAVSTAR space vehicles.

Figure 19 presents the frequency offset for the NAVSTAR 24 cesium clock. The cause of the anomalous behavior occurring before 30 August 1991 (mjd 8498) may be attributed to a period of testing of the space vehicle. Only the data in the span of time from 30 August 1991 (mjd 8498) to 11 November 1991 was used in the calculation of the frequency stability. The aging following mjd 8498 was $2.06 \times 10^{-15}/day$.

A composite of the frequency-stability profiles for all Block II NAVSTAR clocks operating on 11 November 1991 is presented in Figure 20. An individual long-term aging correction was calculated for each NAVSTAR clock and removed before computing the frequency stability. The Block II frequency-stability profiles show that all of the NAVSTAR cesium clocks were within the 2×10^{-13} specification for a one-day sample time and had stabilities of less than the specification for all sample times up to 30-days. The dominant random noise types observed for the cesium clocks was white frequency noise for sample times of one to ten days with a gradual trend towards flicker frequency noise for sample times of 30-days. This was the expected frequency profile for well behaved cesium clocks. Small departures from white frequency noise towards random walk frequency noise were noted for several of the cesium clocks. This is believed to be due to small anomalies in the frequency offset rather than to the presence of any significant component of random walk in the frequency.

CONCLUSIONS

The frequency stability for four of the five Block I NAVSTAR clocks was better than the specification of 2×10^{-13} for Block I cesium clocks for a sample time of one-day. The NAVSTAR-10 cesium clock, which has exceeded the design life, did not meet the one-day frequency-stability specification during 1991.

All Block II NAVSTAR cesium clocks are better than the 2×10^{-13} specification for a one-day sample time. The best frequency stability for a one-day sample time was 8×10^{-14}. The dominant random noise type for the Block II NAVSTAR cesium clocks was white frequency noise for sample times of one to ten days.

The performance for all Block I and Block II clocks operating on 11 November 1991 is summarized in Table 2.

Table 2

PERFORMANCE SUMMARY
GPS BLOCK I AND BLOCK II CLOCKS
U.S. Naval Observatory Monitor Site
Calendar 1991

Navstar Number	Clock Serial	Clock Type	Time Span (*days*)	Frequency Stability 1 day ($pp10^{13}$)	Frequency Stability 10 days ($pp10^{14}$)	Aging 1991 ($pp10^{15}/day$)
3	20	Rb	132	1.8	41.4	28.50
8	2	Cs	314	1.8	4.9	0.37
9	4	Cs	314	1.8	5.4	-0.57
10	5	Cs	314	3.6	9.3	-12.80
11	23	Rb	314	1.5	23.6	-124.00
14	8	Cs	314	1.2	5.2	-0.32
13	14	Cs	314	1.5	4.3	-1.79
16	11	Cs	305	1.4	7.4	-2.61
19	27	Cs	208	1.7	9.6	16.30
17	25	Cs	314	1.1	4.3	-1.40
18	31	Cs	314	1.0	3.7	0.05
20	30	Cs	314	1.3	3.8	1.39
21	6	Cs	327	1.4	5.7	-1.74
15	37	Cs	314	1.7	5.6	-0.28
23	36	Cs	308	1.1	3.3	0.27
24	52	Cs	73	0.8		2.06

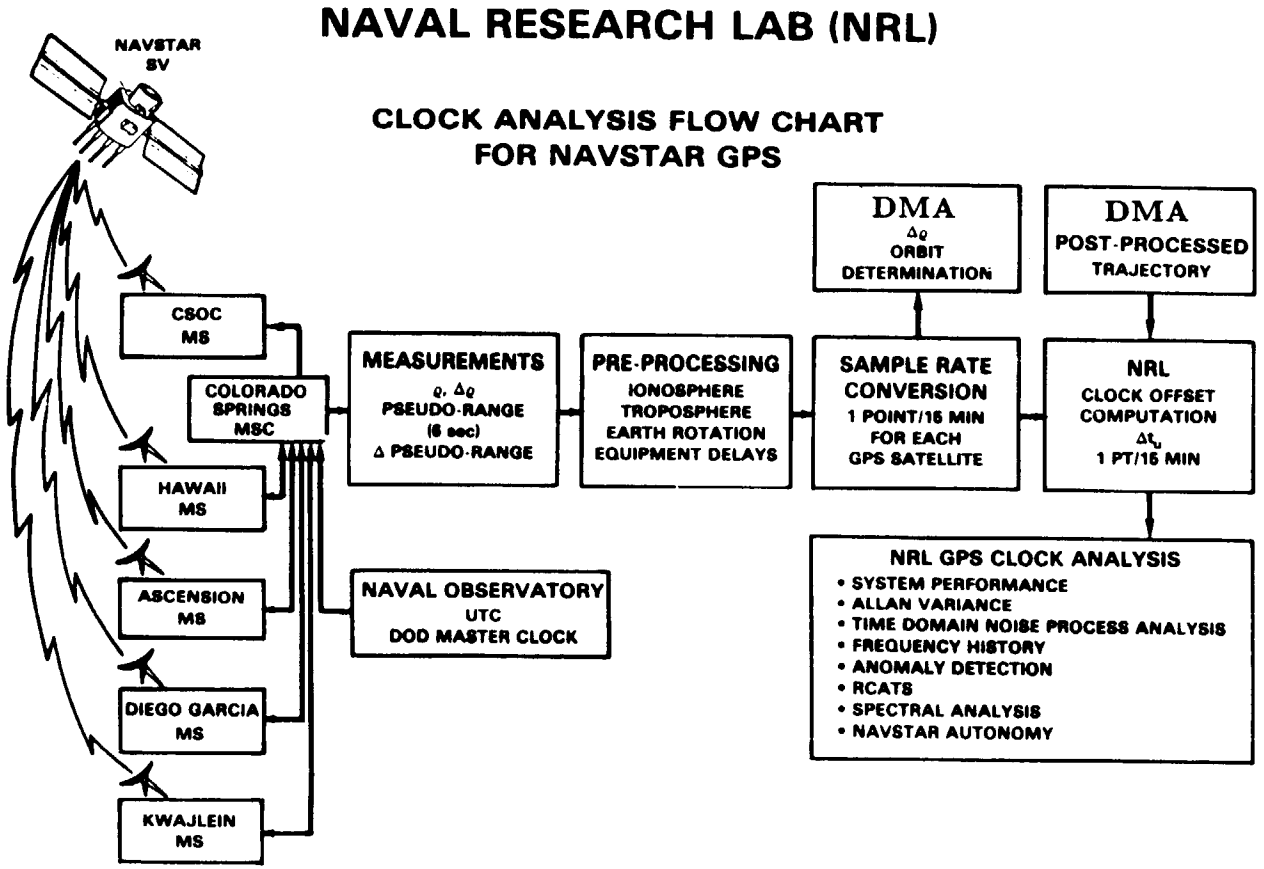

Figure 1. Clock Analysis Flow Chart.

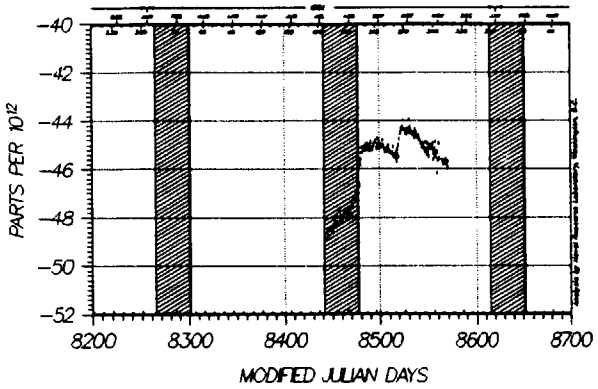

Figure 2. NAVSTAR 3 Frequency Offset.

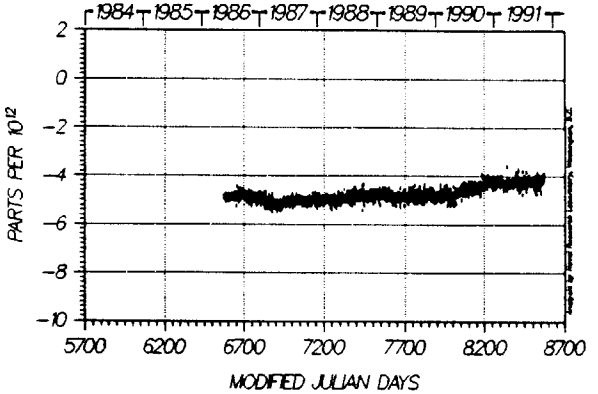

Figure 3. NAVSTAR 8 Frequency Offset.

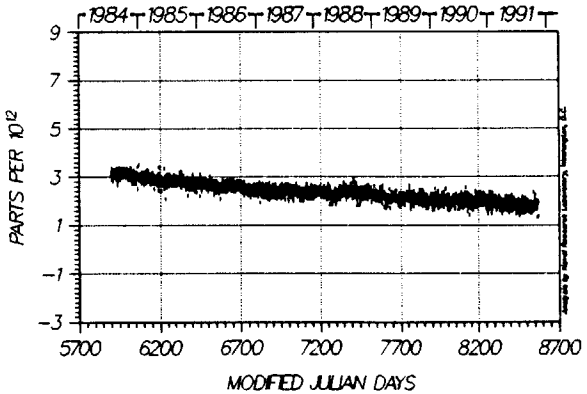

Figure 4. NAVSTAR 9 Frequency Offset.

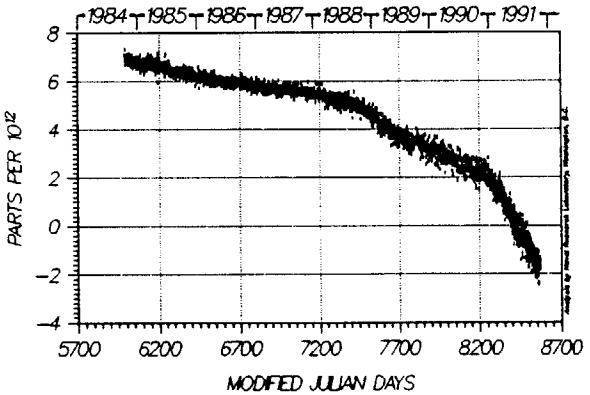

Figure 5. NAVSTAR 10 Frequency Offset.

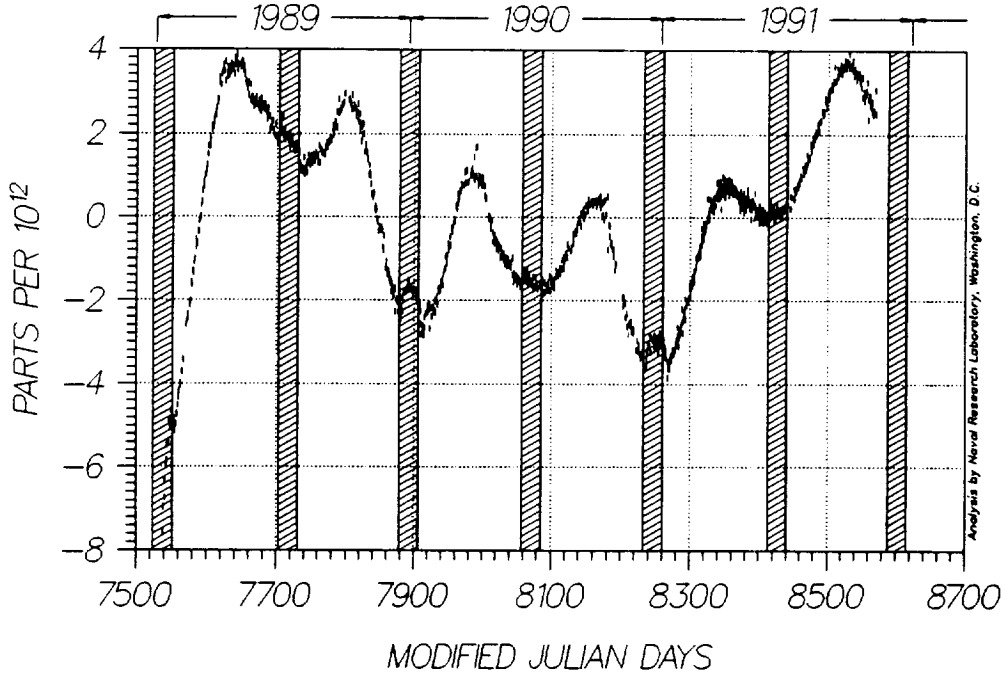

Figure 6. NAVSTAR 11 Frequency Offset.

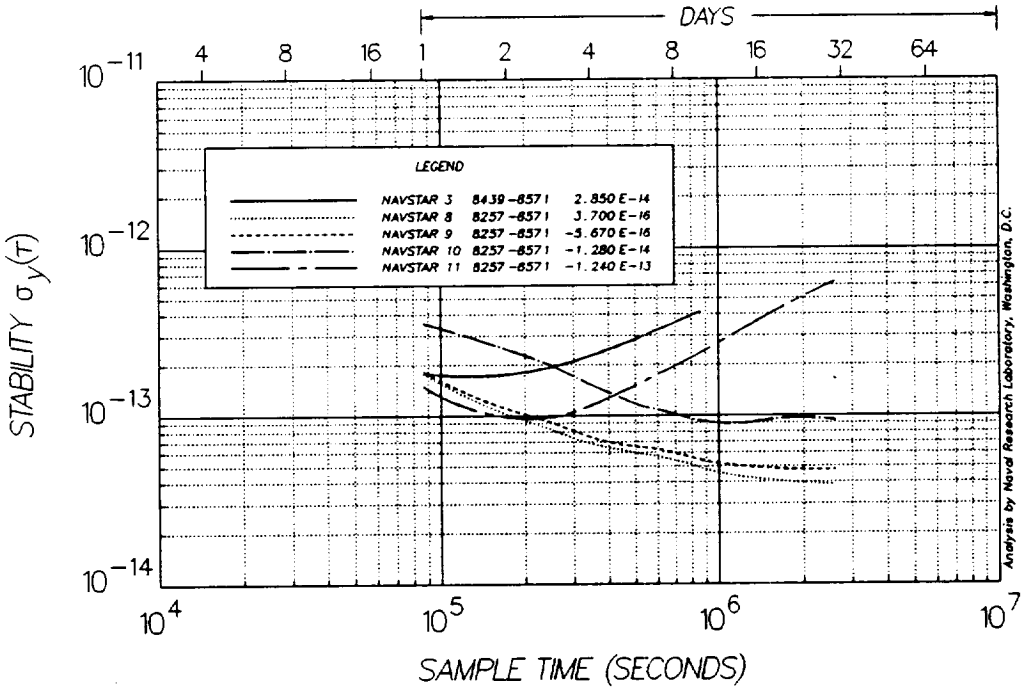

Figure 7. Block I Composite Stability.

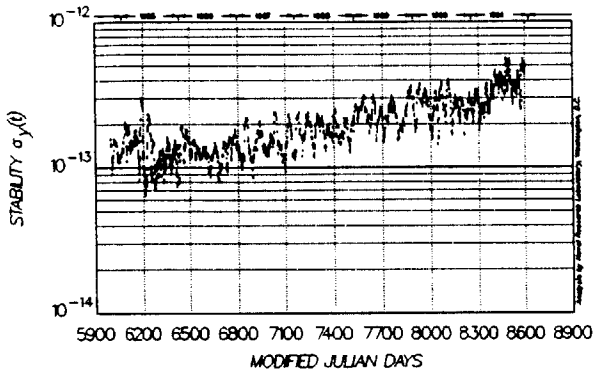

Figure 8. NAVSTAR 10 Stability History.

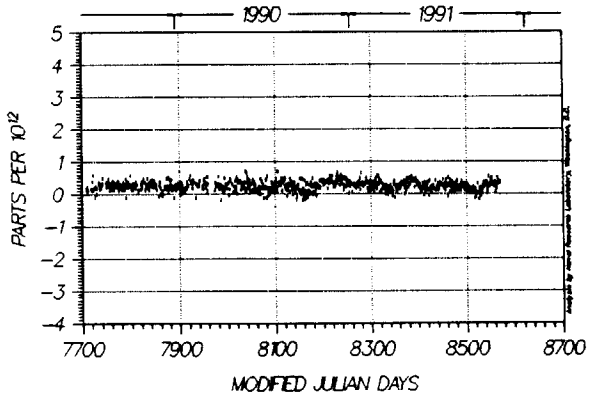

Figure 9. NAVSTAR 14 Frequency Offset.

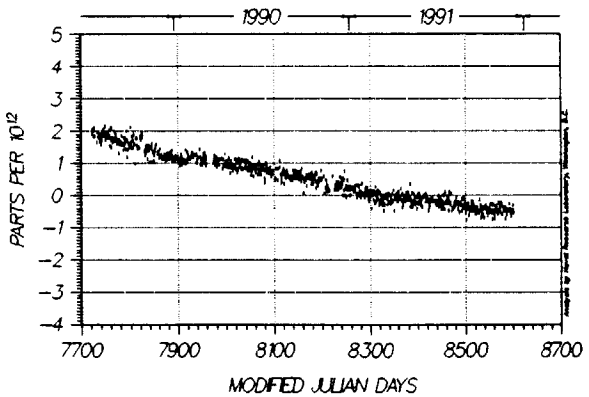

Figure 10. NAVSTAR 13 Frequency Offset.

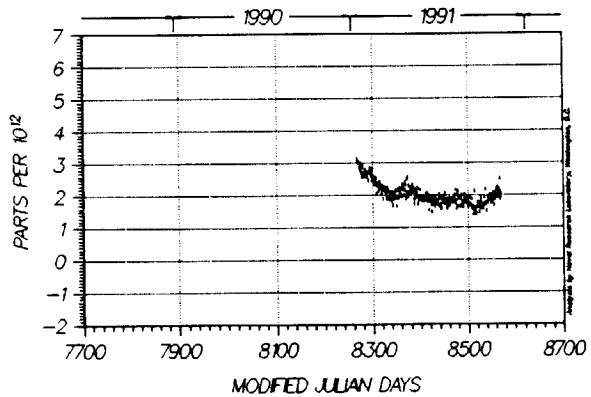

Figure 11. NAVSTAR 16 Frequency Offset.

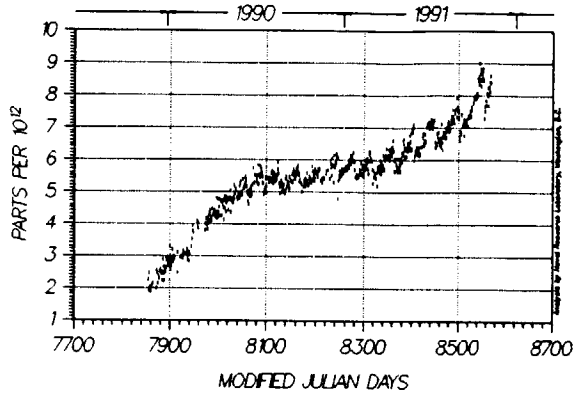

Figure 12. NAVSTAR 19 Frequency Offset.

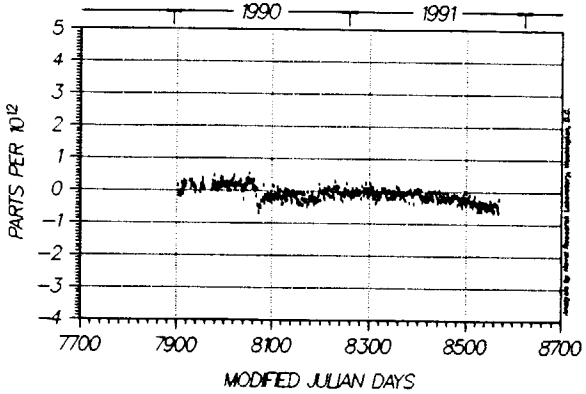

Figure 13. NAVSTAR 17 Frequency Offset.

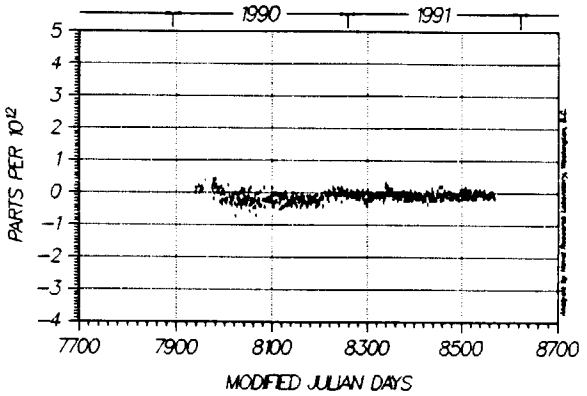

Figure 14. NAVSTAR 18 Frequency Offset.

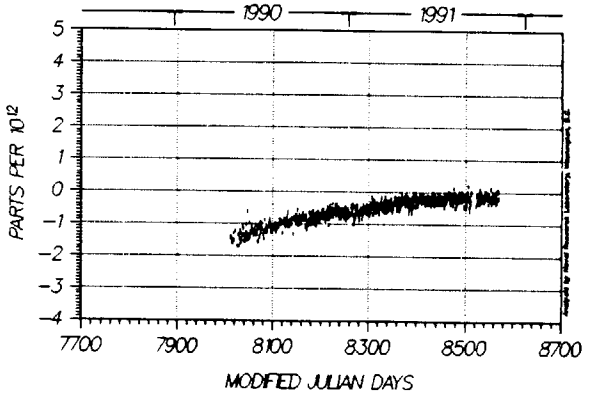

Figure 15. NAVSTAR 20 Frequency Offset.

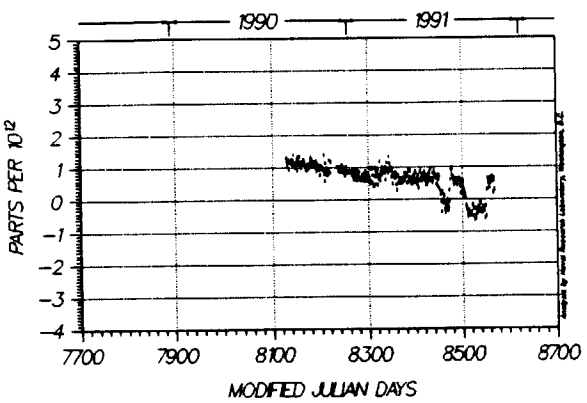

Figure 16. NAVSTAR 21 Frequency Offset.

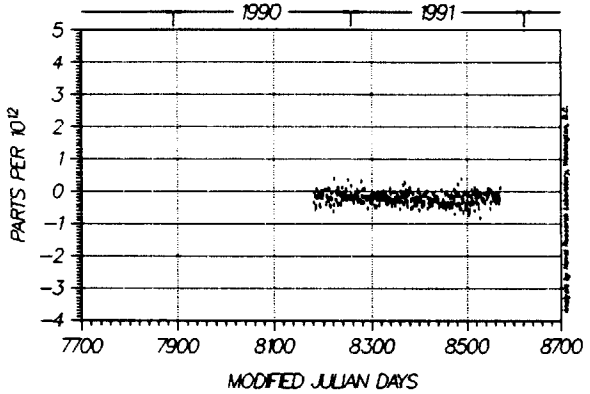

Figure 17. NAVSTAR 15 Frequency Offset.

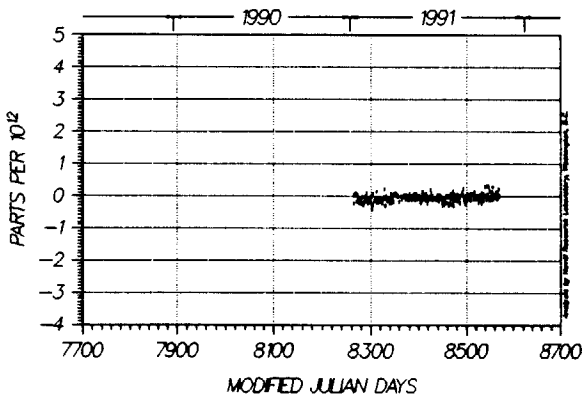

Figure 18. NAVSTAR 23 Frequency Offset.

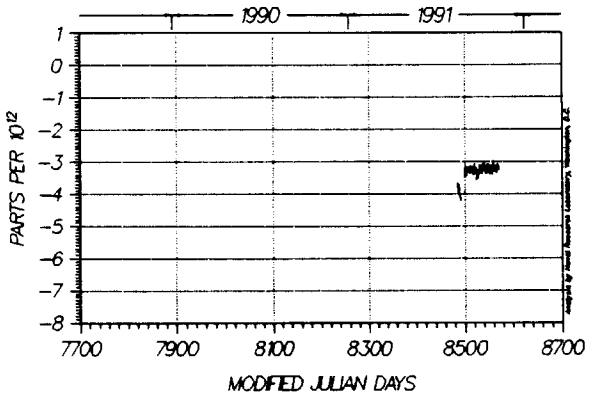

Figure 19. NAVSTAR 24 Frequency Offset.

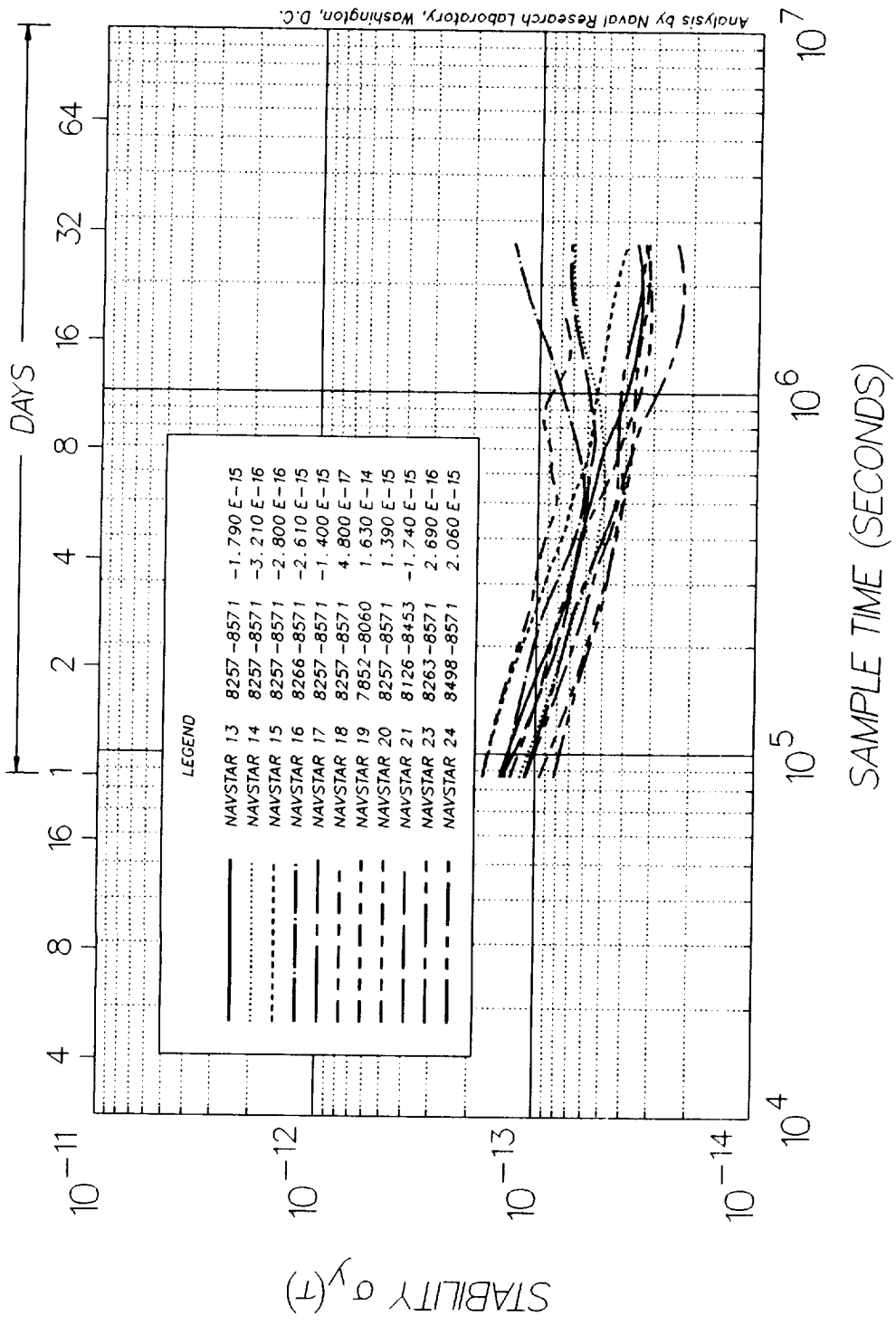

Figure 20. Block II Composite Stability.

THE ROLE OF THE CONSULTATIVE COMMITTEE ON INTERNATIONAL RADIO (CCIR) IN TIME AND FREQUENCY*

Roger E. Beehler
National Institute of Standards and Technology
325 Broadway
Boulder, CO 80303

Abstract

The Consultative Committee on International Radio (CCIR) is a technical advisory group that, within the International Telecommunications Union (ITU), provides formal Recommendations, technical advice, and technical information related to the allocation and use of the radio spectrum. The CCIR does its work through a number of separate Study Groups, each of which deals primarily with one or more radio-based services recognized by the ITU. One of these, Study Group 7, is called "Science Services" and deals with, among other things, time and frequency services and related topics. This part of CCIR is probably best known for its development and implementation of the UTC time system in 1972. The U.S. national Administration develops proposed Recommendations and provides other technical input to the CCIR through an organization of U.S. Study Groups that parallel those functioning internationally. Both the private and government sectors participate actively under the general oversight of the U.S. State Department and its U.S. CCIR National Committee. Current and projected future activities of U.S. and international Study Group 7 will be described, including some examples of current Recommendations, Handbooks, and other documentation that might be useful for those working with time and frequency applications.

INTRODUCTION

The Consultative Committee on International Radio (CCIR) is one of several international organizations that play an important role in time and frequency activities. These organizations may be grouped roughly into three main categories as illustrated in Figure 1: those that deal primarily with the "standards" aspects of time and frequency (for example, the definition of the second); those that are concerned mainly with the scientific aspects; and those that are involved more with the regulatory aspects affecting time and frequency dissemination services. The standards-related organizations shown on the left side of the chart derive from the Treaty of the Meter and include, at the highest level, the General Conference of Weights and Measures (CGPM) and the International

Committee of Weights and Measures (CIPM). These bodies, acting upon the technical advice of its consultative committees, such as those for the definition of the second (CCDS) and the meter (CCDM), adopted the current definition of the second in terms of the cesium atom. The International Bureau of Weights and Measures (BIPM) serves as an international measurement laboratory and includes a Time Section in Paris, which has important responsibilities for the timing community in terms of maintaining and coordinating the international UTC and TAI international atomic time scales. These responsibilities were previously handled by the former International Time Bureau (BIH).

A number of scientifically oriented international organizations also have strong interest in time and frequency and make important contributions to the field. The United Nations Educational, Scientific, and Cultural Organization (UNESCO) includes an International Council of Scientific Unions (ICSU). Two of its member organizations, the International Astronomical Union (IAU) and the International Radio Science Union (URSI), have particularly strong interest in time and frequency from the points of view of astronomical time and radio-signal propagation, respectively. One of the permanent service organizations established by ICSU, the International Earth Rotation Service (IERS), has direct impact on time and frequency services and other operations by having responsibilities for determining and announcing the dates for insertion of leap seconds into the UTC time scale. The IERS also determines and announces the value of the difference between UTC and the UT1 astronomical time scales that is included on most standard time and frequency broadcasts.

The third type of organization important to time and frequency and the principal one of interest for this discussion is the regulatory structure briefly outlined on the right side of Figure 1. The parent organization is the International Telecommunications Union (ITU) which, while maintaining an affiliation with the United Nations, traces its roots back to 1885. Under terms of the International Telecommunications Convention the ITU is charged to, among other things, "study technical and operating questions relating specifically to radiocommunications without limit of frequency range, and to issue recommendations on them ..." The ITU, among many other functions, issues and updates the International Radio Regulations that play a major role in regulating how the radio spectrum, including that used by standard time and frequency broadcast services, is allocated and used. The ITU depends heavily on its technical advisory body, the CCIR, in all of its activities relating to the various radio-based international services. The Consultative Committee on International Telephone and Telegraph (CCITT) performs a similar role in the area of telephone and telegraph communications. One of the CCIR Study Groups, Study Group 7, is assigned specific responsibility for the Standard-Frequency and Time-Signal Service, which includes time and frequency broadcasts operating in the specific frequency bands allocated by the ITU.

CCIR OBJECTIVES, ORGANIZATION, AND WORKING METHODS

The CCIR has three principal objectives:

1. to provide the technical bases for use by administrative radio conferences and radiocommunication services for efficient use of the radio-frequency spectrum and the geostationary-satellite orbit, bearing in mind the needs of the various radio services;

2. to recommend performance standards for radio systems and technical arrangements which assure their effective and compatible interworking in international telecommunications; and

3. to collect, exchange, analyze, and disseminate technical information resulting from studies by the CCIR, and other information available for the development, planning, and operation of radio systems, including any necessary special measures required to facilitate the use of such information in developing countries.

In order to address these objectives the CCIR has formed 10 Study Groups, the majority of which deal with one or more radiocommunication services as defined by the ITU. Other Study Groups deal with more general topics, such as propagation, spectrum management, and inter-service sharing and compatibility issues. As revised by the 1990 CCIR Plenary Assembly, the current Study Groups are:

Study Group 1:	Spectrum Management Techniques
Study Group 4:	Fixed-Satellite Service
Study Group 5:	Propagation in Non-Ionized Media
Study Group 6:	Propagation in Ionized Media
Study Group 7:	Science Services
Study Group 8:	Mobile, Radiodetermination, and Amateur Services
Study Group 9:	Fixed Service
Study Group 10:	Sound Broadcasting Services
Study Group 11:	Television Broadcasting Services
Study Group 12:	Inter-service Sharing and Compatibility

In addition there are two other groups which deal with certain interactions with the CCITT and common CCIR vocabulary issues.

The CCIR's activities relating to time and frequency are now conducted within a recently reorganized Study Group 7, called "Science Services." Prior to May, 1990, this group's responsibilities were carried out in two separate Study Groups: Study Group 2 (Space Research and Radioastronomy) and the old Study Group 7 (Standard Frequencies and Time Signals). The new "Science Services" Study Group 7 is further subdivided into the following 4 working groups, known as Working Parties:

WP 7A:	Time and Frequency Services;
WP 7B:	Space Research;
WP 7C:	Earth Exploration and Meteorological Satellites; and
WP 7D:	Radio and Radar Astronomy.

The 1990 CCIR Plenary Assembly, in setting up this structure, authorized the following "Scope" statement for WP 7A: "Dissemination, reception, and coordination of standard-frequency and time-signal services, including the application of satellite techniques, on a world-wide basis." With a narrow interpretation of this scope statement, the CCIR and Study Group 7 might seem to be interested only in those aspects of time and frequency that relate directly to standard time and frequency broadcast services, such as WWV, that use the specific frequencies allocated to the Standard-Frequency and Time-Signal Service. As will be indicated later, however, the CCIR has traditionally adopted a much broader view of its scope in the time and frequency area and, in fact, has expanded its interests significantly beyond the narrow topic of standard frequency and time broadcasts using the allocated bands.

The international CCIR organization is, for the most part, mirrored in the U.S. by a parallel national structure of Study Groups charged with developing documentation proposals in various forms that reflect the views of U.S. organizations (public and private) and the U.S. government. For example, there is a U.S. Study Group 7 and a U.S. Working Party 7A that deals with time and frequency matters. Participation is open to any organization with interests in the subject involved. Historically, the most active organizations participating in the work of WP 7A include the National Institute of Standards and Technology (NIST), the U.S. Naval Observatory (USNO), the National Aeronautics and Space Administration (NASA), Jet Propulsion Lab (JPL), and the Applied Physics Lab (APL) of Johns Hopkins University.

CCIR working methods are currently undergoing a significant streamlining process, designed to shorten the time required for approval and publication of important Recommendations and to reduce operating costs, particularly at the international level. Typically, proposals for new or revised documentation (for example, Recommendations, Reports, Questions to be studied, Handbook contributions) are generated by various national Administrations. In the case of the U.S. time and frequency area, this occurs in a series of 3-4 meetings of WP 7A conducted before each international CCIR Working Party meeting. Documents approved by WP 7A are then submitted to the full U.S. Study Group 7 for revision or approval. The next step is a review by the U.S. CCIR National Committee, consisting of all U.S. Study Group Chairmen, frequency management personnel, and other private and government representatives. This part of the review process permits coordination with other U.S. Study Groups and the State Department. Approved documents are then forwarded to Geneva as input documents for the next international meeting. U.S. proposals, along with those from other nations, are considered by the international Working Party meetings and then forwarded in appropriate form to the following international Study Group meetings. The full Study Group either accepts or rejects each document. Those that are accepted either go directly to Administrations for final approval by correspondence (urgent Recommendations) or are sent on to the next CCIR Plenary Assembly. The approval process for Recommendations can thus take as little as a few months or as long as several years.

CCIR IMPACT ON TIME AND FREQUENCY ACTIVITIES

CCIR actions can affect time and frequency in several ways: (1) frequency allocations and their use; (2) formal Recommendations relating to the operation of Standard-Frequency and Time-Signal Service broadcasts; (3) other Recommendations relating to time and frequency activities, such as standards, time scales, dissemination, and coordination; and (4) other information outputs in the form of Reports, Recommendation texts, and Handbooks. Each of these aspects is discussed in more detail below.

ALLOCATION ASPECTS

Frequency allocations are usually made by World Administrative Radio Conferences. General WARC's are held at least every 20 years, and special ones dealing with a subset of radio services are held more often as needed. Appropriate CCIR Study Groups prepare technical Reports for these allocation conferences, providing background information on such issues as propagation considerations, sharing possibilities, and preferred frequencies and bandwidths. A complete table of allocations for all frequency bands, including sharing constraints where appropriate, is published

by the ITU as part of the Radio Regulations.

Currently (1991), the following frequency allocations are assigned to the Standard-Frequency and Time-Signal Service:

1. 20 kHz ± 0.05 kHz
2. 14-19.95 kHz, 20.05-70 kHz, 72-84 kHz (Region 1), and 86-90 kHz (Region 1) Stations operating in these bands are permitted by footnote to broadcast time and frequency signals with full protection rights.
3. 2.5 MHz ± 5 kHz
4. 5 MHz ± 5 kHz
5. 10 MHz ± 5 kHz
6. 15 MHz ± 10 kHz
7. 20 MHz ± 10 kHz
8. 25 MHz ± 10 kHz
9. 400.1 MHz ± 25 kHz
10. 4202 MHz ± 2 MHz (space-to-Earth)
    6427 MHz ± 2 MHz (Earth-to-space)
11. 13.4-14.0 GHz (Earth-to-space)
    20.2-21.2 GHz (space-to-Earth)
12. 25.25-27.0 GHz (Earth-to-space)
    30.0-31.3 GHz (space-to-Earth)

Allocation 1 was formerly used by WWVL in the U.S. but is currently inactive. The low-frequency allocations in 2 are footnote allocations under which stations such as WWVB in the U.S., HBG in Switzerland, and DCF77 in Germany operate. Allocations 3-8 are those used by various high-frequency services such as WWV and WWVH in the U.S. Allocation 9 was obtained in 1971 in anticipation of a WWV-type service from satellites. To date it has not been used for this purpose. All these allocations mentioned thus far have "primary" status, which means that they have guaranteed protection under the Radio Regulations and do not have to share with other services. The allocation pairs in allocations 10-12 are footnote allocations and are subject to some constraints according to the Radio Regulations.

While some of the time and frequency allocations are clearly capable of supporting time transfer at the highest possible accuracy levels (for example, the pairs of high-bandwidth satellite allocations), the main use to date has been for the widespread LF and HF broadcast services, providing only modest accuracy capabilities by today's standards. However, such services offer many other advantages in terms of wide coverage, low cost of receivers, reliable reception in many areas, and multiple sources for UTC time. The vast majority of users, even in today's high-technology environment, simply do not require accuracies beyond that offered by many LF and HF services. Thus, these allocations and CCIR's role in generating and maintaining them will continue to have important

impact on large numbers of users in the future. On the other hand, many of the more demanding applications for time and frequency are being served in other ways, particularly by making use of opportunities for time-and-frequency transfer using other available services. Two examples are the use of the Global Positioning System (GPS) satellites of the Radiodetermination Service and two-way time transfer through communication satellites operating in the Fixed-Satellite Service. In these cases, of course, the CCIR also plays an important allocation role through its Study Groups 8 and 4, respectively.

RECOMMENDATIONS ON OPERATING STANDARD TIME AND FREQUENCY SERVICES

The CCIR, through its Study Group 7 and Working Party 7A, formulates various formal Recommendations that relate to the operation of broadcast services using those allocations assigned to the Standard-Frequency and Time-Signal Service. Such Recommendations effectively have the force of international law, at least for the more than 150 member nations of the ITU. In the U.S. these Recommendations apply directly to the WWV, WWVH, and WWVB broadcast services operated by NIST and, in the rest of the world, they impact similar services. In addition, some other time and frequency services that do not operate in the allocated bands nevertheless follow many of these Recommendations. The time code transmitted over the U.S. GOES satellites is an example.

The best known Recommendation of this type is CCIR Recommendation 460, which established the UTC (Coordinated Universal Time) system in 1972. Today, UTC is the time disseminated not only from standard time and frequency stations, but also from virtually every generally available source for precise time. Related Recommendations propose using UTC as the general reference for time and frequency measurements and in all international telecommunication activities. Corresponding recommendations from other international organizations such as URSI and the IAU have supported the intent of the original CCIR recommendations.

Another CCIR Recommendation that has proved very useful is one that recommends use of various existing standard time and frequency broadcasts and certain other available signals, such as Loran-C and Omega Navigation System broadcasts, for precise time and frequency references. Detailed operating characteristics and broadcast formats for the various broadcasts are given in an Annex to this Recommendation. CCIR Study Group 7 makes a strong effort to keep this information updated approximately every two years.

Other CCIR Recommendations that impact standard time and frequency broadcasts and their effective use involve topics such as the use of other frequency bands for broadcast services, the avoidance of interference to these services, the use of the "Modified Julian Date," time scale notations, and the international synchronization of time scales. The latter Recommendation is especially important in today's environment since it recommends that the various timing centers maintain their local UTC time scales to within 1 μs of UTC. This tight tolerance is stated as a "desirable goal".

RECOMMENDATIONS RELATING TO OTHER ASPECTS OF TIME AND FREQUENCY

As mentioned earlier, Study Group 7 has historically taken a rather broad view of its scope as defined by the CCIR. The breadth of the current Working Party 7A work program can be seen

from the following listing of the titles of the 9 formal "Questions" that provide the bases for input documentation and related actions:

1. Methods for Improving Terrestrial Frequency and Time Dissemination
2. Stability of Standard-Frequency and Time-Signal Emissions as Received
3. Time Codes
4. Worldwide Dissemination of Time Signals to an Accuracy of 1 μs or Better for Industrial Purposes
5. Techniques for Time Transfer
6. Performance and Reliability of Frequency Standards and Their Use in Time Scales
7. Standard Frequency and Time Signals from Satellites
8. Two-way Time Transfer Through Communication Satellites

To date Working Party 7A has produced several Recommendations in response to this set of Questions that go somewhat beyond the narrow topic of operating the Standard-Frequency and Time-Signal Service. For example, there is now a rather comprehensive Recommendation on "Frequency and Time (Phase) Instability Measures." The latest version of this Recommendation now includes instability measures for clocks, measurement systems, and dissemination systems. Its Annex contains helpful background information and references on instability characterization. There are two Recommendations relating to satellite techniques; a general encouragement to consider satellite methods and a more specific one relating to the use of GPS satellites for timing under varying conditions of intentional signal degradation. Another Recommendation supports the dissemination of time information in coded form without specifying a particular code format. Working Party 7A also generated a Recommendation providing definitions of more than 60 terms commonly used in CCIR time and frequency activities. While the Glossary of Terms is primarily intended for use within the CCIR, efforts have been made in constructing it to coordinate as closely as possible with other vocabulary efforts, such as that being addressed within the IEEE organization.

In recognition of the current and projected future importance of satellite methods, Working Party 7A also operates a special Task Group 7/2, which is charged to consider developing appropriate Recommendations and other documentation relating to satellite time transfer on an expedited basis (next 1-2 year period). It is likely that this group, working partly by correspondence, will propose future Recommendations on the use of GPS and GLONASS, the use of two-way time transfers through communication satellites, and possibly on methods for calibrating delays through ground-station equipment.

CCIR-GENERATED INFORMATION ON TIME AND FREQUENCY

Aside from formal Recommendations, the CCIR also plays an important role by generating, compiling, and publishing useful technical information in several different forms. The intended audience may vary from document to document. In some cases, the information is intended for a rather

restricted audience, for example, the participants in World Administrative Radio Conferences. Other material may be designed for a more general audience of technical engineers or scientists who are not specialists in the particular technical area. Much of the information is also intended to be useful to personnel in developing countries who are responsible for developing or operating radiocommunication systems.

This technical information is published in several different forms. The principal traditional method is the so-called "Green Books" that are published for each Study Group at the completion of each 4-year CCIR working cycle. These Green Books currently contain all the active Recommendations, Reports, and other documentation of the Study Group. The Reports contain factual technical information and analyses which are helpful in producing Recommendations. Under current CCIR policy, the Report form is being de-emphasized and considered more as a temporary internal working document used in the process of developing Recommendations. As a result, there is a current tendency to annex some of this background technical information to the texts of the formal Recommendations. Occasionally, a Study Group may decide to compile information on a particular topic into a Handbook format, which is then published by the CCIR in Geneva. One better known Handbook, produced by Study Group 4, deals with Satellite Communications. Working Party 7A is currently working on two different Handbooks relating to time and frequency. The first, which is expected to be published in 1992, deals with satellite time dissemination. It includes information both of a background nature on topics such as propagation effects, satellite orbits, signal structures, and relativity considerations, as well as more specific information on satellite systems available for time transfer applications. Working Party 7A has recently (1991) decided to produce a second Handbook, tentatively titled "Selection and Use of Precise Frequency and Time Systems." The content will include material on various frequency standards; operational experiences, problems, and pitfalls; time scale aspects; time and frequency measurements and characterization; and some uses for frequency sources. The Handbook will be prepared by a group of international experts from Working Party 7A.

Any of the ITU/CCIR publications may be ordered directly from the ITU by contacting: International Telecommunications Union, General Secretariat - Sales Section, Place des Nations, CH-1211, Geneva, Switzerland.

CONCLUSION

The CCIR is one of several international organizations that play an important role in international aspects of time and frequency. It is the key organization in matters relating to the allocation and use of the radio spectrum for time and frequency dissemination services. Its impact goes well beyond the formal Standard-Frequency and Time-Signal Service, however, in terms of providing Recommendations and technical information in a variety of forms. The Recommendations and other publications are useful for technical professionals working with time and frequency applications but who are not specialists in the field.

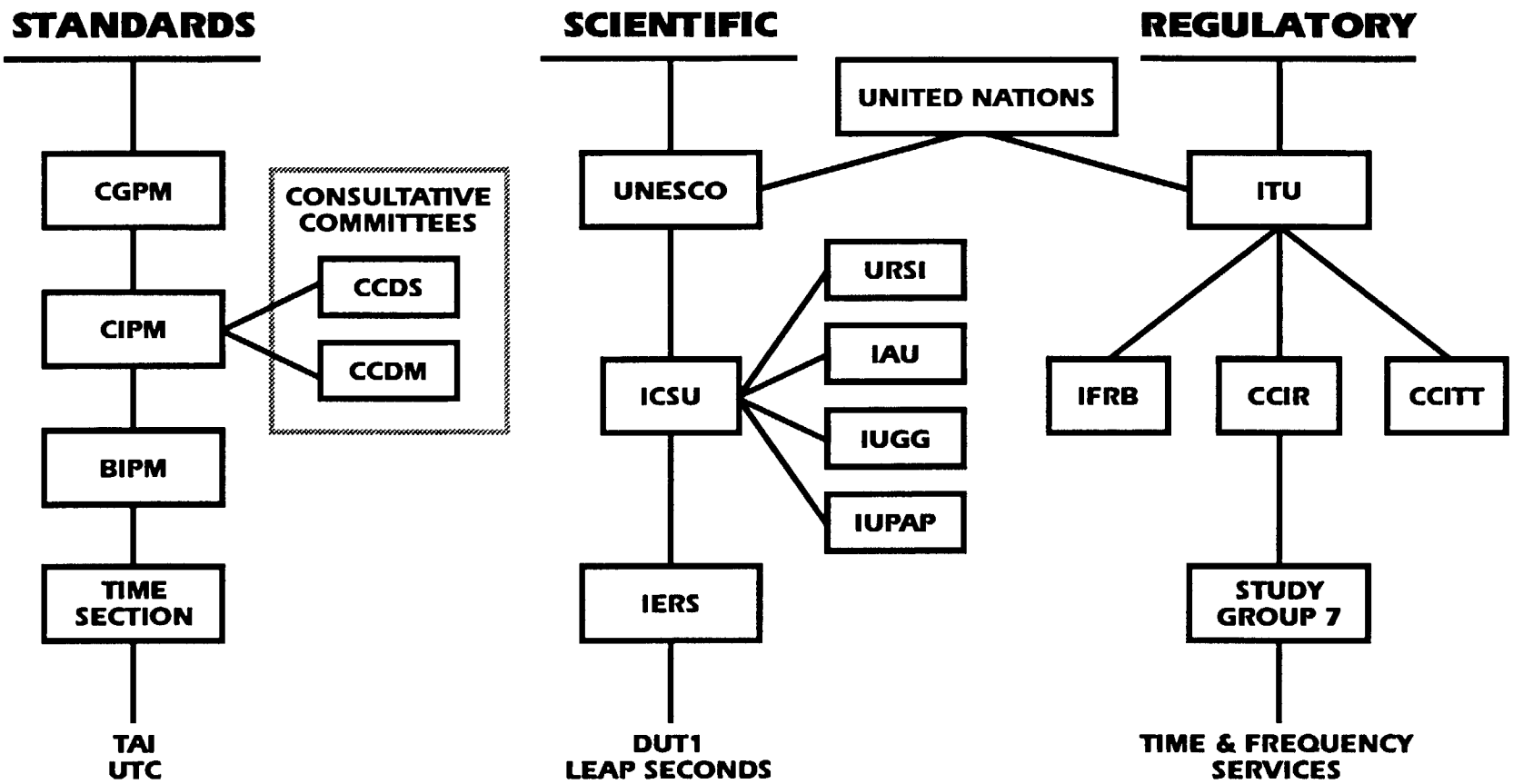

Figure 1. International Organizations With an Impact on Time and Frequency. For simplicity only those suborganizations are shown that are relevant to time and frequency.

QUESTIONS AND ANSWERS

Dr. Gernot Winkler, NIST: Just a suggestion to add to this excellent review. Maybe we should mention the glossary. It is a document which is still under consideration and which needs inputs and coordination with existing vocabularies and which is a real problem like all of these efforts.

Mr. Beehler: Yes, very good, it is certainly an important document. It was listed on one of the slides, but we feel that it is very important that we can agree on definitions of terms that are commonly used in time and frequency. As Dr. Winkler mentioned, we try to coordinate this as much as possible with other activities, so it is a changing document. We keep updating it and, most recently, we have been interacting very strongly with the IEEE vocabulary group. We have been able to agree on definitions for many of the terms in the glossary. I think that there are sixty some now. The IEEE has accepted many of these and we have made a few revisions at their request also.

Clark Wardrip, BFEC: Roger, how does one acquire some of these documentations?

Mr. Beehler: The main mechanism is to acquire them directly from the ITU in Geneva. I have included in the written paper the address to write to. They will send you a price list and so on. As far as I know, they are not generally available in the US.

ACCURACY OF GPS TIME TRANSFER VERIFIED BY CLOSURE AROUND THE WORLD

W. Lewandowski, G. Petit and C. Thomas
Bureau International des Poids et Mesures
Pavillon de Breteuil
92312 Sèvres Cedex, France

Abstract

The precision of time transfer over intercontinental distances by the GPS common-view method, using measurements of ionospheric delays, precise ephemerides provided by the DMA and a consistent set of antenna coordinates, reaches 3-4 ns for a single 13-min measurement, and decreases to 2 ns when averaging several measurements over a period of one day. It is thought that even this level of precision can be bettered by improving the ionospheric measurements, the ephemerides of the satellites and the antenna coordinates.

In the same conditions, an estimation of the accuracy is attained by using three intercontinental links encircling the Earth to establish a closure condition: The three independant time links should add to zero. We have computed such a closure condition over a period of thirteen months using data recorded at the Paris Observatory in Paris (France), at the Communications Research Laboratory in Tokyo (Japan) and at the National Institute for Standards and Technology in Boulder, Colorado (USA). The closure condition is verified to within a few nanoseconds but a bias, varying with time, can be detected.

1. INTRODUCTION

The excellence of worldwide time unification depends on the quality of the clocks kept by national timing centers and on the means of time comparison. Rapid development in the use of the Global Positioning System since 1983 has led to major improvements in the precision and accuracy of the metrology of time. Using commercially available GPS time receivers, time comparisons can easily be performed with an accuracy of 10 to 20 nanoseconds over intercontinental distances. However, it is possible to improve this performance by removal of systematic errors. In GPS time transfer, the three principal sources of error are the local antenna coordinates, the broadcast ionospheric model and the broadcast ephemerides. A thirteen-month experiment in which three long-distance time links are combined with simultaneous reduction of these error sources allows us to check the precision of the time transfer, and its accuracy through satisfaction of a closure condition.

2. THE EXPERIMENT

Three long-distance time transfer links between the Paris Observatory in Paris (OP), the Communication Research Laboratory in Tokyo (CRL), and the National Institute of Standards and

Technology in Boulder, Colorado (NIST) have been computed using the common-view method [1], for a 393-day period, from 1990 June 16 (MJD 48058) to 1991 July 13 (MJD 48450).

The GPS data taken at the three sites correspond to the international schedule issued by the Bureau International des Poids et Mesures for the establishment of TAI. Ionospheric delay measurements are performed by dedicated dual-frequency codeless GPS receivers, and precise ephemerides are provided by the US Defense Mapping Agency. Detailed characteristics of the three time links can be found in [2], with the description of the procedures used to obtain accurate antenna coordinates and to correct for ionospheric and ephemerides errors.

3. RESULTS AND DISCUSSION

The corrections to the antenna coordinates being already introduced, four different cases may be distinguished for each time link and for the closure, which is the sum of the three links:

* non-corrected values.
* values corrected for ephemerides only.
* values corrected for ionosphere only.
* values corrected for both ephemerides and ionosphere.

For each case, a Vondrak smoothing [3] is performed on the values UTC(Lab1) – UTC(Lab2). The smoothing used acts as a low-pass filter with a cut-off period of about 3 days. This period has been chosen as being approximately the limit between the short time intervals, where the measurement noise is dominant, and the longer intervals, where the clock noise prevails. For the closure, the smoothed values are interpolated at normal dates (0h UTC each day) and the interpolated values are simply added.

3.1. PRECISION OF TIME COMPARISONS

A first way to estimate the precision of the measurements is from the standard deviation of the residuals to the smoothed values. This is strictly correct if the smoothing has removed only the measurement noise. Over our whole data set, these residuals range from 10 to 15 ns for the uncorrected data, 8 to 10 ns for the data corrected for ephemerides only, 7 to 12 ns for the data corrected for ionosphere only, and 4 to 5 ns for the data with both corrections.

If the data points are regularly spaced, we can also use the time-domain stability measures $\sigma_y(\tau)$ and $\sigma_x(\tau)$ [4]. Applied to a time link $\sigma_x(\tau)$ allows one to characterize the types of noise that are present. In the case of white noise phase modulation (PM), the value of $\sigma_x(\tau)$ for the data spacing is the standard deviation of the white noise, which directly gives the measurement uncertainty. $\sigma_y(\tau)$ allows us to estimate the frequency stability with which clocks can be compared.

For the link OP–NIST which, being the shortest, has the largest number of data points, we can find two periods of 80 and 75 days respectively without any significant gap in the data. On average there are seven points per day and they are quite regularly spaced, the largest spacing being about 7 hours. Figure 1 presents the values of $\sigma_x(\tau)$ for the data over the period from MJD 48375 to

48450, without correction and with both corrections applied. It appears that white noise phase modulation can be identified for averaging times up to about 3 days without correction, but is not the dominant source for times of one day and over when the corrections are applied. The uncertainty of a single measurement is taken from figure 1 to be about 16 ns without correction, but this value is somewhat biased by the data recorded during the few days around MJD 48440 when Selective Availability was in effect. The measurement uncertainty is about 3 ns when the corrections have been applied.

It should be noted that such a measurement uncertainty makes it possible to access the true performance of the best clocks presently available: by averaging a few measurements over one day, a frequency stability of two or three parts in 10^{14} is realized for the link between two clocks. Thus in figure 2, which represents $\sigma_y(\tau)$ for the link OP−NIST over the same period as in figure 1, the values obtained with corrections applied represent the actual frequency stability of the two clocks for time intervals of one day and over.

For the other 80-day period, from MJD 48080 to 48160, the results are quite similar although the measurement noise is estimated to be at a slightly higher level, as discussed in section 3.3 below.

3.2. ACCURACY TEST: THE CLOSURE AROUND THE WORLD

A test of accuracy is performed by computing the closure around the world via OP, NIST and CRL. Daily values of UTC(OP) − UTC(NIST), UTC(NIST) − UTC(CRL) and UTC(CRL) − UTC(OP) are estimated from the smoothed data points. The resulting daily values of the deviation from closure, for the whole period under study, are shown in figure 3 for the non-corrected data and in figure 4 for the data with both corrections applied.

Figure 4 provides evidence of a gain in accuracy when the time links are computed with both corrections. To characterize and quantify the types of noise involved, figure 5 represents the values of $\sigma_x(\tau)$ for the closure, without correction and with both corrections applied. The gain is by a factor 2 to 3 for all averaging times. If we take into account the fact that the values for one and two days are aliased by the smoothing that has been performed on each link, the closure is relatively well characterized by white noise PM up to 16 days. This is not true for longer averaging times, as it is clear from figure 4 that significant biases exist, and that they vary with time. As an example, the mean value of the closure over consecutive 16-day intervals varies from −2 ns to +9 ns, whereas the standard deviation of the mean, assuming white noise, is 1 ns. The mean values over 16-day intervals have a global average of 4 ns and a standard deviation of 3 ns.

3.3 DISCUSSION OF THE ERROR SOURCES

The major three error sources, that are able to produce both long term biases and short term white noise PM, are those listed earlier in this paper: antenna coordinates, ionospheric delays, satellite ephemerides. While we have tried to minimize these errors, they are still present at some level so we try to estimate them here.

The error on the antenna coordinates has been estimated previously [2]. It could account for a few nanoseconds of residual error in the closure. However this error is roughly constant over the whole period, as the geometry of the common-view observations remains similar for each link. When more

accurate coordinates become available from geodetic campaigns, it will be easy to account for them in the data. Accuracies of a few centimeters should then be obtained, and these will contribute negligibly to the error budget of the time transfer.

The accuracy of the measurements of the ionospheric delay by codeless GPS receivers has been reviewed recently [5]. It is estimated to be a few nanoseconds but it is not easy to characterize the residual effect. It is possible that P-code receivers will be used in the future, but it is not clear how this will improve the measurements. Also, although the global ionospheric activity is going to decrease from its recent maximum, it is not clear if it will be measured more accurately by the GPS receivers.

On the other hand, the ephemerides of the satellites are subject to constant improvement. The DMA processing scheme, for example, is regularly improved [6]. The fact that ephemerides are more accurate in 1991 than in 1990 may be visible in our data: figure 6 represents $\sigma_x(\tau)$ for the link OP−NIST for the two periods of about 80 days mentionned in section 3.1 above. The improvement of the spring-summer 91 period relative to that of summer 90 is quite clear for averaging times of up to one day, where the measurement noise dominates. In the future, ephemerides with sub-meter, or even decimeter, accuracy should become available, which will nearly eliminate this source from the error budget.

Finally it should be noted that the stability of the closure for averaging times of a few days is mainly affected by the many glitches that are apparent in figure 4. A careful review of the data indicates that for the second half of the data set, which corresponds to year 1991, all but one of the glitches are associated with a gap of more than one day in the data of one link. This aliasing effect is less clear for the first half of the data set. This fact also favors an improvement in the quality of the ephemerides with time, although chance cannot be ruled out as an explanation.

4. CONCLUSIONS

Results of a 13-month time transfer experiment indicate that, after corrections for ionosphere and ephemerides have been applied, the precision of a single intercontinental GPS time transfer measurement is about 3-4 nanoseconds, and can be reduced by averaging. The accuracy is estimated also to be 3-4 nanoseconds, but significant biases, which vary with time, are still present. It is thought that the accuracy, as estimated by the closure condition, is improving with time, and will eventually reach 1 ns if the ionospheric contribution can be reduced to below this level.

ACKNOWLEDGEMENTS

The authors are grateful to P. Uhrich at OP, M.A. Weiss at NIST, and M. Imae at CRL for providing ionospheric measurements. They thank also the DMA for providing the GPS precise ephemerides, and the US National Geodetic Survey for providing access to the GPS broadcast ephemerides.

REFERENCES

[1] D. W. Allan, M. A. Weiss, *"Accurate time and frequency transfer during common-view of a GPS satellite"*, Proc. 34th Annual Symposium on Frequency Control, pp. 334-346, 1980.

[2] W. Lewandowski, G. Petit, C. Thomas, M. A. Weiss, *"GPS time closure around the world using precise ephemerides, ionospheric measurements and accurate antenna coordinates"*, Proc. 5th European Frequency and Time Forum, pp. 215-220,1991.

[3] J. Vondrak, *"A contribution to the problem of smoothing observational data"*, Bull. Astron. Inst. Czechoslovakia, 20, pp.349-355, 1969.

[4] D.W. Allan, M.A. Weiss, J.L. Jespersen, *" A frequency-domain view of the time-domain characterization of clocks and time and frequency distribution systems"*, Proc. 45th Annual Symposium on Frequency Control, in press, 1991.

[5] D. Davis, M.A. Weiss, K. Davies, G. Petit, *"Improving GPS time transfer with the NIST ionospheric measurement system"*, Proc. of the 4th ION International Technical Meeting, in press, 1991.

[6] E. R. Swift, personal communication, DMA.

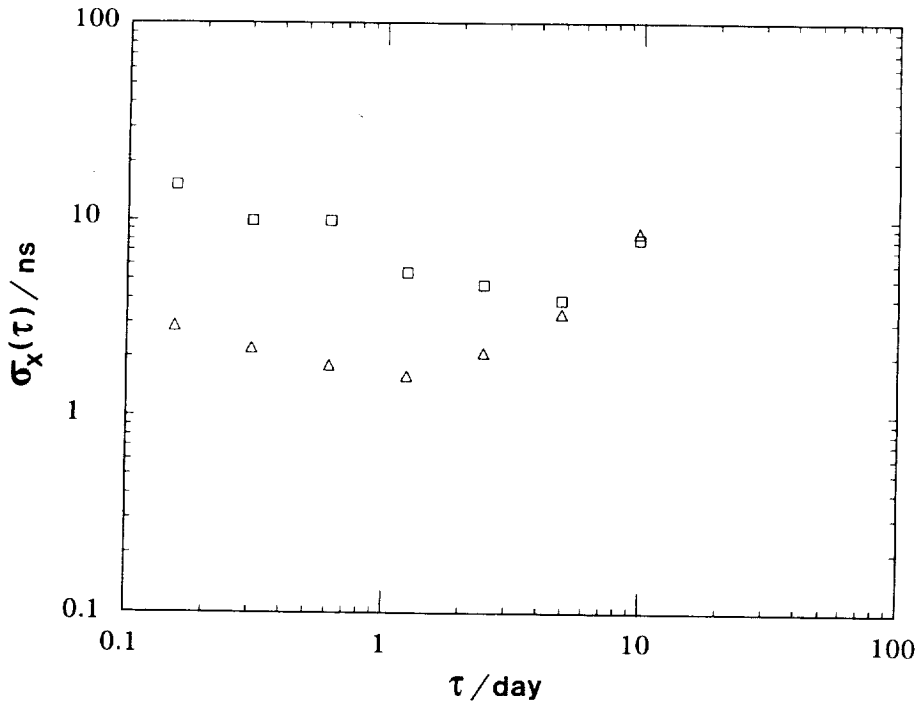

FIGURE 1: *Square root of the time variance $\sigma_x(\tau)$ of the link OP-NIST over the period MJD 48375 to 48450, for data without corrections (squares) and for data corrected using precise ephemerides and measured ionospheric delay (triangles).*

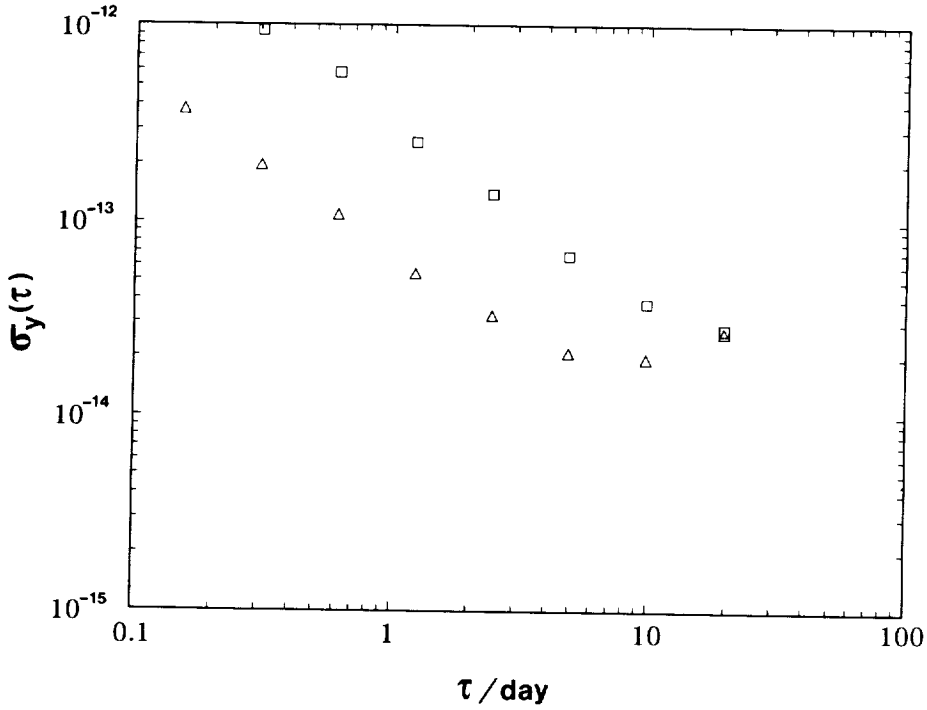

FIGURE 2: *Square root of the two-sample Allan variance $\sigma_y(\tau)$ of the link OP-NIST over the period MJD 48375 to 48450, for data without corrections (squares) and for data corrected using precise ephemerides and measured ionospheric delay (triangles).*

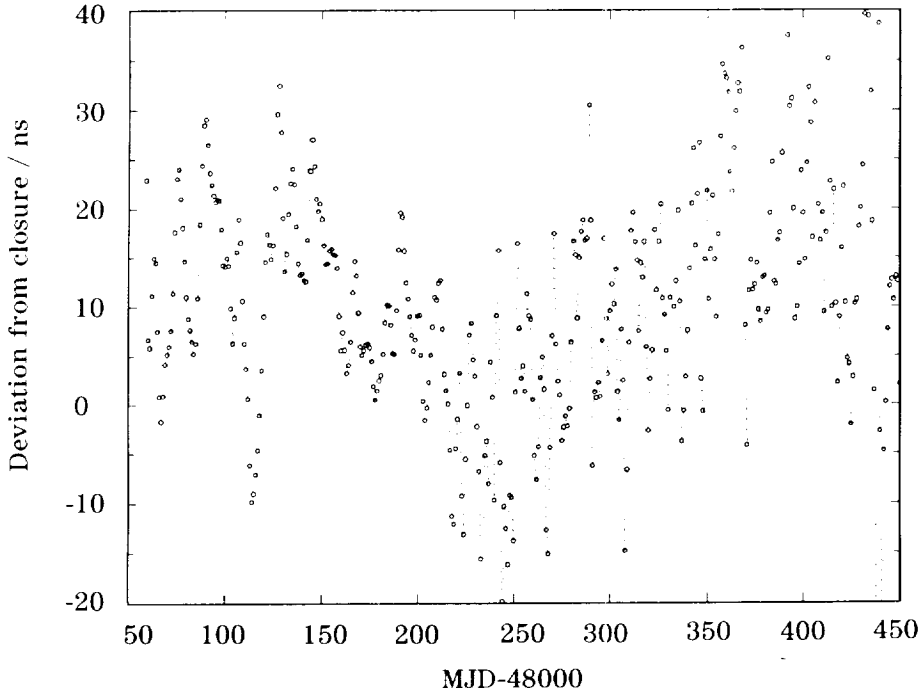

FIGURE 3: *Deviation from closure around the world via OP, NIST and CRL with non-corrected data.*

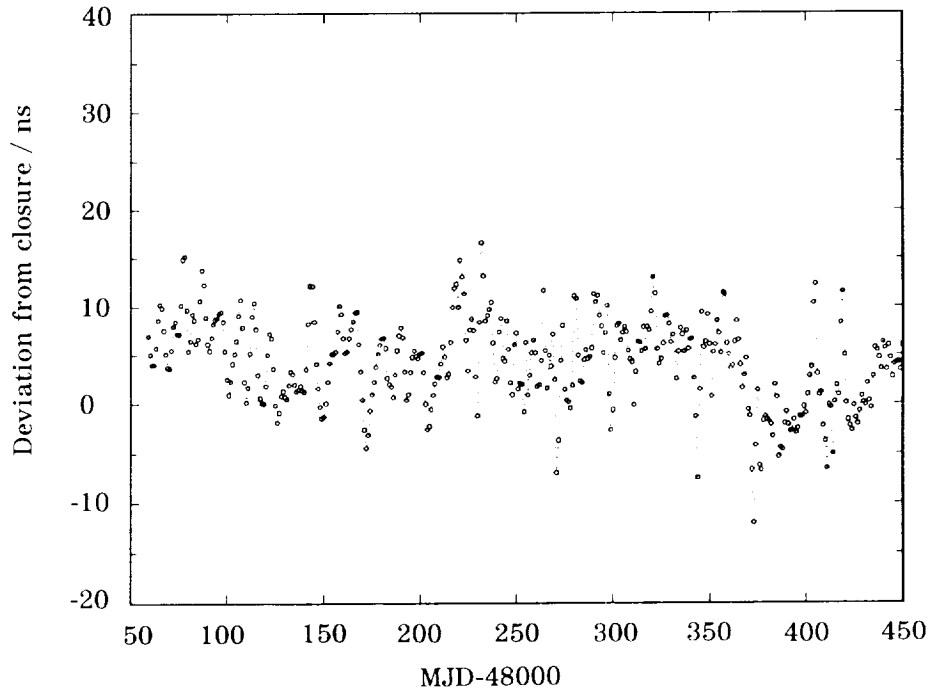

FIGURE 4: *Deviation from closure around the world via OP, NIST and CRL with data corrected for precise ephemerides and measured ionospheric delay.*

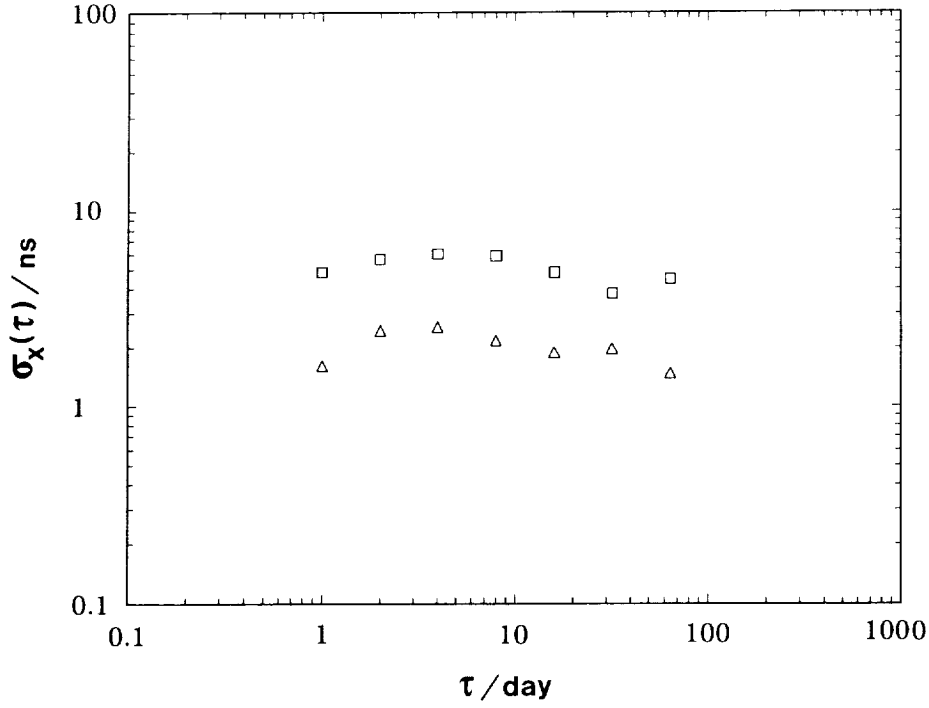

FIGURE 5: *Square root of the time variance $\sigma_x(\tau)$ of the deviation from closure over the period MJD 48058 to 48450, for data without corrections (squares) and for data corrected using precise ephemerides and measured ionospheric delay (triangles).*

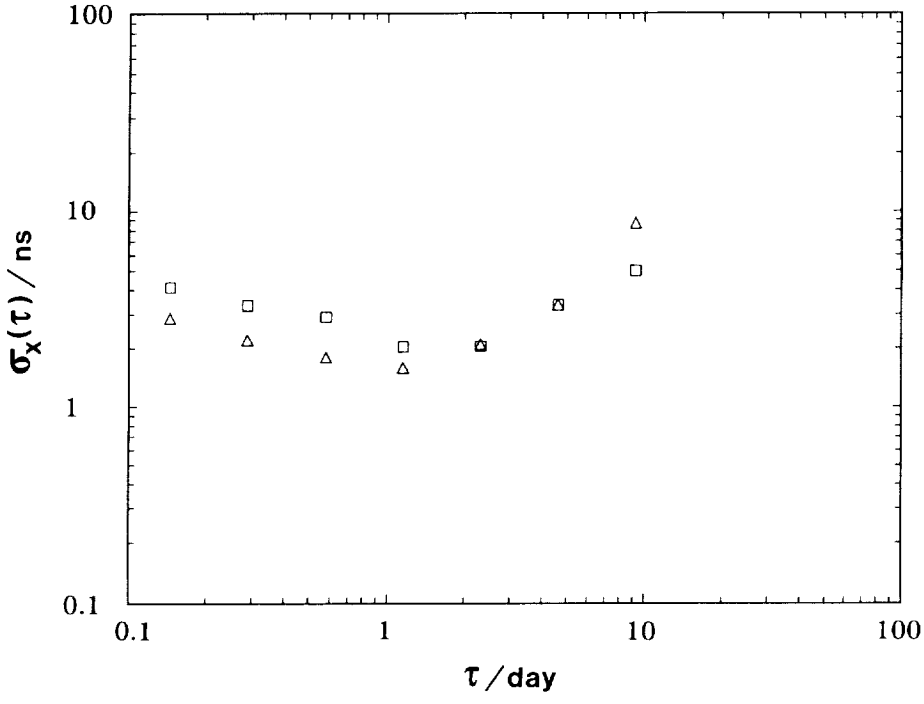

FIGURE 6: *Square root of the time variance $\sigma_x(\tau)$ of the link OP-NIST for data corrected using precise ephemerides and measured ionospheric delay over the periods MJD 48080 to 48160 (squares) and MJD 48375 to 48450 (triangles).*

QUESTIONS AND ANSWERS

David Allan, NIST: Would it not have been better to measure the frequency stability using Mod $\sigma_y(\tau)$? Since you have white PM, you can see the frequency more quickly and actually optimally.

Mr. Petit: We generally use $\sigma_y(\tau)$.

Mr. Allan: But Mod $\sigma_y(\tau)$ gives a better measure of what the clock is doing with white PM.

Dr. Gernot Winkler, USNO: In other words, you are not interested in frequency, but in time interval? Would you like to comment on the possibility of keeping the data at the stations, as with time, it is possible that by using all of the data, to improve your position with respect to the GPS reference system.

Mr. Petit: Yes, of course, that is a way of improving the station coordinates. That has actually been used, but clearly it is not the best way to get good coordinates. I would prefer to get very close to a VLBI or satellite laser ranging station and use precise surveying to obtain the station coordinates. That should give centimeter accuracy and will be done in the very near future.

Dr. Winkler: I agree, but my comment was addressed to the general time user, who cannot easily connect to a such a primary reference point as defined by laser or VLBI. He may well be better served by keeping all the records.

Mr. Petit: That is what we have done. Last June we introduced for all station clocks, a list of coordinates to be used that were derived from the time data themselves. This was because before this time, the station coordinates were uncertain by several meters. This was clearly visible in the time data. We now think that all the time stations are accurate to a level below one meter.

Dr. Martin Levine, SAO: Can you tell me the meaning, on the slide, of "raw data"? Is that the data as output by the receiver? Does it include the built in broadcast ionospheric and tropospheric corrections?

Mr. Petit: Yes, that is the data as it comes. It is the regular output of the receiver, with the built in broadcast corrections, but has not been processed to include our corrections.

COMPARISON OF GLONASS AND GPS TIME TRANSFERS BETWEEN TWO WEST EUROPEAN TIME LABORATORIES AND VNIIFTRI

P. Daly
Department of Electronic and Electrical Engineering
University of Leeds
Leeds LS2 9JT, United Kingdom

N. B. Koshelyaevsky
All Union Institute for Physical, Technical & Radiotechnical Measurements – VNIIFTRI
Mendeleevo, Moscow region, 141570, USSR

and

W. Lewandowski, G. Petit, C. Thomas
Bureau International des Poids et Mesures
Pavillon de Breteuil
92312 Sèvres Cedex
France

Abstract

The University of Leeds built a GPS/GLONASS receiver about five years ago and since then has provided continuous information about GLONASS time and its comparison with GPS time. For the last two years VNIIFTRI and some other Soviet time laboratories have used Soviet-built GLONASS navigation receivers for time comparisons. Since June 1991, VNIIFTRI has been operating a GPS time receiver on loan from the BIPM. This offered, for the first time, an opportunity for direct comparison of time transfers using GPS and GLONASS. This experiment shows that even with relatively imprecise data recording and processing, in terms of time metrology, GLONASS can provide continental time transfer at a level of several tens of nanoseconds.

INTRODUCTION

Two global space navigation systems, the American GPS and the Soviet GLONASS, are at the about same stage in the development of their space segments, but they are unequally used for international time comparisons. GPS, with a large range of time-specialized receivers, has for many years been exploited worldwide for accurate time transfer [1], while GLONASS is still used on an experimental basis by only a few laboratories [2]. Although at present GPS time transfer

fully satisfies the needs of time metrology, it is the sole method which is operationally effective and the lack of redundancy is felt. There is also a growing concern about GPS degradation by Selective Availability. In this context GLONASS is of increasing interest as an excellent additional source.

For about five years the University of Leeds (Leeds, UK) has operated a GPS/GLONASS timing receiver built in-house, and provided continuous information about GLONASS time and its comparison with GPS time. For the last two years VNIIFTRI (Mendeleevo, Moscow Region, USSR) and some other Soviet time laboratories have used Soviet-built GLONASS navigation receivers for time comparisons. Since June 1991, VNIIFTRI has been operating a commercial GPS time receiver on loan from the BIPM. This offers, for the first time, an opportunity for direct comparison of time transfers by GPS and GLONASS between laboratories of West Europe and USSR. Values of UTC(LDS)–UTC(SU) and UTC(OP)–UTC(SU), as provided by GPS and by GLONASS, are reported together with estimates of the errors involved.

This experiment covers the period from July 4 to September 8, 1991. The GPS Block II satellites have been deleted from GPS common-view treatment when they were affected by Selective Availability (beginning of July [3]).

GLONASS AND GPS OBSERVATIONS AT THE UNIVERSITY OF LEEDS

The time laboratory of the University of Leeds is equipped with the three following time receivers:

- **TRIMBLE 5000A**

  This receiver is programmed with the BIPM international common view schedule and refers to UTC(LDS).

- **TRIMBLE 4000A**

  This receiver generates a 1 PPS synchronised on UTC(USNO) as broadcast by GPS satellites with an uncertainty of 100ns [1]. This signal is the external reference of the Leeds University GPS/GLONASS receiver.

- **Leeds University GPS/GLONASS receiver**

  This receiver performs the measurements of UTC(USNO)–GPS time and UTC(USNO)–GLONASS time.

The three receivers are connected to the one omni-directional antenna and use the same set of coordinates expressed in the WGS 84 reference frame with an uncertainty of 3 m.

In the past GLONASS observations by GPS/GLONASS Leeds University receiver provided a series of navigational solutions expressed in the Soviet reference frame (SGS 85) used by GLONASS satellites. These results agreed with WGS 84 coordinates within 5 meters.

The delays of the receivers are known approximately within 20ns. The schema of the whole installation is illustrated in Figure 1.

The GPS/GLONASS receiver performs the measurements almost continuously, observing all available GLONASS satellites and a selection of GPS satellites (all Block I and 2 Block II satellites). For a given satellite, the receiver starts measurements of UTC(USNO)- satellite time and does this once a second for 180s. This data is stored, filtered to remove outliers and averaged. The typical standard deviation for 180s averages is 50ns. During one day the receiver performs roughly 340 tracks of 180s, 75% of them corresponding to GLONASS satellites. Daily averages of tracks have a standard deviation around 50ns for both GPS and GLONASS data. These results are not corrected for ionospheric or tropospheric delays.

The GPS observations produced by the GPS TRIMBLE 5000A receiver are used in this study for common-view time transfer with VNIIFTRI. Previous analysis of common-view time transfer between the University of Leeds and the Paris Observatory showed that the TRIMBLE 5000A data is affected by a noise which limits the uncertainty of such a time transfer to 10- 15ns. This noise is partly due to uncertainty in the coordinates. Several attempts have been made to improve the Leeds antenna coordinates by the BIPM method [4]. All of them produced the coordinates with uncertainties of several meters which indicates other than geometrical error sources. The TRIMBLE 5000A receiver was programmed during this experiment with the 37 13-minute tracks of the BIPM international tracking schedule no 17 including all Block I and Block II satellites. About 25 tracks were available each day for this experiment.

GLONASS AND GPS OBSERVATIONS AT THE VNIIFTRI

The USSR State Time & Frequency Service (VNIIFTRI) is located in Mendeleevo, near Moscow. This organization is responsible for the maintenance of the Soviet national time reference UTC(SU). An ensemble of high-quality atomic clocks, mostly hydrogen masers, is operated.

GLONASS time observations at VNIIFTRI have been carried out, since 1989, using a Soviet-built commercially available receiver A-724 designed for aircraft navigation. The receiver is supplied with 1 PPS and 5 MHz provided by the VNIIFTRI master clock. The readings of the master clock are corrected "a posteriori", to transform them into UTC(SU). The receiver uses a fixed model of the ionospheric delay and does not correct observations for tropospheric delay. The antenna coordinates are expressed in the Soviet Geodetic System 85 (SGS 85) with estimated uncertainty of order 5m provided by a series of navigational solutions.

There are three to five observations per day of UTC(SU)–GLONASS time. All of them are performed at low elevations in the direction of East. With the limited model of ionosphere and the lack of tropospheric correction this particular configuration of observations can produce a bias.

As an estimated uncertainty for the daily averages of UTC(SU)–GLONASS time, we adopted the value of 50ns as already deduced for the observations at the University of Leeds.

Since June 1991 VNIIFTRI has operated a commercial GPS time receiver on loan from the BIPM referred to SU master clock. The delay of the GPS receiver was determined by the comparison with the Paris "on line" GPS receiver [5]. The coordinates of its antenna were determined by the BIPM method [4] and expressed in the ITRF reference frame [6] with an uncertainty of 1m. The receiver is programmed with 37 daily tracks according to the BIPM tracking schedule no 17. About 35 tracks were available each day for this study. The GPS installation at the VNIIFTRI allows the comparison of the UTC(SU) in common view mode to the West European time laboratories with an accuracy of a few ns.

GLONASS TIME TRANSFER BETWEEN MENDELEEVO AND WESTERN EUROPE

To realize time transfer between Leeds and Mendeleevo via GLONASS we use the measurements of UTC(SU)–GLONASS time, UTC(LDS)–GPS time, and GLONASS time–GPS time. Combination of these three values gives UTC(SU)–UTC(LDS).

VNIIFTRI provides the daily values of UTC(SU)–GLONASS time with uncertainty of 50ns and Leeds provides the measurements of UTC(LDS)–GPS time realized by the TRIMBLE 5000A receiver. The 25 or so available daily measurements of UTC(LDS)-GPS time are smoothed at the BIPM to provide daily values at 0h UTC with an uncertainty of 15ns.

To obtain the values of GLONASS time–GPS time we use the daily averages of UTC(USNO)–GLONASS time and UTC(USNO)–GPS time provided by Leeds with uncertainties of 50ns. We believe that these two measurements are affected partly by the same systematic biases (uncertainty of the UTC(USNO) as locally reconstituted, ionospheric delay, coordinates,...). For this reason when we remove UTC(USNO) by differencing the above measurements to obtain the daily values of GLONASS time–GPS time, we adopt the uncertainty of 50ns for this difference.

For the final values of UTC(LDS)–UTC(SU) obtained from this process we adopt an uncertainty of 70ns, which is derived from the quadratic combination of the involved uncertainties.

We have also realized the comparison of UTC(SU) with the Paris Observatory time scale UTC(OP) using both systems GLONASS and GPS. Paris Observatory operates a commercial GPS time receiver connected to UTC(OP). The comparison of UTC(SU) with UTC(OP) via GLONASS was realized in a similar way to that described above, the values UTC(LDS)–GPS time replaced by UTC(OP)–GPS time. The 35 or so available daily measurements of UTC(OP)–GPS time are smoothed at the BIPM to provide daily values at 0h UTC with an uncertainty of 7ns. The final values of UTC(OP)–UTC(SU) via GLONASS are provided with an estimated uncertainty of 70ns.

GPS COMMON-VIEW TIME TRANSFER BETWEEN MENDELEEVO AND WESTERN EUROPE

The common-view time transfer between Mendeleevo and Leeds was realised with about 25 tracks available, and between Mendeleevo and Paris with about 35 daily tracks available. In both cases a Vondrak smoothing [7], which acts as a low-pass filter with a cut-off period of about 3 days, was performed on the common-view values. For this experiment, the smoothed values are interpolated for 0h UTC of each day. The precision of both time links is estimated from the residuals of the smoothed values. Over the period of this study, the residuals ranged from 12 to 15ns for the UTC(LDS)–UTC(SU) and 3 to 4 ns for the UTC(OP)–UTC(SU).

COMPARISON OF GLONASS AND GPS

Time transfer via GLONASS between Mendeleevo and two West European laboratories was realized with an estimated uncertainty of 70ns. The GPS common-view time transfer provided a time link between Mendeleevo and Leeds with an uncertainty of about 15ns and between Mendeleevo and Paris with an uncertainty of about 4ns. Accordingly the comparison of GLONASS with GPS for

the Leeds–Mendeleevo link has an estimated uncertainty of 80ns and for Mendeleevo–Paris, 70ns.

The daily differences between the two methods are presented in figures 2 and 3. Use of the modified Allan variance (Figures 4 and 5) allows us to characterize the noise affecting the values of comparison for each of the two links. For both links the data exhibit white phase noise up to an averaging time of about 4 days. This justifies computation of mean values for periods of duration up to 4 days and corresponding standard deviations of the mean. For a 4-day averaging period the results are as follows:

Period MJD	Mean values of GPS-GLONASS for UTC(OP)-UTC(SU)	Stand. dev.	Mean values of GPS-GLONASS for UTC(LDS)-UTC(SU)	Stand. dev.
	(ns)	(ns)	(ns)	(ns)
48440–48443	-64	2	-91	2
48444–48447	-44	5	-55	13
48448–48451	-54	2	-70	6
48452–48455	-48	2	-44	10
48456–48459	-45	5	-44	5
48460–48463	-40	2		
48464–48467	-43	9		
48468–48471	-43	10	-52	10
48472–48475	-42	6	-42	7
48476–48479	-48	9	-57	12
48480–48483	-44	4	-27	10
48484–48487	-44	9	-43	8
48488–49491	-12	5	-28	17
48492–48495	-2	2	-5	2
48496–48499	12	3	18	4
48500–48503	-3	8	2	15
48504–48507	-3	4	-10	14

This table shows a fairly constant bias of about −45ns between the two techniques for the first period of the experiment (MJD period: 48440–48487) and for the two links. A sharp change then occurs, reducing the bias to roughly 0ns. As we do not know the differential delays between GLONASS equipments, the bias does not have meaning, and this comparison relates only to precision. The sharp change in the bias could be explained by the low elevation of the observations and their orientation in only one direction (far East) at Mendeleevo. In the absence of good estimates of ionospheric delay the changes in solar activity should have a significant effect on the measurements. Also frequent changes in the hour of observations at Mendeleevo could introduce a bias into measurements caused by ionospheric delay. The ionospheric conditions change dramatically between day and night.

One can also observe a lower noise level for the link between Paris and Mendeleevo than that between Leeds and Mendeleevo. This can be explained mainly by more accurate coordinates at Paris.

We have computed the mean values of the differences GPS–GLONASS for each of two links for the 68 days of this experiment. As the noise is not white for this period we adopt the root mean square of the residuals to the mean as an estimation of the confidence of the mean. The mean value for the link Paris–Mendeleevo is −33ns with estimated confidence 24ns and for the link Leeds–Mendeleevo respectively −38ns and 32ns. Both estimates of confidence for the period of this study are significantly lower that for our estimation of the uncertainties of the involved measurements (70ns and 80ns). This indicates that our estimates are too conservative. However, a longer period of comparison is required to obtain more precise specification of the uncertainty of this comparison.

CONCLUSION

This study shows that even with relatively imprecise data recording and processing, in terms of time metrology, GLONASS can provide continental time transfer at a level of several tens of nanoseconds. By introducing common-views, this performance should be significantly improved. Further possible improvements are the, at least partial, removal of ionospheric and tropospheric delays. More precise determination of GLONASS antenna coordinates in the SGS 85 reference frame is another task. The development of automatic GLONASS receivers dedicated especially for time transfer would be a most significant breakthrough.

REFERENCES

[1] W. Lewandowski, C. Thomas, *"GPS time transfer,"* in Proc. of the IEEE, Special Issue on Time and Frequency, pp. 991-1000, July 1991.

[2] P. Daly, G. T. Cherenkov, N. B. Koshelyaevsky, S. Pushkin, *"Satellite time transfer between UTC(USNO) and UTC(SU) using Navstar GPS and GLONASS,"* in Proc. 4th Institute of Navigation Technical Meeting, pp. 199-206, September 1991.

[3] W. Lewandowski, G. Petit, C. Thomas, *"The Need for GPS Standardization,"* in these Proceedings.

[4] B. Guinot, W. Lewandowski, *"Improvement of the GPS Time Comparisons by Simultaneous Relative Positioning of the Receiver Antennas,"* in Bulletin Géodésique, 63, pp. 371-386, 1989.

[5] W. Lewandowski, *"Determination of differential time corrections between the GPS time receivers located at the Observatoire de Paris, the Observatoire de la Cte d'Azur and the Technical University of Graz,"* Rapport BIPM-91/6, 1991.

[6] W. Lewandowski, *"High Accuracy Ground-Antenna Coordinates for GPS Time Transfer,"* in Proc. IAG Symposium G2-Permanent Satellite Tracking Networks for Geodesy and Geodynamics, Vienna, August 1991, in press.

[7] J. Vondrak, *"A Contribution to the Problem of Smoothing Observational Data,"* in Bull. Astron. Inst. Czechoslovakia, 20, pp. 349-355, 1969.

ACRONYMS

BIPM	Bureau International des Poids et Mesures
GLONASS	Global Navigation Satellite System
GPS	Global Positioning System
IERS	International Earth Rotation Service
ITRF	IERS Terrestrial Reference Frame
LDS	University of Leeds, Leeds, United Kingdom
OP	Paris Observatory, Paris, France
SA	Selective Availability of GPS
SGS	Soviet Geodetic System
TAI	International Atomic Time
USNO	US Naval Observatory, Washington D.C.
UTC	Coordinated Universal Time
UTC(LDS)	Coordinated Universal Time realized by the University of Leeds
UTC(OP)	Coordinated Universal Time realized by the Paris Observatory
UTC(SU)	Coordinated Universal Time realized by the VNIIFTRI
VNIIFTRI	Vsiesoiuznyi Naouchno Issliedovatielskii Institut Fiziko Tieknichieskih i Radiotieknichieskih Izmierienii (All Union Institute for Physical, Technical & Radiotechnical Measurements).
WGS	World Geodetic System

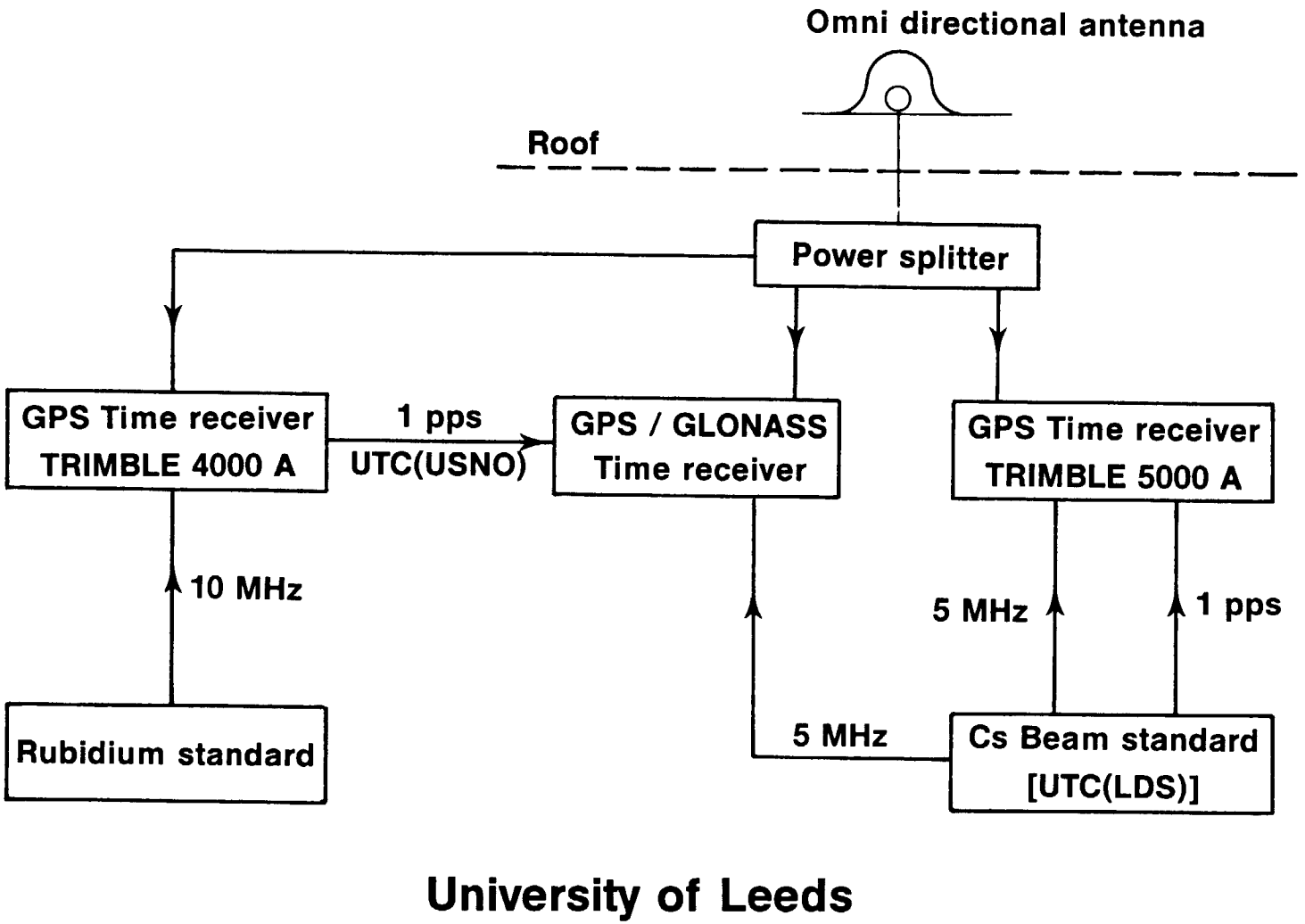

FIGURE 1. *Schema of installation of time receivers at the University of Leeds.*

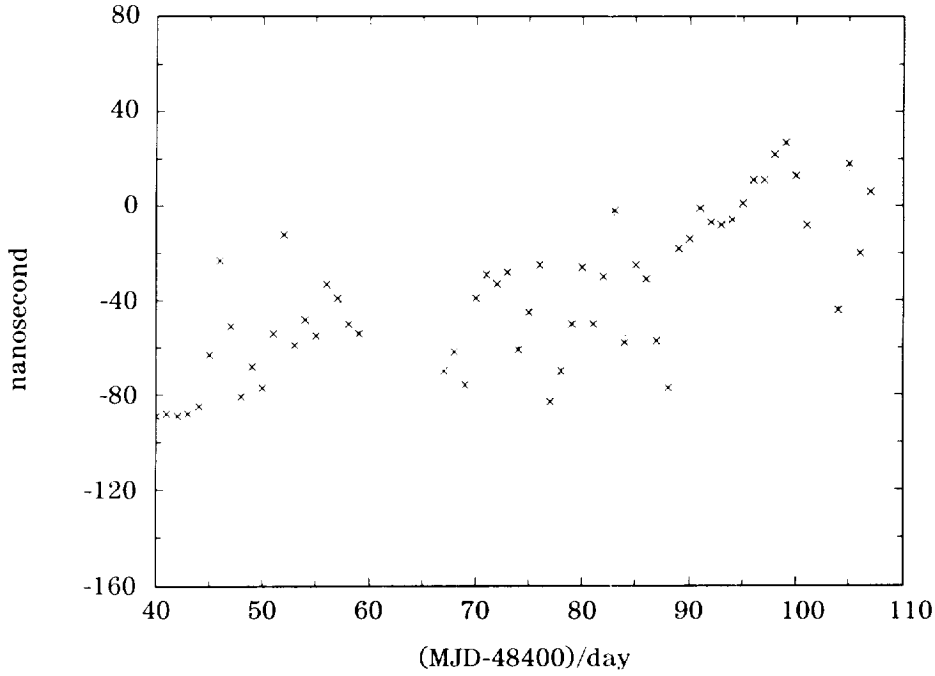

FIGURE 2. *UTC(LDS)-UTC(SU) as obtained by GPS minus UTC(LDS)-UTC(SU) as obtained by GLONASS+GPS. Daily values interpolated for 0h UTC.*

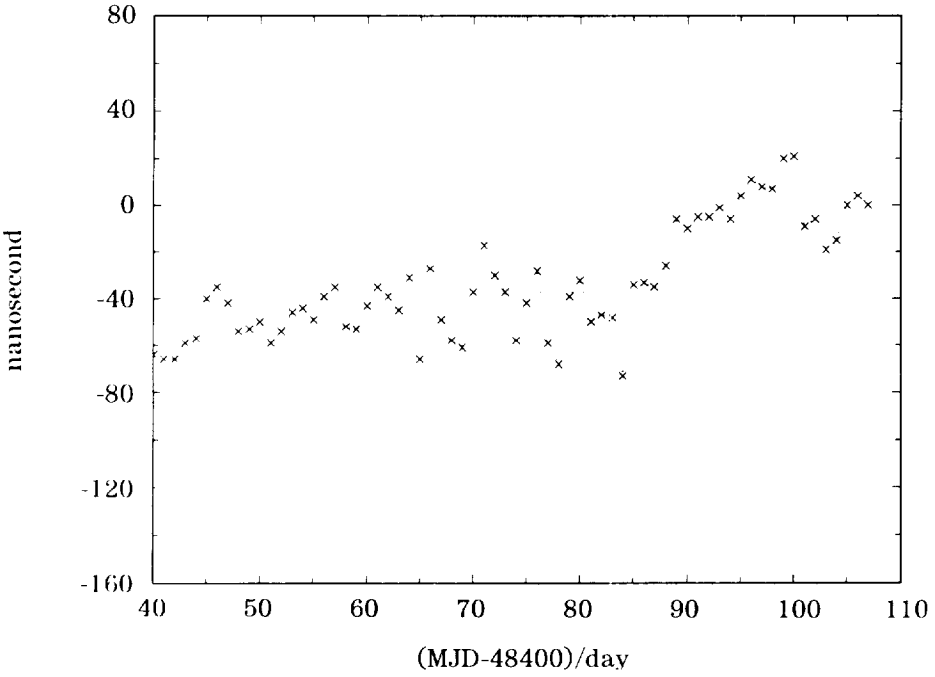

FIGURE 3. *UTC(OP)-UTC(SU) as obtained by GPS minus UTC(OP)-UTC(SU) as obtained by GLONASS+GPS. Daily values interpolated for 0h UTC.*

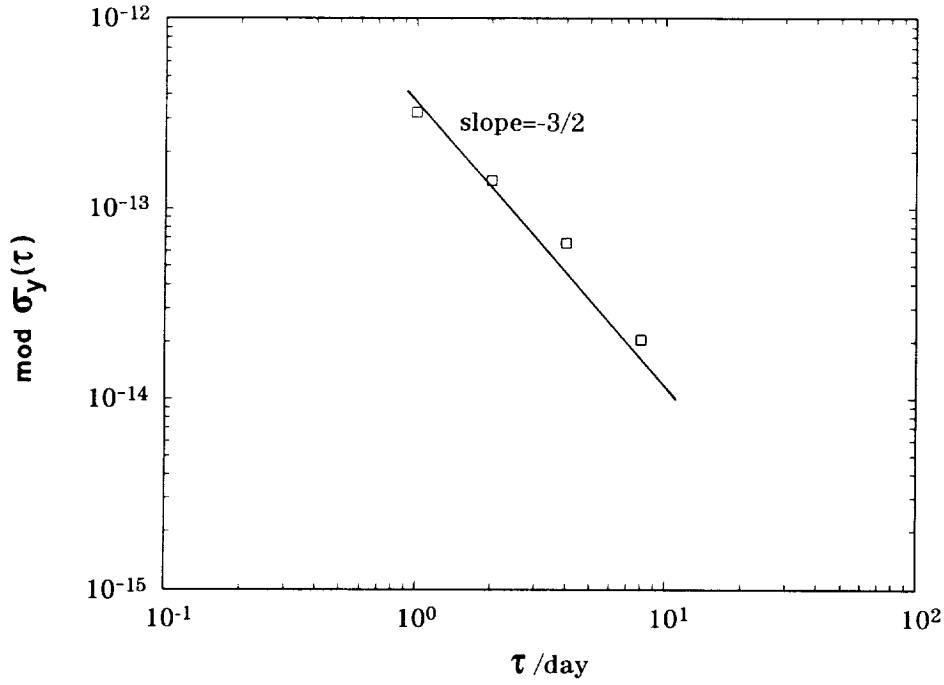

Figure 4. *Square root of the modified Allan variance of the differences presented in Figure 2.*

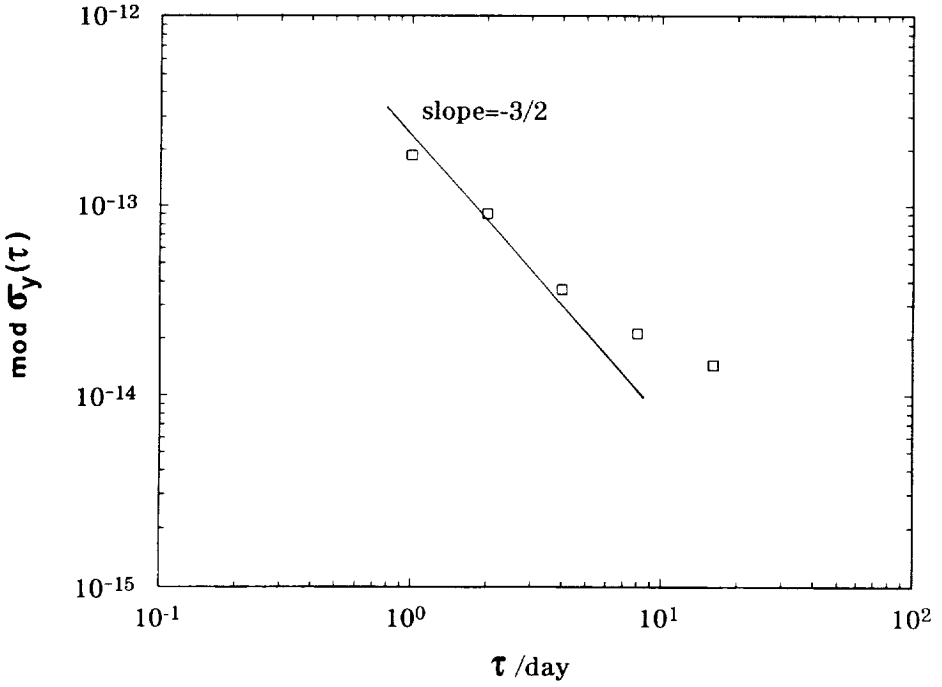

Figure 5. *Square root of the modified Allan variance of the differences presented in Figure 3.*

A Proposed Time Transfer Experiment Between the USA and the South Pacific

John Luck
Australian Surveying and Land Information Group
Canberra, ACT Australia

John Dunkley
Defence Science and Technology Organisation
Salisbury, SA Australia

Tim Armstrong
Department of Scientific and Industrial Research
Lower Hutt, New Zealand

Al Gifford, Paul Landis, Scott Rasmussen and Paul Wheeler
Department of Defense
Washington, DC USA

Tom Bartholomew
The Analytic Sciences Corporation (TASC)
Linthicum, MD USA

Sam Stein
Timing Solutions Corporation
Boulder, CO USA

Abstract

This paper describes the concept, architecture and preliminary details of an experiment directed towards providing continuous Ultra High Precision (UHP) time transfer between Washington, DC; Salisbury, SA Australia; Orroral Valley, ACT Australia; and Lower Hutt, New Zealand. It further describes a proposed method of distributing UTC(USNO) at a high level of precision to passive users over a broad area of the South Pacific.

The concept is based on active two-way satellite time transfer from the United States Naval Observatory (USNO) to the proposed USNO Master Clock West (MCW) in Wahiwa, HI USA at the 1 nanosecond level using active satellite two-way time transfer augmented by Precise Positioning Service (PPS) of the Global Positioning System (GPS). MCW would act as an intermediate transfer/reference station, again linked to Salisbury at the 1 nanosecond level using active satellite two-way time transfer augmented by PPS GPS. From this point, time would be distributed within the region by two methods. The first is an existing TV line sync system using an Australian communications satellite (AUSSAT K1) which is useful to the 20 nanosecond level. The second approach is RF ranging and multilateration between Salisbury, Orroral Observatory, Lower Hutt and the AUSSAT B1 and B2 to be launched in 1992. Orroral Observatory will provide precise laser ranging to the AUSSAT B1/B2 retro reflectors which will reduce ephemeris related time transfer errors to below 1 nanosecond. The corrected position will be transmitted by both the time transfer modem and the existing TV line sync dissemination process. Multilateration has the advantage of being an all weather approach and when used with the laser ranging technique will provide a precise measurement of the propagation path delays. This will result in time transfer performance levels on the order of 10 nanoseconds to passive users in both Australia and New Zealand.

Introduction

The motivation for the proposed time transfer experiment between the USA and the South Pacific is rooted in the Geographic Dependence and Latitude Effects Study (GDLE)[1]. The GDLE Study was conducted over a 12 month period to: 1) investigate and verify the existence of reported anomalies, the so-called "bowing effect", in GPS time recovery; 2) analyze the potential causes; and 3) determine procedures to maximize overall time transfer performance in the geographic area of interest. Based on the preliminary results of the GDLE we have concluded that the major GPS time transfer anomalies result from uncompensated clock and ephemeris errors in the daily GPS uploads. In addition we see evidence of a long term effect which may be seasonal in nature.

As further motivation, the Australian Government has a requirement to coordinate their national time scale to UTC and to disseminate this time nationally and regionally to a high level of accuracy. Their specific aim is to guarantee the general availability of UTC(AUS) at an accuracy approaching 1 nanosecond (1σ) through a low cost operational service. As part of that process they are interested in evaluating alternative methods of acquiring and distributing time. With the advent of SA/AS it has become important to explore independent techniques which can be used to augment GPS.

The proposed experiment is therefore designed to support the participants interests by: 1) providing long term monitoring of GPS one-way time recovery using Standard Positioning Service (SPS) and PPS receivers; 2) implementing a high precision, GPS independent, time transfer linkage between UTC(USNO) and Salisbury Australia; and 3) testing an improved regional TV line synch time dissemination method.

It is believed that the proposed experiment would, in conjunction with the previously described GDLE, eliminate or confirm the presence of long term variations in GPS time transfer to Australia. It would also establish a mechanism for nanosecond level time transfer to Australia and exercise an improved regional precise time distribution methodology.

Concept

Refering to Figure 1, the concept is based on active two-way Ku-band satellite time transfer, using the Satellite Business Systems SBS-5, from the United States Naval Observatory (USNO) in Washington, DC (Figure 2) to the proposed USNO Master Clock West (MCW) in Wahiwa, HI USA (Figure 3). This technique has been used operationally at the sub-nanosecond level and is expected here to be usable to 1 nanosecond. MCW would operate as an intermediate transfer/reference station, again linked to Salisbury at the 1 nanosecond level using active two-way X-band satellite time transfer modems, via the Defense Satellite Communications System (DSCS) Western Pacific Satellites, augmented by SPS and PPS GPS.

From Salisbury (Figure 4), time would be distributed within the region by two methods. The first is an existing TV line sync system using an Australian communications satellite (AUSSAT K1) (Figure 5). With after-the- fact ephemeris correction, this is useful to the 20 nanosecond level. The second approach is an improvement to be implemented with the AUSSAT B1/B2 satellites to be launched in 1992. These satellites will be fitted with retro reflectors. Laser ranging from the Orroral Observatory and RF ranging (clock difference measurements) from Salisbury, Hobart, and Sydney along with ionospheric corrections will ultimately reduce ephemeris related time transfer errors to the 1 nanosecond level. The corrected position will be transmitted by the existing TV line sync dissemination process and the time transfer modem.

As a future enhancement, multilateration (RF ranging) from Salisbury, Orroral Valley and Lower Hutt offers the advantage of all weather operations and when used with he laser ranging technique will provide a higher precision measurement of the propagation path delays. This will result in time transfer performance levels on the order of 10 nanoseconds to passive users in both Australia and New Zealand.

Elements of the Experiment

1. ENSEMBLE

The requirements for time-keeping and frequency control at both MCW and Salisbury will be supported by a system known as ENSEMBLE. It is a multi-clock time system capable of keeping stable time and frequency linked to UTC(USNO) based on the use of the Precise Positioning Service (PPS) of the Global Positioning System (GPS).

ENSEMBLE (see Figure 6) will monitor, weight and combine the outputs of up to 8 clocks in a Kalman filter algorithm known as Kalman Aiding Sources Version 2 (KAS-2), similar to the one in use at the GPS Master Control Station (MCS)[2]. KAS-2 is used to create a paper clock within a controlling computer that is the best estimate of the correct time. The frequencies of 2 of the contributing cesium clocks will be steered long-term to UTC-USNO using highly filtered continuous comparisons with GPS. The short term performance of ENSEMBLE is based on the inherent stability of the cesium clocks. For periods of 24 hours or longer the frequency of the clock ensemble is steered to the GPS constellation with the ENSEMBLE software. The steering correction is integrated over several days to eliminate short term upsets.

To insure reliability there are 3 levels of backup which include: 1) system level redundancy in clocks, receivers, computers and time code generators; 2) manual override and operation of ENSEMBLE; and 3) finally the ability to support the entire system with a single stand-alone clock. ENSEMBLE will provide for performance monitoring and fault detection through a set of outputs which will be remotely interfaced to the USNO.

Using PPS GPS, as it is currently operating, ENSEMBLE will provide an absolute time accuracy of <30 nanoseconds (RMS), not-to-exceed 150 nanoseconds (5σ) with respect to UTC(USNO). The frequency stability at one day will be less than $2x10^{-14}$, at ten days less than $1x10^{-14}$, and less than $5x10^{-15}$ at thirty days.

2. Satellite Two-Way Time Transfer Modem

Two way time transfer uses Very Small Aperture Terminals (VSAT) and communication satellites to link time transfer modems at each location. A pulse is transmitted from each end every second and its time of arrival is measured at the other end relative to the local clock (Figure 7). The measurement is equal to the difference between the two clocks plus the delays of the path and hardware. Typical errors in the process, when care is taken to calibrate the equipment and cables, are about a nanosecond.

$$Measurement_{locationA} = Time_A - Time_B + DELAY_{BtoA}$$

$$Measurement_{locationB} = Time_B - Time_A + DELAY_{AtoB}$$

$$Measurement_A - Measurement_B = 2(Time_A - Time_B)$$

If the delays and hardware are equal the difference in clocks A and B can be found by taking half the difference in the two measurements. In practice the two delays are not equal. They differ because of hardware, ionospheric path delays and earth rotation. The hardware differences can be measured by comparing systems before deployment. Path differences caused by the Sagnac effect can be calculated with approximate knowledge of the equipment and satellite locations. The differences in the ionosphere are under 100 picoseconds at the $12 - 14ghz$ operating frequency and the 2 ghz offset between the transmitting and receiving frequencies.

Typically the two way operation is accomplished with a master site and several slave sites (Figure 8). The slave sites will only respond upon command of the master site. Data measurements are exchanged between the two location over the same link that is transmitting the pulse.

The advantages of the two way technique over GPS time transfer include 1) two way does not need accurate information on antenna or satellite locations, 2) tropospheric effects cancel; and 3) ionospheric path delay errors are less than 100 picoseconds. These result in a more accurate time transfer.

The 100 picosecond number for ionospheric path delay is for Ku-band operation. At X-band the delay in each path is higher due to the inverse frequency effect but the difference between transmission and receiving frequency is less. The projected ionosphere errors at X-band are therefore about 150 picoseconds.

To perform two way time transfers between some locations it is necessary to a use an intermediate relay point. The relay point may be equipped with zero, one or two modems. With zero modems the two terminals are cabled together causing the total link noise to be the sum of the two parts. This saves equipment but does not provide time transfers at the relay point. With one modem, sequential time transfer may be done by using the local clock to flywheel between transfers. With two modems, simultaneous transfers may be done thus eliminating any small errors in the relay clock.

3. Orroral Observatory/AUSSAT Time Dissemination

The Australian national system of precise time comparisons embodied in UTC(AUS) is accomplished by measurement of TV signals from AUSSAT supported by orbit information supplied by AUSSAT Belrose and by time measurements from the GPS which provide the relationship of UTC(AUS) to International Atomic Time (IAT) and UTC(BIPM). Precision and accuracy are currently estimated to be on the order of 50 nanoseconds. Precision improves to about 10 nanoseconds when AUSSAT's orbit is improved using GPS results (Figures 5 and 9). The Orroral Laser Ranging System is being upgraded for ranging to retroreflectors on the AUSSAT B spacecraft with 5 cm precision and accuracy for much better orbits. Locally generated GPS orbits, precise base station location and ionospheric calibration, already planned for a national 'zero-order' geodetic network tied to VLBI and laser ranging sites, will add strength and reliability to the TV method.

ABC TV signals transmitted from AUSSAT K1 provide times of arrival (TOA) of arbitrary but well defined sync pulses. These are measured with respect to local clocks at participating stations as shown in Figure 5. The measurement equipment typically includes a 1.5 meter dish, LNA, B-MAC decoder and sync pulse selector, and an ordinary TV set as shown in Figure 9.

If t_0 is the time of transmission, x_i the measured time of reception, T_i the clock error, d_i the receiver delay, e_i the unmodelled random and systematic error such as ionospheric and relativistic effects, and p_i the propagation delay from satellite to station i, then:

$$x_i = t_0 + T_i + d_i + p_i + e_i$$

whence:

$$x_i - x_j = (T_i - T_j) + (d_i - d_j) + (p_i - p_j) + (e_i - e_j)$$

The relative clock error $T_i - T_j$ is readily determined when the relative propagation delay $p_i - p_j$ has been calculated from supplied orbital and receiver location data, provided the relative receiver delay $d_i - d_j$ has been calibrated. Results for the clock differences between the hydrogen masers at Mount Pleasant Observatory in Hobart and the National Measurements Laboratory (NML) in Sydney show a precision of 70 nanoseconds, which includes error contributions from the clocks, the measurements, the ionosphere and the orbit.

Alternatively, when the relative clock error is already known from independent GPS time comparisons at several 'Master' stations, the relative propagation delays $p_i - p_j$ can be calculated and used as pseudo-range differences to improve the spacecraft's orbit which is then applied to the corrections for 'Remote' stations. For this purpose, measurements are taken hourly. The results, when GPS time results from 'Master' stations at NML, Orroral, Telecom Research Laboratories in Melbourne and Yarragadee SLR have been added to solve for semi-major axis, eccentricity, inclination and relative receiver delays (station biases) show a precision of 13 nanoseconds for a 2-day fit after editing some outliers.

AUSSAT orbital positions measured by radar tracking from the Earth Station at Belrose are accurate to 30 metres. The improvement brought about by combining GPS time measurements with the TV measurements is geometrically weak for perigee, node and anomaly solutions, and under threat from the policy of 'Selective Availability'.

The next generation of AUSSAT's, B1 and B2, will be launched in 1992 and will each carry an array of 14 38 mm diameter retroreflectors (James, Steel and Evans, 1990). The range error from the upgraded Orroral laser will be less than 5 cm with a pointing error of 2-3". It would be highly desirable to upgrade the Yarragadee SLR station as well, to add strength to the solution for in-orbit longitude.

The geodetic positions of the AUSSAT and GPS antennas need to be known to better than 30 centimeters to achieve the 1 nanosecond time transfer goal. All participating locations must be located to that accuracy on a common geodetic datum.

Australian fiducial stations located at Orroral, Yarragadee, Tidbinbilla, Alice Springs, Gnangara, and Towns-ville will become the basis for the "zero-order" national network. This network will be integrated with the timing network and will provide the capability for producing accurate coordinates for time transfer, ionospheric corrections for GPS, and a regional GPS orbit determination service.

4. Salisbury/DMA Installation

The installation at Salisbury will be as shown in Figure 4. The time/frequency reference will consist of a truncated version of ENSEMBLE with a single computer, one measurement system, one GPS PPS time recovery receiver, and a minimum of 3 cesium beam frequency standards, at least one of which will be steerable. The ENSEMBLE computer will be directly interfaced to the NRL satellite time transfer modem which will provide regular time transfers from MCW via the DSCS. This is expected to maintain the local ENSEMBLE estimate of UTC(USNO) to within 2 nanoseconds (RMS). The calibrated ENSEMBLE UHP 1 PPS and 5 Mhz outputs will be buffered and supplied to the AUSSAT TV time dissemination system.

The existing DMA monitor station at Salisbury consists of 2 T14100A receivers, an HP5061 cesium frequency standard, an HP5065A rubidium frequency standard, a LORAN C receiver, a computer and a phone modem. It is expected that the DMA system will be upgraded in 1992.

Data Collection and Analysis

The participants have planned to put the elements of the experiment in place over the next 9-12 months. Operation of MCW will begin in the September 1992 time frame with the remaining segments coming on line as equipment and resources become available. It is hoped that data collection can be maintained over a minimum period of 12 months.

Data collection will be designed to build the following data sets:

- Salisbury
  - UTC(USNO) versus local clock
    - via two-way satellite time transfer modem
    - via GPS one-way broadcast
      - real-time using local ENSEMBLE PPS system
      - real-time using local DMA SPS system
      - post-time using both of the above with post-fit DMA GPS ephemerides
  - UTC (AUS) versus local clock
    - via AUSSAT K1
    - via AUSSAT B1/B2 with ephemeris corrections (when available)
- Hawaii
  - UTC(USNO) versus MCW
    - via two-way satellite time transfer modem
    - via GPS one-way broadcast
      - real-time using local ENSEMBLE SPS system
      - real-time using local ENSEMBLE PPS system
      - post-time using local ENSEMBLE PPS system and DMA post-fit GPS ephemerides
    - via common view with USNO (PPS and SPS)

Preliminary plans for data analysis include:

- Difference and compare Salisbury and MCW data sets
  - $UTC(USNO)_{viaPPS/GPS} - UTC(USNO)_{viaTwoway}$
  - $UTC(USNO)_{viaSPS/GPS} - UTC(USNO)_{viaTwoway}$
  - $UTC(USNO)_{viaPPS/GPS} - UTC(USNO)_{viaSPS/GPS}$
  - $UTC(USNO)_{viaAUSSATK1} - UTC(USNO)_{viaPPS/GPS}$
  - $UTC(USNO)_{viaAUSSATK1} - UTC(USNO)_{viaSPS/GPS}$
- Compare two-way time transfer configurations
  - pass-through method in Hawaii
  - direct retransmission in Hawaii
  - sequential transmissions in Hawaii
- Compare time transfer modem ranging performance to existing ranging systems.

References

[1] Beard, R.,Gifford, A., Stebbins, S., Rasmussen S.,and Bartholomew T. "Interim Report on the Geographic Dependency and Latitude Effects Study," Proceedings of the 45th Annual Symposium on Frequency Control, 29-31 May, 1991, Los Angeles, CA, pp. 608-625.

[2] Stein, S. R., "Kalman Ensembling Algorithm: Aiding sources Approach," Proceedings of the Third International Time Scale Algorithm Symposium, 12-13 september, 1988, turin, Italy, pp. 345-357.

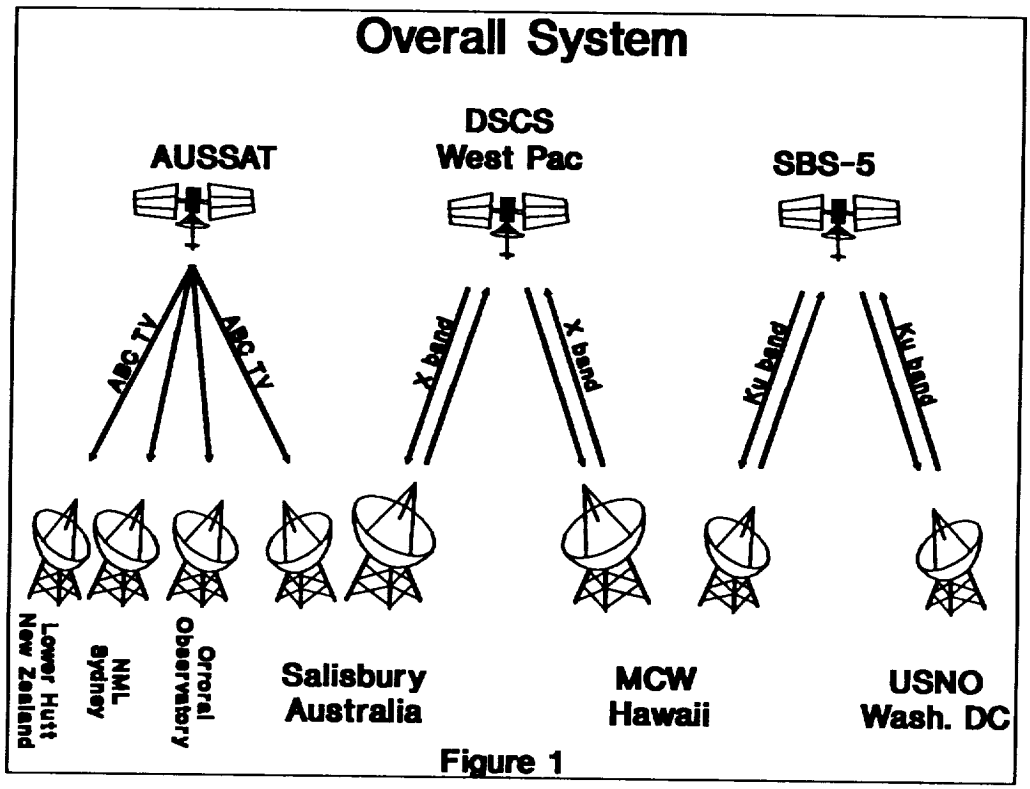

Figure 1

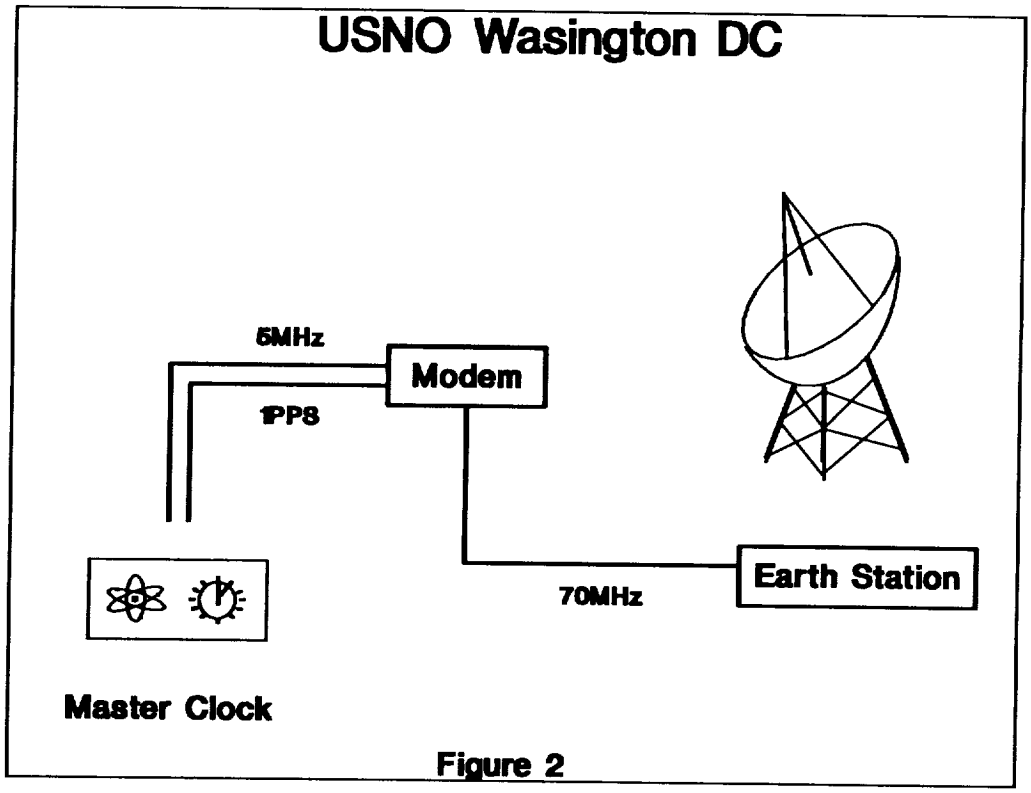

Figure 2

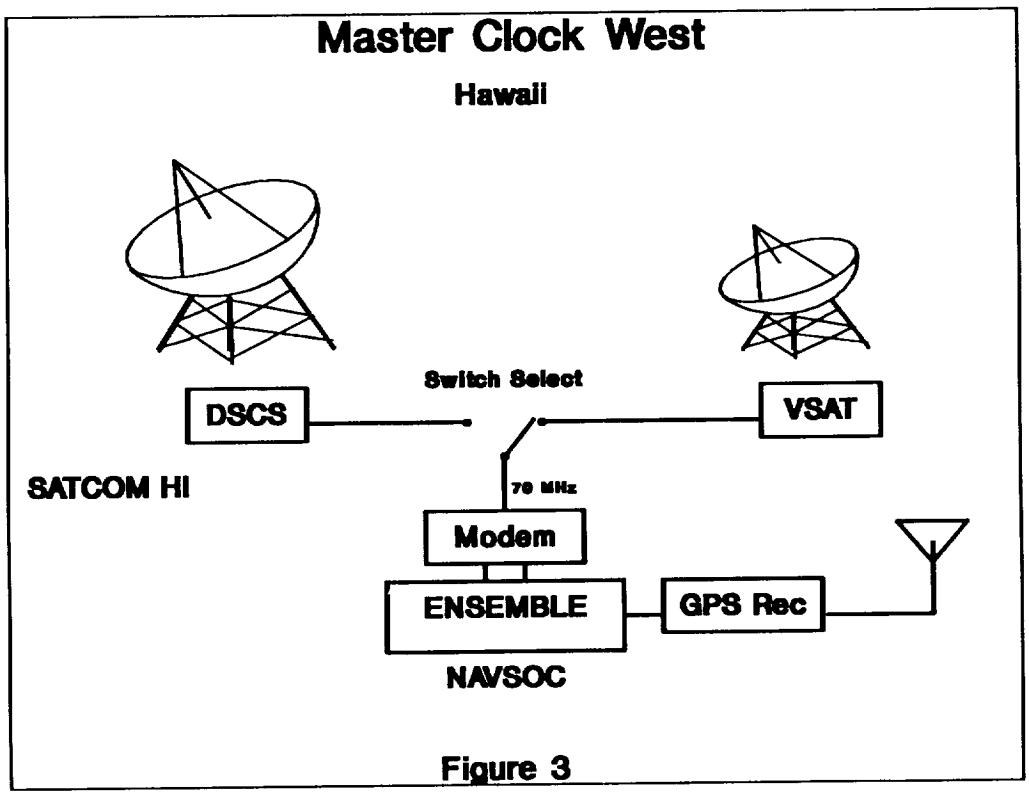

Figure 3

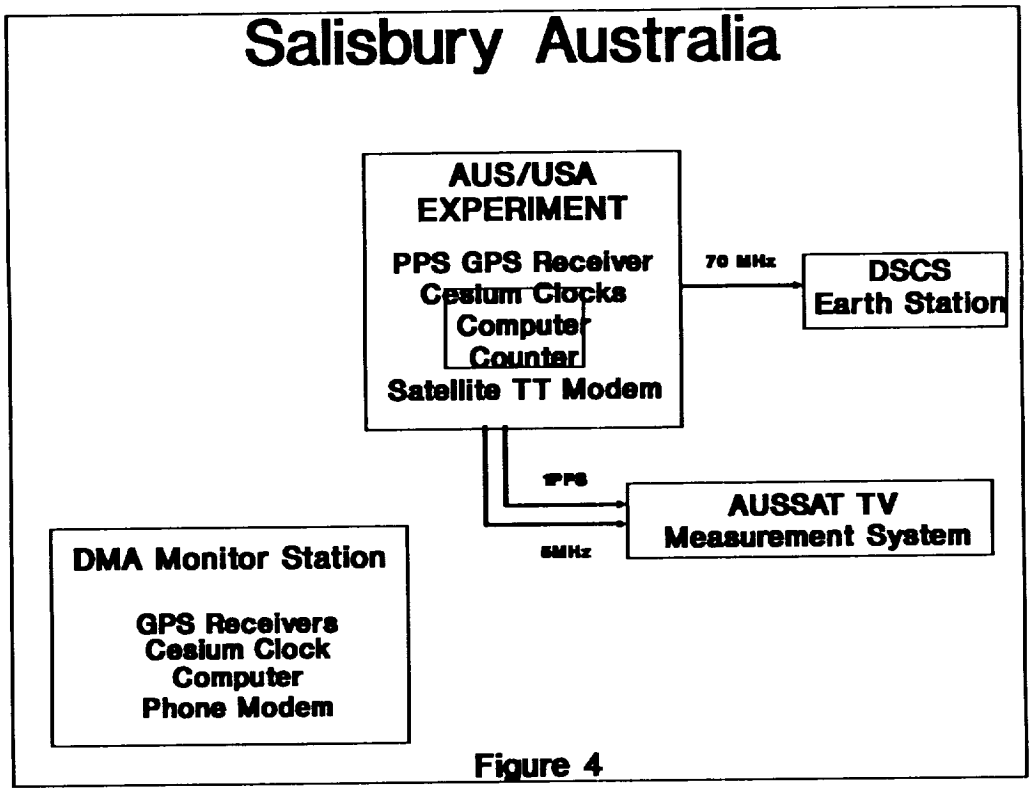

Figure 4

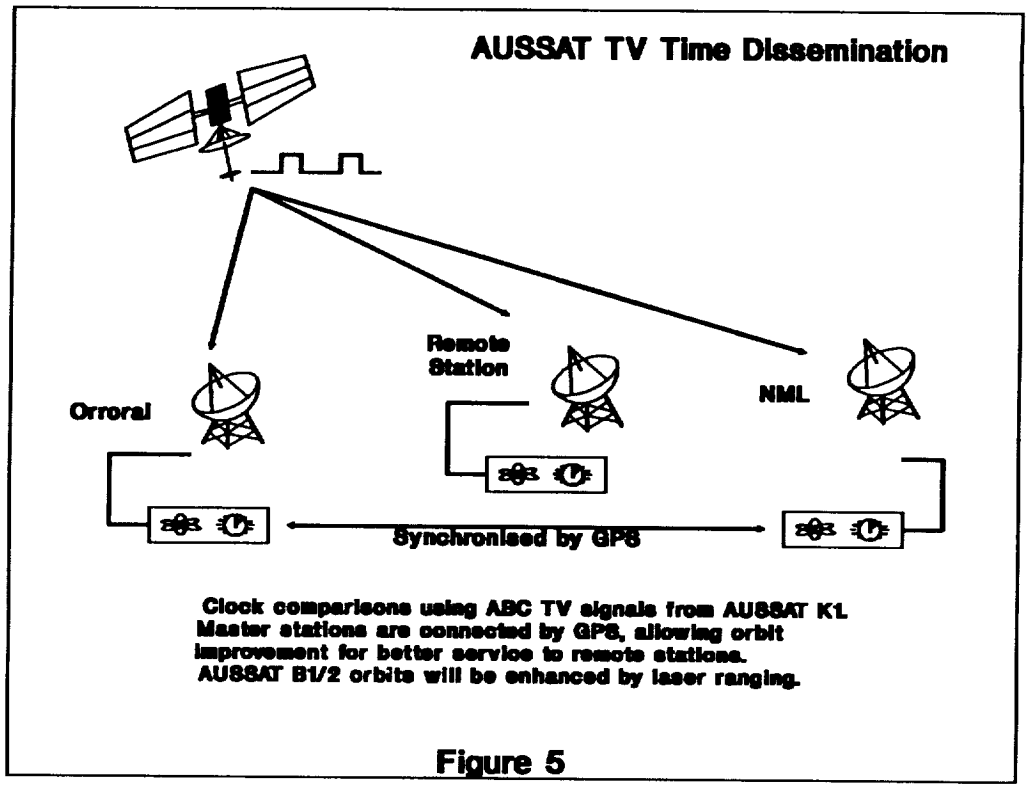

Figure 5

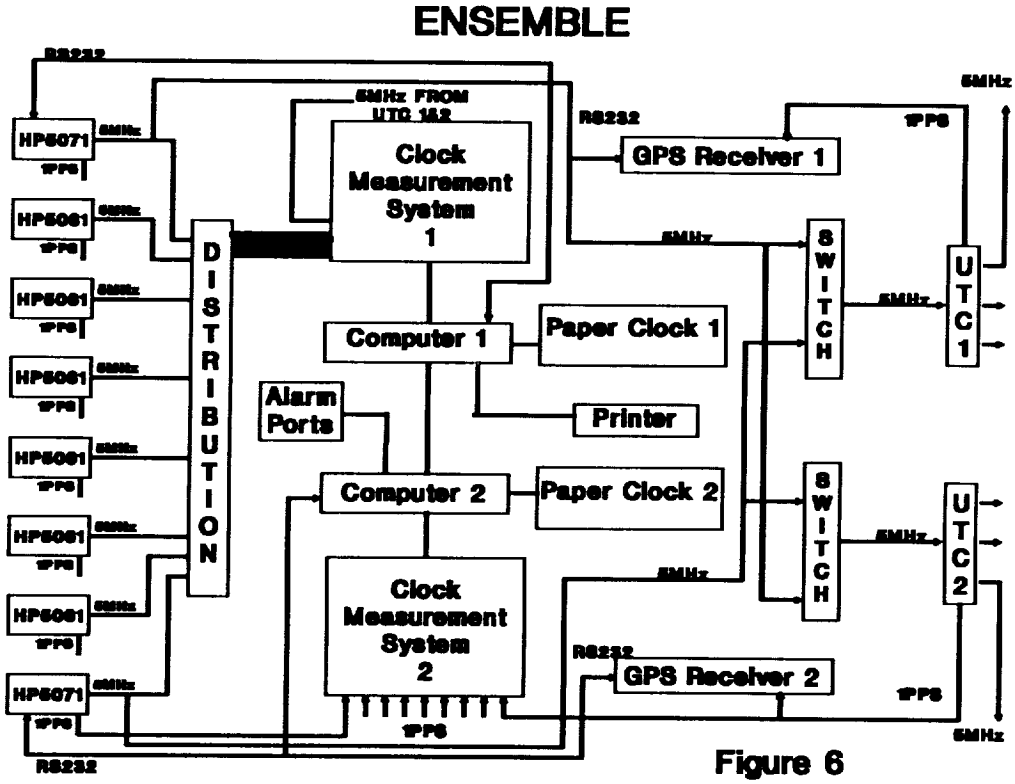

Figure 6

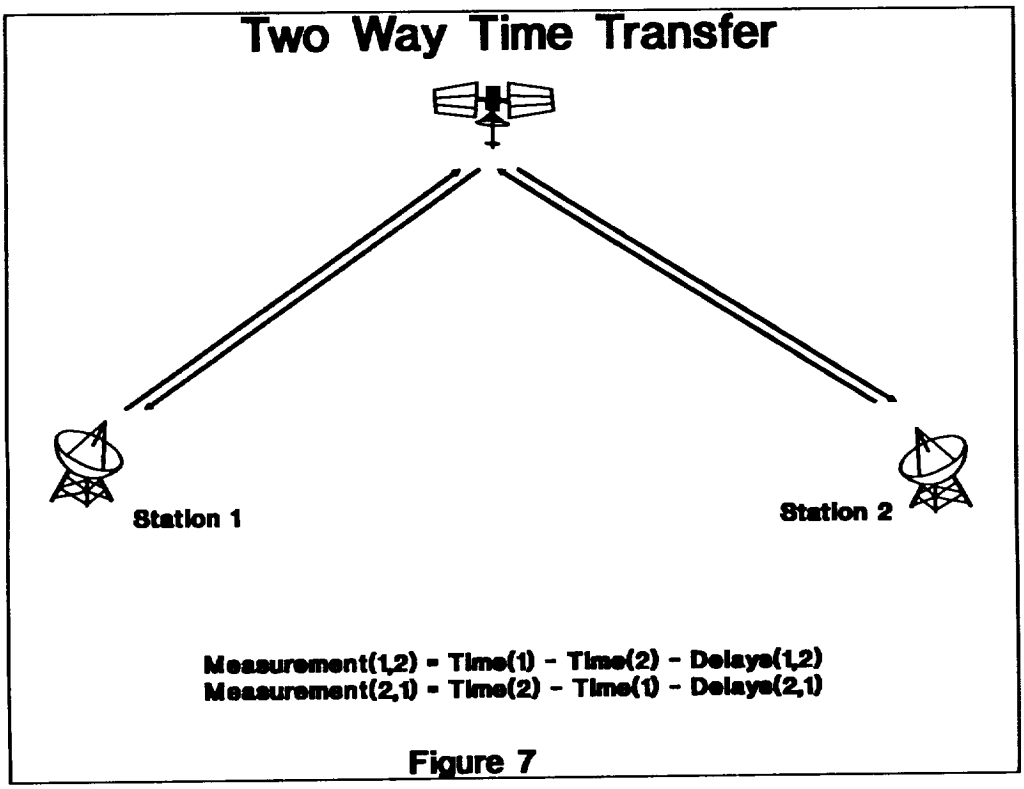

Figure 7

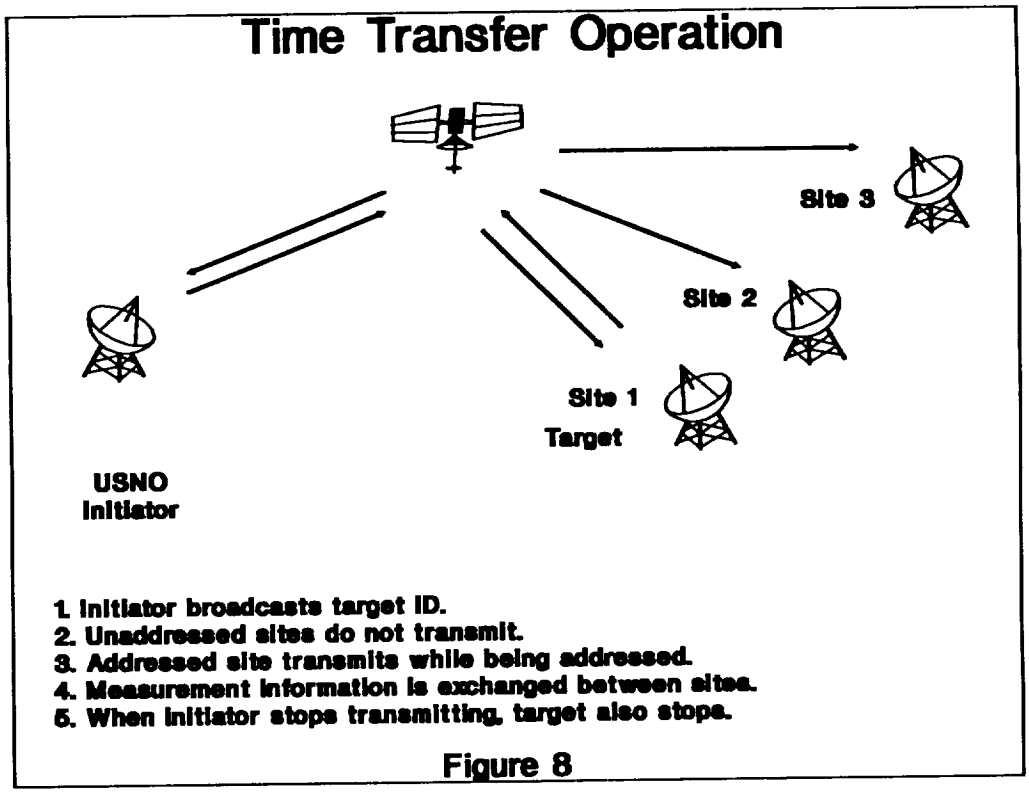

Figure 8

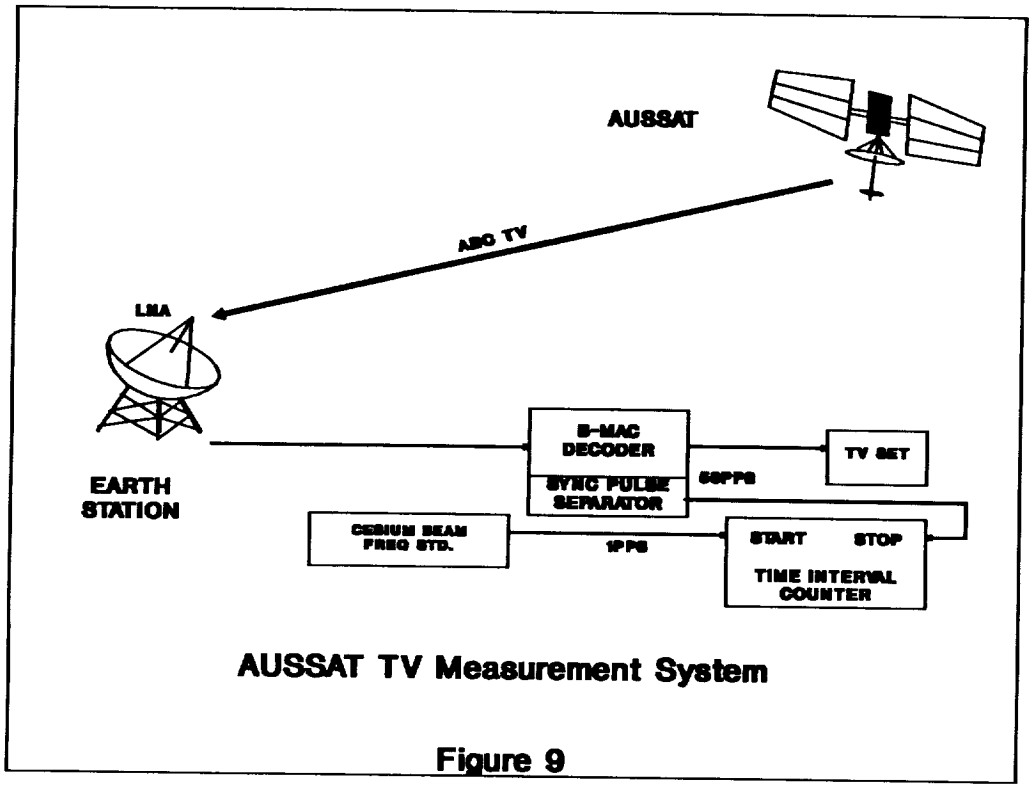

AUSSAT TV Measurement System

Figure 9

QUESTIONS AND ANSWERS

Dr. Claudine Thomas, BIPM: The BIPM is very interested in this experiment because of the difficulty of obtaining a good time transfer link between Australia, New Zealand and America.

Dr. Robert Vessot SAO: Will the modem that you have at NRL, the two-way time transfer modem, operate two-way with more than one station at the same time?

Mr. Gifford: No, not at the same time. It can communicate to a number of stations, but only does time transfer to one at a time.

G. Petit, BIPM: How do you get the precise ephemeris? You need at least three stations to obtain the data. Are there only two stations as shown on your slide?

Mr. Gifford: I only showed two on the slide, but NASA has about five stations in the grid.

GEOSTATIONARY SATELLITE POSITION DETERMINATION FOR COMMON-VIEW TWO-WAY TIME TRANSFER MEASUREMENTS

Zhuang Qixiang and R.J. Douglas
INMS, National Research Council
Ottawa, Canada K1A 0R6

Abstract

In common-view two-way time transfer, each earth station receives an unwanted return signal from its own transmission as well as the desired signal from the other earth station. NRC, NIST and USNO have been cooperating in a three-corner common-view two-way time transfer experiment. Some systematic effects are known to depend on the position of the satellite (Sagnac effect and the cross-correlation pulling of the pseudo-random codes).

A method is presented for deriving accurate satellite ranges from each of three stations doing common-view two-way satellite time transfer measurements, when one (and only one) station also takes ranging measurements on its "unwanted return signal" for a brief period. The method is applied to determine the variations in position of the satellite used over the course of the NRC/NIST/USNO SBS-3 experiment, with ranging data taken at NRC, where no additional hardware was required to automate the process.

The fit and extrapolation which are employed in this method have an estimated precision of 2 m. If the delays of SBS-3 satellite Ku band transponder and earth station equipment were measured accurately as well as the tropospheric refractions were well modeled and corrected, we would expect a ranging accuracy of 2.5 m and satellite positioning accuracy would be 200 m (latitude) 50 m (longitude) and 20 m (height above ellipsoid).

INTRODUCTION

Two-way satellite time transfers are routinely performed between NIST and USNO, NIST and NRC, and between NRC and USNO. The first year of measurements, described here, used the SBS-3 Ku band geosynchronous satellite at 95° W. As shown in Figure 1, these three earth stations are within the -4 dB contour of the continental beam from this satellite. The earth stations are spaced on sufficiently long baselines to allow accurate satellite position determinations from ranging measurements that loop through the satellite. We have used a positioning method that adds only a little overhead to the minimal two-way time transfer when operated from one minimally equipped time-transfer earth station in a two-way time transfer network.

The set-up and all measurements are arranged to fit in a 30 minute period each Monday, Wednesday and Friday morning. As illustrated in Figure 2, three time transfer measurement groups are scheduled: *NIST(1)/USNO(0)*, *NRC(3)/NIST(4)* and *USNO(0)/NRC(1)*, each lasting 300 seconds and typically starting at 10:30, 10:37 and 10:47 respectively. A ranging measurement at NRC, *NRC(4)* which lasts 100 seconds, is inserted between *NRC(3)/NIST(4)* and *USNO(0)/NRC(1)*. For each institute, the number in brackets indicates the receiving code of the Mitrex 2500 modem's pseudorandom noise (PRN) sequence.

A method is described below for deriving accurate range data (of the satellite from the three stations) from two groups of time transfer measurements *NRC(3)/NIST(4)* and *USNO(0)/NRC(1)* as well as one station ranging *NRC(4)*. The synchronism which is required for three-station simultaneous ranging is created by means of polynomial fits and extrapolation of the time transfer data *NRC(3), NIST(4), NRC(1)* and *USNO(0)*. This is a "pseudo synchronism" method which exploits the slow rate change of timing (a few ns/s was typical for SBS-3) and the high precision of the timing (residuals of less than 1 ns for 1 s measurements). After extrapolation, five sets of simultaneous fits (and measurements) *NRC(4), NRC'(3), NIST'(4), NRC'(1)* and *USNO'(0)* are available. The important differences of the equipment configuration at NRC, NIST and USNO are shown in Figure 3: note differences of earth station and time interval counter (TIC) connections.

RANGE EQUATIONS

The range equations are straightforward to write down, starting with the ranging readings at NRC (*NRC(4)*) which can be expressed

$$NRC(4) = TU_{(NRC)} + TD_{(NRC)} + 2R_{(NRC)} + STR \tag{1a}$$

where *TU* and *TD* are the equipment time delays of the uplink path and downlink path at earth station, *R* is the range between earth station and satellite, and *STR* is the satellite transponder time delay. Rearranging equation (1a) gives

$$R_{(NRC)} = [\, NRC(4) - TU_{(NRC)} - TD_{(NRC)} - STR \,] / 2 \; . \tag{1b}$$

The time transfer readings at NRC and NIST can be written respectively

$$NRC'(3) = PPSx_{(NIST)} - dTx_{(NIST)} + TU_{(NIST)} + WE + TD_{(NRC)} - PPSx_{(NRC)} \tag{2}$$

$$NIST'(4) = PPSx_{(NRC)} - dTx_{(NRC)} + TU_{(NRC)} + EW + TD_{(NIST)} - PPSx_{(NIST)} \tag{3}$$

where *PPSx* is the external 1pps from the master clock driving the modem; *dTx* is the modem delay between *PPSx* and *Tx*; *EW* and *WE* are the signal path up to, through and down from the satellite going from east to west and west to east; it is easy to see that

$$WE + EW = 2R_{(NRC)} + 2R_{(NIST)} + 2STR \tag{4}$$

Using a pair of microwave relays and a 2.3 GHz translator, the "station loop delay" at NRC, *SL*, has been measured routinely. *SL* and total station equipment delay *(TU + TD)* are different. From Figure 3, we have

$$SL = TU + TD - 2DH + TRL \tag{5}$$

where *DH* is the antenna time delay which includes the delay of the antenna feed and connecting waveguide and cables; *TRL* is the 2.3 GHz translator delay plus connecting cable delay.

A measurement of the NIST station equipment delay has been done[D.Howe, 1987]. The NIST experiment used a satellite transponder simulator, as illustrated in Figure 4 (1). The $SL_{(NIST)}$ as well as the sum of the simulated *STR* and $TU_{(NIST)} + TD_{(NIST)}$ were obtained,

$$STR + TU_{(NIST)} + TD_{(NIST)} = 1436\,ns$$

$$SL_{(NIST)} = 1359\,ns \tag{6}$$

The experiment at NRC used a compact mixer unit, as illustrated in Figure 4 (2). $SL_{(NRC)}$, the sum of $TU_{(NRC)}$ and $TD_{(NRC)}$ as well as the difference of $TRL_{(NRC)}$ and $2DH_{(NRC)}$ were measured,

$$TU_{(NRC)} + TD_{(NRC)} = 3373.5\,ns$$

$$TRL_{(NRC)} - 2DH_{(NRC)} = 6.6\ ns$$

$$SL_{(NRC)} = 3380.1\ ns \tag{7}$$

Collecting the above equations, the three range equations become

$$R_{(NRC)} = [\,NRC(4) - TU_{(NRC)} - TD_{(NRC)} - 83.6\ ns\,]/2$$

$$= [\,NRC(4) - TRL_{(NIST)} + 2DH_{(NIST)} - 3450.5\ ns\,]/2 \tag{8}$$

$$R_{(NIST)} = [\,NIST'(4) + NRC'(3) - NRC(4) + dTx_{(NRC)} + dTx_{(NIST)} - 1435.5\ ns\,]/2 \tag{9}$$

$$R_{(USNO)} = [NRC'(1) + USNO'(0) - NRC(4) + dTx'_{(NRC)} + TU_{(NIST)} + TD_{(NIST)} - TU_{(USNO)} - TD_{(USNO)} - 1435.5\ ns\,]/2$$

$$= [NRC'(1) + USNO'(0) - NRC(4) + dTx'_{(NRC)} - SL_{(USNO)} + TRL_{(USNO)} - TRL_{(NIST)} + 2DH_{(NIST)} - 2DH_{(USNO)} - 77\ ns\,]/2 \tag{10}$$

Thus the problem reduces to knowing the sum delay of TU and TD at NIST and USNO, these delays could be measured by transporting a compact calibration unit to the NIST and USNO earth station sites.

ALGORITHM OF SATELLITE POSITION DETERMINATION

In general, it is necessary to measure at least four ranges of four observing stations for determining the position and time of a space target. The independent range variable L_i is the function of target coordinates X_s, Y_s, Z_s, observing station coordinates X_i, Y_i, Z_i and measuring time t_i

$$L_i = Y(X_s, Y_s, Z_s, X_i, Y_i, Z_i, t_i) \qquad (i = 1,4) \tag{11}$$

If the clocks of the observing stations have been synchronized precisely and the ranging measurements are conducted at a common time t, then only three observing stations are required for the determination of target coordinates. The weighted observing equation and the weighted least-squares solution

$$\mathbf{G^T W G X = G^T W (O - C)} \tag{12}$$

$$\mathbf{X = (G^T W G)^{-1} G^T W (O - C)} \tag{13}$$

where, **X** is target position improvement matrix; **G** is the measurement matrix; **W** is the weighting matrix; and **O-C** is the matrix of difference between measured and computed ranges. If **G** is square matrix and $\det\mathbf{G} = |\mathbf{G}| \neq 0$, equation (13) becomes

$$\mathbf{X = (WG)^{-1} W (O - C)} \tag{14}$$

In our case, the known numbers are the coordinates of three observing stations, the independent ranges between satellite and three stations and the initial rough position of satellite. The determination of **W** is based on ranging precision at each station, the weighting factor is the reciprocal of ranging precision. Due to the different antenna size of earth stations and the introduction of polynomial extrapolation and conversion equation in range determination, the ranging precisions at three stations become unequal in our case. Based on the error estimates of ranging and time transfer measurements, range conversion as well as extrapolation, the differential weighting matrix **W** has been established. The algorithm employed in the position determination process is a standard differential correction technique of weighted least-square that minimises the observation residuals, i.e. the difference between the measured ranges and calculated ranges. The satellite initial position is iteratively replaced by the corrected satellite position, the iterative process continues until the position converges to within a delta value of error. The covariance matrix

$$\mathbf{P = (G^T W G)^{-1} W} \tag{15}$$

is used to determine the goodness of each solution fit to the data and is used to calculate the Position Dilution Of Precision (PDOP). PDOP is the coherent factor between the position accuracy of satellite and the geometric distribution between satellite and observing stations.

$$PDOP=\sqrt{P_{11}+P_{22}+P_{33}} \tag{16}$$

Where, P_{11}, P_{22} and P_{33} are the diagonal terms of **P** matrix. The individual DOPs (XDOP, YDOP, ZDOP) or (φDOP, λDOP, HDOP) could be derived from P_{11}, P_{22} and P_{33} in the different coordinate systems.

UNCERTAINTY DISCUSSION

The absolute accuracy of satellite position determination is dependent upon knowledge of ranging accuracy, Position Dilution of Precision as well as station position accuracy. Over the course of SBS-3 experiment, the single shot (1 s) precision of ranging measurement at NRC has been about ±1.2 ns under normal circumstances. The "ranging" precisions of NIST and USNO through conversion (but excluding extrapolation errors - discussed below) can be estimated about ±1.6 ns and ±2.2 ns respectively (again for 1 s measurements). It must be emphasized that the absolute accuracy of ranging measurements are subject to many systematic errors. The uncertainties relative to position determination accuracy are discussed and estimated below for our first satellite positioning results. In many cases significant improvements in accuracy could be made with rather modest efforts.

1. Polynomial extrapolation. Figure 5 shows the measurement schedule used at NRC for evaluating the accuracy of the extrapolation. The extrapolation uncertainties have been evaluated at NRC by conducting additional timing and ranging measurements: by "eavesdropping" on the NIST/USNO time transfer and measuring (receive only) timing *NRC(1)* and *NRC(0)*; and by a second ranging session *NRC(4)*. The uncertainties of the extrapolations were evaluated by calculating the rms residual of the observed - extrapolated results, as shown in Figure 5. For extrapolation times of less than 400 seconds, a second order polynomial regression gave the best results, with rms extrapolation residuals of less than 6.8 ns.

2. Propagation delay. No cancelling of path delay exists during ranging measurement. Both the tropospheric and ionospheric refraction effects need to be taken into account. A signal propagating through the troposphere will be absorbed and delayed due to effects of snow, rain, clouds, fog as well as oxygen and water vapour molecules. The refractive correction increases with atmospheric pressure (or partial pressures of important molecules) and increases as the satellite elevation decreases. This kind of time delay could reach to several hundred nanoseconds in the worst cases. With a suitable model of tropospheric refraction, the time delay of tropospheric refraction could be corrected to about 1%. SBS-3 satellite elevations at NRC, NIST and USNO are about 34°, 42° and 41° degrees respectively. The effect of tropospheric refraction would be about 33 ns under normal circumstances. A Ku band radio signal propagating through ionosphere will be refracted, the refractive index is mainly proportional to the electron density integrated along the path and the inverse square of the signal frequency. For a 12 and 14 GHz link, the signal delay of ranging due to ionospheric refraction can be estimated as about 2 ns.

3. Satellite transponder delay. The satellite transponder delay should be available from design and acceptance test specifications and accurate to about 1 ns. In our case, the SBS-3 transponder delay is simulated by the experiment at NIST. The time delay uncertainty between the electrical centre of the satellite transponder and the simulator value was estimated as 10 ns. This effect of this delay on position will be almost the same for the three earth stations, and to first order, will simply displace the attributed position of the electrical centre of the satellite from, say, a reference plane referred to the satellite antenna.

4. Station equipment delay. To know the time delay of earth station equipment, we can measure the sum of up path and down path delay of all station equipments or alternatively the station loop delay,

the difference of antenna delays and the difference of translator delays. Based on modern technique, these equipment delays could be measured accurate to one nanosecond, but one must pay more attention to every aspect of measurement. The station loop delay *SL*, the modem loop delay *ML* and *(SL-ML)* delay have been automatically measured at NRC as a matter of routine. Figure 6 shows the results from April, 1990 to April, 1991. *(SL-ML)* is the total delay of the 70 MHz IF cable, Up/Down converter, 2.3 GHz translator, Tx/Rx relay and associated cables. Most of these units are operated in outdoor conditions, and so suffered environmental effects. The *(SL-ML)* delay with a ±1.52 ns of rms displays more noise than the *ML* delay with variations of ± 0.66 ns rms. The *SL* and *(SL-ML)* delays show obvious seasonal variation, and a sinusoidal function, $y=a\sin(2\pi ct+b)$ fits the data as shown in Figure 6 with a peak-to-peak amplitude of 3.2 ns for the station loop, and 3.8 ns for the delay of the station loop minus the modem loop. The seasonal variation of the station loop delay is expected to be dominated by the temperature coefficient of the long 70 MHz IF cables, which are outdoors and buried at a depth of less than one metre for much of the run. Figure 6 also shows a small systematic drift in the modem loop delay measurements over the one year period. The station loop delay *SL* also has been measured at NIST, and published for a 15 day period [D. Howe, 1987]. Direct station loop delay measurements for USNO were not available. In calculation of USNO range, an estimated value of *SL(USNO)* has been used with an uncertainty of about 50 ns. The differences of translator delay and the differences of antenna delay among NRC, NIST and USNO are ignored in our calculation, thus another error of about 20 ns has been introduced.

5. PDOP. For the geometric distribution among NRC, NIST, USNO and SBS-3, the calculated PDOP is about 80. The sensitivity coefficients of latitudinal, longitudinal and height above ellipsoid position errors with respect to range error are 77.2, 20.0, 8.8 respectively. In most applications, this kind of error magnification is the limitation of the resolution of position determination. It can be reduced only by choosing optimal geometric distribution among satellite and stations.

6. Station coordinates. Errors in station coordinates have a direct effect on satellite position. The station coordinates need to be measured as accurately as possible in a common coordinate system. For the NRC earth station, the WGS-84 coordinates of the principal GPS antenna at NRC were used as the local reference. The location of the antenna of earth station was surveyed relative to the GPS antenna, and the antenna coordinates of NRC earth station were obtained with an accuracy about 7 metres. The adopted antenna coordinates of NIST and USNO earth stations were assumed with the same level of accuracy.

7. Code pulling. The ranging measurements at NRC were normally taken with no other time transfer station transmitting, and so are not expected to have any systematic pulling of the delay-locked loop of the modem's receiver. For the timing measurement runs, two PRN codes are present at the same chip rate (2.5 MHz) and length (10,000 chips). The Mitrex PRN codes are not quite orthogonal, with cross-correlation pulling averaging about 0.7% of the main autocorrelation slope used by the delay-locked loop. Averaged over all relative PRN phases, we expect a code pulling of some 2 ns rms, if the carriers are syntonized and the two signals are matched in power. Power mismatch will reduce the code pulling for the strong signal, and increase the code pulling for the weak signal. For these runs, the as-received carriers from the three earth stations rarely match within the 2 Hz noise bandwidth of the modem, giving a large rejection of the unwanted signal, to the level where code pulling is not an issue for satellite position determination.

Based on the above discussion, the current ranging accuracy is estimated as 20 m and the absolute satellite positioning accuracy is conservatively estimated as 1.6 km. If the equipment delays were measured accurately and tropospheric refractions were well modeled, the accuracy could be improved to 2.5 m (range) and 200 m (position), and only then would be limited by the extrapolation accuracy.

SATELLITE POSITION RESULTS

The satellite position determinations from April 1990 to December 1990 are presented in Figure 7. To calculate each position, a total of five data sets must be measured successfully at three stations. All five are not always available, as evidenced by the gaps in Figure 6. Note that the satellite remains within ±0.03° of a longitude 0.05° W of its nominal position of 95° W. In the periods of most nearly continuous results, shown in Figure 8, the three satellite coordinates exhibit periodic trend every 28 days.

The monthly period is attributed to the perturbing influence of the moon's gravitational force on the geostationary satellite. The moon's perturbing acceleration on a geostationary satellite has been estimated less than about 9×10^{-6}, i.e., about 5.4 km for two days tracking arc. Due to our schedule of time transfer measurements which are performed at a nearly fixed time of a day, the influence of earth's non-sphericity perturbing force are not observed. This offers a chance to see the influence of the moon's perturbation, and presumably station-keeping such as is seen on MJD 48237, indicated by a symbol ↑ in Figure 8.

EFFECTS OF SATELLITE POSITION ON TIME TRANSFER

For each of the satellite positions that were determined, the Sagnac correction was calculated for all three links: NRC/SBS-3/NIST, NRC/SBS-3/USNO and NIST/SBS-3/USNO. The Sagnac corrections are shown in Figure 9, and are indeed small. The variation was less than 20 ps for any one link, and was determined with an accuracy of ±2 ps. This simple positioning method can evaluate and remove Sagnac effect variations at the ps level.

The satellite position can also affect common-view two-way time transfer measurements by varying the time delay between the two signals each earth station receives: the signal transmitted from the other time laboratory, and the unwanted return signal from its own transmission. The unwanted return signal can pull the timing signal by some 4 ns rms, if the carriers are syntonized. If the rf powers and the modems are matched, the code pullings will almost cancel for the two-way time transfer. However, if there is a 3 dB mismatch in powers (as is commonly observed in our experience) a code pulling of about 1 ns rms can be expected if the carriers are syntonized (for these experiments, they rarely are syntonized within the 2 Hz noise bandwidth of the delay locked loop). The relative delay between the two signals depends mostly on the day-to-day variation in satellite position, the other delays are either constant (equipment delays), slowly varying (the UTC time scale differences) or are settable. During a 300 second timing run, the relative delay may vary by several 400 ns chips as the satellite changes position, but all in a deterministic way. If the two-way time transfer runs are supplemented with a ranging measurement, the effects of code pulling might be evaluated within the limits of our extrapolation accuracy estimate of about 7 ns rms (2% of one chip). The upper bound of the effects of code pulling may be seen in Figures 10 through 13.

In Figure 10, the first difference of the autocorrelation function of Mitrex code 0 (a $[2^{15}-1]$ maximal length PRN code, truncated at 10,000 chips) is shown. The early/late discriminator locks the delay locked loop at the zero crossing of the large negative slope at the origin, of 100% in 400 ns. The details of the autocorrelation function away from the origin are only important in the event of significant multipath signals. In Figures 11 through 13, the first difference of the cross-correlations of the pairs of different Mitrex codes are presented for the ranges of relative delays observed in our experiments with SBS-3. The values on these graphs represent an effective zero-shift for the delay-locked loop, in the case where the unwanted carrier is within the modem's 2 Hz noise bandwidth of the locked carrier. For any particular delay time shown in one of the Figures 11 through 13, the associated code pulling may be read from the graph as a percentage of one chip (400 ns). Also shown for each cross-correlation is a histogram of observed range differences determined in this work. This limit on the size of the code pulling effect can be seen to have been better, by chance, for the NRC/NIST link (Figure 11) than for the USNO/NIST link (Figure 13).

With the Mitrex modems, one interesting possibility is for one station in each transfer to choose its transmit time origin so as to use a part of the cross-correlation that has zero code pulling effect. Of the 28 code pairs that might be used, all but 5 have at least one 400 ns wide range of time delay which has zero code pulling (corresponding to the cross-correlation function having 3 successive values the same). For the Mitrex codes, these flat spots are as follows: code [0,1]: none; [0,2]: 2.396 ms; [0,3]: 3.1876 ms; [0,4]: 0.394, 2.7636 and 3.6984 ms; [0,5]: 0.0472 ms; [0,6]: 0.0536 ms; [0,7]: 0.898 & 0.8984, 2.3388 ms; [1,2]: 0.3184, 0.4932, 1.2652 & 1.2656 ms; [1,3]: 0.650 ms; [1,4]: 0.158, 0.8448 ms; [1,5]: 1.304, 2.6956 ms; [1,6]: none; [1,7]: 3.3936 ms; [2,3]: none; [2,4]: 1.3056, 2.214 ms; [2,5]: 1.5908, 3.6324 ms; [2,6]: 1.9692 ms; [2,7]: none; [3,4]: 0.7332, 3.700 ms; [3,5]: 1.794 ms; [3,6]: 1.0472, 1.1728, 2.6804, 3.9388 ms; [3,7]: 1.144, 3.0832 ms; [4,5]: 0.4708 ms; [4,6]: 1.4304 ms; [4,7]: 0.5784 ms; [5,6]: 0.0972, 2.8724 ms; [5,7]: none; and [6,7]: 0.8576 ms. The crosscorrelation flat spots for [i,j] occur for code i leading or lagging code j by the specified amounts, and the code pulling will then be zero at both earth stations. The times specified with an ampersand (and differing by 400 ns) are flat spots having 4 successive cross correlation values the same, and would be the easiest zero code pulling to use with just a programmable delay generator. The different dopplers would still normally permit 100 s of measurement free from code pulling, but the delay generator would have to be set with 2-station relative position information determined just before the time transfer session (just a few seconds worth of initial measurements, on each of the two codes, taken at only one earth station, would suffice to set the delay generator). As may be seen from the histograms in Figures 11 through 13, the day-to-day position variations do not allow us any confidence to hit even an 800 ns wide window for zero code pulling.

Geostationary satellite position determination by these methods also can make signals from the satellite into useable one-way timing references, with accuracy potential at the 10 ns level, limited principally by the need for position determination at the receiver.

ACKNOWLEDGMENT

The authors wish to thank H.F. Lam for the design and maintenance of the earth station's microwave and electronic equipment.

REFERENCES

1. D.A.Howe, "Stability Measurements of Ku-Band Spread Spectrum Two-Way Time Transfer Equipment", Proc. of the 41st Annual Symposium on Frequency Control, p. 149-160, 1987.

2. D.W.Hanson, "Fundamentals of Two-Way Time Transfers by Satellite", Proc. of the 43rd Annual Symposium on Frequency Control, p. 174-178, 1989.

3. G. de Jong, "Accurate Delay Calibration for Two-way Time Transfer Earth Stations", Proceedings of the 21st Annual Precise Time and Time Interval Applications and Planning Meeting, p. 107-115, 1989.

4. R.N.Treuhaft, "Tropospheric Limitations to the Stability of Radio Metric Delay Measurements", Proc. of the 21st Annual Precise Time and Time Interval Applications and Planning Meeting, p. 233-238, 1989.

5. Q. Zhuang, et al., "An Investigation of Three Dimension Position Dilution of Precision", Acta Astronomica Sinica, Vol. 32, No. 2, p. 113-120, 1991.

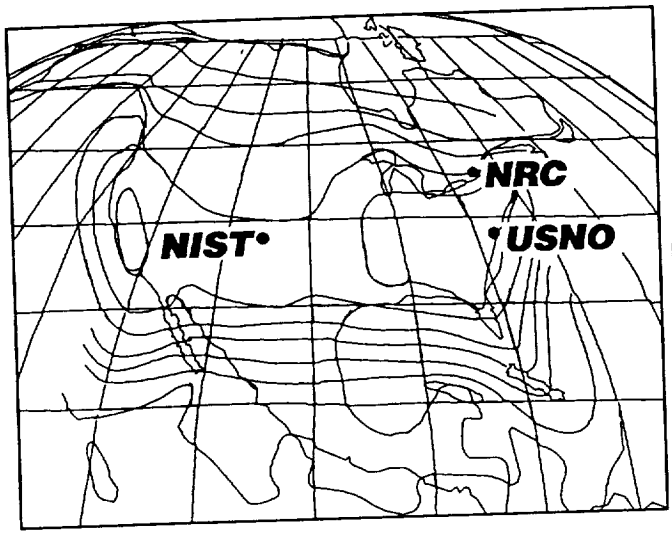

Figure 1. *The locations of the time laboratories of NIST, USNO and NRC within the continental beam of SBS-3. The contours are 2 dB apart.*

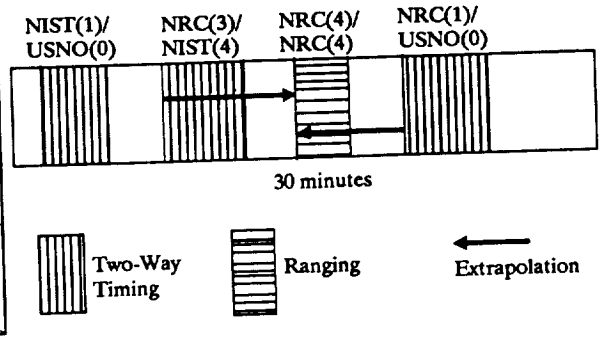

Figure 2. *Measurement Schedule for Time Transfer and Ranging.*

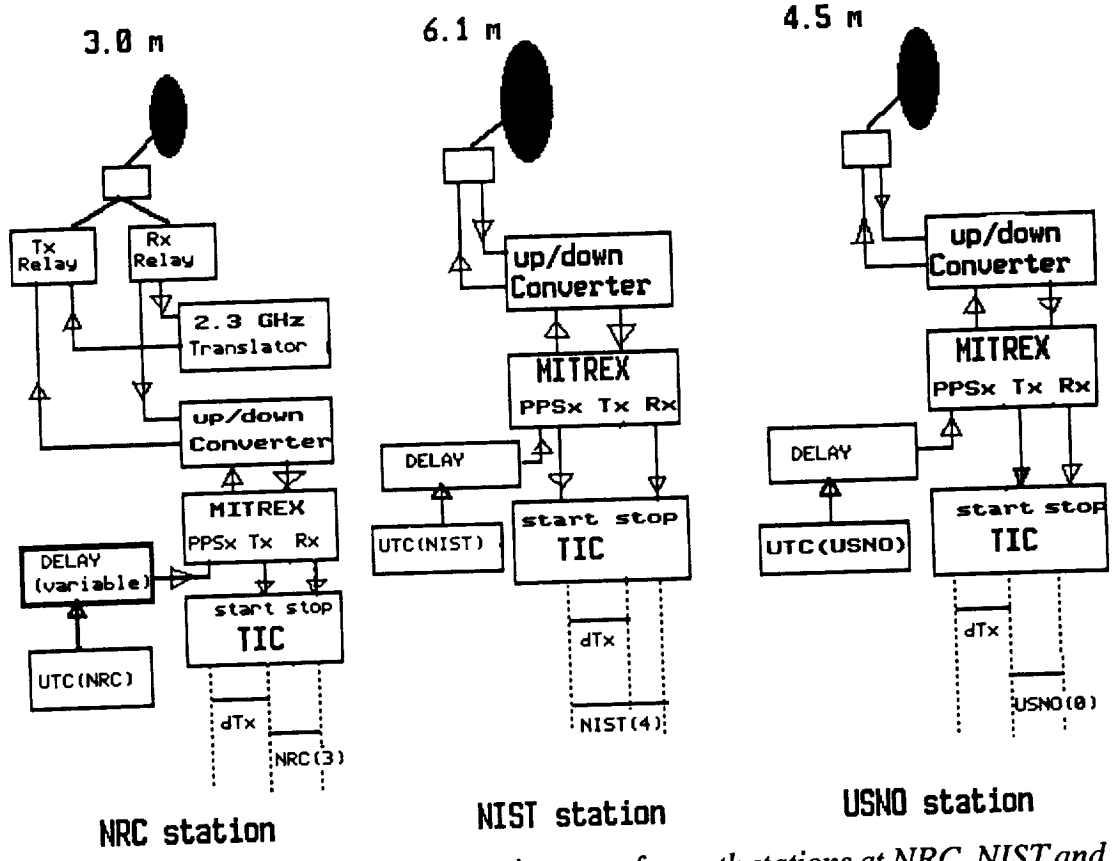

Figure 3. *The electronics at the two-way time transfer earth stations at NRC, NIST and USNO.*

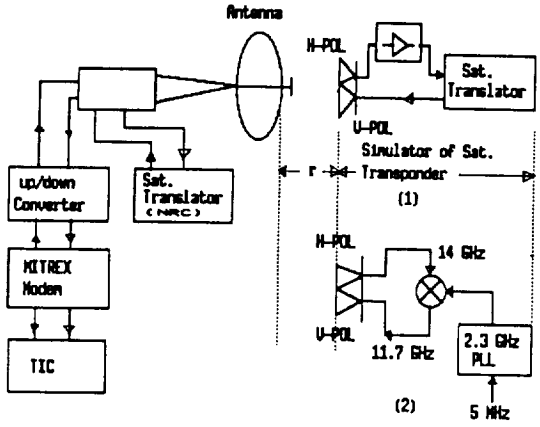

Figure 4. *Station Equipment Delay Measurement at NIST (above) and NRC (below).*

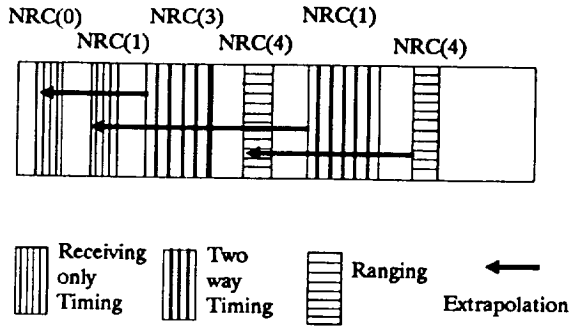

Figure 5. *Measurement Schedule for Extrapolation Evaluation*

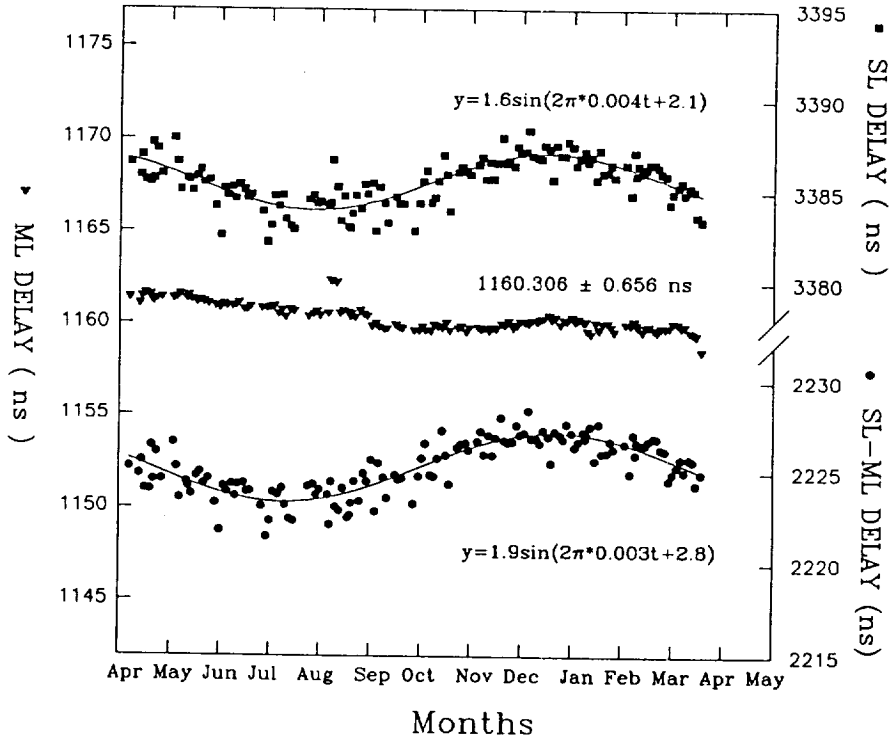

Figure 6. *One year's variation of the Mitrex internal modem loop (ML) and the station loop (SL), measured at NRC's earth station.*

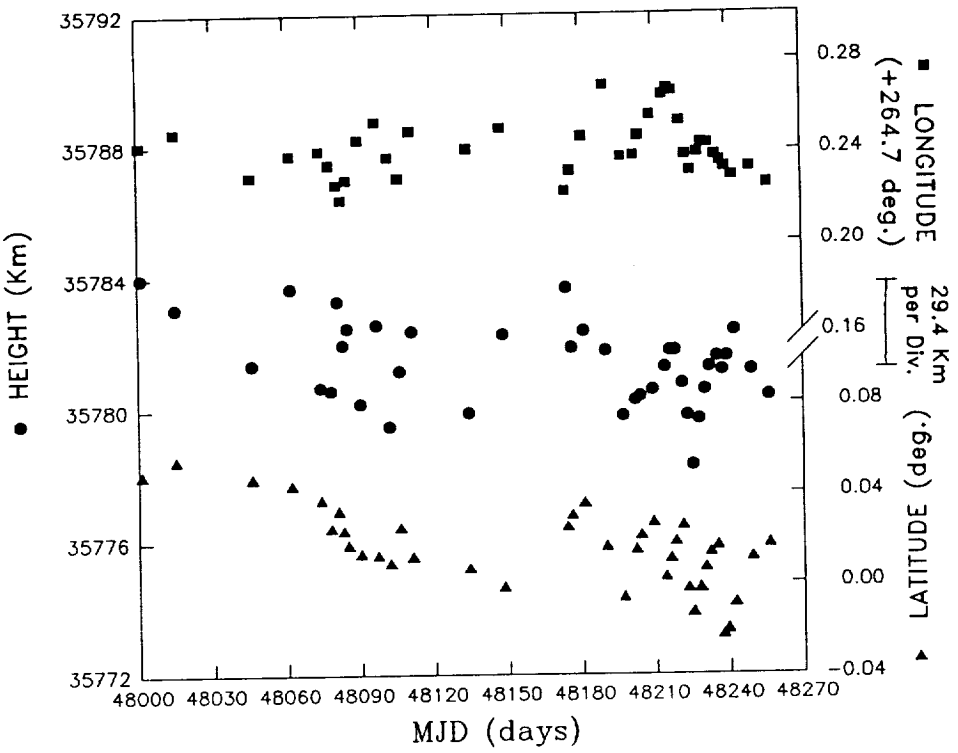

Figure 7. *SBS-3 satellite position determination, measured by ranging at NRC and two-way time transfer with NIST and USNO.*

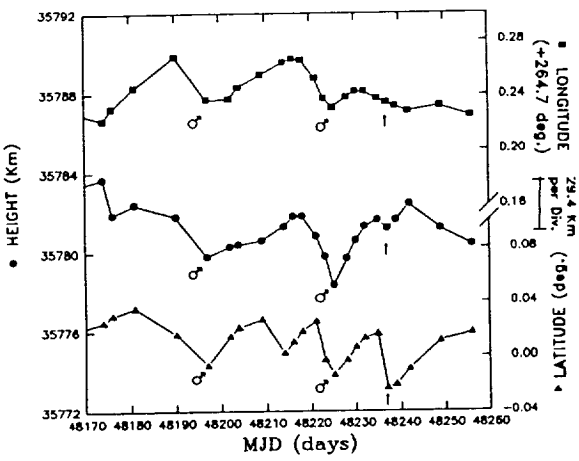

Figure 8. *Detail of SBS-3 position determination, illustrating a monthly cycle.*

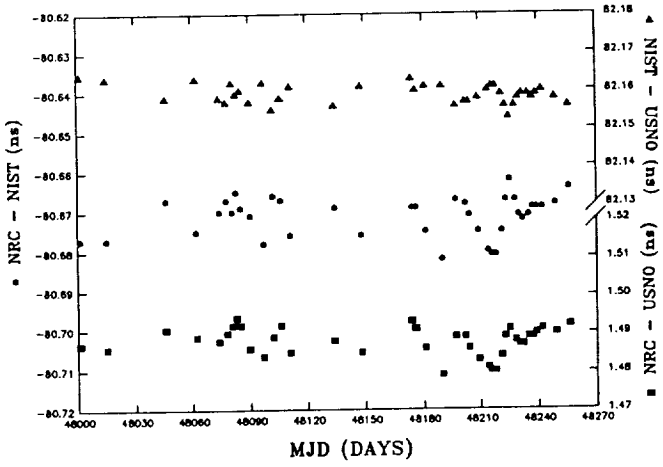

Figure 9. *Sagnac effect corrections for links via SBS-3: NRC/NIST (middle); NIST/USNO (top); and NRC/USNO (bottom)- note that although USNO is W of NRC in longitude, it appears E of NRC when viewed from SBS-3.*

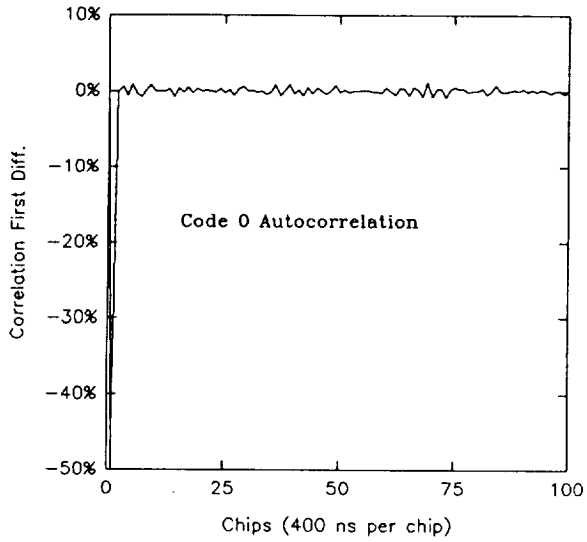

Figure 10. *The first difference of the auto-correlation of the Mitrex modem PRN code 0. The vertical scale is normalized to a scale of 100% in 400 ns.*

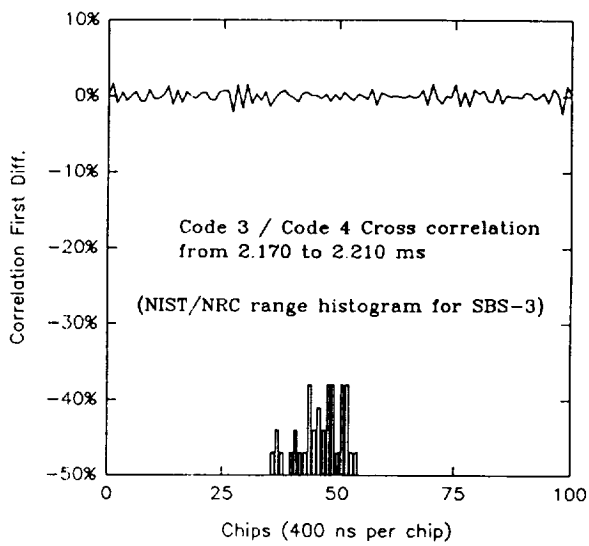

Figure 11. *The first difference of the cross correlation of the Mitrex PRN code 3 with code 4, plotted vs relative delay around the NIST/NRC values. Also shown is a histogram of this link's relative delays changed by the position of SBS-3.*

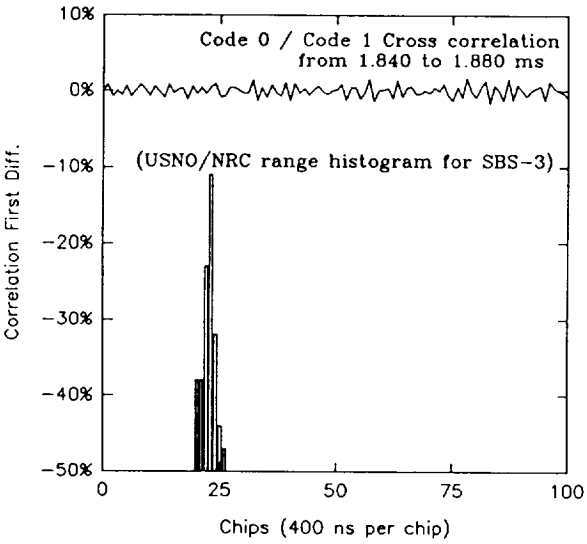

Figure 12. *The first difference of the cross correlation of the Mitrex PRN code 0 with code 1, plotted vs relative delay around the USNO/NRC values. Also shown is a histogram of this link's relative delays changed by the position of SBS-3.*

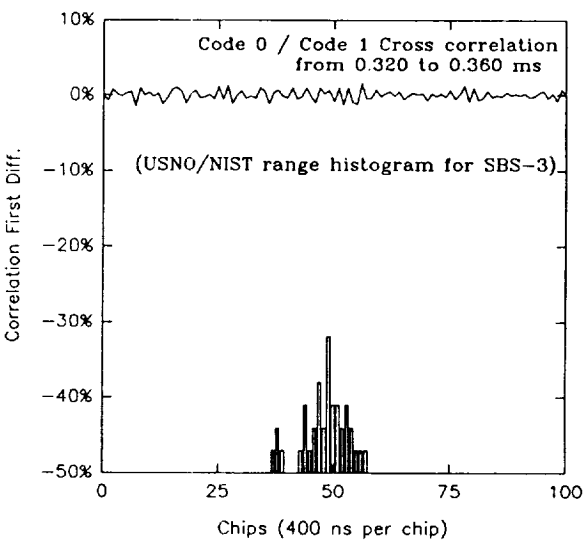

Figure 13. *The first difference of the cross correlation of the Mitrex PRN code 0 with code 1, plotted vs relative delay around the USNO/NIST values. Also shown is a histogram of this link's relative delays changed by the position of SBS-3.*

Millisecond Pulsar Observation System at CRL

Y. Hanado, H. Kiuchi, S. Hama, A. Kaneko and M. Imae
Communications Research Laboratory
Ministry of Posts and Telecommunications
893-1 Hirai Kashima Ibaraki, 314 Japan

Abstract

Millisecond pulsars attract attentions as a future reference clock in place of present atomic clocks, by reason of their highly stable pulse timing. CRL (Communications Research Laboratory) has been developing an observation system to measure the pulse timing of millisecond pulsar precisely, and recently has completed its basic part. By using it, we observed PSR1937+21 at 1.5GHz band and got a pulse timing with a precision of $16\mu sec/\tau$ by 5 days observation.

Introduction

CRL has a responsibility for keeping and supplying the time and frequency standard of Japan, and has been developing atomic clocks such as hydrogen maser and cesium clocks. We search for new methods to get more stable reference time scale, and started a project for establishing a reference clock system using the pulse timing of millisecond pulsars, such as PSR1937+21.

A pulsar is an object which radiates quite periodic pulse signal, which is considered a rotating neutron star. Generally this pulse arrival timing is stable, and especially so called millisecond pulsar has highly stable pulse timing in long term. According to the timing data of millisecond pulsar PSR1937+21 observed at Arecibo Observatory [1], shown in Fig.1, the long term fractional frequency stability reaches up to 10^{-13} ($\tau = 10^7 sec$). This is comparable to the stability of the most stable atomic clock, and it shows the possibility of a new clock using millisecond pulsars.

In the 21st PTTI meeting, we introduced our observation plan of millisecond pulsars [2]. Since then, we have been developing the observation system of millisecond pulsars using the 34m antenna at Kashima Space Research Center, and recently completed its basic part. In this paper, the feature of our system and the results of the observation for PSR1937+21 will be described.

Observation system

An observed pulse arrival time includes the error dt_{obs} , which depends on parameters of an antenna and an observation system. An observation system must be designed to make this error as small as possible. dt_{obs} is given by [3], [4];

$$dt_{obs} = \frac{(dt)^{3/2} \cdot T_{sys}}{\sqrt{B \cdot T \cdot P} \cdot \langle S \rangle \cdot G} \qquad (sec) \qquad (1)$$

where

dt : half width of the observed pulse (sec),
P : pulse period (sec),
T_{sys} : system noise temperature (K),
$\langle S \rangle$: mean flux density of pulse (Jy),
G : antenna gain (K/Jy),
B : observed bandwidth (Hz),
T : integration time (sec).

To decrease dt_{obs} under the given antenna parameters such as T_{sys} and G, we must take the wide observing bandwidth B and long integration time T. Our data acquisition system was designed to meet these requirements.

Fig.2 shows the block diagram of our system. It has 16 channels in order to expand the observation bandwidth reducing the dispersion effect. A signal suffers dispersion delay according to its frequency from inter stellar plasma, which is expressed as follows [5];

$$dt_{DM}(f) = 0.00415 \times f^{-2} \times DM \qquad (sec) \tag{2}$$

where f is the frequency of the radio signal (GHz), and DM is the dispersion measure (pc/cm^3). If one channel's bandwidth becomes wide, the difference of $dT_{DM}(f)$ becomes large and the observed pulse width becomes broad. So we at first receive a pulse signal in narrow band (270kHz for each channel) to get a sharp pulse. Then to get a signal with wide bandwidth, each channel's signal are all added in off-line after canceling of each dispersion delay. Final data corresponds to the data observed by about 4MHz bandwidth.

To average many pulses quickly, we have introduced a data processor which works as both an A/D converter and a box-car averager. It averages pulses of each channel by hardware, which saves calculation time and memory for data storage.

Sampling clocks for A/D conversion and trigger clock for averaging are obtained from a signal generator. It gives an *a priori* frequency corresponding to the pulsar period received at the observation station [6],[7]. The reference signal of this signal generator is the hydrogen maser.

Observation of PSR1937+21

By using above system, the observation of PSR1937+21 was carried out at 1.5GHz band from Oct. 31 to Nov. 4, 1991. Fig.3 shows the detected pulse figure in one period, which is after averaging of about 1.5 million pulses (corresponds to about 40 minutes). The second peak is an interpulse. Observed pulse width is about 70 μsec , which is reasonable value compared with the estimated pulse width 60 μsec . This value is the maximum difference of dispersion delays for 270kHz bandwidth at 1383.67MHz (the lowest frequency band in this observation), and is calculated by Eq.2 where DM = 71 (pc/cm^3).

We got such averaged pulses every 1 hour, and defined their peak points. If the calculated pulsar period was equal to the observed pulsar period, these peaks were to appear at the same point in any interval. At first, however, the peak points seemed to drift as time went, as if they were dominated by some

systematic effect. We considered this was an apparent change caused by incomplete compensation of Doppler effect, and removed this drift by the least square method. Fig. 4 shows the residual of each data from the least square fitting line. The error bar represents a typical dt_{obs} 6.4 μsec calculated by Eq.1, where dt = 70 μsec , P = 1.557806 $msec$ (epoch = 2445303.2940 Julian ephemeris date) [7], T_{sys} = 37 K, B = 270kHz, $< S >$ = 8mJy, G = 0.42 K/Jy, and T = 2400 sec are assumed. The standard deviation calculated from these data is 9.7 μsec .

From the residual shown in Fig.4, we calculated the Allan variance by;

$$\sigma_y^2(\tau) = \frac{1}{2}\left\langle \left[\frac{R(t+\tau) - R(t)}{\tau} - \frac{R(t) - R(t-\tau)}{\tau} \right]^2 \right\rangle \tag{3}$$

where $R(t)$ is a residual at time t, and the angled bracket is an average taken over all available triplets. The $\log \sigma_y(\tau)$ is plotted in Fig.5. Each data is corresponds to τ = 1,2,3,4,5,24, and 48 hours. The value at τ = 48 hours has a large error bar, because the number of samples was very few. Except this one, data seems to be on a straight line with the precision of 16 μsec $/\tau$.

Conclusion

We developed an observation system for millisecond pulsars, and observed the pulse timing of PSR1937+21 with the precision of about 16μsec $/\tau$. Our main purpose is to use the pulsar timing as a most stable clock, so our measurement precision should be better than present value by at least one order. For this improvement, we plan to expand the observation bandwidth B further to decrease dt_{obs} , and investigate some methods. The local sweep method is one of them. By using it, one channel can track one pulse in some frequency band by sweeping a local frequency and shifting its observable frequency band along with the dispersion curve. It is equal to expanding the bandwidth of one channel.

Besides the use as a clock, various applications of a millisecond pulsar's pulse timing are considered. Its high stability is expected to be a good probe of detecting the dispersion fluctuation, gravitational wave and so on. We will study these subjects when we can take timing data with enough precision.

References

[1] M.M. Davis, J.H. Taylor, J.M. Weinsberg, and D.C. Backer, "High-Precision Timing Observations of the Millisecond Pulsar PSR1937+21," Nature, 315, pp.547-550, 1985.

[2] S. Hama, M. Imae, H. Kiuchi, and H. Takaba, and F. Takahashi, "Observation Plan of High-Stable Pulsars in CRL," Proceedings of the 21st PTTI meeting, pp.289-293, 1989.

[3] R.S. Foster and D.C. Backer, "Constructing a Pulsar Timing Array," RAL(Radio Astronomy Laboratory) Preprint No.168, 1990.

[4] H.Ögelman and E.P.J.von den heuvel, Timing Neutron Stars, pp.4-5, Kluwer Academic Publishers,1989.

[5] D.C. Backer and R.W. Hellings, "Pulsar Timing and General Relativity," Ann. Rev. Astron. Astrophys., 24, pp.537-575,1986.

[6] M.L.Meeks, Methods of Experimental Physics, vol.12-part C, pp.308-314, Academic Press, 1976.

[7] L.A. Rawley, J.H. Taylor, M.M. Davis and D.W. Allan, "Millisecond Pulsar PSR1937+21: A Highly Stable Clock," Science, 238, pp.761-765, 1987.

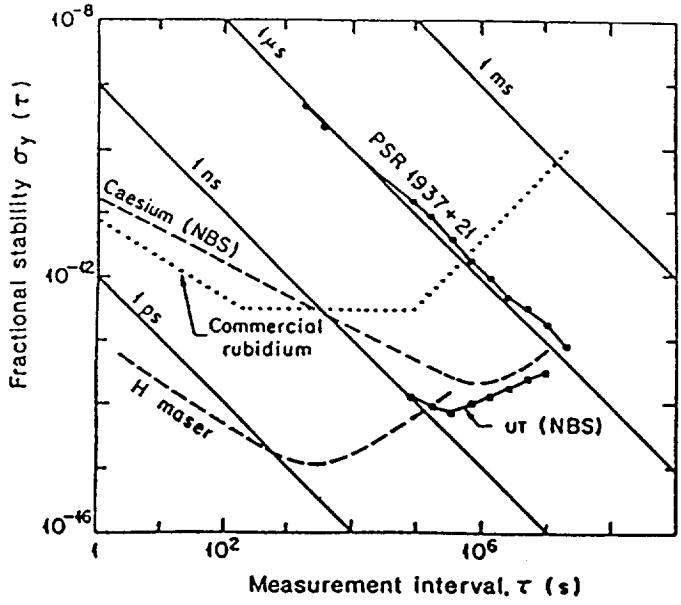

Figure 1 Fractional frequency stability for PSR1937+21 at Arecibo observatory [1]

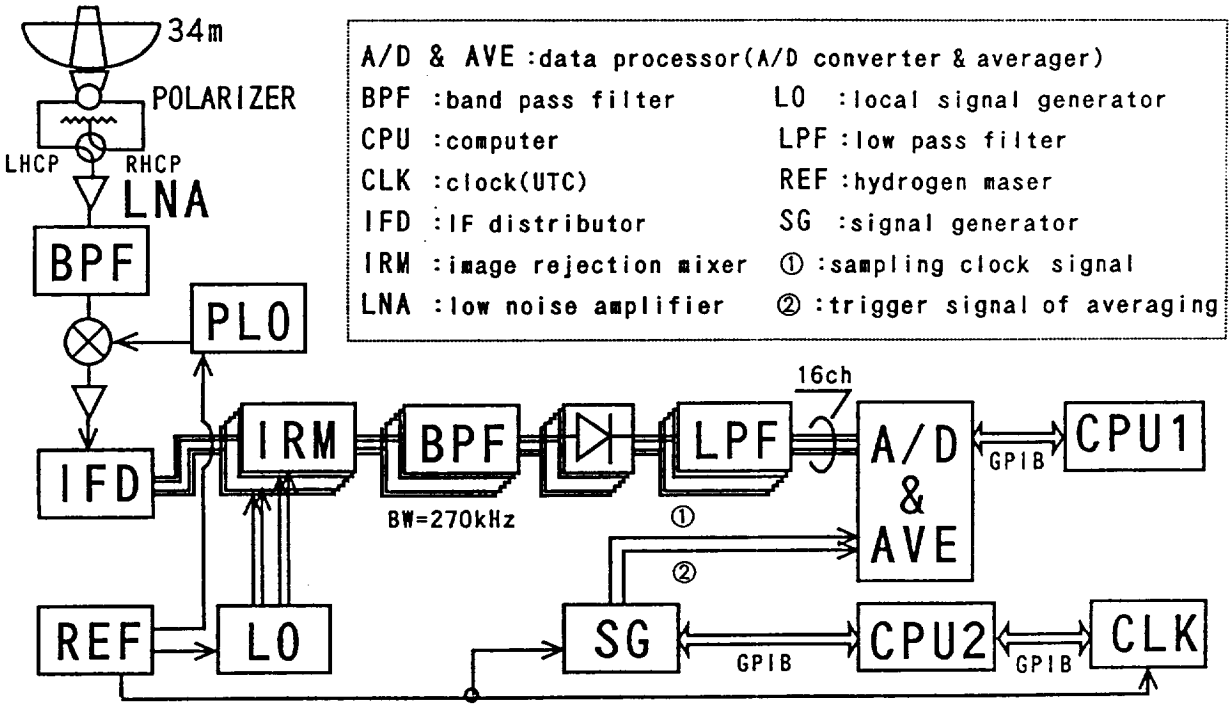

Figure 2. Block diagram of pulsar observation system at CRL.

Pulsar signal from 1.5GHz receiver is down converted at the first mixer to IF-band(100-500MHz). Divided IF signal from IFD is converted to video band at IRM, restricted in 270 kHz bandwidth, then detected. Detected signal is restricted from 150 Hz to 20 kHz at LPF, A/D converted and averaged in data processor, then saved in the host computer(CPU1). Another computer (CPU2) controls clock signals for the data processor . It reads time from CLK and calculates the pulse period received at the observation station in real time, then sends the period to the signal generator.

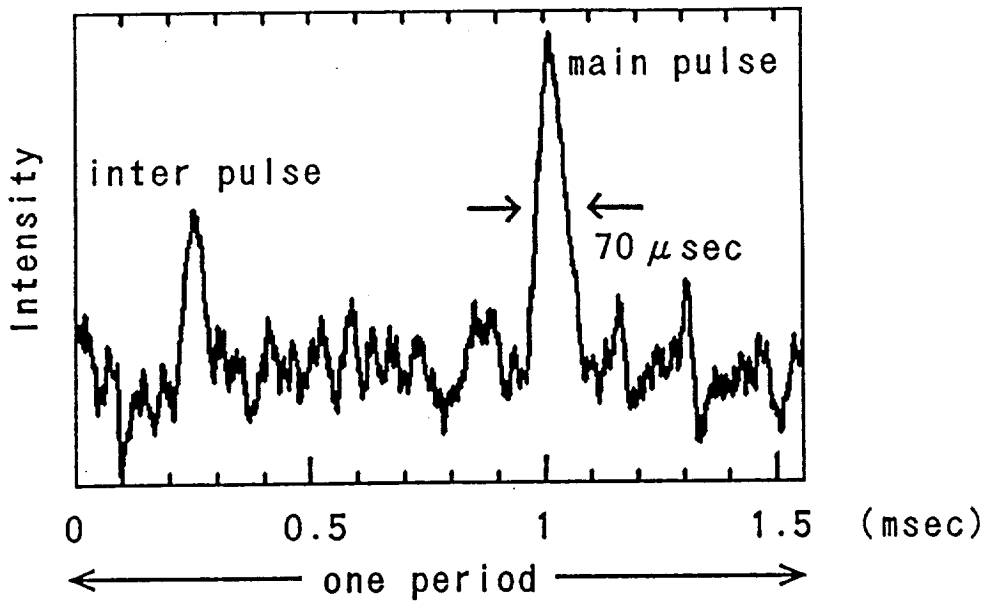

Figure 3. Pulse figure of PSR1937+21 observed at 1.5GHz.

It is acquired after averaging of 1.5 million pulses.

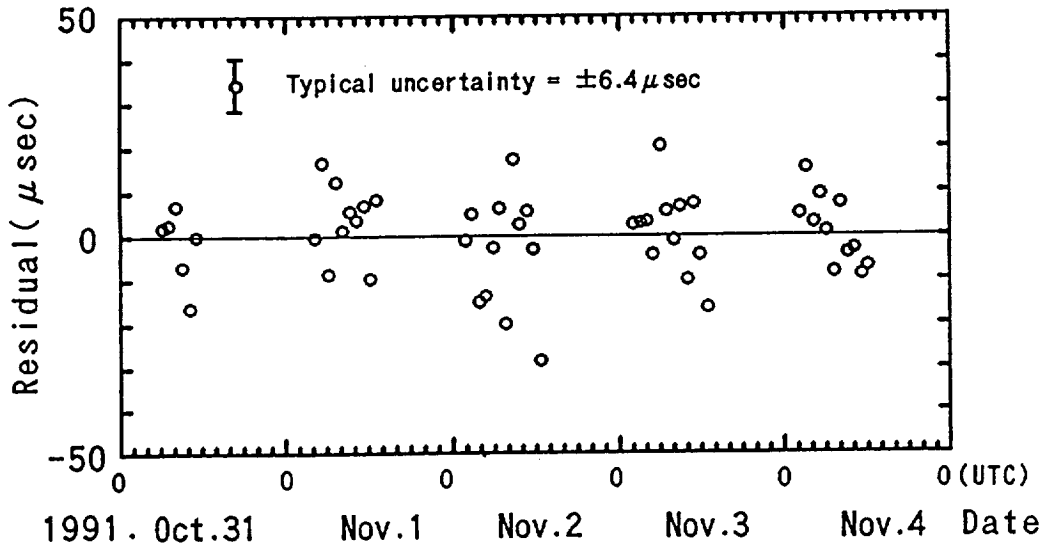

Figure 4. Post-fit arrival time residuals for PSR1937+21.

Arrival times are acquired from the peak points of averaged pulses taken over one hour. The least square fitting is carried out as canceling the drift of data. The residuals are derived from the fitting line.

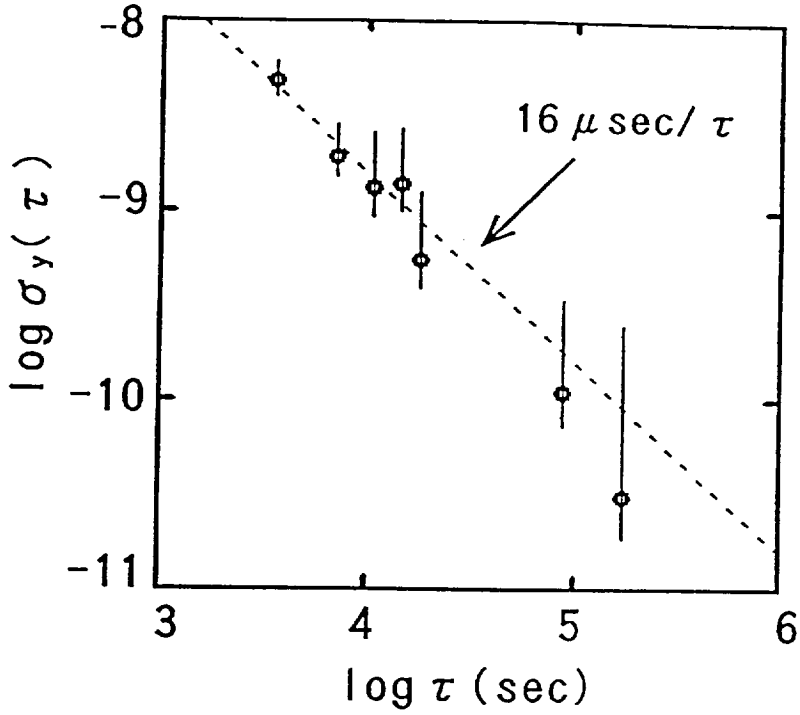

Figure 5. Fractional frequency stability for PSR1937+21 at CRL.

Each circle is calculated from the data of 5 days observation. The broken line corresponds to the precision of our system, 16 μsec/τ.

IN ORBIT DEMONSTRATION OF A H-MASER CLOCK SYSTEM

by

G. Busca, L.G. Bernier
Observatoire de Neuchâtel (ON), Switzerland

S. Starker
Deutsche Forschungsanstalt für Luft und Raumfahrt (DLR)
Oberpfaffenhofen, Germany

S. Feltham
European Space Agency (ESA), Noordwijk, The Netherlands

ABSTRACT

The ESA-NASA technology demonstration flight of a pair of hydrogen masers on the EURECA III mission is planned for 1998. The ESA part of the experiment will have a maser built by Neuchâtel Observatory and a microwave T&F transfer system derived from the existing PRARE system. The NASA part of the experiment will have a maser built by the Smithsonian Astrophysical Observatory and a laser T transfer system. The technology demonstration experiment is described with its expected outcomes and applications.

1.0 INTRODUCTION

This paper reports a proposal submitted by Neuchâtel Observatory (ON) in cooperation with the Deutsche Forschungsanstalt für Luft und Raumfahrt (DLR) to the European Space Agency (ESA) for the space technology demonstration of a H-maser with a microwave Time & Frequency Transfer (T&FT) system to be flown on the EURECA III spacecraft which will be launched in 1998.

The Smithsonian Astrophysical Observatory (SAO) have submitted a similar proposal to the National Space Administration (NASA) for the flight of a SAO built maser with a laser Time Transfer (TT) system to be flown on the same mission. This project was reported in this 23rd PTTI meeting [1].

The high level of redundancy provided by the joint NASA-ESA technology demonstration flight of 2 masers with both a laser TT system and a microwave T&FT system obviously gives a high reliability level to the experiment but, most of all, makes possible a complete evaluation of the contribution of each maser and each transfer system to the overall T&F stability performance.

EURECA III will be a 6 month mission after which the EURECA spacecraft will be retrieved by the Space Shuttle. The ON maser

will be designed for a 10 year lifetime in order to demonstrate the level of performance achievable in future T&F applications in space.

The ESA project will involve Neuchâtel Observatory for the ESA maser physics package and electronics design, DLR and the Institute of Navigation of Stuttgart (INS) in Germany for the microwave T&FT system design and industries for the space qualification of the equipments.

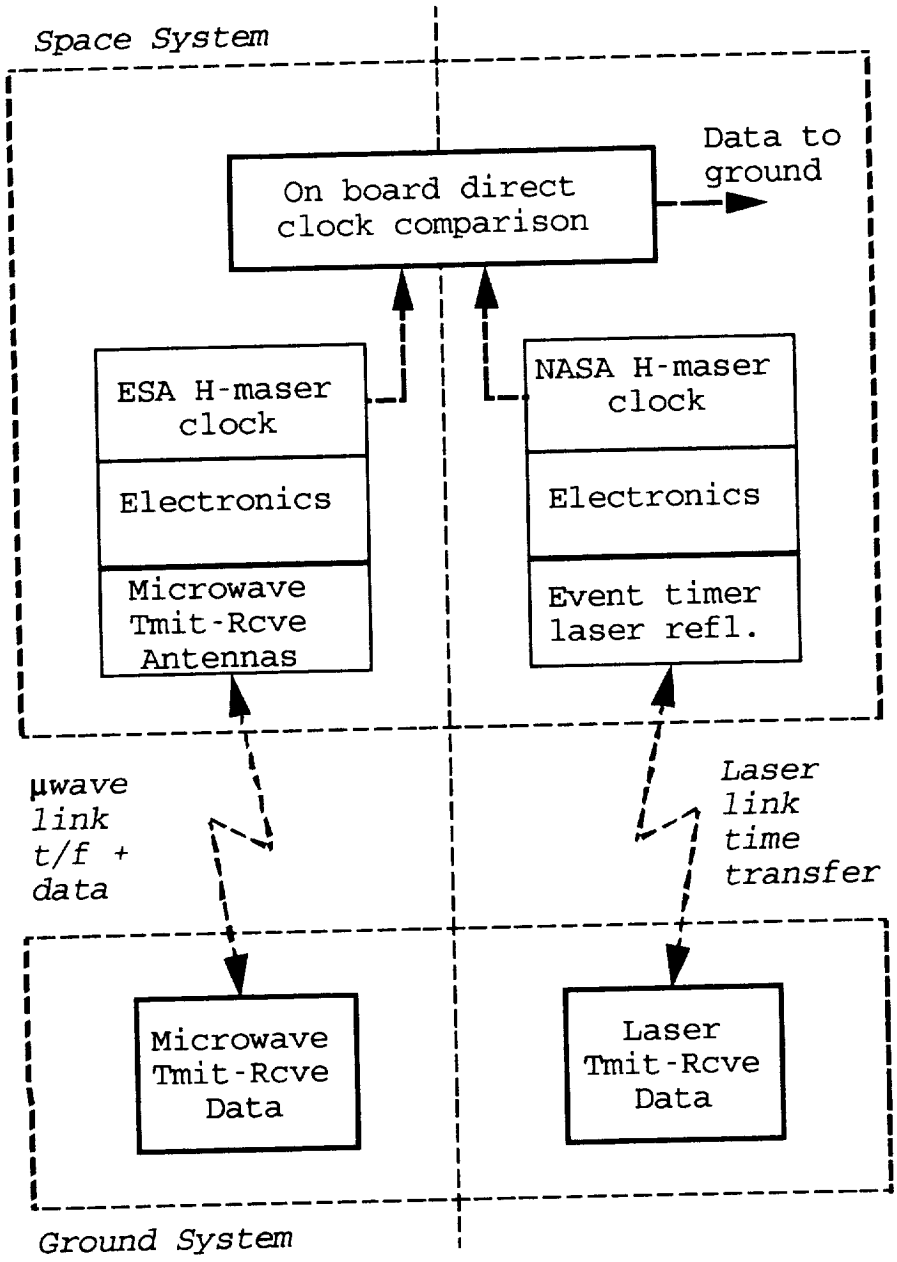

Figure 1
Proposed 2 H-maser T&F Transfer Experiment

The microwave T&FT system will be an extended version of the NAVEX microwave link demonstrated in the 1985 Shuttle mission D1 as a powerful tool for the control of two atomic clocks onboard the Shuttle. This method comprises a precise PRN-code time transfer combined with a simultaneous spread-spectrum data transmission. The extended version with higher carrier frequencies and larger signal bandwidths will be based on existing hardware-facilities of the PRARE ranging system developed by INS for use in ESA ERS-1 satellite.

The T&FT microwave system will be signal compatible with the ground equipment of PRARE and, as the latter, will use both X and S band 1-way links for real time ionospheric correction. Compatibility with PRARE makes the network of already existing PRARE ground stations usable for the present spaceborne masers T&F transfer experiment at the cost of only small modifications to the PRARE ground stations.

2.0 LOCAL & REMOTE T&F TRANSFER & MEASUREMENT CAPABILITIES

Fig.1 shows the schematic diagram of the planned NASA-ESA maser mission on EURECA III.

2.1 LOCAL COMPARISON OF SPACEBORNE H-MASERS

The frequency difference between the ESA and NASA masers is measured continuously during the whole mission (6 to 9 months) using the on board direct clock comparison system. The comparison data is stored locally and transmitted to ground on the telemetry link when tracking stations are visible. The direct comparison will allow the estimation of the relative frequency stability between the 2 H-maser clocks (characterized in the time domain by the classic and modified Allan variances) for averaging periods τ in the range from 1 second to 1 week with a very good statistic confidence.

2.1 LASER REMOTE TIME TRANSFER

The laser TT system [1] allows the remote measurement of the time stability of the space masers. The time comparison is made between a ground maser and the spaceborne maser with a sampling interval equal to the time interval between 2 successive passes of the EURECA spacecraft, i.e. $\tau \geq 5400$ s. These time stability measurements will also make possible the estimation of the long-term frequency stability of the spaceborne masers.

The NASA spaceborne TT system is equipped with a corner laser reflector, a laser detector and a time tagging counter. The laser ground station measures the 2 way time propagation time of the laser pulse using the passive corner reflector. The spaceborne

laser detector and time tagging counter determine the time of arrival of the laser pulse in terms of the spaceborne clock local time.

A propagation time error of ≈ 10 ps is estimated to be achievable in the laser TT system [2]. The time error accumulated by the spaceborne H-maser clock over a full orbit is also ≈ 10 ps. Therefore time transfers with a precision of the order of 10 ps is possible from one laser station ground clock to another even if the EURECA spacecraft is not in common view. State-of-the-art time transfers between ground clocks, using already existing laser ground stations, is indeed a highly attractive application of the spaceborne masers experiment.

2.2 MICROWAVE REMOTE T&F TRANSFERS

The microwave T&F transfer system allows the remote measurement of both the short-term and long-term stability of the spaceborne H-masers. During each contact period, the short term stability is measured continuously from the ground stations that are equipped with both a H-maser and a modified PRARE receiver.

The typical contact period is 10 minutes. Several frequency samples averaged over a τ = 100 s averaging interval can be acquired in a single pass. This allows a frequency transfer to the 1×10^{-14} level over a single pass. Frequency averaging over the whole 10 minutes pass yields a single τ = 600 s frequency sample. In this way the spaceborne H-maser frequency stability with respect to a ground H-maser reference can be measured with a few parts in 10^{15} uncertainty by using multi-pass statistics.

The long-term stability of the spaceborne H-maser is estimated by means of time transfers. The time interval error accumulated by the spaceborne H-maser clock with respect to a ground H-maser clock is sampled at every pass over a ground station equipped with a maser and a PRARE receiver. Note that the time interval error accumulated by the spaceborne H-maser clock during a 600 s contact interval is only 1 ps.

The transmission through the telemetry link of the local frequency comparison between the 2 spaceborne H-masers together with the T&F microwave remote comparison between the spaceborne H-masers and the ground H-maser reference make possible a real time measurement of the microwave T&FT system noise.

The contributions of residuals of the ionospheric propagation model, of the geometric doppler and delay cancellation model, and of the relativistic correction model to the microwave T&FT system accuracy are estimated in the following sections below.

The schematic of the PRARE system, modified to provide two X band channels instead of one, permitting the evaluation of 2 spaceborne hydrogen maser clocks, is shown on Fig.3 and Fig.4.

The standard PRARE T&FT system works as follows. Two one-way signals, one in S band and one in X band, are generated from the spaceborne maser and sent to the ground stations. The signals carry both time information, contained into the spread spectrum PRN code modulation, and frequency information, contained into the carrier phase. By measuring the differential delay and the differential doppler between the same signal propagated simultaneously through X and S bands, the actual ionospheric delay and doppler can be determined by the ground stations. A coherent transponder in the ground station sends the signal back to the spaceborne PRARE system in X band. Again both time and frequency information are transmitted through the PRN code and carrier. The transponded signal is received and processed by the PRARE system aboard the space vehicle and yields the one-way delay and the one-way doppler which are estimated to be half the 2-way delay and half the 2-way doppler respectively. The computed 1-way doppler and delay are transmitted in real time to the ground station via the data link.

In standard PRARE applications, the information provided by the system is used for geodetic purposes. In our application, on the other hand, the knowledge of the 1-way doppler and delay, corrected for the actual ionospheric propagation effects and for the relativistic effects discussed in next sections are used by the ground station in order to compare to a high precision the time and frequency of its reference clock with respect to the space clock.

Note that the PRARE system, contrary to the doppler cancellation system of [7], [8] or to the doppler and delay cancellation system proposed in [9], does not try to compensate in real time and by hardware the ionospheric and geometric delay and doppler. Instead these effects are first measured and then corrected by software.

3.3 PRESENT STATUS AND FORESEEN IMPROVEMENTS OF PRARE

The time transfer error achievable with the standard PRARE ground station of the first generation ERS-1 PRARE, which uses a 60 cm dish antenna, is limited by the S/N ratio to a level of 50 ps for an averaging time of 1 s. By increasing the averaging time to > 10 s, the error can be reduced to a limiting value of about 5 ps [10]. This level of performance is comparable or better than that achievable with a laser TT system. On the other hand the frequency transfer error of the ERS-1 PRARE system is limited by the resolution of the counter on board which is 5×10^{-12} for an averaging time of 1 s. This is not acceptable in view of the maser stability performance which is 1×10^{-13} over the same interval. However the counter resolution can be increased by 1 order of magnitude by a minor modification of the PRARE spaceborne equipment. This modification of the counter would yield a white noise floor of 5×10^{-13} for an averaging time of $\tau = 1s$, improving as $1/\tau$ with the averaging time, and the FT

The laser TT system is expected to track the EURECA spacecraft with a millimeter level range accuracy. The tracking data will be used to calibrate the non-dispersive tropospheric delay in the microwave T&FT system to the corresponding level of time accuracy.

3.0 DETAILED DESCRIPTION OF THE SPACE AND GROUND SYSTEMS

The next sections report the detailed description of the space and ground systems used in the ESA part of the experiment.

3.1 ESA SPACEBORNE MASER

Fig.2 shows a drawing of the spaceborne H-maser to be produced by ON. This preliminary design of the spaceborne physics package is based on our 10 year experience with the original EFOS ground masers [3], that are used in VLBI applications, in addition to our on going recent experience gained in the development of the EFOS-B ground maser for ESTEC [4]. Only the features related specifically to the adaptation of the physics package to the space environment are reported below.

The main design features of the ESA spaceborne maser are as follows. The vacuum system uses a passive getter system for pumping hydrogen. A small ion pump is also necessary in order to pump the residual non-getterable gases present in the vacuum enclosure. The high thermal insulation between the cavity and the base plate that is required by the use of an aluminium microwave cavity is naturally provided by the space vacuum environment. A solid state hydrogen supply is used which is much more reliable and lightweight than the conventional hydrogen bottle and pressure regulator.

An auxiliary mode cavity oscillator is used in the Automatic Cavity Tuning (ACT) system [5]. The output frequency of the TE_{013} auxiliary mode oscillator is measured using a counter. By stabilizing the frequency of the TE_{013} auxiliary mode, the frequency of the TE_{011} main mode is automatically stabilized due to the fact that the frequency ratio of the 2 modes is constant. This type of ACT does not perturb at all the maser signal because it uses a mode of the cavity far from the TE_{011} mode. It has no ambient temperature sensitivity since the oscillator amplifier is secured to the cavity and is thermally controlled by the ACT loop to the same level of thermal stability as the cavity itself.

The size and mass limitations imposed by the space qualification requirements can be satisfied by a careful mechanical design. The main trade-off issue in the mass budget is the choice of the thickness to be used for the 5 layers of magnetic shields. The preliminary overall characteristics of the spaceborne maser are

- 35 cm diameter and 70 cm length
- 70 kg mass including electronics
- 70 W power consumption

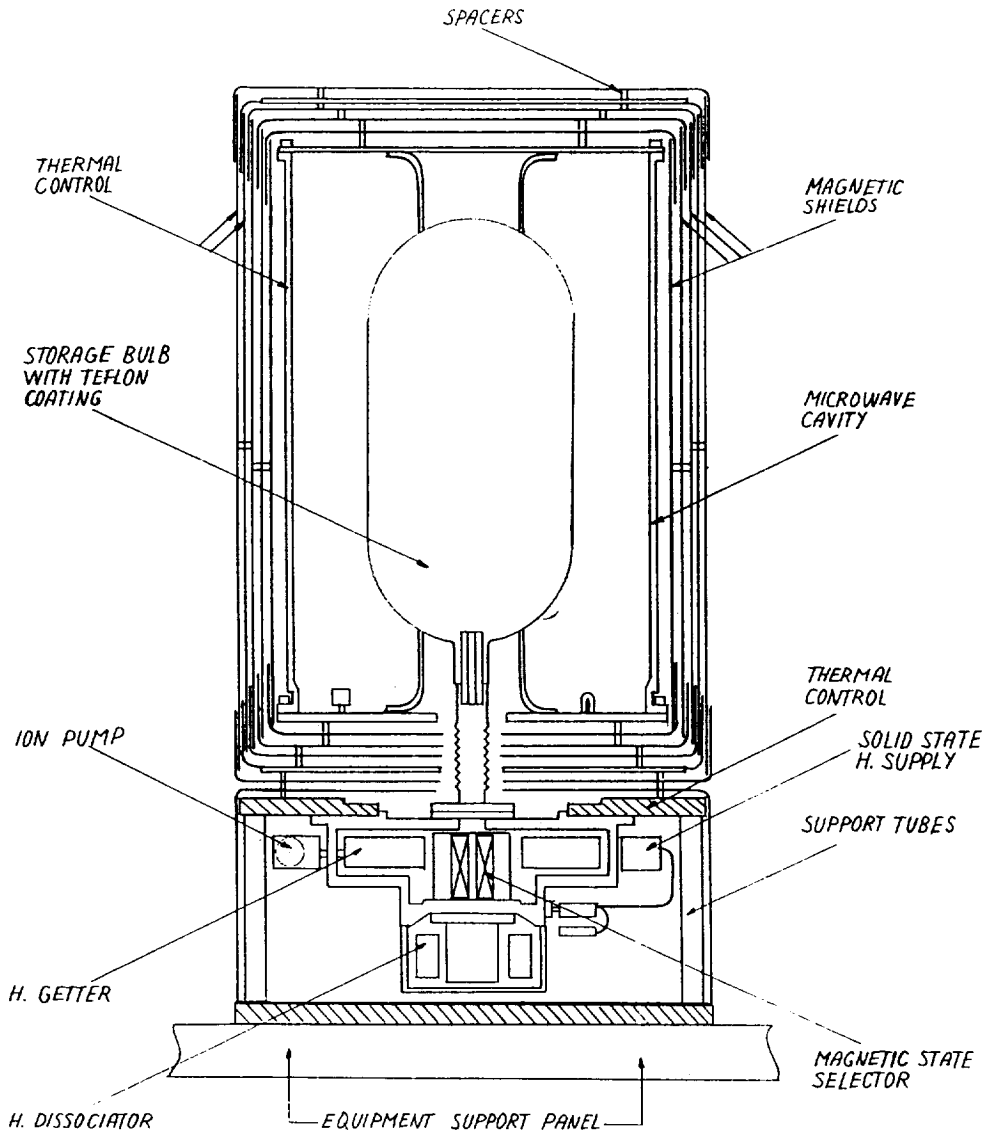

Figure 1
Sketch of Spaceborne H-maser Physics Package

In addition to the drastic vibration and acceleration specifications on the mechanical design imposed by space qualification, the main environmental constraints that are foreseen are thermal and magnetic.

The temperature of the instrument mounting base plate on the EURECA platform is specified to be within a [0 C°, 40 C°] range. Therefore the temperature coefficient of the maser must be very small in order to maintain state-of-the-art frequency stability.

An extremely low thermal sensitivity will be achieved actively by the use of the ACT system.

The magnetic torquers used to control the attitude of the EURECA spacecraft produce magnetic pulses which intensity can reach up to 3 Gauss on the worst area of the instrument mounting panel. In the most favorable area of the panel the pulse strength reaches 50 mGauss. This is to be compared to the 1 mGauss field variations encountered by ground masers under normal operating conditions.

3.2 PRARE T&F MICROWAVE TRANSFER SYSTEM

The development of the microwave T&FT system will be managed by DLR which already has a working experience in this field [6]. The adaptation of the existing PRARE system, which was developed by DLR for use in the ERS-1 satellite, to the requirements of the present maser experiment is a cost-effective alternative to the development of a completely new T&FT system not only from the point of view of the production of the space qualified equipment but also because existing PRARE ground stations become usable for the T&F monitoring of the spaceborne masers at the price of minor modifications.

The schematic of the PRARE system, modified to provide two X band channels instead of one, permitting the evaluation of 2 spaceborne hydrogen maser clocks, is shown on Fig.3 and Fig.4.

The standard PRARE T&FT system works as follows. Two one-way signals, one in S band and one in X band, are generated from the spaceborne maser and sent to the ground stations. The signals carry both time information, contained into the spread spectrum PRN code modulation, and frequency information, contained into the carrier phase. By measuring the differential delay and the differential doppler between the same signal propagated simultaneously through X and S bands, the actual ionospheric delay and doppler can be determined by the ground stations. A coherent transponder in the ground station sends the signal back to the spaceborne PRARE system in X band. Again both time and frequency information are transmitted through the PRN code and carrier. The transponded signal is received and processed by the PRARE system aboard the space vehicle and yields the one-way delay and the one-way doppler which are estimated to be half the 2-way delay and half the 2-way doppler respectively. The computed 1-way doppler and delay are transmitted in real time to the ground station via the data link.

In standard PRARE applications, the information provided by the system is used for geodetic purposes. In our application, on the other hand, the knowledge of the 1-way doppler and delay, corrected for the actual ionospheric propagation effects and for the relativistic effects discussed in next sections are used by the ground station in order to compare to a high precision the

time and frequency of its reference clock with respect to the space clock.

Note that the PRARE system, contrary to the doppler cancellation system of [7], [8] or to the doppler and delay cancellation system proposed in [9], does not try to compensate in real time and by hardware the ionospheric and geometric delay and doppler. Instead these effects are first measured and then corrected by software.

3.3 PRESENT STATUS AND FORESEEN IMPROVEMENTS OF PRARE

The time transfer error achievable with the standard PRARE ground station of the first generation ERS-1 PRARE, which uses a 60 cm dish antenna, is limited by the S/N ratio to a level of 50 ps for an averaging time of 1 s. By increasing the averaging time to > 10 s, the error can be reduced to a limiting value of about 5 ps [10]. This level of performance is comparable or better than that achievable with a laser TT system. On the other hand the frequency transfer error of the ERS-1 PRARE system is limited by the resolution of the counter on board which is 5×10^{-12} for an averaging time of 1 s. This is not acceptable in view of the maser stability performance which is 1×10^{-13} over the same interval. However the counter resolution can be increased by 1 order of magnitude by a minor modification of the PRARE spaceborne equipment. This modification of the counter would yield a white noise floor of 5×10^{-13} for an averaging time of $\tau = 1$s, improving as $1/\tau$ with the averaging time, and the FT system would catch up the maser frequency stability curve for an averaging time of 100 s.

It would be possible to further improve the FT performance of the PRARE system but at the cost of a major redesign. The white phase noise floor due to the S/N alone is 1×10^{-14} $1/\tau$.

The temperature sensibility of the internal delay is about 30 ps/C° and can be compensated with a 20 fold improvement factor by the internal delay calibration system. Therefore a < 10 ps delay stability can be achieved over a full orbital period.

In conclusion the PRARE system happens to match the requirements of our spaceborne masers experiment at the cost of minor modifications. The latter include the addition of a second channel in X band since 2 masers are to be evaluated.

3.4 T&FT SYSTEM DESIGN OPTIONS

Many design options of the T&FT system are open. For reliability reasons the H-maser clocks signals will be cross-switchable. Therefore the clock labeled N°1 in the S band 1-way link of figure 3 may may be switched to either H-maser signal in case the other maser fails. For the same reliability reasons the use of 2 redundant transmitter chains sharing the same antenna is considered.

The use of 2 channels in the X band downlink allows a continuous and simultaneous comparison between the H-maser spaceborne clocks N°1 and N°2. This is necessary for the ground measurement of the relative short-term stability between clock N°1 and clock N°2. The spaceborne hardware could be simplified by the use of only one X band downlink channel, like in the standard PRARE package, but then the clock N°1 vs clock N°2 data is obtained from non-simultaneous clock N°3 vs clock N°2 and clock N°3 vs clock N°1 measurements.

The modification options for the accommodation of the existing PRARE ranging ground equipment to both internal delay calibration and T&FT requirements are still open.

4.0 CINEMATIC AND RELATIVISTIC ASPECTS

The true 1-way delay and 1-way doppler are not half the measured 2-way delay and doppler because of the asymmetry due to the fact that the space vehicle moves during the signal propagation. It can be shown that the frequency offset measured on ground is given by

$$\Delta f/f = \delta f/f + DA^{(1)} + DA^{(2)} + D^{(2)} + GS \qquad (1)$$

where $\Delta f/f$ is the normalized frequency offset between the ground and the spaceborne maser after correction for ionospheric propagation effects, $\delta f/f$ is the true frequency offset between the clocks, $DA^{(1)}$ is the first order doppler asymmetry term, $DA^{(2)}$ the second order doppler asymmetry term, $D^{(2)}$ the second order doppler and GS the gravitational frequency shift.

The different terms are given by

$$DA^{(1)} = \frac{1}{2}\left(\left(\vec{\beta}_1 - \vec{\beta}_G\right)\cdot\vec{r}_{1G} - \left(\vec{\beta}_G - \vec{\beta}_2\right)\cdot\vec{r}_{G2}\right) \qquad (2)$$

$$DA^{(2)} = \left(\left(\vec{\beta}_1\cdot\vec{r}_{1G}\right)^2 - \left(\vec{\beta}_1\cdot\vec{r}_{1G}\right)\left(\vec{\beta}_G\cdot\vec{r}_{1G}\right) - \left(\left(\vec{\beta}_2 - \vec{\beta}_G\right)\cdot\vec{r}_{G2}\right)^2\right) \qquad (3)$$

$$D^{(2)} = \frac{1}{2}\left(\beta_G^2 - \beta_1^2\right) \qquad (4)$$

$$GS = \frac{\phi_G - \phi_1}{c^2} \qquad (5)$$

The $\vec{\beta}_i = \frac{\vec{v}_i}{c}$ are velocity vectors normalized by the velocity of light c. The $\vec{r}_i$ are position vectors. ϕ is the gravitation potential. Index 1 refers to the position and velocity of the satellite, in an inertial system of coordinates, at the time a synchronization pulse is generated in the satellite and sent to the ground. Index G refers to the position and velocity of the ground station at the time the pulse arrives to the ground. Index 2 refers to the position and velocity of the satellite at the time the pulse transponded from the ground arrives to the satellite.

In the planned experiment the gravitational shift is nearly constant, due to the circular orbit, and equal to $\approx 6 \times 10^{-11}$. The second order doppler shift is of the same order of magnitude and nearly constant for the same reason. These conditions are radically different from the conditions of the 1976 red-shift experiment [11] in which the gravitation shift and second order doppler changed by order of magnitudes in the course of a ballistic flight. In the present experiment it is the doppler asymmetry terms that show a high dynamic change in the course of every pass of the space vehicle over a ground station. The first order term $DA^{(1)}$ will reach maximum values of the order of 1×10^{-10}. It will be possible to check the relativistic model of the asymmetry terms to the order of 1×10^{-15}.

5.0 GROUND SEGMENT

At present the only ground station committed to the laser TT aspect of the experiment is the NASA station of Maoi in Hawaii. The Matera station in southern Italy and the Shanghai station in China are showing interest to join. The scientific benefit of the participation of several laser tracking stations is the possibility of time transfer to a 100 ps level of accuracy between distant ground clocks.

As for the microwave T&FT aspect, the commitment of the Mas Palomas station is expected. The participation of ground stations equipped with both laser tracking and PRARE systems allows the precise calibration of the microwave tropospheric delay.

All VLBI stations use hydrogen maser clocks and those located within the EURECA III visibility region could be equipped with mobile PRARE ground equipment. The relevant European stations are Matera and Noto in Italy.

Besides, all existing PRARE stations located within $\pm 30°$ of latitude, i.e. about 10 stations, could participate. The PRARE stations are committed to geodesy work and the benefit they could

draw from the experiment is the mm level position determination accuracy provided by the use of a spaceborne maser reference clock. A very precise tracking of the EURECA III orbit is required in order to make possible the accurate position determinations of the ground PRARE stations. This could be easily achieved if a space qualified GPS receiver is carried aboard the EURECA III spacecraft in addition to the laser ranging system. As a matter of fact, part of the original goals of the ERS-1 PRARE experiment, that failed because of a destructive latch-up in the memory subsystem of the ERS-1 PRARE space package, could be achieved by means of the EURECA III maser experiment.

ACKNOWLEDGEMENTS

We would like to thank Mr. N. Sagna, from Neuchâtel Observatory, for his calculation of the relativistic doppler asymmetry model, and also Prof. P. Hartl and W. Schäfer, from the Institute of Navigation of the University of Stuttgart, for the information about the detailed PRARE performance.

REFERENCES

[1] Vessot R.F.C., Mattison, E.M., Decher R., "Test of an Orbiting Hydrogen Maser Clock System Using Laser Time Transfer", to be published in Proc. 23rd Annual PTTI Planning and Applications Meeting, December 3-5, 1991, Pasadena, CA.

[2] Veillet C., "Lasso: The New Transatlantic Phase", to be published in *Proc. 23rd Annual PTTI Planning and Applications Meeting*, December 3-5, 1991, Pasadena, CA.

[3] Schlüter W., Nottarp K., Feil D., Busca G., "First Experiences with the H-Maser EFOS-1", *Proc. of the 14th Annual PTTI Applications and Planning Meeting*, Greenbelt, November 1982, pp. 393-408.

[4] Bernier L.G., Busca G., "Recent Progress in the Development of the EFOS-B Hydrogen Maser at Neuchâtel Observatory", *Proc. 5th EFTF*, Besançon, March 1991, pp.404-406.

[5] Busca G., Johnson L., "A New Automatic Cavity Tuning for Active H Masers", *Proc. 1st European Time and frequency Forum*, Besançon, March 1987, pp.339-341.

[6] Starker S., Arko D., Hammesfahr J., Nau N., Sappl E., Schild H., Schimmel R., Stelzel F., *Navigation Experiment NAVEX on Spacelab Mission D1*, Final Report, DLR, Institute of Radio Frequency Technology, D-8031 Wessling.

[7] Vessot R.F.C., Levine M., Mueller L., Baker M., "The Design of an Atomic Maser System for Satellite Experiments", *Proc.*

21st Annual Symposium on Frequency Control, Atlantic City, April 1967, pp. 512-542.

[8] Vessot R.F.C., Levine M.W., "Performance Data of Space and Ground Hydrogen Masers and Ionospheric Studies for High-Accuracy Comparisons Between Space and Ground Clocks", *Proc. 28th Annual Symposium on Frequency Control*, Atlantic City, May 1974, pp. 408-414.

[9] Penfield H., Imbier E.,Vessot R.F.C., "Design of the STIFT Time and Frequency Transfer Microwave Ground Terminal", *Proc. 14th Annual PTTI Applications and Planning Meeting*, NASA Goddard Space Flight Center, Greenbelt, Maryland, November 30,December 1-2, 1982, pp. 223-241.

[10] Schäfer W., Institute of Navigation of the University of Stuttgart, private communication.

[11] Vessot R.F.C., Levine M.W., Mattison E.M., Hoffman T.E., Imbier E.A., Têtu M., Nystrom G., Kelt J.J., Trucks H.F., Vaniman J.L., "Space-Borne Hydrogen Maser Design", *Proc. 8th Annual PTTI Applications and Planning Meeting*, Washington, December 1976, pp. 277-233.

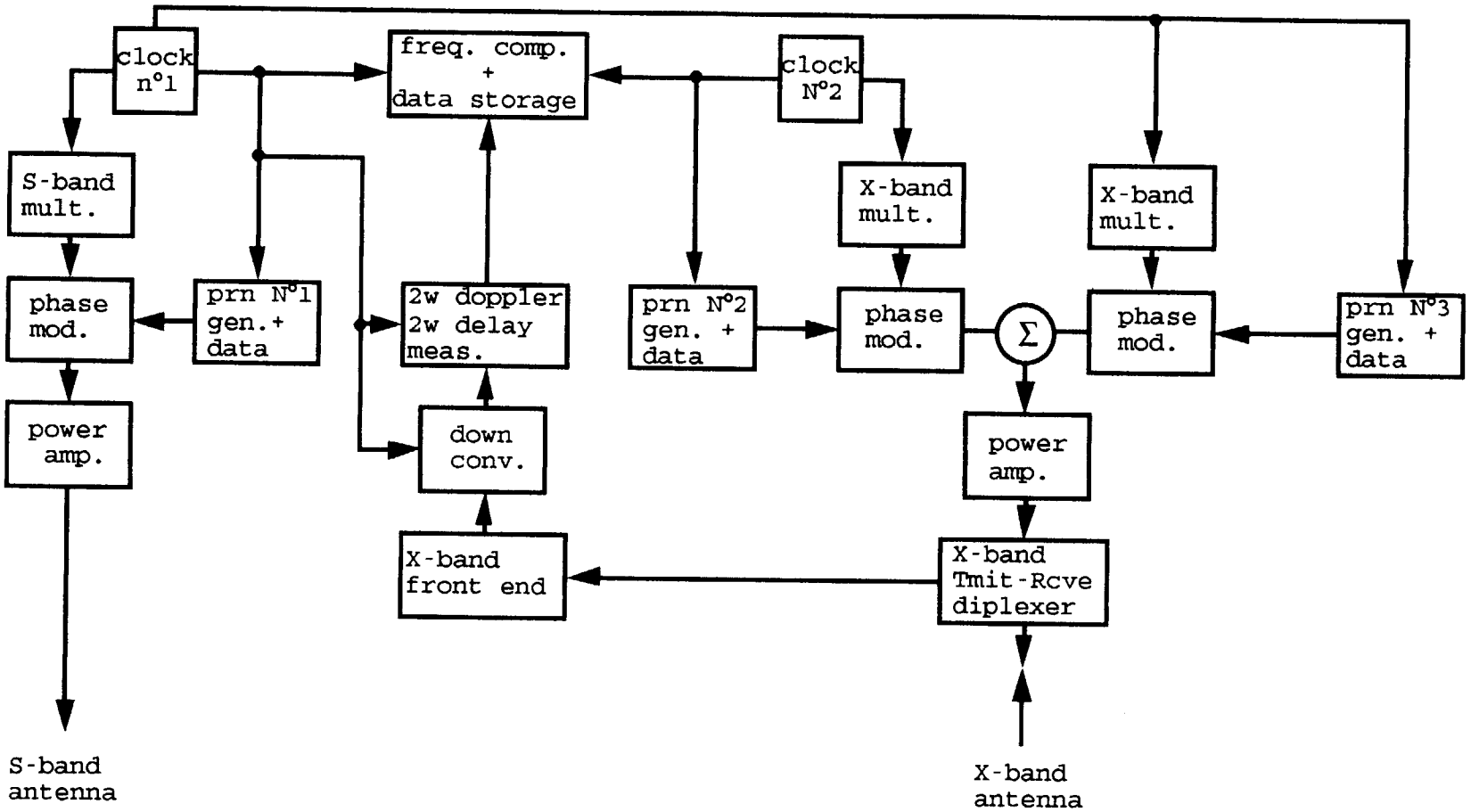

Figure 3
Modified Spaceborne PRARE

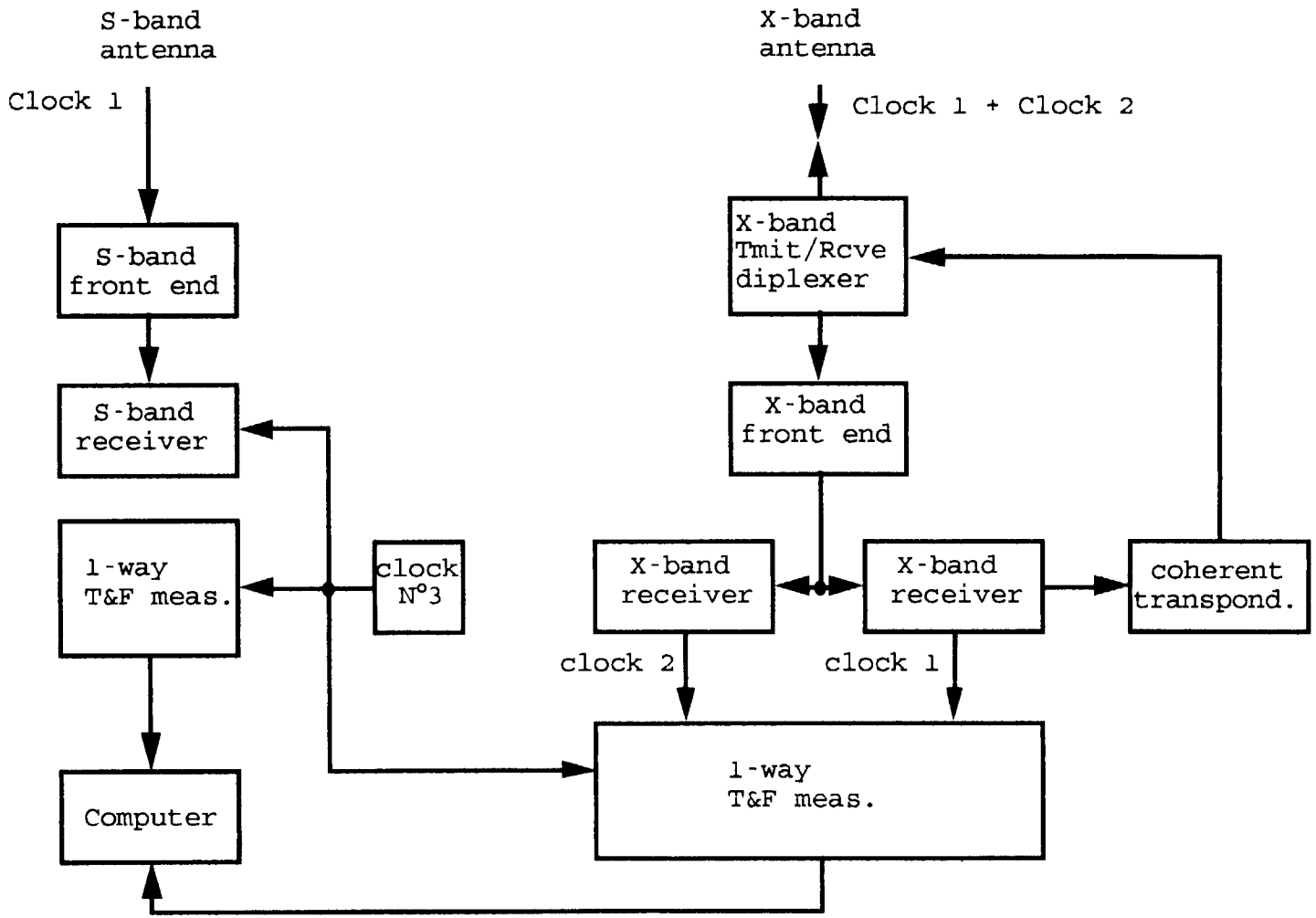

Figure 4
Modified Ground PRARE

TEST OF AN ORBITING HYDROGEN MASER CLOCK SYSTEM USING LASER TIME TRANSFER

Robert F.C. Vessot, Edward M. Mattison, and G.U. Nystrom
Smithsonian Astrophysical Observatory
and

Rudolph Decher

George C. Marshall Space Flight Center
National Aeronautics and Space Administration

Abstract

We describe a joint SAO/NASA program for flight testing an atomic hydrogen maser clock system design for long-term operation in space. The clock system will be carried by a shuttle-launched EURECA spacecraft. Comparisons with earth clocks to measure the clock's long-term frequency stability ($\tau > 10^4$ seconds) will be made using laser time transfer from existing NASA laser tracking stations. We describe the design of the maser clock and its control systems, and the laser timing technique. We discuss the precision of station time synchronization and the limitations in the comparison between the earth snd space time scales owin to gravitational and relativistic effects. We will explore the implications of determining the spacecraft's location by an on-board GPS receiver, and of using microwave techniques for time and frequency transfer. The possibility of a joint SAO/NASA/ESA (European Space Agency) test with a second hydrogen maser and a microwave time and frequency transfer system will be discussed in a separate paper.

INTRODUCTION

A number of future space applications will need high stability oscillators, such as hydrogen masers, having frequency stability better than 10^{-15} for time intervals between 10^3 and 10^5 seconds. Such applications include tests of relativistic gravitation[1], operation of Very Long Baseline Interferometers[2], high precision space tracking, and time synchronization by orbiting clocks[3]. When high-stability microwave signals are transmitted through the earth's atmosphere and compared with a high-stability oscillator, as in earth-based VLBI or microwave Doppler tracking, the measurement accuracy of the system is limited by fluctuations in atmospheric propagation, rather than by the oscillator's frequency stability. Such a system in space, however, would be almost completely free of propagation effects. Under spaceborne operation, measurement precision would depend primarily on the frequency stability of the maser oscillator, and could fully exploit the high frequency stability provided by an H-maser.

A joint NASA/SAO technology experiment to demonstrate the performance of this maser in space is now in progress. The frequency of the space maser will be compared with terrestrial clocks and time scales by means of laser pulse techniques and time measurement. This work, which is supported by the NASA Office of Aeronautics and Exploration Technology (OAET) "In Step" program, is currently in Phase B, during which we are defining the experiment and developing a plan for its implementation.

Development at SAO of an atomic hydrogen maser for space operation began in 1972 with the design and construction of a maser for the 1976 SAO/NASA Gravitational Redshift (Gravity Probe-A, or GP-A) test of the Einstein Equivalence Principle[4], in which a maser was launched by a Scout rocket to an altitude of 10,000 km in a nearly vertical two-hour flight. The next generation of space masers, designed for four years of continuous operation in space, has been under development at SAO, and a preliminary demonstration model has been built and operated.

Figure 1 shows the expected stability of the spaceborne SAO maser, represented by the Allan deviation $\sigma(\tau)$. As an example of the precision attainable with such an oscillator in space, one can consider Doppler ranging measurements. The limits imposed by this level of oscillator frequency stability on hour-to-hour determination of range-rate is 1.8×10^{-5} cm/sec, while the limit on range distance is 0.065 cm. These values are about two orders of magnitude better than can be achieved with current earth-based systems.

Maser frequency stability over short time intervals - less than roughly 10^4 seconds - is governed by the inherent thermal noise within the maser's oscillation linewidth and by the signal power to the receiver system. These characteristics are determined largely by the design of the maser's hydrogen storage bulb and hydrogen beam optics, all of which are similar in the space maser to the design of SAO's VLG-11 terrestrial H-masers. Systematic frequency variations, occurring for times beyond about 10^4 seconds, result in the up-turn in the $\sigma(\tau)$ curve shown in Fig. 1, and are the focus of interest in our investigation. The slanted lines in Fig. 1 represent the limits on frequency stability determination resulting from uncertainties of 20 picoseconds and 50 picoseconds, respectively, in the laser time transfer technique. With a 50 ps system, for example, we will be sensitive to maser frequency variations on the order of 2×10^{-15} for intervals of greater than roughly half a day.

In the planned SAO/NASA Space Maser experiment, the new space maser will be flown on a European Space Agency (ESA) EURECA spacecraft, and frequency measurements will be made by time transfer using existing laser ranging stations. A possible joint NASA/ESA experiment is also being considered, to test simultaneously a second H-maser on the EURECA spacecraft. This maser will be developed by the Neuchatel Observatory, Switzerland, led by G. Busca. In addition to the laser time transfer system, the joint experiment would use a microwave time transfer system developed by the Deutsche Forschungsanstalt für Luft und Raumfahrt (DLR), Oberpfaffenhofen, Germany, led by by S. Starker. This joint project would greatly broaden the technological goals of the experiment to include international time transfer at the sub-nanosecond level.

THE EXPERIMENT CONCEPT

The concept for making frequency comparisons between a spaceborne clock and an earth station originated in the early 1980s with a NASA-sponsored study of a Satellite Time and Frequency Transfer (STIFT)[5] mission, for which a combination of laser time transfer and microwave time and frequency comparison was proposed. Here the idea was to use highly precise laser timing, which is limited to clear sky conditions, to calibrate a pseudo-random-noise modulated microwave time transfer system, which would be useable under nearly all weather conditions. The study involved SAO, the US Naval Observatory, the National Bureau Of Standards, and the University of Maryland.

The present plan is to operate the maser on the EURECA spacecraft, which will be deployed from the NASA Space Shuttle, and boosted to an altitude of 525 km in a 28.5° inclination orbit. The spacecraft will remain in operation for approximately 6 months, after which it will be returned to a lower orbit and retrieved by the shuttle.

The EURECA spacecraft is shown in Fig. 2 with its solar panels extended. Magnetic torquers and cold nitrogen gas jets maintain its orientation in space with its solar panels facing the sun. Because EURECA's earthward-pointing surface will change as the spacecraft circles the earth, laser reflector/detector arrays will be mounted in three places to allow laser time transfer under all orientations. The procedure for time transfer is straightforward. When the spacecraft comes into view of the laser station, laser pulses are fired at the spacecraft. The time of reception of these pulses is recorded at the spacecraft in terms of the time kept by the space maser clock system. In addition, the pulse transmission times (epochs) and their round-trip propagation intervals are recorded on earth. One-half the propagation interval, with appropriate corrections, is then used to determine the spacecraft pulse reception time in terms of the earth clock, thus giving a comparison of time kept by the earth and space clocks.

The space maser's frequency will be measured over averaging intervals of approximately 94 minutes, EURECA's revolution period about the earth, as well as for intervals of a day and longer. Each day the spacecraft will be visible from the Hawaiian laser ranging site during several consecutive passes, separated by 94 minutes. With a laser timing precision of 20 ps, we expect to be able to make short-term frequency measurements with a precision of $\sigma_y(94) \sim 4 \times 10^{-15}$. For longer intervals, the precision improves with the time interval between measurements, as indicated by the straight lines in Fig. 1. The dominant factors likely to limit the frequency comparison precision are errors in correcting for gravitational and relativistic effects, owing to uncertainties in the spacecraft's position and velocity. The random processes that affect the stability of H-masers for periods less than roughly 10^3 seconds are well understood and not likely to be changed by the space environment. In the planned test, the goal is to measure any systematic effects that affect the operation of the maser; these effects will be observable at averaging intervals beyond one day.

Of particular interest are the effects of magnetic field and temperature variations, including the possible long-term effects of radiation in space. Environmental processes will be correlated with systematic variations of frequency. Continuous monitoring will be done of all relevant temperatures, the maser's internal vacuum, hydrogen source pressure and dissociator efficiency, and the maser's output signal level.

Figure 3 shows a block diagram of the experimental system, including the major EURECA electronic systems and the maser's control electronics, r.f. receiver, and clock and event timer. The receiver's frequency synthesizer operates from a 64 bit number-controlled oscillator; its settings can be adjusted by telecommand with a granularity of 7 parts in 10^{18}. The arrival time of the incoming laser pulse is registered by the event timer with a resolution of about 20 picoseconds and is stored in memory for subsequent telemetry to the EURECA ground control station, along with readings of the monitored system parameters.

During the mission, occasional telecommands from earth will be send to the maser's microprocessor to adjust the maser's operating parameters, such as its source H_2 pressure and internal magnetic fields. The microprocessor performs several functions, including controlling maser parameters; monitoring maser operation; and carrying out programmed sequential operations, such as determining the maser's internal magnetic field by varying the Zeeman oscillator's frequency and measuring the corresponding maser output power.

THE SPACE MASER

The internal structure of the second generation SAO space maser is based on design of the maser used in the GP-A mission, in that the cavity resonator, storage bulb and beam optics are similar. Figure 4 shows a cross section view of the new space maser. In the present maser we have substantially improved the thermal control system by taking advantage of the longer mission duration and the vacuum of space, which permits us to use multilayer insulation (MLI). The new thermal design evolved from the development at SAO of small passive masers, sponsored by the U.S. Naval Research Laboratory[6]. This design permits operation under atmospheric conditions, for testing, as well as in the vacuum of space. The technique employs a segmented cylindrical aluminum isothermal oven. The independence of the oven segments allows the oven to control heat flowing through the multilayer insulation, which dominates under atmospheric conditions, as well as heat flowing through structural members, which is most important when the maser is in vacuum.

The maser's cavity resonator is isolated from structural variations in the vacuum belljar that result from the atmospheric pressure change encountered when going from earth to space. Isolation is achieved by mounting the CER-VIT cavity resonator and storage bulb, as a subassembly, on a circular baseplate that is attached to one of the belljar necks near the center of the belljar endcap. The baseplate is almost completely isolated from the belljar, and is not affected by variations in belljar shape. The effects of axial thermal expansion of the cavity mounting structure are minimized by clamping the cavity onto its baseplate with a zero-rate Belleville spring; radial expansion is reduced by supporting the cavity on the baseplate by a quasi-kinematic roller mount. This mounting structure is identical to that used in the GP-A maser, which coped with 60 g shock and 20 g static accelerations generated by the solid fueled Scout rocket system.

A three-section printed-circuit magnetic field solenoid fits closely within the innermost magnetic shield that surrounds the titanium alloy vacuum belljar. The belljar is equipped with two demountable metallic vacuum seals. The cavity resonator's mechanical tuner is adjusted through a port sealed with a gold "O" ring. The belljar is joined by another gold "O" ring to a manifold, made of thin-walled stainless steel, that contains vacuum pumps and the hydrogen beam forming system. Four hydrogen-sorbing cartridges in a cross-shaped array on the manifold surround the hexapole state-selector magnet. A small ion pump scavenges non-hydrogen gases. Extrapolating from our experience with the GP-A maser, which operated continuously for one year with a single hydrogen sorption cartridge, the four sorption cartridges are expected to permit more than four years of continuous operation.

As in the GP-A maser, hydrogen for the maser is obtained from $LiAlH_4$ contained in a thermally-controlled vessel and maintained at about 40 psig. Hydrogen flow is regulated by servo control of the temperature of a palladium-silver diaphragm to maintain a constant pressure in the hydrogen dissociator. Molecular hydrogen is dissociated into atoms by an external r.f. power supply. Heat generated by the r.f. power dissipated in the vacuum-enclosed glass dissociator is conducted through the dissociator's walls to the bottom manifold flange, from which it is dumped to the EURECA heat sinks.

The maser's size, weight and expected power consumption are summarized in Table 1. Because EURECA's magnetic torquers produce magnetic field variations as high as 0.1 Gauss at the location of the maser, we will add a fifth layer of magnetic shielding, enclosing the entire maser, in order to prevent magnetic field inhomogeneity frequency shifts[7] that can result from these field variations.

A photograph of the engineering demonstration model that was built to test the thermal design is shown in Figure 5. Its measured oscillation parameter[8] is $q = 0.14$, its storage bulb relaxation rate

is $\gamma = 2.0\ \mathrm{sec}^{-1}$, and its oscillation line Q is $Q_l = \omega/2\gamma = 2.2\times\ 10^9$. Thermal measurements in room temperature (25°C) air closely follow the design predictions, with 18 watts required for thermal control. In vacuum, we predict a power consumption of 7.5 watts with the maser mounting baseplate held at 20°C and the maser surrounded by MLI. Thermal tests in vacuum will be made on the demonstration model early in 1992 to verify the design.

LASER TIME TRANSFER

The space maser will be compared with ground maser clocks by laser time transfer. Laser transfer is the most accurate method of comparing separated clocks. The principle of laser time transfer is shown in Fig. 3. The laser ground station transmits short laser pulses (~200 ps duration) at a rate of up to 8 Hz that are reflected back to the ground station by corner reflectors mounted on the spacecraft. Timing of the ground station pulses is controlled by a hydrogen maser that is compared with primary time scales by means of GPS time transfer. The emission time t_{e1} and the arrival time t_{e2} of the reflected laser pulse are measured in terms of the time scale t_e of the ground clock. One half the pulse round trip interval $t_{e2} - t_{e1}$ provides the propagation delay to the spacecraft and allows us to predict the time of arrival $(t_{e1} + t_{e2})/2 = (t_{e1} + [t_{e2} - t_{e1}]/2)$ of the laser pulse at the spacecraft as measured in the ground clock's time scale. At the spacecraft, a photodetector located near the corner reflector, senses the arrival of the laser pulse and provides a signal to the event timer controlled by the onboard maser clock. The event timer determines the arrival time $t - s$ of the laser pulse in the time scale of the onboard clock. The difference between the two epochs (onboard and ground pulse times) is the time difference between the ground and space clock. Fig. 6 shows a light-time diagram of the laser time transfer technique. The laser time transfer technique can provide sub-nanosecond accuracy. We expect that a precision of 20 to 50 picoseconds in the comparison of the space and ground clocks should be achievable.

The primary laser ground station is the existing laser ranging station on top of Mt. Haleakala on Maui (Hawaii). Because of Federal Aeronautics Administration regulations, laser ranging is not available below an elevation of 20°. The sun-fixed attitude of the EURECA spacecraft requires three cube-corner reflector arrays on the spacecraft in order to obtain full angular coverage. We expect to perform laser tracking and time transfer during both day and night transits of the spacecraft.

EXPERIMENT OPERATION

The nominal duration of the EURECA mission is 6 months but could last up to 9 months. The EURECA spacecraft will be in a circular orbit of altitude between 525 and 485 km with 28.5° inclination. Onboard experiment data will be transmitted through the EURECA telemetry system to the ESA ground station and relayed to SAO. Several equipment functions will be controlled by command from the ESA ground station, enabling us to perform in-flight diagnostic tests and to adjust parameters for optimal operation of the experiment. Details concerning data collection and data flow from telemetry and laser ground station, distribution of data to the user, and other aspects of the experiment are being defined as part the now ongoing Phase B study.

While the primary ground station for laser time transfer is the existing laser station on Maui, Hawaii, other laser stations, such as at Matera, Italy, and Shanghai, China[**9**], are able to contact the spacecraft, and may participate in the experiment. These laser stations are presently equipped with hydrogen masers and high resolution event timers. Because of the low inclination of the orbit, only

a small number of existing laser stations are able to see the spacecraft. However, there are mobile laser stations available in the USA and in Europe that can be set up in locations providing optimum visibility of the spacecraft.

For the Maui laser station, up to five consecutive contacts with the spacecraft can be anticipated during a 24 hour time period. The maximum period available for time transfer during a spacecraft transit over the station is approximately seven minutes. A sample ground track calculation of consecutive laser contacts with Maui is shown in Figure 7.

Accurate position and velocity data of the spacecraft are needed to determine relativistic corrections. For precision of relative frequency comparison at a level of 1 part in 10^{16}, we require position tracking accuracy of approximately 1 meter, and velocity accuracy of approximately 1mm/sec. At present, the standard ESA tracking process does not provide the required accuracy. Several options are available to obtain the necessary orbit data accuracy, including use of laser tracking data and operation of an onboard GPS receiver.

This experiment could provide an opportunity to perform global high precision (100 picosecond) clock synchronization experiments.

POSSIBLE JOINT NASA/ESA SPACE H-MASER EXPERIMENT

A joint NASA/ESA H-maser space experiment is being studied by ESA and is the topic of another paper at this meeting[**10**]. This experiment would add to the SAO/NASA experiment equipment, a second space H-maser built by the Observatoire Cantonal de Neuchatel and a microwave time and frequency transfer system, probably a modified PRARE ranging system[**11**], provided by the DLR. The combined experiment would permit direct on-board frequency comparison of the two H-maser clocks, as well as and time and frequency transfer to a number of existing PRARE ground stations. While the microwave frequency comparisons would last for only about 7 minutes, and the frequency stability measurement would be correspondingly limited, the resulting time synchronization, using phase modulation of the one-way and two-way microwave links, is expected to be well into the sub-nanosecond domain[**12**]. The possibility of recovering the phase of the microwave carrier signal from orbit to orbit so as to retain the phase coherence of the frequency comparison has been advanced in an earlier publication[**13**]; however, close attention to the tracking requirements and atmospheric propagation delay measurements will be required to enable this "reconnection" of phase. The microwave time transfer, which is essentially independent of weather conditions, would be calibrated with the more precise laser time transfer method.

ACKNOWLEDGEMENTS

This work is supported by the National Aeronautics and Space administration. We thank G. Busca, S. Starker and S. Feltham for many interesting and informative discussions.

Table 1. Space Maser Characteristics

Dimensions	Weight	Power Requirements	
442 mm (17") diam	67 kg	Physics unit:	17 watts
863 mm (34) long		Receiver/synthesizer:	10 watts
		Total:	27 watts

REFERENCES

1. G.S. Levy et al. , *"Results of a Very Long Baseline Interferometry Demonstration using the NASA Tracking and Data Relay Satellite"* Acta Astron. 15, 481 (1986).

2. R. Decher et al., *"A Space System for High Precision Global Time and Frequency Comparison of Clocks"* Proc 12th Annl. Precise Time and Time Interval (PTTI) Applications and Planning Meeting , 99 (1980).

3. R.F.C. Vessot et al., *"Test of Relativistic Gravitation with a Space-Borne Hydrogen Maser"*, Phys. Rev. Lett. 45, 2081 (1980)

4. R. Decher, D.W. Allan, C.O. Alley, R.F.C. Vessot and G.M.R. Winkler, *"Shuttle Experiment to Demonstrate High-Accuracy Global Time and Frequency Transfer"*, Proc 1981 International Geoscience and Remote Sensing Symposium, IGARSS-81 370 (1981)

5. E.M. Mattison, G.U. Nystrom and R.F.C. Vessot, *"Design, construction and testing of a small passive hydrogen maser"*, Proc. 33rd Ann. Symp. on Freq. Control , 549 (1979).

6. S. B. Crampton and H. T. M. Wang, *"Duration of hydrogen-atom spin-exchange collisions"*, Phys. Rev. A 12 ,1305 (1975).

7. D. Kleppner , H. C. Berg, S. B. Crampton, N. F. Ramsey, R. F. C. Vessot, H. E. Peters, and J. Vanier, *"Hydrogen Maser Principles and Techniques"*, Phys. Rev. 138, A972 (1965).

8. S. Lesciutta and F.M. Yang, private communication (1991)

9. G. Busca, S. Starker, and S. Feltham, *"In orbit demonstration of a H-maser system"*, this volume.

10. P. Hartle, W. Shafer, C. Reigber, H. Wilmes, *"Precise range and range rate equipment, PRARE"*, XIX I.U.G.G. General Assembly, International Association of Geodesy Aug. 1987, Vancouver Canada.

11. H. Penfield, E. Imbier and R.F.C. Vessot, *"Design of the Satellite Time and Frequency Transfer (STIFT) Microwave Ground Terminal"*Proc 14th Annl. Precise Time and Time Interval (PTTI) Applications and Planning Meeting , 223 (1982).

12. D.W. Allan, C.O. Alley, N. Ashby, R. Decher, R.F.C. Vessot and G.M.R. Winkler, *"Ultra-Accurate International Time and Frequency Comparison Via an Orbiting Hydrogen Maser Clock"*, Journal de Physique 42, C8-395 (1981).

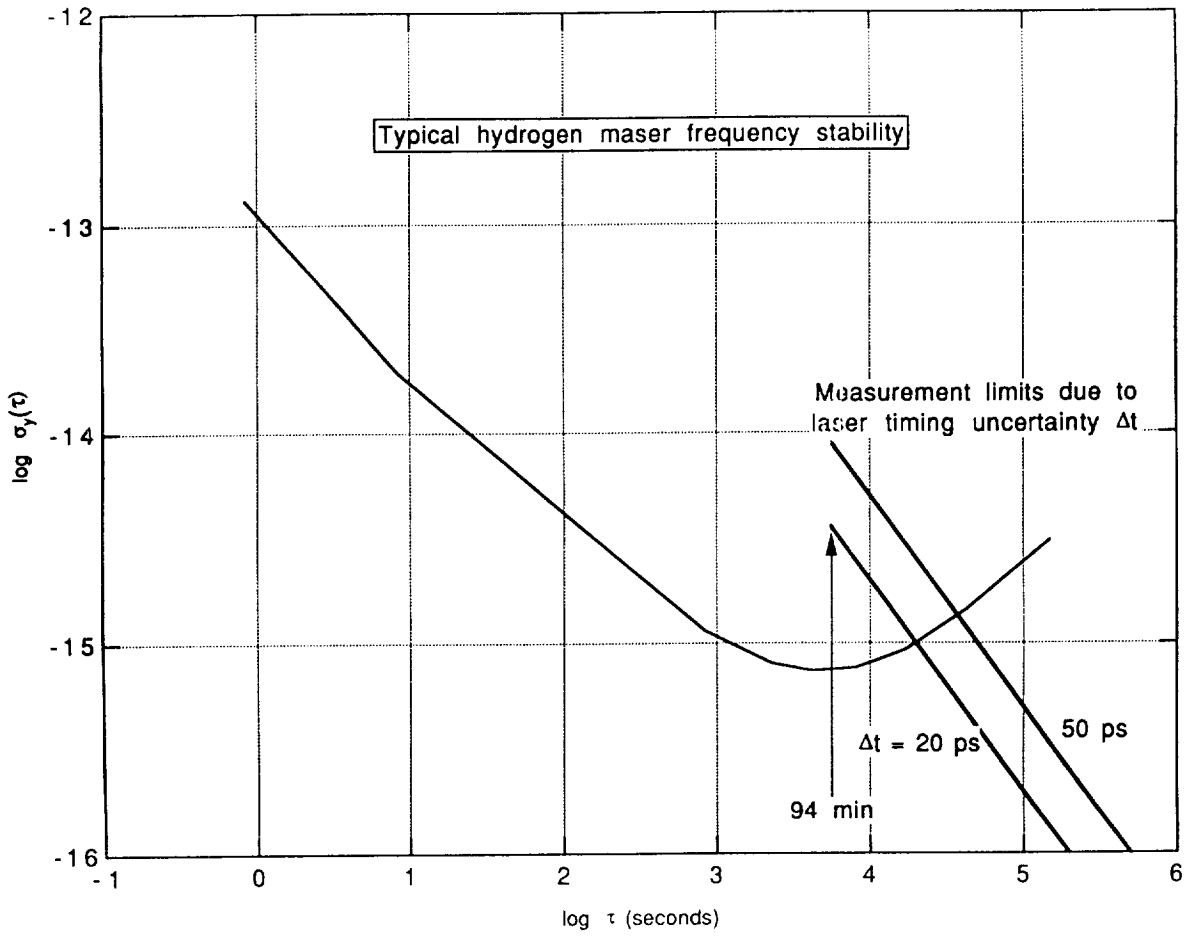

FIGURE 1. TYPICAL H-MASER FREQUENCY STABILITY

The overall EURECA configuration has been primarily determined for a maximum payload volume, while minimizing Shuttle launch costs, both providing an optimum spacecraft length-to-mass ratio and a direct attachment to the Shuttle via a three-point latching system, for a variable positioning of the platform throughout the length of the Shuttle's cargo bay.

The EURECA flight configuration is shown in Figure 2

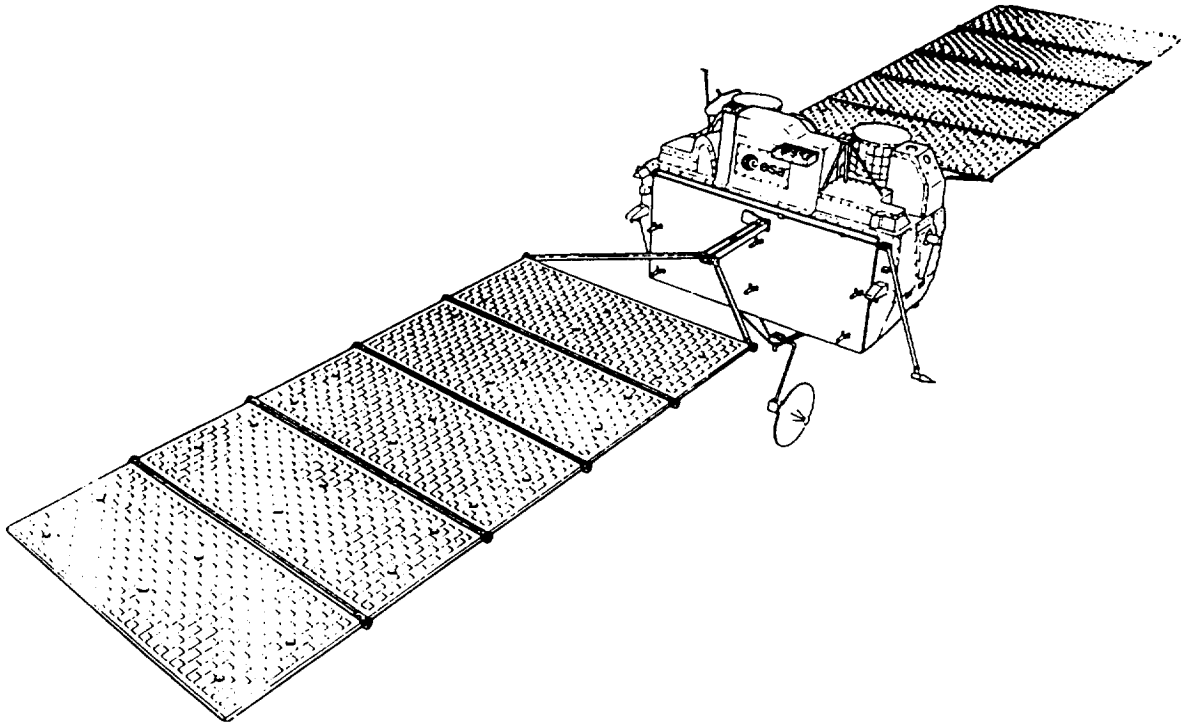

Figure 2 Eureca Flight Configuration

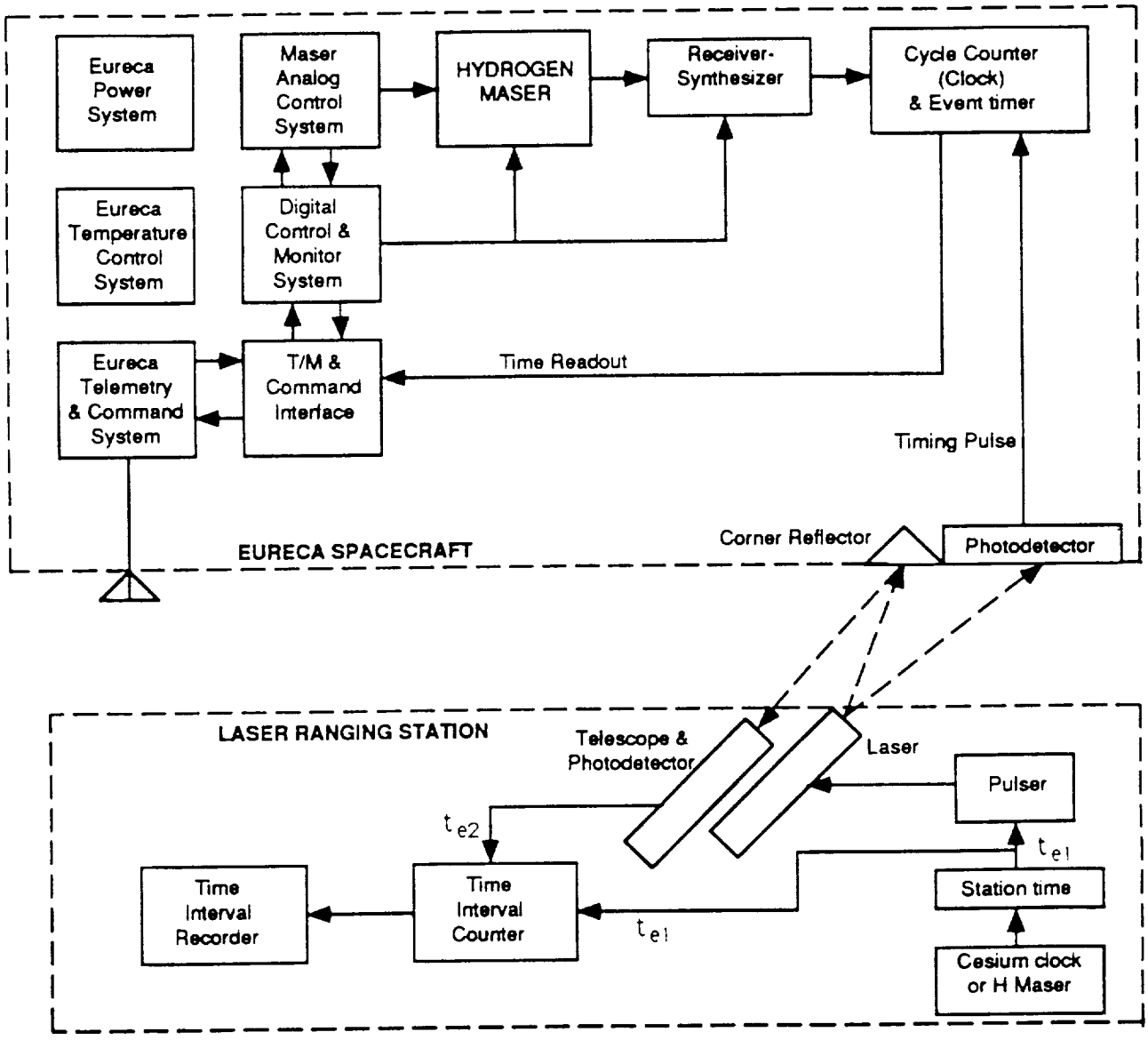

Fig. 3 – Space Maser timing system conceptual block diagram

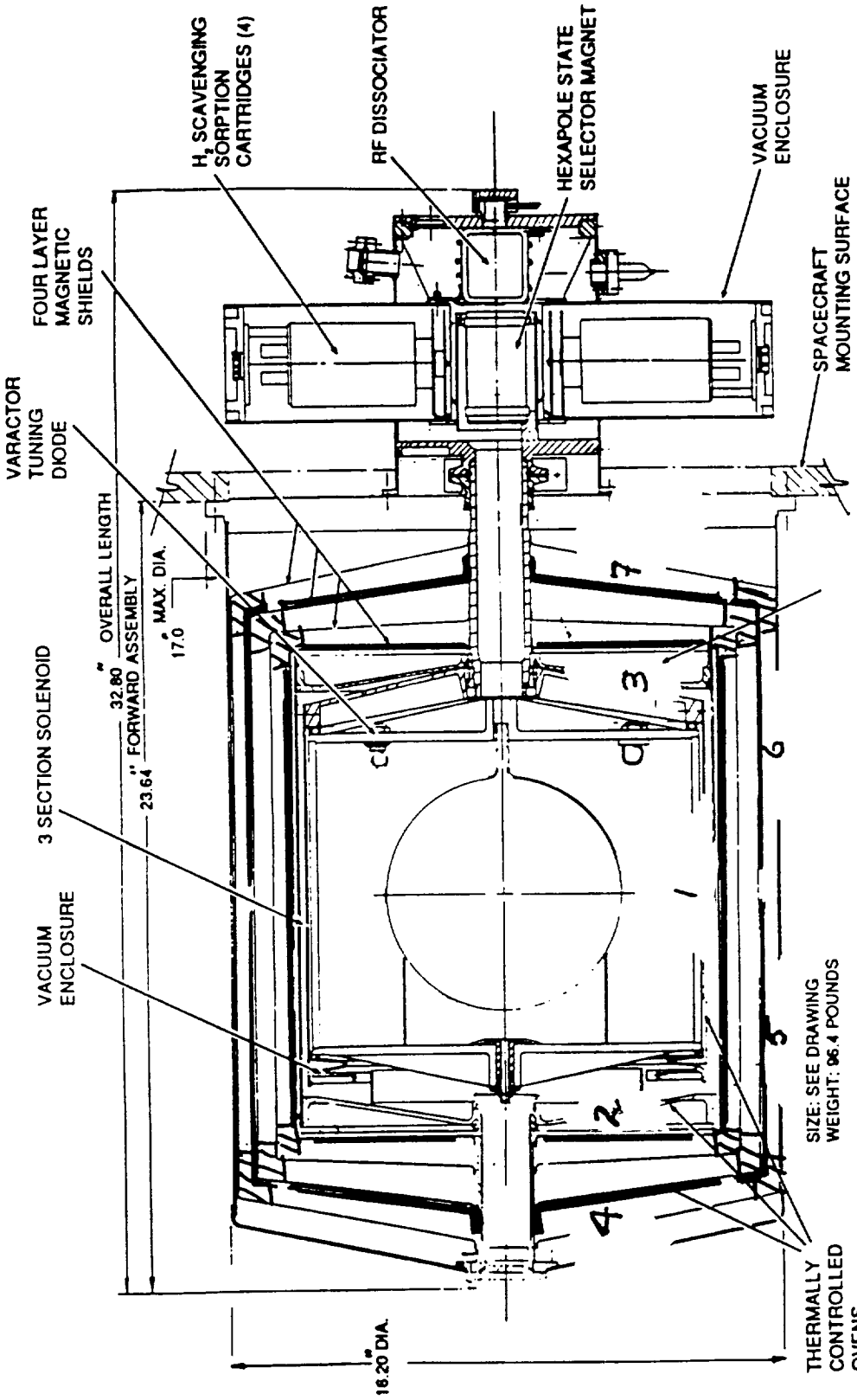

1, 2, and 3 BELL JAR HEATERS

4, 5, 6, and 7 THERMAL GUARD STATIONS

CROSS SECTION VIEW OF SPACE MASER

FIGURE 4.

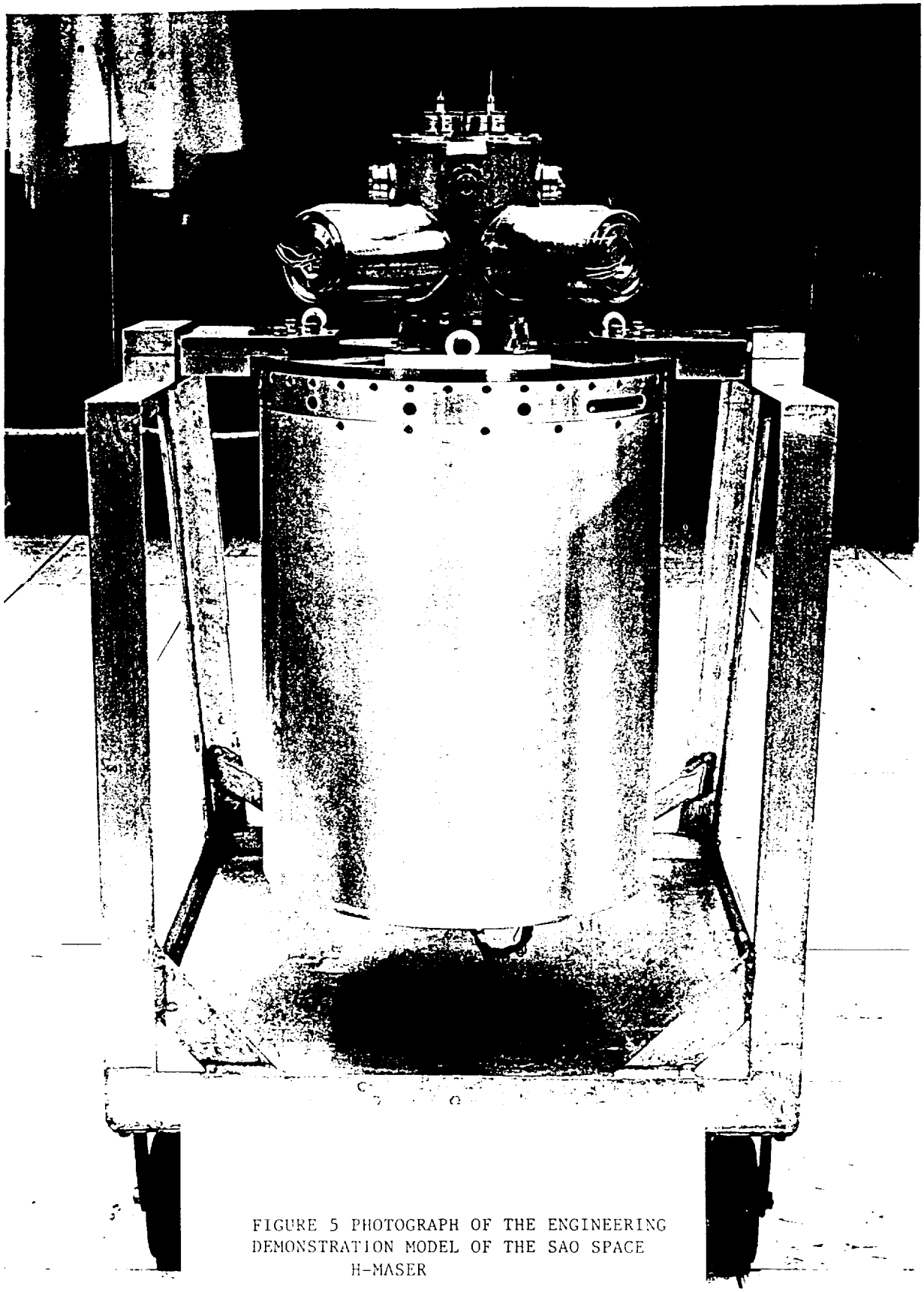

FIGURE 5 PHOTOGRAPH OF THE ENGINEERING DEMONSTRATION MODEL OF THE SAO SPACE H-MASER

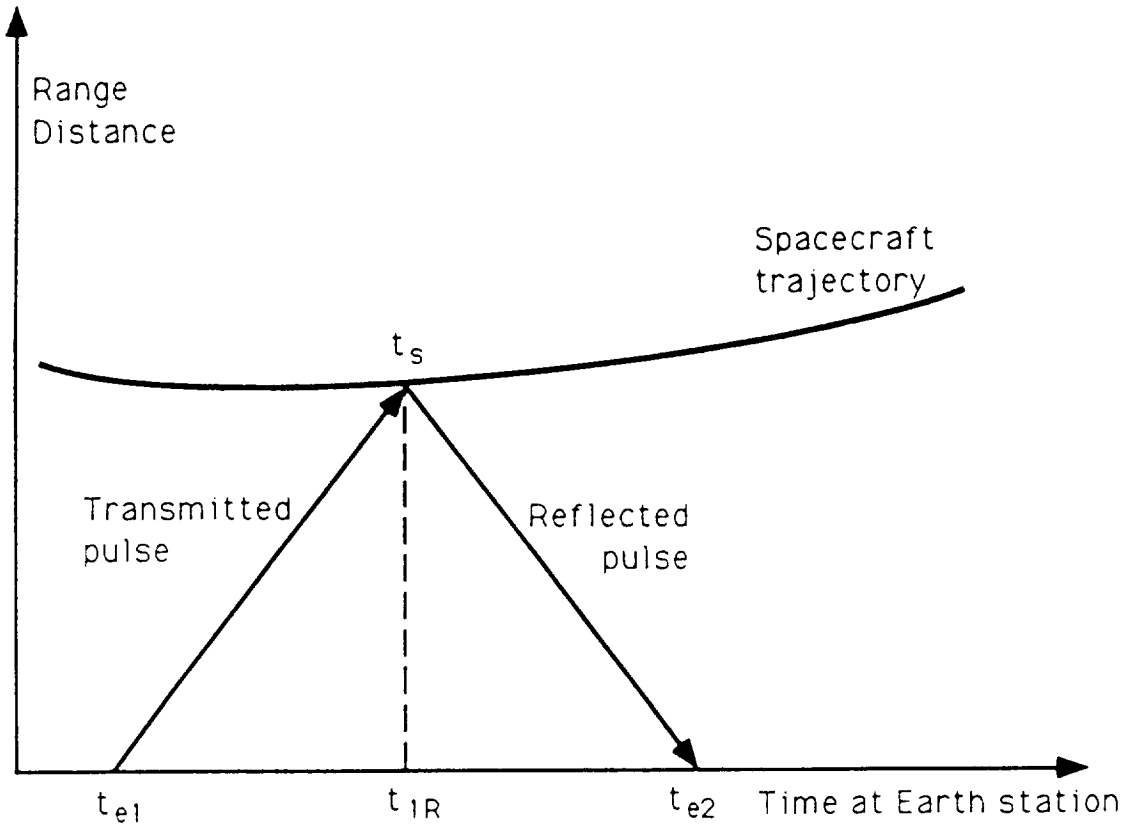

t_{e1} = time of laser pulse transmission as measured by earth station clock

t_s = time of detection at spacecraft as measured by spacecraft clock

t_{1R} = time of pulse arrival at spacecraft in terms of earth clock

$=(t_{e2}-t_{e1})/2$

$\Delta t_{se}=t_s-t_{1R}$ is the difference between the pulse arrival times measured by the space and earth clocks, corrected for propagation delay:

$$\Delta t_{se}=(t_s-t_{1R})=t_s-\left(\frac{t_{e1}-t_{e2}}{2}\right)-t_{e1}=t_s-\left(\frac{t_{e1}+t_{e2}}{2}\right)$$

FIGURE 6 LIGHT TIME DIAGRAM OF LASER TIME TRANSFER TECHNIQUE

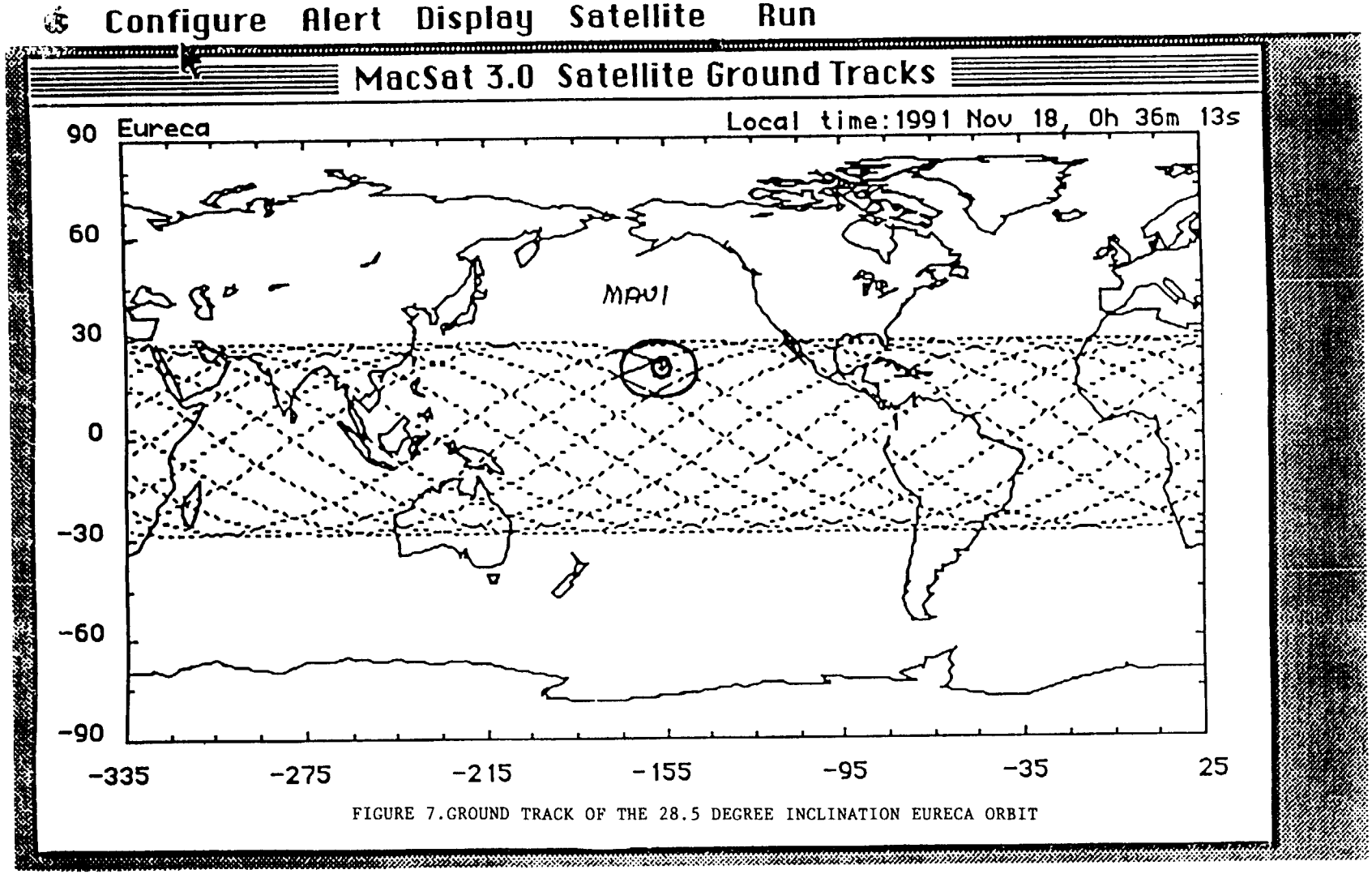

FIGURE 7.GROUND TRACK OF THE 28.5 DEGREE INCLINATION EURECA ORBIT

QUESTIONS AND ANSWERS

Dr. G. John Dick, JPL: First, what do you feel are the most important environmental problems. You have the temperature effects due to coming in and out of sunlight. Secondly, what would you have to say as to the utility of a super time standard in a low orbit like this, as opposed to a geostationary orbit.

Dr. Vessot: The first question is hard to answer, because if we knew what we were looking for, we would test it on the ground. It is usually said that there are combinations of environmental effects that are not possibly realizable in ground testing. I suspect that temperature gradients are likely to be the hardest thing to beat. We will introduce them in testing to determine the response times and the effects. There is also the question of particle radiation. From the discussions with the people who make Teflon, it appears that this type of radiation may even be beneficial. The problem is that a change is not good, so we will watch the wall shift very intently. That is something that we will measure when we recover the vehicle when it comes back to earth. It is likely to be in a powerful radiation belt in the planned orbit. For the second question about applications–there is no real application in this experiment other than to test the clock in this very low orbit. If could have polar orbit at a high altitude, then we could have world-wide coverage, which was the proposal envisioned for STIFT. This should have been able to do sub-nanosecond timing with a microwave system. From what I have seen today, it is not wrong to expect that we could get 100 picoseconds with a laser. The laser would not be an all weather system, but some people would settle for that in order to get 100 picoseconds.

Mr. Busca: I would like to add just one point. For time transfer this will be a really unique situation. We will be able to stay on a cycle of the 10 GHz for a full orbital period. The signal-to-noise and the clocks allow that to be done.

David Allan, NIST: That brings me to my question. I am very happy to hear you say that you can keep track of a cycle, because if you can, going back to the STIFT experiment, we were able to show that, if you can do the relativity well enough, meaning that you have to keep track of the vehicle position to a few meters for the full orbit in order to adjust for all the relativity terms, then you can use the phase, or the zero crossings of the carrier, as a timing edge. That would take you down to the sub-ten picosecond level. You do that from pass to pass and then talk about comparing clocks in parts in the 10^{16}, 10^{17} and 10^{18}. In terms of long term timing we hope that you remember what we tried to wrestle with before. If that could be integrated into this experiment it would be very useful.

Present Status and Future Prospects for Ionospheric Propagation Corrections for Precise Time Transfer Using GPS

John A. Klobuchar
Ionospheric Physics Division
Air Force Geophysics Directorate
Phillips Laboratory
Hanscom Air Force Base, MA 01731

Abstract

The ionosphere can be the greatest variable source of error in precise time transfer using GPS satellites. For single frequency GPS users the iono spheric correction algorithm can provide an approximate 50% r.m.s. correction to the time delay, but users who desire a more complete correction must make actual measurements of ionospheric time delay along the path to the GPS satel lite. Fortunately, at least three commercial GPS receivers, specifically designed to measure and correct for ionospheric time delay, are now, or soon will be, available. Initial operation with two different types of GPS iono spheric receivers has demonstrated a high degree of accuracy in measuring the ionospheric group delay. Results of these measurements will be presented.

For those who use a model to correct for ionospheric time delay, it is tempting to use daily values of solar 10.7 cm radio flux to correct a monthly average ionospheric time delay model for each day's operation. The results of correlation of daily maximum ionospheric time delay against solar radio flux values show a poor correction will be obtained by this procedure. Prospects for improving ionospheric corrections during the declining phase of the present solar cycle will be discussed.

INTRODUCTION

It is well known that attempts to obtain precise time by means of monitoring the clocks on the GPS satellites can be limited by the time delay of the earth's ionosphere. This additional time delay is due to the group delay of the modulation of the 1.023 MHz and 10.23 MHz modulation which carry the modulation, or time information on the signal. The amount of this additional time delay can be expressed as:

$$\Delta t = 40.3/(cf^2)\mathrm{TEC} \qquad \text{(seconds)}$$

where c is the velocity of light, in m/s and f is the carrier frequency, in Hertz.

TEC is the number of free electrons in a unit column, having a cross section of one square meter, the earth's ionosphere along the path between the satellite and the ground monitoring station. One TEC unit is called 1×10^{16} el/m^2.

Typical monthly median values of this additional time delay are shown in Figure 1a for 2000 U. T. for the solar maximum year of 1990. Note that the highest values of ionospheric vertical time delay are 50 nanoseconds. To convert vertical time delay values to those at a slant elevation angle a mean ionospheric height of 400 km is generally used. Thus, at low elevation angles, even as low as 5 degrees, the time delay will be only approximately three times as high as the vertical values.

During a period of minimum solar activity the ionospheric time delay values will be much lower. Figure 1b illustrates the results of a monthly median model of time delay for 1995, a year of expected minimum in solar activity. Note that the maximum value of ionospheric time delay is only 20 nanoseconds, and for much of the time over the entire globe, the maximum median vertical ionospheric time delay is less than 5 nanoseconds. These model representations are of monthly median conditions only.

IONOSPHERIC DAY-TO-DAY VARIABILITY

The variability of ionospheric time delay about the monthly median values for any month is approximately normally distributed about the mean value with a standard deviation from 20 to 25%, especially during the daytime hours when the absolute values are the highest. Figure 2 illustrates the day-to-day variability of ionospheric time delay over an entire year, for a mid-latitude station located near Boston, MA. The units in Figure 3 are in 10^{16} el/m^2 column. To obtain nanoseconds of time delay at L1, the 1.575 GHz GPS freq uency, you must divide the TEC ordinate scale by 1.85. Note that each of the monthly overplots has a relatively large spread about its monthly median values. A similar variability is found for ionospheric time delay measured from other mid-latitude stations.

CORRECTING FOR IONOSPHERIC TIME DELAY

I. THE GPS IONOSPHERIC TIME DELAY ALGORITHM

The GPS satellites transmit, as part of their data message, coefficients designed to correct for approximately 50% of the root mean square, (rms) ionospheric time delay error. Tests of the performance of this algorithm against a large amount of mid-latitude ionospheric electron content data have shown that, indeed, at least a 50% rms correction is achieved. Klobuchar and Doherty, (1990), have looked at the statistics of the behavior of ionospheric time delay for a number of stations, and also have shown the statistics of the residual errors after applying the GPS ionospheric time delay algorithm.

Figure 3a illustrates the statistics of the variability of the earth's mean daytime ionosphere for a low mid-latitude station, Ramey, Puerto Rico. The three seasons of a solar maximum year, 1981, are represented separately in Figure 3a. The solid points represent the actual behavior of ionospheric range error, in meters at L1, versus cumulative probability. One meter represents 3 nanoseconds of time delay. The abscissa is scaled in a manner such that a normal distribution is represented by a straight line in this figure. Note that for all three seasons the ionospheric time delay behavior is approximately normally distributed.

Also shown in Figure 3a is the remaining ionospheric range error after the use of the GPS single frequency user algorithm to correct for ionospheric range error. Note that, for all but the approximate lowest 0.01 fraction of the curves, the use of the algorithm considerably lowered the ionospheric

range error.

Figures 4a and 4b illustrate similar data for a station located in Hamilton, MA also for the solar maximum year of 1981. Again the GPS single frequency user ionospheric algorithm provides a large improvement over the actual data for the daytime values for all three seasons. The large departure from near normal distribution of the data above 0.99 on the cumulative proba bility curve for the equinox daytime values shown in figure 4a is due to a single magnetic storm which occurred during that season.

Other similar comparisons of actual ionospheric measurements against the GPS ionospheric algorithm have been made for stations located in Hawaii and Tromso, Norway. The results of comparisons at all these stations show that the algorithm works best during times when the actual ionospheric range errors are the greatest, which is when it is highly desirable that it should work the best. During the nighttime hours, when the absolute values of ionospheric time delay are low, the algorithm does not correct as well, but during those hours of low absolute values, a poorer correction can more easily be tolerated.

II. MEASUREMENTS OF IONOSPHERIC TIME DELAY

If the residual errors in obtaining precise time from GPS signals, after using the single frequency ionospheric correction algorithm, are still too large for precise time transfer using GPS, then an actual measurement of the ionospheric time delay must be made, preferably along the line of sight from the same GPS satellite from which the time transfer is being attempted. Davis, et. al. (1991) have described a receiving system specifically designed to measure ionospheric time delay from multiple GPS satellites. Figure 5 illustrates an example of TEC data obtained from this type of code-free rec eiving system. Also shown in this figure is the TEC obtained by the Faraday rotation technique. The agreement is excellent, indicating that the NIST ionospheric monitoring system works as desired.

The code-free GPS ionospheric receiving system is relatively inexpensive and has been proven to yield satisfactory values of ionospheric time delay to an approximate accuracy of a few nanoseconds, certainly better that ten nano seconds, but, at present, not as good as one nanosecond. One potential problem for ionospheric corrections is the unknown offset of the 10.23 MHz modulation on the L1 and L2 frequencies on each GPS satellite. Each satellite has a different modulation offset, called tgd, which is transmitted as part of each satellite message. Unfortunately, when compared against other measure ments of ionospheric electron content the transmitted tgd values do not yield as precise absolute ionospheric electron content as desired. Several groups are presently studying ways of improving the accuracy of this bias.

CORRELATION OF IONOSPHERIC TIME DELAY WITH SOLAR RADIO FLUX

Ionization in the earth's ionosphere is produced by ultra-violet, UV, emissions from the sun. Thus, it is tempting to use a standard measure of short term solar activity, the solar radio flux on 10.7 cm wavelength, to correlate with the day-to-day variability of the ionosphere. Unfortunately, this does not work well due to many other complicating factors in the produc tion, loss and transport of ionization in the earth's ionosphere which are still subjects of active research in the ionospheric community.

As an example of attempts to correlate ionospheric time delay against F10.7, Figure 6a illustrates correlations of mean daytime values of TEC against 10.7 cm solar radio flux for each of the 12 months of 1981, a year of very high solar activity. The coefficient of correlation, along with the 95% confidence intervals is given for each month. Note that, for most months, the correlation is low. The highest values of correlation occur during April and December and even during those months the correlation coefficient is only 0.66.

If the magnetically disturbed days are removed from each month, the resulting correlation does not improve significantly, as indicated in Figure 6b. Note that the month of April now has a negligible correlation, while that for May and some of the winter months has improved a bit. Over half the months of the year exhibit a negligible correlation of mean daytime ionospher ic time delay against the standard F10.7 radio measure of solar UV flux.

LONG TERM SOLAR FLUX

We are now in the declining phase of the current 11 year solar cycle, as shown in Figure 7. At present the predictions of long term solar activity are not reliable. Thus, an average solar cycle maximum is perhaps the best that can be predicted at this time. As we approach the end of the current solar cycle, expected to be in the mid-1990s, predictions of the next cycle should be more reliable since the method which has had moderate success in long term predictions has relied on recurrent magnetic storms during the last few years of a solar cycle. During the solar minimum conditions expected in the mid- 1990s the absolute values of ionospheric time delay should be from one half to one fourth their values during solar maximum.

DISCUSSION AND CONCLUSIONS

Ionospheric time delay limits the accuracy of precise time transfer, by using the single frequency signal from the GPS satellites, to a few tens of nanoseconds. The ionospheric time delay algorithm can improve the ionospheric rms error by at least 50%, but the remaining errors may still be too large for time transfer at the ten nanosecond level.

The best method of correcting for the effects of ionospheric time delay is simply to measure it directly by means of a relatively inexpensive code-free receiving system designed specifically for that purpose. The overall accuracy of such a system is certainly better than ten nanoseconds, but probably not yet at the one nanosecond level. Time transfer at the sub-nanosecond level using GPS will be very difficult to accomplish due to the effects of the time delay of the earth's ionosphere.

The long term solar activity of the present solar cycle is now in its declining phase, and can be expected to reach a minimum in activity in the mid-1990s. The best current estimates of the next solar maximum are for it to occur approximately in the year 2000, and to be of average strength. By the mid-1990s the predictions of the strength of the next solar maximum should be greatly improved.

REFERENCES

1. Davis, D., M. A. Weiss, K. Davies, and Gerard Petit, *"Improving GPS Time Transfer with the NIST Ionospheric Measurement System"*, presented at the ION- GPS-91 Symposium,

Albuquerque, NM, September 1991.

2. Klobuchar, J. A. and P. H. Doherty, *"The Statistics of Ionospheric Time Delay for GPS Ranging on L1"*, Proceedings of ION GPS-90, The Institute of Navigation, September 1990.

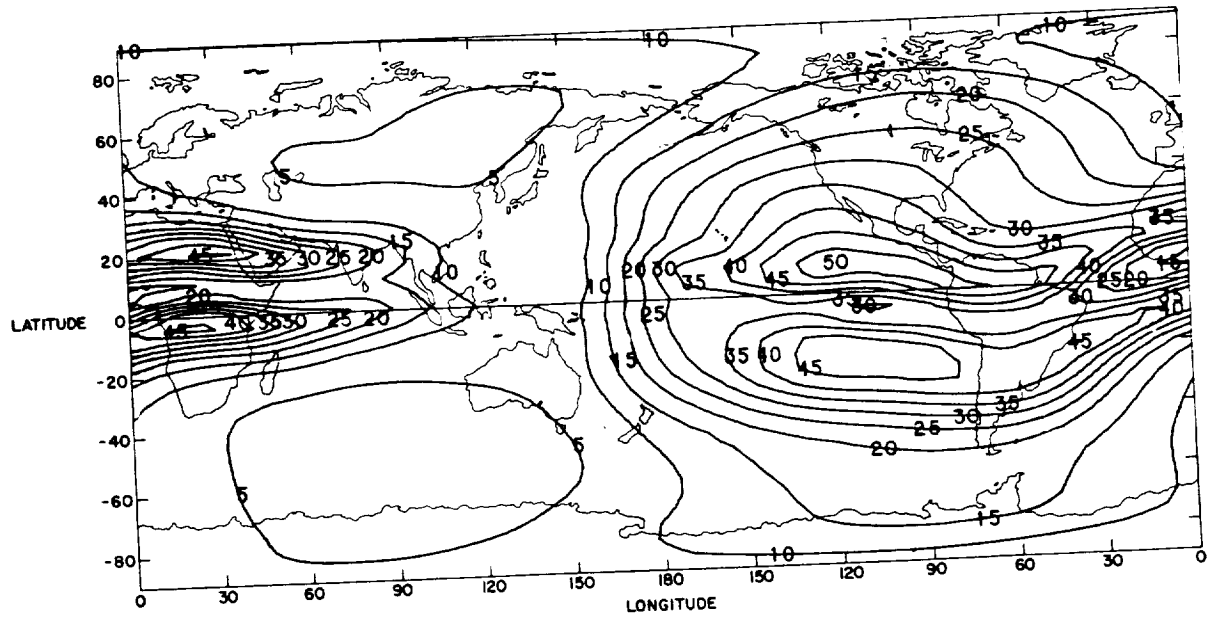

Figure 1a. Contours of world-wide monthly time delay for March 1990, a solar maximum year.

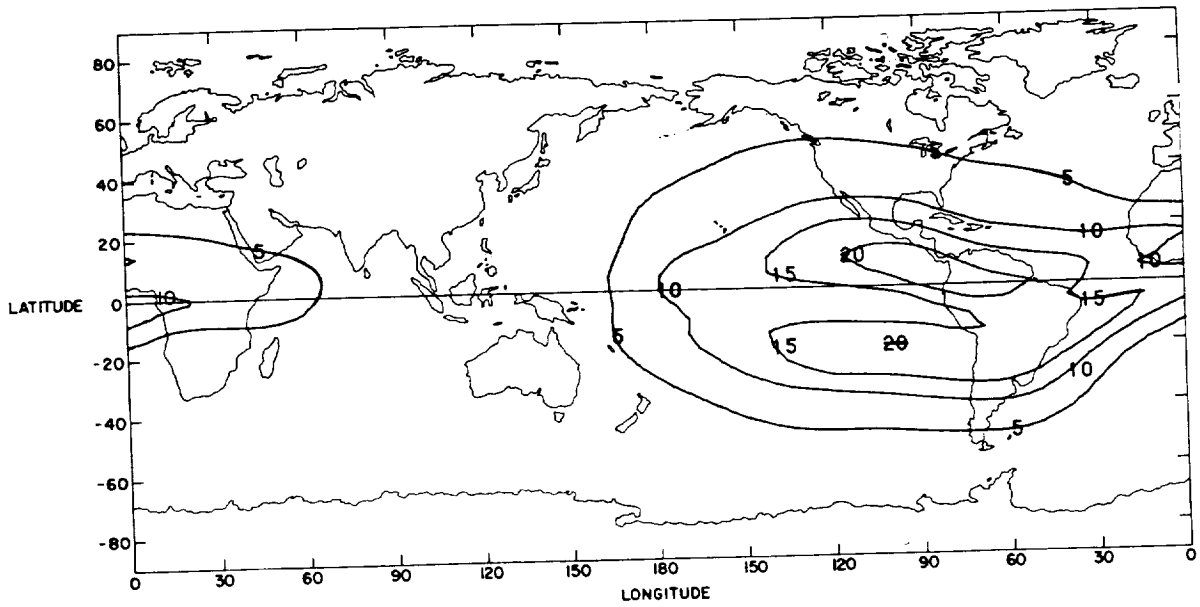

Figure 1b. Contours of world-wide monthly time delay for March 1995, a year of expected solar minimum activity.

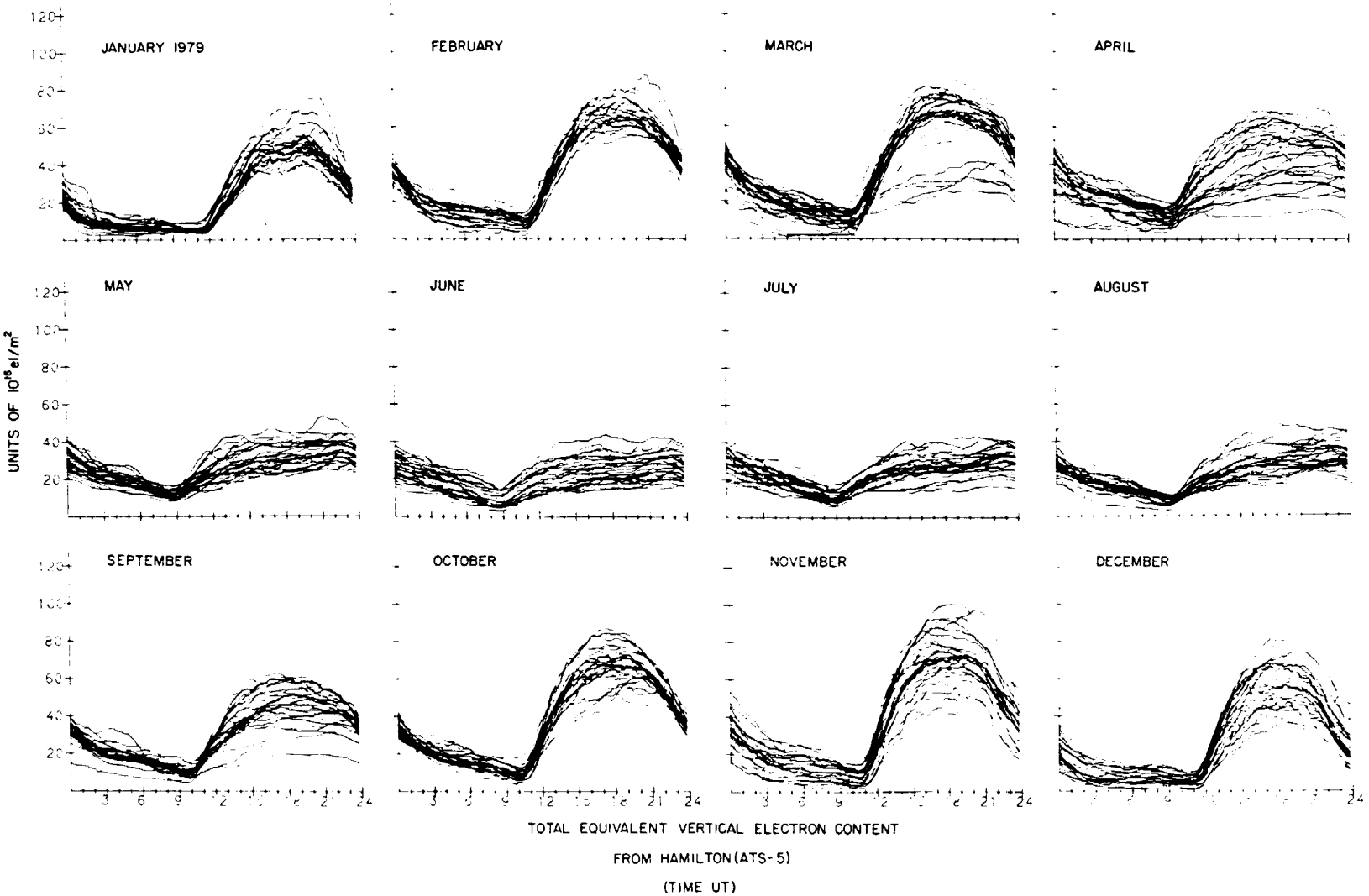

Figure 2. Monthly overplots of ionospheric TEC for 1979, a year of high solar activity.

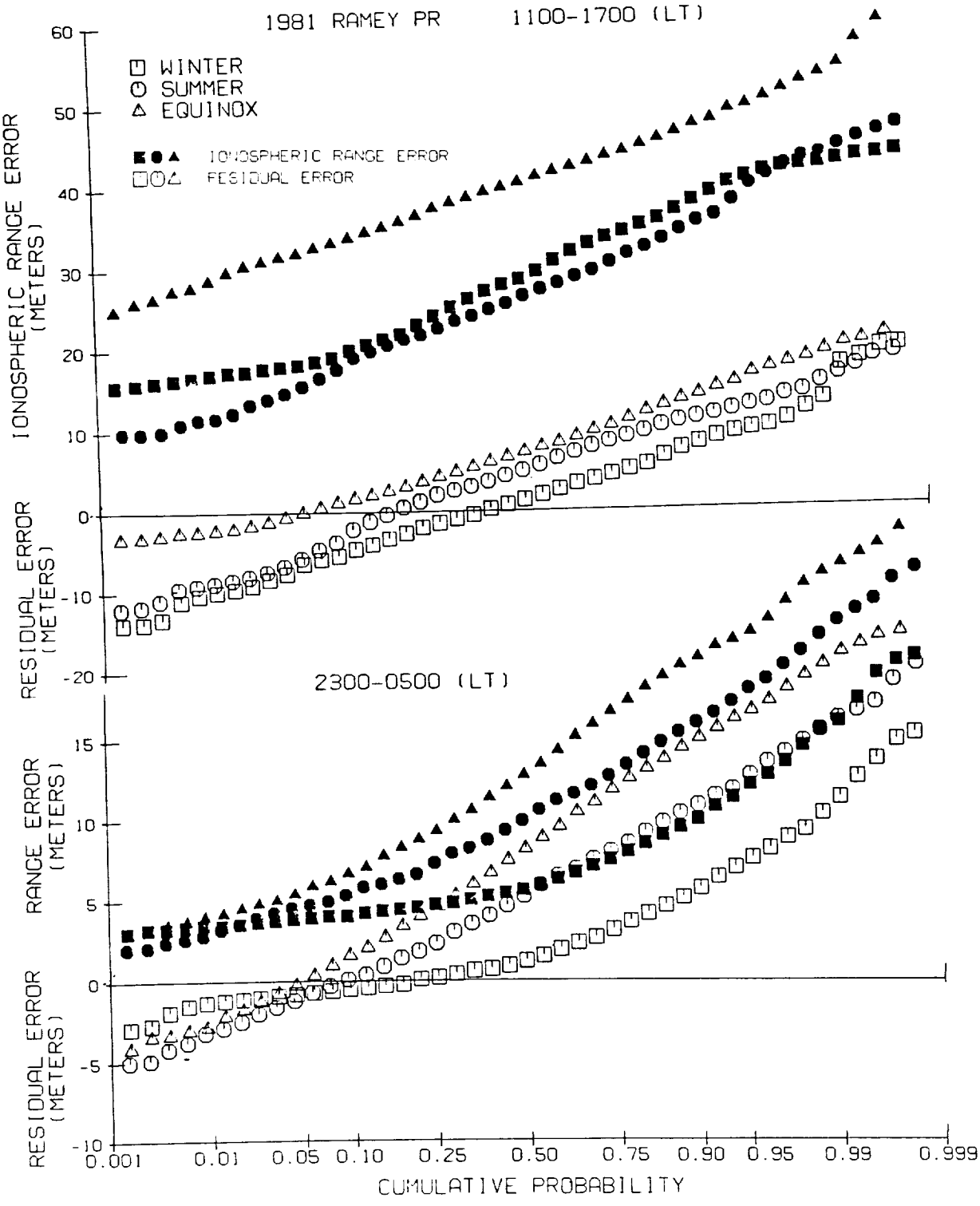

Figure 3. Cumulative probability of ionospheric range error for Ramey, PR for three seasons during 1981, a year of high solar activity. Also shown is the residual error after applying the GPS single frequency user ionospheric error algorithm.
3a, (top) is for mean daytime. 3b, (bottom) is for mean nighttime.

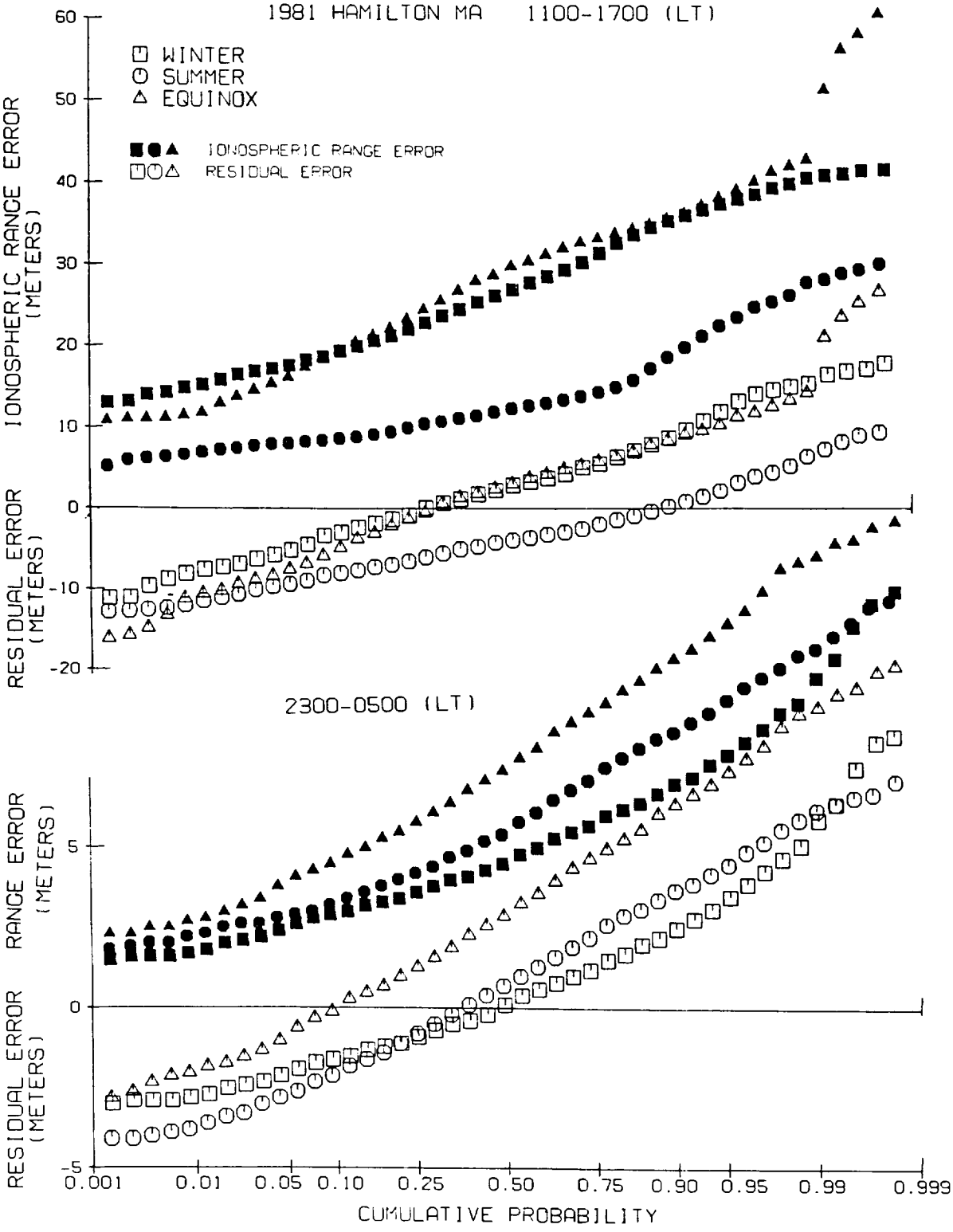

Figure 4. Cumulative probability of ionospheric range error for Hamilton, MA for three seasons during 1981, a year of high solar activity. Also shown is the residual error after applying the GPS single frequency user ionospheric error algorithm.
4a, (top) is for mean daytime. 4b, (bottom) is for mean nighttime.

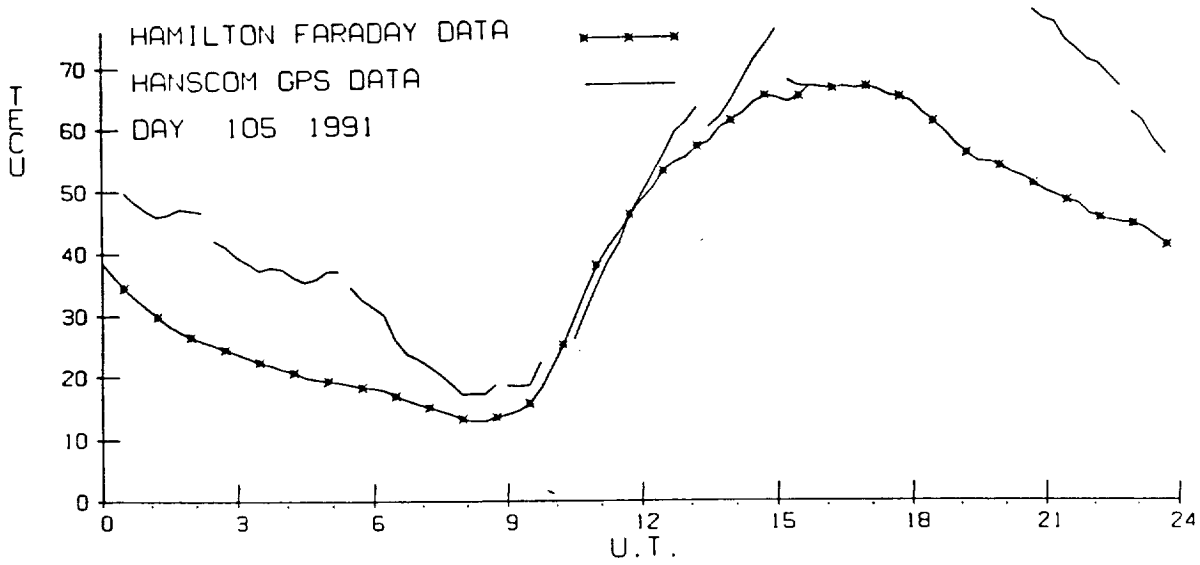

Figure 5. One day of ionospheric time delay received from a code-free GPS receiving system at Hanscom AFB, MA.

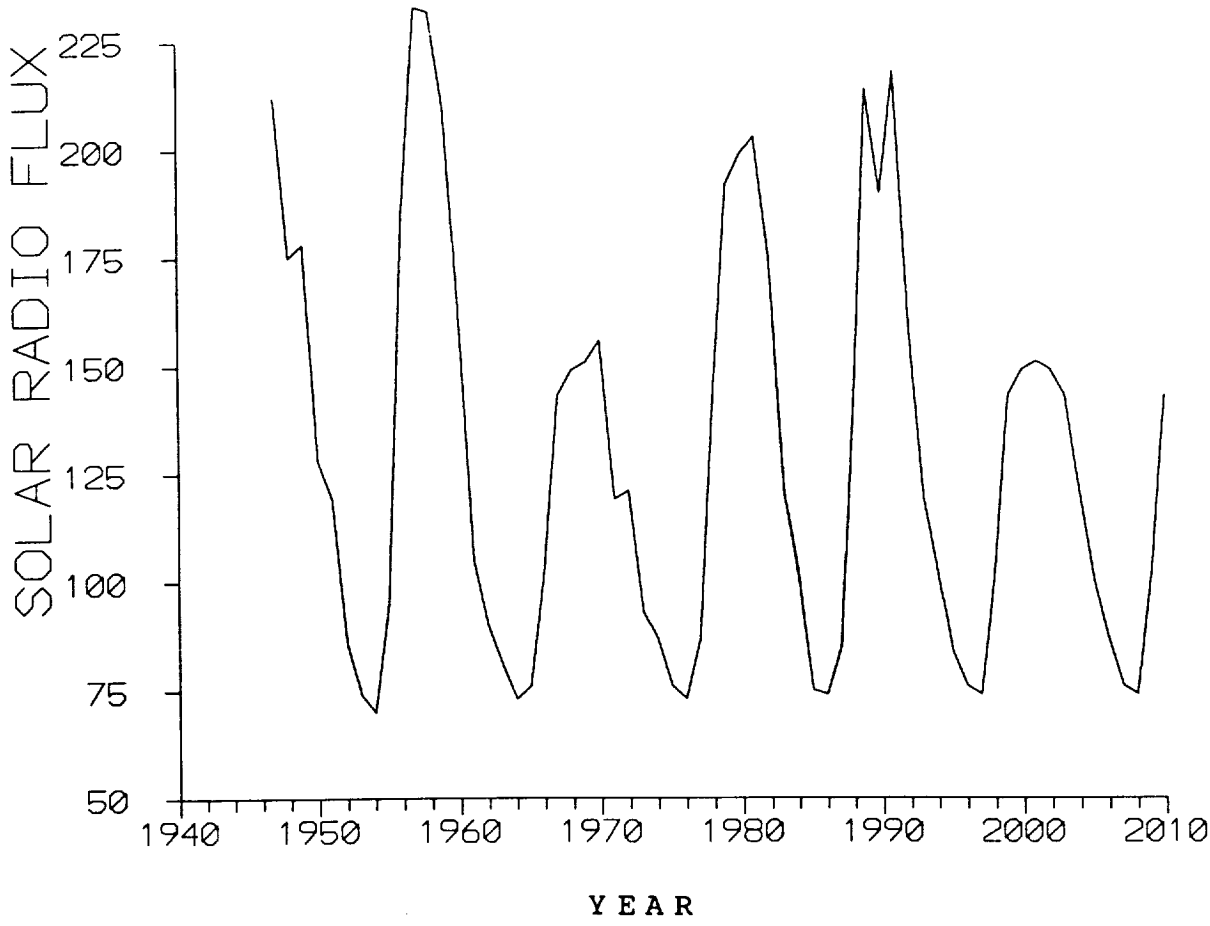

Figure 7. Mean yearly solar activity for the last four solar cycles and projections for the next cycle.

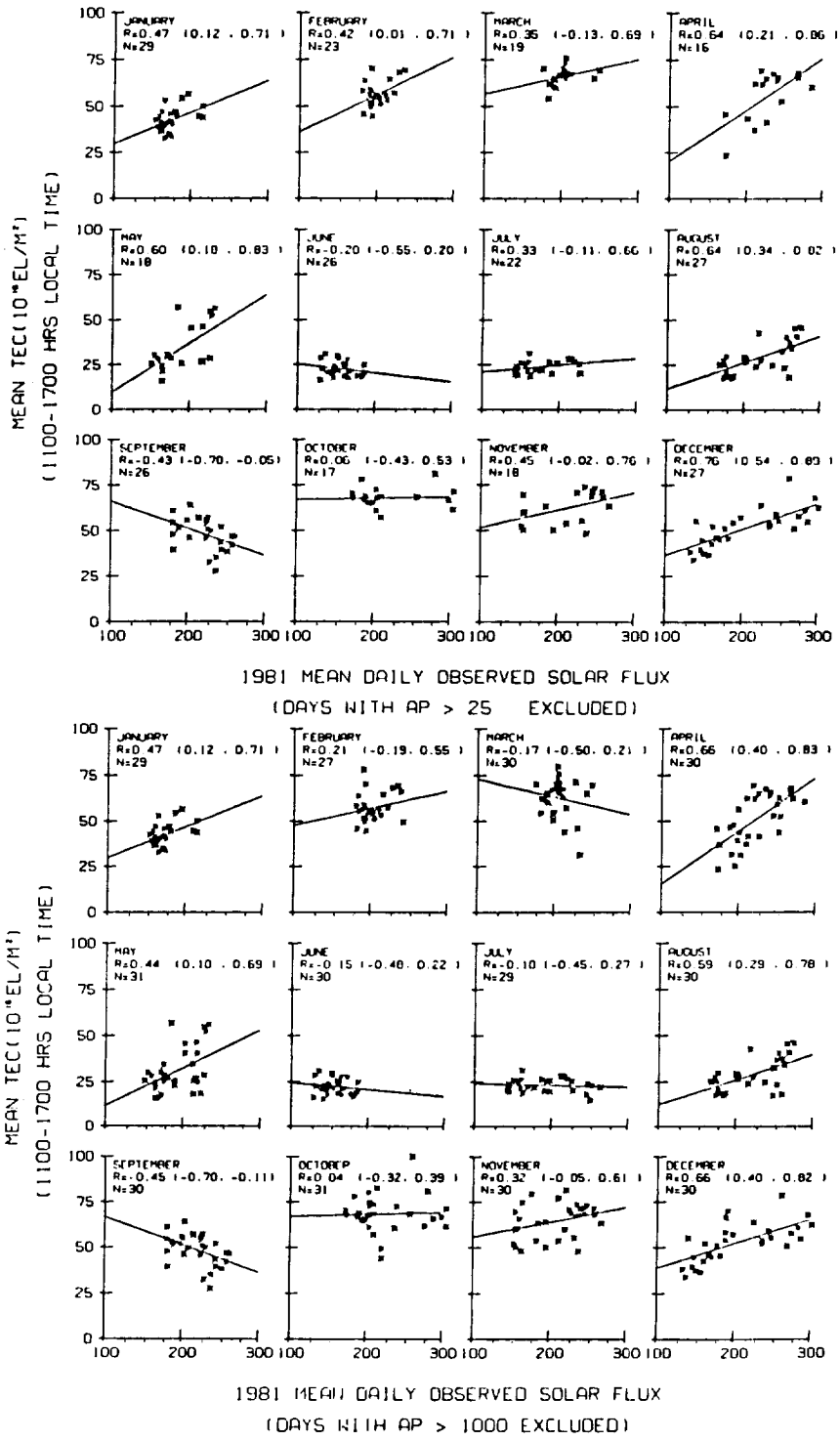

Figure 6. Correlation of mean daytime TEC from Hamilton, MA against $F_{10.7}$ for the twelve months of 1981 for magnetically quiet days (6a, top portion) and with all days included (6b, bottom portion).

QUESTIONS AND ANSWERS

Dr. William Klepczynski, USNO: A comment along the lines of "the ghost of Christmas present". At the ION meeting in September we gave a paper where the problem is even compounded more by the transmitted model by GPS. There is a maximum number for the solar flux unit that can be transmitted. The current values of solar flux exceed that value. There is a truncation problem that makes the transmitted model incomplete when the sun really acts up.

Mr. Klobuchar: Yes, it was very bad during January and February. I don't know what to do about that. If JPO would give a little money to think about it, we could try to update the model. There is a later set of data now that we could use to improve that algorithm, but I don't think that there is much interest at JPO.

Dr. Henry Fliegel, Aerospace: It is not known as well as it should be, perhaps, that JPO no longer directs the day to day operations of GPS. That is really in the hands of Space Command. The one thing that JPO can do, of course, is to revise the software to take care of this truncation problem that Bill and you have just been discussing. I guess that we should work on that so that we will be ready for the next solar maximum. The other comment that I have is that, although frankly the relations between JPO and Space Command have been very, very poor over the last few years, I think that under the new joint command for GPS, the Air Force will be more responsive to things like this.

Mr. Klobuchar: Without getting into the politics of the situation, it is not just a truncation problem. It is because the algorithm coefficients themselves were designed only up to an average solar cycle maximum. We didn't accurate time delay information that incorporated even the 1981 cycle, let alone the present cycle. However, now that is available. It would require a lot of looking at the data and new coefficients and a new model. I think that it is not a problem for the operational side, but for the Space Systems Division side.

Samuel Ward, JPL In looking at the data there, and being aware that the ionization of the atmosphere by the solar flux is a function of the angle that the flux strikes the atmosphere. That angle is a function of the tidal bulge caused by solar, earth, lunar rhythms. Could this cause some of the problems that you see?

Mr. Klobuchar: What causes the long term solar behavior is not something that I don't really want to comment on. Some people have said that most of the angular momentum of the solar system is due to the planet Jupiter, since it is the heaviest planet. So somehow Jupiter "sucks out" the sunspots from the sun. The period of Jupiter is about 11 years. Having said all of that, I shouldn't have because that smacks to me of astrology. The people who are the real solar experts don't have a good handle on what causes the cycles. They are starting to understand the shorter term stuff a little, but not the long term. They know less about forecasting solar cycles than we do about the weather. JPL is starting to give some excellent data on the ionospheric measurements around the world because they are scattering the ROGUE receivers around and are getting a lot of data. With that data, it may be possible to make a world wide model of planetary time delay, directly, within the next five years or so.

Dr. Claudine Thomas, BIPM: You forgot to mention that there is another form of codeless receiver that was developed at BIPM and reported At the PTTI in Redondo Beach. It is now available in commercial form, coupled with a GPS receiver. That receiver is used at BIPM.

Mr. Klobuchar: Yes, I didn't mean to go into the commercial units, but there are several out there. You should realize that the rights to commercial use of them belongs to Pete McDoran, who did the work when he was at JPL. The sequence is probably JPL, NIST with the French group, and the Japanese.

1991 PTTI CONFERENCE
ATTENDEES LIST

Wayne T. Abernethy
U. S. Naval Research Laboratory
P. O. Box 727
635 Telegraph Road
Stafford, VA 22554 USA
703/690-3614

Charles Adams
Hewlett-Packard
5301 Stevens Creek Boulevard
MS/51U/23
Santa Clara, CA 95052 USA
408/553-2440

Martin P. Anguilar
D.O.D.
3925 Foster Avenue
Baltimore, MD 21224-4340 USA

David W. Allan
National Institute of Standards and Technology
Time and Frequency Division
325 Broadway
Boulder, CO 80303 USA

Brad Anderson
Stanford Telecom
2421 Mission College Boulevard
Santa Clara, CA 95056-0968 USA
408/987-5506

William W. Anderson
Fleet Numerical
Oceanography Center
Code 74
Airport Road
Monterey, CA 93943-5005 USA
408/647-4413

Thomas B. Andrews
Hewlett-Packard
5301 Stevens Creek Boulevard
Santa Clara, CA 95052-8059 USA
408/553-7013

Ronald J. Andrukitis
U. S. Naval Observatory
Time Service Substation
11820 Southwest 166th Street
Miami, FL 33177 USA
305/235-0515

Sami Asmar
Jet Propulsion Laboratory
4800 Oak Grove Drive
Pasadena, CA 91109 USA
818/393-0662

Rob Avery
Telecom Solutions
85 West Tasman Drive
San Jose, CA 95134 USA
408/428-7862

James F. Barnaba
A. F. Metrology Center
Newark Air Force Base
Newark, OH 43057-5475 USA
614/522-7792

James A. Barnes
Austron, Incorporated
3011 Broadway
Boulder, CO 80304 USA
303/490-7282

Thomas R. Bartholomew
TASC
1190 Winterson Road
Linthicum, MD 21090 USA
410/850-0070

Francoise S. Baumont
Observatoire de la Cote D'Azur
OCA/CERGA
Avenue Nicolas Copernic
F-06130 Grasse, FRANCE
33 1 93 36 5849

Roger East Beehler
National Institute of Standards and Technology
325 Broadway
Boulder, CO 80303 USA
303/497-3281

Laurent-Guy Bernier
Observatoire Cantonal de Neuchatel
Avenue de Beauregard 3
CH-2036 Cormondreche
SWITZERLAND
41 38 318 831

Martin Bloch
Frequency Electronics Incorporated
55 Charles Lindburgh Boulevard
Mitchell Field, NY 11553 USA
516/794-4500

Stephen G. Boemler
Naval Aviation Depot-Standards Lab
Code 94601/3220
NAS Pensacola, FL 32508 USA
904/452-3277

Richard T. Boswell
Ball Corporation
Efratom Division
3 Parker
Irvine, CA 92718 USA
714/770-5000

Dan E. Brannen
HRB Systems
Science Park Road
P. O. Box 60
State College, PA 16804-0060 USA
814/238-4311

Lee A. Breakiron
U. S. Naval Observatory
Time Service Department
34th and Massachusetts Avenue, Northwest
Washington, DC 20392-5100 USA
202/653-1888

Julian C. Breidenthal
Jet Propulsion Laboratory
4800 Oak Grove Drive
MS/161-228
Pasadena, CA 91109 USA
818/354-3349

Anthony W. Brown
Lockheed Technical Operations Company
P. O. Box 3430
Onizuka Air Force Base, CA 94088 USA
408/752-3132

Edward E. Burkhardt
Burkhardt Monitoring Service
P. O. Box 1411
Glen Allen, VA 23060 USA
804/261-1800

Giovanni Busca
Observatoire Cantonal de Neuchatel
Avenue de Beauregard 3
CH-2036 Cormondreche
SWITZERLAND
41 38 318 831

Edgar W. Butterline
AT&T
Routes 202 and 206 North
Bedminster, NJ 07921 USA
908/234-4545

Troy Caffey
Department of Defense
223 Harbor Drive
Severna Park, MD 21146 USA
410/647-6433

Malcolm D. Calhoun
Jet Propulsion Laboratory
4800 Oak Grove Drive
Pasadena, CA 91109 USA
818/354-9763

William Cashin
Ball Corporation
Efratom Division
3 Parker
Irvine, CA 92718-1605 USA
714/770-5000

Harold Chadsey
U. S. Naval Observatory
Time Service Department
34th and Massachusetts Avenue, Northwest
Washington, DC 20392-5100 USA
202/653-1888

Z. C. Chai
Shanghai Observatory
Chinese Academy of Sciences
80 Nandan Road
Shanghai, CHINA

Yat Chan
The Aerospace Corporation
2350 East El Segundo Boulevard
El Segundo, CA 90245 USA
310/336-7174

Mark J. Chandler
BMC
235 Congress Avenue
Lansdowne, PA 19050 USA
215/622-2833

Rex Chappel
Hewlett-Packard
5301 Stevens Creek Boulevard
Santa Clara, CA 95052 USA
408/553-2402

Li Chengfu
Beijing Institute RM&M
P. O. Box 3930
Beijing, CHINA
83 85 462

Lee Chenoweth
Ball Corporation
Efratom Division
3 Parker
Irvine, CA 92718 USA
714/770-5000

Lisa G. Childers
Hewlett-Packard
5301 Stevens Creek Boulevard
Santa Clara, CA 95052-8059 USA
408/553-2328

Philip A. Clements
Jet Propulsion Laboratory
4800 Oak Grove Drive
Pasadena, CA 91109 USA
818/354-2933

Debra Coleman
Bonneville Power Administration
P. O. Box 3621
Portland, OR 97208-3621 USA
503/230-4533

Carey Conlon
Naval Satellite Operations Center
Building 375
Point Mugu, CA 93042 USA
805/989-4342

Len Cutler
Hewlett-Packard Laboratories
3500 Deer Creek Road
Palo Alto, CA 94303-0867 USA

Kevin Daly
Odetics
Precision Time Division
1515 South Manchester Avenue
Anaheim, CA 92802-2907 USA
714/758-0400

Jim Danaher
35 Navigation
23141 Plaza Pointe Drive
Laguna Hills, CA 92653 USA
714/830-3777

Angela M. Davis
U. S. Naval Observatory
Time Service Department
34th and Massachusetts Avenue, Northwest
Washington, DC 20392-5100 USA
202/653-1528

Kenneth J. Davis
D.O.D. Naval Weapons Center
Code 62541
China Lake, CA 93555 USA
619/939-6768

Patrick Davis
Navstar Electronics, Incorporated
1500 North Washington Boulevard
Sarasota, FL 34236 USA
813/366-9335

Gerrit De Jong
Van Swinden Laboratory
P. O. Box 654
2600 Ar Delft
NETHERLANDS
31 15 631 500

Zhang De Jun
Beijing Institute RM&M
P. O. Box 3930
Beijing, CHINA
83 85 462

Rudolph Decher
NASA/MSFC
Huntsville, AL 35812 USA
205/544-7751

Steven D. Deines
3254 Austin Drive
Colorado Springs, CO 80909 USA
719/630-7532

Edoardo Detoma
SEPA S.p.A (FIAT)
Corso Giulio Cesare, 294-300
Torino 10154, ITALY
39 11 2682 523

G. John Dick
Jet Propulsion Laboratory
4800 Oak Grove Drive
Pasadena, CA 91109 USA
818/354-6393

William A. Diener
Jet Propulsion Laboratory
4800 Oak Grove Drive
Pasadena, CA 91109 USA
818/354-9762

Michael Dienert
TIMETECH GmbH
15 Nobelstr 15
7000 Stuttgart, GERMANY
49 711 687 3575

Barbara A. Donaldson
EG&G
Frequency Divisions
35 Congress Street
Salem, MA 01970-0662 USA

Winfield Donat, III
U. S. Naval Observatory
34th and Massachusetts Avenue, Northwest
Washington, DC 20392-5100 USA
202/653-1538

Robert J. Douglas
National Research Council of Canada
M-36 Institute for National
Measurement Standards
Ottawa, Ontario K1A 0R6, CANADA
613/993-5186

Richard A. Dragonette
Johns Hopkins University
Applied Physics Laboratory
Johns Hopkins Road
Laurel, MD 20723-6099 USA
301/953-5000

Charles Dunn
Jet Propulsion Laboratory
4800 Oak Grove Drive
Pasadena, CA 91109 USA

Frank E. Easton
U. S. Air Force
Building 856, Room E247
Wright-Patterson Air Force Base
Dayton, OH 45433-6508 USA
513/257-4113

Edward Eng
Lockheed Missiles and Space Company
P. O. Box 3504
Sunnyvale, CA 94088 USA
408/756-3989

Thomas English
Ball Corporation
Efratom Division
3 Parker
Irvine, CA 92718-1605 USA
714/770-5000

Sheila Faulkner
U. S. Naval Observatory
Time Service Department
34th and Massachusetts Avenue, Northwest
Washington, DC 20392-5100 USA
202/653-1460

W. A. Feess
The Aerospace Corporation
2350 East El Segundo Boulevard
El Segundo, CA 90245-4691 USA

John Fellner
Ball Corporation
Efratom Division
3 Parker
Irvine, CA 92718 USA
714/770-5000

Mark Fitzgerald
Motorola, Incorporated
8201 East McDowell Road
M/D H2220
Scottsdale, AZ 85252 USA
602/441-8616

Henry F. Fliegel
The Aerospace Corporation
2350 East El Segundo Boulevard
El Segundo, CA 90245-4691 USA
310/336-1710

Earl Fossler
TRAK Systems
4726 Eisenhower Boulevard
Tampa, FL 33634-6391 USA
813/884-1411

Dan Friel
Leitch Incorporated
825K Greenbriar Circle
Chesapeake, VA 23320 USA
804/424-7920

Richard E. Funderburk
Austron, Incorporated
P. O. Box 14766
Austin, TX 78761 USA
512/251-2341

Jean C. Gaignebet
Observatoire de la Cote D'Azur
OCA/CERGA
Avenue Nicolas Copernic
F-06130 Grasse, FRANCE
33 1 93 36 5849

Ivan J. Galysh
U. S. Naval Research Laboratory
4555 Overlook Avenue, Southwest
Washington, DC 20375-5000 USA
202/404-7060

Jerry L. Garcia
NASA/Langley Research Center
MS/488
Hampton, VA 23665-5225 USA
804/864-5888

Mike Gardner
Leitch Incorporated
825K Greenbriar Circle
Chesapeake, VA 23320 USA
804/424-7920

Michael Garvey
Frequency and Time Systems, Incorporated
34 Tozer Road
Beverly, MA 01915 USA
508/927-8220

Robin Giffard
Hewlett-Packard Laboratories
3500 Deer Creek Road
Palo Alto, CA 94303-0867 USA
415/857-5372

Guy A. Gifford
U. S. Naval Research Laboratory
Code 8321
Washington, DC 20375-5000 USA
202/404-7060

Asbjorn M. Gjelsvik
MITRE
Burlington Road
Bedford, MA 01730 USA
617/377-9067

Earl Grant
U. S. Army Information System Command
White Sands Missile Range
White Sands, NM 88002 USA
505/678-1717

Joe C. M. Green
Allied Signal
Bendix Aerospace Corporation
129 North Hill Avenue
Pasadena, CA 91001 USA
818/584-4472

Charles A. Greenhall
1836 Hanscom Drive
South Pasadena, CA 91030 USA
213/258-1017

Robert L. Hamell
Jet Propulsion Laboratory
4800 Oak Grove Drive
Pasadena, CA 91109 USA
818/354-4944

Yuko Hanado
Communications Research Laboratory
893-1 Hirai, Kashimamachi
Ibaraki 314, JAPAN
81 299 82 1211

Hiroshi Hanado
Communications Research Laboratory
893-1 Hirai, Kashimamachi
Ibaraki 314, JAPAN
81 299 82 1211

Robert Hardin
Ball Corporation
Efratom Division
3 Parker
Irvine, CA 92718-1605 USA
714/770-5000

Walter R. Harding
NAVELEX
P. O. Box 55
Portsmouth, VA 23705-0055 USA
804/396-0516

Ilan Havered
Datum, Incorporated
1363 South State College Boulevard
Anaheim, CA 92806 USA
714/533-6333

Helmut Hellwig
Air Force Office of Scientific Research
Bolling Air Force Base
Washington, DC 20332-6448 USA
202/767-5017

Robert J. Hesselberth
Spectracom Corporation
101 Despatch Drive
East Rochester, NY 14445 USA

Richard L. Holstein
U. S. Air Force
6585 TG HSTT TKOD
Hollamon Air Force Base
Alamogordo, NM 88330-5000 USA
505/679-2535

Diana S. Howell
Jet Propulsion Laboratory
MS/161-228
4800 Oak Grove Drive
Pasadena, CA 91109 USA
818/354-0399

Quyen D. Hua
PAQ Communications
607 Shetland Court
Milpitas, CA 95035 USA
408/946-3305

Lim Hudiono
Ball Corporation
Efratom Division
3 Parker
Irvine, CA 92718-1605 USA
714/770-5000

James F. Hungerford
FTS
34 Tozer Road
Beverly, MA 01915 USA
508/927-8220

Jeffrey S. Ingold
Bendix Field Engineering Corporation
One Bendix Road
Columbia, MD 21045 USA
301/964-7188

Bernardo Jaduszliwer
The Aerospace Corporation
P. O. Box 92957, MS/253
Los Angeles, CA 90009 USA
310/336-9217

Nicolette M. Jardine
U. S. Naval Observatory
Time Service Department
34th and Massachusetts Avenue, Northwest
Washington, DC 20392-5100 USA
202/653-1662

James Jespersen
National Institute of Standards and Technology
325 Broadway
Boulder, CO 80303 USA
303/497-3849

Walter A. Johnson
The Aerospace Corporation
2350 East El Segundo Boulevard
El Segundo, CA 90245 USA
310/336-7174

James L. Johnson
Hewlett-Packard
5301 Stevens Creek Boulevard
Santa Clara, CA 95052 USA
408/553-2622

Sarunas K. Karuza
The Aerospace Corporation
2350 East El Segundo Boulevard
El Segundo, CA 90245 USA
310/336-7174

Shalom Kattan
Guide Technology, Incorporated
920 Saratoga Avenue
Suite 215
San Jose, CA 95129 USA
408/246-9905

Nancy E. Key
Jet Propulsion Laboratory
4800 Oak Grove Drive
Pasadena, CA 91109 USA
818/354-5434

Dieter Kirchner
Technische Universitat Graz
12 Inffeldgasse
Graz A-8010 AUSTRIA
43 316 873 7459

Lothar Kirk
Jet Propulsion Laboratory
4800 Oak Grove Drive
Pasadena, CA 91109 USA
818/354-3033

William J. Klepczynski
U. S. Naval Observatory
Time Service Department
34th and Massachusetts Avenue, Northwest
Washington, DC 20392-5100 USA
202/653-1521

John A. Klobuchar
Air Force Phillips Laboratory - GPI
Ionospheric Physics GP-IS
Hanscom Air Force Base, MA 01731 USA
617/377-3988

David J. E. Knight
National Physical Laboratory
Queens Road
Teddington Middlesex TW11 DLW
UNITED KINGDOM
44 81 943 6796

Stephen H. Knowles
NAVSPASUR
Dahlgren, VA 22448 USA
703/663-8191

Greg Kret
TrueTime, Incorporated
3243 Santa Rosa Avenue
Santa Rosa, CA 95407 USA
707/528-1230

Paul F. Kuhnle
Jet Propulsion Laboratory
MS/298-100
4800 Oak Grove Drive
Pasadena, CA 91109 USA
818/354-2715

Paul J. Kushmeider
Bendix Field Engineering Corporation
MS/VLBI
One Bendix Road
Columbia, MD 21045 USA
301/964-7672

Jack Kusters
Hewlett-Packard
5301 Stevens Creek Boulevard
Santa Clara, CA 95052-8059 USA
408/553-2041

G. Paul Landis
U. S. Naval Research Laboratory
Code 8322
Washington, DC 20375-5000 USA
202/404-7067

Julius C. Law
Jet Propulsion Laboratory
MS/298-100
4800 Oak Grove Drive
Pasadena, CA 91109 USA
818/354-2988

Ming C. Lee
Western Test Range/SFD
Vandenberg Air Force Base, CA 93437 USA
805/734-8232

Albert Leong
The Aerospace Corporation
2350 East El Segundo Boulevard
El Segundo, CA 90245 USA
310/336-7174

Sigfrido M. Leschiutta
Politecnico-Elettronica
24 Corso Abruzzi
Torino 10123 ITALY
38 11 56 44 035

Martin W. Levine
Smithsonian Astrophysical Observatory
P. O. Box 1513
Manchester, MA 01944 USA
617/496-7652

Wlodzimierz W. Lewandowski
Bureau International des Poids et Mesures
Pavillon de Breteuil
F-92312 Sevres Cedex, FRANCE
33 1 45 07 7063

Steve Lewis
Jet Propulsion Laboratory
MS/125-B18
4800 Oak Grove Drive
Pasadena, CA 91109 USA
818/354-3033

Fumming Li
Ball Corporation
Efratom Division
3 Parker
Irvine, CA 92718-1605 USA
714/770-5000

Chuck Little
Hewlett-Packard
5301 Stevens Creek Boulevard
Santa Clara, CA 95052-8059 USA
408/553-2506

Roger D. Loiler
Allen Osborne Associates
756 Lakefield - J
Westlake Village, CA 91361 USA
805/495-8420

Robert J. Lopes
AT&T - ADEC
Two Gateway Center
Newark, NJ 07012 USA
201/645-5025

James G. Lopez
Jet Propulsion Laboratory
4800 Oak Grove Drive
Pasadena, CA 91109 USA
818/354-7055

John Luck
Orroral Geodetic Observatory
Auslig
P. O. Box 2
Belconnen ACT 2616 AUSTRALIA

David W. Lupton
U. S. Coast Guard
Omega Nav System Center
7323 Telegraph Road
Alexandria, VA 22310-3998 USA
703/866-3806

George F. Lutes
Jet Propulsion Laboratory
4800 Oak Grove Drive
Pasadena, CA 91109 USA
818/354-6210

George E. Lutz
Hewlett-Packard
MS/51U-23
5301 Stevens Creek Boulevard
Santa Clara, CA 95050 USA
408/553-2558

Ken E. Martin
Bonneville Power Administration
P. O. Box 491
Vancouver, WA 98606 USA
206/690-2694

Edward M. Mattison
Smithsonian Astrophysical Observatory
60 Garden Street, MS/59
Cambridge, MA 02138 USA
617/495-7265

Richard H. Maurea
Johns Hopkins University
Applied Physics Laboratory
Johns Hopkins Road
Laurel, MD 20723 USA
301/953-5000

Thomas B. McCaskill
U. S. Naval Research Laboratory
Code 8323
4555 Overlook Avenue, Southwest
Washington, DC 20375-5000 USA
202/767-2595

Tom McClelland
Frequency Electronics, Incorporated
55 Charles Lindburgh Boulevard
Mitchell Field, NY 11553 USA
516/794-4500

Hunter McConnell, Jr.
2912 Henrietta Avenue
La Crescenta, CA 91214-2054 USA
818/248-3866

Joseph McDonough
Computer Sciences Corporation
P. O. Box 217
Clearfield, UT 84015 USA
801/773-9271

David A. McGillivray
EG&G/EM
P. O. Box 1912
MS/B3-21
Las Vegas, NV 89125 USA
702/295-3094

Marvin Meirs
Frequency Electronics, Incorporated
55 Charles Lindburgh Boulevard
Mitchell Field, NY 11553 USA
516/794-4500

Don Mitchell
TrueTime, Incorporated
P. O. Box 115
Georgetown, TX 78627 USA
512/863-5414

Shawn P. Monaghan
Communications Security Establishment
P. O. Box 9703, Terminal
Ottawa, Ontario K1G 3Z4 CANADA
613/991-7691

Robert D. Montesi
Hewlett-Packard
MS/23
5301 Stevens Creek Boulevard
Santa Clara, CA 95052 USA
408/553-3088

Derek Morris
National Research Council
Montreal Road
Ottawa K1A 0R6 CANADA
613/993-9340

Louis F. Mueller
Hewlett-Packard
5301 Stevens Creek Boulevard
Santa Clara, CA 94306 USA
408/553-2347

Frank Mullen
Frequency and Time Systems
34 Tozer Road
Beverly, MA 01915 USA
508/927-8220

Prem K. Munjal
The Aerospace Corporation
2350 East El Segundo Boulevard
El Segundo, CA 90245 USA
310/336-6406

William J. Murphy
Computer Sciences Corporation
P. O. Box 446
Edwards Air Force Base, CA 93523 USA
805/277-2004

Clyde C. Norris
Computer Sciences Corporation
P. O. Box 217
Clearfield, UT 84015 USA
801/773-9271

Jerry R. Norton
Johns Hopkins University
Applied Physics Laboratory
Johns Hopkins Road
Laurel, MD 20723-6099 USA
301/792-5000

Phillip Norton
Naval Satellite Operations Center
Building 375
Point Mugu, CA 93042 USA
805/989-4338

Dean T. Okayama
National Institute of Standards and Technology
P. O. Box 417
Kekaha, HI 96752 USA
808/335-4361

Binh Ong
Ball Corporation
Efratom Division
3 Parker
Irvine, CA 92718-1605 USA
714/770-5000

David B. Opie
Physical Sciences, Incorporated
635 Slaters Lane
Suite G101
Alexandria, VA 22314 USA
703/548-6410

Skip Osborne
Allen Osborne Associates
756 Lakefield Road, Building J
Westlake Village, CA 91361-2624 USA
805/495-8420

Terry N. Osterdock
Stellar Navigation, Incorporated
19075 Skyline Boulevard
Los Gatos, CA 95030 USA
408/354-0733

Joseph W. Ouellette
The Aerospace Corporation
P. O. Box 92957
Los Angeles, CA 90009-2957 USA
310/336-6994

Chris Pagnanelli
Ball Corporation
Efratom Division
3 Parker
Irvine, CA 92718-1605 USA
714/770-5000

Alfred R. Paiz
Jet Propulsion Laboratory
4800 Oak Grove Drive
Pasadena, CA 91109 USA
818/354-3014

Theo Parisek
Hewlett-Packard
5301 Stevens Creek Boulevard
Santa Clara, CA 95052 USA
408/553-3344

Ralph E. Partridge
Los Alamos National Laboratory
P. O. Box 1663
MS/P947
Los Alamos, NM 87545 USA
505/665-1617

Benjamin Parzen
Consulting Engineer
3634 7th Avenue
San Diego, CA 92103 USA
619/292-0567

Peter Z. Paulovich
NAVELEX Portsmouth
P. O. Box 55
Portsmouth, VA 23320 USA
804/396-0287

Rolando Penabade
TRAK Systems
4726 Eisenhower Boulevard
Tampa, FL 33634-6391 USA
813/884-1411

Bruce M. Penrod
Austron, Incorporated
P. O. Box 14766
Austin, TX 78761 USA
512/251-2341

Trudi Peppler
National Institute of Standards and Technology
325 Broadway
Boulder, CO 80303 USA
303/497-3338

Donald B. Percival
University of Washington
Seattle, WA 98105 USA
206/543-1300

James Perry
NASA/Goddard Space Flight Center
Code 531.3
Greenbelt, MD 20771 USA
301/286-3471

Harry E. Peters
Sigma Tau Standards Corporation
P. O. Box 1877
Tuscaloosa, AL 35403 USA
205/553-0038

Gerard Petit
Bureau International des Poids et Mesures
Pavillon de Breteuil
F-92312 Sevres Cedex, FRANCE
33 1 45 07 7067

Wolfgang Pflaum
Ball Corporation
Efratom Division
3 Parker
Irvine, CA 92718 USA
714/770-5000

Tuan M. Pham
Allied Signal
Bendix Field Engineering Corporation
129 North Hill Avenue
Pasadena, CA 91106 USA

Physikalisch Technische
Bundesanstalt
Library
Bundesallee 100
P. O. Box 100
D-3300 Braunschweig GERMANY

William M. Powell
U. S. Naval Observatory
Time Service Department
34th and Massachusetts Avenue, Northwest
Washington, DC 20392-5100 USA
202/653-1528

Edward D. Powers
Naval Research Laboratory
4555 Overlook Avenue, Southwest
Code 8321
Washington, DC 20375-5000 USA
202/404-7060

Robert E. Price
Bendix Field Engineering Corporation
MS/VLBI
One Bendix Road
Columbia, MD 21043 USA
301/964-7437

William L. Raffel
D.O.D. Naval Weapons Center
Code 62541
China Lake, CA 93555 USA
619/939-6763

Richard A. Rayos
Computer Sciences Raytheon
P. O. Box 4127
CSR 2230
Patrick Air Force Base, FL 32925 USA
407/494-7176

Wilson G. Reid
U. S. Naval Research Laboratory
Code 8324
Washington, DC 20375-5000 USA
202/767-2595

Victor S. Reinhardt
Hughes Aircraft Company
SC/S12/4325
P. O. Box 92919
Los Angeles, CA 90009 USA
310/647-8359

Eugene A. Rheingans
351 Binscarth Road
Los Osos, CA 93402 USA
714/637-1959

William J. Riley
EG&G Components
Frequency Division
35 Congress Street
Salem, MA 09170-0662 USA

Juan Rivera
Loral Space Information Systems
1322 Space Park Drive
Houston, TX 77058 USA
713/335-6571

Harry W. Sadler
Bendix Field Engineering Corporation
One Bendix Road
Columbia, MD 21045 USA
410/964-7425

Safaa Samuel
National Institute for Standards, 92A
Ahmed Orabi Street, El
Mohandeseen
Cairo, EGYPT
2 02 36 12 339

George A. Santana
Allied Signal
Bendix Field Engineering Corporation
129 North Hill Avenue
Pasadena, CA 91106 USA
818/584-4520

Rick Sarrica
Hewlett-Packard
5301 Stevens Creek Boulevard
Santa Clara, CA 95052 USA
408/553-2089

Gary D. Sasaki
Hewlett-Packard
5301 Stevens Creek Boulevard
Santa Clara, CA 95052 USA
408/553-2568

Wolfgang Schaefer
University of Stuttgart
D-7000 Stuttgart
Senefelder Str 26 GERMANY

Mark S. Schenewerk
National Oceanographic and Atmospheric
Administration
11400 Rockville Pike
Room 419, N/OES13
Rockville, MD 20852 USA
301/443-2520

Wally Schnitger
Science Systems
P. O. Box 880
Midway City, CA 92655 USA

Soon Shin
Ball Corporation
Efratom Division
3 Parker
Irvine, CA 92718-1605 USA
714/770-5000

Doug A. Sisk
AT&T - ADEC
Two Gateway Center
Newark, NJ 07102 USA
201/645-5765

Gary Smith
Odetics
Precision Time Division
1515 South Manchester Avenue
Anaheim, CA 92802-2907 USA
714/758-0400

Armin Soering
German Telekom, FTZ
3 AM Kavalleriesand
Darmstadt 6100
GERMANY
49 6151 83 4549

Siegfried K. Starker
DLR
8031 Wessling
Ringstr 14, GERMANY
81 53 28347

Samuel R. Stein
Timing Solutions Corporation
555 Jack Pine Court
Boulder, CO 80304 USA
303/443-5152

Charles S. Stone
Frequency Electronics, Incorporated
55 Charles Lindburgh Boulevard
Mitchell Field, NY 11553 USA
512/794-4500

David A. Stowers
Jet Propulsion Laboratory
MS/298-100
4800 Oak Grove Drive
Pasadena, CA 91109 USA
818/354-7055

Emil R. Straka
Hewlett-Packard
5301 Stevens Creek Boulevard
Santa Clara, CA 95051 USA
408/553-2887

Alvin Strauss
Frequency Electronics, Incorporated
55 Charles Lindburgh Boulevard
Mitchell Field, NY 11553 USA
516/794-4500

Joseph J. Suter
Johns Hopkins University
Applied Physics Laboratory
Johns Hopkins Road
Laurel, MD 20723-6099 USA
301/953-5000

Richard L. Sydnor
Jet Propulsion Laboratory
MS/298-100
4800 Oak Grove Drive
Pasadena, CA 91109 USA
818/354-2763

Philip E. Talley
The Aerospace Corporation
530 Margo Avenue
Long Beach, CA 90803 USA
310/431-3226

Patrizia P. Tavella
Istituto Elettrotecnico Nazionale
91 Strada Delle Cacce
Torino 10135 ITALY
39 11 348 8933

Pierre Tetreault
Geodetic Survey of Canada
615 Booth Street
Ottawa Ontario K1A 0E9 CANADA
613/995-4345

Claudine Thomas
Bureau International des Poids et Mesures
Pavillon de Breteuil
F-92312 Sevres Cedex, FRANCE
33 1 45 07 7073

Alexander Titov
Norell, Incorporated
LSRRI
22 Marlin Lane
Mays Landing, NJ 08330 USA
609/625-2223

Michael Tope
TrueTime, Incorporated
3243 Santa Rosa Avenue
Santa Rosa, CA 95407 USA
707/528-1230

Robert D. Turner
Los Alamos National Laboratory
6890 Vallon Drive
Rancho Palos Verdes, CA 90274 USA

Ricardo A. G. Unglaub
Allied Signal
Bendix Field Engineering Corporation
129 North Hill Avenue
Pasadena, CA 91106 USA
818/584-4458

Marinus J. Van Melle
Rockwell International
8042 Madia
La Palma, CA 90623 USA
310/797-3459

Christian Veillet
Observatoire de La Cote D'Azur
OCA/CERGA
Avenue Nicolas Copernic
F-06130 Grasse FRANCE
33 1 93 36 5849

Robert F. C. Vessot
Smithsonian Astrophysical Observatory
60 Garden Street
Cambridge, MA 02138 USA
617/495-7276

John Vig
U. S. Army Labcom
ATTN: SLCET-EQ
Fort Monmouth, NJ 07703-5601 USA
908/544-4275

Frank J. Voit
The Aerospace Corporation
2350 East El Segundo Boulevard
El Segundo, CA 90245 USA
310/336-7174

Eric P. Vondran
45th Space Wing
Maintenance Sq/Engineering
Building 981
Patrick Air Force Base, FL 32931 USA
407/799-2195

Todd Walter
Gravity Probe B
Hansen Experimental Physics Laboratory
Via Palon Street
Stanford University
Stanford, CA 94305-4085 USA
415/723-7239

Samuel C. Ward
2258 Midlothian Drive
Altadena, CA 91001 USA
818/794-3491

S. Clark Wardrip
Bendix Field Engineering Corporation
726 Foxenwood Drive
Santa Maria, CA 93455 USA
805/734-8232, Ext. 53214

Werner Weidemann
Ball Corporation
Efratom Division
3 Parker
Irvine, CA 92718-1605 USA
714/770-5000

Marc Weiss
National Institute of Standards and Technology
325 Broadway
Boulder, CO 80303 USA
303/497-3261

Paul J. Wheeler
U. S. Naval Observatory
Time Service Department
34th and Massachusetts Avenue, Northwest
Washington, DC 20392-5100 USA
202/653-0516

Warren L. Wilson
Lockheed Missiles and Space Company
707 Spindrift Drive
San Jose, CA 95134-1346 USA
408/743-1213

Robert E. Wilson
University of Idaho
Department of Electrical Engineering
Moscow, ID 83843 USA
203/885-6554

Gernot M. R. Winkler
U. S. Naval Observatory
Time Service Department
34th and Massachusetts Avenue, Northwest
Washington, DC 20392-5100 USA
202/653-1520

Bosco Wong
Hewlett-Packard
5301 Stevens Creek Boulevard
Santa Clara, CA 95052 USA
408/553-2418

James L. Wright
Computer Sciences Raytheon
P. O. Box 4127
CSR 2230
Patrick Air Force Base, FL 32925 USA
407/494-7176

Nicholas F. Yannoni
Rome Laboratory
31 Lafayette Road
Newton, MA 02162 USA
617/377-2206

Colleen H. Yinger
The Aerospace Corporation
P. O. Box 92957
M4-954
Los Angeles, CA 90009 USA
310/336-4386

Curtis M. Younce
Hewlett-Packard
Santa Clara Division
5301 Stevens Creek Boulevard
Santa Clara, CA 95052 USA
408/553-2540

C. Eric Youngberg
Hewlett-Packard
5301 Stevens Creek Boulevard, MS/52/07
Santa Clara, CA 95119 USA
408/553-2308

Ed Yrisarri
Ball Corporation
Efratom Division
3 Parker
Irvine, CA 92718-1605 USA
714/770-5000

Edward M. Zantek
Naval Air Development Center
Warminster, PA 18974 USA

Vadim Zhoinerov
Norell, Incorporated
22 Martin Lane
Mays Landing, NJ 08330 USA
609/625-2223

Qixiang Zhuang
National Research Council
Room 25, M-36
Montreal Road Campus
Ottawa Ontario K1A 0R6 CANADA
613/993-5698

REPORT DOCUMENTATION PAGE

Form Approved
OMB No. 0704-0188

1. AGENCY USE ONLY *(Leave blank)*	2. REPORT DATE	3. REPORT TYPE AND DATES COVERED
	July 1992	Conference Publication

4. TITLE AND SUBTITLE
23rd Annual Precise Time and Time Interval (PTTI) Applications and Planning Meeting

5. FUNDING NUMBERS
C-NAS5-31000

6. AUTHOR(S)
Richard L. Sydnor, Editorial Committee Chairman

7. PERFORMING ORGANIZATION NAME(S) AND ADDRESS(ES)
NASA-Goddard Space Flight Center
Greenbelt, Maryland 20771

8. PERFORMING ORGANIZATION REPORT NUMBER
92B00083

9. SPONSORING/MONITORING AGENCY NAME(S) AND ADDRESS(ES)
National Aeronautics and Space Administration
Washington, D.C. 20546-0001

10. SPONSORING/MONITORING AGENCY REPORT NUMBER
NASA CP-3159

11. SUPPLEMENTARY NOTES
Richard Sydnor: Jet Propulsion Laboratory, Pasadena, CA. Other sponsors: U.S. Naval Observatory, Jet Propulsion Laboratory, Space and Naval Warfare Systems Command, Naval Research Laboratory, Army Electronics Technology and Devices Laboratory, Rome Laboratory, and Air Force Office of Scientific Research.

12a. DISTRIBUTION/AVAILABILITY STATEMENT
Unclassified - Unlimited
Subject Category 70

12b. DISTRIBUTION CODE

13. ABSTRACT *(Maximum 200 words)*

This document is a compilation of technical papers presented at the 23rd Annual PTTI Applications and Planning Meeting, December 3 through 5, 1991, at the Ritz-Carlton Huntington Hotel in Pasadena, California. Papers are in the following categories.

- o Recent developments in rubidium, cesium, and hydrogen-based frequency standards, and in cryogenic and trapped-ion technology.
- o International and transnational applications of precise time and time interval technology with emphasis on satellite laser tracking networks, GLONASS timing, intercomparison of national time scales and international telecommunications.
- o Applications of precise time and time interval technology to the telecommunications, power distribution, platform positioning, and geophysical survey industries.
- o Applications of PTTI technology to evolving military communications and navigation systems.
- o Dissemination of precise time and frequency by means of GPS, GLONASS, MILSTAR, Loran, and synchronous communications satellites.

14. SUBJECT TERMS
Frequency Standards, Hydrogen Masers, Cesium, Rubidium Trapped Ion, Crystals, Time Synchronization, Precise Time, Time Transfer, GPS, GLONASS, Satellite Clocks, Jitter, Phase Noise

15. NUMBER OF PAGES
460

16. PRICE CODE
A20

17. SECURITY CLASSIFICATION OF REPORT	18. SECURITY CLASSIFICATION OF THIS PAGE	19. SECURITY CLASSIFICATION OF ABSTRACT	20. LIMITATION OF ABSTRACT
Unclassified	Unclassified	Unclassified	Unlimited

NSN 7540-01-280-5500

Standard Form 298 (Rev. 2-89)
Prescribed by ANSI Std. 239-18, 298-102

NASA-Langley, 1992

Aeronautics and
Administration
D.C.
Use, $300

NASA